



**HAL**  
open science

# Caractérisation fonctionnelle de la protéine kinase CK1.2 de leishmanie chez le parasite et l'hôte mammifère

Daniel Martel

## ► To cite this version:

Daniel Martel. Caractérisation fonctionnelle de la protéine kinase CK1.2 de leishmanie chez le parasite et l'hôte mammifère. Biochemistry, Molecular Biology. Université Paris Cité, 2019. English. NNT : 2019UNIP7093 . tel-03403086

**HAL Id: tel-03403086**

**<https://theses.hal.science/tel-03403086v1>**

Submitted on 26 Oct 2021

**HAL** is a multi-disciplinary open access archive for the deposit and dissemination of scientific research documents, whether they are published or not. The documents may come from teaching and research institutions in France or abroad, or from public or private research centers.

L'archive ouverte pluridisciplinaire **HAL**, est destinée au dépôt et à la diffusion de documents scientifiques de niveau recherche, publiés ou non, émanant des établissements d'enseignement et de recherche français ou étrangers, des laboratoires publics ou privés.

## Université de Paris

**Ecole doctorale Bio Sorbonne Paris Cité – ED 562**

***Unité de Parasitologie moléculaire  
et Signalisation – INSERM U1201***

***Institut Pasteur de Paris***

# **Functional characterisation of *Leishmania* casein kinase 1.2 in the parasite and the mammalian host**

Par Daniel Martel

Thèse de doctorat d'Infectiologie-Microbiologie

Dirigée par Najma Rachidi

Présentée et soutenue publiquement le 20 septembre 2019

Devant un jury composé de :

Président du jury :	Philippe Silar / PU-DR / Université Paris-Diderot
Rapporteurs :	Mélanie Bonhivers / DR / CNRS, Université de Bordeaux Nicolas Fasel / PU-DR / Université de Lausanne
Examineurs :	Linda Kohl / MC / MNHN Christian Doerig / PU-DR / RMIT Bundoora Olivier Silvie / DR / UPMC
Directrice de thèse :	Najma Rachidi / CR / Institut Pasteur de Paris
Membre invité :	Gerald Späth / DR / Institut Pasteur de Paris









## **Titre : Caractérisation fonctionnelle de la protéine kinase CK1.2 de leishmanie chez le parasite et l'hôte mammifère**

### **Résumé :**

Les parasites *Leishmania* sont les agents responsables des leishmanioses. Au cours de leur cycle de vie, ils alternent entre une forme promastigote, extracellulaire, chez l'insecte vecteur et une forme intracellulaire, amastigote, dans les macrophages de mammifères. Pour survivre dans l'hôte mammifère, les amastigotes doivent manipuler le macrophage à leur avantage. La caséine kinase 1.2 de Leishmanie (LmCK1.2) pourrait être impliquée dans la manipulation de la cellule-hôte, car : (i) elle est exportée dans la cellule-hôte via des exosomes, (ii) elle est essentielle à la survie du parasite intracellulaire, et (iii) elle phosphoryle des protéines de la cellule hôte. Cependant, il existe peu d'informations sur ses fonctions dans le parasite et sur les voies de signalisations qu'elle pourrait réguler dans le macrophage. Lors de ce travail de thèse, j'ai montré que LmCK1.2 était présente dans le cytoplasme, qu'elle était associée au cytosquelette et à divers organelles tels que le corps basal ou le fuseau mitotique. J'ai montré que la présence de régions de faible complexité, présentes dans la partie C-terminale de LmCK1.2, était nécessaire à sa localisation subcellulaire. Afin de mieux comprendre les fonctions de LmCK1.2, j'ai ensuite réalisé des analyses protéomiques qui m'ont permis d'identifier 171 protéines associées à LmCK1.2 (LmCKAPs) dans le parasite. Ces LmCKAPs sont impliquées dans diverses voies. J'ai pu montrer l'implication de LmCK1.2 dans deux voies particulières : l'endocytose via la régulation du complexe AP2, et la cytokinèse via la régulation d'une nouvelle protéine mitotique, LmCKAP1. J'ai également identifié 146 protéines du macrophage associées à LmCK1.2 (LmCKAPhost). Elles sont surreprésentées dans deux voies particulières : le trafic cellulaire et le métabolisme des protéines, qui pourraient correspondre à des voies importantes pour la survie du parasite intracellulaire. Ce travail a considérablement enrichi nos connaissances sur LmCK1.2. En particulier, ces résultats montrent la singulière ressemblance entre LmCK1.2 et les CK1 humaines en ce qui concerne la localisation et la composition des protéines partenaires, suggérant que CK1.2 de leishmanie ait évolué pour imiter les CK1 de mammifères, particulièrement CK1 $\alpha$ . Le contrôle des voies de signalisation de CK1 $\alpha$  pourrait être l'une des clés de la survie intracellulaire de la leishmanie, comme cela a été montré pour d'autres agents pathogènes tels que les virus.

**Mots clefs :** *Leishmania*, casein kinase 1, relations hôte-pathogène, trafic cellulaire, cytokinèse, localisation.

**Title: Functional characterisation of *Leishmania* casein kinase 1.2 in the parasite and the mammalian host**

**Abstract:**

*Leishmania* parasites are responsible for leishmaniasis. During their life cycle, they alternate between extracellular promastigotes in the insect vector and intracellular amastigotes in mammalian macrophages. Survival in the mammalian host implies to subvert the macrophages. *Leishmania* casein kinase 1 isoform 2 (LmCK1.2), as a signalling kinase, could be involved in the manipulation of the host cell, because: (i) it is released into the host cell via exosomes, (ii) it is essential for intracellular parasite survival, (iii) it phosphorylates host proteins. However, little is known about its functions in the parasites and the pathways it may regulate in the macrophage. I first showed that LmCK1.2 was found in the cytoplasm, associated to the cytoskeleton and to various organelles such as the basal body or the mitotic spindle. The subcellular localisations of LmCK1.2 required the presence of the C-terminal low complexity regions, suggesting the importance of protein-protein interactions for this process. To gain insights into LmCK1.2 functions, I then used proteomics to identify 171 LmCK1.2 associated proteins (LmCKAPs) in the parasite, which were involved in various pathways including endocytosis through the regulation of the AP2 complex and cytokinesis through the regulation of a novel cell-cycle regulated protein, LmCKAP1. Finally, I identified 146 mammalian host proteins associated with LmCK1.2 (LmCKAPhost), which are over-represented in proteins involved in cellular trafficking and protein metabolism, highlighting pathways that might be important for intracellular parasite survival. This work considerably increased our knowledge on *Leishmania* CK1.2. These data demonstrate singular similarities in localization and interactome composition between LmCK1.2 and human CK1s, suggesting that *Leishmania* CK1.2 has evolved to mimic mammalian CK1s and particularly CK1 $\alpha$ . Similarly to other pathogens such as viruses, controlling CK1 $\alpha$  pathways might be one of the keys to *Leishmania* intracellular survival.

**Keywords:** *Leishmania*, casein kinase 1, host-pathogen interactions, cellular trafficking, cytokinesis, localisation.



## Acknowledgements

...ou bien remerciements dans la langue de Molière.

Je souhaite tout d'abord remercier ma directrice de thèse, Najma Rachidi. Merci Najma de m'avoir permis de faire cette thèse avec toi, merci pour ce si beau projet, je suis conscient que j'ai eu de la chance de travailler sur un projet si complet avec tant de choses à découvrir. Merci pour ta patience, ta ténacité et ton optimisme inébranlables ; tu as su me pousser vers le haut et m'as permis de finaliser cette thèse, malgré les vents parfois contraires.

Un grand merci également à Gerald F. Späth notre chef d'unité, cette thèse au sein de ton ParSig ce fut quatre années de réel plaisir, merci pour ton soutien et ta joie communicative, merci pour les discussions scientifiques et les encouragements. ParSig, ce cocon de laboratoire : merci à vous toutes et tous, que vous soyez encore au laboratoire ou non, cette thèse vous y avez grandement contribué et je vous en suis grandement redevable. Vous avez résisté un temps à mon humour excellent (si si), mais je sais bien que finalement je vous ai converti (enfin pas tou(te)s). Eric Prina, merci pour tes conseils, ta gentillesse et ta répartie dans l'humour. La team des co-bureaux de la mezzanine en croix (c'est une appellation d'origine protégée), Pascale Pescher, Suzanne Lamotte et Sima Drini. J'ai réellement adoré mes années avec vous dans ce petit terrier exigü, les discussions, les rires, les chants, et j'en passe une tonne parce que je n'ai que deux pages... Suzanne, merci particulièrement pour le soutien et l'amitié, you rock ! Hervé Lecoeur, déjà merci parce que c'est toi qui as aligné les étoiles pour que je puisse faire la thèse avec Najma. Donc tu as ma gratitude éternelle ! Merci aussi pour ta gentillesse et tes petits plats délicieux. La team, du nouveau bureau tropical (là aussi on est dans de l'appellation d'origine protégée), Olivier Leclercq (merci pour ta gentillesse et le travail que tu as fait pour moi), Laura Piel (de la team PhD, je suis à fond avec toi pour ta dernière ligne droite), Giovanni Bussotti, Thibault Rosazza (bon voyage et bonne chance pour ton doctorat écossais), Paya N'Diaye, Delphine Cormontagne (bon courage aussi pour ton doctorat jovacien), merci pour tout le soutien et l'attention ! Enfin, merci à Christine Maillet (reste comme tu es, une perle !), Christel Ricard-Andraos (merci pour ton aide et ton accent du Sud qui me fait si plaisir). Merci aux autres dont la présence manque, Sophie Veillault, Penny Smirlis, Mathieu Cayla, Stewart Pine, Evi Gouzelou, et tous du LeiShield-MATI.

Merci aux membres de mon jury, Philippe Silar, Mélanie Bonhivers, Nicolas Fasel, Christian Doerig, Linda Kohl et Olivier Silvie. Merci pour votre temps, c'est un honneur de vous avoir dans mon jury. Philippe, après vos cours passionnants en Master 1 je vous retrouve quelques années plus tard, un grand merci d'avoir accepté de présider mon jury de thèse.

Je tiens tout particulièrement à remercier Geneviève Milon pour les encouragements, les petites attentions, la bonne humeur et les discussions passionnantes.

A l'Institut Pasteur, je souhaite remercier Audrey Salles, Julien Fernandes, et toute l'équipe d'UTECHS PBI pour votre disponibilité et gentillesse lors des longues heures que j'ai passées aux microscopes de la plate-forme. Merci à Philippe Bastin et son équipe, Thierry Blisnick, Serge Bonnefoy, Moara Lemos et Estefania Calvo-Alvarez ainsi qu'à Brice Rotureau et Jamin Jung pour tous vos conseils, votre aide et votre soutien. Merci à Brice Sperandio, mon tuteur Pasteur, de m'avoir suivi pendant ces quelques années de thèse, d'avoir pris à cœur son rôle de tuteur et avoir toujours eu la gentillesse de me conseiller. Merci à toutes et à tous qui de près ou de loin avez contribué à cette thèse ou facilité son aboutissement.

A l'Institut Pasteur toujours, je souhaite remercier la team volley ASIP1, merci à toute l'EQUIPE, vraiment c'était toujours une bouffée d'oxygène ces sessions du lundi midi et du mercredi soir. Certes ce fut dur de gagner mais qu'importe, j'ai toujours aimé ces moments. En position reggaeton !! Pizza !! Merci aussi aux Générations Spontanées, la troupe d'impro de Pasteur, et à Layla Jebabli (coach !), ces trois années m'ont tellement fait du bien, c'était un moment de pur bonheur les mardis soir !!

Et puis je souhaite remercier ceux qui n'ont pas vraiment pris part à ce travail, enfin pas directement, et pourtant qui ont eu beaucoup d'influence. Merci à Pierre Caumette mon parrain, tu as initié ma curiosité il y a une quinzaine d'années. Les amis d'Orsay, vous vous reconnaitrez, un grand merci pour le soutien et la facilité que vous avez eu à me changer les idées. Ne changez pas, vous êtes les meilleurs ! Merci à tous les amis, les anciens d'ESN, les amis d'Oz, Raph, Sylvain, Emilien, et merci à l'entourage proche tous autant que vous êtes.

Merci à ma famille, vous me connaissez par cœur, vous n'avez jamais douté de moi, vous m'avez toujours soutenu et encouragé, et ça peut sembler normal venant de sa famille, mais je sais que je suis très chanceux d'avoir une famille si chouette.

Enfin, merci à toi Juliette. Tu as en quelque sorte toi aussi vécu cette thèse. Merci de me rendre la vie plus belle au quotidien.

# Table of contents

RESUMÉ : .....	5
ABSTRACT: .....	7
ACKNOWLEDGEMENTS.....	9
TABLE OF CONTENTS .....	11
ABBREVIATIONS.....	17
LIST OF FIGURES.....	23
LIST OF TABLES.....	25
INTRODUCTION.....	27
<b>1. The leishmaniases .....</b>	<b>29</b>
1.1. The clinical manifestations and geographical distribution.....	29
1.2. Diagnosis, treatment and prevention .....	33
1.2.1. Diagnosis.....	33
1.2.2. Vaccination .....	33
1.2.3. Treatments .....	35
1.2.4. Prevention .....	36
<b>2. Vectors and reservoirs.....</b>	<b>37</b>
2.1. Vectors .....	37
2.2. Reservoirs.....	37
<b>3. The <i>Leishmania</i> parasite.....</b>	<b>38</b>
3.1. Taxonomy.....	38
3.2. Life cycle and interaction with the mammalian host .....	38
3.3. <i>Leishmania</i> cell biology .....	42
<b>4. Protein kinases.....</b>	<b>45</b>
4.1. Eukaryotes.....	45
4.2. Trypanosomatids.....	47
4.3. Casein kinase 1 family .....	48
4.3.1. General description of the CK1 family.....	49
4.3.2. Structure of casein kinase 1.....	49
4.3.3. Specificity of CK1 .....	52
4.3.4. Regulation of CK1 activity.....	52

4.3.5. CK1s in parasites species .....	53
4.3.6. CK1s in infectious diseases .....	55
4.4. <i>Leishmania</i> casein kinase 1 .....	56
4.4.1. Generalities.....	56
4.4.2. LmCK1.2 .....	57
<b>5. PhD objectives.....</b>	<b>60</b>
<b>MATERIALS &amp; METHODS .....</b>	<b>61</b>
<b>Materials.....</b>	<b>63</b>
1. Chemicals .....	63
2. DNA vectors.....	68
2.1. pLEXSY-hyg2 .....	68
2.2. pLEXSY-neo2 .....	69
2.3. pBAD/Thio-TOPO .....	70
2.4. pPLOT and pT plasmids.....	71
<b>Methods.....</b>	<b>73</b>
1. Bioinformatics methods .....	73
1.1. Gene and protein sequence information .....	73
1.2. Multiple Sequence Alignments and Phylogenetic Analyses .....	73
1.3. 3D structure prediction .....	73
1.4. Reactome pathways analysis.....	74
1.5. DAVID pathways analysis.....	74
2. Molecular biology methods.....	74
2.1. Restriction digestion.....	74
2.2. DNA ligation.....	74
2.3. Agarose gel electrophoresis and DNA purification.....	74
2.4. Transformation of <i>E. coli</i> .....	75
2.5. Plasmid extraction .....	75
3. Cell biological methods .....	76
3.1. Cell cycle arrest with flavopiridol .....	76
3.2. Isolation, culture and lysis of bone marrow-derived macrophages .....	76
3.3. Chromatographic conditions for mass spectrometry analysis .....	77
<b>RESULTS.....</b>	<b>79</b>
<b>CHAPTER I.....</b>	<b>81</b>
<b>Presentation .....</b>	<b>83</b>
Contributions to the work.....	83
<b>1. Investigating LmCK1.2 localisation in <i>Leishmania</i> parasites - article .....</b>	<b>84</b>
1.1. Article title, authors and keywords .....	84
1.2. Abstract .....	85
1.3. Introduction.....	86
1.4. Materials and Methods .....	89
1.4.1. Contact for reagent and resource sharing.....	89
1.4.2. Experimental model and subject details .....	89
1.4.3. Methods details .....	90
1.4.4. Quantification and statistical analysis .....	98
1.4.5. Key resources table .....	99

1.5. Results .....	103
1.5.1. <i>Leishmania</i> CK1.2 localisation is ubiquitous .....	103
1.5.2. CK1.2 localises to the basal body.....	104
1.5.3. CK1.2 localises to the flagellum and to the flagellar pocket.....	106
1.5.4. CK1.2 is localised in the granular zone of the nucleolus and redistributed to the mitotic spindle during mitosis. ....	107
1.5.5. CK1.2 co-localises with chaperone proteins to specific organelles .....	109
1.5.6. CK1.2 has a similar localisation in axenic amastigotes as in promastigotes.....	111
1.5.7. The C-terminal and the N-terminal domains of CK1.2 are, respectively, essential for its correct localisation and its stability, but not for its activity.....	112
1.6. Discussion.....	115
1.6.1. Basal body and flagellum.....	116
1.6.2. Nucleolus and chromosome segregation .....	117
1.6.3. Flagellar pocket.....	120
1.6.4. Regulation of CK1.2 localisation .....	121
1.6.5. <i>Leishmania</i> CK1 mimics mammalian CK1 .....	122
1.7. Acknowledgments .....	124
1.8. Figure legends .....	125
1.9. Figures .....	134
1.10. Supplemental figure legends.....	145
1.11. Supplemental figures.....	148
1.12. References.....	154
<b>CHAPTER II .....</b>	<b>165</b>
<b>Presentation .....</b>	<b>167</b>
<b>1. Identification of LmCK1.2 binding partners reveals its role in endocytosis in <i>Leishmania</i> - article .....</b>	<b>168</b>
1.1. Article title, authors and keywords .....	168
1.2. Contributions to the work .....	169
1.2. Abstract .....	170
1.3. Introduction.....	171
1.4. Materials and Methods .....	173
1.4.1. Parasite culture.....	173
1.4.2. Parasite transfection.....	173
1.4.3. CRISPR-Cas9 gene tagging and knockouts.....	174
1.4.4. Genotype characterization .....	174
1.4.5. Analysis of parasite concentration, cell death and mNeonGreen fluorescence intensity.....	175
1.4.6. Immuno-fluorescence microscopy .....	175
1.4.7. Plasmids for recombinant protein production .....	176
1.4.8. Bacterial expression and purification of recombinant proteins .....	176
1.4.9. Protein kinase assays.....	177
1.4.10. Protein extraction, SDS-PAGE and Western Blot analysis .....	178
1.4.11. Immunoprecipitation.....	178
1.4.12. Identification of LmCK1.2-V5-His <sub>6</sub> associated proteins by nanoLC-MS/MS analysis.....	179
1.4.13. AP2 phylogenetic analysis .....	181
1.4.14. FM4-64FX staining .....	181
1.5. Results .....	182
1.5.1. Identification of candidate LmCK1.2-associated proteins.....	182
1.5.2. The LmCK1.2 interactome reveals numerous novel and amastigote stage-specific associated proteins .....	189
1.5.3. Identification of LmCKAPs implicated in vesicular or protein trafficking. ....	198
1.5.4. The AP2 complex is conserved in <i>Leishmania spp.</i> .....	201
1.5.5. $\beta$ 2-adaptin is phosphorylated by LmCK1.2. ....	204

1.5.6. $\alpha$ 2-, $\beta$ 2- or $\mu$ 2-adaptin subunits, expressed in logarithmic and stationary phase are part of one complex. ....	206
1.5.7. The AP2 complex plays a vital role in axenic amastigotes. ....	208
1.5.8. The deletion of $\beta$ 2-adaptin leads to a defect in endocytosis. ....	211
1.6. Discussion .....	213
1.6.1. The subcellular localisation of LmCK1.2 is consistent with the functions of LmCKAPs .....	213
1.6.2. Potential functions of LmCK1.2 in the nucleus .....	214
1.6.3. Novel functions for CK1 family members: Regulation of the Nuclear Pore Complex.....	215
1.6.4. LmCK1.2 might be loaded into exosomes through the regulation of vesicular trafficking. ....	216
1.7. Acknowledgments .....	219
1.8. Supplementary information .....	220
1.8.1. Supplemental tables .....	220
1.8.2. Supplemental figures.....	225
1.8. References.....	228
<b>2. Characterisation of LmCKAP1 .....</b>	<b>235</b>
2.1. Introduction.....	235
2.2. Characterisation of LdBPK_080130.1 (LmCKAP1) using bioinformatics.....	235
2.2.1. Annotation of LmCKAP1. ....	235
2.2.2. Paralogs and orthologs of LdBPK_080130.1 (LmCKAP1) .....	236
2.2.3. Knowledge from other parasites .....	239
2.2.4. Post-translational regulation .....	239
2.3. Expression and localisation of LmCKAP1-mNG in <i>L. donovani</i> .....	240
2.3.1. LmCKAP1 is expressed at low level in <i>L. donovani</i> .....	240
2.3.2. LmCKAP1-mNG is expressed in dividing parasites.....	241
2.4. Knockout of LmCKAP1-mNG in <i>L. donovani</i> . ....	244
2.4.1. LmCKAP1 null mutants are larger cells and have minor growth defect as axenic amastigotes .....	244
2.4.2. Low ectopic overexpression of LmCK1.2 in $\Delta$ LmCKAP1 parasites leads to an increase in cell death only in axenic amastigotes .....	246
2.4.3. Analysis of $\Delta$ LmCKAP1 (+ LmCK1.2-V5) mutants shows aberrant mitotic parasites .....	248
2.4.4. Localisation of LmCK1.2-V5 in $\Delta$ LmCKAP1 cell line.....	249
2.5. Discussion and perspectives.....	250
<b>3. Development of LmCK1.2 immunoprecipitation conditions for mass spectrometry analysis.....</b>	<b>253</b>
3.1. LmCK1.2-V5-His <sub>6</sub> immunoprecipitation from promastigotes cell lysates .....	253
3.2. LmCK1.2-V5-His <sub>6</sub> immuno-precipitation from amastigotes cell lysates .....	259
<b>4. Adaptation of the CRISPR-Cas9 toolkit to <i>Leishmania donovani</i> and characterisation of LmCK1.1 .....</b>	<b>263</b>
<b>5. Conclusion.....</b>	<b>281</b>
<b>CHAPTER III .....</b>	<b>283</b>
<b>A role for LmCK1.2 in host-pathogen interactions .....</b>	<b>285</b>
<b>1. Development of an <i>ex vivo</i> method to identify the LmCKAPhost proteins.....</b>	<b>287</b>
1.1. Generation of the recombinant proteins and macrophage lysates .....	287
1.1.1. Production of rLmCK1.2-V5 .....	287
1.1.2. Production of the recombinant control protein thioredoxin-V5-His <sub>6</sub> .....	288
1.1.3. Production of macrophage extracts .....	290
1.2. Optimisation of the protocol to immuno-precipitate rLmCK1.2-V5 from BMDM lysates.....	290
<b>2. Identification of LmCKAPhost proteins .....</b>	<b>295</b>
2.1. Immuno-precipitation of rLmCK1.2-V5 from BMDM lysates. ....	295
2.2. Analysis of the proteins identified by MS analysis .....	297

2.2.1. Selection criteria used for the identification of LmCK1.2 binding partners. ....	297
2.2.2. Identification of 18 LmCKAHost proteins that also interact with mammalian CK1 .....	300
2.2.3. LmCKAHost proteins are implicated in multiple cellular pathways .....	302
2.2.4. Enrichment of LmCKAHost dataset in proteins involved in membrane trafficking. ....	304
2.2.5. Enrichment of LmCKAHost dataset in proteins involved in oxidative phosphorylation pathway. ....	306
2.2.6. More than a third of LmCKAHost proteins might play a role during <i>Leishmania</i> infection .....	308
<b>3. Conclusion and perspectives .....</b>	<b>313</b>
<b>4. Appendices of Chapter III .....</b>	<b>317</b>
<b>CONCLUSION &amp; PERSPECTIVES.....</b>	<b>321</b>
<b>REFERENCES.....</b>	<b>325</b>
<b>APPENDICES.....</b>	<b>351</b>
<b>APPENDIX 1.....</b>	<b>353</b>
<b>IP from promastigotes.....</b>	<b>355</b>
<b>IP from axenic amastigotes .....</b>	<b>368</b>
<b>APPENDIX 2.....</b>	<b>377</b>
<b>APPENDIX 3.....</b>	<b>397</b>



## Abbreviations

°C	Degree Celsius
a	Coenzyme A
AGC	Serine/threonine protein kinases that contains the PKA, PKG, PKC families
AIFM1	Apoptosis inducing factor mitochondria associated 1
AMP	Adenosine monophosphate
AMPK1	5' AMP-activated protein kinase
AP1	Adaptor protein complex 1
AP17	Adaptor protein 17
AP2	Adaptor protein complex 2
AP2A1	Adaptor protein Alpha 1
AP2B1	Adaptor protein Beta 1
aphA1	Aminoglycoside 3'-phosphotransferase
aPK	atypical Protein Kinases
AraC	Arabinose operon regulatory protein
ASE1	Anaphase spindle elongation protein 1
ATP	Adenosine triphosphate
AU	Arbitrary units
Auto-P	Auto-phosphorylation
AW	Äkta washing buffer
BB	Basal body
BIP	binding protein 1
BMDM	Bone-marrow-derived macrophages
BS3	Bis(sulfosuccinimidyl)suberate
BSA	Bovine serum albumine
BSF	Bloodstrem form
CAC	Chromatic Aberration Corrector
CaMK	Ca <sup>2+</sup> /calmodulin-dependent protein kinase
cAMP	cyclic adenosine monophosphate
Cas9	CRISPR associated protein 9
CCD	charge-coupled device
CCP	Clathrin-coated pits
CDK	Cyclin-dependent kinase
CEN	Centrin
CK	Casein kinase
CK1 or CKI	Casein kinase 1
CK2 or CKII	Casein kinase 2
CL	Cutaneous leishmaniasis
CLTC	Clathrin heavy chain 1
CMLE	Classic Maximum Likelihood Estimation
CRISPR	Clustered Regularly Interspaced Short Palindromic Repeats

CYC1	Cytochrome C1
D4476	4-[4-(2,3-dihydro-benzo[1,4]dioxin-6-yl)-5-pyridin-2-yl-1H-imidazol-2-yl]benzamide
DDX3	DEAD-box RNA helicase
DEPC	Dishevelled/EGL-10/Pleckstrin domain-containing
DFC	Dense fibrillar component
DMSO	Dimethyl sulfoxide
DNA	Deoxyribonucleic acid
DPBS	Dulbecco's Phosphate Buffer Saline
DTT	Dithiothreitol
DUF1669	Domain of unknown function 1669
DUF3608	Domain of unknown function 3608
DYNLL1	Dynein Light Chain LC8-Type 1
DYRK	Dual-specificity tyrosine phosphorylation-regulated kinase
EDTA	Ethylenediaminetetraacetic acid
EF1 $\alpha$	Elongation Factor 1 alpha
EGFR	Epidermal growth factor receptor
EGTA	Ethylene glycol tetraacetic acid
eIF6	Eukaryotic translation initiation factor 6
ELISA	Enzyme-Linked Immunosorbent Assay
ePKs	eukaryotic Protein Kinases
ESCRT	Endosomal sorting complex required for transport
ESYT1	Extended synaptotagmin-1
FACS	Fluorescence-activated cell sorting
FAM83	FAMily with sequence similarity 83
FAZ	Flagellum attachment zone
FAZ2	Flagellum attachment zone protein 2
FC	Fibrillar centre
FCS	Fetal calf serum
FDR	False discovery rate
FGFR	Fibroblast growth factor receptor
FIBP	Acidic fibroblast growth factor intracellular-binding protein
FITC	Fluorescein isothiocyanate
FP	Flagellar pocket
FPN	Flagellar pocket neck
FSC	Forward scatter
FYVE	Domain from the proteins Fab1, YOTB/ZK632.12, Vac1, and EEA1
GC	Granular component
GFP	Green fluorescent protein
GIPLs	Glycoinositolphospholipids
GNB2	Guanine nucleotide-binding protein G(I)/G(S)/G(T) subunit beta-2
GP63	<i>Leishmania</i> major surface glycoprotein
GTP	Guanosine triphosphate
H	Hoechst 33342
HCD	Higher-energy collisional dissociation

HDAC	Histone deacetylase
HEPES	4-(2-Hydroxyethyl)-1-piperazine ethanesulfonic acid
HF	Homology Flanks
HNRNPM	Heterogeneous nuclear ribonucleoprotein M
HPI	hydrophobic pocket II
HRII	hydrophobic region II
Hrr25	HO and Radiation Repair 25. Yeast CK1 $\delta/\epsilon$
Hsc70	Heat shock cognate 71 kDa
Hsp40	Heat shock protein 40
HSP60	Heat shock protein 60
HSP70	Heat shock protein 70
Hsp90	Heat shock protein 90
HYG	Hygromycin b
IAV	Influenza A virus
IFA	Immuno-fluorescence analysis
IFN	Interferon
IFNAR1	Interferon alpha and beta receptor subunit 1
IFNGR1	Interferon gamma receptor 1
IFN $\alpha$	Interferon alpha
IFN $\gamma$	Interferon gamma
IFT	Intra-flagellar transport
IFT172	Intraflagellar Transport 172
IP	Immuno-precipitation
IRAK	Interleukin-1 receptor-associated kinase
JAK	Just Another Kinase
K	Kinetoplast
kDa	kilo Dalton
kDNA	Kinetoplast DNA
KHD	Kinesin homology domain
LB	Lysogeny broth
LCL	Localised Cutaneous Leishmaniasis
LCR	Low Complexity Regions
LCRs	Low complexity regions
LDS	Lithium dodecyl sulfate
LES	Late endosomes
LmCK1.1	<i>Leishmania</i> casein kinase 1 isoform 1
LmCK1.2	<i>Leishmania</i> casein kinase 1 isoform 2
LmCK1.3	<i>Leishmania</i> casein kinase 1 isoform 3
LmCK1.4	<i>Leishmania</i> casein kinase 1 isoform 4
LmCK1.5	<i>Leishmania</i> casein kinase 1 isoform 5
LmCK1.6	<i>Leishmania</i> casein kinase 1 isoform 6
LmCKAP	LmCK1.2-associated protein
LmCKAP1	LmCK1.2-associated protein 1
Lmkin 17	<i>Leishmaniakinesin</i> 17

LmKin 21	<i>Leishmaniakinesin 21</i>
LmKin	<i>Leishmaniakinesin</i>
LmKin 30	<i>Leishmaniakinesin 30</i>
LPG	Lipophosphoglycan
LRR	<i>Leucine-rich repeat</i>
MAPK	Mitogen-activated protein kinases
MBP	<i>Myelin basic protein</i>
MCL	Mucocutaneous Leishmaniasis
MeCN	Acetonitrile
MES	2-(N-morpholino)ethanesulfonic acid
Mg132	Carbobenzoxy-Leu-Leu-leucinal
MGT1	Magnesium transporter 1
MIP	Maximum intensity projection
MLCK	Myosin light chain kinases
mM	Millimolar
mNG	mNeonGreen
MOPS	Morpholinepropanesulfonic acid
mPep	Mean value of peptides
mRNA	Messenger RNA
MS	Mass spectrometry
MSA	Multiple sequence alignment
MSP	Major sperm protein
Mtb	<i>Mycobacterium tuberculosis</i>
MTOC	Microtubule-organising centre
MUSCLE	MUltiple Sequence Comparison by Log-Expectation
MVB	Multivesicular bodies
MW	Molecular Weight
N	Nucleus
NA	Numerical Aperture
NADH	1,4-Dihyronicotinamide adenine dinucleotide
NDUFS	NADH dehydrogenase [ubiquinone] iron-sulfur protein
NEO	Neomycin
NFAT	Nuclear factor of activated T-cells
NF-kB	Nuclear factor-kappa B
NLS	Nuclear Localisation Signal
NP40	Nonidet-P40
NPC	Nuclear pore complex
Nup	Nuclear pore protein
NuSap2	Nucleus and spindle associated protein 2
ORF	Open reading frame
PBS	Phosphate buffered saline
PBST	Phosphate buffered saline with Tween 20
PCR	Polymerase Chain Reaction
PDB	Protein data bank

Pen/Step	Penicillin/Streptomycin
PFA	Paraformaldehyde
PFR2	Paraflagellar rod protein 2
PHD	Plant homeodomain
PI	Propidium iodide
PI3P	Phosphatidylinositol 3-phosphate
PIP2	Phosphatidylinositol 4,5-bisphosphate
PKDL	Post-kala-azar dermal leishmaniasis
PM	Peritrophic matrix
PMSF	Phenylmethylsulfonyl fluoride
PPP1C	Serine/threonine-protein phosphatase PP1 catalytic subunit
PSG	Promastigote secreting gel
PTMs	Post-translational modifications
PV	Parasitophorous vacuoles
PVDF	Polyvinylidene difluoride
RBD	RNA-binding domain
RCC1	Regulator of chromosome condensation
RCG	Receptor Guanylate Cyclase
RIPA	Radioimmunoprecipitation assay buffer
RMD	Relative Mean Delta
RNA	Ribonucleic acid
RNAi	RNA interference
ROI	Region of interest
RPMI	Roswell Park Memorial Institute medium
RRID	Research Resource Identifier
SD	Standar deviation
SDS	Sodium dodecyl sulfate
SDS-PAGE	Sodium dodecyl sulphate-polyacrylamide gel electrophoresis
sgRNA	Single guide RNA
SIP1	SMN-interacting protein 1
SL	Splice leader
SMN	Survival motor neuron
Smo	Smoothened
SNARE	Soluble N-éthylmaleimide-sensitive-factor Attachment protein Receptor
spp.	Species
STAT1	Signal transducer and activator of transcription 1
T7RNAP	T7 RNA polymerase
TAC	Tripartite attachment complex
Tb	<i>Trypanosoma brucei</i>
TBE	Tris/Borate/EDTA
TBS-T	Tris/Borate/EDTA with Tween 20
TF	Transcription factor
TK	Tyrosine Kinase
TKL	Tyrosine Kinase Like

TMD	Transmembrane domain
TNF	Tumor necrosis factor
Trans	Transmission image
TTBK	Tau tubulin kinase family
Tub	Tubulin
UTR	Untranslated region
VL	Visceral leishmaniasis
WHO	World Health Organization
WT	Wild type
μg	Microgram
μL	Microlitre
μM	Micromolar

## List of figures

Hereafter are listed all the figures from this manuscript, with the exception of figures inserted in the articles.

Fig. 1 – The different clinical manifestations of leishmaniasis.....	31
Fig. 2 – Global distribution of cutaneous and mucocutaneous leishmaniasis, in 2016.....	32
Fig. 3 – Global distribution of visceral leishmaniasis in 2016. ....	32
Fig. 4 – Life cycle of <i>Leishmania</i> parasite. ....	40
Fig. 5 – Overview of exosome biogenesis and secretion in mammalian cells. ....	42
Fig. 6 – The main <i>Leishmania</i> forms.....	44
Fig. 7 – Dendrogram of 491 ePK catalytic domains from 478 protein kinases genes. ....	47
Fig. 8 – Schematic alignment of human CK1 isoforms $\alpha$ , $\gamma$ 1–3, $\delta$ , and $\epsilon$ . ....	50
Fig. 9 – 3D structure of CK1 $\delta$ .....	51
Fig. 10 – Amino acid sequence alignment of <i>Leishmania</i> Casein Kinase I proteins.....	58
Fig. 11 – Schematic map of pLEXS <sub>Y</sub> -CK1.2, pLEXS <sub>Y</sub> -CK1.2 $\Delta$ C10-V5-His <sub>6</sub> , pLEXS <sub>Y</sub> -CK1.2 $\Delta$ C43-V5-His <sub>6</sub> and pLEXS <sub>Y</sub> -CK1.2 $\Delta$ N7-V5-His <sub>6</sub> plasmids. ....	69
Fig. 12 – Schematic map of pLEXS <sub>Y</sub> -CK1.2-V5-His <sub>6</sub> (NEO) plasmid. ....	70
Fig. 13 – Schematic map of the plasmids for the expression of recombinant proteins. ....	71
Fig. 14 – Domain structure of LmCKAP1. ....	236
Fig. 15 – Multiple alignment of LmCKAP1 protein sequences from different trypanosomatids species. ....	239
Fig. 16 – Growth curve, cell survival and mNG intensity of promastigotes expressing mNG-tagged LmCKAP1. ....	240
Fig. 17 – Gating of the mNG fluorescent proteins among the parasite population highlights the bigger cells. ....	241
Fig. 18 – Analysis of LmCKAP1-mNG localisation by fluorescence live microscopy. ....	242
Fig. 19 – Proportion of LmCKAP1-mNG positive cells increases upon flavopiridol treatment. ....	243
Fig. 20 – Growth curve, cell survival and forward scatter area of $\Delta$ LmCKAP1 promastigotes or amastigotes. ....	245

Fig. 21 – Characterisation of the $\Delta$ LmCKAP1 (+ LmCK1.2-V5) cells.....	247
Fig. 22 – IFA of $\Delta$ LmCKAP1 cells show aberrant mitotic parasites.....	249
Fig. 23 – LmCK1.2-V5 immunoprecipitation. ....	254
Fig. 24 – LmCK1.2-V5 immunoprecipitation. ....	255
Fig. 25 – LmCK1.2-V5 immunoprecipitation with magnetic beads.....	257
Fig. 26 – LmCK1.2-V5 immunoprecipitation with magnetic beads.....	258
Fig. 27 – LmCK1.2-V5 immunoprecipitation for mass spectrometry (PRO).....	259
Fig. 28 – LmCK1.2-V5 immunoprecipitation with magnetic beads.....	260
Fig. 29 – LmCK1.2-V5 immunoprecipitation with magnetic beads from 18 mg total protein lysate. ....	261
Fig. 30 – LmCK1.2-V5 immunoprecipitation for mass spectrometry (axAMA).....	262
Fig. 31 – Elution fractions of the purification of recombinant LmCK1.2-V5. ....	288
Fig. 32 – Production of recombinant Thioredoxin-V5-His <sub>6</sub> protein. ....	289
Fig. 33 – Immunoprecipitation of host proteins by recombinant LmCK1.2-V5 from macrophage lysates.....	291
Fig. 34 – Immunoprecipitation of host proteins by recombinant LmCK1.2-V5 from macrophage lysates.....	292
Fig. 35 – Immunoprecipitation of host proteins by recombinant LmCK1.2-V5 from macrophage lysates.....	293
Fig. 36 – Immunoprecipitation for mass spectrometry analysis of host proteins with recombinant LmCK1.2-V5 from macrophage lysates, in three biological replicates.....	296
Fig. 37 – Venn diagram of the proteins detected by MS alysis.....	297
Fig. 38 – Interaction network of LmCK1.2 and host proteins. ....	299
Fig. 39 – Genome-wide overview of the results of the LmCKAPhost pathway analysis and comparison with human CK1 interactors.....	303
Fig. 40 – Over-representation of the membrane trafficking pathway among the LmCKAPhost proteins (Reactome pathway analysis). ....	305
Fig. 41 – Over-representation of proteins from the energy metabolism in the LmCKAPhost proteins (DAVID pathway analysis). ....	307

## List of tables

Table 1 – Main <i>Leishmania</i> species of clinical interest with their geographic area. ....	31
Table 2 – Groups of eukaryotic protein kinases (Manning et al., 2002).....	46
Table 3 – The CK1 protein kinases from <i>Leishmania</i> . ....	56
Table 4 – List of the chemicals used in this document. ....	63
Table 5 – Annotation of LmCKAP1 and orthologs in trypanosomatids.....	237
Table 6 – LmCKAPhost proteins also described as human CK1 interactors.....	300
Table 7 – Selection of LmCKAPhost proteins with potential physiological relevance. ....	310
Table 8 – List of LmCKAPhost proteins identified by mass spectrometry. ....	317
Table 9 – List of curated human CK1 interactors obtained from BioGRID v3.5 database.....	320



# Introduction

---



# 1. The leishmaniases

The leishmaniases are a group of diseases caused by protozoan parasites of the genus *Leishmania*. Clinical manifestations are diverse, depending upon several factors such as parasite species or the immune status of the patient. The leishmaniases belong to the tropical neglected diseases identified by the World Health Organization (WHO), and affects poor people in developing countries. The disease is associated with malnutrition, poor housing, population displacement, a weak immune system and lack of financial resources (Alvar et al., 2006; Ranjan et al., 2005). Furthermore, several environmental changes can favour leishmaniasis outbreaks such as deforestation, irrigation schemes, building of dams, urbanization and also climate change. In the latest WHO report (2017), it was shown to be endemic in 97 countries, mainly in developing countries, with an estimated 700 000 to 1 million new cases including 26 000 to 65 000 deaths occurring annually. However, only a small fraction of those infected by *Leishmania* parasites will eventually develop the disease. Endemic regions can be divided geographically into the New World (the Americas), and the Old World (Africa, Asia and Europe) (Alvar et al., 2012). There are three main forms of the disease: cutaneous (CL), muco-cutaneous (MCL) and visceral leishmaniasis (VL).

## 1.1. The clinical manifestations and geographical distribution

The clinical manifestations could be multiple but are divided into three particular forms (Fig. 1):

- Cutaneous leishmaniasis is the most common form of leishmaniasis and can be localised (LCL) or diffuse (DCL). This form is non-lethal and the pathology mainly presents dermatological manifestations such as skin lesions or ulcers on exposed parts of the body, leaving life-long scars and serious disability or stigma. The evolution of skin lesions can be slow (months or years), but heal spontaneously without treatment, leaving, however, important traumas for the patients (Al-Kamel, 2016; Kassi et al., 2008). CL is caused by different *Leishmania* species of the Old and New World, such as *L. major*, *L. braziliensis*, *L. amazonensis* or *L. tropica* (Table 1). According to WHO, the

global incidence of CL is between 600 000 to 1 million new cases annually. In 2016, most of new CL cases (over 84%) occurred in 10 countries: Afghanistan, Algeria, Brazil, Colombia, Iraq, Pakistan, Peru, the Syrian Arab Republic, Tunisia and Yemen (Table 1 and Fig. 2).

- Muco-cutaneous leishmaniasis (MCL) can be lethal in case of a bacterial secondary infection. Its clinical manifestations are physically impacting, causing also dramatic socio-economic burden (Okwor and Uzonna, 2016). MCL causes partial or total destruction of mucous membranes of the nose, mouth and throat. The species causing most of MCL cases is *L. braziliensis*. This species can lead to CL or MCL, and one of the factors favouring MCL over CL seems to be the presence of a *Leishmania* RNA virus (Ives et al., 2011). Only few cases are reported every year and over 90% of MCL cases occur in Bolivia, Brazil, Ethiopia and Peru (Table 1 and Fig. 2).
- Visceral leishmaniasis (VL), also known as kala-azar (black fever in Sanskrit) is the most devastating form of leishmaniasis. VL is lethal in 95% of the cases if left untreated. Two species are responsible for most of the VL cases worldwide: *L. donovani* and *L. infantum* (or *L. chagasi*). Parasites propagate in macrophages of internal organs such as the liver, the spleen, the bone marrow, and the lymph nodes. The disease is characterised by irregular fever, anemia, weight loss, hepato- and splenomegaly as well as hypergammaglobulinemia (Guerin et al., 2002). In 2016, 90% of new VL cases were reported in seven countries: Brazil, Ethiopia, India, Kenya, Somalia, South Sudan and Sudan (Table 1 and Fig. 3). There is a possibility that, after the clinical cure of *L. donovani*, VL patients develop a complication, termed post-kala-azar dermal leishmaniasis (PKDL). This clinical form appears as macular, popular or nodular rash often on the face, upper arms, trunks and other parts of the body. It usually appears months or years after apparent cure of VL (Fig. 1).

**Table 1 – Main *Leishmania* species of clinical interest with their geographic area.**

Sub-genera	Species	Disease form	Area	Distribution
<i>Leishmania</i>	<i>L. aethiopica</i>	LCL, DCL	Old World	East Africa
	<i>L. amazonensis</i>	LCL, DCL, MCL	New World	South America
	<i>L. donovani</i>	VL, PKDL	Old World	Central Africa, South-East Asia, Middle East, India
	<i>L. infantum</i>	VL, CL	Old and New World	Mediterranean basin, South Europe, Middle East, Central Asia, Americas
	<i>L. major</i>	CL	Old World	Central and Northern Africa, Middle East, Central Asia
	<i>L. mexicana</i>	LCL, DCL	New World	Americas
	<i>L. tropica</i>	LCL, VL	Old World	Central and Northern Africa, Middle East, Central Asia, India
	<i>L. venezuelensis</i>	LCL	New World	South America
<i>Viannia</i>	<i>L. braziliensis</i>	LCL, MCL	New World	South America
	<i>L. guyanensis</i>	LCL, MCL	New World	South America
	<i>L. lainsoni</i>	LCL	New World	South America
	<i>L. lindenbergi</i>	LCL	New World	South America
	<i>L. naiffi</i>	LCL	New World	South America
	<i>L. panamensis</i>	LCL, MCL	New World	Central and South America
	<i>L. peruviana</i>	LCL, MCL	New World	South America
<i>L. shawi</i>	LCL	New World	South America	

VL, Visceral Leishmaniasis; CL, Cutaneous Leishmaniasis (LCL, localised cutaneous leishmaniasis; DCL, diffuse cutaneous leishmaniasis); MCL, Mucocutaneous Leishmaniasis; PKDL, Post Kala-azar Dermal Leishmaniasis.

**Fig. 1 – The different clinical manifestations of leishmaniasis.**

From left to right: cutaneous, mucocutaneous, visceral and post-kala-azar leishmaniasis. (Images sources: WHO/M. Saeedi)

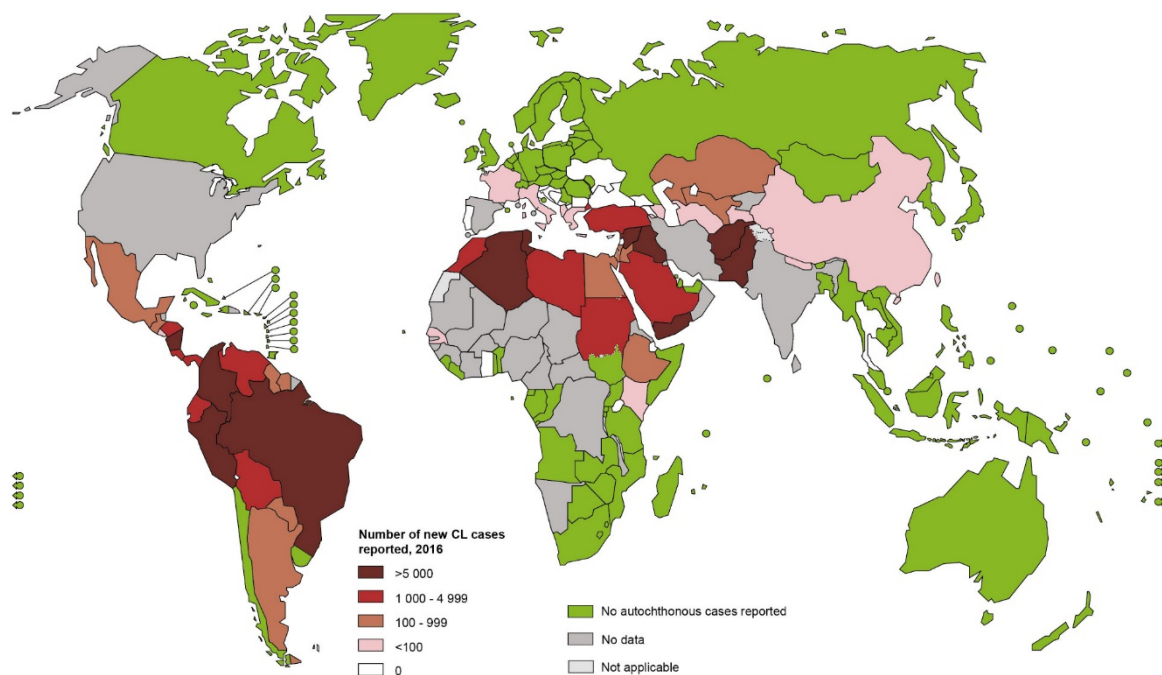


**Fig. 2 – Global distribution of cutaneous and mucocutaneous leishmaniasis, in 2016.**

The colour code correspond to the number of reported cases in 2016. (Data source: WHO)

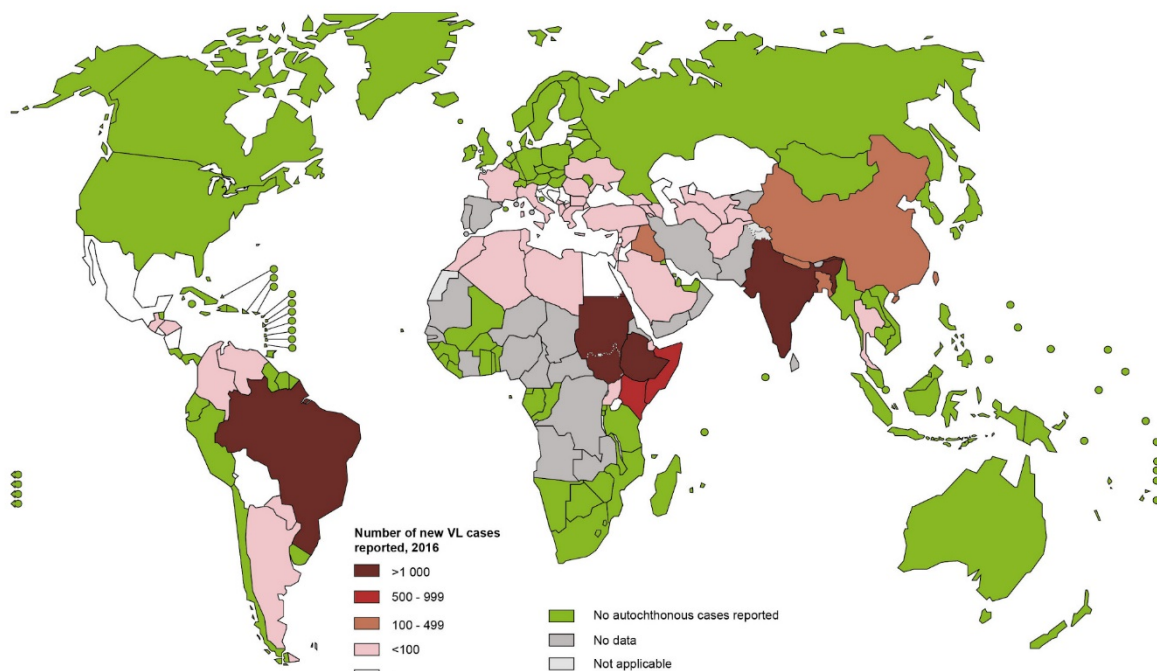


**Fig. 3 – Global distribution of visceral leishmaniasis in 2016.**

The colour code correspond to the number of reported cases in 2016. (Data source: WHO)

## 1.2. Diagnosis, treatment and prevention

### 1.2.1. Diagnosis

Because of the large number of species that could potentially affect humans, and the different forms of diseases associated with leishmaniasis, a good diagnosis is crucial to prescribe the adapted treatment to patients. Diagnosis is based on clinical manifestations coupled with epidemiological features and analyses. In laboratories, diagnosis of leishmaniasis can be direct or indirect by searching for the presence of parasites, or host antibodies, respectively. Depending on the country, different methods are being used which differ in sensitivity, specificity and cost (Guerin et al., 2002).

Detection for parasites can be performed by microscopy using Giemsa staining, from a clinical sample, such as skin smear (CL), spinal smear, peripheral blood or spleen aspirates (for VL). Culturing the parasites can also be carried out in biphasic or monophasic medium, for subsequent analyses. Indirect tests can improve diagnosis, with a combination of immunological and molecular analyses. Immunological or serological tests are performed mostly for VL, and are easy and precise, but may be insufficient to distinguish two closely related species or for immuno-compromised patients. These tests show the presence of circulating antibodies using immunofluorescence tests, Enzyme-Linked Immunosorbent Assay (ELISA), Western blotting or flow cytometry. Direct tests are primarily based on molecular tests mainly based on Polymerase Chain Reaction (PCR) and allow the quantification of parasites and the characterization of the species from clinical samples (Galluzzi et al., 2018).

### 1.2.2. Vaccination

Natural infections of CL and VL leads to robust immunity in most of the human cases, and *Leishmania* parasites do not show antigenic variation in contrast to *T. brucei* that causes sleeping sickness, therefore several bodies of research have aimed to develop *Leishmania* vaccines to control *Leishmania* infection. A successful *Leishmania* vaccine should induce a Th1 immune response, provide long-term immunity and protection against parasites causing VL and CL (Nagill and Kaur, 2011). For now, there is no such vaccine available for humans, but some vaccines (such as Leishmune® and CaniLeish®) generate robust protective immunity in dogs and are used globally (Moafi et al., 2019).

The first technique for vaccination was leishmanisation, or deliberate infection with virulent parasites. It was successfully used in the past as a live-vaccine against CL and gave protection against a secondary *Leishmania* infection in endemic areas. However, this strategy was stopped due to major complications including non-healing skin lesions, exacerbation of skin diseases, and the potential fatal impact of immuno-suppression (Seyed et al., 2018). First generation of vaccines consisted in the injection of whole-killed parasites, fractionated *Leishmania* antigen or and live-attenuated pathogens. Their effectiveness and their protective effect were variable, depending on hardly controllable parameters such as *in vitro* culture of the parasites. The use of recombinant proteins produced through genetically engineered-cells, is termed as “second generation vaccines.” Proteins from the parasites, produced in bacteria and purified, or injected with the bacteria, have been tested, conferring some degree of protective immunity against natural infection (Moafi et al., 2019).

A combination of recombinant antigens from *Leishmania* and sandfly saliva antigens has been found to increase the immune response at early stages of infection (Carregaro et al., 2013; Reed et al., 2016; Teixeira et al., 2014). Immunogenic sandfly saliva antigens includes LJM19 (a 11kDa salivary protein with unknown function), LJL143 (a 38kDa salivary protein with anticoagulant activity), the yellow-related protein PPTSP44, Lufaxin (the protein component in saliva that inhibits the alternative pathway of the complement system) (Cecilio et al., 2017; Fiuza et al., 2016; Mendes-Sousa et al., 2017; Tlili et al., 2018). An innovative multivalent vaccine candidate against human VL, composed of Virus-Like-Particles (VLP) loaded with three different recombinant proteins (LJL143 from *Lutzomyia longipalpis* saliva, and KMP11 and LeishF3+, as parasite-derived antigens) was assessed and proved the immunogenicity of the formulation (Cecilio et al., 2017). This innovative formulation would need to be tested in the context of infection. However the main drawback of these second generation vaccines is their price. Alternatively, a combination of live-attenuated *L. donovani* Centrin1 knockout parasites with sandfly salivary protein LJM19 used as adjuvant and intradermal route of immunisation conferred long lasting protection against VL (Fiuza et al., 2016).

DNA vaccines are third generation vaccines that transmit specific *Leishmania* immunogenic antigens via adenoviruses to allow the production of the antigen by the human cells. A recent vaccine was developed against VL and PKDL, ChAd63-KH DNA, providing protection against *Leishmania* infection (Osman et al., 2017); however, it should be further

evaluated in other clinical trials. Some of the risks with third generation vaccines are integration into the genome of the patient, auto-immune response and cancer (Dunning, 2009).

### 1.2.3. Treatments

In contrast to the lack of human vaccine so far, there is a repertoire of drugs for the treatment of leishmaniasis. Since the 1940s, pentavalent antimony has been the first-line of treatment against all forms of leishmaniasis, and is still used today with the same two forms: meglumine antimoniate (Glucantime®) and sodium stibogluconate (Pentostam® or Stibanate®). However, antimonials are highly toxic drugs, related to arsenic, and can sometimes cause life-threatening side effects making the treatment dangerous. Emergence of treatment failures to pentavalent antimony, particularly in some regions in India (Sundar et al., 2000), have pointed the need for development of alternative treatments against leishmaniasis. Several anti-leishmanial compounds replacing or used in combination with antimonials have been identified over the past two decades, such as Amphotericin B, Miltefosine, Paromomycin and Pentamidine.

Amphotericin B is an effective anti-leishmanial drug and has been used for the treatment of all forms of the disease. However its toxicity and the complicated treatment protocol involving intravenous and intramuscular administration for four weeks has led to the development of a less toxic formulation by incorporation of amphotericin B into liposomes (Wasan et al., 1994). This formulation, termed AmBisome® is a potent anti-leishmanial drug, however its use is limited due to the cost of the treatment that remains unaffordable in endemic areas. In 2011, a partnership between WHO and Gilead®, that produce AmBisome®, has led to its free distribution in endemic regions, and in 2016 the agreement was extended in until 2021. Amphotericin B is the first-line treatment for VL in South Asia, the Mediterranean Basin, Middle East, Central Asia and South America (World Health Organization, 2010).

Miltefosine has been successful in treating CL and VL and is the first oral drug for treatment of leishmaniasis (Croft and Olliaro, 2011). This is particularly important for treatment of leishmaniasis in regions where intravenous and intramuscular injections are difficult to conduct. Miltefosine has been approved to treat CL and VL, including in Indian regions where VL is endemic and there is treatment failure to pentavalent antimonials

(Bhattacharya et al., 2007; Jha et al., 1999). There is a high risk for emergence of miltefosine resistance in *L. infantum* and *L. donovani* in the future, due to increase use for canine leishmaniasis in Europe and inappropriate application for human treatment in the Indian subcontinent (Mondelaers et al., 2016).

Paromomycin is efficient for treatment of CL and VL (Sundar et al., 2009). It is an antibiotic with good anti-leishmanial activity, and it usually used in combination with other drugs like antimonials, that allows for the reduction of treatment duration and a higher efficacy. This drug offers great potential as a new, simple and easily applicable treatment for CL (Ben Salah et al., 2013). However, the availability of the drug is limited, thus restricting its use to endemic regions (Singh et al., 2012; Thakur, 2003).

In conclusion, treatments for the various forms of leishmaniasis are limited, mostly toxic, and the availability and affordability of the treatments is reduced in some isolated endemic regions. Moreover, there is a risk for parasite resistance due to the adaptability of the parasite (Barja et al., 2017). It is therefore crucial to accelerate the development of new and better treatments.

#### 1.2.4. Prevention

The main prevention methods for leishmaniasis are based on the control of vectors and host reservoirs. The contact between humans and the vector needs to be minimised; different actions are possible to do so: (i) physical actions, such as using insecticides (DTT or pyrethroids) in houses and adapted bed nets; (ii) changes in behaviour such as restraining from going out at dusk and wear covering clothing; and (iii) separating the livestock from the homes and fill back soil and wall cracks to avoid proliferation of sand flies near houses (Kishore et al., 2006). Emergence of insecticide resistances have already been observed, and the massive use of these chemicals have an impact on the environment (Dinesh et al., 2010). For reservoir control, impregnated dog collars are used and recommended, as well as vaccination. Elimination campaigns of infected dogs have already taken place, with contrasting results and raising ethical questions (Werneck et al., 2014).

## 2. Vectors and reservoirs

### 2.1. Vectors

*Leishmania* transmission occurs by the bite of an infected female sand fly during its blood meal. In addition to act as vector, it is important to stress that sand flies are hosts for *Leishmania*, where a complex differentiation process occur for the parasites (Dostálová and Volf, 2012). Moreover, sand flies are important for the development of the disease via the transmission of gut bacteria and saliva content that includes anticoagulants, vasodilators, anti-platelet agents and immuno-modulatory and anti-inflammatory molecules (Andrade et al., 2007). Sand flies belong to the order Diptera and the Phlebotominae subfamily, which is composed of 800 known species. About 98 seem able to transmit *Leishmania* parasites to vertebrate hosts, and 30 have been shown to act as vectors. Phlebotomus genera are found in the Old World (Europe, Northern Africa, Middle East, Asia) whereas Lutzomyia are found in the New World (Killick-Kendrick, 1999; Maroli et al., 2013; Ready, 2013). Sand flies are soundless and small flying insects, very small in size (no more than 3 mm in length), and most species bite at dusk and at night, although some also bite during daytime. Sand flies can very easily adapt to new environments; they are found in semi-arid regions and desert, as well as tropical and sub-tropical areas. Sand flies feed on vegetable sugars, only the female require blood to complete its gonotrophic cycle.

### 2.2. Reservoirs

Reservoir hosts of *Leishmania* can be diverse but restricted to mammals. About 70 mammalian species could act as reservoir hosts of *Leishmania*, including humans, dogs, rodents, monkeys or bats (Roque and Jansen, 2014). *Leishmania* parasite develops in all mammalian hosts; and in the vast majority of cases it will be asymptotically, which renders them potential reservoirs. Reservoir hosts can lead to zoonotic transmission, with wild animals acting as the reservoirs, anthrozo-zoonotic transmission, where humans and animals are reservoirs, and anthroponotic transmission, where humans are the sole reservoirs during the *Leishmania* life cycle, mostly for *L. donovani* and *L. tropica* (Molina et al., 2003). Due to the

wide range of species that could act as reservoir hosts, living in various types of environment, transmission is favoured.

### 3. The *Leishmania* parasite

#### 3.1. Taxonomy

*Leishmania* parasites are protozoan parasites belonging to the order *Kinetoplastidae* and the *Trypanosomatidae* family (Simpson et al., 2006). The kinetoplastids are a group of protists that contain a range of ubiquitous free-living species, pathogens of vertebrates, invertebrates and some plants. Members of the kinetoplastid order cause, among others, African sleeping sickness, Chagas disease, leishmaniases. There are 53 species of *Leishmania*, from which twenty are responsible for human leishmaniases. Each *Leishmania* species is associated with the development of a clinical form of the disease, a specific geographic distribution that range from very localised to distributed to different regions (New and Old World), to specific hosts (vector or mammalian) and intrinsic characteristics including biochemical, molecular and immunological (Akhoundi et al., 2016; Banuls et al., 2007).

#### 3.2. Life cycle and interaction with the mammalian host

*Leishmania* parasite alternate between two main stages that are morphologically different, the extracellular promastigote stage within the invertebrate host (sand flies) and the intracellular amastigote stage within the vertebrate host (e.g. humans, Fig. 4). The promastigotes are highly motile parasites that measures 12-20  $\mu\text{m}$  in length for 1-4  $\mu\text{m}$  in width, and possess a centrally located nucleus, a long flagellum at the anterior end of the cell emerging from the flagellar pocket and that can reach up to 20  $\mu\text{m}$  in length. Promastigotes are front-flagellated swimmers, adapted for extracellular survival inside the digestive tract of sand flies. After a blood meal on an infected reservoir host, amastigotes differentiate in the abdominal midgut inside the peritrophic matrix (PM), a chitin-based structure that envelops the blood meal and differentiate into procyclic promastigotes. Procyclics are highly

proliferative, and present long cell body and flagellum (nectomonads). They secrete chitinases allowing the rupture of the PM, to be released in the midgut lumen and attach to the microvilli of the sand fly midgut epithelium with their flagellum (Pimenta et al., 1992; Schlein et al., 1991). Then, the nectomonads reduce in size to become leptomonads and finally differentiate into two distinct stages: infectious and non-replicative metacyclic promastigotes, and haptomonad promastigotes that migrate to the stomodeal valve. The parasites secrete a gel composed of filamentous proteophosphoglycan, the promastigote secreting gel (PSG), which obstructs the gut. This obstruction and the destruction of the valve by the chitinase secreted by parasites, which facilitates the reflux of parasites (Dostálová and Volf, 2012; Gossage et al., 2003). The metacyclic promastigotes, the only infectious promastigote form, are different from the procyclic forms as they are pre-adapted for survival in the mammalian host: they express stage-specific surface molecules (including metacyclic lipophosphoglycan, LPG) and become complement-resistant (Besteiro et al., 2007). The different stages of differentiation between the first blood meal on infected hosts and the transmission of infectious metacyclic promastigotes in the next blood meal takes about ten days.

Once injected in the mammalian host through the bite of the sand fly, promastigotes are phagocytised by resident or recruited cells of the dermis, although the main host cell is the macrophage (Fig. 4). Parasite- or sand fly-derived components facilitates the establishment of intracellular infection, such as sand fly saliva, parasite PSG, and parasite exosomes co-egested during the blood meal (Atayde et al., 2015; Gomes and Oliveira, 2012; Ilg, 2000). *Leishmania* parasites invade macrophages by receptor-mediated endocytosis, for example via complement components that are cleaved by parasite proteases (Shao et al., 2019; Stuart et al., 2008). Following internalisation, metacyclic promastigotes are located in the early phagosomes that will mature to late phagosomes and ultimately fuse with lysosomes to become acidic phagolysosomes termed parasitophorous vacuoles (PV) (with an internal pH 4.5 – 5.5) (Antoine et al., 1990).

These conditions – acidic pH and mammalian body temperature (33-37°C) – trigger promastigote differentiation into the intracellular amotile amastigote form, a process that takes about 24-72 hours (Rosenzweig et al., 2008a; Tsigankov et al., 2012; Zilberstein and Shapira, 1994). Amastigotes are round or oval body shaped parasites and are highly adapted to the PV: they are intracellular and non-motile parasites, with a reduced size (2 – 4 µm in

diameter), a shorter flagellum that does not emerge from the flagellar pocket. Amastigotes are also acidophilic and have an adapted energy metabolism (Besteiro et al., 2007). Remarkably, amastigotes are covered by a densely packed glycocalyx composed of glycoinositolphospholipids (GIPLs) that form a highly hydrophilic barrier (Forestier et al., 2015). *Leishmania* differentiation in amastigote is also accompanied by changes in mRNA and protein abundance, and with the expression of amastigote-specific genes (Charest et al., 1996; Rosenzweig et al., 2008b; Saxena et al., 2007).

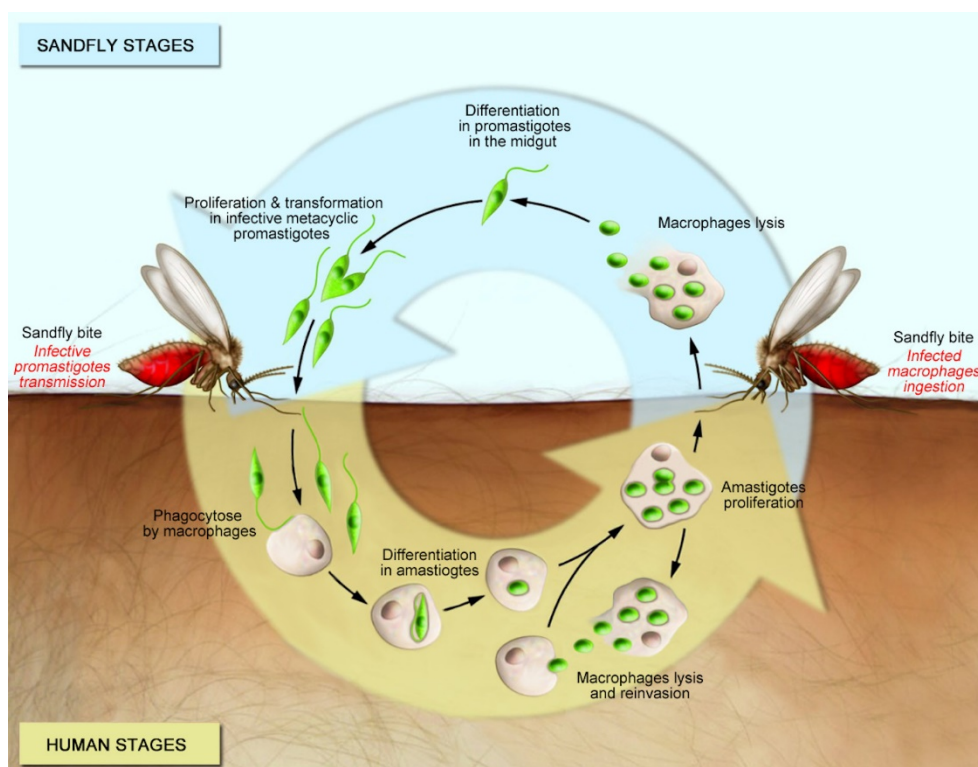


**Fig. 4 – Life cycle of *Leishmania* parasite.**

Sand flies inoculate infective promastigotes (metacyclics) into a mammalian host during a blood meal. Promastigotes are phagocytosed by macrophages where they differentiate into pathogenic intracellular amastigotes in response to low pH and elevated temperature. The amastigotes multiply, and infect other phagocytic cells. The life cycle is completed when infected macrophages are taken up by another sand fly during feeding. Ingested amastigotes convert to promastigotes within the sand fly midgut, which then transform into highly infectious metacyclic promastigotes. (Data source: modified from (Stuart et al., 2008)).

A method has been developed to perform host-cell free differentiation of promastigotes into amastigote-like parasites (axenic amastigotes), with a combination of acidic conditions (pH 5.5) and high temperature (37°C) (Doyle et al., 1991; Hodgkinson et al., 1996). This system has been well established for *L. donovani* (Barak et al., 2005), and although

axenic and host-derived amastigotes are not identical, it remains a useful tool for research. Differentiation into axenic amastigotes is in two phases: a differentiation process during the first 24h and a proliferation step from 24 to 192h (Barak et al., 2005).

Remarkably, *Leishmania* amastigotes are able to evade the major microbicidal mechanisms of macrophages by, for instance, transient inhibition of phagosome maturation (Scianimanico et al., 1999; Vinet et al., 2009), or inhibition of macrophage activation. The *Leishmania* parasite releases proteins and glycolipid effectors into the host cell and target host cell signalling proteins implicated in anti-microbial responses. To illustrate this, the *Leishmania* Elongation Factor 1 alpha (EF1 $\alpha$ ), but not the host EF1 $\alpha$ , has been shown to bind and activate SHP-1, a negative regulator of macrophage activation that inhibit TNF secretion and NO production (Hardin et al., 2006; Nandan et al., 2002). How *Leishmania* secretes key molecules that modulate the host cell and allow for long-term survival and persistence in the host organism has been debated. Increasing evidences suggest that *Leishmania* secretes virulence factors via exosomes (Dong et al., 2019; Silverman et al., 2008, 2010a, 2010b). In mammalian cells, exosomes are generated within the endosomal system. During the process of maturation from early to late endosomes or multivesicular bodies (MVBs), the endosomal membrane invaginates to generate intraluminal vesicles in the lumen of the endosomes. Then, MVBs can either fuse with the lysosome for degradation or with the plasma membrane to release the vesicles in the extracellular environment (Fig. 5) (Bobrie et al., 2011). In *Leishmania*, the mechanisms of exosomes biogenesis and release are unknown to date. Proteomics studies have identified proteins involved in intracellular survival, signal transduction, transport processes and proteins with immunosuppressive functions among *L. donovani* exosomes (Silverman et al., 2008, 2010a). Research of the exosome biogenesis mechanism in *Leishmania* is interesting because it could lead to the identification of therapeutic targets (Atayde et al., 2016).

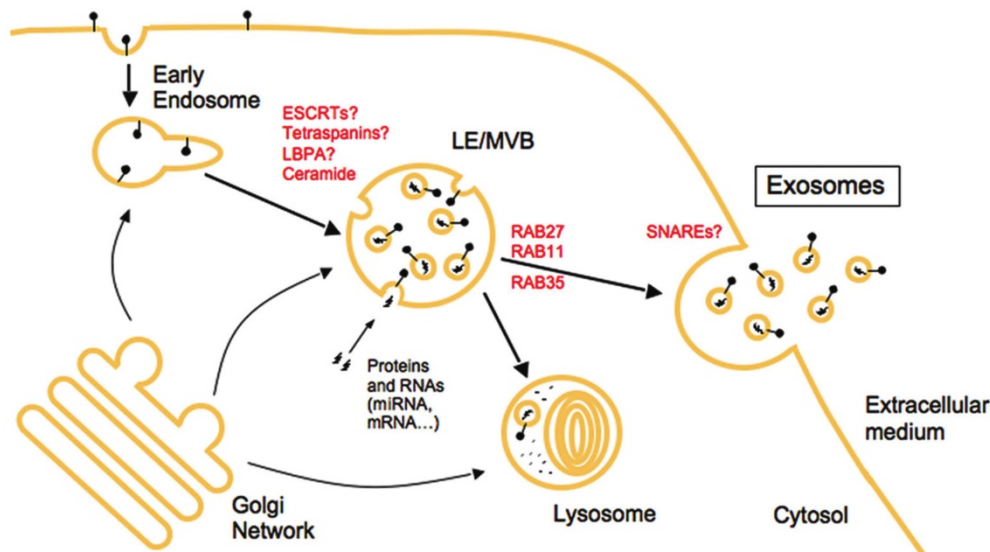


**Fig. 5 – Overview of exosome biogenesis and secretion in mammalian cells.**

Exosomes originate from internal multivesicular compartments called MVBs which are also late endosomes (LEs). Formation of the internal vesicles of MVBs has been shown to require ESCRT proteins, tetraspanins and the lipid LBPA, but the role of all these molecules in exosome biogenesis is still unclear. The lipid ceramide has also recently been shown to allow formation of internal vesicles and to be required for exosome secretion. Several Rab proteins, RAB11, RAB27, RAB35, known to be involved in trafficking of vesicles between intracellular compartments, have been shown to play a role in exosome secretion. The final step required for exosome secretion, i.e. fusion of MVBs with the plasma membrane, most probably involves a complex of SNARE proteins, but the nature of this complex is not known. (Data source: (Bobrie et al., 2011))

### 3.3. *Leishmania* cell biology

Although the two life stages are different in morphology, the basic cellular architecture is conserved in *Leishmania* and is defined by cross-linked sub-pelicular corset microtubules that are maintained throughout the cell cycle. Cellular components include single-copy organelles, such as the mitochondrion and Golgi apparatus (see Fig. 6). The kinetoplast, which corresponds to the mitochondrial DNA, is positioned anteriorly to the nucleus, and is directly connected to the basal body from which the flagellum extends (Sunter and Gull, 2017). The mitochondria is characterized by conventional external and internal membranes. There is only one mitochondrion per cell, which is large and elongated. The set of mitochondrial DNA, called kDNA, is condensed in a substructure, the kinetoplast (Fig. 6), which is located at the base of the flagellum. This kDNA represents 10 to 20% of the total DNA. It is a concatenated circular DNA network, divided into two classes: homogeneous maxi-circles (~ 25-50 molecules of 20 to 40 kb) and many copies of the heterogeneous mini-circles (0.5 to 1 kb). Maxi circles encode

mitochondrial proteins and mini-circles are known to produce a specific RNA, called a guide RNA, which decode the network of maxi circles by RNA editing. The flagellar pocket, at the base of the flagellum, is an invagination of the cell membrane and forms a vase-like structure (Fig. 6). This flagellar pocket is the only site for endocytosis and exocytosis, and therefore a crucial interface with the extracellular environment (mammalian host cell or vector midgut) (Longenecker et al., 1996). In addition, there are small organelles called glycosomes (Fig. 6), which are specific to Kinetoplastidae. They play an important role in parasite metabolism, harboring several steps of glycolysis.

In higher eukaryotes, gene transcription is regulated by elements such as promoters and facilitating regions leading to the production of monocistronic pre-messenger RNAs, which contain exons (coding sequences) and introns (non-coding sequences). These RNAs are then subjected to a cis-splicing reaction leading to the excision of the introns and the formation of the messenger RNAs (mRNA). In contrast, *Leishmania*, like all trypanosomatids, possess a different mechanism for gene expression. Indeed, this expression occurs in the absence of conventional cis-regulators or conventional transcription factors (TFs) (Boucher et al., 2002; Matkin et al., 2001; Smith et al., 2007). In these organisms, almost all genes are organized in polycistrons and do not include introns (Tamar et al., 2000). These polycistrons can contain many genes but unlike bacteria, genes in a polycistronic unit in *Leishmania* are not generally functionally related. The polycistronic unit is transcribed and in parallel cleaved into monocistronic mRNA by the action of two simultaneous intergenic RNA cleavage reactions, trans-splicing and polyadenylation (Boucher et al., 2002; Papadopoulou et al., 1994; Tamar et al., 2000). Trans-splicing adds a 39 nucleotide sequence called the splice leader to the 5' ends of the mRNAs and the polyadenylation adds a 3' polyadenylated tail to the mRNAs (Ullu et al., 1993).

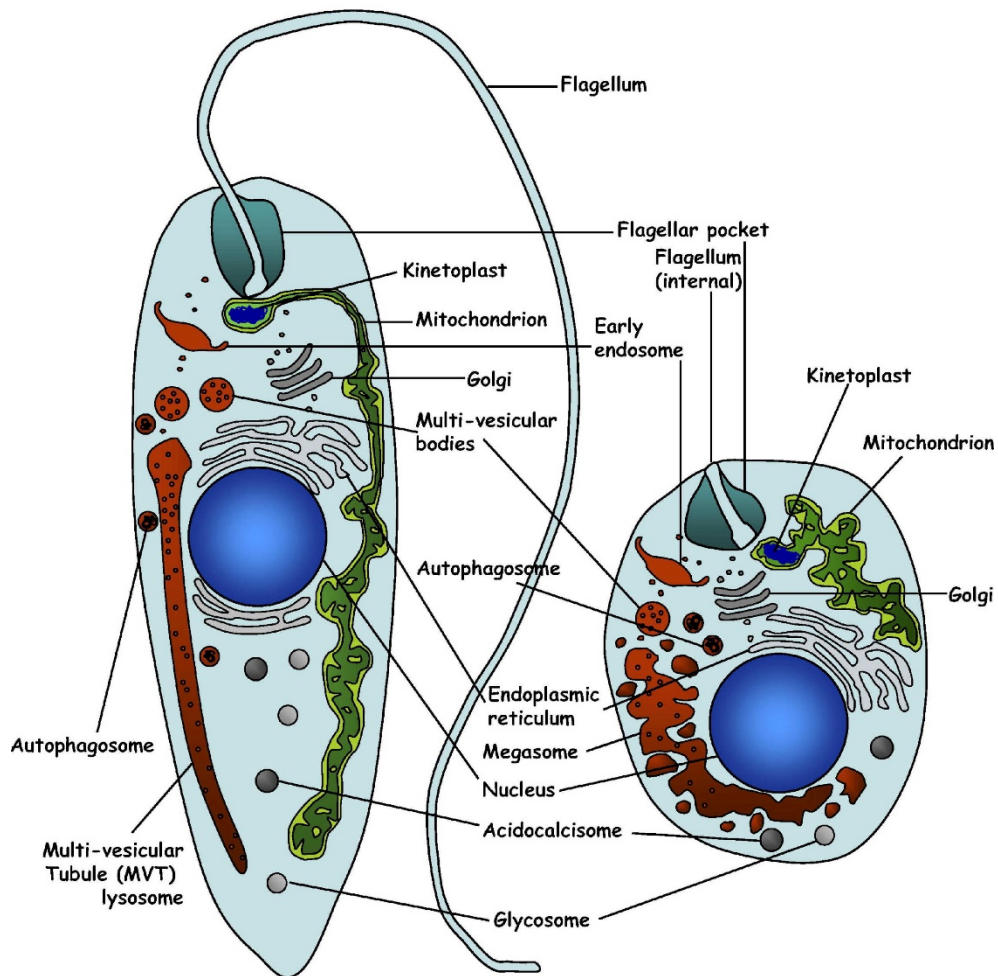


**Fig. 6 – The main *Leishmania* forms.**

Schematic representation of the main intracellular organelles from *Leishmania* promastigote (left) or amastigote (right) stages. The flagellar pocket marks the anterior end of the cell. (Data source: (Besteiro et al., 2007)).

## 4. Protein kinases

### 4.1. Eukaryotes

Protein phosphorylation is one of the most important and common post-translational modifications (PTMs) (Li et al., 2013; Sacco et al., 2012). More than two-third of the 21,000 proteins encoded by the human genome have been shown to be phosphorylated, according to the Kinexus PhosphoNET website (<http://www.phosphonet.ca/>). Phosphorylation of cellular proteins is involved in multiple stimuli controlling most aspect of life and death. It allows for activation or inactivation of cellular proteins, and their association with other proteins resulting in the assembly or disassembly of protein complexes. Protein phosphorylation is a reversible reaction and is catalysed by the members of one of the largest protein families, the protein kinases (Ardito et al., 2017). Protein kinases represent approximately 2% of the proteins encoded by the human genome, and are conserved across eukaryotes, suggesting essential functions for all eukaryotic cells (Manning et al., 2002). Activation or inactivation of kinases is mediated by autophosphorylation, phosphorylation by other kinases, by binding to an activator/inhibitor protein or by their subcellular sequestration and localisation (Ardito et al., 2017). Protein kinases have been shown to differ in their specificity, some kinases phosphorylating hundreds of proteins, while others being very specialised (Ptacek et al., 2005; Ubersax et al., 2003). The human kinome consists of 478 eukaryotic protein kinases (ePKs) and 40 atypical protein kinases (aPK) (Manning et al., 2002).

The ePKs catalyse the transfer of the terminal ( $\gamma$ ) phosphate group of adenosine or guanosine tri-phosphate (ATP or GTP, respectively) to the hydroxyl moiety in the respective amino acid residue (serine, threonine or tyrosine). A divalent cation such as  $Mg^{2+}$  or  $Mn^{2+}$  is required for this reaction (Roskoski, 2015). Serine and threonine residues contain an alcoholic side chain whereas tyrosine contains a phenolic side chain. The ePKs are classified in two categories based upon the nature of the phosphorylated  $-OH$  group (alcohol or phenol): the serine/threonine protein kinases (the majority), and the tyrosine protein kinases (Manning et al., 2002). There is a third category of protein kinases that exhibits dual specificity, capable of phosphorylating both tyrosine and serine/threonine residues, for instance the dual-specificity tyrosine phosphorylation–regulated kinase (DYRK) (Lindberg et al., 1992).

The catalytic domain (kinase domain) of the ePKs is highly conserved and ranges from 250 to 300 residues (Hanks et al., 1988; Taylor and Radzio-Andzelm, 1994). This kinase core consists of two-subdomains, a small N- and a large C-terminal, that forms a bilobal protein (Schwartz and Murray, 2011). Both subdomains are connected by a peptide strand (the hinge) that forms a cleft, which corresponds to the active site with a front (catalytic residues) and a back pocket (Schwartz and Murray, 2011). A conserved lysine and a “gatekeeper” residue control the access to the back pocket. Phosphorylation of the activation loop or an allosteric mechanism lead to the activation of the catalytic domain (Ardito et al., 2017). Apart from the highly conserved catalytic domain, ePKs have non-catalytic N- and C-terminus, which differ in lengths and amino acid composition, and are mostly required for regulation and localisation of the ePKs (Nishi et al., 2014).

The ePKs are divided in nine groups, based on the characteristics of their catalytic domains, their substrate specificity and their regulations (Hanks and Hunter, 1995; Manning et al., 2002). The different groups are presented in [Table 2](#) and [Fig. 7](#). The number of kinases in every subgroup varies depending on the eukaryotes, and is linked to the different biological functions that were selected during evolution.

**Table 2 – Groups of eukaryotic protein kinases (Manning et al., 2002)**

Protein kinase family	Description
AGC	Subgroup of serine/threonine protein kinases that contains the PKA, PKG, PKC families as well as Akt1/2/3 (PKB1/2/3), Aur1/2/3 (Aurora kinase), PDK1 (phosphoinositide-dependent kinase) and RSK1/2/3/4 (ribosomal protein S6 kinase).
CaMK	The CaMK kinases transfer phosphates from ATP to serine or threonine residues in proteins in response to increase in concentration of intracellular calcium ions. Important for the expression of various genes due to their activity on transcription factors when they are activated. Members of this group contains calcium/calmodulin-dependent protein kinases including CaMK1/2/4, PhK $\gamma$ 1/2 (phosphorylase kinase), MAPKAPK2/3/5 (mitogen-activated protein kinase activating protein kinases), Nek1–11 (Never in mitosis kinases), and MLCK (myosin light chain kinases).
CK1	Group containing the monomeric serine/threonine protein kinases CK1 $\alpha$ / $\gamma$ / $\delta$ / $\epsilon$ (casein kinase 1), the TTBK1/2 (tau tubulin kinase) and the VRK1/2/3 (vaccinia-related kinase) families, see <a href="#">Section 4.3</a> .
CMGC	Group that contains the CDK (cyclin-dependent protein kinases, CDK1–11), MAPK (mitogen activated protein kinases, ERK1–5), GSK3 (glycogen synthase kinase) and CDKL (CDK like, CDKL1–5) families. It contains also CK2.
STE	Group that contains three main families involved in MAPK cascade phosphorylation, sequentially activating each other to then activate the MAPK family (Ste7/MAP2K, Ste11/MAP3K, and Ste20/MAP4K).
TK	Group that contains kinases that specifically phosphorylate tyrosine residues and are thus distinct from dual specificity kinases (phosphorylates serine/threonine and tyrosine). TKs are mostly cell surface receptors (RTKs, e.g., EGFR, FGFR, Flt, InsulinR, PDGFR) but many others are non-receptors tyrosine kinases (e.g., Abl, Eph, JAK, and Src).
TKL	Group of serine/threonine protein kinases that resembles to tyrosine kinases. Members of this family includes MLK1–4 (mixed-lineage kinases), LISK (LIMK/TESK for LIM (Lin-11, Isl-1, Mec-3) kinase and testes-expressing serine kinase), IRAK (interleukin-1 receptor-associated kinase), Raf, RIPK (receptor-interacting protein kinase, or RIP), and STRK (activin and transforming growth factor receptors).
RCG	Group that includes the receptor guanylyl cyclase, and that are similar in sequence to tyrosine kinases.
OTHER	Diverse group containing unclassified kinases.

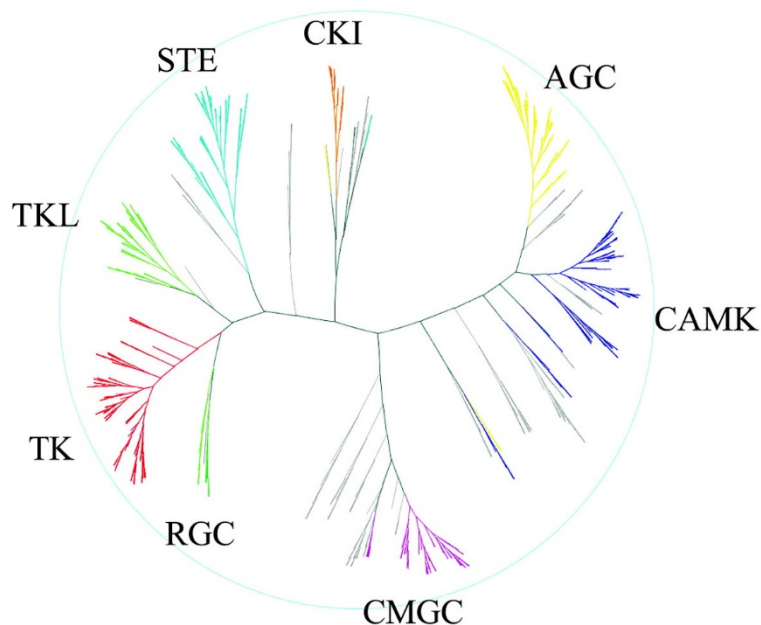


**Fig. 7 – Dendrogram of 491 ePK catalytic domains from 478 protein kinases genes.**

Major groups are labelled and coloured. (Data source: (Manning et al., 2002)).

## 4.2. Trypanosomatids

Bioinformatic analysis of the genome of the main trypanosomatid parasites has uncovered 176 protein kinases (PKs) in *T. brucei*, 190 in *T. cruzi*, and 199 in *L. major* (Parsons et al., 2005). Recently, a new analysis has been performed and revealed an increase in the number of kinases identified: 221 kinases in *L. braziliensis* and 224 in *L. infantum* (Borba et al., 2019; Parsons et al., 2005), consisting of ePKs and aPKs. The trypanosomatid kinome represents 33-43% of the human kinome. Both kinomes represent approximately 2% of their respective genomes, highlighting a key role of protein phosphorylation in the parasite biology. By comparison, *Saccharomyces cerevisiae* contains 119 kinases, and the apicomplexan parasites *Plasmodium falciparum* and *Toxoplasma gondii* 65 and 135 kinases, respectively (Talevich et al., 2013; Ward et al., 2004).

The kinases identified in trypanosomatids have been classified into six of the nine ePKs groups previously described: AGC, CAMK, CK1, STE, CMGC and “OTHER”. The Tyrosine Kinase (TK), Tyrosine Kinase Like (TKL), and the Receptor Guanylate Cyclase (RGC) groups are not represented in trypanosomatids. However, phosphorylation of tyrosine residues has been

reported in trypanosomatids (Nett et al., 2009a, 2009b; Parsons et al., 1991; Tsigankov et al., 2013), and was linked to aPKs and dual-specificity protein kinases (Boynak et al., 2013; Mottram and Smith, 1995). About 8% of the ePKs are predicted to be catalytically inactive, as they lack essential amino acid residues for catalytic activity (Parsons et al., 2005). Moreover, most of the trypanosomatid ePKs lack accessory domains (additional pfam) in the non-catalytic regions that are mainly involved in protein-protein interactions (Parsons et al., 2005).

Comparing the kinome of *L. major*, *L. infantum* and *L. braziliensis* to that of human revealed that the CAMK and AGC groups are poorly represented (CAMK: 16, 23, 23 versus 74 members, and AGC: 11, 12, 10 versus 63 members, respectively). By contrast, CMGC and STE groups are expanded, both groups representing together about 40% of the trypanosomatid kinome and only 20% in human. The CK1 group, although one of the smallest groups, is well represented in trypanosomatids with 7 conserved members in the three *Leishmania* species (6 members of the CK1 family and 1 member of tau tubulin kinase family (TTBK)) compared to 12 members in the human kinome (Borba et al., 2019; Manning et al., 2002; Parsons et al., 2005). By comparison, *P. falciparum* only contains one member of the CK1 group (Talevich et al., 2012; Ward et al., 2004). As signalling kinases, casein kinase 1 family members are particularly attractive as they regulate key pathways such as cell cycle, DNA damage, apoptosis (Knippschild et al., 2014).

### 4.3. Casein kinase 1 family

The discovery of casein kinase 1 is associated with the discovery of protein phosphorylation. It was late in the 19<sup>th</sup> Century that the milk protein casein was unexpectedly found to contain phosphorus, which led to the designation of a new class of proteins named “phosphoproteins” (Hammarsten, 1883). It was not until 1954 that the biochemical mechanism explaining casein phosphorylation was discovered by Burnett and Kennedy, where they showed the phosphorylation activity from an enzyme preparation isolated from liver against exogenous casein (Burnett and Kennedy, 1954). This activity was due to two distinct enzymes, that were termed CK1 (casein kinase 1, or also known as CKI) and CK2 (also known as CKII). However, this demonstration was not reflected by the *in vivo* phosphorylation of casein by these enzymes, this role was later found to be performed by a “genuine” casein

kinase, G-CK particularly expressed in the Golgi apparatus of the lactating mammary gland (Lasa et al., 1997). Thus the name “casein kinase” was kept for the latter kinase, and only the acronyms were conserved for the two protein kinases CK1 and CK2. Nowadays however, for CK1 and CK2, “CK” is still referred in the literature as “casein kinase”, but also “cell kinase”. The present work focuses on a member of the CK1 family, and the main features of this family are described hereafter.

#### 4.3.1. General description of the CK1 family

CK1 protein kinases have been classified in the ePK group CK1. It is important to note that CK1 and CK2 are positioned in distantly related branches in the kinome tree, CK2 is part of the CMGC group whereas CK1 family belongs to the CK1 group with its closest relatives the tau tubulin kinases 1 and 2 (TTBK1/2) and the vaccinia-related kinases 1-3 (VRK1-3) (Miranda-Saavedra and Barton, 2007). CK1 are monomeric and constitutively active serine/threonine protein kinases that are evolutionarily conserved across all eukaryotes and are ubiquitously expressed (Knippschild et al., 2014). CK1 family members play a major role in fundamental cellular processes that range from cell cycle progression, membrane trafficking to DNA damage repair, and cellular functions such as immune response and inflammation, circadian rhythm and apoptosis (reviewed in (Knippschild et al., 2014), citations therein). Consequently, impairment in CK1 activity, regulation, cellular sequestration or the presence of mutation have been associated with important diseases such as cancer, neurodegenerative diseases or sleeping disorders (Jiang et al., 2018; Knippschild et al., 2005a; Schittek and Sinnberg, 2014). In mammals, seven distinct genes encoding for CK1 paralogs  $\alpha$ ,  $\beta$ ,  $\gamma$ 1,  $\gamma$ 2,  $\gamma$ 3,  $\delta$  and  $\epsilon$ , as well as several splice variants, have been characterised (CK1 $\beta$  is the only isoform not expressed in humans). The budding yeast *S. cerevisiae* encodes four different CK1 isoforms: Yck1p, Yck2p, Yck3p and Hrr25p (yeast CK1 $\delta/\epsilon$ ) (DeMaggio et al., 1992; Hoekstra et al., 1991; Robinson et al., 1992; Wang et al., 1992, 1996). The following will highlight some of the most significant features of CK1, mostly coming from studies undertaken on mammalian and yeast CK1.

#### 4.3.2. Structure of casein kinase 1

In mammals, all paralogs share a highly conserved kinase domain (of about 300 amino acids) which differs from most of the other protein kinases by the presence of a S-I-N sequence

instead of the conserved A-P-E in the kinase subdomain VIII (Hanks and Hunter, 1995). Most of the sequence divergence between the CK1 family members is found outside the kinase domain, with differences in length and amino acid composition of both N- and C-termini (Fig. 8, (Knippschild et al., 2014)) CK1 $\delta$  and CK1 $\epsilon$  are the most closely related isoforms and form the  $\delta/\epsilon$  subfamily characterized by a long C-terminal tail that has been shown to be important for auto-inhibition. CK1 $\alpha$  is closely related to the  $\delta/\epsilon$  subfamily, and although, its C-terminal domain is shorter it also undergoes auto-inhibitory phosphorylation (Budini et al., 2009). The CK1 $\gamma$  subfamily is less studied, but displays the ability to anchor to the plasma membrane through a unique C-terminal palmitoylation site (Davidson et al., 2005).

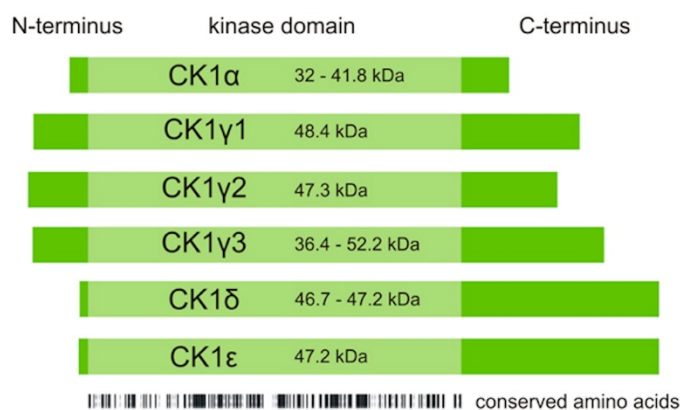


**Fig. 8 – Schematic alignment of human CK1 isoforms  $\alpha$ ,  $\gamma$ 1–3,  $\delta$ , and  $\epsilon$ .**

Their molecular weight varies between 32 (CK1 $\alpha$ ) and 52.2 kDa (CK1 $\gamma$ 3). When transcription variants have been reported for one isoform, the molecular weight is given as range from the smallest to the largest variant. All CK1 isoforms are highly conserved within their kinase domains (light green box, 286 aa), but differ within their variable N- (4–40 aa) and C-terminal (39–122 aa) non-catalytic domains (dark green boxes). (Data source: (Knippschild et al., 2014)).

Crystal structures of the catalytic domain of CK1 $\delta$ ,  $\gamma$  and more recently CK1 $\alpha$  paralogs have been solved revealing the typical 3D bilobal structure of PKs, an N-terminal lobe composed of  $\beta$ -sheets and a larger C-terminal lobe mainly constituted of  $\alpha$ -helices (Fig. 9, representing CK1 $\delta$  structure, (Longenecker et al., 1996; Minzel et al., 2018; Petzold et al., 2016; Xu et al., 1995)). The main structural features of CK1 kinase domain are:

- A  $\alpha$ -helix ( $\alpha$ -A helix) in the N-terminal lobe that is required for conformational regulation of kinase activity.
- A conserved glycine-rich loop (bridge between strands  $\beta$ 1 and  $\beta$ 2); ceiling of the ATP active site.

- A kinesin homology domain (KHD) within the T-loop (L-9D), that is thought to be the domain of interaction of CK1 isoforms with components of the cytoskeleton (Behrend et al., 2000; Tuazon and Traugh, 1991).
- A putative dimerization domain (DD, containing various amino acids of strands  $\beta 1$ ,  $\beta 2$ ,  $\beta 5$ , hinge region,  $\beta 7$ , and  $\alpha B$ )

The structures of the N- and C-terminal domains have not been solved, as they are not structured.

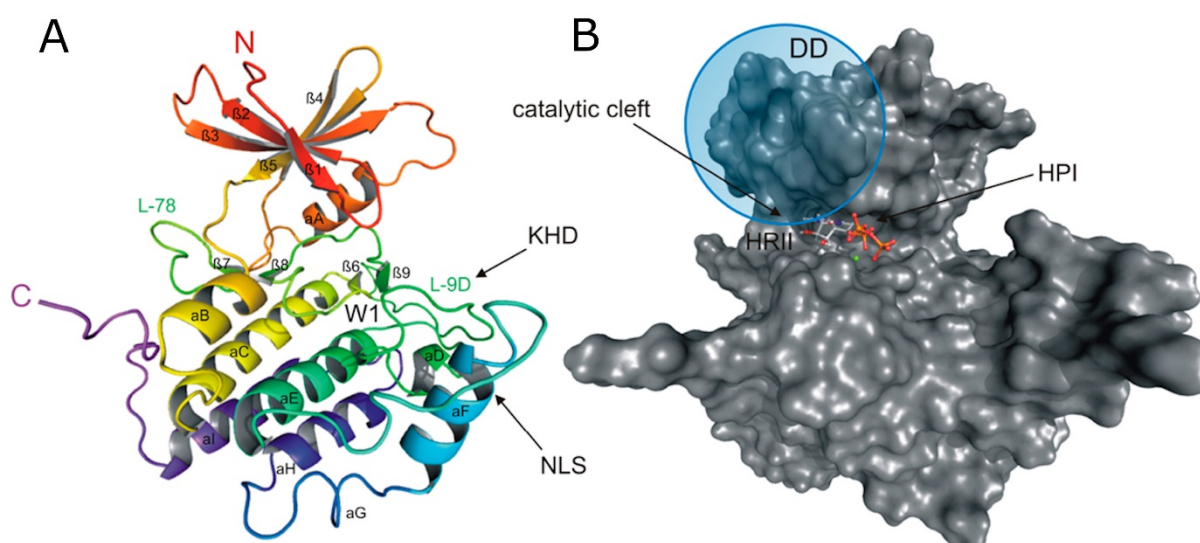


**Fig. 9 – 3D structure of CK1 $\delta$ .**

Ribbon (A) and surface (B) diagram of the molecular structure of CK1 $\delta$  (PDB code 4HGT) modelled in complex with Mg<sup>2+</sup>-ATP at a resolution of 1.80 Å. The catalytic domain folds into two lobes primarily containing strands (N-terminal) and helices (C-terminal) connected by a hinge region forming a catalytic cleft that represents the ATP binding pocket substrate binding site. KHD indicates the kinesin homology domain within L-9D. DD refers to a putative dimerization domain containing various amino acids of  $\beta 1$ ,  $\beta 2$ ,  $\beta 5$ , L-5B,  $\beta 7$ , and  $\alpha B$ , whereas NLS displays a putative nuclear localization signal sequence at the junction between L-EF and  $\alpha F$ . A tungstate molecule binding site identifies a specific phosphate moiety binding motif (W1). The active site contains a deep hydrophobic pocket (HPI) and a spacious hydrophobic region (HR11). (Data source: (Knippschild et al., 2014)).

### 4.3.3. Specificity of CK1

The activity of CK1s are not dependent upon second messengers, such as cAMP diacylglycerol or calcium contrary to other PKs (Tuazon and Traugh, 1991). CK1 is described as acidotropic, as it mainly recognises substrates containing acidic or phosphorylated amino acid residues. The canonical consensus sequence for CK1 protein kinases is pS/T-X-X(X)-S/T, with pS/T corresponding to a serine or threonine residue phosphorylated by a priming kinase. However, phospho-priming is not essential for CK1 kinase activity, as it was observed that pS or pT could be replaced by clusters of acidic residues, (D/E-X-X(X)-pS/T (Marin et al., 1994; Songyang et al., 1996). Furthermore, non-canonical consensus sequences have also been described, such as the pSLS motif with an acidic cluster in n+7, found in  $\beta$ -catenin and nuclear factor of activated T-cells (NFAT), or the motif K/R-X-K/R-X-X-pS/T present in sulfatide and cholesterol-3-sulfate (SCS) binding proteins (Kawakami et al., 2008; Marin et al., 2003). To date, more than 150 substrates for CK1 isoforms have been reported which points towards the pleiotropic character of the family (Knippschild et al., 2014; Xu et al., 2019). The substrate recognition motifs of CK1 are very commonly found in cellular proteins, suggesting that CK1 members could phosphorylate hundreds of substrates. To insure the specificity of the kinase, regulatory mechanisms have been identified.

### 4.3.4. Regulation of CK1 activity

CK1 family members are ubiquitously expressed and constitutively active *in vitro*. However they show differences in expression levels and activity depending on the tissue/cell type or the environment (Löhler et al., 2009; Tuazon and Traugh, 1991; Utz et al., 2010). Several mechanisms regulating their activity and expression have been described: (i) structure-related regulation, (ii) post-translational modifications, (iii) subcellular localisation/compartmentalisation and (iv) interaction with other proteins (Knippschild et al., 2014). For instance, cell stimulation with viral transformation or insulin, as well as treatment with topoisomerase inhibitors or  $\gamma$ -irradiation result in elevated CK1 activity and/or protein levels (Cobb and Rosen, 1983; Hirner et al., 2012; Knippschild et al., 1997). By contrast, CK1 $\alpha$  activity in erythrocytes and neuronal cells was shown to be reduced due to an increase in the membrane concentration of phosphatidylinositol 4,5-bisphosphate (PIP<sub>2</sub>) (Gross et al., 1995).

CK1 activity can be regulated via auto-phosphorylation or site-specific phosphorylation by upstream kinases. The auto-phosphorylation of the C-terminal domain of human CK1 paralogs has been shown to inhibit their activity. For CK1 $\delta/\epsilon$ , auto-phosphorylation generates a sequence motif that acts as pseudo-substrate and thus blocks the catalytic domain of the kinase (Budini et al., 2009; Gietzen and Virshup, 1999; Graves and Roach, 1995; Rivers et al., 1998; Zhai et al., 1995). CK1 isoforms are also phosphorylated by upstream kinases, and the dephosphorylation of CK1 by specific serine/threonine phosphatases resulted in an increase in kinase activity, suggesting the important role of phosphorylation to control CK1 activity (Bischof et al., 2013; Cegielska et al., 1998; Giamas et al., 2007; Gietzen and Virshup, 1999). Several phospho-sites have been identified by mass spectrometry (visit <sup>1</sup> for details), but the upstream kinases were not all identified.

CK1 members are also regulated by subcellular localisation and compartmentalisation, which is crucial to allow the kinase to access to its substrates (Sillibourne et al., 2002; Vancura et al., 1994; Wang et al., 1994). Recently, the FAM83 protein family have been shown to specifically bind to CK1 paralogs and deliver CK1 to unique subcellular compartments (Bozatzki and Sapkota, 2018; Fulcher et al., 2018). Different FAM83 members appear to deliver CK1 paralogs to specific compartments. For example FAM83D was shown to direct CK1 $\alpha$  to the mitotic spindle to regulate spindle positioning (Fulcher et al., 2019).

Finally, CK1 activity could be regulated by interaction with proteins. This is particularly true for the DDX3 (DEAD-box RNA helicase 3) protein that was identified as a regulatory subunit of CK1 in the Wnt/ $\beta$ -catenin network. The interaction of the two proteins stimulates the activity of CK1 (Cruciat et al., 2013).

#### 4.3.5. CK1s in parasites species

CK1 family members are found in parasites responsible for human diseases such as malaria (*Plasmodium falciparum*), toxoplasmosis (*Toxoplasma gondii*), human African trypanosomiasis (HAT, *Trypanosoma brucei*), Chagas disease (*Trypanosoma cruzi*) and leishmaniasis, with different paralogs, their numbers depending on the species.

---

<sup>1</sup> <https://www.phosphosite.org/simpleSearchSubmitAction.action?searchStr=casein%20kinase%201>

*P. falciparum* encodes a single member of the CK1 family, PfCK1, whereas *T. gondii*, which also belongs to the apicomplexans, encodes three CK1 paralogs. Among trypanosomatid species, *T. brucei* and *T. cruzi* have five CK1 paralogs. Interestingly, TcCK1.2 is a multigene family. CK1 paralogs from *Leishmania* species are described in details in the following [Section 4.4](#). The conservation of CK1 in parasites suggests an important role for this kinase family.<sup>2</sup>

PfCK1 encoded gene is expressed in two alternative transcripts and detected in all parasite life stages (Aslett et al., 2010; Barik et al., 1997; Dorin-Semblat et al., 2015). Cellular sequestration appears to be important for PfCK1 regulation. For instance, PfCK1 localises to the surface of infected erythrocytes at early infection stages, and is restricted to the parasite in mature trophozoites, or to a single dot in merozoites (Dorin-Semblat et al., 2015). PfCK1 interacts with proteins involved in multiple functions, such as invasion or metabolism (Dorin-Semblat et al., 2015), suggesting a role in these processes. Moreover, this kinase is phosphorylated at serine 17 and serine 19, which could inhibit kinase activity (Dorin-Semblat et al., 2015). Finally, PfCK1 seems to be essential for the erythrocyte asexual cycle (Solyakov et al., 2011).

TgCK1 $\alpha$  and TgCK1 $\beta$  are the two isoforms that have been characterised in *T. gondii*, TgCK1 $\gamma$  remains so far not studied. TgCK1 $\alpha$  is more abundant and more active than TgCK1 $\beta$  in tachyzoites, suggesting a different post-translational regulation (Donald et al., 2005). Their localisation differ slightly, with both being localised to the cytoplasm whereas TgCK1 $\beta$  is also present at the plasma membrane (Donald et al., 2005). TgCK1 $\alpha$  is not essential, and the deletion of this paralog increases the virulence of transgenic parasites in mice (Wang et al., 2016). This contrasts with its orthologs in *Plasmodium* or *T. brucei*, which were essential.

In *T. brucei*, the only isoforms that have been studied are TbCK1.1 and TbCK1.2. Both genes are adjacent on chromosome 5, and one of the difference between these paralogs is the presence of an unusual QQQQQQQQQQ motif in TbCK1.2 (Urbaniak, 2009). TbCK1.2 protein is detected in both bloodstream form (BSF) and procyclic form (PCF) and was described to be essential for the BSF (Urbaniak, 2009) and the PCF (Minia and Clayton, 2016),

---

<sup>2</sup> Because this work is solely focused on *Leishmania* CK1.2, the knowledge presented here concerning CK1 from other parasite species presuppose that the life cycles and other basic knowledge of these parasite species are known to the reader.

in contrast to TbCK1.1, which is non-essential (Urbaniak, 2009). TbCK1.2 was recently found to negatively regulate the stability of a CCCH zinc finger protein, ZC3H11, required for stabilizing stress response mRNAs upon heat shock (Minia and Clayton, 2016).

In *T. cruzi*, TcCK1.1 and TcCK1.2 are the most studied, and are highly similar with 94% amino acid identity within the kinase domain (Spadafora et al., 2002). TcCK1.1 expression was shown to be stage-regulated, with drastic increased mRNA amounts in trypomastigote compared to epimastigote, while TcCK1.2 expression was found constant, with slight increased mRNA amounts in amastigotes compared to epimastigotes (Spadafora et al., 2002).

#### 4.3.6. CK1s in infectious diseases

Several studies have linked CK1 with infectious diseases through the manipulation of the host CK1 signalling pathways by intracellular pathogens, either by exploiting the host CK1s or by exporting their own CK1. First, several pathogens, including *Mycobacterium* and viruses, have been shown to manipulate host signalling pathways by exploiting the host CK1. Indeed, during *Mycobacterium tuberculosis* (Mtb) infection, the knockdown of CK1 $\delta$  or  $\epsilon$  leads to a decrease in bacteria burden (Jayaswal et al., 2010). Xia et al. have shown that influenza A virus (IAV) evaded the immune systems by targeting IFNGR1, the type II IFN receptor 1 (IFN- $\gamma$ ) as well as IFNAR1, the type I IFN receptor 1 (IFN- $\alpha/\beta$ ) for degradation through phosphorylation of those receptors by CK1 $\alpha$ . Their degradations impaired the transduction signal (type I and II IFNs) creating favourable conditions for viral propagation (Xia et al., 2018). Second, several parasites are thought to manipulate host CK1 pathways by exporting their own CK1 into the host cell. PfCK1, the only CK1 paralog in *P. falciparum* is an ectokinase targeted to the membrane of the host erythrocyte in the early stages of infection (Dorin-Semblat et al., 2015). *Leishmania* CK1.2 (LmjF.35.1010) was also shown to be exported in the host (in macrophages or in the midgut of the insect vector) by the parasites as free proteins or via exosomes (Atayde et al., 2015; Santarém et al., 2013; Silverman et al., 2008, 2010a). For these two parasites, the function of CK1 in their respective host cell has not been elucidated. LmCK1.2 functions in host-pathogen interactions are further described in [Chapter III](#).

## 4.4. *Leishmania* casein kinase 1

### 4.4.1. Generalities

*Leishmania* genome encodes for six CK1 paralogs, namely LmCK1.1, LmCK1.2, LmCK1.3, LmCK1.4, LmCK1.5 and LmCK1.6 (Table 3). They are conserved across *Leishmania* species for which genomic information is currently available, and their protein size range from 37-62 kDa in *L. donovani* (LmCK1.1 and LmCK1.4, respectively), with the main differences observed in the non-catalytic C-terminal domain. Phylogenetic analyses using the conserved catalytic domain showed that LmCK1.1 and LmCK1.2 are the most closely related, probably the consequence of duplication and subsequent independent evolution (both genes are adjacent in chromosome 35 in *L. donovani*) (Rachidi et al., 2014). LmCK1.3 and LmCK1.4 are also related to each other and form a separate clade from other CK1 isoforms (Dan-Goor et al., 2013). Interestingly, LmCK1.2 and, in a lesser extent, LmCK1.1 are more closely related to the mammalian CK1 paralogs (from 59 to 71% identity) than to the other *Leishmania* paralogs (from 36 to 55% identity) (Rachidi et al., 2014).

**Table 3 – The CK1 protein kinases from *Leishmania*.**

CK1 isoform	Accession ( <i>L. donovani</i> )	Protein length (aa)	MW (kDa)	C-terminal domain size (aa)	Observations in literature for <i>Leishmania</i> isoforms
LmCK1.1	LdBPK_351020.1	324	37.2	38	-
LmCK1.2	LdBPK_351030.1	353	39.8	70	(Durieu et al., 2016; Rachidi et al., 2014)
LmCK1.3	LdBPK_041230.1	368	41.3	80	-
LmCK1.4	LdBPK_271680.1	568	62.3	152	(Dan-Goor et al., 2013)
LmCK1.5	LdBPK_251640.1	518	58.9	174	-
LmCK1.6	LdBPK_303530.1	376	42.2	74	-

Accession, protein length and molecular weight (MW) were obtained from TriTrypDB. C-terminal domain size was calculated by subtracting the protein length to the last amino acid of the protein kinase domain detected by ProSiteProfiles database in TriTrypDB.

With the exception of LmCK1.2, none of the other *Leishmania* CK1s were identified in published proteomics studies (Paape et al., 2010; Silverman et al., 2008, 2010a), and little information has been published on these proteins, as most of the data focused on LmCK1.2 partly due to its attractiveness as putative drug target. There are several hypothesis that could

explain the non-detection of these paralogs by MS: (i) their level might be below MS detection; (ii) LmCK1.4 was shown to be secreted in promastigotes, therefore the cell extracts might not have recovered detectable level of the kinase (Dan-Goor et al., 2013); (iii) some isoforms might be regulated and/or expressed in specific life stages. Transcriptomics analyses of *L. major* developmental stages in the sand fly suggests that LmCK1.3 is up-regulated in metacyclic promastigotes, and LmCK1.6 is up-regulated in nectomonad and metacyclic promastigotes (Inbar et al., 2017).

#### 4.4.2. LmCK1.2

Previous work from our laboratory has highlighted the importance of LmCK1.2 as a target for drug discovery (Durieu et al., 2016; Rachidi et al., 2014).

LmCK1.2 is highly conserved among *Leishmania* species with more than 99% sequence identity, with minor differences only observed in the last 13 C-terminal amino acids (Fig. 10A), suggesting a very strong purifying selection against mutations within LmCK1.2, probably pointing to important functions (Rachidi et al., 2014). This particularity is unique to LmCK1.2. Moreover, LmCK1.2 is the kinase with the highest similarity to its human ortholog (Fig. 10B, (Rachidi et al., 2014)).

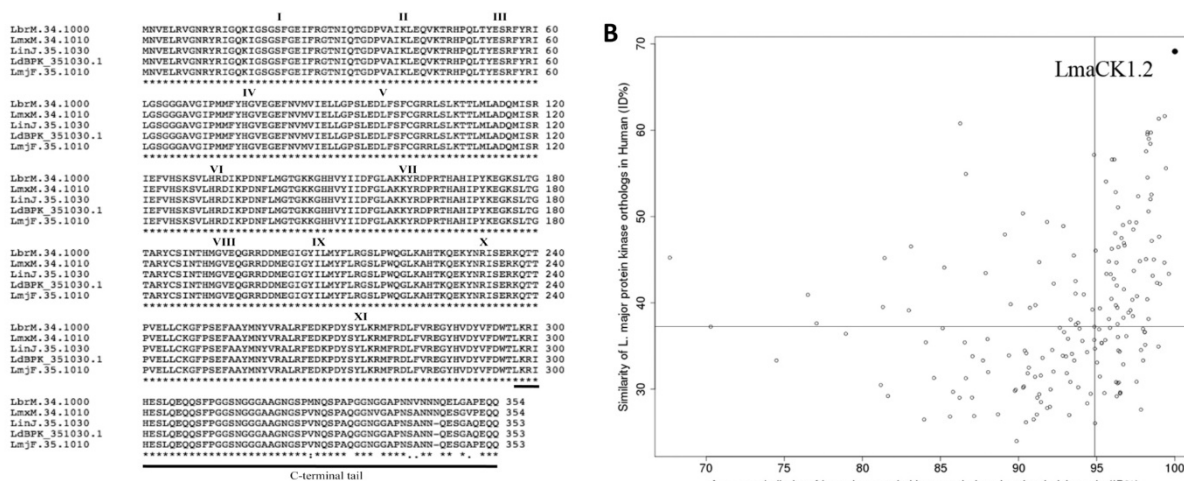


**Fig. 10 – Amino acid sequence alignment of *Leishmania* Casein Kinase I proteins.**

A. The amino acid sequences of LmjF.35.1010 (*L. major* CK1.2), LbrM.34.1000 (*L. braziliensis* CK1.2), LinJ.35.1030 (*L. infantum* CK1.2), LdBPK\_351030.1 (*L. donovani* CK1.2) and LmXM.34.1010 (*L. mexicana* CK1.2) have been compared using ClustalW2 program. \* corresponds to amino acid residues that are invariant in all four CK1s. B. Differential conservation of *L. major* protein kinases in other *Leishmania* or in human. The average similarity of *L. major* protein kinase sequences in *L. braziliensis*, *L. infantum* and *L. mexicana* is plotted against the similarity of the best human homologs. The vertical black line corresponds to the median of the average similarity of *L. major* proteins to other *Leishmania* (95%). The horizontal black line corresponds to the median of the average similarity of *L. major* proteins to human homologs (37%). (Data source: (Rachidi et al., 2014)).

LmCK1.2 is expressed in promastigotes and axenic amastigotes, and active in both life stages (Rachidi et al., 2014). An established CK1 inhibitor, the D4476 (4-[4-(2,3-dihydro-1,4-benzodioxin-6-yl)-5-(2-pyridinyl)-1H-imidazol-2-yl]benzamide), is able to inhibit transgenic LmCK1.2 purified from parasite extract or recombinant LmCK1.2 kinase activity. Only a cytostatic effect was observed using D4476 at the 50% effective concentration (EC50) dose in promastigotes, whereas a cytotoxic effect was observed in axenic amastigotes (Rachidi et al., 2014). In addition, inhibition of LmCK1.2 by D4476 significantly decreased the parasite burden of infected macrophages (Durieu et al., 2016; Rachidi et al., 2014).

LmCK1.2 has been identified as an ecto-kinase excreted in the host cell as free protein or through exosomes similarly to virulence factors (Sacerdoti-Sierra and Jaffe, 1997; Silverman et al., 2008, 2010a; Vieira et al., 2002). Although the functions of LmCK1.2 in the host cell have not been investigated, a first study showed that LmCK1.2 phosphorylates the IFNAR1 leading to attenuation of the cellular responses to IFN $\alpha$  *in vitro* (Liu et al., 2009).

These findings suggest that LmCK1.2 carries functions outside of the parasite. Our working hypothesis is thus that LmCK1.2 is released by the parasite, via the exosomes, to

phosphorylate host substrates and thus modify the host cell biology and immune response. The subversion of the host cell is necessary to allow the intracellular parasite to survive.

## 5. PhD objectives

The working hypothesis is that LmCK1.2 is released by the parasite, via the exosomes, to phosphorylate host substrates and thus modify the host cell biology and immune response. The subversion of the host cell is necessary to allow the intracellular parasite to survive. The aim of my PhD was to investigate this hypothesis through the characterisation of LmCK1.2 and the identification of its potential functions in the parasite and in the host cell:

- Objective 1 was to characterise exhaustively the localisation of LmCK1.2 in the parasite to gain insights into its cellular functions. The results are presented in [Chapter I](#).

- Objective 2 was to identify and characterise LmCK1.2 binding partners involved in cellular trafficking to gain insights into the mechanisms involved in its exosomal loading. The results are presented in [Chapter II](#).

- Objective 3 was to investigate the putative functions of LmCK1.2 in the host cell through the identification of the host binding partners of *Leishmania* CK1.2. The results are presented in [Chapter III](#).

# Materials & Methods

---



# Materials

## 1. Chemicals

All the chemicals used for the experiments described in this thesis were purchased from Sigma-Aldrich, NEB, USB, Invitrogen, Fluka, ThermoFisher Scientific, VWR Chemicals or Calbiochem, and were analytical grade or above. Media for cell culture were cell culture grade, i.e. sterile and endotoxin tested, and purchased from Gibco or Sigma-Aldrich. The pH of the buffers was measured at room temperature.

**Table 4 – List of the chemicals used in this document.**

Application	Description	Composition
General Use	Dulbecco's Phosphate-Buffered Saline (pH 7.4)	137 mM NaCl
		2.7 mM KCl
		8 mM Na <sub>2</sub> HPO <sub>4</sub>
		1.4 mM KH <sub>2</sub> PO <sub>4</sub>
		Purchased from Gibco
	Distilled Water for cell culture	Purchased from Gibco
	Tris-HCl (pH 8.0)	1 M Tris, pH adjusted to 8.0 with HCl
	Tris-HCl (pH 7.5)	1 M Tris, pH adjusted to 7.5 with HCl
Agarose gel electrophoresis	50X TAE buffer (pH 8.3)	2 M Tris-HCl, pH 8.0
		1 M acetic acid, pH 8.0
		50 mM EDTA
		Purchased from EuroMedex
	10X BlueJuice Gel Loading buffer	65% (w/v) Sucrose
		10 mM EDTA (pH 8.0)
		0.3 % (w/v) Bromophenol blue
		10 mM Tris-HCl (pH 7.5) Purchased from Invitrogen
	6X Gel Loading Dye, Purple	Purchased from NEB
	Ethidium bromide solution	Ethidium bromide solution (0.7 mg/mL) purchased from Eurobio
	SmartLadder DNA ladder	Purchased from Eurobio
DNA Ligation	T4 DNA ligase buffer	40 mM Tris-Hcl (pH 7.8) 10 mM MgCl <sub>2</sub>

		10 mM DTT 0.5 mM ATP Purchased from Promega
<b>DNA purification</b>	Wizard SV Gel and PCR Clean-Up System	Purchased from Promega
<b>Plasmid preparation</b>	NucleoBond Xtra Midi	Purchased from Macherey-Nagel
	NucleoSpin Plasmid	Purchased from Macherey-Nagel
<b><i>Leishmania</i> transfection</b>	Electroporation buffer (pH 7.6)	0,15 mM CaCl <sub>2</sub> 120 mM KCl 10 mM KH <sub>2</sub> PO <sub>4</sub> 5 mM MgCl <sub>2</sub> 25 mM HEPES (pH 7.5) 2 mM EDTA, pH adjusted to 7.6
	1X Tb-BSF buffer (for Amaxa transfection)	90 mM sodium phosphate 5 mM potassium chloride 0.15 mM calcium chloride 50 mM HEPES, pH adjusted to 7.3
	Dynabeads Protein G (30 mg/mL)	Purchased from Thermo Scientific
	DPBS-tween buffer	0.02% Tween-20 in DPBS, pH adjusted to 7.4
	BS <sup>3</sup> buffer	2 mg Bis(sulfosuccinimidyl) suberate (BS <sup>3</sup> ) 20 mM Sodium Phosphate 150 mM NaCl in distilled H <sub>2</sub> O
<b>Immuno-precipitation</b>	Conjugation buffer	20 mM Sodium Phosphate pH 7.4 150 mM NaCl in distilled H <sub>2</sub> O
	Washing buffer (beads buffer)	50 mM Tris pH 7.4 5 mM Sodium Fluoride 250 mM NaCl 5 mM EDTA pH 8 0.1% NP-40 Complete protease inhibitor cocktail in distilled H <sub>2</sub> O
	NuPAGE loading buffer	7.5µL LDS Sample Buffer 3 µL Sample Reducing Agent 19.5 µL H <sub>2</sub> O
	Glycine elution buffer	33.33 mM glycine pH 2.8 0.33X LDS Sample Buffer 0.33X Sample Reducing Agent

<b>Production of recombinant protein</b>	Lysis	60 mM $\beta$ -glycerophosphate 1 mM sodium vanadate 1 mM sodium fluoride 1 mM disodium phenylphosphate 150 mM NaCl 10 mM imidazole 0.1% Triton X-100 supplemented with protease inhibitor cocktail in DPBS
	Washing buffer	60 mM $\beta$ -glycerophosphate 1 mM sodium vanadate 1 mM sodium fluoride 1 mM disodium phenylphosphate 300 mM NaCl 30 mM imidazole 0.1% Triton X-100 supplemented with protease inhibitor cocktail in DPBS, pH adjusted to 7.5
	Elution buffer	60 mM $\beta$ -glycerophosphate 1 mM sodium vanadate 1 mM sodium fluoride 1 mM disodium phenylphosphate 300 mM imidazole supplemented with protease inhibitor cocktail in DPBS, pH adjusted to 7.5
<b>Protein lysis</b>	RIPA lysis buffer	150 mM NaCl 1% Triton X-100 20 mM Tris/HCl (pH 7.4) 1% NP-40 1 mM EDTA 1 mM sodium vanadate 1 mM PMSF supplemented with protease inhibitor cocktail in H <sub>2</sub> O, pH adjusted to 7.4
<b>SDS-PAGE</b>	MES SDS running buffer	50 mM MES 50 mM Tris-HCl (pH 7.3) 0.1 % (w/v) SDS 1 mM EDTA Prepared from NuPAGE <sup>®</sup> MES SDS Running buffer (20X) from Invitrogen
	Pre-stained Protein Standard	Purchased from Invitrogen

<b>Protein staining</b>		Bio-Safe Coomassie Stain Purchased from Bio-Rad
	Coomassie blue staining solution	Coomassie Brilliant Blue R-250 Dye (purchased from ThermoFischer Scientific)
	Coomassie blue unstaining solution	10% (v/v) ethanol 7% (v/v) acetic acid 83% ddH <sub>2</sub> O
	SYPRO Ruby Protein Gel stain	Purchased from ThermoFischer Scientific
	SYPRO Ruby Protein Gel unstaining solution	10% (v/v) ethanol 7% (v/v) acetic acid 83% ddH <sub>2</sub> O
<b>Western blot</b>	Transfer buffer	48 mM TrisBase 39 mM Glycine 20% (v/v) methanol
	BSA Blocking buffer	5 g BSA in 100 mL of PBS-T buffer
	Milk blocking buffer	5 g Milk powder in 100 mL of TBS-T buffer
	PBS-T washing buffer	PBS 1X supplemented with 0.25 % Tween-20
	TBS-T washing buffer	100 mM Tris-HCl (pH 7.4) 150 mM NaCl 0.075% (v/v) Tween-20
	Restore Western Blot Stripping buffer	Purchased from Thermo Scientific
<b><i>In vitro</i> kinase assay</b>	Kinase buffer C (pH 7.5)	5X solution. Final concentrations in 1X: 50 mM MOPS pH 7.5 5 mM EGTA 15 mM MgCl <sub>2</sub> 1 mM dithiothreitol 0.1 mM sodium vanadate
<b>Cell culture</b>	<i>E. coli</i> strains DH5 $\alpha$ , XL10 Gold, Rosetta	Purchased from Invitrogen Purchased from Promega Purchased from VWR
	Liquid medium (LB)	0.5% (w/v) Yeast extract 1% (w/v) Tryptone 0.5% (w/v) NaCl
	Solid medium (LB agar)	1.5% (w/v) agar in LB
	<i>L. donovani</i> promastigote (LD1Spro)	M199 medium supplemented with 10% (v/v) FBS

	20 mM HEPES (pH 6.9) 100 µM Adenine 100 U/mL Penicillin/Streptomycin 2 mM L-glutamine 10 µg/mL folic acid 30 µM Hemin 0.5 µg/mL Biotin 8 µM 6-biopterin 4.1 mM NaHCO <sub>3</sub> 7.5% 1x RPMI 1640 vitamins solutions (Sigma) pH adjusted to 7.4 with HCl
<i>L. donovani</i> axenic amastigote (LD1Sama)	RPMI 1640 + GlutaMAX™ -I medium (Gibco) supplemented with 20% (v/v) FBS 28 mM MES 2 mM L-glutamine 1x RPMI 1640 amino acid mix (Sigma) 1x RPMI 1640 vitamins solutions (Sigma) 10 µg/mL folic acid 100 µM Adenine 100 U/mL Penicillin/Streptomycin pH adjusted to 5.5 with HCl
Carbobenzoxy-Leu-Leu-leucinal (MG132)	10 µM, purchased from Sigma-Aldrich
Ammonium chloride (NH <sub>4</sub> Cl)	20 mM, purchased from VWR Chemicals
Flavopiridol	5 µM in LD1Spro
<b>FACS</b>	
FM4-64FX	5 µg/mL in DPBS, purchased from ThermoFisher Scientific
LysoTracker Red DND-99	100 mM in LD1Spro, purchased from ThermoFisher Scientific
Propidium iodide	For cell death: 2 µg/mL in PBS
<b>Immuno-fluorescence</b>	
Slides preparation	Poly-lysine solution 10 µg/mL in PBS
Slides fixation	4% paraformaldehyde solution in PBS Ice cold Methanol
Blocking of aldehyde groups	50 mM NH <sub>4</sub> Cl prepared in H <sub>2</sub> O
Cell permeabilization and blocking after PFA fixation	0.5 mg/mL of saponin 10 % FCS in DPBS
Blocking after Methanol fixation	10 % FCS in DPBS

	Incubation of antibodies after PFA fixation	0.5 mg/mL of saponin 0.5 % BSA PBS
	Incubation of antibodies after Methanol fixation	0.5 % BSA PBS
	DNA staining	0.5 µg/mL of Hoechst 33342 dye Purchased from Sigma-Aldrich
	Mounting medium	SlowFade Gold Antifade Mountant Purchased from ThermoFisher Scientific
<b>Antibiotics</b>	Ampicillin	100 µg/mL in LB (liquid), or 100 µg/mL in LBagar (solid) from a 100 mg/mL stock solution in ddH <sub>2</sub> O Purchased from Fisher Bioreagents
	Hygromycin B	30 µg/mL in LD1S medium from a 50 mg/mL stock solution in DPBS Purchased from ThermoFisher Scientific
	Puromycin dihydrochloride	30 µg/mL in LD1S medium Purchased from Sigma-Aldrich
	Blasticidin S hydrochloride	20 µg/mL in LD1S medium Purchased form ThermoFisher Scientific
	Geneticin G418	100 µg/mL in LD1S medium Purchased from ThermoFisher Scientific

## 2. DNA vectors

### 2.1. pLEXSY-hyg2

This expression vector (Jena Biosciences) for *Leishmania* carries a hygromycin B phosphotransferase (HYG) gene conferring hygromycin B resistance and the bla gene conferring ampicillin resistance. Hygromycin B is used for positive selection in *Leishmania*. This vector was previously used for the expression of LmCK1.2 with a V5-tag and His<sub>6</sub>-tag (V5-His<sub>6</sub>) in C-terminus in *Leishmania* (pLEXSY-CK1.2, (Rachidi et al., 2014)). The pLEXSY-CK1.2 construct was used to study LmCK1.2 localisation in *L. donovani* (see [Chapter I](#)), as well as to identify LmCK1.2 binding partners from promastigotes and axenic amastigotes (see [Chapter II](#)) (see [Fig. 11](#)).

The pLEXY-hyg2 vector was modified by Stuart Pine, an intern in the laboratory, to insert a V5-His<sub>6</sub>-tag and further modified to insert truncated version of LmCK1.2: CK1.2ΔC10, CK1.2ΔC43, and CK1.2ΔN7. The resulting plasmids, pLEXY-CK1.2ΔC10-V5-His<sub>6</sub>, pLEXY-CK1.2ΔC43-V5-His<sub>6</sub> and pLEXY-CK1.2ΔN7-V5-His<sub>6</sub> were used to study the localisation and expression of each truncated proteins in *L. donovani* (see Chapter I) (see Fig. 11).

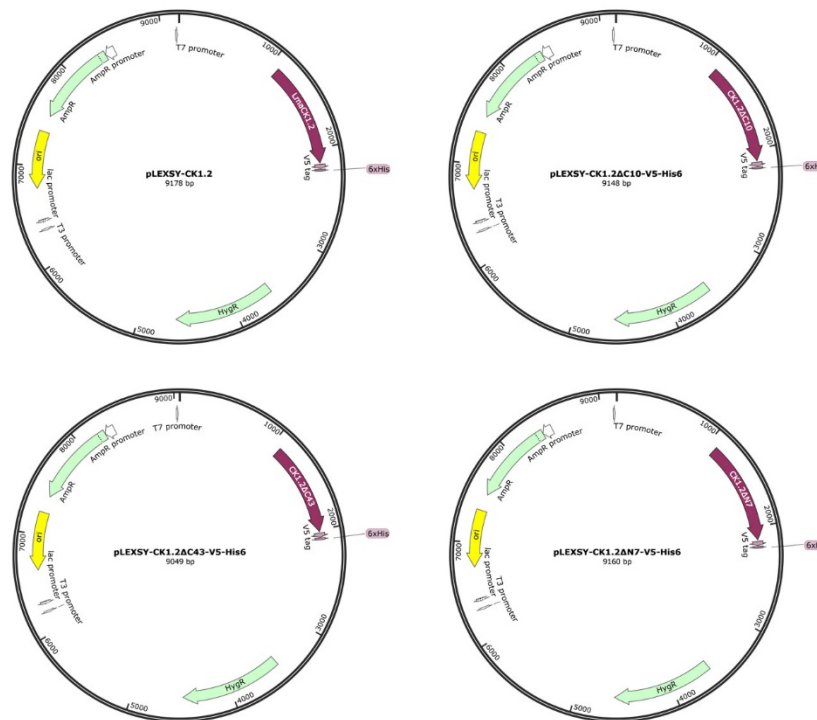


**Fig. 11 – Schematic map of pLEXY-CK1.2, pLEXY-CK1.2ΔC10-V5-His<sub>6</sub>, pLEXY-CK1.2ΔC43-V5-His<sub>6</sub> and pLEXY-CK1.2ΔN7-V5-His<sub>6</sub> plasmids.**

These plasmids express WT, ΔC10, ΔC43 and ΔN7 versions of LmCK1.2 and were generated for C-terminal V5-His<sub>6</sub> tagging of these proteins.

## 2.2. pLEXY-neo2

This expression vector (Jena Biosciences) for *Leishmania* is identical to the pLEXY-hyg2 except that it carries a *neo* marker gene encoding aminoglycoside (3') phosphotransferase APH (3')-Ia (aphA1) that provides resistance to geneticin (G418). Geneticin is used for positive selection in *Leishmania*. I used this vector to transfer the *neo* marker to the pLEXY-CK1.2 plasmid, to replace the hygromycin B resistance gene (see Chapter II). I used the obtained plasmid, pLEXY-CK1.2-V5-His<sub>6</sub> (NEO) (Fig. 12) to study the localisation of LmCK1.2 in the

parasite cell line used for CRISPR-Cas9 gene editing, particularly for the study of LmCKAP1, a LmCK1.2 associated protein (see [Chapter II](#)).

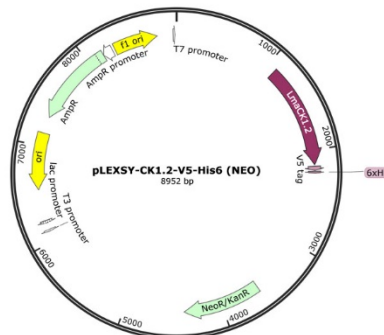


**Fig. 12 – Schematic map of pLEXSY-CK1.2-V5-His<sub>6</sub> (NEO) plasmid.**

This plasmid was generated for C-terminal V5-His<sub>6</sub> tagging of LmCK1.2.

### 2.3. pBAD/Thio-TOPO

This vector was used to generate the His-Patch thioredoxin N-terminal fusion proteins and V5-His<sub>6</sub> C-terminal tagging, for expression and purification of fusion proteins produced in *E. coli*. Expression in *E. coli* is driven by the araBAD promoter (P<sub>BAD</sub>). The AraC gene product encoded on the pBAD/Thio-TOPO plasmid (ThermoFisher Scientific) positively regulates this promoter. The thioredoxin fusion can significantly increase the solubility of many difficult-to-express proteins and improve the yield of protein production.

For the production of recombinant LmCK1.2 truncations CK1.2ΔC10, CK1.2ΔC43, and CK1.2ΔN7, Stewart Pine from our laboratory generated the following pBAD/Thio-TOPO constructs: pBAD-thio-topo-LmCK1.2ΔC10-V5-His<sub>6</sub>, pBAD-thio-topo-LmCK1.2ΔC43-V5-His<sub>6</sub> and pBAD-thio-topo-LmCK1.2ΔN7-V5-His<sub>6</sub> (see [Chapter I](#)) ([Fig. 13](#)). For the production of recombinant α2 adaptin (LdBPK\_070060.1), β2-adaptin (LdBPK\_110990.1) and γ2-adaptin (LdBPK\_363180.1), I generated the following constructs: pBADthio-α2-adaptin-V5-His<sub>6</sub>, pBADthio-β2-adaptin-V5-His<sub>6</sub> or pBADthio-μ2-adaptin-V5-His<sub>6</sub> plasmids (see [Chapter II](#)) ([Fig. 13](#)).

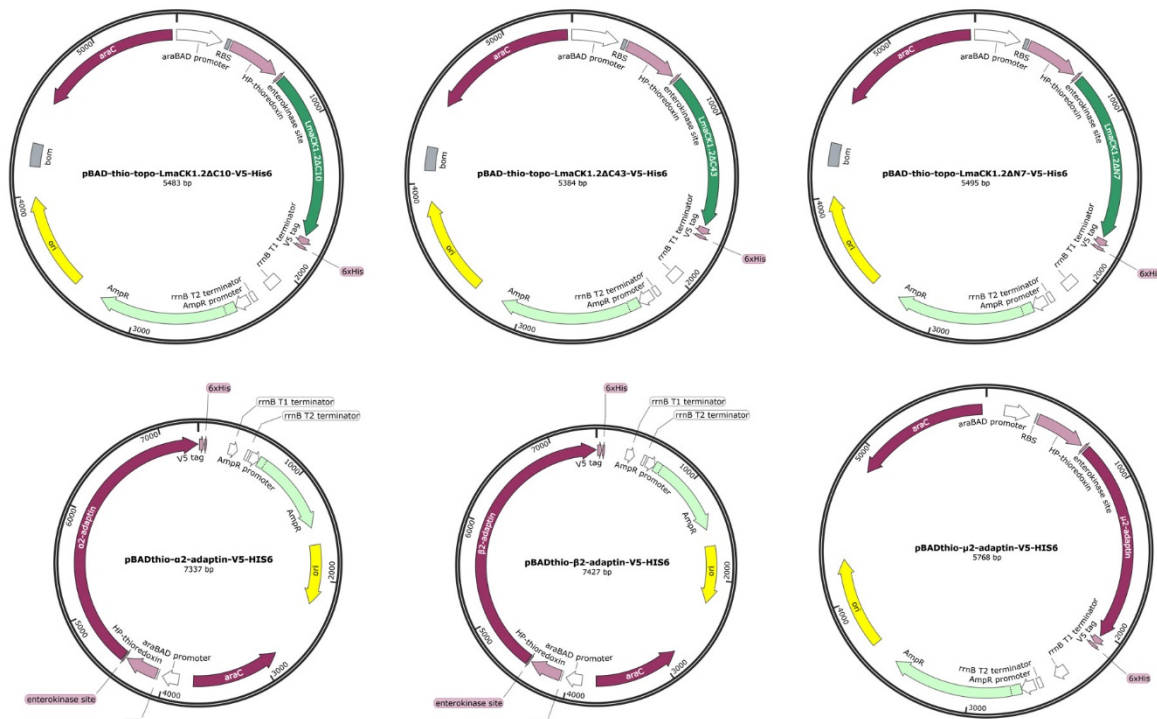


**Fig. 13 – Schematic map of the plasmids for the expression of recombinant proteins.**

The plasmids pBAD-thio-topo-LmaCK1.2ΔC10-V5-His<sub>6</sub>, pBAD-thio-topo-LmaCK1.2ΔC43-V5-His<sub>6</sub> and pBAD-thio-topo-LmaCK1.2ΔN7-V5-His<sub>6</sub> are shown on top (right to left), and pBADthio-α2-adaptin-V5-His<sub>6</sub>, pBADthio-β2-adaptin-V5-His<sub>6</sub> or pBADthio-μ2-adaptin-V5-His<sub>6</sub> plasmids are shown on the bottom.

## 2.4. pPLOT and pT plasmids

The pPLOT and pT plasmids are used for the CRISPR-Cas9 toolkit for gene tagging (pPLOT) or knockout (pT) (Beneke et al., 2017). I used the pPLOTv1 puro-mNeonGreen-puro to tag proteins of interest with mNeonGreen fluorescent protein at the C-terminus, and the plasmids pTPuro\_v1 and pTBlast\_v1 to generate double allele deletion (PuroR and BlastR) mutants (see [Chapter II](#)). For details of the different plasmids, see LeishGEdit website (<http://www.leishgedit.net/>).



## Methods

In this section, only the methods that refers to the sections that are not formatted as articles are provided. Related sections are: [Chapter II section 2 and section 3](#), and [Chapter III](#). For the other results, the corresponding methods are given in the body of the articles. For the [Chapter II section 2 and section 3](#), several methods were identical to ones from the article that starts the chapters I and II, thus they are not provided here.

### 1. Bioinformatics methods

#### 1.1. Gene and protein sequence information

Gene and protein sequences of *Leishmania*, *Trypanosoma* and *Crithidia* were retrieved from the web databases TriTrypDB (<http://tritrypdb.org/tritrypdb/>) along with information about the predicted domains.

#### 1.2. Multiple Sequence Alignments and Phylogenetic Analyses

Multiple amino acid sequence alignments were obtained with MUSCLE (MUltiple Sequence Comparison by Log-Expectation) (<https://www.ebi.ac.uk/Tools/msa/muscle/>) (Madeira et al., 2019). Full size protein sequences were submitted to MUSCLE server version 3.8 under the default parameters. The percentage of identity matrix was generate from the multiple sequence alignment provided by MUSCLE.

#### 1.3. 3D structure prediction

Prediction of 3D structure were obtained with I-TASSER (Iterative Threading ASSEmbly Refinement) server (<https://zhanglab.ccmb.med.umich.edu/I-TASSER/>), with the default parameters (Roy et al., 2010). The server provides a TM-score that corresponds to a metric for measuring the similarity of two protein structures. TM-score measures the global fold similarity and is less sensitive to the local structural variations and magnitude of TM-score for random structure pairs is length-independent. TM-score values ranges from 0 to 1, where 1 indicates a perfect match between two structures.

#### 1.4. Reactome pathways analysis

LmCKAHost identifiers (human orthologs to the mice proteins identified in the experiments) or mammalian CK1 identifiers obtained from BioGRID were submitted to Reactome website (<https://reactome.org/>) (Fabregat et al., 2018), in order to get an over-representation analysis merged to the Reactome pathways. The default settings were used.

#### 1.5. DAVID pathways analysis

LmCKAHost identifiers (human orthologs to the mice proteins identified in the experiments) were submitted to DAVID Functional Annotation Bioinformatics Microarray Analysis website (<https://david.ncifcrf.gov/>), to identify the enriched pathways in the LmCKAHost dataset. The default settings were used.

## 2. Molecular biology methods

### 2.1. Restriction digestion

10 µg DNA was digested with 20 units of restriction enzyme BamHI-HF, supplemented with CutSmart buffer (NEB) in a total volume of 20 µL. The reaction mixtures were incubated at 37°C overnight on a thermomixer (Eppendorf) with shaking at 800 rpm. Digested fragments were analysed by agarose gel electrophoresis and the size was determined by comparison to a DNA ladder (Eurogentec).

### 2.2. DNA ligation

50 ng of vector backbone were mixed with DNA insert at 1:1 molar ratio and added to 1x T4 DNA ligase buffer and 5 units of T4 DNA ligase (Fermentas). The reaction was incubated overnight at 4°C. The ligated products were then transformed into competent bacteria.

### 2.3. Agarose gel electrophoresis and DNA purification

DNA samples (PCR products or digested DNA products) were mixed with 10X BlueJuice Loading buffer (Invitrogen) and separated by agarose gel electrophoresis. A drop of ethidium

bromide solution (Eurobio) was added to 1 % agarose gels in order to allow DNA detection. After visualizing under UV light, gel slices containing the target fragments were excised from the gel and purified using Wizard SV PCR and Gel Clean-up Kit (Promega), according to the manufacturer's instructions.

## 2.4. Transformation of *E. coli*

Competent *E. coli* (50  $\mu$ L) XL10-Gold ultracompetent cells (Stratagene) were transformed with 3  $\mu$ L of ligation product. XL10-Gold bacteria are incubated for 30 min on ice, exposed to heat shock at 42°C for 30 s (XL10-Gold), and then chilled on ice for 5 min. The cells were supplied with 950  $\mu$ L of LB or SOB medium and incubated at 37°C for 1 h on a shaker (250 rpm). After brief spinning (1 000  $\times$  g for 3 min), the cells were plated on LB agar containing 50  $\mu$ g/mL ampicillin and incubated at 37°C overnight. Colonies were inoculated in LB medium with 100  $\mu$ g/mL ampicillin and incubated overnight at 37°C on a shaker with shaking speed at 250 rpm.

## 2.5. Plasmid extraction

- Small-scale plasmid preparation (miniprep)

Single bacterial colonies were transferred from agar plates into 5 mL of LB medium containing 100  $\mu$ g/mL of ampicillin. Bacterial cultures were incubated at 37°C overnight on a shaker (250 rpm). Two mL of culture were harvested by centrifugation at 6 000  $\times$  g for 5 min. The resulting bacterial pellet was subject of the small-scale plasmid preparation using the NucleoSpin Plasmid Kit (Macherey-Nagel) following the manufacturer's instructions. The plasmids were eluted with 30  $\mu$ L of H<sub>2</sub>O (Nuclease-free, Ambion) at room temperature. The concentration of DNA was determined with the Nanodrop system (Thermo Scientific).

- Large-scale plasmid preparation (midiprep)

250 mL of overnight culture of bacteria were centrifuged at 6 000  $\times$  g for 10 min. The plasmid preparation was carried out with the kit NucleoBond Xtra Midi (Macherey-Nagel) according to the supplier's instructions. The DNA was resuspended with 100  $\mu$ L H<sub>2</sub>O (Nuclease-free, Ambion) at room temperature and stored at -20°C. The concentration of DNA was determined with the Nanodrop system (Thermo Scientific).

### 3. Cell biological methods

#### 3.1. Cell cycle arrest with flavopiridol

Logarithmic phase promastigotes were resuspended at  $8 \times 10^6$  in 1 mL of LD1Spro medium, and incubated for 18h at 26°C with either 5  $\mu$ M flavopiridol (in 1 % DMSO final concentration) or 1% DMSO. Arrested parasites were then diluted in DPBS and incubated with 2  $\mu$ g/mL propidium iodide (Sigma-Aldrich). Cells were analyzed with a CytoFLEX flow cytometer (Beckman Coulter, Inc.) to determine the cell concentration, forward scatter area values (FSC-A), the incorporation of propidium iodide (ex $\lambda$  = 488 nm; em $\lambda$  = 617 nm) and monitor mNG intensities (ex $\lambda$  = 506 nm; em $\lambda$  = 517 nm). The parasites strains assayed were: *LdB* pTB007 (parental strain) and *LdB* pTB007 LmCKAP1::mNG::3xMyc (LmCKAP1-mNG).

#### 3.2. Isolation, culture and lysis of bone marrow-derived macrophages

Bone marrow cell suspensions were recovered from tibias and femurs of six-week old female BALB/c ByJRj mice (Janvier Labs, Le Genest-Saint-Isle, France) by flushing with DMEM medium (Gibco, Life technologies) and cultured in medium complemented with mouse recombinant colony stimulating factor 1 (mrCSF-1, ImmunoTools) (de La Llave et al., 2011). One million cells per ml were incubated in bacteriologic petri dish (Corning Life Science) at 37°C in a 7.5% CO<sub>2</sub> atmosphere for 6 days with 75 ng/mL mrCSF-1. After detachment with 25 mM EDTA, macrophages were lysed with RIPA buffer supplemented with anti-protease inhibitors.

### 3.3. Chromatographic conditions for mass spectrometry analysis

The chromatographic conditions for mass spectrometry analysis that allowed the identification of LmCKAHost proteins are described hereafter:

	C18 Precolumn	Loading Buffer	Loading flow	Column	Column Buffer		Gradient		Column Flow	Column Temperature	Mass range
					A	B	%	Time			
<b>IP host Replicate 1</b>	300 µm inner diameter x 5 mm; Dionex	5% MeCN, 0.1% TFA	20 µl/min	nanoViper Acclaim PepMap™ RSLC, 2 µm, 100Å, Thermo Scientific	2% MeCN, 0.1% HCOOH	100% MeCN, 0.085% HCOOH	5 to 30%	100 min	300 nl/min	55°C	400-1500 m/z
<b>IP host Replicate 2</b>	75 µm inner diameter x 2 cm; nanoViper Acclaim PepMap™ 100, Thermo Scientific	2% MeCN, 0.1% HCOOH	2.5 µl/min	nanoViper Acclaim PepMap™ RSLC, 2 µm, 100Å, Thermo Scientific	2% MeCN, 0.1% HCOOH	100% MeCN, 0.085% HCOOH	Multi steps gradient 5 to 30%	151 min	300 nl/min	55°C	400-1500 m/z
<b>IP host Replicate 3</b>	75 µm inner diameter x 2 cm; nanoViper Acclaim PepMap™ 100, Thermo Scientific	2% MeCN, 0.1% HCOOH	2.5 µl/min	nanoViper Acclaim PepMap™ RSLC, 2 µm, 100Å, Thermo Scientific	2% MeCN, 0.1% HCOOH	100% MeCN, 0.085% HCOOH	Multi steps gradient 5 to 30%	152 min	300 nl/min	55°C	400-1500 m/z



# Results

---



# Chapter I

---



## Presentation

In order to gain insights into the cellular functions of LmCK1.2 in the parasite, I first characterised exhaustively the localisation of LmCK1.2 in *L. donovani* promastigotes and axenic amastigotes. The results in this chapter are presented formatted as an article. This article is under submission process.

## Contributions to the work

All experiments shown in this article were performed by me, except those described below for which I provide the contributions:

- *In vitro* kinase assays of LmCK1.2 using HSP70 as substrate were performed by Najma Rachidi using recombinant Hsp70 produced by Katharina Bartsch from the Bernhard Nocht Institute for Tropical Medicine, Hamburg, Germany.
- Generation of pLEXY-CK1.2 $\Delta$ C10-V5-His<sub>6</sub>, pLEXY-CK1.2 $\Delta$ C43-V5-His<sub>6</sub> and pLEXY-CK1.2 $\Delta$ N7-V5-His<sub>6</sub> plasmids, as well as transfection of *LdBob* strain with these plasmids for expression of truncated versions of LmCK1.2, CK1.2 $\Delta$ C10, CK1.2 $\Delta$ C43 and CK1.2 $\Delta$ N7, were performed by Stewart Pine from our laboratory.

# 1. Investigating LmCK1.2 localisation in *Leishmania* parasites - article

## 1.1. Article title, authors and keywords

### Article title:

The low complexity regions in the C-terminus are essential for the subcellular localisation of casein kinase 1 but not for its activity

### Authors:

Daniel MARTEL<sup>1,2</sup>, Stewart PINE<sup>1</sup>, Katharina BARTSCH<sup>3</sup>, Joachim CLOS<sup>3</sup>, Gerald F. SPÄTH<sup>1</sup>, and Najma RACHIDI<sup>1\*</sup>,

<sup>1</sup> Institut Pasteur and INSERM U1201, Unité de Parasitologie moléculaire et Signalisation, Paris, France;

<sup>2</sup> Université Paris Diderot, Sorbonne Paris Cité, Paris, France; <sup>3</sup> Bernhard Nocht Institute for Tropical Medicine, Hamburg, Germany.

**Running Title:** *Casein Kinase I localisation to the nucleolus, the basal body, and the flagellum requires its C-terminus.*

**\*To whom correspondence should be addressed:** Najma Rachidi.

Institut Pasteur and INSERM U1201, Unité de Parasitologie Moléculaire et Signalisation, Paris, France. Tel: +33144389231; Fax: +330145688332; E-mail: [najma.rachidi@pasteur.fr](mailto:najma.rachidi@pasteur.fr)

**Keywords:** Casein kinase I, CK1.2, Localisation, C-terminus, *Leishmania*.

## 1.2. Abstract

Casein Kinase 1 (CK1) family members are serine/threonine protein kinases, ubiquitously expressed in eukaryotic organisms and involved in crucial cellular processes. Defects in CK1 regulation or localisation are associated with important diseases such as cancer or Alzheimer's diseases. CK1 pathways have also been shown to play an important role in infectious diseases through the manipulation of host cell CK1 signalling pathways by intracellular pathogens. Due to its broad spectrum of action, CK1 activity and expression is tightly regulated by a number of mechanisms, including subcellular localisation, which allows the kinase to be brought into close proximity with its substrate. Despite its importance, little is known about the precise cellular localisation of CK1 as most of the knowledge has been obtained indirectly through the study of individual substrates or binding partners of CK1. Here, we present the first exhaustive localisation study of CK1 using the protozoan *Leishmania* as a model. *Leishmania* CK1.2 is an ecto/exokinase released into the mammalian cell to phosphorylate its CK1 substrates. As it performs functions of human CK1s, *Leishmania* CK1.2 is an excellent model to study this kinase family. In this study, we showed that CK1.2 is a ubiquitous kinase, present in the cytoplasm, but also associated to the cytoskeleton as well as to various organelles, such as the basal body, the flagellum, and the mitotic spindle. We uncovered CK1.2 as the first CK1 family member localised to the nucleolus, potentially regulating ribosome processing and chromosome segregation. Using truncated mutants, we demonstrated that the two low complexity regions (LCRs) present at the C-terminus are essential for subcellular localisation of CK1.2 but not for its kinase activity. Furthermore, we showed that the N-terminal domain of CK1.2 is essential to maintain its cellular level. Altogether, our data demonstrate the similarity of localisation between *Leishmania* CK1.2 and human CK1s, highlighting that *Leishmania* CK1.2 has evolved to mimic mammalian CK1s and uncover the importance of LCRs in the localisation of CK1 family members.

### 1.3. Introduction

Casein Kinase 1 (CK1) family members are serine/threonine protein kinases that are ubiquitously expressed in eukaryotic organisms [1]. They are involved in a variety of important cellular processes, such as cell cycle progression, cytokinesis, membrane trafficking, circadian rhythm, DNA repair and vesicular transport in organisms from yeast to humans [1]. Due to its broad spectrum of action, CK1 activity and expression is tightly regulated by a number of mechanisms, including inhibitory autophosphorylation, phosphorylation by other kinases, interactions with various cellular structures or proteins, and subcellular sequestration [1]. The correct subcellular localisation of CK1 allows the kinase to be brought into close proximity with its substrates [2]. Defects in CK1 regulation, localisation or the introduction of mutations in the CK1 coding sequence are often associated with important diseases such as cancer, Alzheimer's and Parkinson's diseases as well as sleeping disorders [2] [3] [4]. There is also increasing evidence suggesting that CK1 plays a role in infectious diseases. Manipulation of host cell CK1 signalling pathways by intracellular pathogens, either by exporting the CK1 of the pathogen into the host cell (*Plasmodium* and *Leishmania*) or by exploiting the host CK1 (*Mycobacteria* and viruses) have been reported [5] [6] [7] [8] [9]. These data suggest that CK1 is an important protein kinase, however two areas remained understudied: its precise localisation and its functions in non-conventional eukaryotes such as *Leishmania* or *Plasmodium* parasites.

Most of the knowledge available on CK1 localisation has been obtained indirectly through the study of individual substrates or binding partners of CK1 but not through the exhaustive study of CK1 localisation. Consistent with its various roles, CK1 is associated with many sub-cellular structures. In mammalian cells, CK1 $\delta$  has been detected at the centrosomes and the *trans*-Golgi network, performing an important role as a mediator of ciliogenesis and being required for Wnt3a-dependent neurite outgrowth [10] [11]. The interaction of huCK1 $\delta$  and ScHrr25/CK1 $\delta$ ,

its yeast ortholog with A-kinase anchor protein 450 and  $\gamma$ -tubulin complex is required to address the kinase to the centrosome [12, 13]. CK1 $\delta$  as well as CK1 $\alpha$  also interact with membrane structures of the endoplasmic reticulum, the Golgi and various transport vesicles [14] [10] [15] [13]. Moreover, in budding yeast, ScHrr25/CK1 $\delta$  is localised to the bud neck, where it is essential for proper cytokinesis, and to endocytic sites, where it is required for their initiation and stabilisation [16] [17] [18]. Lastly, Zhang *et al.* have shown that ScHrr25/CK1 $\delta$  is recruited to cytoplasmic processing bodies (P-bodies), which protects the active kinase from the cytoplasmic degradation machinery during stress [19]. These few examples show how strongly CK1 localisation is associated with its functions, suggesting that investigating further its localisation may increase our knowledge on this kinase and allow the identification of novel functions.

*Leishmania*, as the causing agent of *Leishmaniasis*, represents an excellent model to study the localisation and thus get new insights into the roles of CK1. This parasite has two developmental stages, an extracellular promastigote stage in the insect vector, and an intracellular amastigote stage in the mammalian host that resides inside the phagolysosomes of macrophages. In *Leishmania*, there are six members of the CK1 family and little is known about their localisations or functions. LCK1.4, which unlike the other *Leishmania* CK1s contains a putative secretion signal, seems to be secreted by the parasites. This kinase is mainly localised in the cytoplasm and seems to be excluded from the nucleus [20]. Surprisingly, the localisation of CK1.2, the most abundant member of the CK1 family in *Leishmania* has not been studied despite its importance. Indeed, CK1.2 is the *Leishmania* kinase most closely related to its human orthologs and is essential for parasite survival in mammalian cells [6]. Moreover, *Leishmania* CK1.2, an ecto/exokinase released in the host cell as free protein or via exosomes has been shown to phosphorylate host proteins [21]. CK1.2, similarly to human CK1 $\alpha$  has been shown to phosphorylate IFNAR1 (a receptor for alpha/beta interferon), leading to its

degradation and the attenuation of the cellular responses to IFN- $\alpha$  [22]. These data suggest that *Leishmania* CK1.2 phosphorylates host proteins to subvert macrophages and favours parasite survival, making this kinase an excellent model to study CK1.

In this study, we showed that CK1.2 is a ubiquitous kinase, present in the cytoplasm, but also associated to the cytoskeleton as well as to various organelles, such as the basal body, the flagellum, or the mitotic spindle. For the first time, we showed that a CK1 family member is localised to the nucleolus. Using truncated mutants, we showed for the first time that the two low complexity regions (LCR) present in the C-terminus were essential for the sub-cellular localisation of CK1.2 but not for its kinase activity. Furthermore, we showed that the deletion of the N-terminus leads to a dramatic decrease of CK1.2 abundance.

## 1.4. Materials and Methods

### 1.4.1. Contact for reagent and resource sharing

Further information and requests for resources and reagents should be directed to and will be fulfilled by the Lead Contact, Najma Rachidi ([najma.rachidi@pasteur.fr](mailto:najma.rachidi@pasteur.fr)).

### 1.4.2. Experimental model and subject details

- *Leishmania* cell lines

All the parasite cell lines used in this study were derived from *L. donovani* axenic 1S2D (MHOM/SD/62/1S-CL2D) clone LdBob, obtained from Steve Beverley, Washington University School of Medicine, St. Louis, MO. Promastigotes were cultured and differentiated into axenic amastigotes as described previously [23]. Parasites cell lines were grown in media with 30 µg/mL hygromycin B (ThermoFisher Scientific Cat# 10687010) to maintain the pLEXSY-CK1.2-V5 or the empty pLEXSY plasmids.

The transgenic *L. donovani* cell lines containing either the pLEXSY or pLEXSY-CK1.2-V5-HIS<sub>6</sub> (pLEXSY-CK1.2-V5) vectors, corresponding to the mock or expressing *Leishmania major* CK1.2 tagged with V5 and HIS<sub>6</sub>, respectively, have been described previously [24].

- Plasmids

For the generation of CK1.2ΔC10-V5-His<sub>6</sub>-, CK1.2ΔC43-V5-His<sub>6</sub>- and CK1.2ΔN7-V5-His<sub>6</sub>- expressing cell lines, we first amplified the V5-His<sub>6</sub> fragment from pBAD-thio-topo-CK1.2 [24] using the following primers: 5'-gatggcattctagaatcgatgatatccccggggtaagcctatcc-3' and 5'-gcatggatcgcggccgctcaatggtg-3'. Then we digested the PCR fragment with XbaI and NotI and cloned it into the pLEXSY-Hyg plasmid (Jena bioscience) digested with the same enzymes to obtain pLEXSY-V5-His<sub>6</sub> plasmid. Next, we amplified CK1.2ΔC10, CK1.2ΔC43 and CK1.2ΔN7 from pLEXSY-CK1.2 [24] with the following primers for CK1.2ΔC10: 5'-

gatggcatcggatccatgaacgttgagctgcgtgt-3' and 5'-gcatggatctctagagtttgcgctgttcggagc-3'; for CK1.2ΔC43: 5'-gatggcatcggatccatgaacgttgagctgcgtgt-3' and 5'-gcatggatctctagagctttgctgttcctgcag-3'; for CK1.2ΔN7: 5'-gatggcatcggatccatgggtaatcgctatcgattgg-3', 5'-gcatggatctctagattgttgcggtgcgccg-3'. We digested the PCR fragments with BglIII and XbaI and cloned them into the pLEXSY-V5-His<sub>6</sub> digested with the same enzymes to obtain respectively pLEXSY-CK1.2ΔC10-V5-His<sub>6</sub>, pLEXSY-CK1.2ΔC43-V5-His<sub>6</sub> and pLEXSY-CK1.2ΔN7-V5-His<sub>6</sub>. Finally, these vectors were transfected in LdBob.

We generated *E.coli* strains containing pBAD-thio-topo-LmaCK1.2ΔC10-V5-His<sub>6</sub>, pBAD-thio-topo-LmaCK1.2ΔC43-V5-His<sub>6</sub> or pBAD-thio-topo-LmaCK1.2ΔN7-V5-His<sub>6</sub> by amplifying the whole pBAD-thio-topo-LmaCK1.2-V5-His<sub>6</sub> except the last 30 bp, the last 129 bp or the first 18bp, respectively, using the following primers for CK1.2ΔC10: His<sub>6</sub> 5'-AAGGGCGAGCTTGAAGGTAAG-3' and 5'-GTTTGCGCTGTTCCGAGCG-3'; for CK1.2ΔC43: 5'-AAGGGCGAGCTTGAAGGTAAG-3' and 5'-GAAGCTTTGCTGTTCTGC-3'; and for CK1.2ΔN7: 5'-GGTAATCGCTATCGTATTGGTC-3' and 5'-CATAAGGGCGAGCTTGTCATC-3'. The linear PCR products were circularised by ligation with T4 DNA ligase (Promega Cat#M180A) (O/N, 4°C). Finally the plasmids pBADthio-LmaCK1.2ΔC10-V5-His<sub>6</sub>, pBADthio-LmaCK1.2ΔC43-V5-His<sub>6</sub> and pBADthio-LmaCK1.2ΔN7-V5-His<sub>6</sub> were transformed in *Escherichia coli* Rosetta (DE3) pLysS Competent Cells (Merck Cat# 70956) for bacterial expression.

### 1.4.3. Methods details

- Immunofluorescence

Logarithmic phase promastigotes or axenic amastigotes (48h after shift at 37°C and pH5.5) were resuspended at  $2 \times 10^6$  parasites per mL in Dulbecco's Phosphate Buffer Saline (DPBS)

(Gibco) and 500  $\mu\text{L}$  were added to poly-L-lysine-coated coverslips placed in a 24-well plate. Plates were centrifuged 10 min at 1200 g at room temperature to settle parasites onto the coverslips. For fixation alone, cells were washed three times with DPBS and fixed in 4% paraformaldehyde (PFA) in DPBS for 15 min at room temperature. For cytoskeleton preparation, the protocol was adapted from [25]. Briefly, cells were washed three times with DPBS, treated with 0.125% Nonidet 40 (Fluka BioChemika Cat# 74385) in PIPES buffer (100 mM piperazine-N,N-bis(2-ethanesulfonic acid) (PIPES) pH6.8, 1 mM  $\text{MgCl}_2$ ) for 2 minutes at room temperature and washed twice for 5 minutes in PIPES buffer. Cells were fixed in 4% PFA in DPBS for 15 min at room temperature. After PFA fixation, cells were washed three times in DPBS, neutralised 10 min with  $\text{NH}_4\text{Cl}$  (50 mM in DPBS), and washed again three times in DPBS. For the immuno-labelling of PFA-fixed cells or cytoskeleton preparations, the samples were blocked with 10% filtered heat-inactivated fetal calf serum (FCS) containing  $0.5 \text{ mg}\cdot\text{mL}^{-1}$  saponin in DPBS for 30 min at room temperature and then washed for 5 min in DPBS. The cells were then incubated with primary antibodies diluted in DPBS with 0.5% Bovine Serum Albumin (BSA) and  $0.5 \text{ mg}\cdot\text{mL}^{-1}$  saponin for 1h at room temperature. Three washes of 10 min were performed and the secondary antibody diluted in DPBS with 0.5% BSA and  $0.5 \text{ mg}\cdot\text{mL}^{-1}$  saponin was added. After one hour incubation at room temperature in the dark, cells were washed twice for 10 min in DPBS with 0.5% BSA and  $0.5 \text{ mg}\cdot\text{mL}^{-1}$  saponin, and then twice in DPBS. Parasites were incubated with  $5 \mu\text{g}\cdot\text{mL}^{-1}$  Hoechst 33342 in DPBS for 8 min in the dark, washed twice with DPBS, one time with distilled water, air-dried, then mounted with slides using SlowFade Gold Antifade Mountant (ThermoFisher Scientific Cat# S36937). For methanol fixation, logarithmic phase promastigotes were washed twice in DPBS and resuspended at  $2 \times 10^7$  parasites per mL.  $10^6$  parasites were spread onto poly-L-lysine coated slides, and allowed to settle for 30 min in a humid chamber. Parasites were then fixed in methanol at  $-20^\circ\text{C}$  for 3 minutes and rehydrated for 10 min in DPBS at room temperature. For

immuno-labelling of methanol-fixed parasites, samples were blocked with 10% filtered heat-inactivated FCS in DPBS for 15 min at room temperature and washed for 5 min in DPBS. Then the cells were treated similarly as those fixed by PFA.

The antibodies used were: mouse IgG2a anti-V5 tag monoclonal antibody (Thermo Fisher Scientific Cat# R960-25, RRID:AB\_2556564) diluted at 1/200 (in PFA and methanol fixed parasites) or at 1/300 (in cytoskeleton preparations); rabbit anti-V5 tag polyclonal antibody (Abcam Cat# ab9116, RRID:AB\_307024) diluted at 1/400; rabbit anti-LdCentrin polyclonal antibody (kind gift from Hira L. Nakhasi) diluted at 1/2000 [26]; mouse IgG1 anti-IFT172 monoclonal antibody diluted at 1/200 [27]; mouse anti-PFR2 L8C4 clone antibody diluted at 1/10 [28]; mouse L1C6 anti-TbNucleolus monoclonal antibody diluted at 1/100 (kind gift from Keith Gull [29]); mouse IgG1 anti- $\alpha$ -tubulin monoclonal DM1A antibody (Sigma-Aldrich Cat# T9026, RRID:AB\_477593) diluted at 1/400; chicken anti-Hsp70 and chicken anti-Hsp90 antibodies diluted at 1/200 [30]. IgG subclass-specific secondary antibodies coupled to different fluorochromes were used for double labelling: anti-mouse IgG (H+L) coupled to AlexaFluor488 (1/200 (PFA- or methanol-fixed parasites)) or 1/300 (cytoskeleton preparations), Thermo Fisher Scientific Cat# A-21202, RRID:AB\_141607); anti-mouse IgG2a coupled to Cy3 (1/600; Jackson ImmunoResearch Labs Cat# 115-165-206, RRID:AB\_2338695); anti-mouse IgG1 coupled to AlexaFluor647 (1/600; Thermo Fisher Scientific Cat# A-21240, RRID:AB\_2535809); anti-rabbit IgG (H+L) coupled to AlexaFluor488 (1/400; Thermo Fisher Scientific Cat# A-21206, RRID:AB\_2535792); anti-mouse IgG (H+L) coupled to AlexaFluor594 (1/200; Thermo Fisher Scientific Cat# A-21203, RRID:AB\_2535789); anti-mouse IgG2a coupled to AlexaFluor488 (1/300; Thermo Fisher Scientific Cat# A-21131, RRID:AB\_2535771); anti-mouse IgG1 coupled to AlexaFluor594 (1/300; Thermo Fisher Scientific Cat# A-21125, RRID:AB\_2535767); anti-chicken IgY coupled to AlexaFluor594 (1/200; Jackson ImmunoResearch Labs Cat# 703-586-155,

RRID:AB\_2340378) and anti-rabbit IgG (H+L) coupled to AlexaFluor594 (1/400; Thermo Fisher Scientific Cat# A-21207, RRID:AB\_141637).

- Confocal microscopy

Images were visualised using a Leica SP5 HyD resonant scanner Matrix screener inverted microscope equipped with a HCX PL APO CS 63x, 1.4 NA oil objective (Leica, Wetzlar, Germany). Triple or quadruple immunofluorescence was imaged with Leica Application Suite AF software (LAS AF; Leica Application Suite X, RRID:SCR\_013673) after excitation of the Hoechst 33342 dye with a diode at a wavelength of 405 nm (452/75 Emission Filter), excitation of the AlexaFluor488 with an argon laser at a wavelength of 488 nm (525/50 Emission Filter), excitation of AlexaFluor594 with a diode DPSS at a wavelength of 561 nm (634/77 Emission Filter), excitation of Cy3 with a diode DPSS at a wavelength of 561 nm (595/49 Emission Filter), and excitation of AlexaFluor647 with a helium-neon laser at a wavelength of 633 nm (706/107 Emission Filter). Images were scanned sequentially to minimise cross excitation between channels and each line was scanned twice and averaged to increase the signal-to-noise ratio. The pinhole aperture was set to 1 airy. Images were acquired with 8x zoom at a resolution of 1024×1024. Z-stacks were acquired at 0.082  $\mu\text{m}$  intervals, deconvolved and rendered using either Fiji (RRID:SCR\_002285) or Icy (RRID:SCR\_010587) software [31] (<http://icy.bioimageanalysis.org/>).

- Deconvolution of z-stacks and chromatic aberration correction

All confocal images were processed and analysed by using the Huygens Professional software version 19.04 (Scientific Volume Imaging, Huygens Software, RRID:SCR\_014237). Deconvolution of confocal z-stacks was optimised using the following settings: automatic estimation of the average background with the mode “Lowest” and area radius = 0.7, deconvolution algorithm CMLE, maximum number of iterations = 40, signal to noise ratio

(SNR) = 20, quality change threshold = 0.05, iteration mode = optimised, brick layout = automatic. Theoretical point spread function (PSF) values were estimated for each z-stack.

All deconvolved images were corrected for chromatic shifts and for rotational differences between different channels using the Chromatic Aberration Corrector (CAC) from Huygens Professional software (Scientific Volume Imaging, Huygens Software, RRID:SCR\_014237). To calibrate the image corrections, multifluorescent 0.2  $\mu\text{m}$  TetraSpeck microspheres (ThermoFisher Scientific Cat#T7280) mounted on SlowFade Gold Antifade mountant (ThermoFisher Scientific Cat# S36937) were imaged with identical acquisition parameters. Images were deconvolved similarly, and were used to perform the chromatic aberration estimations with the cross correlation method in CAC software. Corrections were saved as templates and applied for correction of the similarly acquired and deconvolved images in CAC.

- Co-localisation analysis of confocal images

Co-localisation analysis was performed with the Co-localisation Analyzer plug-in of the Huygens Professional software (Scientific Volume Imaging, Huygens Software, RRID:SCR\_014237, v19.04). Processed cross-section images (deconvolved and corrected for chromatic aberrations) of the parasites were opened with this plug-in and Pearson coefficients were calculated for each parasite. Specific areas of the parasite were cropped from the whole image (basal body area, flagella pocket area, mitotic spindle and reduced mitotic spindle areas, flagellar pocket neck area and flagellar tip area) and Pearson coefficients were calculated for these images.

Pearson coefficients of the co-localisation in the basal body and flagellar pocket areas of (i) CK1.2-V5 with Centrin (CEN), IFT172, and DNA (Hoechst 33342, H); or (ii) CEN with IFT172, from 14 images were plotted in scattered dot plots with the mean and standard deviation using GraphPad Prism 8.1.1 (GraphPad Software, GraphPad Prism, RRID:SCR\_002798). Pearson coefficients of the co-localisation of CK1.2-V5 with tubulin in

the mitotic spindle and reduced mitotic spindle areas from seven images were plotted similarly. Pearson coefficients of the co-localisation of CK1.2-V5 with Hsp90 from seven images and with Hsp70 from ten images were also plotted similarly.

- Epifluorescence microscopy and automated parasite detection

Images were visualised using a Zeiss upright widefield microscope equipped with Apotome2 grids and a Pln-Apo 63x, 1.4 NA oil objective (Zeiss). Light source used was a Mercury Lamp HXP 120, and following filters were used: DAPI (Excitation G365; dichroic FT 395; emission BP 420-470), FITC-A488-GFP (Excitation BP 455-495; dichroic FT 500; emission BP 505-555) and A594-TexasRed-mCherry-HcRed-mRFP (Excitation BP 542-582; dichroic FT 593; emission BP 604-644). Images were captured on an Axiocam MRm camera using ZEN Blue software. For comparison of different cell lines, identical parameters of acquisition were applied on all samples.

For the analysis of the fluorescence intensity in the parasite body of different cell lines (mock, WT and domain-deleted mutants), we used the graphical programming plugin Protocols in Icy software (Icy, RRID:SCR\_010587 [32]). A screenshot of the protocol that was applied on the epifluorescence images is shown in Figure S6. Briefly, maximum intensity projection in Z was generated in all channels. Nuclei were segmented with HK-Means plugin (in the nucleus specific channel [33]), and the regions of interest (ROI) generated were used as input for automatically segment the boundary of the parasite body stained with V5 antibody (in all the cell lines) with Active Contours plugin [34]. The recovered ROIs were verified and corrected manually if needed. Properties of the ROI (e.g. sum fluorescence intensity, roundness, and interior) were obtained and used for analysis. Dot plots were generated with GraphPad Prism 8.1.1 (GraphPad Software, GraphPad Prism, RRID:SCR\_002798).

- Protein extraction, SDS-PAGE and Western blot analysis

Logarithmic phase promastigotes were washed in DPBS and protein extraction was performed as described previously [35]. Ten micrograms of total protein were denatured, separated by SDS-PAGE, and transferred onto polyvinylidene difluoride (PVDF) membranes (Pierce). Membranes were blocked with 5% BSA in DPBS supplemented with 0.25% Tween20 (PBST) and incubated over night at 4°C with primary antibody mouse IgG2a anti-V5 tag monoclonal antibody (1/1000; Thermo Fisher Scientific Cat# R960-25, RRID:AB\_2556564) in 2,5% BSA in PBST. Membranes were then washed in PBST and incubated with secondary antibody anti-mouse IgG (H+L) coupled to horseradish peroxidase (1/20000; ThermoFisher Scientific Cat# 32230, RRID:AB\_1965958). Proteins were revealed by SuperSignal™ West Pico Chemiluminescent Substrate (ThermoFisher Scientific Cat# 34580) using the PXi image analysis system (Syngene) at various exposure times. Membranes were then stained with Bio-Safe Coomassie (Bio-Rad Cat #1610786) to serve as loading controls.

- Proteasome and lysosome inhibition assays

Logarithmic phase promastigotes expressing CK1.2-V5-His<sub>6</sub>, CK1.2ΔC10-V5-His<sub>6</sub>, CK1.2ΔC43-V5-His<sub>6</sub>, CK1.2ΔN7-V5-His<sub>6</sub> or mock control (pLEXSY empty plasmid) were resuspended into fresh M199-supplemented promastigote medium at  $5 \times 10^6$  parasites per mL with or without either 10 μM MG132 (Sigma-Aldrich Cat# M7449) or 20 mM NH<sub>4</sub>Cl (VWR Chemicals Cat# 21235.297). Drug selection was maintained with 30 μg hygromycin B (Invitrogen). Parasites were grown for 24h at 26°C and were then lysed for protein extraction as described before. Western blot analysis of ten micrograms of total protein was performed as described before.

Ten micrograms of total proteins treated with or without MG132 were also subjected to Western blot analysis to detect ubiquitinated proteins. Membrane was blocked with 5% BSA in DPBS supplemented with 0.25% Tween20 (PBST) and incubated over night at 4°C with primary

mouse mono- and polyubiquitinated conjugates FK2 monoclonal antibody (1/500; Enzo Life Sciences Cat# BML-PW8810, RRID:AB\_10541840) in 2,5% BSA in PBST. Following washing in PBST, the membrane was incubated with secondary antibody anti-mouse IgG (H+L) coupled to horseradish peroxidase (1/20000; ThermoFisher Scientific Cat# 32230, RRID:AB\_1965958). The immunoblot was revealed with SuperSignal™ West Pico PLUS Chemiluminescent Substrate (ThermoFisher Scientific Cat# 34580) using the PXi image analysis system (Syngene) with 5 min exposure time. The membrane was then stained with Bio-Safe Coomassie G-250 stain (Bio-Rad Cat #1610786) to serve as loading control.

To validate lysosomal inhibition by NH<sub>4</sub>Cl treatment, parasites were sampled prior cell lysis and stained to access lysosomal pH. Treated or untreated parasites were incubated with 100 mM LysoTracker™ Red DND-99 (ThermoFisher Scientific Cat# L7528) in culture medium for 30 min at 26°C and analysed with a CytoFLEX flow cytometer (Beckman Coulter, Inc.) to test for acidic pH of lysosomes upon treatment (exλ = 577 nm; emλ = 590 nm). LysoTracker fluorescence intensity was measured for 15000 parasites using CytExpert software (CytExpert Software, RRID:SCR\_017217, Beckman Coulter, v2.2.0.97). Graphs representing mean LysoTracker fluorescence intensity were generated with GraphPad Prism 8.1.1 (GraphPad Software, GraphPad Prism, RRID:SCR\_002798).

- Recombinant expression, purification of CK1.2-V5-His<sub>6</sub>, CK1.2ΔC10-V5-His<sub>6</sub>, CK1.2ΔC43-V5-His<sub>6</sub> and CK1.2ΔN7-V5-His<sub>6</sub> and protein kinase assay

*Escherichia coli* Rosetta (DE3) pLysS Competent Cells (Merck Cat# 70956) containing pBAD-thio-topo-LmaCK1.2-V5-His<sub>6</sub>, pBAD-thio-topo-LmaCK1.2ΔC10-V5-His<sub>6</sub>, pBAD-thio-topo-LmaCK1.2ΔC43-V5-His<sub>6</sub> or pBAD-thio-topo-LmaCK1.2ΔN7-V5-His<sub>6</sub> were grown at 37°C and induced with arabinose (0,02% final) for 4h at room temperature [6]. Cells were harvested by centrifugation at 10,000 g for 10 min at 4°C and the recombinant proteins were purified as

described previously [6] [36]. The eluates were supplemented with 15% glycerol and stored at  $-80^{\circ}\text{C}$ . The kinase assays were performed as described previously [6] [36].

#### 1.4.4. Quantification and statistical analysis

Statistical analyses were performed with GraphPad Prism 8.1.1 (GraphPad Software, GraphPad Prism, RRID:SCR\_002798) using unpaired t test (parametric test). Graphs were drawn using the same software. All errors correspond to the 95% confidence interval. Statistically significant differences are indicated with three ( $p<0.01$ ), four ( $p<0.001$ ) or five asterisks ( $p<0.0001$ ). The number of samples analysed for each experiment is indicated in figure legends.

## 1.4.5. Key resources table

REAGENT or RESOURCE	SOURCE	IDENTIFIER
Antibodies		
Anti-V5 tag IgG2a mouse monoclonal	Thermo Fisher Scientific	Cat# R960-25, RRID:AB_2556564
Anti-Centrin from <i>L. donovani</i> rabbit polyclonal	[26]	N/A
Anti-IFT172 from <i>T. brucei</i> IgG1 mouse monoclonal	[27]	N/A
Anti-V5 tag IgG rabbit polyclonal	Abcam	Cat# ab9116, RRID:AB_307024
Anti-PFR2 from <i>T. brucei</i> mouse polyclonal (L8C4)	[28]	N/A
Anti-nucleolus IgG from <i>T. brucei</i> mouse monoclonal (L1C6)	Keith Gull, University of Oxford, UK	N/A
Anti-alpha-tubulin IgG1 mouse monoclonal DM1A	Sigma-Aldrich	Cat# T9026, RRID:AB_477593
Anti-Hsp90 from <i>L. donovani</i> IgY chicken polyclonal	[30]	N/A
Anti-Hsp70 from <i>L. donovani</i> IgY chicken polyclonal	[30]	N/A
Anti-mono- and polyubiquitinated conjugates mouse monoclonal (FK2)	Enzo Life Sciences	Cat# BML-PW8810, RRID:AB_10541840
Anti-mouse IgG (H+L) coupled to AlexaFluor488	Thermo Fisher Scientific	Cat# A-21202, RRID:AB_141607
Anti-mouse IgG2a coupled to Cy3	Jackson ImmunoResearch Labs	Cat# 115-165-206, RRID:AB_2338695
Anti-mouse IgG1 coupled to AlexaFluor647	Thermo Fisher Scientific	Cat# A-21240, RRID:AB_2535809
Anti-rabbit IgG (H+L) coupled to AlexaFluor488	Thermo Fisher Scientific	Cat# A-21206, RRID:AB_2535792
Anti-mouse IgG (H+L) coupled to AlexaFluor594	Thermo Fisher Scientific	Cat# A-21203, RRID:AB_2535789

Anti-mouse IgG2a coupled to AlexaFluor488	Thermo Fisher Scientific	Cat# A-21131, RRID:AB_2535771
Anti-mouse IgG1 coupled to AlexaFluor594	Thermo Fisher Scientific	Cat# A-21125, RRID:AB_2535767
Anti-chicken IgY coupled to AlexaFluor594	Jackson ImmunoResearch Labs	Cat# 703-586-155, RRID:AB_2340378
Anti-rabbit IgG (H+L) coupled to AlexaFluor594	Thermo Fisher Scientific	Cat# A-21207, RRID:AB_141637
Anti-mouse IgG (H+L) coupled to horseradish peroxidase	Thermo Fisher Scientific	Cat# 32230, RRID:AB_1965958
<b>Bacterial Strains</b>		
<i>Escherichia coli</i> Rosetta (DE3) pLysS Competent Cells	Merck	Cat# 70956
<b>Experimental Models: Organisms/Cell lines</b>		
<i>LdBob</i> cells with pLEXSY vector (mock)	[6]	N/A
<i>LdBob</i> cells with pLEXSY-CK1.2-V5-His <sub>6</sub> vector, expressing <i>LmaCK1.2-V5-His<sub>6</sub></i>	[6]	N/A
<i>LdBob</i> cells with pLEXSY-CK1.2ΔC10-V5-His <sub>6</sub> vector, expressing <i>LmaCK1.2ΔC10-V5-His<sub>6</sub></i>	This study	N/A
<i>LdBob</i> cells with pLEXSY-CK1.2ΔC43-V5-His <sub>6</sub> vector, expressing <i>LmaCK1.2ΔC43-V5-His<sub>6</sub></i>	This study	N/A
<i>LdBob</i> cells with pLEXSY-CK1.2ΔN7-V5-His <sub>6</sub> vector, expressing <i>LmaCK1.2ΔN7-V5-His<sub>6</sub></i>	This study	N/A
<b>Chemicals, Peptides, and Recombinant Proteins</b>		
Nonidet P40 (NP40)	Fluka BioChemika	Cat# 74385
Ammonium Chloride (NH <sub>4</sub> Cl)	VWR Chemicals	Cat# 21235.297
Carbobenzoxy-Leu-Leuleucinal (MG132)	Sigma-Aldrich	Cat# M7449
SlowFade Gold Anti-Fade	ThermoFisher Scientific	Cat# S36937
Recombinant thio- <i>LmaCK1.2-V5-His<sub>6</sub></i>	This study, (5)	N/A

Recombinant thio- <i>Lma</i> CK1.2ΔC10-V5-His <sub>6</sub>	This study	N/A
Recombinant thio- <i>Lma</i> CK1.2ΔC43-V5-His <sub>6</sub>	This study	N/A
Recombinant thio- <i>Lma</i> CK1.2ΔN7-V5-His <sub>6</sub>	This study	N/A
Recombinant MBP	Sigma-Aldrich	Cat# M1891
Oligonucleotides		
Primer: pBADthio- <i>Lma</i> CK1.2ΔC10-V5-His <sub>6</sub> and pBADthio- <i>Lma</i> CK1.2ΔC43-V5-His <sub>6</sub> forward: AAGGGCGAGCTTGAAGGTAAG	This study	N/A
Primer: pBADthio- <i>Lma</i> CK1.2ΔC10-V5-His <sub>6</sub> reverse: GTTTGCGCTGTTCCGAGCG	This study	N/A
Primer: pBADthio- <i>Lma</i> CK1.2ΔC43-V5-His <sub>6</sub> reverse: GAAGCTTTGCTGTTCCCTGC	This study	N/A
Primer: pBADthio- <i>Lma</i> CK1.2ΔN7-V5-His <sub>6</sub> forward: GGTAATCGCTATCGTATTGGTC	This study	N/A
Primer: pBADthio- <i>Lma</i> CK1.2ΔN7-V5-His <sub>6</sub> reverse: CATAAGGGCGAGCTTGTCATC	This study	N/A
Recombinant DNA		
Plasmid: pLEXY-hyg2 (HygR)	Jena Bioscience	Cat# EGE-232
Plasmid: pLEXY-CK1.2-V5-His <sub>6</sub> (HygR)	(5)	N/A
Plasmid: pLEXY-CK1.2ΔC10-V5-His <sub>6</sub> (HygR)	This study	N/A
Plasmid: pLEXY-CK1.2ΔC43-V5-His <sub>6</sub> (HygR)	This study	N/A
Plasmid: pLEXY-CK1.2ΔN7-V5-His <sub>6</sub> (HygR)	This study	N/A
Plasmid: pBADthio- <i>Lma</i> CK1.2-V5-His <sub>6</sub>	This study,	N/A

Plasmid: pBADthio- <i>Lma</i> CK1.2ΔC10-V5-His <sub>6</sub>	This study	N/A
Plasmid: pBADthio- <i>Lma</i> CK1.2ΔC43-V5-His <sub>6</sub>	This study	N/A
Plasmid: pBADthio- <i>Lma</i> CK1.2ΔN7-V5-His <sub>6</sub>	This study	N/A
Software and Algorithms		
Icy	Icy	RRID:SCR_010587
GraphPad Prism	GraphPad	RRID:SCR_002798
CytExpert Software	Beckman Coulter	RRID:SCR_017217, v2.2.0.97
Fiji	Fiji	RRID:SCR_002285
Huygens Professional	Scientific Volume Imaging	RRID:SCR_014237
Leica Application Suite AF (LAS AF)	Leica	RRID:SCR_013673

## 1.5. Results

### 1.5.1. *Leishmania* CK1.2 localisation is ubiquitous

We investigated *Leishmania donovani* CK1.2 localisation in promastigotes using parasites expressing an episomal copy of CK1.2 tagged with V5-His<sub>6</sub> at the C-terminus (CK1.2-V5) [6]. This cell line has been validated in a previous study where we showed that CK1.2-V5 is active, and functional as it can compensate for a decrease of endogenous CK1.2 activity [6]. These findings suggest that CK1.2-V5 is properly folded and thus localises similarly to the endogenous CK1.2. We first performed immunofluorescence assays on parasites fixed with paraformaldehyde (PFA) and revealed CK1.2-V5 localisation by confocal microscopy using an anti-V5 antibody. As shown in Fig. 1A, we detected intense punctate staining in the cytoplasm, in the nucleus and in the flagellum, specific to CK1.2-V5 as the control parasites expressing the empty plasmid only showed weak background fluorescence (Fig. 1B). We compared the sum of the fluorescence intensity in the cell body for each CK1.2-V5 expressing parasite to that of the control and confirmed that it was significantly higher for the cell line expressing CK1.2-V5 ( $1\,712\,899 \pm 85\,178$ , n=256) than for the control ( $893\,556 \pm 16\,256$ , n=154) (Fig. 1C). This punctated pattern is similar to the cytoplasmic localisation of CK1 in human cells [37].

To determine whether we could uncover specific localisations masked by the cytoplasmic staining, we first treated *LdBob* parasites with methanol for different lengths of time in order to gradually permeabilise the parasite and lose part of the cytosolic material. As shown Fig. S1, after 3 minutes of methanol treatment, CK1.2-V5 could be detected primarily in organelles such as the flagellar pocket or the basal body, and less in the cytoplasm. To characterise those additional localisations, we performed a detergent treatment in order to release loosely attached cytoplasmic components and maintain cytoskeleton-bound proteins. To this end, *LdBob* promastigotes were treated with 0,125% NP-40 prior to PFA fixation and staining. We detected

a signal (i) adjacent to the kinetoplast, which could correspond to the basal body (Fig. 1D, CK1.2-V5); (ii) in the flagellar pocket region and along the flagellum; (iii) in the Hoechst-unstained region of the nucleus that corresponds to the nucleolus; and (iv) in the cytoplasm as punctated structures (Fig. 1D, CK1.2-V5). To confirm these locations, we performed co-localisation studies with specific markers.

### 1.5.2. CK1.2 localises to the basal body

In detergent-treated parasites, CK1.2-V5 was invariably detected between the kinetoplast and the flagellar pocket, in close proximity to the kinetoplast. In kinetoplastids, this region corresponds to the basal body or to the loading area of flagellar proteins into the flagellum [27]. The basal body (BB) is a microtubule-based organelle responsible, among other roles, for cilia and flagellum assembly in eukaryotes [38]. The basal body and its pro-basal body are attached to the kinetoplast through the tripartite attachment complex (TAC) [39] but also to the flagellar pocket [38]. The BB is involved in the duplication of the kinetoplast, which corresponds to the mitochondrial DNA. To investigate whether CK1.2-V5 co-localises with the basal body, we used an anti-centrin antibody, which recognises *L. donovani* centrin-4 (LdBPK\_221260.1) [26]. Centrins are cytoskeletal calcium binding (EF-hand) proteins, which in trypanosomatids are localised to the basal body and to a bilobe structure close to the Golgi, where they contribute to their duplication during mitosis [40] [26] [41]. We performed immunofluorescence assays on parasites treated with detergent and fixed with PFA, using anti-V5 (Fig. 2A, CK1.2-V5) and anti-centrin-4 antibodies (Fig. 2A, CEN). We showed that centrin localises in close proximity to the kinetoplast as one or two dots, depending on the cell cycle stage, which correspond to basal bodies (Fig. 2A, CEN, white arrow). Surprisingly for cells supposed to be mainly in G1, the number of cells containing two basal bodies is largely superior to that containing one basal body. Indeed, 75% of the cells contain two BBs, 10% contain dividing BB and only 10% of

cells contain one BB (Fig. S2A, CEN). This finding indicates that the division of the BB could be the earliest event of cell division and suggests that cells are mainly in mitosis. A signal was also observed in the flagellar pocket region, which could correspond to the bilobe structure (Fig. 2A, CEN, yellow arrow) [42] [40]. Using the anti-V5 antibody, we showed that CK1.2-V5 co-localises with centrin (Fig. 2B panel a, white arrows) as measured by a mean Pearson coefficient of  $0.741 \pm 0.050$  (n=14, Fig. 2C). This result indicates that CK1.2 co-localises with the basal bodies. Interestingly, CK1.2-V5 does not co-localise with centrin staining next to the Golgi, as judged by the mean Pearson coefficient below 0.5 ( $0.47 \pm 0.074$ , n=14; Fig. 2C), suggesting that CK1.2 is not associated with the bilobe structure. Furthermore, CK1.2-V5 seems to localise between the kinetoplast DNA and the basal body but does not co-localise with the kinetoplast DNA (mean Pearson coefficient of  $0.27 \pm 0.164$ , n=14, Fig. 2C), suggesting that it could also co-localise with the TAC. This structure connects the basal body to the kDNA and is involved in its segregation [43]. Altogether, these data suggest that CK1.2, besides the basal body, could regulate the segregation of the kDNA.

Next, we investigated whether CK1.2-V5 localises also to the transition fibres (TF). The flagellum represents a specific compartment and proteins that are destined for this compartment are recruited to the TFs, a platform where they are recognised as molecular cargo by the intra-flagellar transport (IFT) machinery [44]. The TFs are symmetric, nine-bladed, propeller-like fibrous structures, positioned at the ciliary base. These structures are also required for ciliogenesis initiation and connect the basal body to the flagellar pocket [45]. To determine whether CK1.2 localises to this selection platform, we first compared the localisation of centrin with IFT172, a major component of the IFT trains using anti-centrin and anti-IFT172 antibodies [26, 27]. In detergent-treated promastigotes, we observed three dots located between the flagellar pocket and the basal bodies (Fig. 2A, IFT172). As shown Fig. 2B panel b, part of the IFT172 signal co-localises with centrin as determined by the mean Pearson coefficient of 0.63

$\pm 0.1$  (n=14, **Fig. 2C**). The dots are situated on both sides of each basal body, which may correspond to the position of the transition fibres (**Fig. 2B panel b**). We then determined the localisation of CK1.2-V5 compared to IFT172 and revealed that part of CK1.2-V5 co-localises with IFT172 (**Fig. 2B panel c**, white arrow), as shown by the yellow staining and as measured by the mean Pearson coefficient of  $0,805 \pm 0,06$  (n=14, **Fig. 2C**). Lastly, we merged the three channels to represent in 3D the localisation of CK1.2-V5 with the kinetoplast, the basal body and the transition fibres (3D video in **Fig. S2B**). This 3D model revealed that the basal bodies are in-between CK1.2, which is also in close proximity to the kinetoplast, and the pool of IFT172 (**Fig. 2D, 3D view**). These findings suggest that CK1.2 is perfectly located (i) to regulate basal body functions such as the coordination of kinetoplast/basal body segregation, and (ii) to be loaded onto the flagellum and/or regulate the loading of flagellar proteins [45].

### 1.5.3. CK1.2 localises to the flagellum and to the flagellar pocket

We have previously shown that CK1.2-V5 also localises in an area that could correspond to the flagellar pocket (FP). To determine whether it localises inside the flagellar pocket or in the membrane, we compared the localisation of CK1.2-V5 with that of PFR2, a major component of the filamentous paraflagellar rod (PFR), which is situated inside the flagellar pocket from the pocket collar to the pocket neck (**Fig. 3A panel a** [46]). As judged by the z-stack images shown in **Fig. 3A panel b**, CK1.2-V5 does not co-localise with PFR2 but is located around it, suggesting that CK1.2 localises around the flagellar pocket, which is consistent with an association with the FP

membrane and a release via exosomes. Similarly, CK1.2-V5 does not co-localise with PFR2 in the flagellum but alongside the PFR2 signal (**Fig. 3A panel c**), suggesting that it could be on the axoneme. To confirm this hypothesis, we compared the localisation of CK1.2-V5 to that of IFT172. As in detergent-treated promastigotes, most of the flagellar IFT172 staining is lost (**Fig.**

2A), we performed the experiment using PFA-fixed cells (Fig. 3B). Both proteins were detected as dotted staining perfectly aligned along the flagellum, suggesting that CK1.2-V5 is located on the axoneme (Fig. 3B, 3D view). Moreover, according to the punctated staining we observed for both proteins, CK1.2 might also be transported in the flagellum similarly to IFT172 and not be part of fixed structures. However, because CK1.2-V5 does not co-localise with IFT172, as the two proteins seem to be intercalated, it is unlikely that CK1.2 would be a cargo of the IFT trains. Instead CK1.2 could be (i) directly associated to the kinesins/dyneins that drive the IFT trains or (ii) localised on different doublets than that of the IFTs [47, 48], which in *Trypanosoma brucei* have been shown to be doublet 4 and 7 [49].

#### 1.5.4. CK1.2 is localised in the granular zone of the nucleolus and redistributed to the mitotic spindle during mitosis.

As shown Fig. 1D, CK1.2-V5 was detected in a sub-nuclear location not stained by Hoechst, which may correspond to the nucleolus, the site for rRNA synthesis and processing as well as ribosome assembly [50]. To ascertain this hypothesis, we compared the localisation of CK1.2-V5 in detergent-treated promastigotes with that of L1C6 antibody that specifically recognises an unknown nucleolar protein [51]. We detected the L1C6-targeted antigen in the centre of the Hoechst-unstained area in the nucleus, which corresponds to the dense fibrillar zone of the nucleolus and is thought to be involved in rDNA transcription (Fig. 4, merged image, red staining) [50]. CK1.2-V5 was also detected in the nucleolus as dotted staining, however it is localised around the L1C6 staining, at the periphery of the nucleolus (Fig. 4, merged image, green staining). This localisation corresponds to the granular component of the nucleolus, which contains mainly RNA and is thought to be involved in the last steps of rRNA processing and ribosome biogenesis. These findings suggest that CK1.2 could be involved in the regulation of rRNA processing rather than that of rDNA transcription. We uncovered a potential novel role for CK1 family members; as, to our knowledge, such a localisation and its potentially associated

function have not been described for other eukaryote. CK1.2 may also play an additional role in the nucleolus, not linked to ribosome processing. Indeed, in dividing cells, we noticed that CK1.2-V5 staining seemed to elongate similarly to the nucleolus as defined by the Hoechst-unstained area, which was not the case for L1C6 staining (Fig. 5A, H and L1C6). The L1C6 antigen follows the classical segregation pattern described for the nucleolus by Ogbadoyi *et al.* (Fig. 5A rows a-f, merge) [52]. The spherical nucleolus elongates to a bar-shaped form and splits into two entities (Fig. 5A row d, CK1.2-V5, H and L1C6). Conversely, CK1.2 elongates from a wheel-shaped to a bar-shaped form that reaches both ends of the cell, similarly to the nucleolar region. These elongations are concomitant to nuclear division, suggesting their involvement in chromosome segregation. To investigate this hypothesis, we asked whether CK1.2 also co-localises with the mitotic spindle and whether the spindle is assembled in the nucleolus. To this end, we compared the localisation of CK1.2-V5 to that of  $\alpha$ -tubulin in dividing cells (Fig. 5B rows a-e). As shown in Fig. 5B panel a (Merge), CK1.2-V5 co-localises with the mitotic spindle in defined areas. Indeed, we only detected co-localisation, as judged by a mean Pearson coefficient (mPc) above 0.5, when considering part of the mitotic spindle (Fig. 5C). During anaphase, CK1.2-V5 is localised at each end of the elongated mitotic spindle (Fig. 5B row d). These findings suggest that CK1.2 may be involved in the regulation of chromosome segregation. Evidence from other eukaryotes support such a role for CK1 in mitosis and its recruitment to the spindle [53]. Surprisingly, the mitotic spindle co-localises also with the nucleolus as determined by the Hoechst-unstained region, suggesting that nucleolar proteins could be involved in chromosome segregation in the absence of visible centrosomes. Similar processes have been described in *Trypanosoma brucei* [54]. Thus, we identified CK1.2 as another nucleolar protein that relocates from the nucleolus to the mitotic spindle during mitosis.

### 1.5.5. CK1.2 co-localises with chaperone proteins to specific organelles

Exosomes are vesicles of endosomal origin released by cells from multivesicular bodies into their extracellular environment and known to promote cell-to-cell communications [55]. CK1.2 has been identified in exosomes by proteomic analyses, suggesting a role of this kinase in the host cell. In an attempt to visualise the exosomal fraction of CK1.2, we compared the localisation of CK1.2 with that of Hsp90 and Hsp70, two proteins shown to be, among other functions, cargos of *Leishmania* exosomes [21]. Moreover, their human orthologs are known substrates of human CK1 [56].

- *CK1.2 is localised with Hsp90 at the flagellar pocket neck.*

We have recently shown that *Leishmania* CK1.2 phosphorylates Hsp90 similarly to the human CK1 [57], suggesting that they could be localised in similar organelles. We thus performed co-localisation studies between CK1.2-V5 and Hsp90 on detergent-treated promastigotes. Compared to PFA-fixed parasites (Fig. S3A), most of Hsp90 has been removed from the parasite body by the detergent treatment, indicating that the major fraction of Hsp90 is cytoplasmic (Fig. 6A). Only a small fraction of Hsp90 is associated with the cytoskeleton at the flagellar pocket neck (Fig. 6A). This fraction also co-localises with CK1.2-V5, as confirmed by a Pearson coefficient above threshold (Fig. 6B). The two proteins seem to form a horseshoe shape as judged by the 3D view (Fig. 6C) and the movie (Fig. S3B). These results suggest that CK1.2 and Hsp90 could have specific functions linked to endo- or exocytosis, as the flagellar pocket neck has been shown to be the site of endocytosis regulation [58].

- *CK1.2 co-localises with Hsp70, its substrate, to the basal body, the flagellar pocket and flagellar tip.*

The human Hsp70 C-terminal domain is phosphorylated by human CK1, suggesting that this kinase regulates certain functions of Hsp70 [56]. Muller *et al.* suggested that phosphorylation of Hsp70 acts as a switch for regulating co-chaperone binding, leading to folding

(phosphorylation) or degradation (dephosphorylation) of client proteins. We first observed the localisation of Hsp70 and compared it to that of CK1.2. As expected and similarly to Hsp90, Hsp70 is mainly localised in the cytoplasm, as judged by Fig. S4A. However, we uncovered a novel localisation for Hsp70. In detergent-treated parasites, we observed a cytoskeleton-bound fraction of Hsp70, which is weakly localised in the flagellum as punctuated stainings but strongly associated with the flagellar tip (Fig. 7A, Hsp70). Hsp70 is also localised in the flagellar pocket and the basal body regions as well as around the nucleus and in the nucleolus (Fig. 7A, Hsp70). As shown in Figure 7A (Merge) and confirmed by the Pearson coefficient (Fig. 7B), Hsp70 co-localises with CK1.2-V5 at the basal body, in the flagellar tip and in the flagellar pocket. However, based on the Pearson coefficient, it seems that Hsp70 co-localises with CK1.2 across the whole parasite, which was not observed for Hsp90. Hsp70 might thus be one of the main components of CK1.2 complexes. To determine whether *Leishmania* Hsp70, similarly to its human orthologs, was phosphorylated by CK1.2, we performed an *in vitro* kinase assay using recombinant Hsp70 and CK1.2-V5 (Fig. 7C). We showed that in the presence of CK1.2,  $^{32}\text{P}$  was incorporated into Hsp70, suggesting that CK1.2 phosphorylated Hsp70; result further supported by the loss of  $^{32}\text{P}$  incorporation following the addition of D4476, a specific inhibitor of CK1.2 [6]. To exclude the possibility that the incorporation of  $^{32}\text{P}$ -ATP could be linked to the ATPase activity of Hsp70, we performed the experiment without adding the kinase. We did not observe any incorporation, suggesting that Hsp70 is phosphorylated *in trans* by CK1.2 (Fig. 7C). These data suggest that Hsp70 may be regulated by CK1.2-mediated phosphorylation and contribute to its localisation.

Altogether, the co-localisation of CK1.2 with Hsp90 and Hsp70, although providing valuable information on CK1.2 potential functions and regulations, did not provide any elements that could increase our knowledge on the mechanisms leading to the loading of proteins into exosomes.

### 1.5.6. CK1.2 has a similar localisation in axenic amastigotes as in promastigotes

We next investigated whether the localisation of CK1.2 is modified during stage conversion. To this end, we determined the localisation of CK1.2-V5 in axenic amastigotes and showed that in PFA-fixed cells, the localisation of CK1.2-V5 is similar to that observed in promastigotes. CK1.2-V5 is revealed as intense fluorescent dots in the cytoplasm and at the flagellar tip (Fig. 8A, white arrows). We next treated the parasites with detergent prior to PFA fixation. In these parasites, CK1.2-V5 is localised at the basal body, the flagellum or the flagellar pocket, the nucleolus and the flagellar pocket neck, similarly to its localisation in promastigote (Fig. 8B). Contrary to non-treated axenic amastigotes, in detergent-treated axenic amastigotes CK1.2-V5 seems excluded from the flagellar tip and restricted to the flagellar pocket neck as judged by Figure 8C and 3D view (green staining). Indeed, in non-treated parasites, we detected CK1.2 at the flagellar tip of 82% of CK1.2 positive cells, whereas in detergent-treated parasites, we detected CK1.2 at the flagellar tip of only 8% of CK1.2 positive cells. This result suggests that CK1.2 is not associated with the cytoskeleton at the flagellar tip contrary to what we observed in promastigotes. CK1.2-V5 is strongly detected at the flagellar pocket neck, where it forms a horseshoe shape (Fig. 8C, & 3D view). Next, because in axenic amastigotes the flagellum is shorter, we compared the localisation of CK1.2-V5 with IFT172 and centrin. CK1.2-V5 also co-localised at the basal body with both centrin and IFT172 (Fig. 8C, merge). Interestingly, IFT172 proteins, which clearly accumulate at the transitional fibres, were also found along the short flagellum and at the flagellar tip (Fig. 8C, IFT172). This data is surprising and suggests that IFTs might be required for transporting proteins that are not required to build the flagellum. Altogether, these data show clearly that CK1.2 displays multiple localisation patterns, which are likely to be linked to different functions. However, apart from a non-functional nuclear localisation signal, there are no addressing sequences that could explain such a wide range of

localisations [1]. Moreover, *Leishmania* CK1.2 is constitutively active, contrary to human CK1 $\delta$ ,  $\epsilon$  and to a lesser extent CK1 $\alpha$ , thus requires a tighter regulation of its localisation to avoid inappropriate phosphorylation of its substrates [1].

1.5.7. The C-terminal and the N-terminal domains of CK1.2 are, respectively, essential for its correct localisation and its stability, but not for its activity.

In higher eukaryotes, CK1 is mainly regulated through its N- and C-terminal domains [1, 59]. To determine how CK1.2 is regulated, we investigated which domains were required for its localisation. Among *Leishmania* CK1 paralogs, CK1.2 and CK1.1 are highly similar but differ in their N- and C-terminus [6, 35]. We identified important deletions in the N- and C-terminal domains of CK1.1 compared to CK1.2, which might explain the differences in regulation and localisation. Indeed, in contrast to CK1.1, CK1.2 is released into the host cell via exosomes and is essential for parasite survival [6] [21]. We thus generated N- and C-terminal truncations of CK1.2, based on the alignment with CK1.1 to determine the importance of these domains for the localisation and regulation of CK1.2 [35]. As shown in Fig. 9A, the three truncated CK1.2 proteins were (i) lacking the last ten amino acids (aa) at the C-terminus that share almost no similarity to CK1.1 (CK1.2 $\Delta$ C10), (ii) lacking the last 43 aa of the C-terminus that correspond to the LCRs, (CK1.2 $\Delta$ C43), or (iii) lacking the seven first aa at the N-terminus (CK1.2 $\Delta$ N7). We first tested whether these truncated mutants were still active kinases. Indeed, the C-terminal domain is important for kinase activity [59]. To this end, we expressed these mutants as recombinant proteins in *E.coli*, purified them on a cobalt resin and performed a kinase assay using MBP as canonical substrate [6]. CK1.2 is active, as demonstrated by the incorporation of <sup>32</sup>P into MBP. CK1.2 $\Delta$ C10, CK1.2 $\Delta$ C43 and CK1.2 $\Delta$ N7 are also active as they phosphorylate MBP with the same efficiency as CK1.2 (Fig. 9B, top panel). This finding indicates that the N- or the C-terminal domains of CK1.2 are not essential for its activity. Next, we transfected

LdBob promastigotes with a pLEXSY plasmid containing CK1.2, CK1.2 $\Delta$ C10, CK1.2 $\Delta$ C43 or CK1.2 $\Delta$ N7 genes to produce V5-tagged versions of these proteins. We used the empty vector as control. We confirmed the expression of the three truncated proteins by Western blot analysis (Fig. 9C). CK1.2 $\Delta$ C10-V5 and CK1.2 $\Delta$ C43-V5 levels were similar to that of CK1.2-V5, whereas the level of CK1.2 $\Delta$ N7 was lower (Fig. 9C). There are at least two possible hypotheses to explain the low abundance of CK1.2 $\Delta$ N7, either the deletion of the N-terminus leads to structural instability or without its N-terminus, the mutant protein is prone to degradation. We excluded the first possibility, since CK1.2 $\Delta$ N7 was easily produced as recombinant protein in bacteria (Fig. 9B, coomassie). To investigate the second hypothesis, we first tested whether CK1.2 $\Delta$ N7 could be degraded by the proteasome, by treating the transgenic parasites with Mg132, a proteasome inhibitor. We showed that the level of CK1.2 $\Delta$ N7 as well as that of CK1.2 and the other mutants was similar in the presence or in the absence of Mg132 (Fig. 9D panel a). To confirm that the proteasome was blocked, we controlled whether we could detect an increase in ubiquitinated proteins by performing a Western blot analysis using an anti-ubiquitin antibody. As judged by Fig. S5A, the level of ubiquitinated proteins was increased in presence of Mg132, confirming that the proteasomal degradation is blocked. We next investigated whether the mutant proteins could be degraded in the lysosomes. To this end, we treated the transgenic parasites with ammonium chloride (NH<sub>4</sub>Cl), which increases the pH in the lysosome rendering proteases inactive [60]. We showed that the level of CK1.2 $\Delta$ N7 remained low despite the inhibition of lysosomal proteases (Fig. 9D panel b). We confirmed the alkalisation of the lysosome by NH<sub>4</sub>Cl using a LysoTracker, which stains acidic compartments of living cells, and we observed a decrease in LysoTracker staining, indicating an increased in pH (Fig. S5B). The low level of CK1.2 $\Delta$ N7 protein is thus not the consequence of degradation by the proteasome or by the lysosome. We also excluded autophagy, which is ultimately a lysosome-mediated degradation [61].

To assess the importance of the N- and C-terminal domains for CK1.2 localisation, we performed immunofluorescence studies either on PFA-fixed cells or on detergent-treated PFA-fixed cells as previously described. To determine whether the mutants could localise similarly to the wild type (WT), we measured the sum fluorescence of each parasite in the WT and the three mutant parasites. In PFA-fixed cells (Fig. 9E panel a), we could not detect any statistically significant differences between CK1.2, and CK1.2 $\Delta$ C10 or CK1.2 $\Delta$ C43. In contrast, we could measure a statistically significant difference between CK1.2 and CK1.2 $\Delta$ N7, with CK1.2 $\Delta$ N7 level being similar to that of the background control. This data is consistent with the results obtained from the Western blot analyses. We then performed the same experiment with parasites treated with detergent prior to PFA-fixation to evaluate the ability of the mutant proteins to associate with the cytoskeleton (Fig. 9E panel b). We showed that there was no significant difference in fluorescence intensity between CK1.2 and CK1.2 $\Delta$ C10, suggesting that the two transgenic parasites have similar level of proteins remaining in the cell. Conversely, we could detect a significant difference in fluorescence intensity between CK1.2 and CK1.2 $\Delta$ C43 or CK1.2 $\Delta$ N7, suggesting that the level of CK1.2 $\Delta$ C43 and CK1.2 $\Delta$ N7 detected in the cells after detergent treatment was lower than that of the WT. These data suggest that the C-terminal domain between aa 343 and 353 is not implicated in CK1.2 cellular localisation, contrary to the domain between aa 310 and 343, which corresponds to low complexity regions that are deleted in CK1.1. We cannot conclude on the importance of the N-terminal domain between aa 1-7 for CK1.2 localisation as the protein cannot be detected by immunofluorescence and can only be detected weakly in Western blot analysis. Our data suggests that deleting the C-terminal domain prevents the mutant protein from associating with organelles and the cytoskeleton, causing it to remain in the cytoplasm.

## 1.6. Discussion

CK1.2 has been shown to be essential for promastigote, axenic and intra-macrophagic amastigotes, but little is known about the essential functions it performs in the parasite [6]. The data presented here suggest that CK1.2 displays a pleiotropic localisation, consistent with its involvement in multiple processes. This finding is similar to the data obtained with its eukaryotic orthologs [1]. As shown for higher eukaryotes, localisation of CK1 is linked to its functions and regulates its specificity towards its substrates. Therefore, studying its localisation is important to get insights into CK1 functions [1].

We detected CK1.2 in punctate structures in the cytoplasm of promastigote as well as amastigotes. The origins of these structures in *Leishmania* are unclear but based on similar localisation of CK1 in human cells there are several hypotheses. Human CK1 $\alpha$  has also been localised to cytoplasmic speckles through its interaction with FAM83H [37], which could be disassembled keratin speckles [62]. We excluded this possibility, as no ortholog of keratin has been described in *Leishmania*. They could be P-bodies, which are non-membranous compartments resulting from the accumulation of specific mRNA and proteins to discrete sites in the cytoplasm [63]. This is a strong possibility as human CK1 $\delta$  and HRR25, its *Saccharomyces cerevisiae* ortholog have been shown to localise to P-bodies [19]. Zhang *et al.*, showed that it protects the kinase from degradation, especially during stress [19]. Moreover, CK1.2 in *Trypanosoma brucei* has been recently shown to regulate ZC3H11, a protein involved in the stabilisation of stress response mRNAs [64]. Surprisingly in axenic amastigotes, there is a concentration of those punctate structures at the tip of the shorter flagellum. This localisation could be linked to the excretion of CK1.2; this hypothesis will be studied in the future. We showed that part of these CK1.2-containing punctate structures is not extracted by detergent treatment suggesting that they could be associated to the cytoskeleton such as microtubules or

actin. CK1.2 also localises to other organelles besides these speckles, which could be associated to specific functions.

### 1.6.1. Basal body and flagellum

CK1.2 is localised to the basal body, which is similar to the localisation of human CK1 $\epsilon$ , where it plays a role in primary cilia disassembly [65]. Moreover, we showed that CK1.2 is localised to the region situated above the basal bodies, which corresponds to the tripartite attachment complex (TAC). Our data suggests that CK1.2 is localised more specifically to the exclusion zone filaments, which is the cytoplasmic component of the TAC, as we did not see any co-localisation with the kDNA [66]. This finding indicates that CK1.2 could be part of the exclusion zone filaments and thus involved in the duplication of the kDNA.

Another localisation we revealed for CK1.2 is the transition fibres (TFs), where it co-localises with the IFTs. The TFs connect the basal body to the flagellar pocket and are the docking sites for IFTs and thus for flagellar proteins [44]. There are two possible explanations for this localisation, which are not mutually exclusive. First, CK1.2 could be involved in the selection of flagellar proteins, similarly to mammalian CK1, as it was shown that human CK1 $\alpha$  phosphorylates mammalian Smoothed (Smo) leading to its accumulation in the cilia [67]. Second, it could be localised to the TFs because as a flagellar protein, it needs to be loaded onto the flagellum.

We showed that CK1.2 localises on the axoneme of the flagellum, which is supported by proteomic data [68] [69]. With *Chlamydomonas reinhardtii*, *Leishmania* is the only eukaryote where a flagellar localisation of CK1 has been observed [70]. We showed that CK1.2 is strongly associated to the axoneme, as it is not displaced as easily as IFT172 in presence of detergent [27]. This finding and the fact that CK1.2 does not co-localise with IFTs, suggest that they might not be traveling on the same doublet and thus that CK1.2 might not be transported by

IFT trains [49]. These findings raise the question on how CK1.2 is transported along the axoneme and what its role might be. CK1.2 could be involved in motility, similarly to CK1 in *Chlamydomonas reinhardtii*, which phosphorylates the Inner Dynein Arm II Intermediate Chain 138 to regulate flagellum motility [70] or sensing. Indeed, CK1.2 accumulates at the distal end of the flagellum both in promastigotes and in axenic amastigotes, although in promastigotes, it seems to be linked to the cytoskeleton whereas in axenic amastigotes it is not. We also showed that Hsp70 co-localises with CK1.2, suggesting that both proteins are in a complex. The localisation of these two proteins in promastigotes is resistant to detergent, suggesting that they bind to a specific structure, already identified in *T. brucei* but never formally characterised [68]. Such a localisation has also been shown for Hsp70 in *Chlamydomonas* [71] [72]. Protein localisation at the flagellar distal tip could be involved in microtubule assembly, stability or dynamics [68, 71, 72]. Moreover, the flagellum has been identified as a sensory organelle, and the distal tip as important in signal transduction [73, 74]. CK1 is a signalling kinase known to transduce signals and to phosphorylate substrates to target them for degradation [75]. The localisation of CK1 at the flagellum could thus have a similar function as that in cilia.

### 1.6.2. Nucleolus and chromosome segregation

The mammalian nucleolus has three components: the fibrillar centre (FC), where rDNA transcription occurs; the dense fibrillar component (DFC), where pre-ribosomal RNA transcripts are spliced and modified; and, at the periphery of the nucleolus, the granular component (GC), where final maturation of the pre-ribosomal ribonucleoproteins and assembly with ribosomal proteins take place [76]. In trypanosomatids, the organisation of the nucleolus is slightly different, as no clear differences have been identified between the FC and the DFC [52]. Contrary to our nucleolar marker, we showed that CK1.2 localises at the periphery of the nucleolus corresponding to the granular component. This finding indicates that the kinase could

be involved mostly in the regulation of the last steps of ribosomal processing in the nucleolus but not in rDNA transcription. This is slightly different from previous data related to yeast and human CK1, showing that these kinases are implicated in the maturation of pre-40S ribosomes in the cytoplasm [77] [78]. Nevertheless, human CK1 $\alpha$  and  $\delta$  have been identified in the proteome of the nucleolus, suggesting that, similarly to *Leishmania* CK1.2, they localise in the nucleolus and thus could play a role in this organelle [79].

Apart from its potential involvement in ribosome processing CK1.2 might have another function in the nucleolus. We observed, like others, that the nucleolus is also the site of mitotic spindle elongation and thus of chromosome segregation [80] [81]. We could co-localise nucleolar CK1.2 with tubulin from the assembly of the mitotic spindle to its elongation unlike the nucleolar marker protein, suggesting that CK1.2 could be involved in chromosome segregation. The redistribution of nucleolar proteins onto the mitotic spindle has been described for TbNOP86, a protein potentially involved in chromosome segregation in *T. brucei* [54]. Moreover, seventeen nucleolar proteins are associated to the mitotic spindle in *Trypanosoma brucei* and more than half of the 700 human nucleolar proteins are not involved in ribosome biogenesis but involved in functions such as mitotic progression [81, 82]. This finding is quite surprising as in human cells, the microtubule-organising centre (MTOC) organises the assembly of the mitotic spindle, not the nucleolus. Despite having a basal body, no structural equivalents of human centrosomes have been identified in Trypanosomatids [83] [84, 85]. Contrary to the mammalian basal body, which migrates near the nucleus to be part of the centrosome upon primary cilia disassembly, we showed that the *Leishmania* basal body does not migrate and thus does not participate to nuclear segregation [86]. Instead, chromosome segregation seems to rely on an atypical MTOC, which is located in the nucleolus. We could show that the nucleolar pool of CK1.2 is redistributed onto the mitotic spindle within the elongated nucleolus. This finding suggests that the nucleolus contains a structure that acts as a MTOC and could organise the

mitotic spindle and regulate its positioning. Our results are consistent with those of Kumar *et al.*, who showed that the nucleolar twinfilin-like protein, an actin-binding protein, is redistributed to the mitotic spindle and controls mitotic spindle elongation [80]. Moreover, it has been shown in *Naegleria* that specific nucleolar binding sites for microtubules could allow mitotic spindle formation and attachment [87]. Our data increases the number of identified nucleolar proteins that are redistributed to the mitotic spindle and strongly suggest that CK1.2 could be implicated in the regulation of these processes. It will be interesting in the future to investigate whether CK1.2 regulates this relocation by phosphorylating key proteins. This phenomenon, which seems to be specific to centrosome-less organisms such as kinetoplastids could be explained by the fact that the basal body in *Leishmania* and *Trypanosoma brucei*, does not contribute to chromosome segregation. Therefore, our findings support the hypothesis that chromosome segregation is mediated by an alternative mechanism, involving the nucleolus and CK1.2 [88].

The involvement of CK1 in proper spindle positioning has been recently described for human CK1 $\alpha$ . The human kinase is recruited to the spindle by FAM83D, which is essential for spindle positioning and timely cell division [89]. FAM83D is part of the FAM83A-H protein family that has been recently identified as partners of CK1 in cells, acting as subcellular anchors for CK1 isoforms through the conserved N-terminal domain of unknown function 1669 (DUF1669). There are no orthologs of these proteins in *Leishmania* as judged by protein alignment [37]. Surprisingly, in axenic amastigotes, following the retraction of the flagellum, we observed the migration of the basal bodies nearer to the nucleus but with no evidence of involvement in chromosome segregation as it was still initiated in the nucleolus. This phenomenon is similar to that observed for the cilia where the BB migrates to a position near the nucleus, as primary cilia are disassembled to be part of the centrosome during the cell cycle

[86]. However, because the BB is not involved in chromosome segregation, its migration remains to be elucidated.

### 1.6.3. Flagellar pocket

We have shown that CK1.2 localises around the flagellar pocket, probably associated with its membrane. The flagellar pocket is an invagination of the plasma membrane located in the anterior part of the parasite [90]. Contrary to the rest of the parasite body, it lacks the sub-pellicular microtubule and thus is thought to be the site of exo-endocytosis [90]. Moreover, all vesicular trafficking originate from the FP, rendering this organelle crucial for host-pathogen interactions. The localisation of CK1.2 at the flagellar pocket suggests that the kinase could be exported by and/or could regulate endocytosis. There are evidences supporting the two hypotheses: (i) CK1.2 is exported by exosomes, probably through the FP [21]; and (ii) Hrr25, as well as human CK1 $\delta/\epsilon$  promotes initiation of clathrin-mediated endocytosis through its recruitment to endocytic sites [18]. Therefore, similarly to other eukaryotes, CK1.2 could regulate endocytosis. We identified two other proteins that are located to the flagellar pocket, Hsp70 and Hsp90, the latter being specifically recruited to the neck. Moreover, both proteins are phosphorylated by CK1.2 and their human orthologs by human CK1 ([56] [57], our data). This is the first time that a localisation of Hsp90 to a specific organelle is observed in *Leishmania*. The detection of CK1.2 and Hsp90 at the flagellar pocket neck (FPN) is consistent with a potential role of these proteins in endocytosis. The FPN, mainly described in *T. brucei*, facilitates the entry of macromolecules, nucleates the flagellum attachment zone (FAZ) and regulates endocytosis [58, 91]. *Trypanosoma brucei* PIPKA, which is implicated in endocytosis, shows a localisation at the FPN comparable to that of CK1.2 and Hsp90 [58]. The localisation of CK1.2 and Hsp90 to the FPN suggests that the two proteins might play a role in endocytosis. This is in accordance with known functions of mammalian CK1 but would to be a novel role for Hsp90 [18, 92]. Another role associated with FPN localisation is the regulation of

cytokinesis. Indeed, the deletion of *Trypanosoma brucei* Smeel1, a protein part of the hook complex and localised to the FPN, leads to a cytokinesis defect [91]. *S. pombe* CK1 has been shown to be required for the mitotic checkpoint that delays cytokinesis [93]; thus *Leishmania* CK1.2 could have a similar role. To discriminate between these potential functions, further analyses will be required.

#### 1.6.4. Regulation of CK1.2 localisation

The subcellular localisation of mammalian CK1 is dependent on interacting partners [1], suggesting that the domains in CK1.2 involved in protein-protein interactions could be crucial for regulating its localisation. We showed that the C-terminal domain of CK1.2 is essential for the specific localisation of CK1.2 as it is lost if part of the C-terminus is deleted. This domain between the amino acids 310 and 343 may contribute to the binding of interacting partners as it corresponds to the Low Complexity Regions (LCR). LCRs were shown to be more abundant in highly connected proteins, such as signalling kinases [94]. Removing these domains considerably reduced the ability of CK1.2 to localise to organelles and subcellular structures. These LCRs are also present in the C-terminal domain of CK1 $\alpha$ , CK1 $\delta$ , CK1 $\epsilon$ , as well as in the C- and N-terminal of CK1 $\gamma$ 1, CK1 $\gamma$ 2, CK1 $\gamma$ 3, suggesting that they might also be crucial for the localisation of human CK1s (<http://repeat.biol.ucy.ac.cy/sequenceserver> [95]). This finding suggests that protein-protein interactions are crucial for CK1 localisation. Thus identification of CK1.2 binding partners will be critical to understand how CK1.2 traffics through the cell and is released in the host cell to perform its various functions. Surprisingly, this domain is deleted from the C-terminus of *Leishmania* CK1.1; instead a LCR is present at the N-terminus [96]. Knowing that CK1.1 is not excreted via exosomes contrary to CK1.2 and that the absence of this domain is the major difference between the two proteins, it is possible that these LCR domains are important for CK1.2 excretion and thus its functions in the host cell. Moreover, the different positions of the LCRs in CK1.2 and CK1.1 suggest that they probably interact with

different partners. One of CK1.2 interactors could be Hsp70, as it seems to co-localise with CK1.2 across the whole parasite. Moreover, we have shown that Hsp70 is a substrate of CK1.2, which is consistent with what has been observed for human Hsp70 [56]. Human CK1 has been described to phosphorylate Hsp70 at its C-terminal domain to regulate the balance between folding and degradation. Our data suggest that Hsp70 could be the main binding partner of CK1.2 and might be involved in the regulation of its localisation. We also showed that the last 10 amino acids of CK1.2 are not essential as their removal does not alter activity, localisation or stability. In contrast, the removal of the seven first amino acids renders the protein undetectable in the cell. We excluded proteasomal, lysosomal or autophagosomal degradation, as well as degradation by cathepsin B or calpain-like cysteine peptidase, off targets of Mg132, but we did not explore the possibility that the protein might be directly excreted into the extracellular environment [97]. This hypothesis is supported by the fact that CK1.2 but also CK1.4 in *Leishmania* and PfCK1 in *Plasmodium* have been shown to be ectokinases that could be shedded in the extracellular medium [98] [20] [5]. Interestingly, these seven amino acids are absent in CK1.1 protein sequence. This finding is consistent with the two proteins being regulated differently.

#### 1.6.5. *Leishmania* CK1 mimics mammalian CK1

The similarity between *Leishmania* and human CK1s in terms of structure, activity, regulation and now localisation is in line with the high level of identity observed between their protein sequences and consistent with these kinases having similar functions [99] [6]. These findings supports the hypothesis of a role of *Leishmania* CK1.2 in the mammalian host cell as a substitute to the mammalian CK1s, but to which of the seven mammalian paralogs, *Leishmania* CK1.2 is the closest. The sequence alignment data suggests that CK1.2 is more closely related to CK1 $\delta$ , but its sensitivity to IC261 (CK1 inhibitor) is closer to CK1 $\alpha$  [24]. The localisation data supports these first observations by showing that CK1.2 localises similarly to CK1 $\alpha$ ,  $\delta$  and

$\epsilon$  and thus suggests that *Leishmania* CK1.2 could potentially replace all three mammalian paralogs in the infected macrophage. However, Isnard *et al.* showed that during a *Leishmania* infection, only CK1 $\alpha$  is down regulated suggesting that *Leishmania* might only compensate for this paralog [100]. This will have to be investigated further.

Altogether, our data demonstrate the pleiotropic localisations of CK1.2 and thus its potential involvement in multiple processes, making this kinase an essential signalling molecule for the parasite. Moreover, our present and previous data demonstrate the similarity of localisation, structure, activity, regulation between *Leishmania* CK1.2 and human CK1s, highlighting that *Leishmania* CK1.2 is an excellent model to study mammalian CK1s (this data, [99] [6] [36]). Indeed, we uncovered a potential novel localisation of CK1 family members to the nucleolus and revealed the importance of LCRs for CK1 family member localisation. Finally, to date CK1.2 is the only signalling kinase shown to be exported into the host cell via exosomes and to have the ability to regulate multiple host cell processes, suggesting that it could be a key player for host-pathogen interactions and parasite survival.

## 1.7. Acknowledgments

This work was supported by the ANR-13-ISV3-0009. Daniel Martel was supported by the French Government's Investissements d'Avenir program Laboratoire d'Excellence Integrative Biology of Emerging Infectious Diseases (grant no. ANR-10-LABX-62-IBEID studentship). Part of the work was supported by the Deutsche Forschungsgemeinschaft Grant Cl 120/8-1. We thank Frauke Fuchs for technical assistance. The authors would like to thank Hira L Nakhasi, U.S. FDA, for the anti-*Ldc*centrin antibody; Philippe Bastin, Institut Pasteur, for the anti-*TbIFT172* and anti-*TbPFR2* (L8C4) antibodies; Keith Gull, University of Oxford for the L1C6 antibody; the Unit of Technology and Service - Photonic BioImaging (UTechS PBI) from the Institut Pasteur, for the help with confocal microscopy and analyses of co-localisations, in particular Audrey Salles, Julien Fernandes and Anne Danckaert. Finally, we would like to thank Brice Rotureau, Thierry Blisnick and Philippe Bastin for fruitful discussions and advices.

## 1.8. Figure legends

### **Fig. 1: *Leishmania* CK1.2 localisation is ubiquitous**

(A) IFA of *LdBob* pLEXSY-CK1.2-V5 and (B) *LdBob* pLEXSY (mock) promastigotes, fixed with PFA and stained with anti-V5 antibody to detect CK1.2-V5 localisation. The confocal images were acquired under the same conditions and show the anti-V5 staining (CK1.2-V5 or V5), Hoechst 33342 staining (H), a merge of the anti-V5 (green) and Hoechst 33342 (blue) signals and the transmission image (Trans). Scale bar, 2  $\mu$ m. The pictures are maximum intensity projection (MIP) of the confocal stacks containing the parasites.

(C) Analysis of different parameters extracted from ROI of the promastigotes parasite bodies. Scatter dot plots showing the sum of fluorescence intensity (for the V5 signal) of CK1.2-V5-expressing or mock control cell lines.

(D) IFA of *LdBob* pLEXSY-CK1.2-V5 promastigotes obtained after detergent treatment followed by PFA fixation and detection with the anti-V5 antibody labeling CK1.2-V5. The confocal images show the anti-V5 staining (CK1.2-V5, normal or saturated image), Hoechst 33342 staining (H), a merge of the anti-V5 (green) and Hoechst 33342 (blue) signals and the transmission image (Trans). Scale bar, 2  $\mu$ m. The pictures are MIP of the confocal stacks containing the parasites.

See also Figure S1 and S7.

### **Fig.2: CK1.2 localises to the basal bodies**

IFA of *LdBob* pLEXSY-CK1.2-V5 promastigotes obtained after detergent treatment followed by PFA fixation and stained with the anti-V5, anti-centrin 4 or anti-IFT172 antibodies.

(A) Single channel images of the CK1.2-V5, Hoechst 33342 (H), centrin 4 (CEN) or IFT172 signals and the transmission image (Trans). The white arrow highlights the basal bodies and the yellow arrow the bilobe region.

(B) The left panel shows CK1.2-V5 signal (green) merged with H (Hoechst 33342, blue), CEN (centrin 4, red) and IFT172 (cyan). The three right panels show a magnification of region 1 with H signal (blue) merged with (a) CK1.2-V5 (green) and CEN (red), (b) CEN (green) and IFT172 (red) and (c) IFT172 (red) and CK1.2-V5 (green) signals. Scale bar, 2  $\mu\text{m}$  or 1  $\mu\text{m}$  for magnified images. These pictures are single stacks extracted from deconvolved confocal stacks corrected for chromatic aberration. The white arrows highlight the basal bodies and the yellow arrow the bilobe region.

(C) Dot plots showing Pearson's covariation coefficients in the basal body (BB) or the flagellar pocket (FP) regions for different combination of signals: CK1.2-V5 signal versus CEN, IFT172 or H in the BB region or versus CEN in the FP region. The Pearson's covariation coefficients were also measured for CEN signal versus IFT172 in the BB region. Pearson's covariation coefficients were measured from  $n=14$  different confocal stacks which were deconvolved and corrected for chromatic aberration with Huygens Professional software. The plot was generated with GraphPad Prism software and the mean values are represented with red bold segments.

(D) 3D-reconstruction of the basal body region from the merged image (B), showing CK1.2-V5 signal (green) merged with CEN (red), IFT172 (blue) or H (white). All confocal stacks containing the parasite were used to generate this picture.

See also Figure S2.

### **Fig. 3: CK1.2 localises to the flagellar pocket and the axoneme of the flagellum**

(A) IFA of *LdBob* pLEXSY-CK1.2-V5 promastigotes obtained after detergent treatment followed by PFA fixation and staining with the anti-V5 and anti-PFR2 antibodies. (a) The following images show CK1.2-V5, PFR2, Hoechst 33342 (H) signals, the transmission image (Trans), and finally the merge of CK1.2-V5 (green), PFR2 (red) and H (blue) signals. (b) 2D images from the confocal stack of the flagellar pocket (white square in (a)) showing CK1.2-V5

signal (green) merged with PFR2 (red) and H (blue). (c) 3D-reconstruction (3D view) of the flagellum (white square in (a)), showing CK1.2-V5 signal (green) merged with PFR2 (red).

(B) IFA of *LdBob* pLEXSY-CK1.2-V5 promastigotes fixed by PFA and stained with the anti-V5 and anti-IFT172 antibodies. The left panels display the single channel images of the CK1.2-V5, IFT172, Hoechst 33342 (H) signals, the transmission image (Trans), and a merge of CK1.2-V5 (green), IFT172 (red) and H (blue) signals. The right panel shows a 3D-reconstruction (3D view) of the flagellum (region 1), with CK1.2-V5 signal (green) merged with IFT172 (red).

Scale bars, 2  $\mu\text{m}$  or 1  $\mu\text{m}$  for 2D images. Pictures in (Aa) and (B, left panels) are single stacks extracted from deconvolved confocal stacks corrected for chromatic aberration. All confocal stacks containing the parasite were used for pictures (Ab, Ac) and (B, 3D view).

**Fig. 4: CK1.2 localises in the nucleolus**

IFA pictures of *LdBob* pLEXSY-CK1.2-V5 promastigotes obtained after detergent treatment followed by PFA fixation and stained with the anti-V5 antibody and L1C6 antibody targeting the nucleolus. The images show the single channel images of the transmission image (Trans) and CK1.2-V5, Hoechst 33342 (H) and L1C6 signals. The merged panel displays CK1.2-V5 (green), L1C6 (red) and H (blue) signals. The right panel show a magnification of the nucleus region with H signal (blue) merged with CK1.2-V5 (green) and L1C6 (red) signals. Scale bar, 2  $\mu\text{m}$ . These pictures are single stacks extracted from deconvolved confocal stacks corrected for chromatic aberration.

**Fig. 5: CK1.2 is redistributed to the mitotic spindle during mitosis**

(A) IFA pictures of *LdBob* pLEXSY-CK1.2-V5 promastigotes obtained after detergent treatment followed by PFA fixation and stained with anti-V5 (CK1.2-V5) and anti-L1C6 (nucleolus, L1C6) antibodies. Confocal images representing sequential events of mitosis

revealed different localisation patterns of L1C6 nucleolar marker and CK1.2-V5. (a – f) The images correspond to the transmission (Trans), the merged containing CK1.2-V5 (green), Hoechst 33342 (H) (blue) and L1C6 (red) signals. The following four images show a magnification of the nuclear region with the merged and single channel images. N=nucleus, K=kinetoplast. Scale bar, 2  $\mu\text{m}$  or 1  $\mu\text{m}$  for magnified images. These pictures are single stacks extracted from deconvolved confocal stacks corrected for chromatic aberration.

(B) IFA pictures of *LdBob* pLEXSY-CK1.2-V5 promastigotes obtained after detergent treatment followed by PFA fixation and stained with anti-V5 and anti- $\alpha$ -tubulin antibodies. Sequential images of various stages of cell division (a – e) showing the single channel images for CK1.2-V5, H and  $\alpha$ -tubulin signals, the merged images showing CK1.2-V5 (green), H (blue) and  $\alpha$ -tubulin (red) signals, and the transmission image (Trans). Scale bar, 2  $\mu\text{m}$ . These pictures are single stacks extracted from deconvolved confocal stacks corrected for chromatic aberration.

(C) Dot plots showing Pearson's covariation coefficients for different combination of signals in the entire mitotic spindle region and in a reduced mitotic spindle region containing also CK1.2-V5 signal. For both regions, CK1.2-V5 signal was compared with  $\alpha$ -tubulin (TUB) or Hoechst 33342 (H). The signal of TUB was also compared with H. Pearson's covariation coefficients were measured from  $n=7$  different confocal stacks which were deconvolved and corrected for chromatic aberration with Huygens Professional software. The plot was generated with GraphPad Prism software and the mean values are represented with red bold segments.

**Fig. 6: CK1.2 and Hsp90 co-localise to the flagellar pocket neck**

(A) IFA pictures of *LdBob* pLEXSY-CK1.2-V5 promastigotes obtained after detergent treatment followed by PFA fixation and stained with anti-V5 and anti-*LdHsp90* antibodies targeting CK1.2-V5 and Hsp90, respectively. (a and b) The left panel shows the transmission

images merged with (a) Hoechst 33342 (H, blue) and CK1.2-V5 (green) signals, or (b) with H (blue) and Hsp90 (red) signals. The left panel in (c) shows a merged image of H (blue) with CK1.2-V5 (green) and Hsp90 (red) signals. The right panels show a magnification of the flagellar pocket and basal body region (white square) for their respective left panel. Scale bar, 2  $\mu\text{m}$ . These pictures are single stacks extracted from deconvolved confocal stacks corrected for chromatic aberration.

(B) Dot plots showing Pearson's covariation coefficients for CK1.2-V5 and Hsp90 signals at the FPN or in the whole parasite region (WP). Pearson's covariation coefficients were measured from  $n=7$  different confocal stacks, which were deconvolved and corrected for chromatic aberration with Huygens Professional software. The plot was generated with GraphPad Prism software and the mean values are represented with red bold segments.

(C) 3D-reconstruction of the anterior end of the parasite body from image (A) panel (c) (white rectangle region), showing CK1.2-V5 signal (green) merged with Hsp90 (red) and H (blue). All confocal stacks containing the parasite were used for this picture.

See also Figure S3.

**Fig. 7: Hsp70 co-localises with CK1.2 to the flagellum, to the flagellar tip and to the basal body**

(A) IFA pictures of *LdBob* pLEXSY-CK1.2-V5 promastigotes obtained after detergent treatment followed by PFA fixation and stained with anti-Hsp70 and anti-V5 (CK1.2-V5) antibodies and Hoechst 33342 (the nucleus, H). Single channel images show Hsp70, H and CK1.2-V5 signals, and the transmission image (Trans). The merged image contains CK1.2-V5 (green) signal with Hsp70 (red) and H (blue) signals. Region (1) shows a magnification of the flagellum (white square region) of the merged panel. The pictures are maximum intensity projection (MIP) of the confocal stacks containing the parasites, after removal of the stacks in

contact with the glass coverslip. Confocal stacks were deconvolved and corrected for chromatic aberration. Scale bar, 2  $\mu\text{m}$ . The white arrow highlights Hsp70 and CK1.2 signal to the flagellar tip.

(B) Dot plots showing Pearson's covariation coefficients for CK1.2-V5 and Hsp70 signals in the flagellar tip, flagellar pocket, basal body regions or the whole parasite region. Pearson's covariation coefficients were measured from  $n=10$  different confocal stacks which were deconvolved and corrected for chromatic aberration with Huygens Professional software. The plot was generated with GraphPad Prism software and the mean values are represented with red bold segments.

(C) *In vitro* kinase assay Hsp70.

HSP70 was incubated with or without rCK1.2 and with rCK1.2 + D4476 (CK1 inhibitor) in presence of buffer C and  $\gamma\text{-}^{32}\text{P}\text{-ATP}$ . Kinase assays were performed at  $30^\circ\text{C}$  for 30 min and reaction samples were separated by SDS-PAGE, gels were stained by Coomassie (right panel), and signals were revealed by autoradiography (left panel). The position of marker proteins is indicated at the left, the positions of CK1.2 and HSP70 are indicated on the right. Results are representative of two independent experiments.

### **Fig. 8: CK1.2 localisation in amastigotes**

(A and B) IFA of *LdBob* pLEXSY-CK1.2-V5 axenic amastigotes, fixed with PFA (A) or obtained after detergent treatment (B) and stained with anti-V5 antibody (CK1.2-V5). The single channel images show CK1.2-V5 and Hoechst 33342 (H) signals, and the transmission image (Trans). The merged image contains CK1.2-V5 (green) signal with H (blue) signal. Scale bar, 2  $\mu\text{m}$ . The pictures are maximum intensity projection (MIP) of the confocal stacks

containing the parasites. Confocal stacks were deconvolved and corrected for chromatic aberration.

(C) IFA of *Ld*Bob pLEXSY-CK1.2-V5 axenic amastigotes obtained after detergent treatment followed by PFA fixation and stained with anti-V5, anti-centrin 4 or anti-IFT172 antibodies. The single channel images show CK1.2-V5, Hoechst 33342 (H), centrin 4 (CEN) or IFT172 signals and the transmission image (Trans). The merged images are combinations of different channels showing H, CK1.2-V5, CEN and IFT172, as written on the images. Scale bar, 2  $\mu$ m. These pictures are single stacks extracted from deconvolved confocal stacks corrected for chromatic aberration.

(D) 3D-reconstruction of the flagellar pocket region and its neck from image (C), which has been rotated, showing CK1.2-V5 signal (green) merged with CEN (red) and IFT172 (blue). All confocal stacks containing the parasite were used for this picture.

**Fig. 9: The C-terminal domain of CK1.2 is essential for its localisation to specific organelles, but not for its activity**

(A) Cartoon representing the domain structure of *Lm*CK1.2 (GenBank: CBZ38008.1). The protein structure contains a kinase domain (yellow) and a C-terminal tail with two low complexity regions (LCR) (purple). The cartoon also shows a schematic representation of three domain-deletion mutants: CK1.2 $\Delta$ C10, CK1.2 $\Delta$ C43 and CK1.2 $\Delta$ N7.

(B) *In vitro* kinase assay using recombinant thio-CK1.2-V5 (WT, 55.9 kDa) and the truncated kinase mutants thio-CK1.2- $\Delta$ C10-V5 ( $\Delta$ C10, 54.9 kDa), thio-CK1.2- $\Delta$ C43-V5 ( $\Delta$ C43, 52.1 kDa) and thio-CK1.2- $\Delta$ N7-V5 ( $\Delta$ N7, 55.2 kDa). Results are representative of three independent experiments. Purified proteins were incubated with MBP as substrate, with or without CK1.2 canonical inhibitor D4476. Kinase assays were performed at the same time for 30 min at pH 7.5 and 30°C and reaction samples were separated by SDS-PAGE, gels were stained by

Coomassie (bottom), and signals were revealed by autoradiography (top). The brackets indicate auto-phosphorylation (Auto-P) and the arrows substrate phosphorylation (MBP-P) signals. MW= Molecular Weight.

(C) Western blot analysis. Proteins were extracted from *LdBob* pLEXSY-CK1.2-V5 (WT, 42.8 kDa) or expressing truncated kinase mutants *LdBob* pLEXSY-CK1.2- $\Delta$ C10-V5 ( $\Delta$ C10, 41.8 kDa), *LdBob* pLEXSY-CK1.2- $\Delta$ C43-V5 ( $\Delta$ C43, 39.0 kDa) and *LdBob* pLEXSY-CK1.2- $\Delta$ N7-V5 ( $\Delta$ N7, 42.1 kDa) in logarithmic phase promastigotes. Twenty micrograms were analysed by Western blotting (WB) using the anti-V5 antibody ( $\alpha$ -V5) (top panel). The Coomassie-stained membrane of the blot is included as a loading control (bottom panel). MW= Molecular Weight. The blot is representative of three independent experiments.

(D) Logarithmic phase promastigotes from the same cell lines as in (C) were treated by the proteasome inhibitor MG132 (a) or by ammonium chloride (NH<sub>4</sub>Cl), an inhibitor of lysosomal degradation (b), for 18h. Proteins from treated and untreated control were extracted and twenty micrograms were analysed by Western blotting (WB) using the anti-V5 antibody ( $\alpha$ -V5) (top panel). The Coomassie-stained membrane of the blot is included as a loading control (bottom panels). MW= Molecular Weight. The blots are representative of three independent experiments.

(E) Measurement of the sum of fluorescence intensity extracted from ROI of the promastigote parasite bodies in the mock, wild type and three domain-deletion mutants (same cell lines as in (C)). Scatter dot plots showing the sum fluorescence intensity (for the V5 signal) in the different cell lines in PFA-fixed (a) or detergent-treated (b) parasites. Data originates from n=54 (Mock, PFA), n=88 (WT, PFA), n=63 ( $\Delta$ C10, PFA), n=80 ( $\Delta$ C43, PFA), n=68 ( $\Delta$ N7, PFA), n=62 (Mock, det. treated), n=77 (WT, det. treated), n=55 ( $\Delta$ C10, det. treated), n=78 ( $\Delta$ C43, det. treated) and n=74 ( $\Delta$ N7, det. treated). The mean values and the 95% confidence intervals are

indicated with bold segments. Statistically significant differences are indicated with two ( $p < 0.01$ ), three ( $p < 0.001$ ) or four asterisks ( $p < 0.0001$ ). ns. = non-significant.

See also Figure S5.

## 1.9. Figures

Figure 1

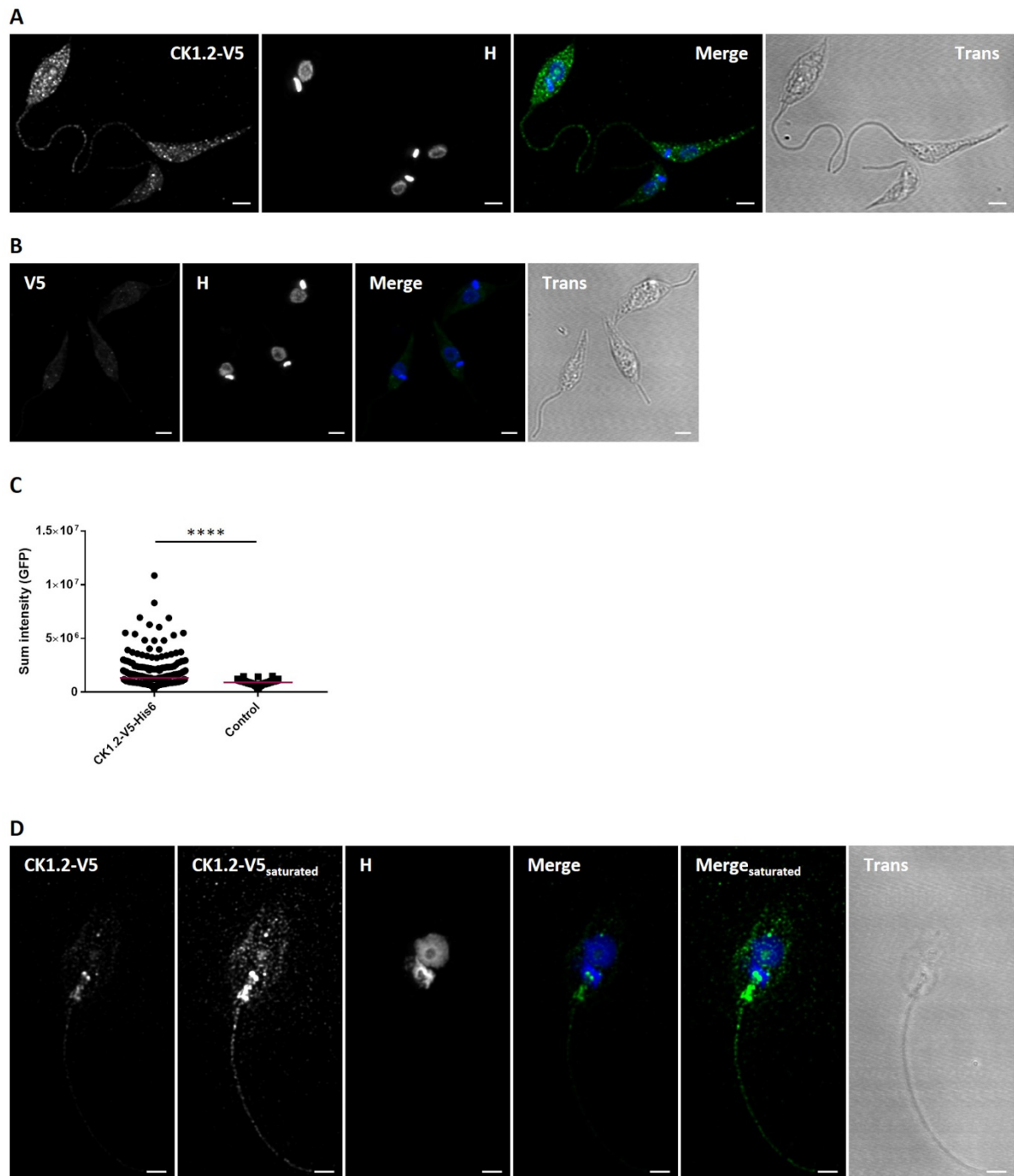


Figure 2

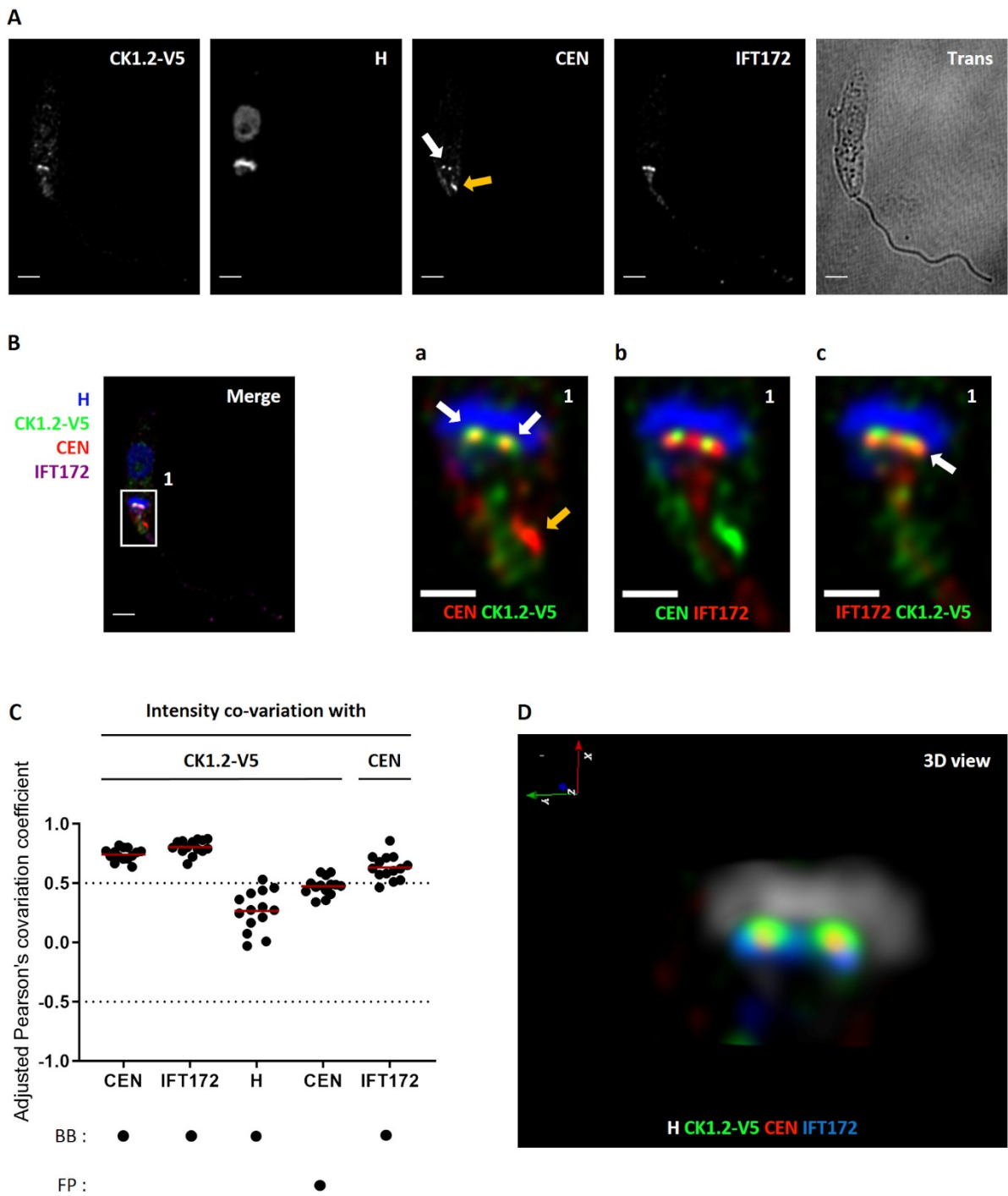
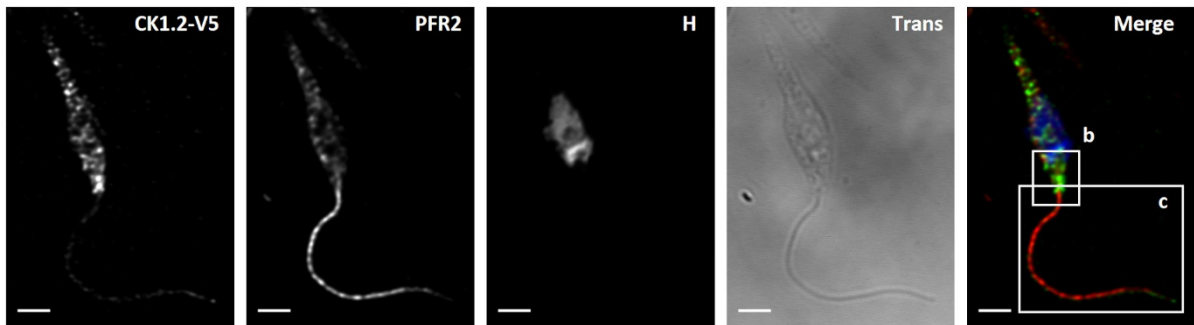


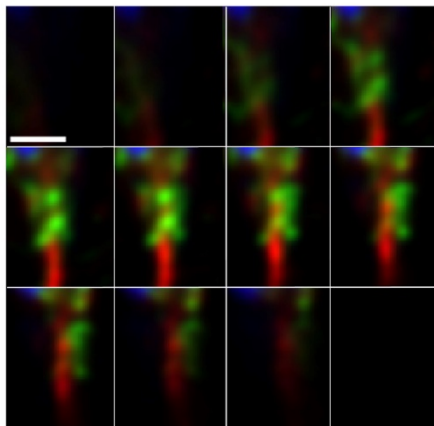
Figure 3

A

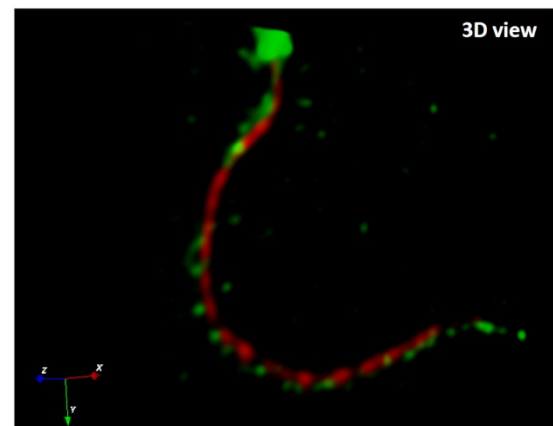
a



b



c



B

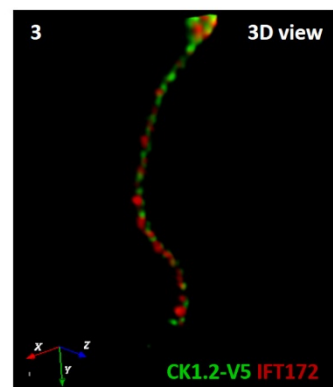
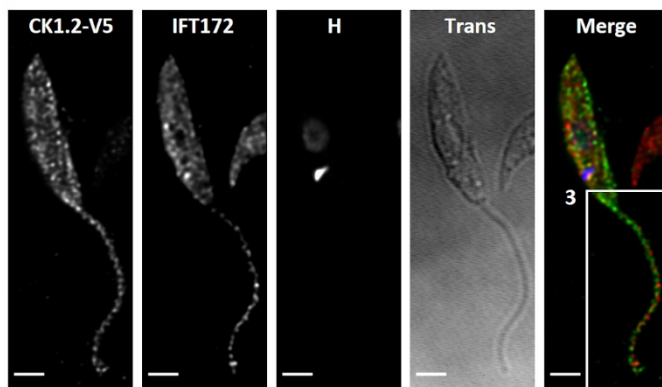


**Figure 4**

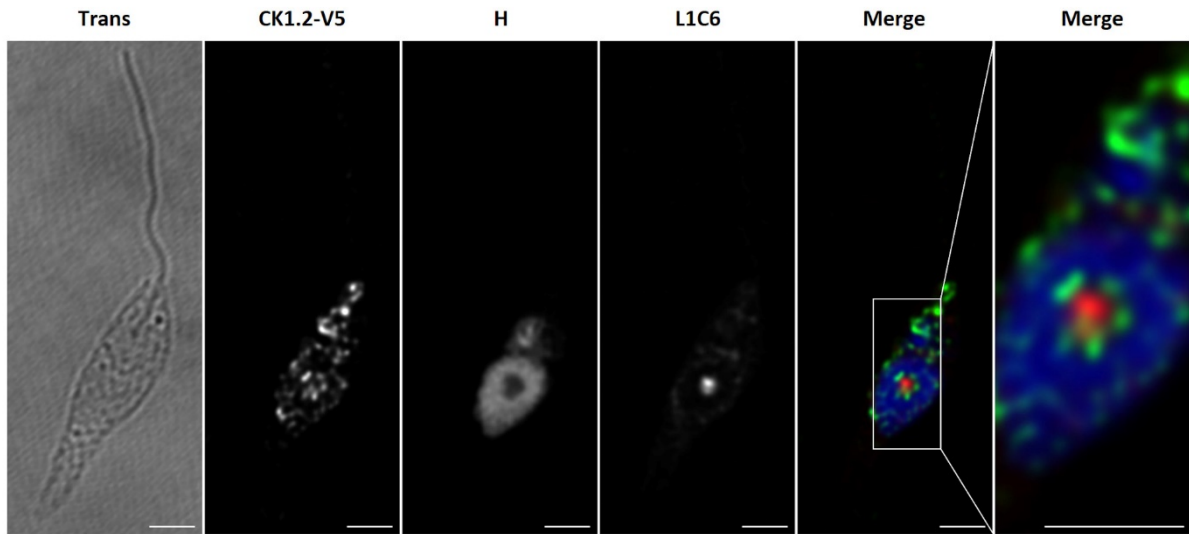
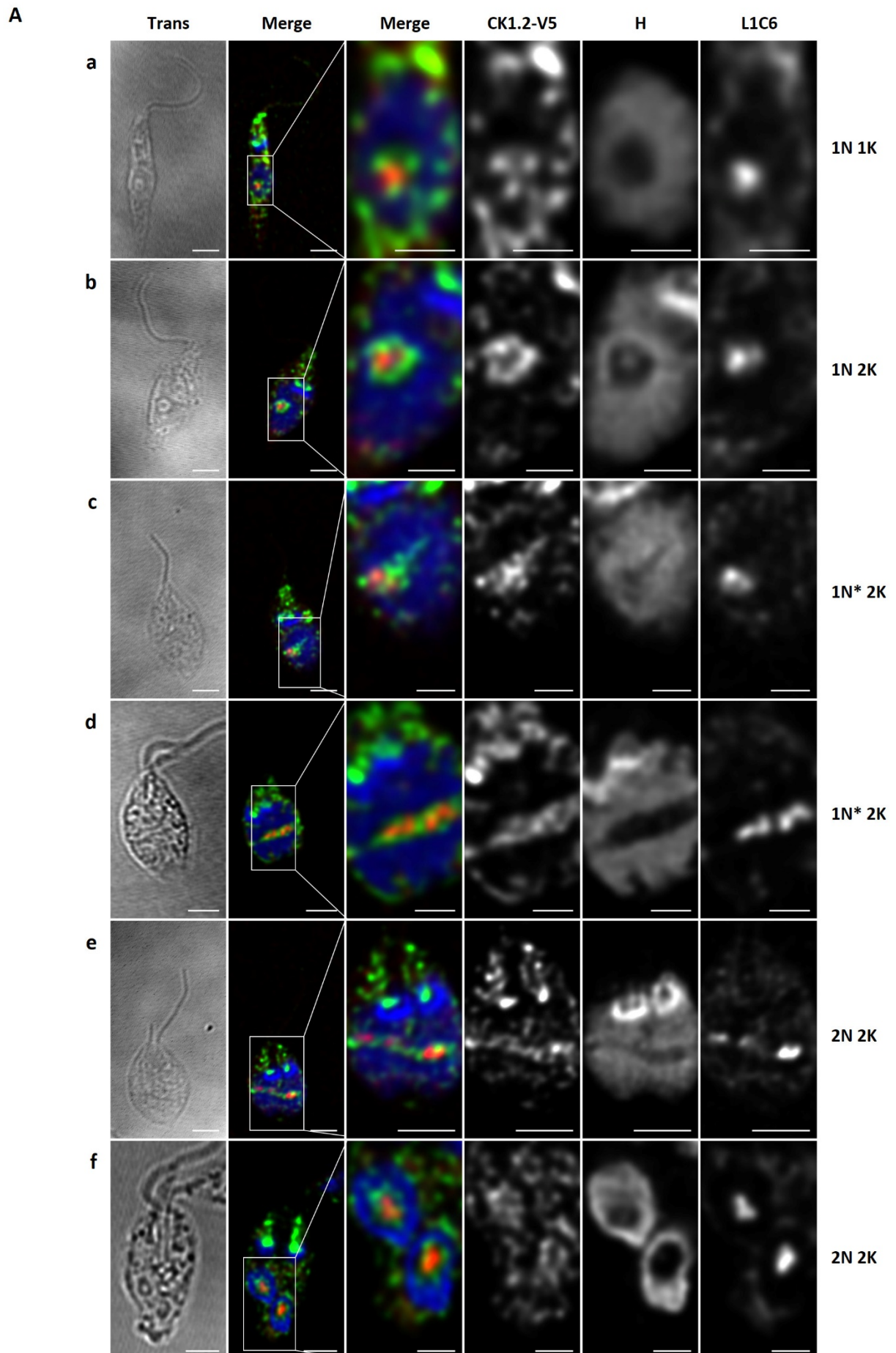
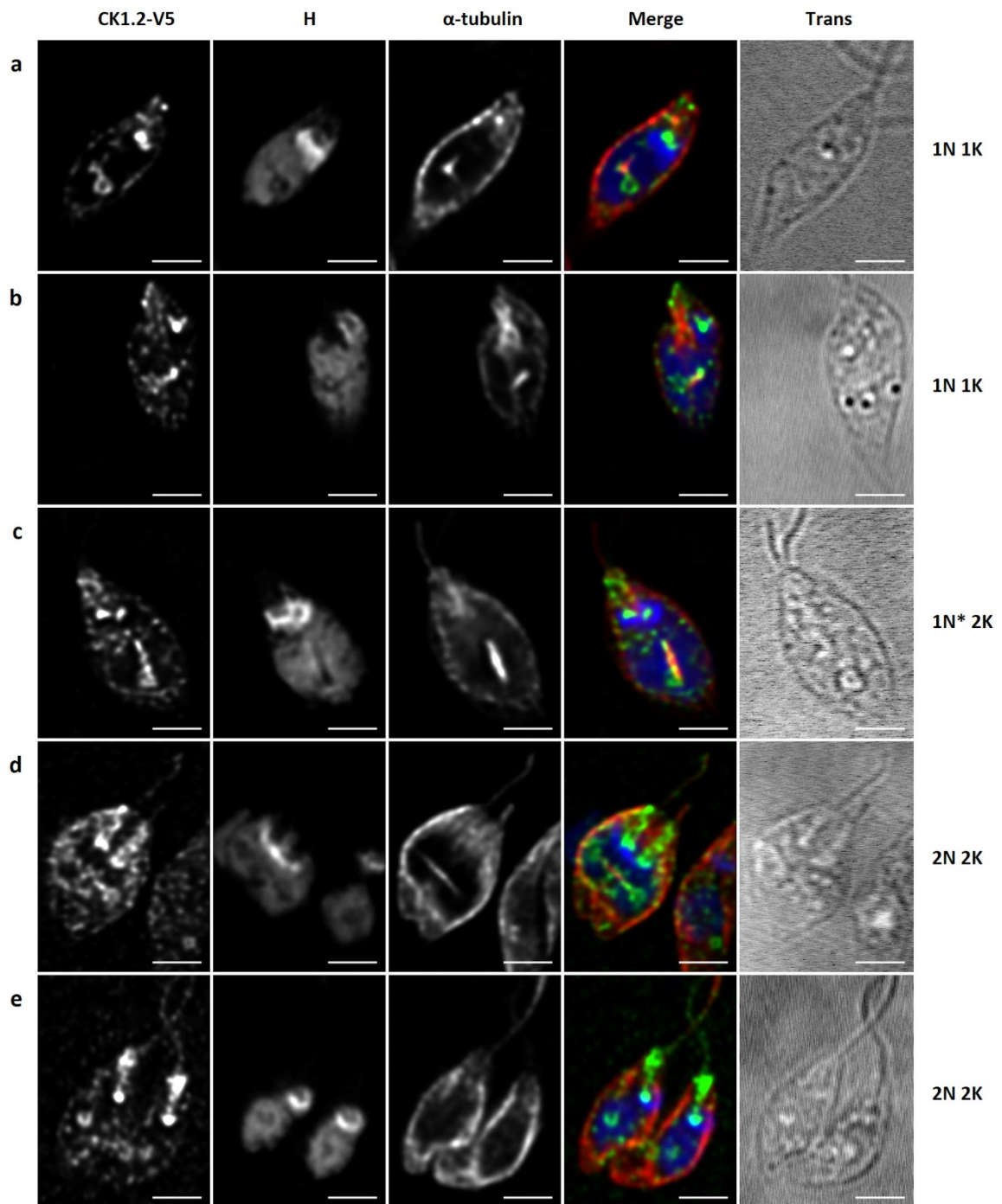


**Figure 5**



B



C

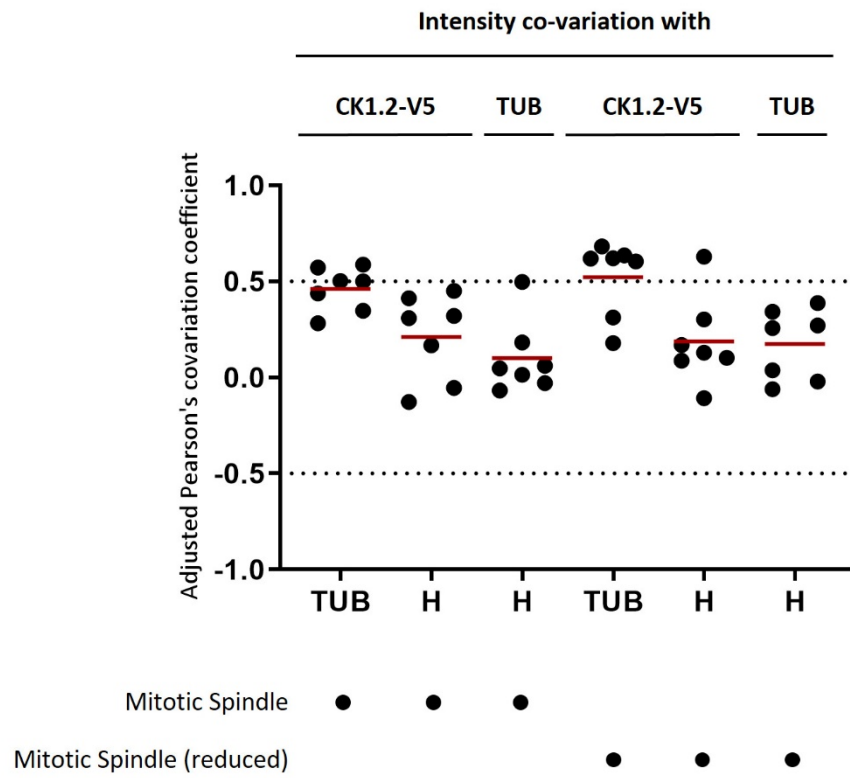


Figure 6

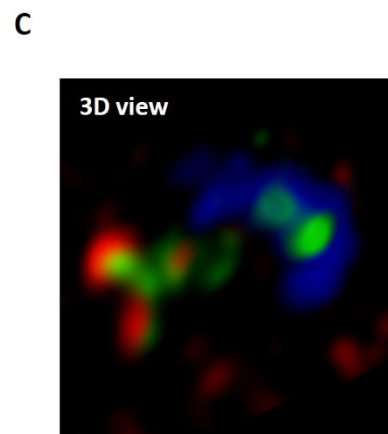
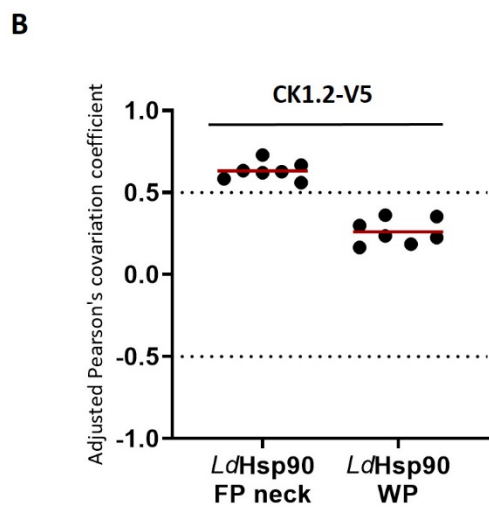
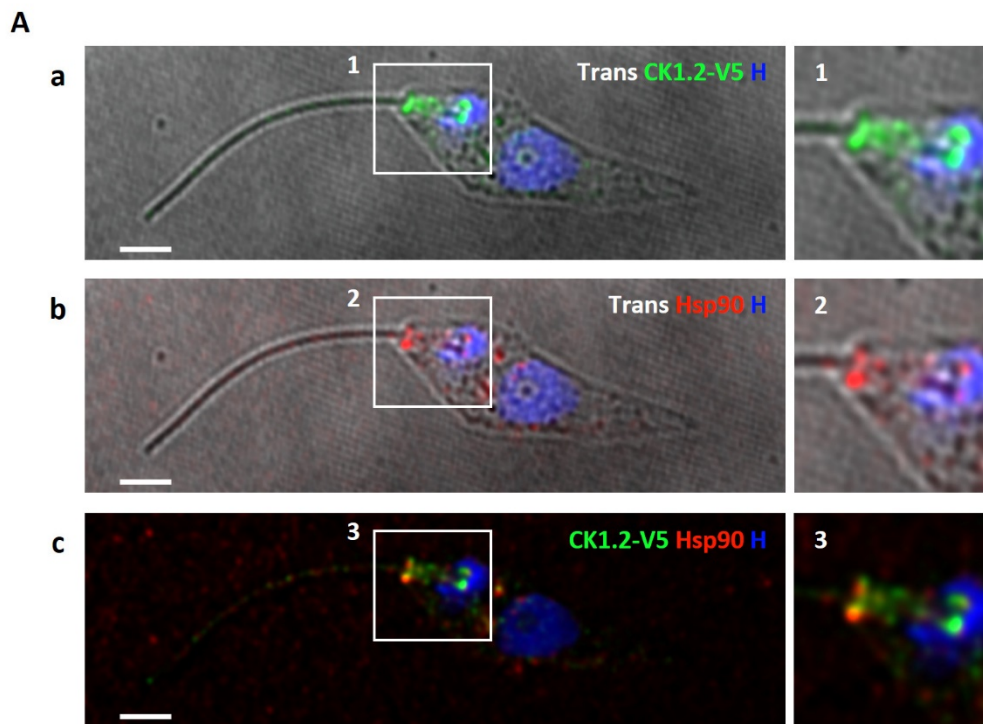


Figure 7

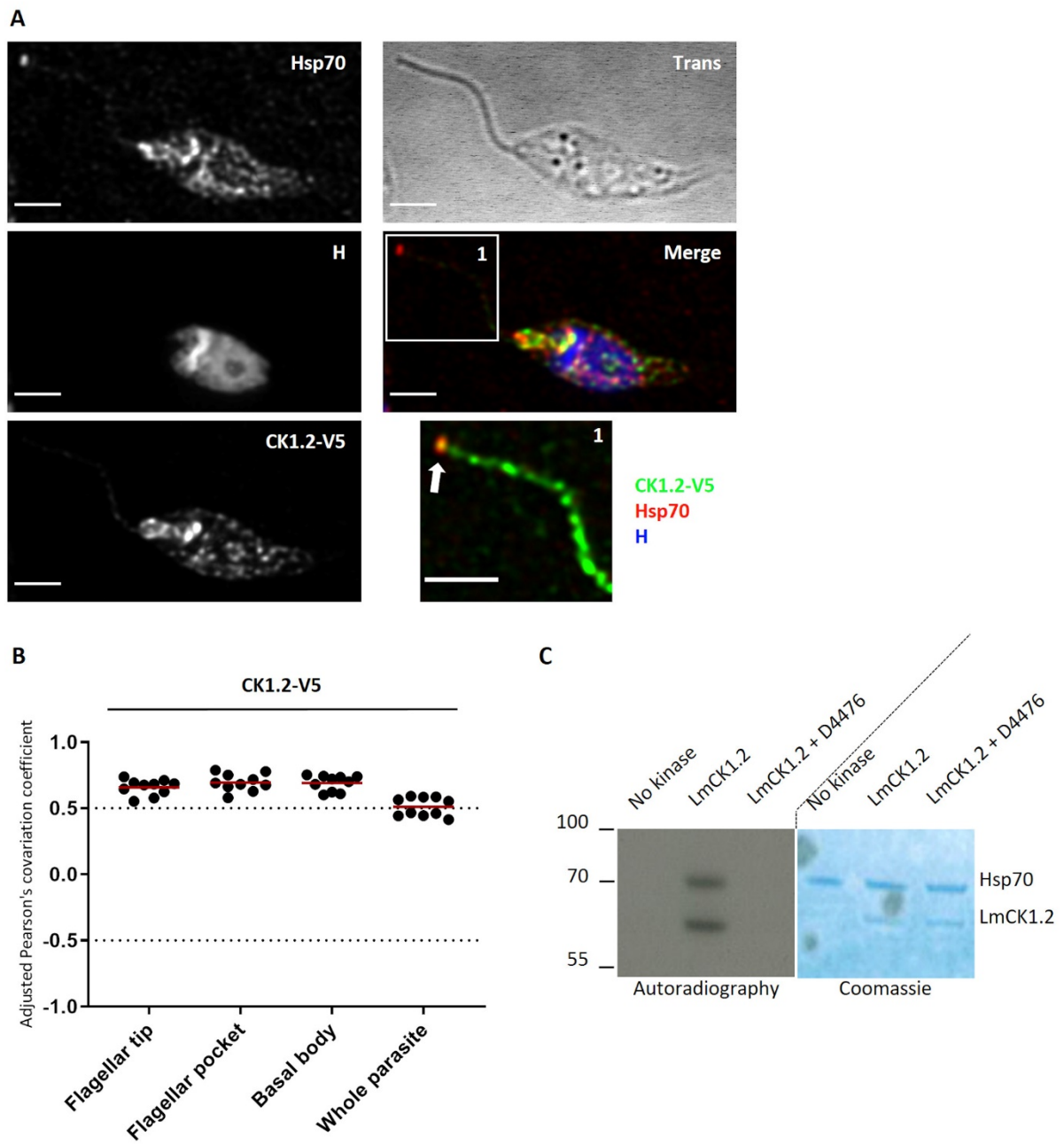


Figure 8

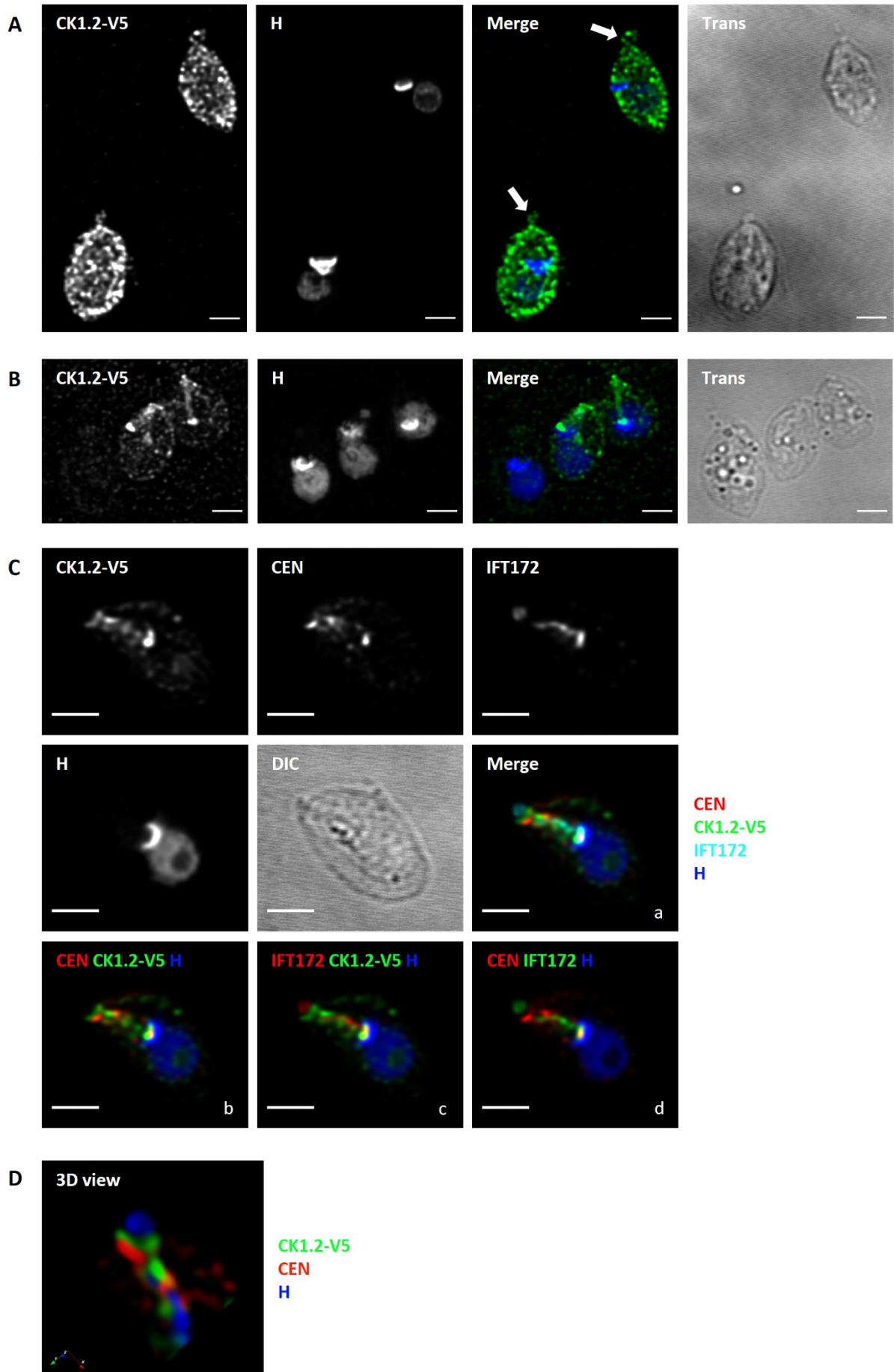
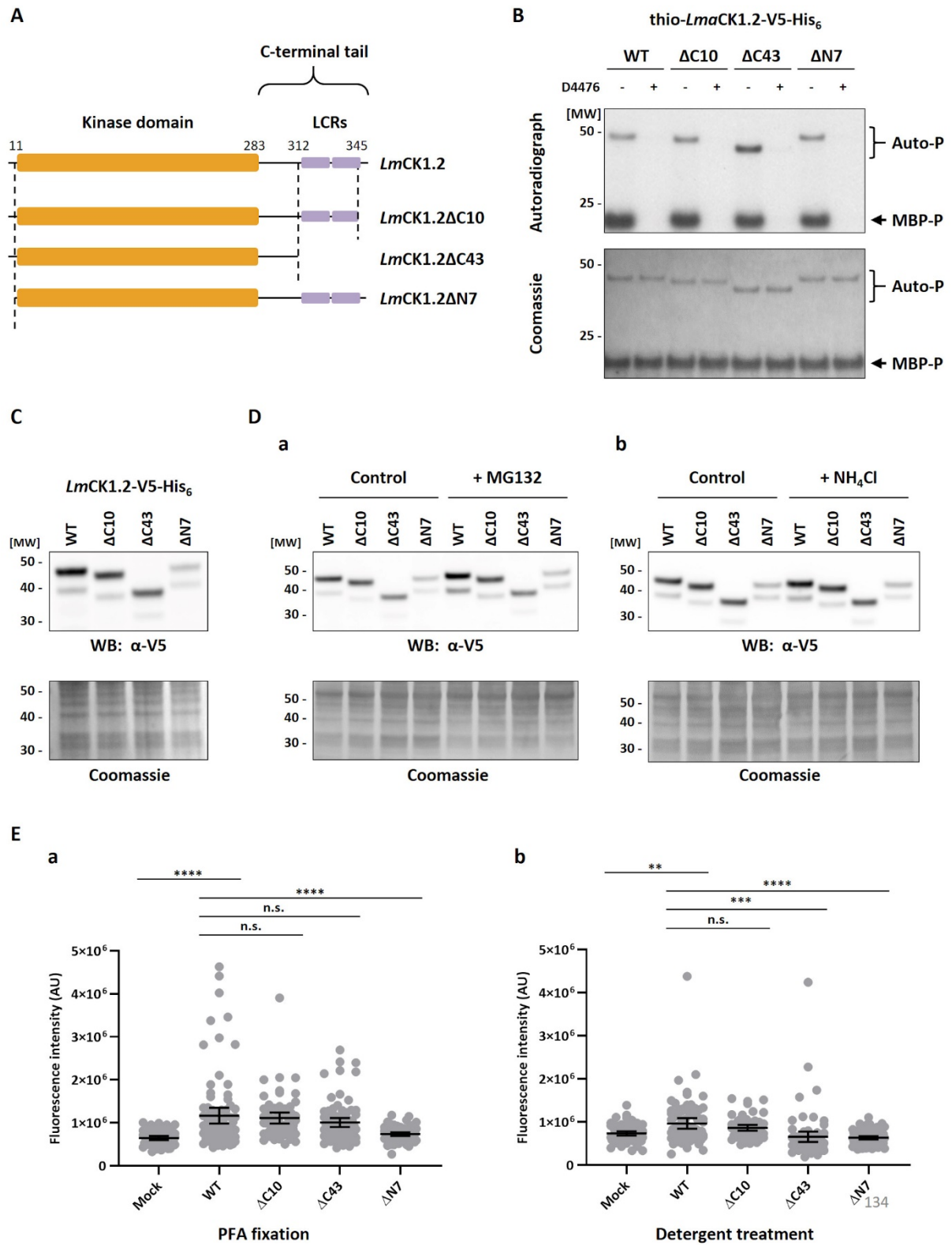


Figure 9



## 1.10. Supplemental figure legends

### **Fig. S1: CK1.2-V5 localisation in methanol-fixed promastigotes, Related to Fig. 1**

(A and B) IFA of *LdBob* pLEXSY-CK1.2-V5 (A) and *LdBob* pLEXSY (mock) (B) promastigotes, fixed in ice-cold methanol for 3 minutes and stained with anti-V5 antibody to detect CK1.2-V5 localisation. The epifluorescence images were acquired under the same conditions and show the anti-V5 staining (CK1.2-V5 or V5), Hoechst 33342 staining (H), a merge of the anti-V5 (green) and H (red) signals and the transmission image (Trans). Scale bar, 5  $\mu\text{m}$ . The pictures are maximum intensity projection (MIP) of the stacks containing the parasites.

### **Fig. S2: Centrin 4 localisation to a single basal body, Related to Fig. 2**

(A) IFA of *LdBob* pLEXSY-CK1.2-V5 promastigotes obtained after detergent treatment followed by PFA fixation and stained with anti-V5, anti-centrin 4 antibodies. The single channel images show centrin 4 (CEN) and Hoechst 33342 (H) signals and the transmission image (Trans). The merged images show CEN (red) signal with H (green) or the transmission image. The single basal body (1 bb) is highlighted with a white arrow. Scale bar, 2  $\mu\text{m}$ . These pictures are single stacks extracted from deconvolved confocal stacks corrected for chromatic aberration.

(B) Video of the 3D-reconstruction of the basal body region (from Figure 2b), sequentially showing Hoechst 33342 (H, white) signal with IFT172 (blue), centrin 4 (CEN, red) and CK1.2-V5 (green) signals. All confocal stacks containing the parasite were used to generate this reconstruction. 3D-reconstruction generated by the 3D VTK viewer. The video was recorded with Video recorder plugin from ICY software (icy, RRID:SCR010587).

**Fig. S3: Hsp90 localisation, Related to Fig. 6**

(A) IFA of *LdBob* pLEXSY-CK1.2-V5 promastigotes fixed with PFA without detergent treatment, and stained with anti-*LdHsp90* antibody to detect Hsp90 localisation. The single channel images show Hsp90 and Hoechst 33342 (H) signals and the transmission image (Trans). The merged channel shows Hsp90 (red) and H (blue) signals. Scale bar, 2  $\mu\text{m}$ . These pictures are single stacks extracted from deconvolved confocal stacks corrected for chromatic aberration.

(B) Video of the 3D-reconstruction of the flagellar pocket neck (from Figure 6Ac) in rotation, showing CK1.2-V5 signal (green) merged with Hsp90 (red). All confocal stacks containing the parasite were used for this picture. 3D-reconstruction generated by the 3D VTK viewer and a 360° rotation was generated by 3D Rotation plugin from ICY software (icy, RRID:SCR010587).

**Fig. S4: Hsp70 localisation, Related to Fig. 7**

IFA of *LdBob* pLEXSY-CK1.2-V5 promastigotes fixed with PFA without detergent treatment, and stained with anti-Hsp70 antibody. The single channel images show Hsp70 and Hoechst 33342 (H) signals and the transmission image (Trans). The merged channel shows Hsp70 (red) and H (blue) signals. Scale bar, 2  $\mu\text{m}$ . These pictures are single stacks extracted from deconvolved confocal stacks corrected for chromatic aberration.

**Fig. S5: Inhibition of proteasomal and lysosomal degradation, Related to Fig. 9**

(A) Verification of the accumulation of ubiquitinated proteins upon proteasome inhibition. Logarithmic phase promastigotes from *LdBob* pLEXSY-CK1.2-V5 (WT) or expressing truncated kinase mutants *LdBob* pLEXSY-CK1.2- $\Delta$ C10-V5 ( $\Delta$ C10), *LdBob* pLEXSY-CK1.2- $\Delta$ C43-V5 ( $\Delta$ C43) and *LdBob* pLEXSY-CK1.2- $\Delta$ N7-V5 ( $\Delta$ N7) were treated with the

proteasome inhibitor MG132 for 18h. Proteins from treated and untreated samples were extracted and twenty micrograms were analysed by Western blotting using the mono- and poly-ubiquitinated conjugates monoclonal (FK2) antibody ( $\alpha$ -Ubiquitin) (left panel). The Coomassie-stained membrane of the blot is included as a loading control (right panel). MW= Molecular Weight. The blot is representative of two independent experiments.

(B) Logarithmic phase promastigotes from *LdBob* pLEXSY-CK1.2-V5 (WT) or expressing truncated kinase mutants *LdBob* pLEXSY-CK1.2- $\Delta$ C10-V5 ( $\Delta$ C10), *LdBob* pLEXSY-CK1.2- $\Delta$ C43-V5 ( $\Delta$ C43) and *LdBob* pLEXSY-CK1.2- $\Delta$ N7-V5 ( $\Delta$ N7) were treated with ammonium chloride for 18h to inhibit the lysosomal degradation. Untreated parasites were used as control. Lysosomes of the parasites were then stained with 100 mM LysoTracker™ Red DND-99 for 30 min at 26°C. Mean fluorescence intensity of the LysoTracker accumulation in lysosomes was measured by flow cytometry in treated (black) and untreated (grey) parasites for ~15000 parasites. The data are representative of two independent experiments. The graph was generated with GraphPad Prism software.

**Fig. S6: Protocol for automatic segmentation of parasite bodies, Related to Fig. 1**

Screenshot of the protocol applied on the epifluorescence images to analyse diverse parameters of the parasite body of *LdBob* pLEXSY-CK1.2-V5, mock or domain-deleted mutants, stained with the anti-V5 antibody to detect CK1.2-V5 localisation. Protocol is a graphical programming plugin in Icy software (Icy, RRID:SCR010).

## 1.11. Supplemental figures

Figure S1

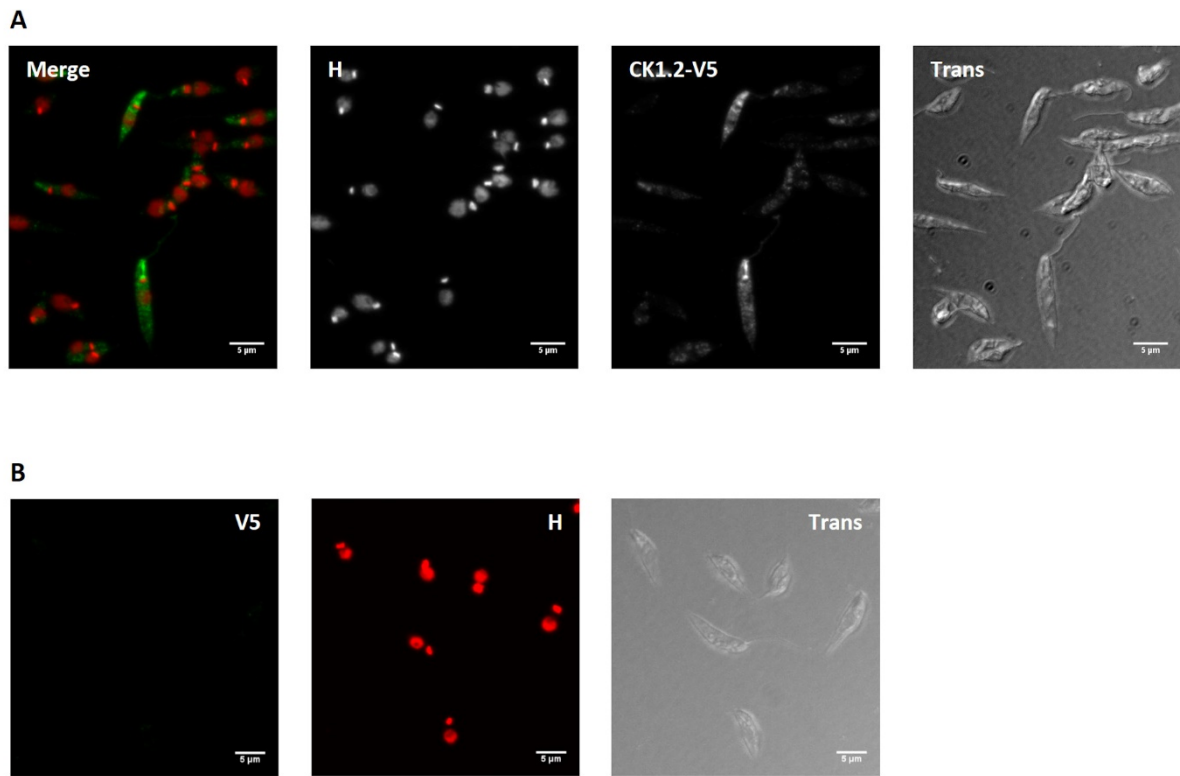
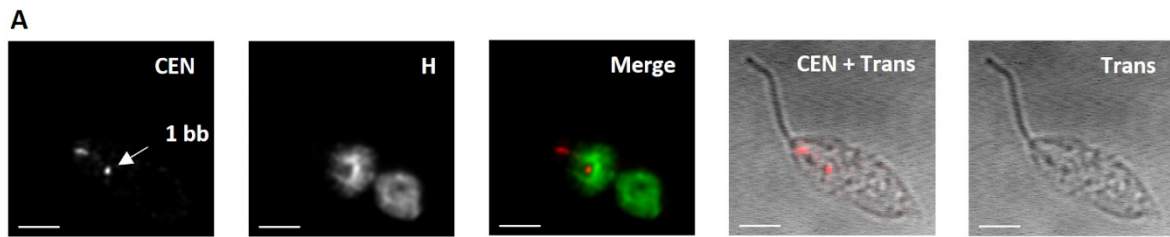


Figure S2



**B**

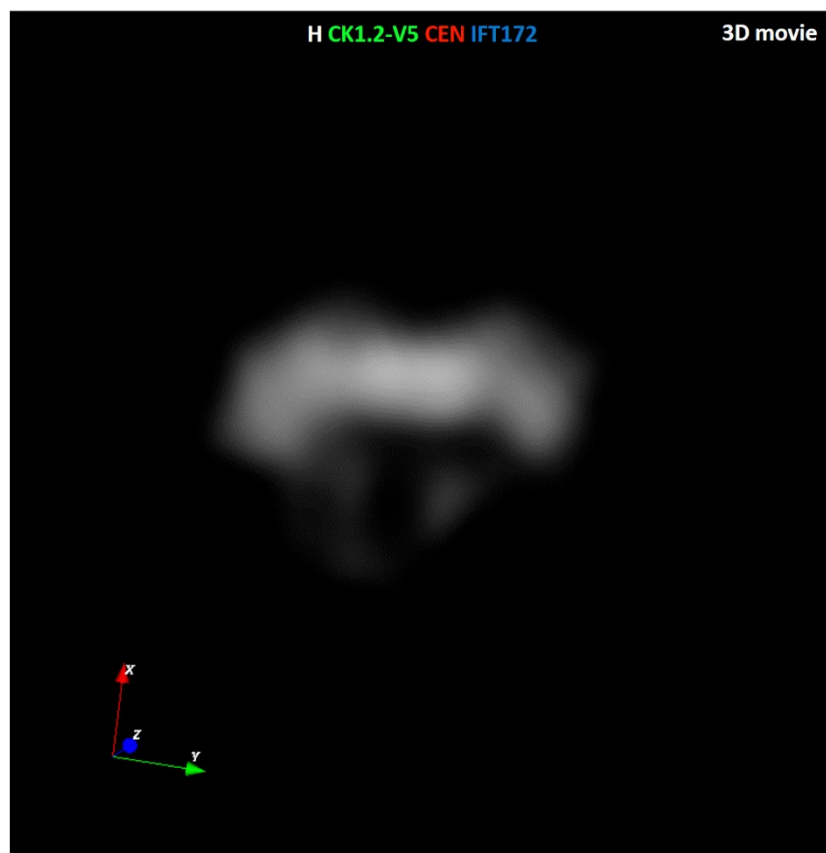


Figure S3

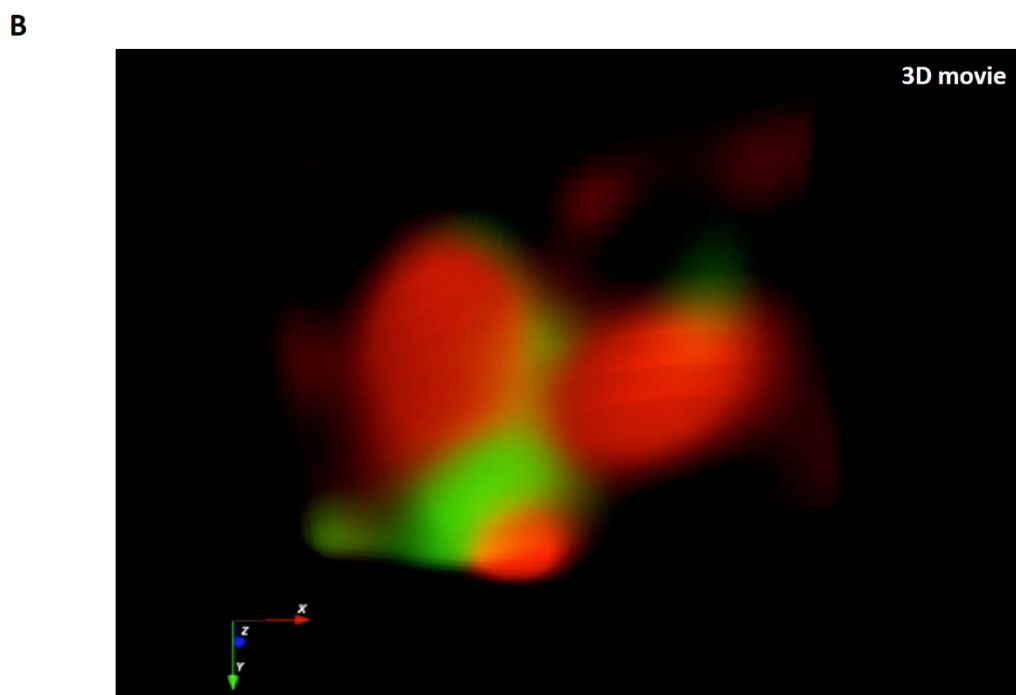
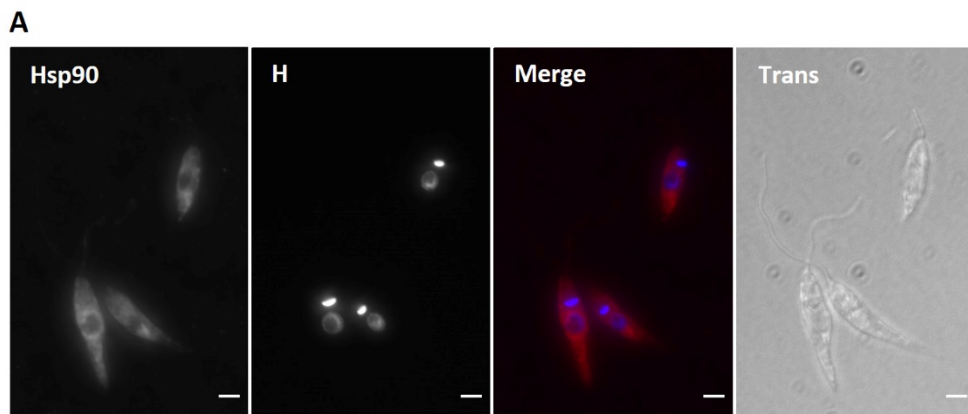


Figure S4

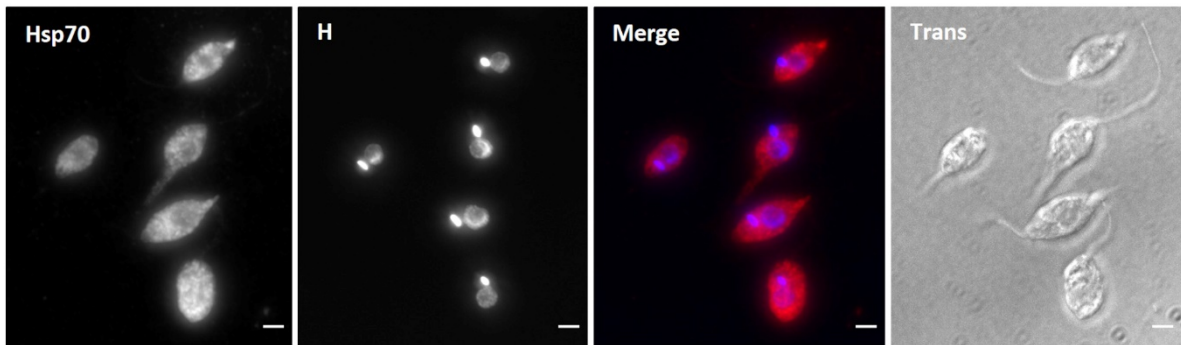


Figure S5

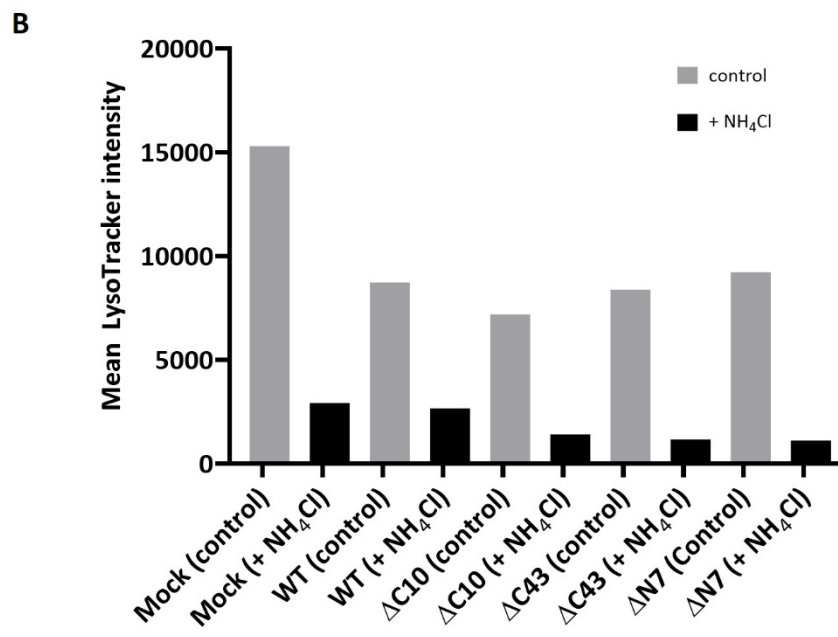
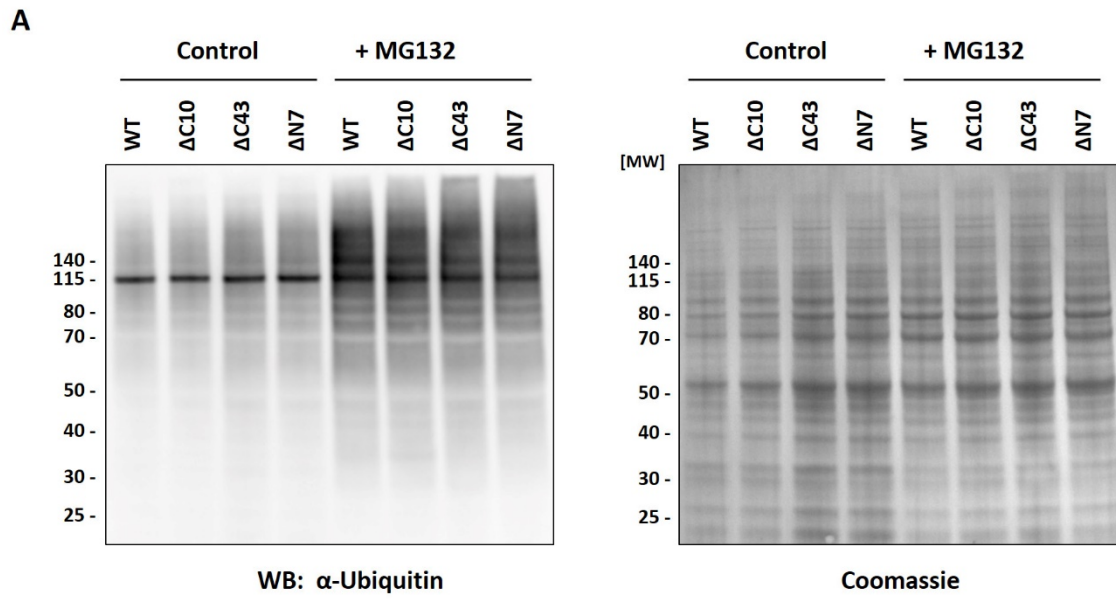
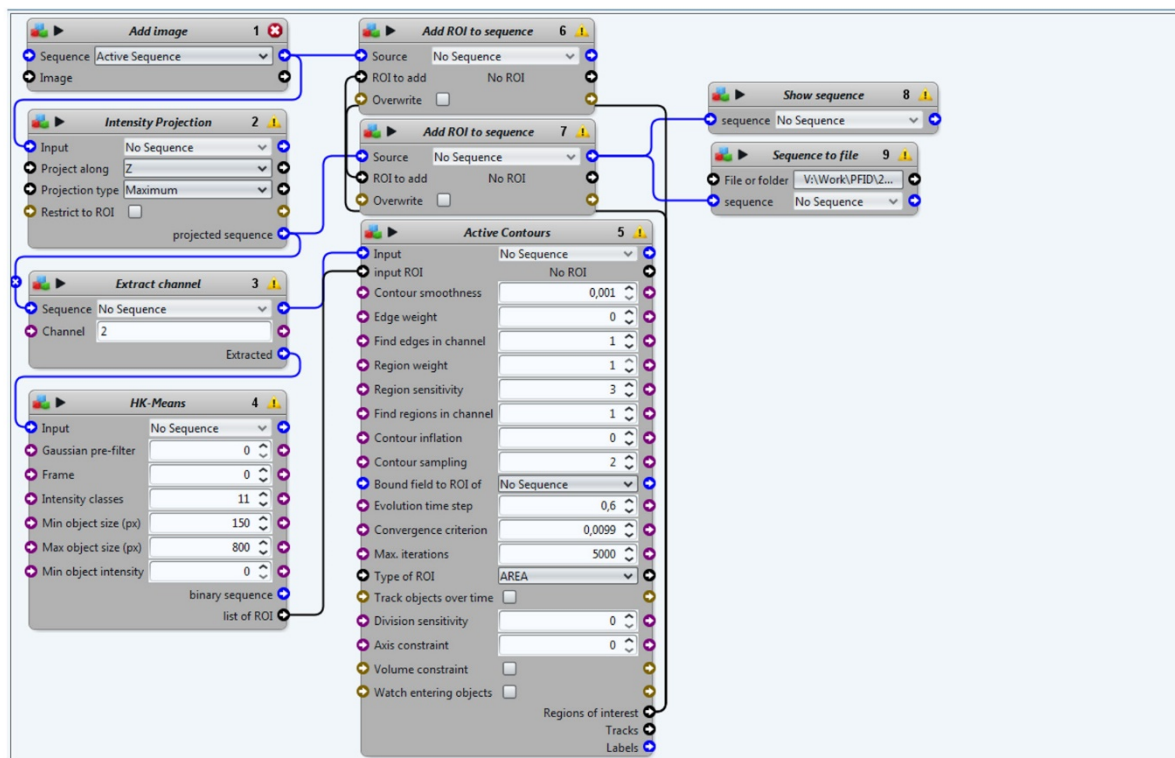


Figure S6



## 1.12. References

1. Knippschild, U., Kruger, M., Richter, J., Xu, P., Garcia-Reyes, B., Peifer, C., Halekotte, J., Bakulev, V., and Bischof, J. (2014). The CK1 Family: Contribution to Cellular Stress Response and Its Role in Carcinogenesis. *Frontiers in oncology* *4*, 96.
2. Knippschild, U., Gocht, A., Wolff, S., Huber, N., Lohler, J., and Stoter, M. (2005). The casein kinase 1 family: participation in multiple cellular processes in eukaryotes. *Cell Signal* *17*, 675-689.
3. Schitteck, B., and Sinnberg, T. (2014). Biological functions of casein kinase 1 isoforms and putative roles in tumorigenesis. *Mol Cancer* *13*, 231.
4. Jiang, S., Zhang, M., Sun, J., and Yang, X. (2018). Casein kinase 1alpha: biological mechanisms and theranostic potential. *Cell Commun Signal* *16*, 23.
5. Dorin-Semblat, D., Demarta-Gatsi, C., Hamelin, R., Armand, F., Carvalho, T.G., Moniatte, M., and Doerig, C. (2015). Malaria Parasite-Infected Erythrocytes Secrete PfCK1, the Plasmodium Homologue of the Pleiotropic Protein Kinase Casein Kinase 1. *PloS one* *10*, e0139591.
6. Rachidi, N., Taly, J.F., Durieu, E., Leclercq, O., Aulner, N., Prina, E., Pescher, P., Notredame, C., Meijer, L., and Spath, G.F. (2014). Pharmacological assessment defines the *Leishmania donovani* casein kinase 1 as a drug target and reveals important functions in parasite viability and intracellular infection. *Antimicrob Agents Chemother* *58*.
7. Silverman, J.M., and Reiner, N.E. (2010). Exosomes and other microvesicles in infection biology: organelles with unanticipated phenotypes. *Cell Microbiol* *13*, 1-9.
8. Jayaswal, S., Kamal, M.A., Dua, R., Gupta, S., Majumdar, T., Das, G., Kumar, D., and Rao, K.V. (2010). Identification of host-dependent survival factors for intracellular *Mycobacterium tuberculosis* through an siRNA screen. *PLoS pathogens* *6*, e1000839.
9. Xia, C., Wolf, J.J., Vijayan, M., Studstill, C.J., Ma, W., and Hahm, B. (2018). Casein Kinase 1alpha Mediates the Degradation of Receptors for Type I and Type II Interferons Caused by Hemagglutinin of Influenza A Virus. *J Virol* *92*.

10. Greer, Y.E., Westlake, C.J., Gao, B., Bharti, K., Shiba, Y., Xavier, C.P., Pazour, G.J., Yang, Y., and Rubin, J.S. (2014). Casein kinase 1delta functions at the centrosome and Golgi to promote ciliogenesis. *Molecular biology of the cell* 25, 1629-1640.
11. Greer, Y.E., and Rubin, J.S. (2011). Casein kinase 1 delta functions at the centrosome to mediate Wnt-3a-dependent neurite outgrowth. *J Cell Biol* 192, 993-1004.
12. Sillibourne, J.E., Milne, D.M., Takahashi, M., Ono, Y., and Meek, D.W. (2002). Centrosomal anchoring of the protein kinase CK1delta mediated by attachment to the large, coiled-coil scaffolding protein CG-NAP/AKAP450. *Journal of Molecular Biology* 322, 785-797.
13. Peng, Y., Moritz, M., Han, X., Giddings, T.H., Lyon, A., Kollman, J., Winey, M., Yates, J., 3rd, Agard, D.A., Drubin, D.G., et al. (2015b). Interaction of CK1delta with gammaTuSC ensures proper microtubule assembly and spindle positioning. *Molecular biology of the cell* 26, 2505-2518.
14. Brockman, J.L., Gross, S.D., Sussman, M.R., and Anderson, R.A. (1992). Cell cycle-dependent localization of casein kinase I to mitotic spindles. *Proceedings of the National Academy of Sciences* 89, 9454-9458.
15. Gross, S.D., Hoffman, D.P., Fiset, P.L., Baas, P., and Anderson, R.A. (1995). A phosphatidylinositol 4,5-bisphosphate-sensitive casein kinase I alpha associates with synaptic vesicles and phosphorylates a subset of vesicle proteins. *The Journal of Cell Biology* 130, 711-724.
16. Kafadar, K.A., Zhu, H., Snyder, M., and Cyert, M.S. (2003). Negative regulation of calcineurin signaling by Hrr25p, a yeast homolog of casein kinase I. *Genes Dev* 17, 2698-2708.
17. Lusk, C.P., Waller, D.D., Makhnevych, T., Dienemann, A., Whiteway, M., Thomas, D.Y., and Wozniak, R.W. (2007). Nup53p is a target of two mitotic kinases, Cdk1p and Hrr25p. *Traffic* 8, 647-660.
18. Peng, Y., Grassart, A., Lu, R., Wong, C.C.L., Yates, J., 3rd, Barnes, G., and Drubin, D.G. (2015a). Casein kinase 1 promotes initiation of clathrin-mediated endocytosis. *Dev Cell* 32, 231-240.

19. Zhang, B., Shi, Q., Varia, S.N., Xing, S., Klett, B.M., Cook, L.A., and Herman, P.K. (2016). The Activity-Dependent Regulation of Protein Kinase Stability by the Localization to P-Bodies. *Genetics* 203, 1191-1202.
20. Dan-Goor, M., Nasereddin, A., Jaber, H., and Jaffe, C.L. (2013). Identification of a secreted casein kinase 1 in *Leishmania donovani*: effect of protein over expression on parasite growth and virulence. *PloS one* 8, e79287.
21. Silverman, J.M., Clos, J., de'Oliveira, C.C., Shirvani, O., Fang, Y., Wang, C., Foster, L.J., and Reiner, N.E. (2010). An exosome-based secretion pathway is responsible for protein export from *Leishmania* and communication with macrophages. *J Cell Sci* 123, 842-852.
22. Liu, J., Carvalho, L.P., Bhattacharya, S., Carbone, C.J., Kumar, K.G., Leu, N.A., Yau, P.M., Donald, R.G., Weiss, M.J., Baker, D.P., et al. (2009). Mammalian casein kinase 1 $\alpha$  and its leishmanial ortholog regulate stability of IFNAR1 and type I interferon signaling. *Mol Cell Biol* 29, 6401-6412.
23. Martel, D., Beneke, T., Gluenz, E., Späth, G.F., and Rachidi, N. (2017). Characterisation of Casein Kinase 1.1 in *Leishmania donovani* Using the CRISPR Cas9 Toolkit. In *BioMed research international*.
24. Rachidi, N., Taly, J.F., Durieu, E., Leclercq, O., Aulner, N., Prina, E., Pescher, P., Notredame, C., Meijer, L., and Späth, G.F. (2014). Pharmacological assessment defines *Leishmania donovani* casein kinase 1 as a drug target and reveals important functions in parasite viability and intracellular infection. *Antimicrobial Agents and Chemotherapy* 58, 1501-1515.
25. Florimond, C., Sahin, A., Vidilaseris, K., Dong, G., Landrein, N., Dacheux, D., Albisetti, A., Byard, E.H., Bonhivers, M., and Robinson, D.R. (2015). BILBO1 Is a Scaffold Protein of the Flagellar Pocket Collar in the Pathogen *Trypanosoma brucei*. *PLoS pathogens* 11, e1004654.
26. Selvapandiyan, A., Duncan, R., Debrabant, A., Bertholet, S., Sreenivas, G., Negi, N.S., Salotra, P., and Nakhasi, H.L. (2001). Expression of a mutant form of *Leishmania donovani* centrin reduces the growth of the parasite. *J Biol Chem* 276, 43253-43261.

27. Absalon, S., Blisnick, T., Kohl, L., Toutirais, G., Dore, G., Julkowska, D., Tavenet, A., and Bastin, P. (2008). Intraflagellar transport and functional analysis of genes required for flagellum formation in trypanosomes. *Mol Biol Cell* *19*, 929-944.
28. Kohl, L., Sherwin, T., and Gull, K. (1999). Assembly of the Paraflagellar Rod and the Flagellum Attachment Zone Complex During the *Trypanosoma brucei* Cell Cycle. *Journal of Eukaryotic Microbiology* *46*, 105-109.
29. Devaux, S., Kelly, S., Lecordier, L., Wickstead, B., Perez-Morga, D., Pays, E., Vanhamme, L., and Gull, K. (2007). Diversification of function by different isoforms of conventionally shared RNA polymerase subunits. *Mol Biol Cell* *18*, 1293-1301.
30. Hombach, A., Ommen, G., Chrobak, M., and Clos, J. (2013). The Hsp90–Sti1 interaction is critical for *Leishmania donovani* proliferation in both life cycle stages. *Cellular Microbiology* *15*, 585-600.
31. Schindelin, J., Arganda-Carreras, I., Frise, E., Kaynig, V., Longair, M., Pietzsch, T., Preibisch, S., Rueden, C., Saalfeld, S., Schmid, B., et al. (2012). Fiji: an open-source platform for biological-image analysis. *Nature methods* *9*, 676-682.
32. de Chaumont, F., Dallongeville, S., Chenouard, N., Herve, N., Pop, S., Provoost, T., Meas-Yedid, V., Pankajakshan, P., Lecomte, T., Le Montagner, Y., et al. (2012). Icy: an open bioimage informatics platform for extended reproducible research. *Nature methods* *9*, 690-696.
33. Dufour, A., Meas-Yedid, V., Grassart, A., and Olivo-Marin, J.- (2008). Automated quantification of cell endocytosis using active contours and wavelets. 19th International Conference on Pattern Recognition, 1-4.
34. Dufour, A., Thibeaux, R., Labruyere, E., Guillen, N., and Olivo-Marin, J.C. (2011). 3-D active meshes: fast discrete deformable models for cell tracking in 3-D time-lapse microscopy. *IEEE transactions on image processing : a publication of the IEEE Signal Processing Society* *20*, 1925-1937.
35. Martel, D., Beneke, T., Gluenz, E., Spath, G.F., and Rachidi, N. (2017). Characterisation of Casein Kinase 1.1 in *Leishmania donovani* Using the CRISPR Cas9 Toolkit. *BioMed research international* *2017*, 4635605.

36. Durieu, E., Prina, E., Leclercq, O., Oumata, N., Gaboriaud-Kolar, N., Vougianniopoulou, K., Aulner, N., Defontaine, A., No, J.H., Ruchaud, S., et al. (2016). From Drug Screening to Target Deconvolution: a Target-Based Drug Discovery Pipeline Using Leishmania Casein Kinase 1 Isoform 2 To Identify Compounds with Antileishmanial Activity. *Antimicrob Agents Chemother* *60*, 2822-2833.
37. Fulcher, L.J., Bozatz, P., Tachie-Menson, T., Wu, K.Z.L., Cummins, T.D., Bufton, J.C., Pinkas, D.M., Dunbar, K., Shrestha, S., Wood, N.T., et al. (2018). The DUF1669 domain of FAM83 family proteins anchor casein kinase 1 isoforms. *Science signaling* *11*.
38. Vaughan, S., and Gull, K. (2015). Basal body structure and cell cycle-dependent biogenesis in *Trypanosoma brucei*. *Cilia* *5*, 5.
39. Selvapandiyani, A., Debrabant, A., Duncan, R., Muller, J., Salotra, P., Sreenivas, G., Salisbury, J.L., and Nakhasi, H.L. (2004). Centrin gene disruption impairs stage-specific basal body duplication and cell cycle progression in *Leishmania*. *J Biol Chem* *279*, 25703-25710.
40. Shi, J., Franklin, J.B., Yelinek, J.T., Ebersberger, I., Warren, G., and He, C.Y. (2008). Centrin4 coordinates cell and nuclear division in *T. brucei*. *Journal of cell science* *121*, 3062-3070.
41. He, C.Y., Pypaert, M., and Warren, G. (2005). Golgi duplication in *Trypanosoma brucei* requires Centrin2. *Science* *310*, 1196-1198.
42. Selvapandiyani, A., Kumar, P., Morris, J.C., Salisbury, J.L., Wang, C.C., Nakhasi, H.L., and Cohen-Fix, O. (2007). Centrin1 Is Required for Organelle Segregation and Cytokinesis in *Trypanosoma brucei*. *Molecular Biology of the Cell* *18*, 3290-3301.
43. Hoffmann, A., Jakob, M., and Ochsenreiter, T. (2016). A novel component of the mitochondrial genome segregation machinery in trypanosomes. *Microbial cell* *3*, 352-354.
44. Deane, J.A., Cole, D.G., Seeley, E.S., Diener, D.R., and Rosenbaum, J.L. (2001). Localization of intraflagellar transport protein IFT52 identifies basal body transitional fibers as the docking site for IFT particles. *Current Biology* *11*, 1586-1590.
45. Wei, Q., Ling, K., and Hu, J. (2015). The essential roles of transition fibers in the context of cilia. *Curr Opin Cell Biol* *35*, 98-105.

46. Wheeler, R.J., Gluenz, E., and Gull, K. (2015). Basal body multipotency and axonemal remodelling are two pathways to a 9+0 flagellum. *Nat Commun* 6, 8964.
47. Gokhale, A., Wirschell, M., and Sale, W.S. (2009). Regulation of dynein-driven microtubule sliding by the axonemal protein kinase CK1 in *Chlamydomonas* flagella. *The Journal of cell biology* 186, 817-824.
48. Wirschell, M., Yamamoto, R., Alford, L., Gokhale, A., Gaillard, A., and Sale, W.S. (2011). Regulation of ciliary motility: conserved protein kinases and phosphatases are targeted and anchored in the ciliary axoneme. *Arch Biochem Biophys* 510, 93-100.
49. Bertiaux, E., Mallet, A., Fort, C., Blisnick, T., Bonnefoy, S., Jung, J., Lemos, M., Marco, S., Vaughan, S., Trepout, S., et al. (2018). Bidirectional intraflagellar transport is restricted to two sets of microtubule doublets in the trypanosome flagellum. *The Journal of cell biology*.
50. Motta, M.C.M., Souza, W.d., and Thiry, M. (2003). Immunocytochemical detection of DNA and RNA in endosymbiont-bearing trypanosomatids. *FEMS Microbiology Letters* 221, 17-23.
51. Názer, E., and Sánchez, D.O. (2011). Nucleolar Accumulation of RNA Binding Proteins Induced by ActinomycinD Is Functional in *Trypanosoma cruzi* and *Leishmania mexicana* but Not in *T. brucei*. *PloS one* 6, e24184.
52. Ogbadoyi, E., Ersfeld, K., Robinson, D., Sherwin, T., and Gull, K. (2000). Architecture of the *Trypanosoma brucei* nucleus during interphase and mitosis. *Chromosoma* 108, 501-513.
53. Stoter, M., Bamberger, A.-M., Aslan, B., Kurth, M., Speidel, D., Loning, T., Frank, H.-G., Kaufmann, P., Lohler, J., Henne-Bruns, D., et al. (2005). Inhibition of casein kinase I delta alters mitotic spindle formation and induces apoptosis in trophoblast cells. *Oncogene* 24, 7964-7975.
54. Boucher, N., Dacheux, D., Giroud, C., and Baltz, T. (2007). An essential cell cycle-regulated nucleolar protein relocates to the mitotic spindle where it is involved in mitotic progression in *Trypanosoma brucei*. *J Biol Chem* 282, 13780-13790.
55. They, C., Ostrowski, M., and Segura, E. (2009). Membrane vesicles as conveyors of immune responses. *Nat Rev Immunol* 9, 581-593.
56. Muller, P., Ruckova, E., Halada, P., Coates, P.J., Hrstka, R., Lane, D.P., and Vojtesek, B. (2012). C-terminal phosphorylation of Hsp70 and Hsp90 regulates alternate binding to co-

- chaperones CHIP and HOP to determine cellular protein folding/degradation balances. *Oncogene*.
57. Hombach-Barrigah, A., Bartsch, K., Smirlis, D., Rosenqvist, H., MacDonald, A., Dingli, F., Loew, D., Spath, G.F., Rachidi, N., Wiese, M., et al. (2019). Leishmania donovani 90 kD Heat Shock Protein - Impact of Phosphosites on Parasite Fitness, Infectivity and Casein Kinase Affinity. *Scientific reports* 9, 5074.
  58. Demmel, L., Schmidt, K., Lucast, L., Havlicek, K., Zankel, A., Koestler, T., Reithofer, V., de Camilli, P., and Warren, G. (2016). The endocytic activity of the flagellar pocket in *Trypanosoma brucei* is regulated by an adjacent phosphatidylinositol phosphate kinase. *J Cell Sci* 129, 2285.
  59. Schitteck, B., and Sinnberg, T. (2014). Biological functions of casein kinase 1 isoforms and putative roles in tumorigenesis. *Mol Cancer* 13, 231.
  60. Qin, H., Shao, Q., Igdoura, S.A., Alaoui-Jamali, M.A., and Laird, D.W. (2003). Lysosomal and proteasomal degradation play distinct roles in the life cycle of Cx43 in gap junctional intercellular communication-deficient and -competent breast tumor cells. *J Biol Chem* 278, 30005-30014.
  61. Besteiro, S. (2017). Autophagy in apicomplexan parasites. *Current opinion in microbiology* 40, 14-20.
  62. Kuga, T., Kume, H., Kawasaki, N., Sato, M., Adachi, J., Shiromizu, T., Hoshino, I., Nishimori, T., Matsubara, H., and Tomonaga, T. (2013). A novel mechanism of keratin cytoskeleton organization through casein kinase Ialpha and FAM83H in colorectal cancer. *J Cell Sci* 126, 4721-4731.
  63. Hubstenberger, A., Courel, M., Benard, M., Souquere, S., Ernoult-Lange, M., Chouaib, R., Yi, Z., Morlot, J.B., Munier, A., Fradet, M., et al. (2017). P-Body Purification Reveals the Condensation of Repressed mRNA Regulons. *Mol Cell* 68, 144-157 e145.
  64. Minia, I., and Clayton, C. (2016). Regulating a Post-Transcriptional Regulator: Protein Phosphorylation, Degradation and Translational Blockage in Control of the Trypanosome Stress-Response RNA-Binding Protein ZC3H11. *PLoS pathogens* 12, e1005514.

65. Lee, K.H., Johmura, Y., Yu, L.R., Park, J.E., Gao, Y., Bang, J.K., Zhou, M., Veenstra, T.D., Yeon Kim, B., and Lee, K.S. (2012). Identification of a novel Wnt5a-CK1 $\epsilon$ -Dvl2-Plk1-mediated primary cilia disassembly pathway. *The EMBO journal* *31*, 3104-3117.
66. Schneider, A., and Ochsenteiter, T. (2018). Failure is not an option - mitochondrial genome segregation in trypanosomes. *J Cell Sci* *131*.
67. Chen, Y., Sasai, N., Ma, G., Yue, T., Jia, J., Briscoe, J., and Jiang, J. (2011). Sonic Hedgehog dependent phosphorylation by CK1 $\alpha$  and GRK2 is required for ciliary accumulation and activation of smoothened. *PLoS biology* *9*, e1001083.
68. Subota, I., Julkowska, D., Vincensini, L., Reeg, N., Buisson, J., Blisnick, T., Huet, D., Perrot, S., Santi-Rocca, J., Duchateau, M., et al. (2014). Proteomic analysis of intact flagella of procyclic *Trypanosoma brucei* cells identifies novel flagellar proteins with unique sub-localization and dynamics. *Molecular & cellular proteomics : MCP* *13*, 1769-1786.
69. Beneke, T., Demay, F., Hookway, E., Ashman, N., Jeffery, H., Smith, J., Valli, J., Becvar, T., Myskova, J., Lestinova, T., et al. (2018). Genetic dissection of a *Leishmania* flagellar proteome demonstrates requirement for directional motility in sand fly infections. *bioRxiv*, 476994.
70. Boesger, J., Wagner, V., Weisheit, W., and Mittag, M. (2012). Application of phosphoproteomics to find targets of casein kinase 1 in the flagellum of *Chlamydomonas*. *International journal of plant genomics* *2012*, 581460.
71. Bloch, M.A., and Johnson, K.A. (1995). Identification of a molecular chaperone in the eukaryotic flagellum and its localization to the site of microtubule assembly. *J Cell Sci* *108 (Pt 11)*, 3541-3545.
72. Pedersen, L.B., Geimer, S., Sloboda, R.D., and Rosenbaum, J.L. (2003). The Microtubule plus end-tracking protein EB1 is localized to the flagellar tip and basal bodies in *Chlamydomonas reinhardtii*. *Current biology : CB* *13*, 1969-1974.
73. Landfear, S.M., and Zilberstein, D. (2019). Sensing What's Out There - Kinetoplastid Parasites. *Trends Parasitol* *35*, 274-277.

74. Haycraft, C.J., Banizs, B., Aydin-Son, Y., Zhang, Q., Michaud, E.J., and Yoder, B.K. (2005). Gli2 and Gli3 localize to cilia and require the intraflagellar transport protein polaris for processing and function. *PLoS genetics* *1*, e53.
75. Liu, J., Carvalho, L.P., Bhattachariya, S., Carbone, C.J., Kumar, K.G., Leu, N.A., Yau, P.M., Donald, R.G., Weiss, M.J., Baker, D.P., et al. (2009). Mammalian casein kinase Ialpha and its leishmanial ortholog regulate stability of IFNAR1 and Type I interferon signaling. *Mol Cell Biol* *29*, 6401-6412.
76. Boisvert, F.M., van Koningsbruggen, S., Navascues, J., and Lamond, A.I. (2007). The multifunctional nucleolus. *Nature reviews. Molecular cell biology* *8*, 574-585.
77. Zemp, I., Wandrey, F., Rao, S., Ashiono, C., Wyler, E., Montellese, C., and Kutay, U. (2014). CK1delta and CK1epsilon are components of human 40S subunit precursors required for cytoplasmic 40S maturation. *J Cell Sci* *127*, 1242-1253.
78. Ghalei, H., Schaub, F.X., Doherty, J.R., Noguchi, Y., Roush, W.R., Cleveland, J.L., Stroupe, M.E., and Karbstein, K. (2015). Hrr25/CK1delta-directed release of Ltv1 from pre-40S ribosomes is necessary for ribosome assembly and cell growth. *J Cell Biol* *208*, 745-759.
79. Andersen, J.S., Lam, Y.W., Leung, A.K., Ong, S.E., Lyon, C.E., Lamond, A.I., and Mann, M. (2005). Nucleolar proteome dynamics. *Nature* *433*, 77-83.
80. Kumar, G., Kajuluri, L.P., Gupta, C.M., and Sahasrabudde, A.A. (2016). A twinfilin-like protein coordinates karyokinesis by influencing mitotic spindle elongation and DNA replication in *Leishmania*. *Mol Microbiol* *100*, 173-187.
81. Zhou, Q., Lee, K.J., Kurasawa, Y., Hu, H., An, T., and Li, Z. (2018). Faithful chromosome segregation in *Trypanosoma brucei* requires a cohort of divergent spindle-associated proteins with distinct functions. *Nucleic acids research* *46*, 8216-8231.
82. Pederson, T., and Tsai, R.Y. (2009). In search of nonribosomal nucleolar protein function and regulation. *J Cell Biol* *184*, 771-776.
83. Ogbadoyi, E., Ersfeld, K., Robinson, D., Sherwin, T., and Gull, K. (2000). Architecture of the *Trypanosoma brucei* nucleus during interphase and mitosis. *Chromosoma* *108*, 501-513.

84. Ambit, A., Woods, K.L., Cull, B., Coombs, G.H., and Mottram, J.C. (2011). Morphological Events during the Cell Cycle of *Leishmania major*. *Eukaryot Cell* *10*, 1429-1438.
85. Harmer, J., Towers, K., Addison, M., Vaughan, S., Ginger, M.L., and McKean, P.G. (2018). A centriolar FGR1 oncogene partner-like protein required for paraflagellar rod assembly, but not axoneme assembly in African trypanosomes. *Open biology* *8*.
86. Kobayashi, T., and Dynlacht, B.D. (2011). Regulating the transition from centriole to basal body. *J Cell Biol* *193*, 435-444.
87. Walsh, C.J. (2012). The structure of the mitotic spindle and nucleolus during mitosis in the amoeba-flagellate *Naegleria*. *PloS one* *7*, e34763.
88. da Silva, M.S., Monteiro, J.P., Nunes, V.S., Vasconcelos, E.J., Perez, A.M., Freitas-Junior, L.d.H., Elias, M.C., and Cano, M.I.N. (2013). *Leishmania amazonensis* promastigotes present two distinct modes of nucleus and kinetoplast segregation during cell cycle. *PloS one* *8*, e81397.
89. Fulcher, L.J., He, Z., Mei, L., Macartney, T., Wood, N., Prescott, A.R., Whigham, A., Varghese, J., Gourlay, R., Ball, G., et al. (2018). FAM83D directs protein kinase CK1 $\alpha$  to the mitotic spindle for proper spindle positioning. *bioRxiv*, 480616.
90. Gull, K. (2003). Host-parasite interactions and trypanosome morphogenesis: a flagellar pocketful of goodies. *Current opinion in microbiology* *6*, 365-370.
91. Perry, J.A., Sinclair-Davis, A.N., McAllaster, M.R., and de Graffenried, C.L. (2018). TbSmee1 regulates hook complex morphology and the rate of flagellar pocket uptake in *Trypanosoma brucei*. *Mol Microbiol* *107*, 344-362.
92. Chen, C.Y., and Balch, W.E. (2006). The Hsp90 chaperone complex regulates GDI-dependent Rab recycling. *Mol Biol Cell* *17*, 3494-3507.
93. Johnson, A.E., Chen, J.S., and Gould, K.L. (2013). CK1 is required for a mitotic checkpoint that delays cytokinesis. *Current biology : CB* *23*, 1920-1926.
94. Coletta, A., Pinney, J.W., Solis, D.Y., Marsh, J., Pettifer, S.R., and Attwood, T.K. (2010). Low-complexity regions within protein sequences have position-dependent roles. *BMC systems biology* *4*, 43.

95. Kirmitzoglou, I., and Promponas, V.J. (2015). LCR-eXXXplorer: a web platform to search, visualize and share data for low complexity regions in protein sequences. *Bioinformatics* *31*, 2208-2210.
96. Aslett, M., Aurrecochea, C., Berriman, M., Brestelli, J., Brunk, B.P., Carrington, M., Depledge, D.P., Fischer, S., Gajria, B., Gao, X., et al. (2010). TriTrypDB: a functional genomic resource for the Trypanosomatidae. *Nucleic acids research* *38*, D457-462.
97. Crawford, L.J., Walker, B., Ovaa, H., Chauhan, D., Anderson, K.C., Morris, T.C., and Irvine, A.E. (2006). Comparative selectivity and specificity of the proteasome inhibitors BzLLLLCOCHO, PS-341, and MG-132. *Cancer Res* *66*, 6379-6386.
98. Sacerdoti-Sierra, N., and Jaffe, C.L. (1997). Release of ecto-protein kinases by the protozoan parasite *Leishmania major*. *J Biol Chem* *272*, 30760-30765.
99. Bohm, T., Meng, Z., Haas, P., Henne-Bruns, D., Rachidi, N., Knippschild, U., and Bischof, J. (2019). The kinase domain of CK1delta can be phosphorylated by Chk1. *Bioscience, biotechnology, and biochemistry*, 1-13.
100. Isnard, A., Christian, J.G., Kodiha, M., Stochaj, U., McMaster, W.R., and Olivier, M. (2015). Impact of *Leishmania* infection on host macrophage nuclear physiology and nucleopore complex integrity. *PLoS pathogens* *11*, e1004776.

# Chapter II

---



## Presentation

I previously demonstrated that LmCK1.2 pleiotropic localisation seems to rely on protein-protein interactions with the LCR domains present in its C-terminus. To get insights into the proteins important for its localisation and more generally into its functions in the parasite, I identified LmCK1.2 binding partners in *L. donovani* promastigotes and axenic amastigotes.

This chapter is presented in three parts: (1) The main results formatted as an article, although it has not been submitted yet, as it still requires additional experiments to finalize the article; (2) the characterisation of an interacting partner of LmCK1.2 involved in cytokinesis; (3) additional results explaining in detail the optimisation steps of the immunoprecipitation that was use in the two previous parts.

# 1. Identification of LmCK1.2 binding partners reveals its role in endocytosis in *Leishmania* - article

## 1.1. Article title, authors and keywords

### Article title:

Casein kinase 1 is involved in the regulation of endocytosis through the phosphorylation of the  $\beta$ 2-adaptin subunit of the AP2 complex.

### Authors:

Daniel MARTEL<sup>1, 2</sup>, Paya NDIAYE<sup>1</sup>, Florent DINGLI<sup>3</sup>, Olivier LECLERCQ<sup>1</sup>, Guillaume ARRAS<sup>3</sup>, Damarys LOEW<sup>3</sup>, Gerald F. SPÄTH<sup>1</sup>, and Najma RACHIDI<sup>1\*</sup>.

### Authors address:

<sup>1</sup> Institut Pasteur and INSERM U1201, Unité de Parasitologie moléculaire et Signalisation, Paris, France; <sup>2</sup> Université de Paris, Sorbonne Paris Cité, Paris, France; <sup>3</sup> Laboratoire de Spectrométrie de Masse Protéomique, Centre de Recherche, Institut Curie, Paris, France.

**Running title:** Casein Kinase 1 regulates multiple pathways including endocytosis.

**\*To whom correspondence should be addressed:** Najma Rachidi.

Institut Pasteur and INSERM U1201, Unité de Parasitologie Moléculaire et Signalisation, Paris, France. Tel: +33144389231; Fax: +330145688332; E-mail: [najma.rachidi@pasteur.fr](mailto:najma.rachidi@pasteur.fr)

**Keywords:** Casein kinase I, CK1.2, binding partners, endocytosis, adaptins, AP2 complex, cellular trafficking, *Leishmania*.

## 1.2. Contributions to the work

Most of the work presented here was performed by me. However, to be transparent, I provide here the contributions that were performed by others.

- The gel filtration experiments corresponding to Fig. 5B were performed by Olivier Leclercq, technician in our laboratory.
- The generation of mNG-tagged and KO cells for the genes LmKin17, LmKin21, LmKin30 and LmDYNLL1 as well as all the verification steps for these genes and the immunofluorescence analysis were performed by Paya N'Diaye, former intern from our laboratory.
- Mass spectrometry analyses were performed by Florent Dingli (mass spectrometry ingeneer) and Damarys Loew (platform manager) from the Laboratoire de Spectrométrie de Masse Protéomique, Centre de Recherche, Institut Curie, Paris, France.

## 1.2. Abstract

Casein kinase 1 (CK1) is a highly conserved serine/threonine protein kinase ubiquitously expressed in eukaryotes and playing major roles in most cellular processes. Impairment in CK1 activity, regulation or cellular sequestration can lead to diseases such as cancer or neurodegeneration. Moreover, increasing evidences have linked CK1 to infectious diseases via the manipulation of host CK1 pathways by intracellular pathogens. As a signalling kinase, hundreds of substrates have been reported and its canonical consensus site can be found in a wide range of proteins. Thus, other regulatory mechanisms are required to insure specificity, including inhibitory auto-phosphorylation, subcellular sequestration, and interaction with various proteins. Several studies have demonstrated the importance of interacting partners to regulate the localization or the activity of CK1, such as FAM83 proteins. We have recently shown that LmCK1.2 localisation to very specific cell compartments requires low complexity regions present at the C-terminus, suggesting that protein-protein interaction might be important for these localizations. In this study, using proteomics we identified 171 interacting proteins in promastigotes and axenic amastigotes. We focused on proteins involved in cellular trafficking and particularly the AP2 complex. We showed that LmCK1.2 phosphorylated  $\beta$ 2-adaptin and confirmed that  $\alpha$ 2-,  $\beta$ 2-,  $\mu$ 2-adaptin and LmCK1.2 co-fractionated in the same complex. While the null mutant of  $\alpha$ 2-adaptin was lethal, those of  $\beta$ 2- and  $\mu$ 2-adaptin presented only a severe growth defect in axenic amastigotes. Finally, we showed that parasites deleted for  $\beta$ 2-adaptin presented an endocytosis defect. Our findings are consistent with LmCK1.2 regulating endocytosis through the interaction with and phosphorylation of the AP2 complex.

### 1.3. Introduction

Casein kinase 1 (CK1) family members are highly conserved serine/threonine protein kinases ubiquitously expressed in eukaryotes (Knippschild et al., 2014) showing constitutive phospho-transferase activity (Venerando et al., 2014). They play a major role in fundamental cellular processes that range from cell cycle progression and membrane trafficking to DNA damage repair (reviewed in (Knippschild et al., 2014), citations therein). Impairment in CK1 activity, regulation, cellular sequestration or the presence of mutation have been associated with important diseases such as cancer, neurodegeneration or sleep disorders (Jiang et al., 2018; Knippschild et al., 2005a; Schitteck and Sinnberg, 2014). Furthermore, increasing evidences have linked CK1 with infectious diseases through the manipulation of host CK1 signalling pathways by intracellular pathogens (Dorin-Semblat et al., 2015; Jayaswal et al., 2010; Rachidi et al., 2014; Silverman et al., 2010b; Xia et al., 2018). In human, six distinct genes encode for CK1 paralogs and their transcription variants (Knippschild et al., 2014), that show a highly conserved kinase domain and a divergent C-terminal domain both in length and in primary structure (Knippschild et al., 2014). These features are conserved in orthologs from for example yeast or protozoan parasites.

Hundreds of substrates have been reported for the different human CK1 paralogs, which is consistent with a role of CK1 in signal transduction. Moreover, canonical and non-canonical consensus sites targeted by CK1, are present in a wide range of proteins, suggesting that other mechanisms exist to regulate CK1 such as inhibitory auto-phosphorylation, phosphorylation by upstream kinases, interaction with various cellular structures or proteins and subcellular sequestration (Agostinis et al., 1989; Flotow and Roach, 1991; Flotow et al., 1990; Kawakami et al., 2008; Knippschild et al., 2014; Marin et al., 2003). Several studies have shown the importance of interacting partners for the localization of CK1 paralogs, and to either enhance or inhibit their activity (Behrend et al., 2000; Bischof et al., 2013; Cruciat et al., 2013; Fulcher et al., 2018; McKenzie et al., 2006; Sillibourne et al., 2002; Wolff et al., 2005, 2006; Yin et al., 2006). Recently, the FAM83 proteins were shown to interact with CK1 $\alpha$ ,  $\alpha$ -like,  $\delta$ , and  $\epsilon$  isoforms in mammalian cells through the conserved DUF1669 domain. Mutations in this domain not only impaired the interaction with the kinase but also the subcellular localization of the FAM83 members (Fulcher et al., 2018). It is therefore crucial to identify the interacting proteins of CK1 to gain insights into its cellular functions.

*Leishmania* parasite is the causative agent of leishmaniases and has two life cycle stages: the promastigote stage in the insect vector (blood feeding phlebotomine sand flies) where the parasites are extracellular and flagellated, and the amastigote stage in the mammalian host where the immotile parasites reside inside the phagolysosome of macrophages. There are six CK1 paralogs in *Leishmania*, from LmCK1.1 to LmCK1.6 (Dan-Goor et al., 2013). The most studied paralogs, LmCK1.2, has been identified in the secretome, in the proteome of *L. donovani* exosomes and in the midgut exo-proteome of *L. major*-infected sandflies (Atayde et al., 2015; Silverman et al., 2008, 2010a). We have recently shown that the localisation of LmCK1.2 in very specific cellular compartments (e.g. the basal bodies, the flagellum and the nucleolus) requires the low complexity regions (LCRs) present at its C-terminus (Martel et al., submitted). The absence of peptide signal but the requirement of low complexity regions within the C-terminal domain suggests that LmCK1.2 localization might be driven by the interaction with binding partners. These results point towards the importance of interacting partners in bringing CK1 to its substrates, in organisms as divergent as vertebrates, fungi or protozoan parasites (Knippschild et al., 2014), and suggest that *Leishmania* CK1.2 represent an excellent model to study CK1 functions.

In this study, we used a comprehensive proteomics approach to uncover the interacting partners of LmCK1.2 in promastigote and axenic amastigote stages. We identified 171 interacting proteins with pleiotropic functions. We focused on proteins involved in cellular trafficking and particularly on the AP2 complex. We showed that LmCK1.2 phosphorylated  $\beta$ 2-adaptin and confirmed that  $\alpha$ 2-,  $\beta$ 2-adaptin and LmCK1.2 co-fractionated in the same complex. While the null mutant of  $\alpha$ 2-adaptin was lethal, that of  $\beta$ 2- and  $\mu$ 2-adaptin presented only a severe growth defect in axenic amastigotes. Finally, we showed an endocytosis defect in cells deleted for  $\beta$ 2-adaptin. Our findings are consistent with LmCK1.2 being involved in endocytosis through the regulation of the AP2 complex.

## 1.4. Materials and Methods

### 1.4.1. Parasite culture

All the parasite cell lines used in this study were derived from *L. donovani* axenic strain 1S2D (MHOM/SD/62/1S-CL2D) clone LdBob, from Steve Beverley (Washington University School of Medicine, St. Louis, MO). Promastigotes were cultured and differentiated into axenic amastigotes as described previously (Martel et al., 2017). Briefly, logarithmic promastigotes at  $10^5$  parasites per mL were incubated at 26°C in M199 media (Gibco) supplemented with 10% heat-inactivated FCS, 20 mM HEPES, pH 6.9, 4.1 mM NaHCO<sub>3</sub>, 2 mM glutamine, 8 µM 6-biopterin, 10 µg/mL folic acid, 100 µM adenine, 30 µM hemin, 1X RPMI 1640 vitamins solutions (Sigma), 100 U/mL of Penicillin/Streptomycin (Pen/Step), and adjusted at pH 7.4. Axenic amastigotes were generated by incubating  $10^6$  logarithmic promastigotes per mL at 37°C and 5% CO<sub>2</sub> in RPMI 1640 + GlutaMAX™ -I medium (Gibco) supplemented with 20% of heat-inactivated FCS, 28 mM MES, 2 mM glutamine, 1x RPMI 1640 amino acid mix (Sigma), 1X RPMI 1640 vitamins solutions (Sigma), 10 µg/mL folic acid, 2 mM glutamine, 100 µM adenine, 100 U/mL of Pen/Step, and adjusted at pH 5.5. When appropriate, axenic amastigote cell aggregates were dispersed by passing cell suspensions five times through a 27-gauge needle before analysis.

Transgenic *L. donovani* cell lines LdBob pLEXY and LdBob pLEXY-CK1.2-V5-His<sub>6</sub> (Rachidi et al., 2014) (mock or expressing *Leishmania major* CK1.2 tagged with V5 and His<sub>6</sub>, respectively) or LdB pTB007 (Martel et al., 2017) (expressing Cas9 and T7 RNA polymerase) were cultured in M199 supplemented with 30 µg/mL hygromycin B (Invitrogen). For the mutants generated with the CRISPR-Cas9-toolkit, the relevant selective drugs were added to the medium at the following concentrations: 30 µg/mL puromycin dihydrochloride (Sigma) and/or 20 µg/mL blasticidin S hydrochloride (Invitrogen).

### 1.4.2. Parasite transfection

Parasite transfections for gene tagging or knockout using the CRISPR-Cas9 toolkit were performed as described previously (Martel et al., 2017), adapted from (Beneke et al., 2017).  $2 \times 10^7$  LdB pTB007 promastigotes in logarithmic phase were transfected with PCR reactions in 1X Tb-BSF buffer (90 mM sodium phosphate, 5 mM potassium chloride, 0.15 mM

calcium chloride, 50 mM HEPES, pH 7.3) (Schumann Burkard et al., 2011) using 2 mm gap cuvettes (MBP) with program X-001 of the Amaxa Nucleofector IIb (Lonza Cologne AG, Germany). Transfected cells were immediately transferred into 10 mL prewarmed promastigotes medium in 25 cm<sup>2</sup> flasks and left to recover at 26°C overnight before addition of the appropriate selection drugs. Drug-resistant transfectants became apparent about 7–10 days after transfection.

### 1.4.3. CRISPR-Cas9 gene tagging and knockouts

The methods used for CRISPR-Cas9 gene tagging and knockout in *L. donovani* in this study were described previously (Martel et al., 2017), adapted from the work of Beneke *et al.* (Beneke et al., 2017). Gene tagging was achieved by insertion of a drug-selectable marker cassette (puromycin resistance) and fluorescent mNeonGreen gene into the endogenous gene locus to produce an in-frame gene fusion at the C-terminus. Gene deletions were achieved by replacing the endogenous genes with two distinct drug-selectable marker cassettes (one in each allele, puromycin and blasticidin resistance genes) containing their own UTRs. The EuPaGDT primer design tool (Peng and Tarleton, 2015) was used to design primers for amplification of gene-specific 5' or 3' sgRNA templates (3' for gene tagging; 5' and 3' for gene deletion) using sequences from the loci of the targeted genes from the *L. donovani* 1S2D reference genome (accession: PRJNA396645). Primer G00 (sgRNA scaffold) was used in combination with the gene-specific 5' or 3' sgRNA template primer to generate the sgRNA templates PCR products. *L. donovani* 1S2D reference genome was also used to design primers for amplification of donor DNA (5' HF forward, 3' HF forward, 3' HF reverse; HF, homology flanks) from pPLOTv1 puro-mNeonGreen-puro (for mNeonGreen tagging, puromycin resistance marker) or pTPuro and pTBlast (for gene knockouts, puromycin and blasticidin resistance). Primer sequences are detailed in [Table S1](#) in [Supplementary Information](#).

### 1.4.4. Genotype characterization

To estimate the loss of the target gene in the knockout cell lines, parasites were passaged at least twice after transfection and genomic DNA was then extracted with the DNeasy Blood & Tissue kit (Qiagen). The presence or absence of the target gene ORF as well as the correct integration of the drug-resistance genes in the knockout and parental cell lines

was verified by a diagnostic PCR. Primers were designed (i) to amplify about 1000 kb within the gene ORF, or (ii) to amplify a fragment diagnostic for insertion of the resistance cassette. Primer sequences are detailed in [Table S1](#) in [Supplementary information](#).

#### 1.4.5. Analysis of parasite concentration, cell death and mNeonGreen fluorescence intensity

Analysis of parasite concentration, cell death and mNeonGreen fluorescence intensity was performed as described previously (Martel et al., 2017). Briefly, parasites in culture were diluted in DPBS (Gibco) and incubated with 2 µg/mL propidium iodide (Sigma-Aldrich). Cells were analyzed with a CytoFLEX flow cytometer (Beckman Coulter, Inc.) to determine the cell concentration, the incorporation of propidium iodide (exλ = 488 nm; emλ = 617 nm) and monitor mNG intensities (exλ = 506 nm; emλ = 517 nm). The parasite strains analysed were : *LdB pTB007* (parental strain), *LdB pTB007 α2-adaptin::mNG::3xMyc*, *LdB pTB007 β2-adaptin::mNG::3xMyc* and *LdB pTB007 μ2-adaptin::mNG::3xMyc*, *LdB pTB007 Δβ2-adaptin<sup>Puro/Blast</sup>*, *LdB pTB007 Δμ2-adaptin<sup>Puro/Blast</sup>*. The percentage of cell death, cell growth, and the mean mNeonGreen (mNG) fluorescence intensity were calculated using CytExpert software (CytExpert Software, RRID:SCR\_017217, Beckman Coulter, v2.2.0.97). Graphs were generated with GraphPad Prism (v7.03).

#### 1.4.6. Immuno-fluorescence microscopy

*LdB pTB007* promastigotes expressing the fluorescent fusion proteins α2-adaptin-mNG-myc, β2-adaptin-mNG-myc or μ2-adaptin-mNG-myc were imaged by live microscopy. Parasites were harvested from logarithmic phase cultures by centrifugation and washed 3 times in PBS with Hoechst 33342 (ThermoFisher Scientific Cat# H3570) at 5 µg/mL. Parasites were resuspended in 50 µL PBS, and 2 µL was allowed to settle on a slide and a coverslip was applied. The parasites were immediately imaged with a 60x NA 1.42 plan-apochromat oil immersion objective lens (Olympus AMEP4694) on an EVOS FL microscope (Thermo Fischer Scientific, AMF4300) with an ICX445 monochrome charge-coupled device (CCD) camera (Sony) at room temperature.

### 1.4.7. Plasmids for recombinant protein production

The open reading frames of *L. donovani* homologs of the AP2 complex, LdBPK\_070060.1 ( $\alpha$ 2-adaptin), LdBPK\_110990.1 ( $\beta$ 2-adaptin) and LdBPK\_363180.1 ( $\mu$ 2-adaptin) were cloned into the bacterial expression vector pBAD/Thio-TOPO (ThermoFisher Scientific) to produce the recombinant fusion proteins thio- $\alpha$ 2-adaptin-V5-His<sub>6</sub>, thio- $\beta$ 2-adaptin-V5-His<sub>6</sub> and thio- $\mu$ 2-adaptin-V5-His<sub>6</sub>. The procedure was performed as follows: pBADthio-V5-His<sub>6</sub> plasmid backbone was PCR amplified with Platinum SuperFi DNA Polymerase (ThermoFisher Scientific) from pBAD/Thio-TOPO plasmid using the following primers: 5'-AAGGGCGAGCTTGAAGGTAAG-3' and 5'-AAGGGCGAGCTTGTCATCGTC-3'. The 2883-bp  $\alpha$ 2-adaptin, 2973-bp  $\beta$ 2-adaptin and the 1314-bp  $\mu$ 2-adaptin coding sequences (omitting the stop codon) were amplified by PCR with Platinum SuperFi DNA Polymerase (ThermoFisher Scientific) from *L. donovani* LD1S genomic DNA using the respective following primers: 5'-ATGGACATGCGAGGTCTCGCCCA-3' and 5'-TTGTAGGGCGAACTTGATTGTGTGCGAG-3'; 5'-ATGCCGAACGTGTTTGTCACTG-3' and 5'-GTCCGTCGATAGCGGACACAAG-3'; 5'-ATGCTATCAGTTTTGATGTTCC-3' and 5'-TATGCGGCACTGATAATCAC-3'. Phosphate groups were added to the 5' end of PCR-amplified DNA fragments with T4 polynucleotide kinase (New England BioLabs). PCR-amplified fragments and plasmid backbone were ligated to obtain pBADthio- $\alpha$ 2-adaptin-V5-His<sub>6</sub>, pBADthio- $\beta$ 2-adaptin-V5-His<sub>6</sub> or pBADthio- $\mu$ 2-adaptin-V5-His<sub>6</sub> plasmids. The resulting constructs were verified by DNA sequencing prior to expression in bacteria.

### 1.4.8. Bacterial expression and purification of recombinant proteins

Recombinant expression and purification of thio-CK1.2-V5-His<sub>6</sub>, thio- $\alpha$ 2-adaptin-V5-His<sub>6</sub>, thio- $\beta$ 2-adaptin-V5-His<sub>6</sub> and thio- $\mu$ 2-adaptin-V5-His<sub>6</sub> was performed as described previously (Martel et al., submitted)(Rachidi et al., 2014). *Escherichia coli* Rosetta (DE3) pLysS Competent Cells (Merck Cat# 70956) transformed with pBADthio- $\alpha$ 2-adaptin-V5-His<sub>6</sub>, pBADthio- $\beta$ 2-adaptin-V5-His<sub>6</sub> or pBADthio- $\mu$ 2-adaptin-V5-His<sub>6</sub> were grown at 37°C and induced with arabinose (0.02% final) for 4h at room temperature. Cells were harvested by centrifugation at 10,000 g for 10 min at 4°C. The bacterial pellets were resuspended in DPBS containing 60 mM  $\beta$ -glycerophosphate, 1 mM sodium vanadate, 1 mM sodium fluoride, 1 mM disodium phenylphosphate, 150 mM sodium chloride, 10 mM imidazole supplemented with

protease inhibitor cocktail (Complete EDTA free tablets, Roche Applied Science) (lysis buffer). Samples were sonicated at 20 V for two cycles of 2 min (10/10 s ON/OFF; 30/30 s ON/OFF). Triton X-100 (0.1% final) was then added. The samples were placed for 30 min at 4°C with rotation and then centrifuged 30 min at 15,000 g at 4°C. The supernatants were purified on cobalt beads (HisPur Cobalt Resin, ThermoFisher Scientific Cat# 89964) pre-equilibrated in lysis buffer. After 2 h incubation at 4°C with agitation, the beads were washed four times in DPBS containing 60 mM  $\beta$ -glycerophosphate, 1 mM sodium vanadate, 1 mM sodium fluoride, 1 mM disodium phenylphosphate, 300 mM sodium chloride, 30 mM imidazole, 1% Triton X-100 at pH 7.5 and supplemented with protease inhibitor cocktail (Complete EDTA free tablets, Roche Applied Science). Recombinant proteins were eluted for 30 min at 4°C with 300 mM imidazole in elution buffer at pH 7.5 supplemented with protease inhibitor cocktail (Complete EDTA free tablets, Roche Applied Science) (DPBS containing 60 mM  $\beta$ -glycerophosphate, 1 mM sodium vanadate, 1 mM sodium fluoride, 1 mM disodium phenylphosphate). Glycerol was added to the elution fractions (15% v/v final concentration) and samples were stored at -80°C.

#### 1.4.9. Protein kinase assays

Protein kinase assays were performed as described previously (Martel et al., submitted). Briefly, purified recombinant thio-CK1.2-V5-His<sub>6</sub> was incubated on a shaker at 30°C for 30 min with 2  $\mu$ g myelin basic protein (MBP) substrate or an equivalent amount of thio- $\alpha$ 2-adaptin-V5-His<sub>6</sub>, thio- $\beta$ 2-adaptin-V5-His<sub>6</sub> or thio- $\mu$ 2-adaptin-V5-His<sub>6</sub>, and 15  $\mu$ M ATP, 50 mM morpholinepropanesulfonic acid (MOPS) pH 7.5, 5 mM EGTA, 15 mM MgCl<sub>2</sub>, 1 mM dithiothreitol, 0.1 mM sodium vanadate and 1  $\mu$ Ci [ $\gamma$ <sup>32</sup>P] adenosine-triphosphate (ATP) (3000 Ci/mmol) in final volume of 20  $\mu$ l. DMSO 1% or casein kinase 1 inhibitor D4476 (selective ATP-competitive inhibitor of CK1) at 10  $\mu$ M in 1% DMSO were added to the proteins. The phosphotransferase reaction was stopped by addition of 1x NuPAGE LDS Sample Buffer and NuPAGE Sample Reducing Agent and 5 min denaturation at 95°C. Reaction samples were separated by SDS-PAGE and the gel was stained by Bio-Safe Commassie (Bio-Rad) then dried. Incorporation of  $\gamma$ <sup>32</sup>P was monitored by exposing the dried gel on an X-ray sensitive film (Roche) at -80°C.

#### 1.4.10. Protein extraction, SDS-PAGE and Western Blot analysis

Logarithmic phase promastigotes or axenic amastigotes were washed in DPBS and protein extraction was performed in RIPA buffer as described previously (Martel et al., 2017). Twenty micrograms of total proteins were denatured, separated by SDS-PAGE, and transferred onto polyvinylidene difluoride (PVDF) membranes (Pierce). Membranes were blocked with 5% milk or BSA in DPBS supplemented with 0.25% Tween20 (PBST) and incubated overnight at 4°C with primary antibody mouse IgG2a anti-V5 tag monoclonal antibody (1/1,000; Thermo Fisher Scientific Cat# R960-25, RRID:AB\_2556564) in 2,5% BSA in PBST. Membranes were then washed in PBST and incubated with secondary antibody anti-mouse IgG (H+L) coupled to horseradish peroxidase (1/20,000; ThermoFisher Scientific Cat# 32230, RRID:AB\_1965958). Proteins were revealed by SuperSignal™ West Pico Chemiluminescent Substrate (Thermo Scientific) using the PXi image analysis system (Syngene) at various exposure times. Membranes were then stained with Bio-Safe Coomassie (Bio-Rad Cat #1610786) to serve as loading controls.

#### 1.4.11. Immunoprecipitation

To immuno-precipitate LmCK1.2 from parasite extracts we used the transgenic *L. donovani* cell lines containing either the plasmid pLEXY or pLEXY-CK1.2-V5-His<sub>6</sub>, mock or expressing *L. major* CK1.2-V5-His<sub>6</sub>, respectively. Logarithmic phase promastigotes or axenic amastigotes (48 h after temperature and pH shift) were washed in DPBS and protein extraction was performed as described previously (Martel et al., 2017). Unless stated otherwise, all the following steps were performed at 4°C. Briefly, parasites were lysed with RIPA lysis buffer (150 mM NaCl, 1% Triton X-100, 20 mM Tris HCl [pH 7.4], 1% NP-40, 1 mM EDTA, complete protease inhibitor cocktail (Roche Applied Science, IN) and supplemented with 1 mM sodium orthovanadate and 1 mM PMSF), vortexed and, after sonication, clarified by centrifugation. For immunoprecipitation of CK1.2-V5-His<sub>6</sub> from promastigote or axenic amastigote lysates, 6 mg or 14 mg total proteins, respectively, were used at 2 mg/mL concentration in RIPA lysis buffer. Clarified lysates were pre-cleared for 30 min with 1.5 mg fresh magnetic beads coupled to protein G (ThermoFisher Scientific Cat# 10003D) that were washed thrice with DPBS-tween buffer (DPBS with 0.02% Tween-20, adjusted at pH 7.4). Magnetic beads were discarded and the pre-cleared lysates were mixed for 30 min at 4°C with

crosslinked anti-V5-coupled magnetic beads prepared as follows. Fresh magnetic beads (1.5 mg) were washed thrice with DPBS-tween buffer and mixed with 3 µg mouse IgG2a anti-V5 tag monoclonal antibody (ThermoFisher Scientific Cat# R960-25, RRID:AB\_2556564) in DPBS-tween buffer. After 10 min incubation at room temperature, the anti-V5-coupled magnetic beads were washed thrice in DPBS-tween buffer and the interaction was crosslinked using the bis(sulfosuccinimidyl)suberate (BS<sup>3</sup>) crosslinking reagent. Briefly, anti-V5-coupled magnetic beads were washed twice with conjugation buffer (20 mM sodium phosphate, 150 mM NaCl [pH 7.4]), incubated 30 min with BS<sup>3</sup> buffer (5 mM BS<sup>3</sup> (ThermoFisher Scientific Cat# 21580), 20 mM sodium phosphate, 150 mM NaCl [pH 7.4]) at room temperature, and reaction quenched for 15 min with 1 M Tris-HCl [pH 7.4] (50 mM Tris-HCl final concentration) at room temperature. Crosslinked anti-V5-coupled magnetic beads were then washed thrice with washing buffer (50 mM Tris-HCl [pH 7.4], 5 mM NaF, 250 mM NaCl, 5 mM EDTA [pH 8.0], 0.1% NP-40, complete protease inhibitor cocktail (Roche Applied Science, IN)) and ready to use with pre-cleared lysates. After incubation with pre-cleared lysates, beads were washed with 20x beads volume of washing buffer for six times 5 min at 4°C, then transferred to a new tube and the bound proteins were eluted. Elution conditions were as follows unless otherwise stated: elution at 70°C for 10 min with glycine elution buffer (33.33 mM glycine [pH 2.8], 0.33X NuPAGE LDS Sample Buffer (ThermoFisher Scientific Cat# NP0007), 0.33X NuPAGE Sample Reducing Agent (ThermoFisher Scientific Cat# NP004)) and for axenic amastigote IP, an additional elution condition was performed at 95°C for 5 min with NuPAGE loading buffer (1X NuPAGE LDS Sample Buffer (ThermoFisher Scientific Cat#NP0007), 1X NuPAGE Sample Reducing Agent (ThermoFisher Scientific Cat# NP004)). Elutions were kept at -80°C before mass spectrometry analysis.

#### 1.4.12. Identification of LmCK1.2-V5-His<sub>6</sub> associated proteins by nanoLC-MS/MS analysis

After IP elution of LmCK1.2-V5-His<sub>6</sub> and its interacting partners from promastigotes, samples were separated on SDS-PAGE gels (Invitrogen) and stained with colloidal blue staining (LabSafe GEL Blue™ GBiosciences). Gel slices were excised and proteins were reduced with 10 mM DTT prior to alkylation with 55 mM iodoacetamide. After washing and shrinking the gel pieces with 100% MeCN, in-gel digestion was performed using trypsin/Lys-C

(Promega) overnight in 25 mM NH<sub>4</sub>HCO<sub>3</sub> at 30 °C. Peptides were then extracted using 60/35/5 MeCN/H<sub>2</sub>O/HCOOH and vacuum concentrated to dryness. Samples were chromatographically separated using an RSLCnano system (Ultimate 3000, Thermo Scientific) coupled to an Orbitrap Fusion mass spectrometer (Q-OT-qIT, Thermo Fisher Scientific). Chromatographic conditions for each samples are described in [Table S2](#).

We acquired Survey MS scans in the Orbitrap with the resolution set to a value of 120,000 and a 4 × 10<sup>5</sup> ion count target. Each scan was recalibrated in real time by co-injecting an internal standard from ambient air into the C-trap. Tandem MS was performed by isolation at 1.6 Th with the quadrupole, HCD fragmentation with normalized collision energy of 35, and rapid scan MS analysis in the ion trap. The MS2 ion count target was set to 104 and the max injection time was 100 ms. Only those precursors with charge state 2–7 were sampled for MS2. The dynamic exclusion duration was set to 60 s with a 10 ppm tolerance around the selected precursor and its isotopes. The instrument was run in top speed mode with 3 s cycles.

Data were searched against the in house databases containing uniprot *L. infantum*, *L. donovani* and keratin proteins (8293 sequences for *L. intantum*, 7960 sequences for *L. donovani* and 417 keratins) by using SequestHT from Proteome Discoverer (version 1.4 or 2.1). Enzyme specificity was set to trypsin and a maximum of two miss cleavages was allowed. Oxidized methionine, N-terminal acetylation and carbamidomethyl cysteine were set as variable modifications. The mass tolerances in MS and MS/MS were set to 10 ppm and 0.6 Da, respectively. The resulting files were further processed using myProMS myProMS (Pouillet et al., 2007) where we fixed the FDR for all peptide and protein identification to less than 1%.

We calculated for each identified protein a selection criteria, the relative mean delta (RMD), allowing the comparison of IP results from LmCK1.2-V5 strain (CK) and mock control (Mock) in PRO or axAMA. We used the mean of peptides (mPep) identified in the three replicates from the CK strain or Mock.

$$RMD = \frac{mPep\ CK - mPep\ Mock}{mPep\ CK + mPep\ Mock} \times 100$$

For the co-IP from axAMA lysates, we pooled the number of peptides identified in elutions 1 and 2 of each replicate in order to obtain a total number of peptides identified per replicate that was then used to generate the mPep and RMD.

#### 1.4.13. AP2 phylogenetic analysis

Phylogenetic percent identity matrix of *L. donovani*  $\alpha$ 2-,  $\beta$ 2-,  $\mu$ 2- and  $\sigma$ 2-adaptin of the AP2 complex and six trypanosomatids orthologs were generated using the MULTiple Sequence Comparison by Log-Expectation (MUSCLE) 3.8 multiple sequence alignment program for proteins (Madeira et al., 2019) (RRID:SCR\_011812). Protein sequences were obtained from TriTrypDB release 43 (Aslett et al., 2010) (RRID:SCR\_007043). TriTrypDB accession numbers are provided in Supplementary Table S3. UniprotKB sequences (RRID:SCR\_004426) used for figure illustrations are provided in Supplementary Table S3. The illustrations were taken from Pfam (RRID:SCR\_004726) database where the sequences were subjected for analysis and subsequently modified.

#### 1.4.14. FM4-64FX staining

Endocytic compartments were labeled with the vital dye FM4-64FX (ThermoFischer Scientific Cat#F34653). The procedure was adapted from previously describe method (Mullin et al., 2001). Logarithmic phase *LdB* pTB007  $\Delta\beta$ 2-adaptin<sup>Puro/Blast</sup> or parental promastigotes were incubated in 5  $\mu$ g/ $\mu$ L FM4-64FX for 30 minutes at 26°C, then parasites were diluted at 1:10 in ice cold DPBS and assessed by flow cytometry to monitor FM4-64FX internalisation (ex $\lambda$  = 565 nm; em $\lambda$  = 744 nm). The fluorescence intensity was plotted as histograms with CytExpert software (CytExpert Software, RRID:SCR\_017217, Beckman Coulter, v2.2.0.97).

## 1.5. Results

### 1.5.1. Identification of candidate LmCK1.2-associated proteins

LmCK1.2 possesses low complexity regions (LCRs) in its C-terminus, which are implicated in protein-protein interactions (Martel et al., submitted) (Fig. 1A). To identify LmCK1.2-associated proteins (LmCKAP) in both *Leishmania* life stages, we used the transgenic *L. donovani* cell lines LdBob pLEXY and LdBob pLEXY-CK1.2-V5-His<sub>6</sub>, referred to in the following as mock or CK1.2-V5, respectively (Rachidi et al., 2014) (Martel et al., submitted). The episomal expression of transgenic *L. major* LmCK1.2-V5-His<sub>6</sub> in this strain is half that of the wild type with no growth or cell cycle defects associated (Rachidi et al., 2014). Moreover, the transgenic kinase has a similar activity to that of the wild type (Rachidi et al., 2014). It is worth noting that both CK1.2 orthologs from *L. donovani* and *L. major* share 99% amino acid sequence identity, the only difference being one amino acid difference at the C-terminus (P350Q *L. major* : *L. donovani*).

We performed immuno-precipitations (IP) on logarithmic phase promastigotes (PRO) and axenic amastigotes (axAMA) cell lysates, using a mouse monoclonal anti-V5 antibody. We eluted the purified proteins with one elution buffer for promastigotes and axenic amastigotes, and one additional elution buffer for axenic amastigotes to increase the number of purified proteins. As an example of purification, see Fig. 1B and Materials and Methods. Three independent IPs were performed and the eluted samples were used for nanoscale liquid chromatography coupled to tandem mass spectrometry (nanoLC-MS/MS, or MS). Peptide sequences predicted by MS were used to query the in-house Uniprot databases containing the *L. infantum* JPCM5 and *L. donovani* BPK282A1 reference genomes and keratin proteins. We used both *Leishmania* species in an attempt to identify the maximum of annotated proteins as the Sudanese *L. donovani* Bob strain used in this study displays similarities to both the Nepalese *L. donovani* strain and *L. infantum* strain (unpublished data).

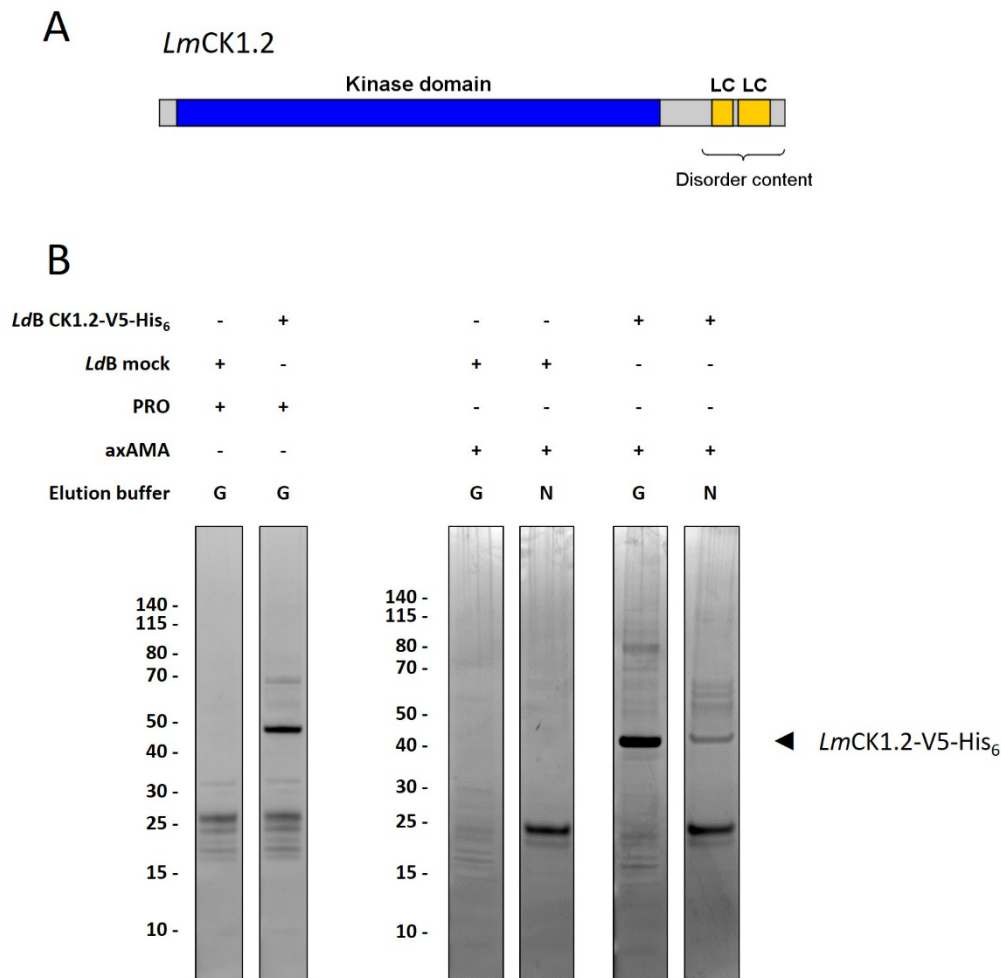


**Fig. 1**– Immunoprecipitation of stage specific *LmCK1.2* interacting proteins, example of purification.

(A) Schematic representation of the domain structure of *LmCK1.2* (GenBank: CBZ38008.1). The protein structure contains a kinase domain (blue) and a disordered C-terminal tail with two low complexity regions (LC) (yellow). (B) *LmCK1.2-V5* immunoprecipitation with magnetic beads. Representative experiment of the IP performed for mass spectrometry analysis. Promastigotes or axenic amastigotes from mock or CK1.2-V5 cell lines were used to purify *LmCK1.2-V5-His<sub>6</sub>* and associated proteins. Four elutions were performed successively with different elution buffers, and only the conditions kept for the IP destined to MS analysis are shown here. Glycine elution buffer was used for elution 1 (G) and NuPAGE loading buffer (N) for elution 2. The proteins were separated by SDS-PAGE and revealed by SYPRO Ruby staining. Molecular weights are shown on the left part of the gels. IP *LmCK1.2-V5-His<sub>6</sub>* is indicated with a black arrow.

To classify candidate *LmCKAPs*, we applied two levels of stringency. In the first level (S1), we classified the proteins identified in at least two independent experiments in the CK1.2-V5 strain but absent in the mock strain. In the second level (S2), we selected proteins that were identified in the CK1.2-V5 strain in at least two independent experiments and with a RMD  $\geq 50\%$  (relative mean delta, see **Materials and Methods**). We assumed for each protein that the detection of more peptides was associated to an increase in protein abundance. We

applied the two selection criteria on *L. donovani* and *L. infantum* protein lists and compared the result to establish the final lists. All the results are presented in [Table 1](#) (PRO), [Table 2](#) (axAMA) and the corresponding raw data are displayed in [Table S4](#).

**Table 1:** Accession numbers and annotations of putative LmCKAPs in promastigotes identified from MS – Selections 1 & 2.

Gene ID	Protein name	mPep (CK) ± SD	RMD (%) ± SD	no. Rep	Also found in axAMA co-IP <sup>+</sup>	Size (kDa)
<b>Selection 1</b>						
LdBPK_151330.1	MGT1 magnesium transporter	22,00 ± 12,53		3	Yes	92,6
LdBPK_361350.1	hypothetical protein, conserved Survival motor neuron (SMN) interacting protein 1 (SIP1), putative	20,00 ± 5,57		3	Yes	208,9
LdBPK_081300.1	histone deacetylase 4, putative	15,67 ± 2,52		3	Yes	67,5
LdBPK_352220.1	Hypothetical protein, conserved	12,67 ± 12,42		3	Yes	55,2
LdBPK_341610.1	hypothetical protein, conserved	11,33 ± 5,51		3	Yes	114,9
LdBPK_290210.1	SNF2 family N-terminal domain/Helicase conserved C- terminal domain containing protein, putative	10,33 ± 5,51		3	Yes	66,9
LdBPK_363660.1	hypothetical protein, conserved	9,33 ± 5,51		3	Yes	89,8
LdBPK_252460.1	hypothetical protein, conserved	7,00 ± 2,00		3	Yes	41,6
LdBPK_180100.1	hypothetical protein, conserved	5,00 ± 3,00		3	Yes	88,6
LdBPK_330990.1	hypothetical protein, conserved	3,67 ± 2,08		3	Yes	50,2
LdBPK_100800.1	hypothetical protein, conserved	3,33 ± 2,08		3	Yes	39,7
LdBPK_321780.1	hypothetical protein, conserved	3,33 ± 2,52		3	Yes	174,2
LdBPK_130650.1	C2 domain containing protein, putative	2,67 ± 2,08		3	Yes	122,1
LdBPK_250870.1	hypothetical protein, conserved	2,33 ± 0,58		3	Yes	218,0
LdBPK_333240.1	hypothetical protein, unknown function	1,00 ± 0,00		3	Yes	230,2
LdBPK_341080.1	hypothetical protein, conserved	3,67 ± 5,51		2	Yes	66,9
LdBPK_321890.1	hypothetical protein, conserved survival of motor neuron (SMN)-like protein	2,00 ± 1,73		2	Yes	16,7
LdBPK_290470.1	hypothetical protein, conserved	1,00 ± 1,00		2	Yes	78,4
LdBPK_353750.1	Gim5A protein, putative	1,00 ± 1,00		2	Yes	24,8
LdBPK_351020.1	CK1.1	0,67 ± 0,58		2	Yes	37,2
LdBPK_341880.1	ubiquitin-like protein	0,67 ± 0,58		2	Yes	8,7
<b>Selection 2</b>						
LdBPK_351030.1	CK1.2 (Casein Kinase 1 isoform 2)	64,00	88,24	3	Yes	39,8
LdBPK_281310.1	luminal binding protein 1 (BiP), putative (HSPA5)	4,67	75,00	3	Yes	71,8
LdBPK_131400.1	chaperonin TCP20, putative	3,00	63,64	3	No	58,8
LdBPK_261220.1	heat shock protein 70-related protein (HSP70.4) (HSPA2)	12,33	60,87	3	Yes	70,4
LdBPK_211300.1	40S ribosomal protein S23, putative	4,33	52,94	3	No	15,9
LdBPK_283000.1	heat-shock protein hsp70, putative (HSPA1B)	41,33	51,22	3	Yes	71,3
LdBPK_362140.1	chaperonin HSP60, mitochondrial precursor	2,00	50,00	3	Yes	59,3

LdBPK_367240.1	T-complex protein 1, theta subunit, putative	2,67	77,78	2	No	58,2
LdBPK_363930.1	60S ribosomal protein L34, putative	1,33	60,00	2	Yes	19,2
LdBPK_291600.1	Nodulin-like, putative	2,33	55,56	2	No	73,8
LdBPK_010790.1	Eukaryotic initiation factor 4A-1	1,00	50,00	2	No	45,3
LdBPK_050510.1	ATP synthase F1, alpha subunit, putative	1,00	50,00	2	Yes	62,5
LdBPK_160560.1	orotidine-5-phosphate decarboxylase/urotate phosphoribosyltransferase, putative	1,00	50,00	2	No	49,7
LdBPK_332600.1	Present in the outer mitochondrial membrane proteome 11	1,00	50,00	2	Yes	42,5

\* LmCKAPs found in both PRO and axAMA co-IP are indicated with “Yes”, if not found in axAMA they are indicated with “No”.

**Table 2:** Accession numbers and annotations of putative LmCKAPs in axenic amastigotes identified from MS – Selection 1 & 2.

Gene ID	Protein name	mPep (CK)	RMD (%)	no. Rep	Also found in PRO co-IP*	Size (kDa)
<b>Selection 1</b>						
LdBPK_151330.1	MGT1 magnesium transporter	93,33		3	Yes	92,6
LdBPK_100800.1	hypothetical protein, conserved	65,33		3	Yes	208,9
LdBPK_361350.1	hypothetical protein, conserved	64,67		3	Yes	67,5
	Survival motor neuron (SMN) interacting protein 1 (SIP1), putative					
LdBPK_341610.1	hypothetical protein, conserved	57,33		3	Yes	55,2
LdBPK_352220.1	hypothetical protein, conserved	53,00		3	Yes	114,9
LdBPK_081300.1	histone deacetylase 4, putative	28,67		3	Yes	66,9
LdBPK_321780.1	hypothetical protein, conserved	28,67		3	Yes	89,8
LdBPK_250870.1	hypothetical protein, conserved	27,00		3	Yes	41,6
LdBPK_363660.1	hypothetical protein, conserved	25,67		3	Yes	88,6
LdBPK_070060.1	alpha-adaptin-like protein	25,33		3	No	107,7
LdBPK_110990.1	adaptin-related protein-like protein	21,00		3	No	108,5
LdBPK_261220.1	heat shock protein 70-related protein (HSP70.4) (HSPA2)	20,00		3	Yes	70,4
LdBPK_210900.1	Temperature dependent protein affecting M2 dsRNA replication, putative	20,00		3	No	115,9
LdBPK_341080.1	hypothetical protein, conserved	18,67		3	Yes	66,9
LdBPK_180100.1	hypothetical protein, conserved	18,00		3	Yes	50,2
LdBPK_252460.1	hypothetical protein, conserved	13,67		3	Yes	39,7
LdBPK_366240.1	hypothetical protein, unknown function	13,33		3	No	46,7
LdBPK_290210.1	SNF2 family N-terminal domain/Helicase conserved C-terminal domain containing protein, putative	12,00		3	Yes	174,2
LdBPK_350400.1	40S ribosomal protein S3A, putative	11,33		3	No	30,0
LdBPK_363180.1	clathrin coat assembly protein-like protein	10,33		3	No	48,9
LdBPK_290470.1	hypothetical protein, conserved	9,67		3	Yes	78,4
LdBPK_362640.1	Nucleoporin NUP96	9,33		3	No	97,1
LdBPK_322920.1	Nucleoporin NUP109	9,33		3	No	115,2
LdBPK_367220.1	Nucleoporin NUP144	9,33		3	No	143,8
LdBPK_330990.1	hypothetical protein, conserved	7,33		3	Yes	122,1
LdBPK_301580.1	protein kinase, putative	7,33		3	No	181,7
LdBPK_181410.1	chaperone DNAJ protein, putative	7,00		3	No	121,9
LdBPK_352100.1	hypothetical protein, conserved	7,00		3	No	80,3

Gene ID	Protein name	mPep (CK)	RMD (%)	no. Rep	Also found in PRO co-IP*	Size (kDa)
LdBPK_321890.1	hypothetical protein, conserved survival of motor neuron (SMN)-like protein	6,33		3	Yes	16,7
LdBPK_261940.1	Thioesterase-like superfamily, putative	6,33		3	No	37,7
LdBPK_151320.1	ubiquitin hydrolase, putative	6,33		3	No	154,7
LdBPK_332160.1	Nucleoporin NUP89	6,00		3	No	86,6
LdBPK_242380.1	cullin-like protein-like protein	5,67		3	No	85,5
LdBPK_210300.1	hexokinase, putative	5,67		3	No	51,7
LdBPK_130650.1	C2 domain containing protein, putative	5,33		3	Yes	218,0
not annotated LINF_070014600	hypothetical protein - conserved	5,33		3	No	239,5
LdBPK_270390.1	Nuclear pore complex protein 158	5,33		3	No	159,1
LdBPK_323320.1	ribosomal protein L3, putative (fragment)	5,00		3	No	12,0
LdBPK_342370.1	Coiled-coil and C2 domain-containing protein	4,67		3	No	100,1
LdBPK_072500.1	glycosomal phosphoenolpyruvate carboxykinase, putative	4,67		3	No	58,3
LdBPK_170290.1	Regulator of chromosome condensation (RCC1) repeat, putative	4,67		3	No	121,5
LdBPK_292620.1	ATP-dependent 6-phosphofructokinase, glycosomal	4,33		3	No	54,0
LdBPK_350370.1	ATP-dependent DEAD-box RNA helicase, putative	4,00		3	No	46,4
LdBPK_351600.1	Nucleoporin NUP82	4,00		3	No	84,4
LdBPK_351020.1	CK1.1	3,67		3	Yes	37,2
LdBPK_080800.1	hypothetical protein, unknown function	3,67		3	No	32,6
not annotated LINF_150018200	Ribosomal protein L6e - putative	3,67		3	No	21,1
LdBPK_110600.1	3-methylcrotonoyl-CoA carboxylase beta subunit, putative	3,33		3	No	58,4
LdBPK_300120.1	alkyldihydroxyacetonephosphate synthase	3,33		3	No	69,5
LdBPK_251280.1	hypothetical protein, conserved	3,33		3	No	235,3
LdBPK_270700.1	hypothetical protein, conserved	3,00		3	No	62,6
LdBPK_323680.1	hypothetical protein, conserved	3,00		3	No	67,4
LdBPK_242050.1	Nucleoporin NUP76	3,00		3	No	81,0
LdBPK_211910.1	Exocyst complex component EXO99	2,67		3	No	102,2
LdBPK_342300.1	hypothetical protein, conserved	2,67		3	No	56,8
LdBPK_050100.1	phosphoprotein phosphatase, putative	2,67		3	No	71,8
LdBPK_366860.1	protein-l-isoaspartate o-methyltransferase, putative	2,67		3	No	28,5
LdBPK_271890.1	small nuclear ribonucleoprotein protein, putative	2,67		3	No	11,8
LdBPK_120720.1	Flagellum attachment zone protein 2	2,33		3	No	144,0
LdBPK_230050.1	peroxidoxin	2,33		3	No	25,4
LdBPK_221030.1	WD domain, G-beta repeat, putative	2,33		3	No	130,2
LdBPK_260160.1	60S ribosomal protein L7, putative	2,00		3	No	28,9
LdBPK_070550.1	60S ribosomal protein L7a, putative	2,00		3	No	39,1
LdBPK_320240.1	dynein light chain, flagellar outer arm, putative	2,00		3	No	10,6
LdBPK_091010.1	hypothetical protein, conserved	2,00		3	No	63,5
LdBPK_311930.1	ubiquitin-fusion protein	2,00		3	No	14,7
LdBPK_081060.1	Exocyst complex component Sec3, putative	1,67		3	No	126,9
LdBPK_272350.1	heat shock protein DNAJ, putative	1,67		3	No	43,6
LdBPK_342380.1	hypothetical protein, unknown function	1,67		3	No	68,6
LdBPK_323110.1	nucleoside diphosphate kinase b	1,67		3	No	16,6
LdBPK_100700.1	hypothetical protein, unknown function	1,33		3	No	41,7
LdBPK_251850.1	3-oxo-5-alpha-steroid 4-dehydrogenase, putative	1,33		3	No	34,2
LdBPK_251210.1	ATP synthase subunit beta, mitochondrial, putative	1,33		3	No	56,3
LdBPK_352650.1	hypothetical protein, unknown function	1,33		3	No	34,8
LdBPK_231720.1	Inositol hexakisphosphate, putative	1,33		3	No	187,3
LdBPK_272040.1	MSP (Major sperm protein) domain containing protein, putative	1,33		3	No	36,5

Gene ID	Protein name	mPep (CK)	RMD (%)	no. Rep	Also found in PRO co-IP*	Size (kDa)
LdBPK_341880.1	ubiquitin-like protein	1,00		3	Yes	8,7
LdBPK_060410.1	60S ribosomal protein L19, putative	1,00		3	No	28,1
LdBPK_170570.1	hypothetical protein, unknown function	1,00		3	No	107,1
LdBPK_364480.1	Nucleoporin NUP152	5,33		2	No	178,6
LdBPK_080130.1	hypothetical protein, conserved	3,67		2	No	121,2
LdBPK_210580.1	Nucleoporin NUP41	3,33		2	No	47,3
LdBPK_320050.1	protein transport protein SEC13	3,00		2	No	36,4
LdBPK_260530.1	hypothetical protein, conserved	2,67		2	No	74,1
LdBPK_220260.1	Nucleoporin NUP132	2,33		2	No	138,0
LdBPK_041170.1	fructose-1,6-bisphosphatase, cytosolic, putative	2,00		2	No	38,9
LdBPK_071070.1	Protein of unknown function (DUF3608), putative	2,00		2	No	269,4
LdBPK_320640.1	hypothetical protein, conserved	1,67		2	No	39,6
LdBPK_310450.1	cytoskeleton-associated protein CAP5.5, putative	1,33		2	No	80,0
LdBPK_050560.1	hypothetical protein, conserved	1,33		2	No	44,4
LdBPK_150840.1	hypothetical protein, conserved	1,33		2	No	225,5
LdBPK_261960.1	hypothetical protein, conserved	1,33		2	No	89,0
LdBPK_301510.1	kinesin, putative	1,33		2	No	133,0
LdBPK_130250.1	Nucleoporin NUP48 (ALADIN)	1,33		2	No	56,3
LdBPK_111190.1	Organic solute transporter Ostalpha, putative	1,33		2	No	77,0
LdBPK_050510.1	ATP synthase F1, alpha subunit, putative	1,00		2	Yes	62,5
LdBPK_270681.1	hypothetical protein, conserved	1,00		2	No	52,3
LdBPK_363360.1	14-3-3 protein 1, putative	1,00		2	No	29,7
LdBPK_220004.1	60S ribosomal protein L11 (L5, L16)	1,00		2	No	21,7
LdBPK_220790.1	hypothetical protein, conserved	1,00		2	No	91,4
LdBPK_251880.1	hypothetical protein, conserved	1,00		2	No	106,1
LdBPK_302320.1	hypothetical protein, conserved	1,00		2	No	52,5
LdBPK_322820.1	hypothetical protein, conserved	1,00		2	No	41,9
LdBPK_366150.1	hypothetical protein, conserved	1,00		2	No	208,8
LdBPK_250270.1	Nucleoporin NUP110	1,00		2	No	126,6
LdBPK_221370.1	40S ribosomal protein L14, putative	0,67		2	No	26,0
LdBPK_291820.1	Acyl-coenzyme A thioesterase, putative	0,67		2	No	39,5
LdBPK_364930.1	Alpha/beta hydrolase family, putative	0,67		2	No	106,2
LdBPK_351720.1	casein kinase II, putative	0,67		2	No	42,6
LdBPK_342100.1	clathrin coat assembly protein AP17, putative	0,67		2	No	16,8
LdBPK_282390.1	cyclin dependent kinase-binding protein, putative	0,67		2	No	99,7
LdBPK_220009.1	heat shock protein DNAJ, putative	0,67		2	No	36,5
LdBPK_354880.1	Histidine phosphatase superfamily (branch 1), putative	0,67		2	No	36,5
LdBPK_060950.1	hypothetical protein, conserved	0,67		2	No	48,9
LdBPK_282490.1	hypothetical protein, conserved	0,67		2	No	94,9
LdBPK_302710.1	hypothetical protein, conserved	0,67		2	No	96,7
LdBPK_323200.1	hypothetical protein, conserved TbAIR9-like	0,67		2	No	96,2
LdBPK_352020.1	hypothetical protein, unknown function	0,67		2	No	150,5
LdBPK_351380.1	Iron-binding zinc finger CDGSH type, putative	0,67		2	No	13,7
LdBPK_365620.1	NADH dehydrogenase, putative	0,67		2	No	57,5
LdBPK_354200.1	polyadenylate-binding protein 2	0,67		2	No	64,6
LdBPK_342240.1	ribosomal protein l35a, putative	0,67		2	No	16,5
<b>Selection 2</b>						
LdBPK_351030.1	CK1.2 (Casein Kinase 1 isoform 2)	119,33	99,44	3	Yes	39,8
LdBPK_291160.1	ribosomal protein L1a, putative	9,33	86,67	3	No	41,1
LdBPK_110970.1	40S ribosomal protein S5	4,00	83,33	3	No	21,3
LdBPK_170270.1	kinesin motor domain containing protein, putative	3,67	83,33	3	No	114,9
LdBPK_302440.1	hypothetical protein, conserved	3,33	81,82	3	No	128,6
LdBPK_252520.1	hypothetical protein, conserved	13,00	81,40	3	No	109,3
LdBPK_354190.1	conserved hypothetical protein	12,67	80,95	3	No	59,7
LdBPK_151000.1	Nucleus and spindle associated protein 2 (NuSAP2), putative	25,00	80,72	3	No	129,2

Gene ID	Protein name	mPep (CK)	RMD (%)	no. Rep	Also found in PRO co-IP*	Size (kDa)
LdBPK_281310.1	luminal binding protein 1 (BiP), putative (HSPA5)	26,67	79,78	3	Yes	71,8
LdBPK_322830.1	ribosomal protein L27, putative	2,67	77,78	3	No	15,4
LdBPK_351450.1	60S ribosomal protein L2, putative (fragment)	2,33	75,00	3	No	10,8
LdBPK_340270.1	hypothetical protein, conserved	4,67	75,00	3	No	42,7
LdBPK_181270.1	mitochondrial carrier protein, putative	2,00	71,43	3	No	26,2
LdBPK_323080.1	tubulin-tyrosine ligase-like protein	2,33	71,43	3	No	71,6
LdBPK_130330.1	alpha tubulin	13,33	70,21	3	No	49,8
LdBPK_170750.1	GRAM domain containing protein, putative	5,67	70,00	3	No	48,2
LdBPK_283000.1	heat-shock protein hsp70, putative (HSPA1B)	46,33	65,48	3	Yes	71,3
LdBPK_271740.1	Dual specificity phosphatase, catalytic domain containing protein, putative	6,33	65,22	3	No	180,9
LdBPK_081290.1	beta tubulin (fragment)	5,67	61,90	3	No	15,9
LdBPK_171300.1	hypothetical protein, conserved	5,67	61,90	3	No	90,3
LdBPK_332600.1	Present in the outer mitochondrial membrane proteome 11	1,67	60,00	3	Yes	42,5
LdBPK_212190.1	60S ribosomal protein L37a, putative	1,33	60,00	3	No	10,3
LdBPK_352610.1	hypothetical protein, conserved	1,33	60,00	3	No	24,3
LdBPK_361020.1	hypothetical protein, unknown function	1,33	60,00	3	No	99,3
LdBPK_211280.1	kinesin, putative	2,67	60,00	3	No	231,1
LdBPK_364650.1	asparaginase-like protein	4,67	57,14	3	No	41,2
LdBPK_161220.1	60S ribosomal protein L39, putative	3,00	55,56	3	No	6,5
LdBPK_211160.1	histone H2A	2,33	55,56	3	No	13,9
LdBPK_181340.1	hypothetical protein, conserved	2,33	55,56	3	No	107,7
LdBPK_320270.1	Serine/threonine-protein kinase Nek1-related, putative	9,33	55,56	3	No	147,0
LdBPK_363570.1	short chain dehydrogenase-like protein	2,33	55,56	3	No	33,1
LdBPK_362140.1	chaperonin HSP60, mitochondrial precursor	3,33	53,85	3	Yes	59,3
LdBPK_190710.1	glycosomal malate dehydrogenase	3,33	53,85	3	No	33,6
LdBPK_050770.1	hypothetical protein, unknown function	7,33	51,72	3	No	139,6
LdBPK_363930.1	60S ribosomal protein L34, putative	1,00	50,00	3	Yes	19,2
LdBPK_363020.1	40S ribosomal protein S24e	4,00	50,00	3	No	15,8
LdBPK_340910.1	60S ribosomal protein L13a, putative (fragment)	1,00	50,00	3	No	10,8
LdBPK_160610.1	histone H3, putative (fragment)	1,00	50,00	3	No	12,0
LdBPK_090120.1	flagellar pocket cytoskeletal protein bilbo1	3,00	63,64	2	No	65,7
LdBPK_210760.1	dual specificity protein phosphatase, putative	1,33	60,00	2	No	66,8
LdBPK_301900.1	hypothetical protein, unknown function	1,00	50,00	2	No	66,4
LdBPK_361050.1	40S ribosomal protein S10, putative	1,00	50,00	2	No	18,6

\* LmCKAPs found in both PRO and axAMA co-IP are indicated with “Yes”, if not found in PRO they are indicated with “No”.

### 1.5.2. The LmCK1.2 interactome reveals numerous novel and amastigote stage-specific associated proteins

As expected, LmCK1.2 (LdBPK\_351030.1) was identified in promastigotes and axenic amastigotes immuno-precipitations (IP) with the highest mean of peptide (mPep) (Table 1, 2 and S4). Few peptides were identified in the mock control for both replicates, resulting in LmCK1.2 being classified in S2, with a high RMD of 88.24 % and 99.44 % for PRO and axAMA, respectively (Table 1 and 2). In addition to LmCK1.2, we identified 34 LmCKAP in PRO and 163 in axAMA (Fig. 2A, Table 1 and 2). In promastigotes, 21 proteins were classified in S1 and 13 proteins in S2 (Fig. 2Aa), whereas in axAMA, 122 proteins were classified in S1 and 41 proteins in S2 (Fig. 2Ab). We found that 26 of the 34 LmCKAP identified in promastigotes were also detected in axenic amastigotes, indicating only 8 PRO-specific proteins (Fig. 2B and Table 1). By contrast, 137 proteins were identified as axAMA-specific LmCKAP (Fig. 2B and Table 2).

The 171 proteins selected as LmCKAP in PRO and axAMA were listed and searched for PANTHER protein class (<http://www.pantherdb.org/>) using *L. major* orthologs as input, or manually annotated using TriTrypDB (Table 3). Consistent with the pleiotropic localisations and functions of CK1 family members in eukaryotes, the LmCKAPs belonged to a wide range of protein classes (Fig. 2C), with an over-representation of proteins involved in post-translational modification, nucleic acid binding and hypothetical proteins. Proteins identified in PRO were particularly clustered in chaperone, nucleic acid binding and hypothetical protein classes, whereas proteins identified in axAMA were mainly clustered in nucleic acid binding, transporters and hypothetical protein classes (Fig. 2D). Identification of these proteins gave us insights into the potential functions of LmCK1.2 in the parasites. For instance, we identified (1) two mRNA splicing factors, SMN-like (LdBPK\_321890.1) and Gemin-2 (SMN interacting protein 1 (SIP1), LdBPK\_361350.1), and a 60S ribosomal protein L34 (LdBPK\_363930.1), suggesting that LmCK1.2 could be implicated in the regulation of the spliceosome (Table 3); and (2) two proteins involved in transcriptional regulation or DNA repair, histone deacetylase 4 (HDAC, LdBPK\_081300.1) and SNF2 helicase (LdBPK\_290210.1) (Table 3), suggesting that LmCK1.2 could be implicated in chromatin remodelling. We identified several complexes that co-precipitate with LmCK1.2 (Fig. 2D and Table 2 and 3).

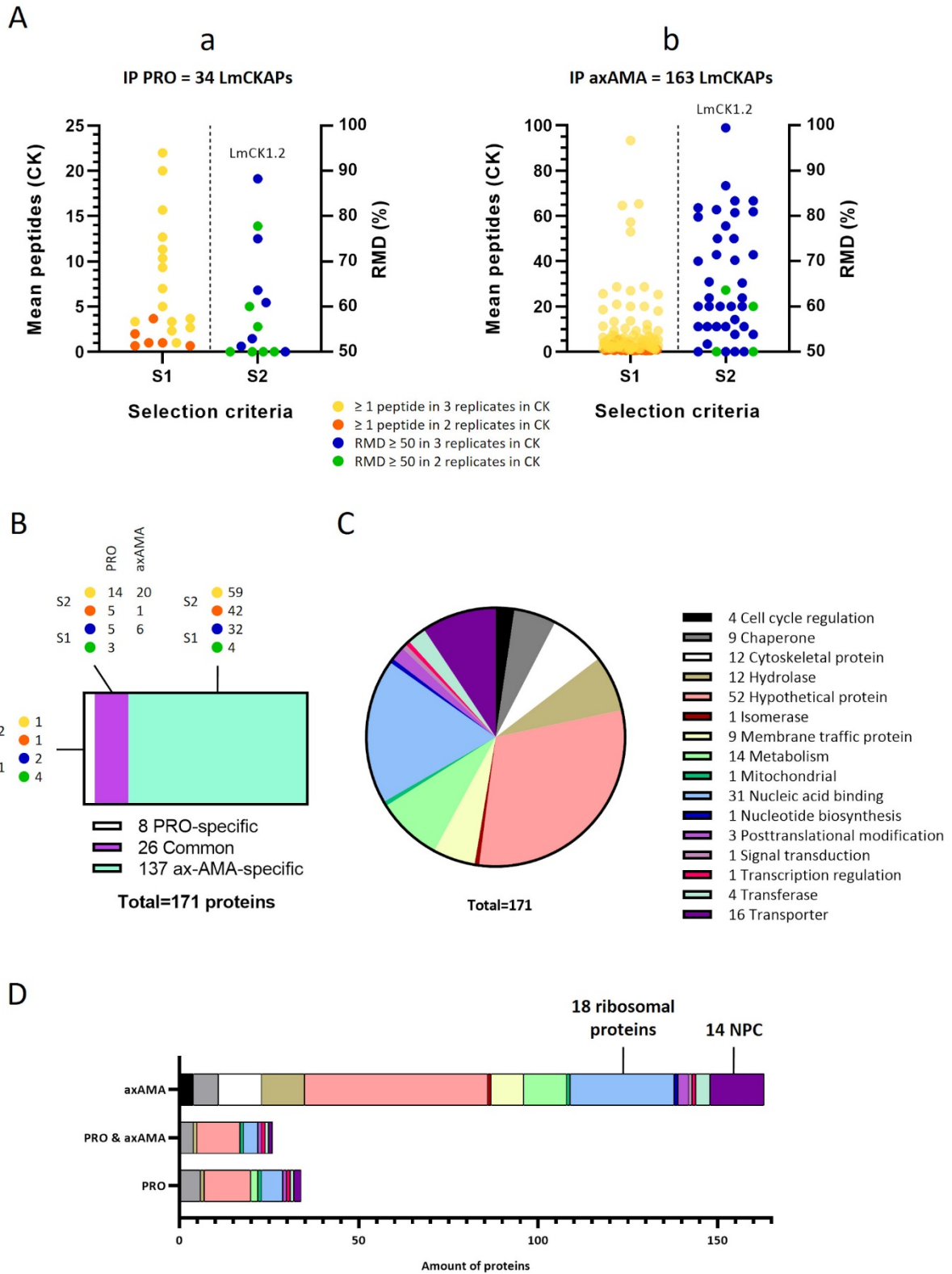


**Fig. 2** – The LmCK1.2 interactome reveals numerous novel and amastigote stage-specific binding partners.

(A) Dot plot representing the LmCK1.2 associated proteins (LmCKAPs) identified in the promastigote (PRO) IP (a) or axenic amastigotes (axAMA) IP (b). LmCK1.2, together with the 34 LmCKAPs in PRO and 163 LmCKAPs in axAMA are plotted according to their selection criteria. Selection 1 proteins (left part), only found in the IP from LmCK1.2-V5-His<sub>6</sub>-expressing parasites (CK), are plotted according to their mean peptide number, and proteins differentiated by two criteria: found with  $\geq 1$  peptide in 3 replicates in CK (yellow), or found with  $\geq 1$  peptide in 2 replicates in CK (orange). Selection 2 proteins (right part), found in the IP from LmCK1.2-V5-His<sub>6</sub>-expressing parasites (CK) and mock, are plotted according to their relative mean delta (RMD) values, and proteins differentiated by two criteria: found with RMD  $\geq 50$  in 3 replicates (blue), or found with RMD  $\geq 50$  in 2 replicates in CK (green). The dot corresponding to LmCK1.2 is provided.

(B) Comparison of the LmCKAPs found in PRO or axAMA IP, with representation of the PRO-specific (cyan), axAMA-specific (light green) and common LmCKAPs (magenta). For each categories, the detailed composition of proteins identified from the two selection criteria (S1 and S2, identical colour code as in (A)) are indicated.

(C) Pie chart representing the protein classes of all identified LmCKAPs from PRO and axAMA IP. Proteins classes were determined based on searches in PantherDB with *L. major* orthologs and manually annotated using TriTrypDB. Colour code and number of proteins identified in each categories are shown in the legend.

(D) Detailed representation of the protein classes of axAMA-specific, PRO-specific or common LmCKAPs, applying the colour code of the pie chart in (C).

The major complex contains eighteen 40S and 60S ribosomal proteins. The interaction of LmCK1.2 with ribosomal proteins is consistent with the role of its human orthologs in the cytoplasmic maturation steps of 40S subunit precursors (Zemp et al., 2014). LmCK1.2 also seems to interact with the nuclear pore complex (NPC) as fourteen members were co-precipitated with LmCK1.2 (Fig. 2D and Table 3). We identified all the components of the outer ring (Sec13, Nup41, Nup82, Nup89, Nup109, Nup132, Nup152, and Nup158) as described in *T. brucei* (Obado et al., 2016). We also detected two additional proteins, described as part of the nuclear pore complex in eukaryotes but not yet identified in kinetoplastid nuclear pores: a putative Seh1 protein, which is part of the outer ring; and Nup48/ALADIN, which has only been found in the human cytoplasmic regions of the NPC (Table 3, (Knockenbauer and Schwartz, 2016; Obado et al., 2016)). Finally, we identified two inner ring components, Nup144 and Nup96, and one component from the nuclear basket, Nup110. The purification of LmCK1.2 with all the components of the outer ring complex, suggests that LmCK1.2 is part of this complex, which has never been shown in eukaryotes. Indeed, CK1 has mostly been shown to phosphorylate proteins to allow their nucleo-cytoplasmic trafficking (Biswas et al., 2011). Moreover, we identified four proteins that bring additional evidences towards a role of LmCK1.2 in mitosis: regulator of chromosome condensation (LdBPK\_170290.1), the spindle-

associated protein NuSap2 (LdBPK\_151000.1), NEK1 (putative NIMA-related kinase LdBPK\_320270.1) and a putative CDK-binding protein (LdBPK\_282390.1) (Table 3).

Our findings not only confirm the data on LmCK1.2 localisation but also provide clues on the functions performed by LmCK1.2 (Martel et al., submitted).

LmCK1.2 was shown to be loaded into exosomes, and we could link this localisation with the identification of LmCK1.2 interacting partners detected in the secretome and/or in exosomes (Silverman et al., 2008, 2010a). Nine proteins were detected in the proteome of exosomes, three proteins in the secretome and 31 in both (Table 3). Compared to the percentage of secreted proteins (1.8%) and exosomal proteins (4%) identified in the genome (8272 ORFs), they represent, respectively, 19% and 23% of LmCK1.2 binding partners, suggesting that they are enriched in our dataset (Table 3) (Silverman et al., 2008). This is consistent with the excretion of LmCK1.2 via exosomes and suggests that several binding partners might be implicated in the loading of the kinase into the exosomes, or in its functions in the host cells.

**Table 3:** Protein classes of the selected LmCKAPs

Protein class Gene ID	Protein name	Copurifies in		Identified in <i>Leishmania</i> secretome or exoproteome
		PRO	axAMA	
<b>Cell cycle regulation</b>				
LdBPK_170290.1	Regulator of chromosome condensation (RCC1) repeat, putative		Yes	
LdBPK_282390.1	cyclin dependent kinase-binding protein, putative		Yes	
LdBPK_151000.1	Nucleus and spindle associated protein 2 (NuSAP2), putative		Yes	
LdBPK_320270.1	Serine/threonine-protein kinase Nek1-related, putative		Yes	
<b>Chaperone</b>				
LdBPK_261220.1	heat shock protein 70-related protein (HSP70.4) (HSPA2)		Yes	E+S
LdBPK_181410.1	chaperone DNAJ protein, putative HSP40 J37 class III	Yes	Yes	
LdBPK_272350.1	heat shock protein DNAJ, putative HSP40 J2 class I		Yes	E+S
LdBPK_220009.1	heat shock protein DNAJ, putative HSP40 J66 class IV		Yes	
LdBPK_281310.1	luminal binding protein 1 (BiP), putative (HSPA5)	Yes	Yes	E+S
LdBPK_283000.1	heat-shock protein hsp70, putative (HSPA1B)	Yes	Yes	
LdBPK_362140.1	chaperonin HSP60, mitochondrial precursor	Yes	Yes	E+S
LdBPK_131400.1	chaperonin TCP20, putative	Yes		Eo
LdBPK_367240.1	T-complex protein 1, theta subunit, putative	Yes		E+S
<b>Cytoskeletal protein</b>				
LdBPK_342370.1	Coiled-coil and C2 domain-containing protein		Yes	
LdBPK_120720.1	Flagellum attachment zone protein 2		Yes	
LdBPK_320240.1	dynein light chain, flagellar outer arm, putative		Yes	So
LdBPK_260530.1	hypothetical protein, conserved Tripartite attachment complex 60 (TAC60)		Yes	
LdBPK_301510.1	kinesin, putative		Yes	
LdBPK_310450.1	cytoskeleton-associated protein CAP5.5, putative		Yes	Eo
LdBPK_170270.1	kinesin motor domain containing protein, putative		Yes	

Protein class Gene ID	Protein name	Copurifies in		Identified in <i>Leishmania</i> secretome or exoproteome
		PRO	axAMA	
LdBPK_323080.1	tubulin-tyrosine ligase-like protein TTLB		Yes	
LdBPK_130330.1	alpha tubulin		Yes	E+S
LdBPK_081290.1	beta tubulin (fragment)		Yes	E+S
LdBPK_211280.1	kinesin, putative		Yes	
LdBPK_090120.1	flagellar pocket cytoskeletal protein bilbo1		Yes	So
<b>Hydrolase</b>				
LdBPK_210900.1	Temperature dependent protein affecting M2 dsRNA replication, putative		Yes	
LdBPK_151320.1	ubiquitin hydrolase, putative		Yes	
LdBPK_261940.1	Thioesterase-like superfamily, putative		Yes	
LdBPK_050100.1	phosphoprotein phosphatase, putative		Yes	Eo
LdBPK_231720.1	Inositol hexakisphosphate, putative Possible protein tyrosine phosphatase		Yes	
LdBPK_251210.1	ATP synthase subunit beta, mitochondrial, putative		Yes	E+S
LdBPK_050510.1	ATP synthase F1, alpha subunit, putative	Yes	Yes	E+S
LdBPK_291820.1	Acyl-coenzyme A thioesterase, putative		Yes	
LdBPK_364930.1	Alpha/beta hydrolase family, putative		Yes	
LdBPK_271740.1	Dual specificity phosphatase, catalytic domain containing protein, putative		Yes	
LdBPK_364650.1	asparaginase-like protein		Yes	
LdBPK_210760.1	dual specificity protein phosphatase, putative		Yes	
<b>Hypothetical protein</b>				
LdBPK_100800.1	hypothetical protein, conserved	Yes	Yes	
LdBPK_341610.1	hypothetical protein, conserved	Yes	Yes	
LdBPK_352220.1	hypothetical protein, conserved	Yes	Yes	
LdBPK_321780.1	hypothetical protein, conserved	Yes	Yes	
LdBPK_250870.1	hypothetical protein, conserved	Yes	Yes	
LdBPK_363660.1	hypothetical protein, conserved	Yes	Yes	
LdBPK_341080.1	hypothetical protein, conserved	Yes	Yes	
LdBPK_180100.1	hypothetical protein, conserved,	Yes	Yes	
LdBPK_252460.1	hypothetical protein, conserved	Yes	Yes	
LdBPK_366240.1	hypothetical protein, unknown function		Yes	
LdBPK_290470.1	hypothetical protein, conserved	Yes	Yes	
LdBPK_330990.1	hypothetical protein, conserved	Yes	Yes	
LdBPK_352100.1	hypothetical protein, conserved		Yes	
LdBPK_130650.1	C2 domain containing protein, putative	Yes	Yes	
LINF_070014600	hypothetical protein - conserved		Yes	
LdBPK_080800.1	hypothetical protein, unknown function		Yes	
LdBPK_251280.1	hypothetical protein, conserved		Yes	
LdBPK_270700.1	hypothetical protein, conserved		Yes	
LdBPK_323680.1	hypothetical protein, conserved		Yes	
LdBPK_342300.1	hypothetical protein, conserved		Yes	
LdBPK_221030.1	WD domain, G-beta repeat, putative		Yes	
LdBPK_091010.1	hypothetical protein, conserved		Yes	
LdBPK_342380.1	hypothetical protein, unknown function		Yes	
LdBPK_100700.1	hypothetical protein, unknown function		Yes	
LdBPK_352650.1	hypothetical protein, unknown function		Yes	
LdBPK_170570.1	hypothetical protein, unknown function		Yes	
LdBPK_080130.1	hypothetical protein, conserved		Yes	
LdBPK_071070.1	Protein of unknown function (DUF3608), putative		Yes	
LdBPK_050560.1	hypothetical protein, conserved		Yes	
LdBPK_150840.1	hypothetical protein, conserved		Yes	
LdBPK_261960.1	hypothetical protein, conserved		Yes	E+S
LdBPK_251880.1	hypothetical protein, conserved		Yes	
LdBPK_270681.1	hypothetical protein, conserved		Yes	
LdBPK_322820.1	hypothetical protein, conserved		Yes	
LdBPK_366150.1	hypothetical protein, conserved		Yes	
LdBPK_060950.1	hypothetical protein, conserved		Yes	Eo
LdBPK_282490.1	hypothetical protein, conserved		Yes	
LdBPK_302710.1	hypothetical protein, conserved		Yes	
LdBPK_323200.1	hypothetical protein, conserved TbAIR9-like		Yes	E+S

Protein class Gene ID	Protein name	Copurifies in		Identified in <i>Leishmania</i> secretome or exoproteome
		PRO	axAMA	
LdBPK_352020.1	hypothetical protein, unknown function		Yes	
LdBPK_302440.1	hypothetical protein, conserved		Yes	
LdBPK_252520.1	hypothetical protein, conserved		Yes	
LdBPK_354190.1	conserved hypothetical protein		Yes	
LdBPK_340270.1	hypothetical protein, conserved		Yes	
LdBPK_170750.1	GRAM domain containing protein, putative		Yes	
LdBPK_171300.1	hypothetical protein, conserved		Yes	
LdBPK_352610.1	hypothetical protein, conserved		Yes	
LdBPK_361020.1	hypothetical protein, unknown function		Yes	
LdBPK_181340.1	hypothetical protein, conserved		Yes	
LdBPK_050770.1	hypothetical protein, unknown function		Yes	
LdBPK_301900.1	hypothetical protein, unknown function		Yes	
LdBPK_333240.1	hypothetical protein, unknown function	Yes		
<b>Isomerase</b>				
LdBPK_354880.1	Histidine phosphatase superfamily (branch 1), putative		Yes	
<b>Membrane traffic protein</b>				
LdBPK_070060.1	alpha-adaptin-like protein		Yes	
LdBPK_110990.1	adaptin-related protein-like protein		Yes	
LdBPK_363180.1	clathrin coat assembly protein-like protein		Yes	
LdBPK_211910.1	Exocyst complex component EXO99		Yes	
LdBPK_081060.1	Exocyst complex component Sec3, putative		Yes	
LdBPK_272040.1	MSP (Major sperm protein) domain containing protein, putative		Yes	
LdBPK_320050.1	protein transport protein SEC13		Yes	
LdBPK_320640.1	hypothetical protein, conserved Nucleoporin SEH1 potentially		Yes	
LdBPK_342100.1	clathrin coat assembly protein AP17, putative		Yes	
<b>Metabolism</b>				
LdBPK_210300.1	hexokinase, putative		Yes	
LdBPK_072500.1	glycosomal phosphoenolpyruvate carboxykinase, putative		Yes	
LdBPK_292620.1	ATP-dependent 6-phosphofructokinase, glycosomal	Yes		E+S
LdBPK_110600.1	3-methylcrotonoyl-CoA carboxylase beta subunit, putative		Yes	
LdBPK_300120.1	alkyldihydroxyacetonephosphate synthase		Yes	
LdBPK_230050.1	peroxidoxin		Yes	E+S
LdBPK_251850.1	3-oxo-5-alpha-steroid 4-dehydrogenase, putative		Yes	
LdBPK_041170.1	fructose-1,6-bisphosphatase, cytosolic, putative		Yes	
LdBPK_365620.1	NADH dehydrogenase, putative		Yes	
LdBPK_181270.1	mitochondrial carrier protein, putative (TbMCP12)		Yes	
LdBPK_363570.1	short chain dehydrogenase-like protein		Yes	
LdBPK_190710.1	glycosomal malate dehydrogenase		Yes	E+S
LdBPK_160560.1	orotidine-5-phosphate decarboxylase/orotate phosphoribosyltransferase, putative PYR6/5	Yes		
LdBPK_353750.1	Gim5A protein, putative	Yes		E+S
<b>Mitochondrial</b>				
LdBPK_332600.1	Present in the outer mitochondrial membrane proteome 11	Yes	Yes	
<b>Nucleic acid binding</b>				
LdBPK_361350.1	hypothetical protein, conserved Survival motor neuron (SMN) interacting protein 1 (SIP1), putative	Yes	Yes	
LdBPK_290210.1	SNF2 family N-terminal domain/Helicase conserved C-terminal domain containing protein, putative	Yes	Yes	
LdBPK_350400.1	40S ribosomal protein S3A, putative		Yes	E+S
LdBPK_321890.1	hypothetical protein, conserved survival of motor neuron (SMN)- like protein	Yes	Yes	
LdBPK_323320.1	ribosomal protein L3, putative (fragment)		Yes	E+S
LdBPK_350370.1	ATP-dependent DEAD-box RNA helicase, putative DHH1		Yes	E+S
LINF_150018200	Ribosomal protein L6e - putative		Yes	E+S
LdBPK_271890.1	small nuclear ribonucleoprotein protein, putative SmB, interact with SMN		Yes	
LdBPK_070550.1	60S ribosomal protein L7a, putative		Yes	E+S
LdBPK_260160.1	60S ribosomal protein L7, putative		Yes	E+S
LdBPK_060410.1	60S ribosomal protein L19, putative		Yes	Eo
LdBPK_220004.1	60S ribosomal protein L11 (L5, L16)		Yes	E+S
LdBPK_221370.1	40S ribosomal protein L14, putative		Yes	E+S

Protein class Gene ID	Protein name	Copurifies in		Identified in <i>Leishmania</i> secretome or exoproteome
		PRO	axAMA	
LdBPK_342240.1	ribosomal protein l35a, putative		Yes	E+S
LdBPK_302320.1	hypothetical protein, conserved RNA methyltransferase		Yes	
LdBPK_220790.1	hypothetical protein, conserved Nitrogen permease regulator 2		Yes	
LdBPK_354200.1	polyadenylate-binding protein 2 PABP2		Yes	So
LdBPK_291160.1	ribosomal protein L1a, putative		Yes	Eo
LdBPK_110970.1	40S ribosomal protein S5		Yes	
LdBPK_322830.1	ribosomal protein L27, putative		Yes	E+S
LdBPK_351450.1	60S ribosomal protein L2, putative (fragment)		Yes	
LdBPK_212190.1	60S ribosomal protein L37a, putative		Yes	Eo
LdBPK_211160.1	histone H2A		Yes	
LdBPK_161220.1	60S ribosomal protein L39, putative		Yes	
LdBPK_363930.1	60S ribosomal protein L34, putative	Yes	Yes	E+S
LdBPK_160610.1	histone H3, putative (fragment)		Yes	
LdBPK_340910.1	60S ribosomal protein L13a, putative (fragment)		Yes	
LdBPK_363020.1	40S ribosomal protein S24e		Yes	E+S
LdBPK_361050.1	40S ribosomal protein S10, putative		Yes	
LdBPK_211300.1	40S ribosomal protein S23, putative	Yes		E+S
LdBPK_010790.1	Eukaryotic initiation factor 4A-1	Yes		E+S
<b>Nucleotide biosynthesis</b>				
LdBPK_323110.1	nucleoside diphosphate kinase b		Yes	E+S
<b>Posttranslational modification</b>				
LdBPK_242380.1	cullin-like protein-like protein, TbCul5		Yes	
LdBPK_311930.1	ubiquitin-fusion protein, Rad60 SUMO-like/Ribosomal L40e family		Yes	Eo
LdBPK_341880.1	ubiquitin-like protein NEDD8	Yes	Yes	
<b>Signal transduction</b>				
LdBPK_363360.1	14-3-3 protein 1, putative		Yes	E+S
<b>Transcription regulation</b>				
LdBPK_081300.1	histone deacetylase 4, putative	Yes	Yes	
<b>Transferase</b>				
LdBPK_301580.1	Eukaryotic translation initiation factor 2-alpha kinase 3, putative		Yes	
LdBPK_351020.1	CK1.1	Yes	Yes	
LdBPK_366860.1	protein-l-isoaspartate o-methyltransferase, putative		Yes	
LdBPK_351720.1	casein kinase II, putative		Yes	
LdBPK_351030.1	CK1.2 (Casein Kinase 1 isoform 2)	Yes	Yes	E+S
<b>Transporter</b>				
LdBPK_151330.1	MGT1 magnesium transporter	Yes	Yes	
LdBPK_322920.1	Nucleoporin NUP109		Yes	
LdBPK_362640.1	Nucleoporin NUP96		Yes	
LdBPK_367220.1	Nucleoporin NUP144		Yes	
LdBPK_332160.1	Nucleoporin NUP89		Yes	
LdBPK_270390.1	Nuclear pore complex protein 158		Yes	
LdBPK_351600.1	Nucleoporin NUP82		Yes	
LdBPK_242050.1	Nucleoporin NUP76		Yes	
LdBPK_364480.1	Nucleoporin NUP152		Yes	
LdBPK_210580.1	Nucleoporin NUP41		Yes	
LdBPK_220260.1	Nucleoporin NUP132		Yes	
LdBPK_111190.1	Organic solute transporter Ostalpha, putative		Yes	
LdBPK_130250.1	Nucleoporin NUP48 (ALADIN)		Yes	
LdBPK_250270.1	Nucleoporin NUP110		Yes	
LdBPK_351380.1	Iron-binding zinc finger CDGSH type, putative		Yes	
LdBPK_291600.1	Nodulin-like, putative	Yes		Eo

So: found only in *L. donovani* secretome (Silverman et al., 2008, 2010a); E+S: found in both *Leishmania* exoproteome and secretome (Silverman et al., 2010a); Eo: found only in *Leishmania* exoproteome (Silverman et al., 2010a).

Finally, 52 LmCKAP were classified as hypothetical proteins: 39 were specifically identified in axAMA, one in promastigotes, and 12 in both life stages. To gain insights into the potential functions of these hypothetical proteins, we collected data from InterProScan domain associations and from orthologs in TriTrypDB (version 43) and TrypTag (Table 4). Some proteins could be annotated, but for others only domains could be found. We identified seven proteins containing transmembrane domains, which could be involved in trafficking; three potential new NUPs; three WD domains-containing proteins, which favours protein-protein interactions; and C2-, VASt-, or GRAM-containing proteins, involved in membrane-associated processes. We also found proteins that could be involved in flagellum assembly such as microtubule-associated protein, a FAZ protein and a flagella connector protein 1 (Table 4). These potential elements need to be confirmed experimentally.

**Table 4:** Hypothetical proteins among the LmCKAPs: InterProScan annotation and TriTrypDB annotation from orthologs (including TrypTag)

Gene ID	Protein name	InterProScan annotation	TriTrypDB annotation from orthologs (including TrypTag)
LdBPK_050560.1	hypothetical protein, conserved	1 TMD	N/A
LdBPK_050770.1	hypothetical protein, unknown function	SP	<i>Leish. spe.</i>
LdBPK_060950.1	hypothetical protein, conserved	N/A	N/A
LINF_070014600	hypothetical protein - conserved	TAT; SP	Flagella connector protein 1 ( <i>T. brucei</i> ); flagella connector localisation; <a href="http://www.tryptag.org/?id=Tb927.8.940">http://www.tryptag.org/?id=Tb927.8.940</a>
LdBPK_071070.1	Protein of unknown function (DUF3608), putative	Vacuolar membrane-associated protein lml1; DEPC 5	N/A
LdBPK_080130.1	hypothetical protein, conserved	Zinc finger, RING/FYVE/PHD-type; SP	<i>Leish. spe.</i>
LdBPK_080800.1	hypothetical protein, unknown function	N/A	<i>Leish. spe.</i>
LdBPK_091010.1	hypothetical protein, conserved	N/A	Nuclear protein, potentially nuclear pore; <a href="http://www.tryptag.org/?id=Tb927.11.13080">http://www.tryptag.org/?id=Tb927.11.13080</a>
LdBPK_100700.1	hypothetical protein, unknown function	Coiled coil domain	<i>Leish. spe.</i>
LdBPK_100800.1	hypothetical protein, conserved	Coiled coil domains; disordered	N/A
LdBPK_130650.1	C2 domain containing protein, putative	C2 domain; C2CDC5	Endocytic; cytoplasm; <a href="http://www.tryptag.org/?id=Tb927.11.4160">http://www.tryptag.org/?id=Tb927.11.4160</a>
LdBPK_150840.1	hypothetical protein, conserved	Coiled coil domains; PTHR43939	Nuclear pore protein; <a href="http://www.tryptag.org/?id=Tb927.9.6460">http://www.tryptag.org/?id=Tb927.9.6460</a>
LdBPK_170570.1	hypothetical protein, unknown function	Coiled coil domain; SP	<i>Leish. spe.</i>
LdBPK_170750.1	GRAM domain containing protein, putative	GRAM domain; Ysp2/Lam4-like; SP	2 TMD (LmjF.17.0730);
LdBPK_171300.1	hypothetical protein, conserved	Coiled coil domains	Endocytic; flagellum (complex); <a href="http://www.tryptag.org/?id=Tb927.5.2500">http://www.tryptag.org/?id=Tb927.5.2500</a>
LdBPK_180100.1	hypothetical protein, conserved	N/A	Maybe centrosomal; <a href="http://www.tryptag.org/?id=Tb927.10.13640">http://www.tryptag.org/?id=Tb927.10.13640</a>

Gene ID	Protein name	InterProScan annotation	TriTrypDB annotation from orthologs (including TrypTag)
LdBPK_181340.1	hypothetical protein, conserved	Coiled coil domains; PTHR34491	Hook complex; <a href="http://www.tryptag.org/?id=Tb927.10.12720">http://www.tryptag.org/?id=Tb927.10.12720</a>
LdBPK_221030.1	WD domain, G-beta repeat, putative	3 WD40 repeat; WD40/YVTN repeat-like-containing domain; G-beta repeat	N/A
LdBPK_250870.1	hypothetical protein, conserved	PH domain	<i>Leish. &amp; T. cruzi</i>
LdBPK_251280.1	hypothetical protein, conserved	2 WD40 repeats; MIOS/Sea4; Coiled coil domains	Endocytic; <a href="http://www.tryptag.org/?id=Tb927.3.1310">http://www.tryptag.org/?id=Tb927.3.1310</a>
LdBPK_251880.1	hypothetical protein, conserved	2 TMD	<i>Leish. spe.</i>
LdBPK_252460.1	hypothetical protein, conserved	Coiled coil domain	<i>Leish. spe.</i>
LdBPK_252520.1	hypothetical protein, conserved	P-loop containing nucleoside triphosphate hydrolase; Kinesin motor domain; Homeobox-like domain; TAD2B; PH domain; Coiled coil domains	N/A
LdBPK_261960.1	hypothetical protein, conserved	Coiled coil domains	Nucleolar protein (NOP86) ( <i>T. brucei</i> ); TrypTag localisation non nucleolar; <a href="http://www.tryptag.org/?id=Tb927.9.2470">http://www.tryptag.org/?id=Tb927.9.2470</a>
LdBPK_270681.1	hypothetical protein, conserved	Coiled coil domain	<i>Leish. spe.</i>
LdBPK_270700.1	hypothetical protein, conserved	N/A	Class I transcription factor A, subunit 3 (CITFA-3) ( <i>T. brucei</i> ); nucleus localisation; <a href="http://www.tryptag.org/?id=Tb927.11.1410">http://www.tryptag.org/?id=Tb927.11.1410</a>
LdBPK_282490.1	hypothetical protein, conserved	Disordered	<i>Leish. spe.</i>
LdBPK_290470.1	hypothetical protein, conserved	Coiled coil domains; disordered	N/A
LdBPK_301900.1	hypothetical protein, unknown function	Coiled coil domain	<i>Leish. spe.</i>
LdBPK_302440.1	hypothetical protein, conserved	Coiled coil domain; disordered	<i>Leish. spe.</i>
LdBPK_302710.1	hypothetical protein, conserved	Coiled coil domains; disordered	N/A
LdBPK_321780.1	hypothetical protein, conserved	Coiled coil domain; SP	<i>Leish. spe.</i>
LdBPK_322820.1	hypothetical protein, conserved	VASt domain; 2 TMD	Flagellum attachment zone; <a href="http://www.tryptag.org/?id=Tb927.11.15870">http://www.tryptag.org/?id=Tb927.11.15870</a>
LdBPK_323200.1	hypothetical protein, conserved TbAIR9-like	5 LRR; AMPK1_CBM	AIR9-like protein (microtubule-associated protein / Internalin-A) ( <i>T. brucei</i> );
LdBPK_323680.1	hypothetical protein, conserved	2 TPR-like domains	N/A
LdBPK_330990.1	hypothetical protein, conserved	FIBP; disordered	N/A
LdBPK_333240.1	hypothetical protein, unknown function	N/A	<i>Leish. spe.</i>
LdBPK_340270.1	hypothetical protein, conserved	Coiled coil domain; disordered	<i>Leish. &amp; T. cruzi</i>
LdBPK_341080.1	hypothetical protein, conserved	SP	N/A
LdBPK_341610.1	hypothetical protein, conserved	Coiled coil domain	<i>Leish. spe.</i>
LdBPK_342300.1	hypothetical protein, conserved	3 WD40 repeat-like; 1 TMD	N/A
LdBPK_342380.1	hypothetical protein, unknown function	Coiled coil domains	<i>Leish. spe.</i>
LdBPK_352020.1	hypothetical protein, unknown function	3 EF-hand domains; EF-hand calcium-binding site	<i>Leish. spe.</i>
LdBPK_352100.1	hypothetical protein, conserved	Coiled coil domain	<i>Leish. spe.</i>
LdBPK_352220.1	hypothetical protein, conserved	N/A	<i>Leish. spe.</i>
LdBPK_352610.1	hypothetical protein, conserved	Coiled coil domain	N/A
LdBPK_352650.1	hypothetical protein, unknown function	Ubiquitin domain; DNA binding domain with preference for A/T rich regions	<i>Leish. spe.</i>
LdBPK_354190.1	conserved hypothetical protein	Disordered	<i>Leish. spe.</i>
LdBPK_361020.1	hypothetical protein, unknown function	4 TMD	<i>Leish. &amp; T. cruzi</i>

Gene ID	Protein name	InterProScan annotation	TriTrypDB annotation from orthologs (including TrypTag)
LdBPK_363660.1	hypothetical protein, conserved	Coiled coil domains	Nucleus; possibly kinetochores; <a href="http://www.tryptag.org/?id=Tb927.11.9950">http://www.tryptag.org/?id=Tb927.11.9950</a>
LdBPK_366150.1	hypothetical protein, conserved	2 TMD	<i>Leish. spe.</i>
LdBPK_366240.1	hypothetical protein, unknown function	RBD; WW domain	<i>Leish. spe.</i>

TMD: transmembrane domain; SP: signal peptide; TAT: twin arginine translocation signal profile; DEPC: Dishevelled/EGL-10/Pleckstrin (DEP) domain-containing; C2CD5: C2 domain-containing protein 5, also known as CDP138 or KIAA0528, is a C2 domain-containing phosphoprotein; PTHR43939: PANTHER family not named; GRAM: intracellular protein-binding or lipid-binding signalling domain; Ysp2/Lam4-like: membrane-anchored lipid-binding protein Ysp2/Lam4-like; PTHR34491: PANTHER family not named; PH: Pleckstrin homology domain; MIOS/Sea4: family that includes MIOS protein of the GATOR complex, Sea4 of the SEACAT complex in budding yeast; TAD2B: Transcriptional adapter 2-beta; VAST: VAD1 Analog of Star-related lipid transfer; predominantly associated with lipid binding domains such as GRAM, C2 and PH domains; LRR: Leucine-rich repeats; AMPK1\_CBM: AMP-activated protein kinase, glycogen-binding domain; TPR-like: Tetratricopeptide-like helical domain; FIBP: acidic fibroblast growth factor intracellular-binding protein; RBD: RNA-binding domain; WW domain: short conserved region in a number of unrelated proteins, which folds as a stable, triple stranded beta-sheet; *Leish. spe.*: specific to *Leishmania* species; *Leish. & T. cruzi*: found in *Leishmania* species and *T. cruzi*.

### 1.5.3. Identification of LmCKAPs implicated in vesicular or protein trafficking.

LmCK1.2 has been shown to be exported, as free protein or via exosomes either in macrophages or in the midgut of the insect vector, but the mechanisms involved in these processes are still unknown (Atayde et al., 2015; Santarém et al., 2013; Silverman et al., 2008, 2010a). To gain insight into these mechanisms, we first selected eleven LmCKAPs potentially involved in protein trafficking based on the literature, or on the presence of putative domains implicated in trafficking (Table 5). We selected:

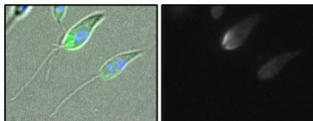
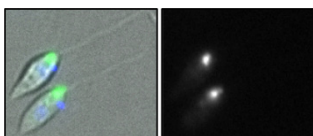
- One hypothetical protein, LdBPK\_080130.1 (LmCKAP1), which contains a FYVE domain necessary to bind to phosphatidylinositol-3-phosphate and to allow the protein to be inserted into cell membranes (Table 4 and 5);
- Sec3 (LdBPK\_081060.1), a protein part of the exocyst complex important to tether vesicles at the plasma membrane;
- The four components of the adaptin protein complex 2 (AP2) that were identified in our dataset: the two large  $\alpha$ 2-adaptin (LdBPK\_070060.1) and  $\beta$ 2-adaptin (LdBPK\_110990.1) subunits, the medium  $\mu$ 2-adaptin subunit (LdBPK\_363180.1) and the small  $\sigma$ 2-adaptin subunit (LdBPK\_342100.1) (Table 5). This complex is involved in endocytosis and trafficking of proteins towards the early endosomes (Mettlen et al., 2018);

- Three putative kinesins, LdBPK\_170270.1 (LmKin17), LdBPK\_211280.1 (LmKin21), and LdBPK\_301510.1 (LmKin30), as well as one dynein light chain, LdBPK\_320240.1 (LmDYNLL1), ortholog to *T. brucei* DYNLL1 (Table 5).

We used the CRISPR-Cas9 toolkit to generate the transgenic parasites expressing in locus mNeonGreen (mNG) epitope-tagged proteins and the corresponding null mutants (Beneke et al., 2017; Martel et al., 2017). We confirmed the correct tagging of mNG-tagged proteins by Western blot analysis (Fig. S1A) and the correct deletion of the corresponding genes by PCR (Fig. S1B).

All the results are summarised Table 5. Only four proteins displayed a localisation consistent with a role in protein trafficking: three members of the AP2 complex and Sec3, which all localise to the flagellar pocket. We selected the AP2 proteins for further characterisation, as they could be involved in the loading of proteins into exosomes.

**Table 5:** Accession numbers and annotations of LmCKAPs identified from MS and involved in membrane trafficking

Gene ID	Protein name (with annotation)	MW	Name	Images	Localisation	Null mutant
LdBPK_080130.1	Hypothetical protein, conserved FYVE / PH domain	121,2	LmCKAP1		Plasma membrane	Viable
LdBPK_070060.1	Alpha-adaptin-like protein, ARM repeat	107,7	$\alpha$ 2-adaptin		Flagellar pocket	Lethal?
LdBPK_110990.1	Adaptin related-like protein, ARM repeat	108,5	$\beta$ 2-adaptin		Flagellar pocket	Viable
LdBPK_363180.1	Clathrin coat assembly-like protein MHD domain	48,9	$\mu$ 2-adaptin		Flagellar pocket	Viable

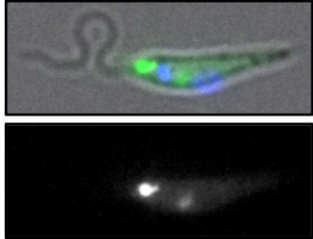
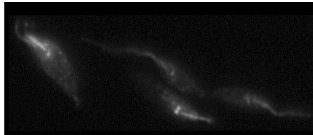
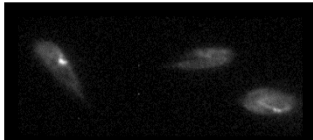
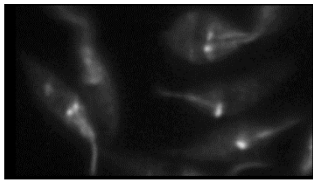
LdBPK_342100.1	Clathrin coat assembly protein AP17	16,8	$\sigma$ -adaptin	n.d.	n.d.	n.d.
LdBPK_081060.1	Exocyst complex component Sec3	126,9	LmSec3		Flagellar pocket	Lethal?
LdBPK_170270.1	Putative Kinesin	114,8	LmKin17		Basal body & flagellum	Lethal?
LdBPK_211280.1	Putative Kinesin	231,1	LmKin21		unknown	Lethal?
LdBPK_301510.1	Kinesin, putative Kinesin motor domain, PH domain	133,0	LmKin30		unknown	Viable
LdBPK_320240.1	Dynein light chain, flagellar outer arm, putative	10,6	LmDYNLL1		Basal body & flagellum	Lethal?

Table showing the LmCKAPs selected for their potential role in protein trafficking, based on the literature or on the presence of putative domains implicated in trafficking. Gene ID (*L. donovani* BPK282A1 strain), annotation, predicted or curated domains, molecular weight (MW) and names are represented, as well as the outcome of CRISPR-Cas9 targeting for mNeonGreen epitope tagging or generation of null mutants. The outcome of null mutant generation is indicated as viable (green) or lethal (red). Live microscopy images of *L. donovani* promastigotes expressing  $\alpha$ 2-adaptin-mNG-myc3,  $\beta$ 2-adaptin-mNG-myc3,  $\mu$ 2-adaptin-mNG-myc3, LmCKAP1-adaptin-mNG-myc3, LmSec3-adaptin-mNG-myc3, LmKin17-adaptin-mNG-myc3, LmKin21-adaptin-mNG-myc3, LmKin30-adaptin-mNG-myc3 or LmDYNLL1-adaptin-mNG-myc3 are presented. Each panel shows the mNeonGreen fluorescence (mNG, green) with/without Hoechst 33342 staining (H, blue) and/or a merged image of mNG, H and the brightfield image. The description of the localisation is provided in the column on the right of the images.

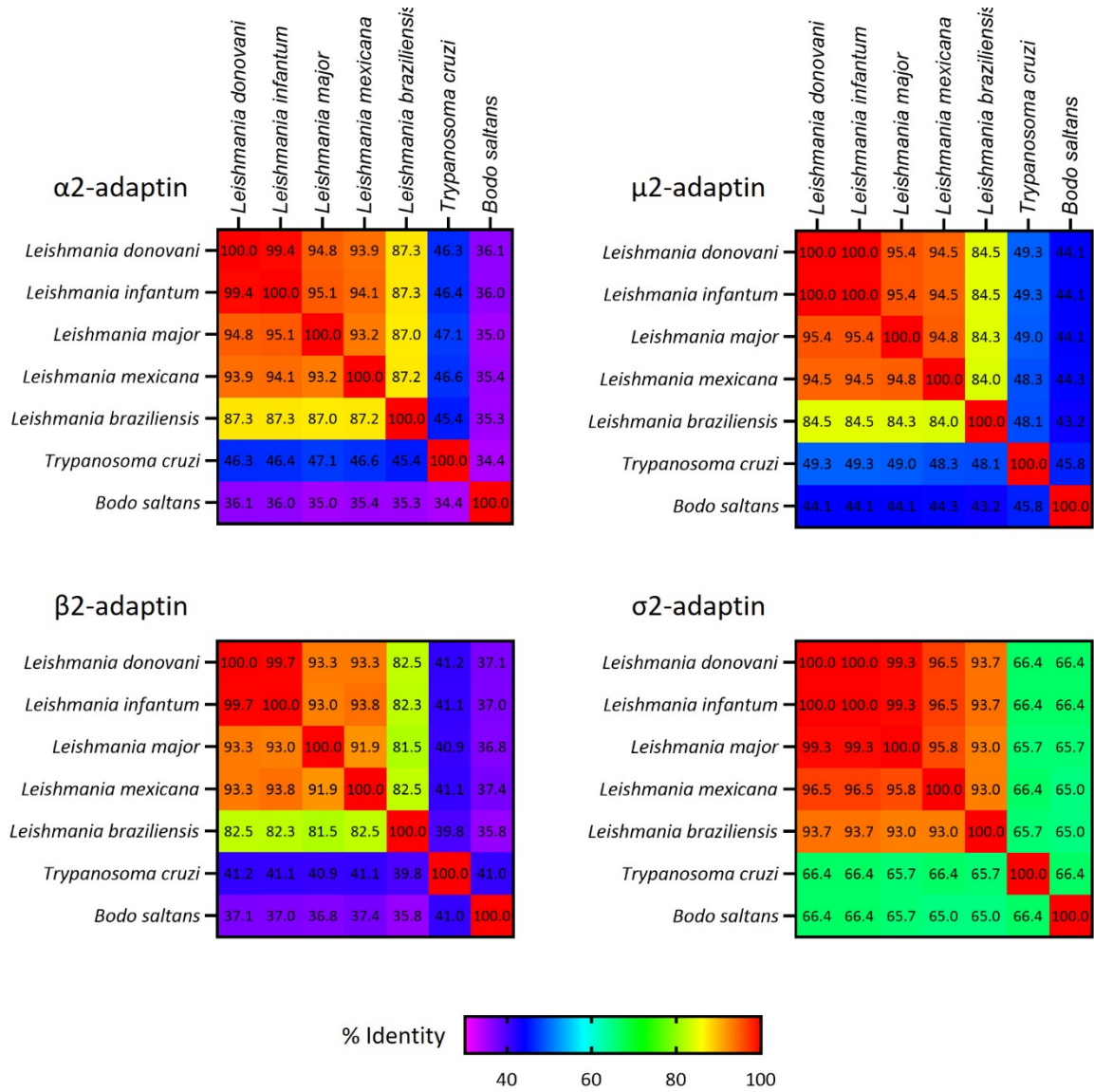
#### 1.5.4. The AP2 complex is conserved in *Leishmania spp.*

There are at least two mechanisms described to load cargo proteins into exosomes in mammalian cells. (1) Subsequently to endocytosis of membrane proteins, vesicles generated at the plasma membrane deliver their cargo to early endosomes, which mature to become late endosomes / multivesicular bodies (MVB). These MVBs can either fuse with lysosomes leading to the degradation of their content or with the plasma membrane to release exosomes (Desdín-Micó and Mittelbrunn, 2017). (2) Through endosomal microautophagy-like processes (Desdín-Micó and Mittelbrunn, 2017; Sahu et al., 2011). A soluble cytoplasmic protein binds to Hsc70, then the complex binds to the endosomal-limiting membrane through Hsc70-electrostatic interactions (Sahu et al., 2011). This mechanism is ATP dependent and does not required protein unfolding (Sahu et al., 2011). The AP2 complex could be implicated in the first mechanism. Indeed, the AP2 complex is involved in the transport of cargos from the plasma membrane to early endosomes through endocytosis by binding to clathrin-coated vesicles (Collins et al., 2002). The AP2 complex, which coordinates clathrin-coated pits (CCP) formation and binds to cargo proteins is targeted to the plasma membranes through its binding to phosphatidylinositol 4,5-bisphosphate (PIP2) (Cocucci et al., 2012; Jackson et al., 2010). Moreover, AP2 complex subunits  $\alpha$ -1 and  $\beta$ -1 (AP2A1 and AP2B1) have been consistently identified as components of exosomes (Simpson et al., 2008), and recent studies showed that AP2, through its association with an RNA-binding ubiquitin FeF ligase MEX3C, was involved in selective sorting of microRNA miR-451a into exosomes (Lu et al., 2017).

Four AP2 subunits were identified as LmCKAPs, exclusively in the assay and not in the control (Table 2). They correspond to the AP2 complex, which is a heterotetramer (Boehm and Bonifacino, 2001). LmCK1.2 seems to interact with the whole complex and not just individual proteins. All subunits were specifically recovered in axAMA, suggesting that the interaction with LmCK1.2 could be stage-specific (Table 2). To better characterise the AP2 complex in *Leishmania spp.*, we carried out a phylogenetic analysis of the four subunits of the AP2 complex from different trypanosomatids species, *Leishmania donovani*, *Leishmania infantum*, *Leishmania major* and *Leishmania mexicana* (from the *Leishmania* subcomplex), *Leishmania braziliensis* (from the *Viannia* subcomplex), *Trypanosoma cruzi* and *Bodo saltans* (see Table S3 for accession numbers). AP2 complex subunits are well conserved in *Leishmania* species, with more than 80% of identity in protein sequence, and up to 93% of identity for the *Leishmania*

*Leishmania* subcomplex (Fig. 3A). AP2 subunits are also conserved in distant trypanosomatids, but with higher divergence (34-67% identity depending on the subunit, Fig. 3A). The small  $\sigma$ -adaptin is the most conserved subunit (around 65% of identity, Fig. 3A). Surprisingly, AP2 was lost in *Trypanosoma brucei*, as these genes were also present in the early-branching trypanosomatid *Paratrypanosoma confusum* (Flegontov et al., 2013), suggesting that *T. brucei* parasites might use clathrin-independent pathways for endocytosis (Manna et al., 2013; Morgan et al., 2002).

A



B

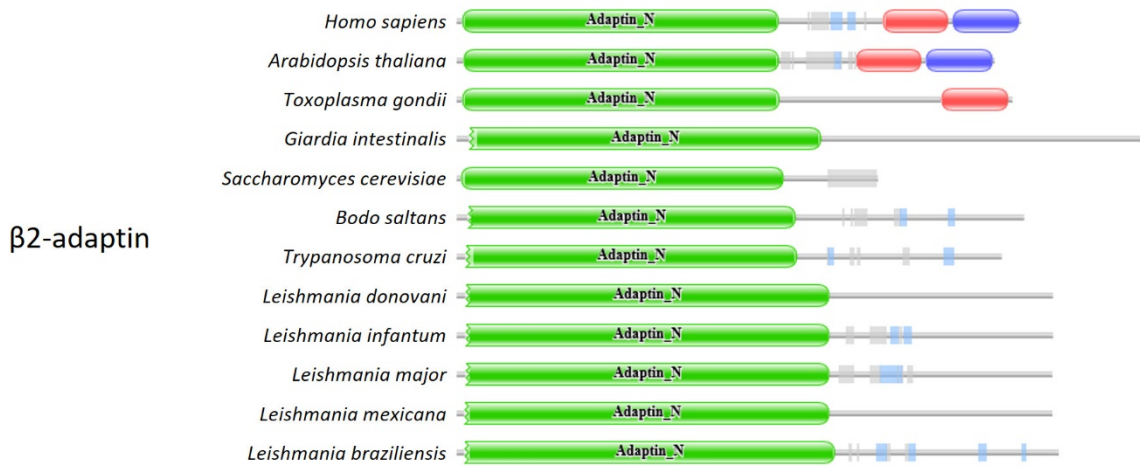


**Fig. 3** – Sequence and functional relationships among AP2 complex homologs.

(A) Pairwise percentage of identity heat matrix of seven AP2 homologs in trypanosomatids, for  $\alpha$ 2-adaptin,  $\beta$ 2-adaptin,  $\mu$ 2-adaptin and  $\sigma$ 2-adaptin (MUSCLE v3.8). Rainbow colormap.

(B) Cartoon showing the domain composition of twelve  $\beta$ 2-adaptin homologs, revealing the absence of a C-terminal domain implicated in clathrin binding in trypanosomatids. The domains are: N-terminal adaptin domain (green, pfam01602),  $\alpha$ 2-adaptin C2 domain (red, pfam02883). Disorder content (gray) or low complexity regions (blue) and  $\beta$ 2-adaptin appendage (blue, pfam09066). Disordered content (gray) and low complexity regions (light blue) are also depicted.

Although *Leishmania* possesses an AP2 complex, it might be clathrin-independent similarly to that of *T. cruzi* (Kalb et al., 2016). To investigate this hypothesis, we compared in **Fig. 3B** the structure of the trypanosomatid  $\beta$ 2-adaptins to that of clathrin-dependent AP2  $\beta$ 2-adaptin (*Homo sapiens*, *Arabidopsis thaliana* and *Toxoplasma gondii*) or clathrin-independent AP2  $\beta$ 2-adaptin (*Giardia intestinalis* and *Saccharomyces cerevisiae*). The structure of all trypanosomatid AP2  $\beta$ 2-adaptins were similar to that of the clathrin-independent AP2, as judged by the absence of the two C-terminal domains (pfam02883 and pfam09066) involved in clathrin binding and polymerization (**Fig. 3B**) (Lemmon and Traub, 2012). This finding suggests that despite having an AP2 complex, endocytosis in *Leishmania* spp. might be clathrin independent.

#### 1.5.5. $\beta$ 2-adaptin is phosphorylated by LmCK1.2.

Next, in order to determine which AP2 subunit is regulated by LmCK1.2, we performed kinase assays. To this end, we expressed *L. donovani*  $\alpha$ 2-,  $\beta$ 2- and  $\mu$ 2-adaptins as V5-His<sub>6</sub>-tagged recombinant proteins in *E. coli*, and purified them using cobalt beads. As a positive control, we used MBP, a canonical substrate and showed its phosphorylation by recombinant LmCK1.2 only in absence of D4476 (a specific CK1 inhibitor, **Fig. 4A**), indicating that the kinase is active. Then, we performed an *in vitro* kinase assays with each adaptin and showed that only  $\beta$ 2-adaptin was successfully phosphorylated by LmCK1.2, as demonstrated by the incorporation of <sup>32</sup>P into the recombinant protein (**Fig. 4B**, band at ~ 115 kDa). The phosphorylation is LmCK1.2-specific, as it was inhibited by D4476 and not detected in the absence of the kinase (**Fig. 4B**). This finding reveals that LmCK1.2 interacts with the AP2 complex, but phosphorylates only the  $\beta$ 2 subunit. Because interaction with the substrate is

not necessary for phosphorylation, we cannot conclude that  $\beta 2$  adaptin is also the only interacting partner of LmCK1.2 in the AP2 complex.

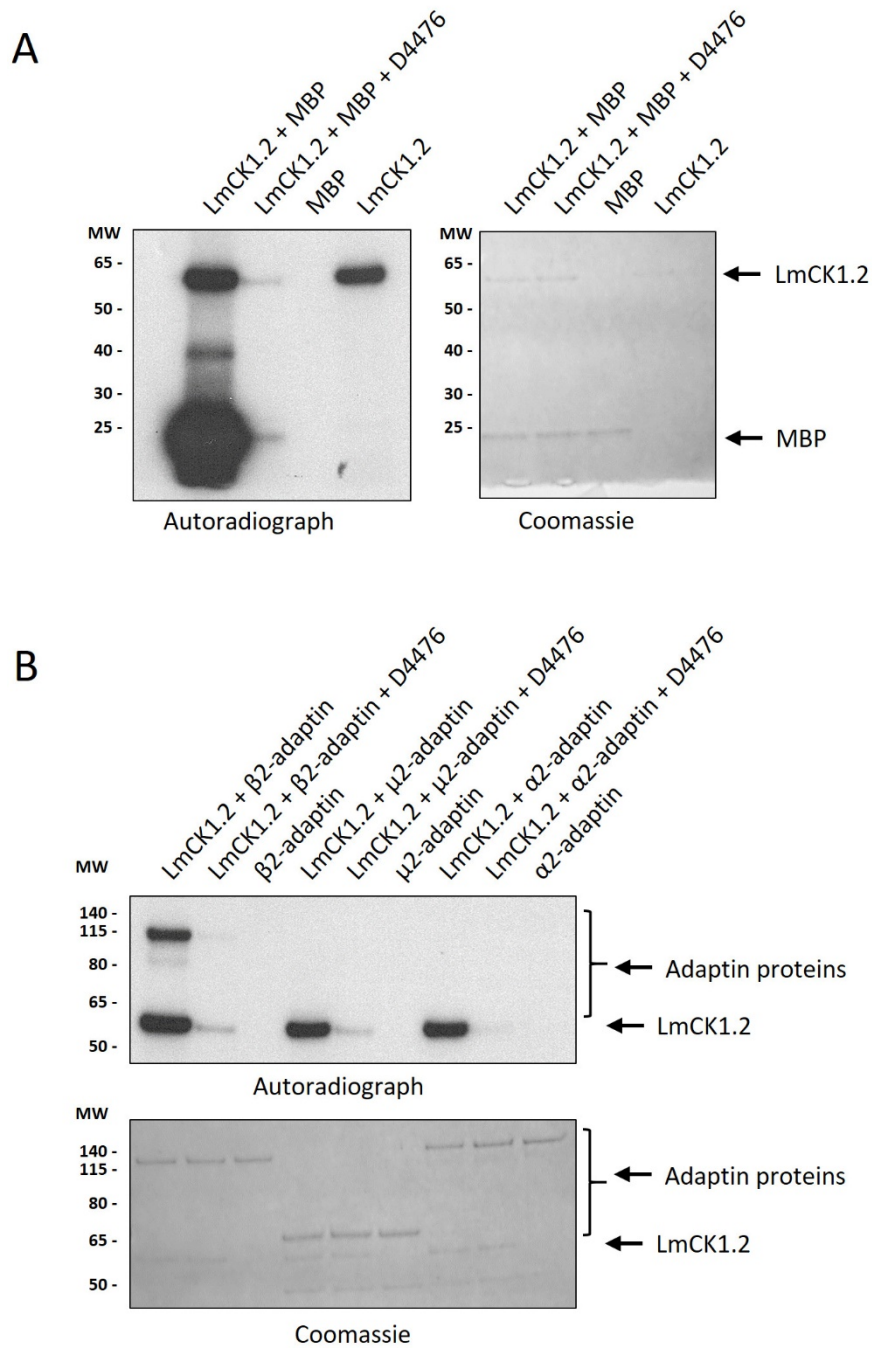


**Fig. 4** –  $\beta$ 2-adaptin (but not  $\alpha$ 2- or  $\mu$ 2-adaptin) is a substrate for LmCK1.2.

*In vitro* kinase assays using recombinant thio-LmCK1.2-V5 (LmCK1.2, 55.9 kDa) and using MBP (A) as substrate or recombinant AP2 adaptins (B): thio- $\alpha$ 2-adaptin-V5 ( $\alpha$ 2-adaptin, 123.7 kDa), thio- $\beta$ 2-adaptin-V5 ( $\beta$ 2-adaptin, 124.7 kDa) or thio- $\mu$ 2-adaptin-V5 ( $\mu$ 2-adaptin, 65.1 kDa). Purified substrates and MBP were incubated with purified kinase, with or without LmCK1.2 canonical inhibitor D4476. A control without the kinase was added. Kinase assays were performed at the same time for 30 min at pH 7.5 and 30°C and stopped by addition of NuPAGE loading buffer. The reaction samples were separated by SDS-PAGE, the gel stained by Coomassie, and the signals were revealed by autoradiography. The brackets indicate AP2 adaptins phosphorylation signals or proteins revealed by Coomassie staining. Arrows indicates whether LmCK1.2 auto-phosphorylation or MBP phosphorylation, and corresponding Coomassie bands. MW, molecular weight. Results are representative of two independent experiments.

### 1.5.6. $\alpha$ 2-, $\beta$ 2- or $\mu$ 2-adaptin subunits, expressed in logarithmic and stationary phase are part of one complex.

To determine the function of the AP2 complex in *Leishmania*, we studied the transgenic parasites expressing either  $\alpha$ 2-,  $\beta$ 2- or  $\mu$ 2-adaptin-mNG. We did not observed any growth defect in promastigotes, except for  $\alpha$ 2-adaptin-mNG expressing promastigotes, which displayed an increase in the percentage of cell death in late stationary phase, reaching about 60% compared to 20% for the mock (Fig. S2). We measured the fluorescence intensity of the different tagged subunits by flow cytometry using the parental strain as negative control to define the background (Fig. 5A, back line). We observed a higher intensity for  $\alpha$ 2- and  $\beta$ 2-adaptin subunits compared to that for the  $\mu$ 2-adaptin subunit, which is constant during parasite growth (Fig. 5A, dark green, light green and blue). These findings suggest that the first two proteins might be more abundant than the last subunit, which is consistent with the Western blot data (Fig. S1Aa).

Next, we performed gel filtration experiments to obtain additional evidence that the three AP2 subunits were part of the same complex and to determine its size. We fractionated 3 mg of total protein from axenic amastigotes on a superdex 200 10/300 GL column and collected 96 fractions of 250  $\mu$ L each. Two hundred microliters of each fraction were blotted on a nitrocellulose membrane to perform a slot blot analysis using an anti-LmCK1.2 antibody and an anti-myc antibody to identify either  $\alpha$ 2-,  $\beta$ 2- and  $\mu$ 2-adaptin subunits. We detected LmCK1.2 in at least four complexes as judged by Fig. 5B (red dots), with sizes ranging from 200 to more than 2000 kDa. One of the complexes at approximately 2000 kDa also contains  $\alpha$ 2- and  $\beta$ 2- and  $\mu$ 2-adaptin. The size of this complex is well above the size of the four individual

proteins combined (139.4, 140.4, 80.7 and 40kDa for  $\alpha$ 2-,  $\beta$ 2- and  $\mu$ 2-adaptin, and LmCK1.2-V5, respectively), suggesting that other proteins could be part of this complex.

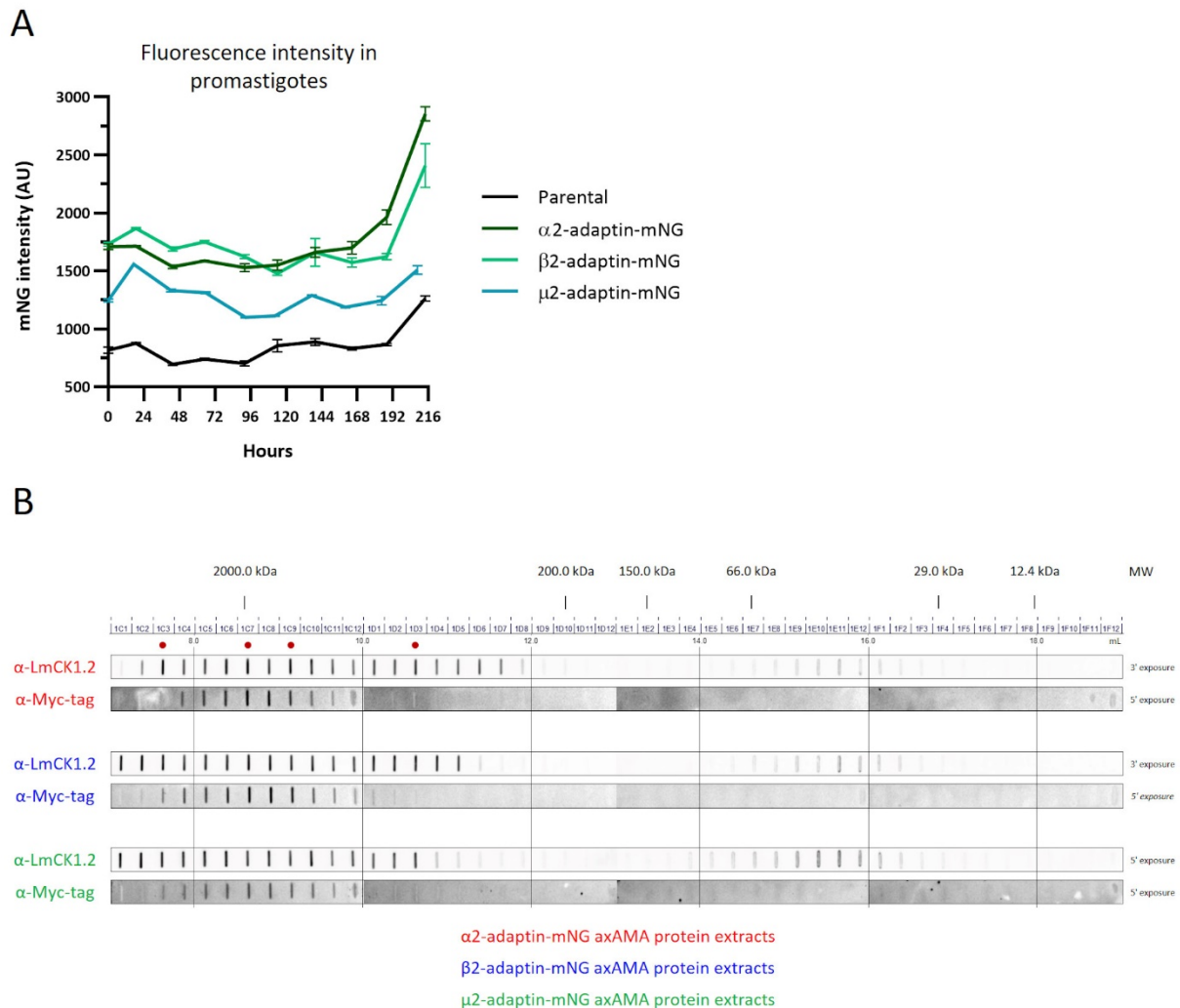


**Fig. 5** – AP2 subunits belong to the same complex, together with LmCK1.2

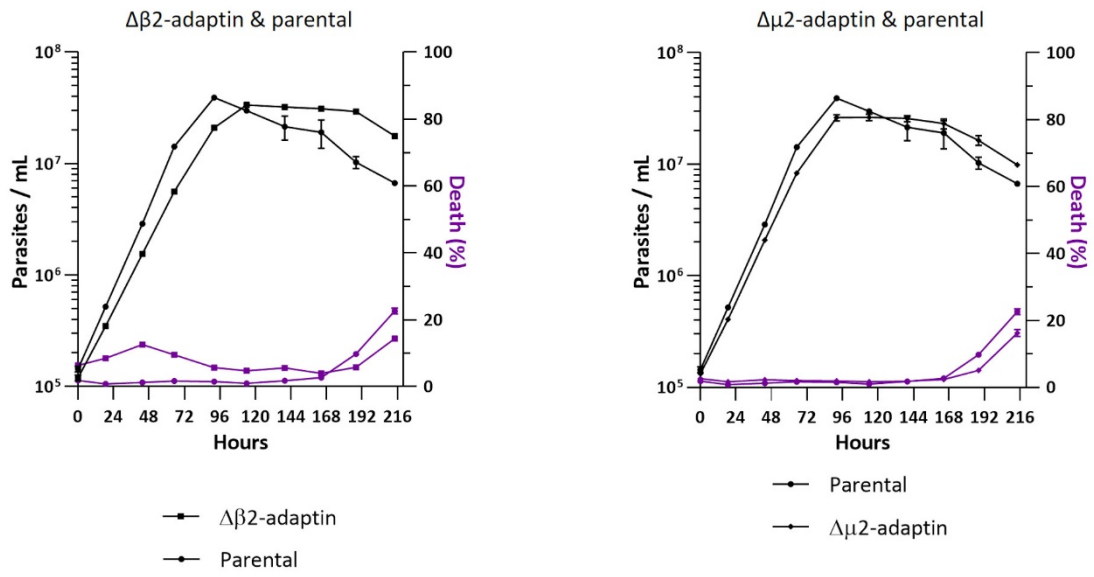
(A) Promastigotes were seeded at  $1 \times 10^5$  cells/mL and cultured for 9 days. Samples were collected every 24 h to assess mNeonGreen fluorescence intensity by flow cytometry in triplicate. Each value displays the mean of triplicates and SD error bars. Cell lines: parental (black) and  $\alpha$ 2-,  $\beta$ 2- and  $\mu$ 2-adaptin-mNG (green, light green and blue, respectively). Representative of two independent experiments. (B) Protein complexes in  $\alpha$ 2-adaptin-mNG (red),  $\beta$ 2-adaptin-mNG (blue) and  $\mu$ 2-adaptin-mNG (green) axenic amastigote extracts were assessed by gel filtration on a superdex 200 10/300 GL column. 96 fractions of 250  $\mu$ L were collected and 200  $\mu$ L were applied on a nitrocellulose membrane to perform a slot blot analysis using an anti-LmCK1.2 antibody and an anti-myc antibody to detect endogenous LmCK1.2 or  $\alpha$ 2-,  $\beta$ 2- and  $\mu$ 2-adaptin-mNG subunits. Results for one experiment.

### 1.5.7. The AP2 complex plays a vital role in axenic amastigotes.

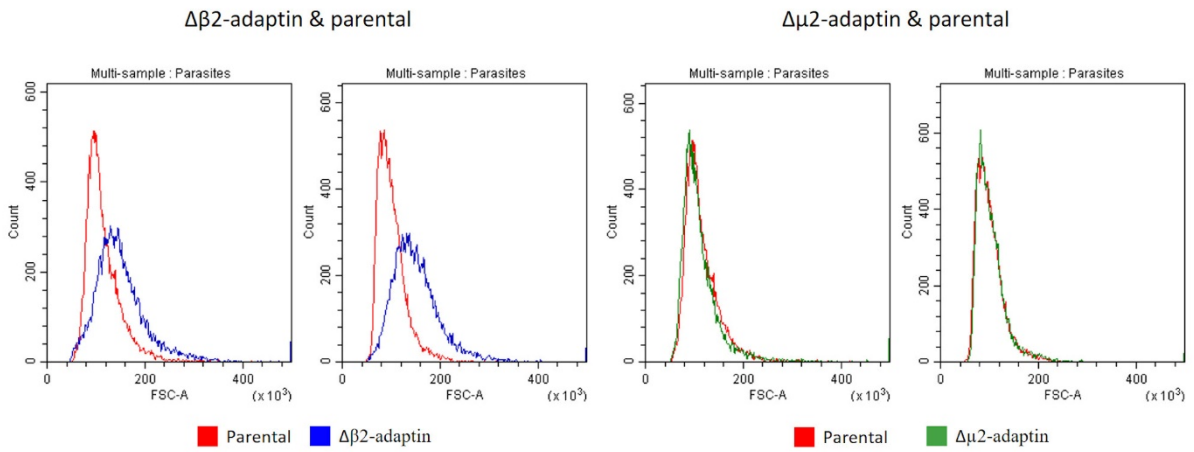
To determine whether this AP2 complex plays an important role in parasite biology, we deleted the genes coding for the three subunits in *LdB* pTB007 cells using CRISPR Cas9 toolkit (Beneke et al., 2017). Only the deletion mutant for the  $\alpha$ 2-adaptin subunit could not be obtained despite several attempts, suggesting that this protein might be essential. This finding supports also the hypothesis that  $\alpha$ 2-adaptin could have additional roles compared to  $\beta$ 2- and  $\mu$ 2-adaptins for which we obtained viable null mutants. We confirmed, by PCR, the deletions of the two alleles, which were successfully replaced with the puromycin and blasticidin-resistance genes (Fig. S1B panels c and d). The generation of homozygous  $\Delta\beta$ 2- and  $\Delta\mu$ 2-adaptin parasites indicates that both genes are non-essential for promastigote survival. Nevertheless, both mutants were slightly slower than the parental strain to reach stationary phase in promastigotes (Fig. 6A). This was especially true for the  $\Delta\beta$ 2-adaptin cell line, which displayed a higher percentage of cell death than that of the parental cell line (WT), in particular during logarithmic phase, as measured by propidium iodide (PI) incorporation (12.5% cell death at 48h compared to 1.2% for the parental strain) (Fig. 6A, square). Moreover, we noticed that  $\Delta\beta$ 2-adaptin mutant cells appeared to be bigger than the wild type cells. To investigate this phenotype, we compared the forward scatter area (FSC-A), which corresponds to cell size, of individual parasites by flow cytometry for the knockout and the parental cell lines. We found that the FSC-A values of the  $\Delta\beta$ 2-adaptin mutant cells were higher than those of the parental cells at 48h (Fig. 6B, panel 1) as well as at 96h (Fig. 6B, panel 2). We did not observe such differences for  $\Delta\mu$ 2-adaptin mutant cells (Fig. 6B, panel 3 and 4). This finding suggests that the deletion of  $\beta$ 2-adaptin leads to an increase in cell size in promastigotes. We next asked whether  $\beta$ 2- and  $\mu$ 2-adaptin were required for axenic amastigote differentiation or growth, as we identified the AP2 complex mainly in axenic amastigote. Although  $\Delta\beta$ 2-adaptin mutant cells were able to differentiate into axenic amastigote, they grew much slower than the WT as they reached stationary phase with a 48h delay (Fig. 6C, left panel). Moreover, they grew to lower densities than WT. This phenotype could be explained by a higher percentage of cell death compared to WT during differentiation (35% for  $\Delta\beta$ 2 and 10% for WT 0-24h). We also measured a higher percentage of cell death during proliferation (48h- 192h), suggesting that the mutant cells were more sensitive to the axenic culture conditions compared to the WT (Fig. 6C, left panel). The  $\Delta\mu$ 2-adaptin cell line also showed an increased in cell death only

during axenic amastigote differentiation, which resulted in a delay in cell growth (Fig. 6C, right panel). However,  $\Delta\mu 2$ -adaptin cells reached the same density in stationary phase than the parental cell line, in contrast to  $\Delta\beta 2$ -adaptin cell line (Fig. 6C, right panel). This result suggests that the deletion of both  $\beta 2$ - and  $\mu 2$ -adaptin genes has a moderate effect on promastigotes, but has a major impact on axenic amastigotes differentiation and growth. This finding is particularly interesting as the AP2 complex components only co-precipitated with LmCK1.2 in axenic amastigotes suggesting that this process could be regulated by LmCK1.2.

A



B



C

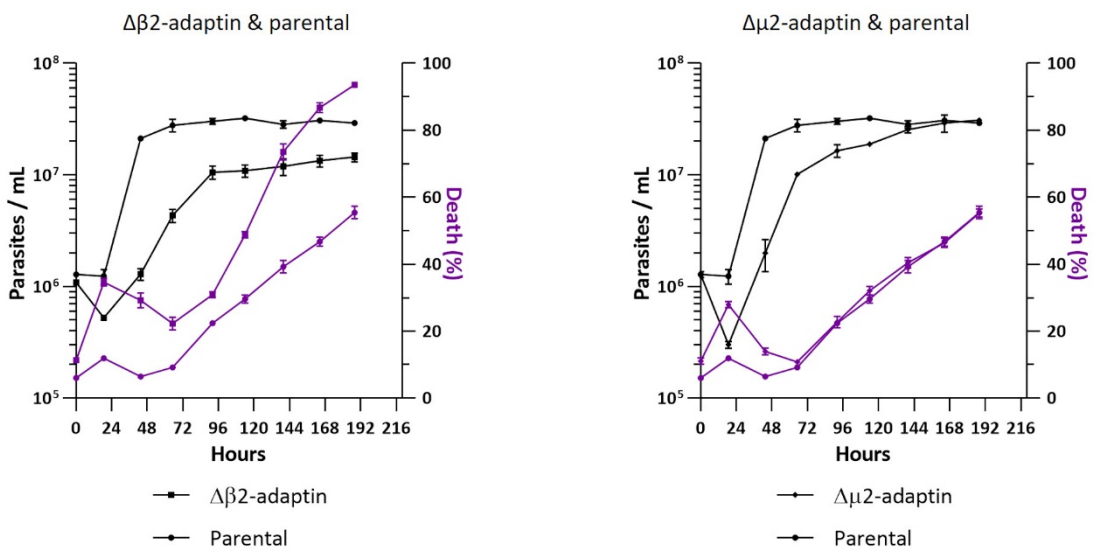


**Fig. 6** – AP2  $\beta$ 2- and  $\mu$ 2-adaptin are required for axenic amastigotes differentiation.

Characterisation of CRISPR-Cas9-mediated null mutants of the *L. donovani*  $\beta$ 2- and  $\mu$ 2-adaptin. (A) Promastigotes were seeded at  $1 \times 10^5$  cells/mL and cultured for 9 days. Samples were collected every 24 h to assess cell concentration (black symbols) and percentage of cell death (magenta symbols) by flow cytometry in triplicate in two independent experiments. Each value display the mean of triplicates and SD error bars. Cell lines: parental (circle),  $\Delta\beta$ 2-adaptin (square) and  $\Delta\mu$ 2-adaptin (diamond).

(B) Histograms showing the forward scatter area (FSC-A) values for parental and the null mutants, at 48h (left panels) and 96h (right panels) of growth, assessed by flow cytometry, related to the samples from (A). Represent  $\sim 15000$  parasites and are representative of triplicate experiments. Cell lines: parental strain (red) or  $\Delta\beta$ 2-adaptin (blue) and  $\Delta\mu$ 2-adaptin (green).

(C) Promastigotes were seeded at  $1 \times 10^6$  cells/mL and shifted to 37°C and pH 5.5 and cultured for 8 days for axenic amastigotes differentiation. Samples were collected every 24 h to assess cell concentration (black symbols) and percentage of cell death (magenta symbols) by flow cytometry in triplicate in two independent experiments. Each values display the mean of triplicates and SD error bars. Cell lines: parental (circle),  $\Delta\beta$ 2-adaptin (square) and  $\Delta\mu$ 2-adaptin (diamond).

### 1.5.8. The deletion of $\beta$ 2-adaptin leads to a defect in endocytosis.

Finally, we investigated the role of the AP2 complex and its implication in endocytosis. To this end, we used the tracer FM4-64FX to assess the volume of the flagellar pocket of the two  $\beta$ 2- and  $\mu$ 2-adaptin mutants (Vince et al., 2008).  $\Delta\beta$ 2- and  $\Delta\mu$ 2-adaptin promastigotes were treated with FM4-64FX for 30 min at 26°C and then the fluorescence intensity was assessed by flow cytometry. FM4-64 rapidly labelled the flagellar pocket and weakly the plasma membrane (Fig. 7A). We measured the difference in FM4-64 uptake by measuring the fluorescence intensity of individual parasites by flow cytometer (Fig. 7B). We noticed a difference in fluorescence intensity between the parental and the  $\beta$ 2-adaptin mutant cells, suggesting that more dye was accumulated in the flagellar pocket (Fig. 7B, left panel). We did not observe such a difference for  $\mu$ 2-adaptin mutant (Fig. 7, right panel). These results indicate that the flagellar pocket of  $\beta$ 2-adaptin mutant might be bigger than that of the parental cell line, suggesting that deletion of  $\beta$ 2-adaptin could affect endocytosis. However, as the size of  $\beta$ 2-adaptin deleted cells are bigger than that of the parental cells, we cannot exclude that this difference could be due to the incorporation of FM4-64FX in the plasma membrane. We will perform additional experiments with different dyes that do not stain the plasma membrane to test this hypothesis.

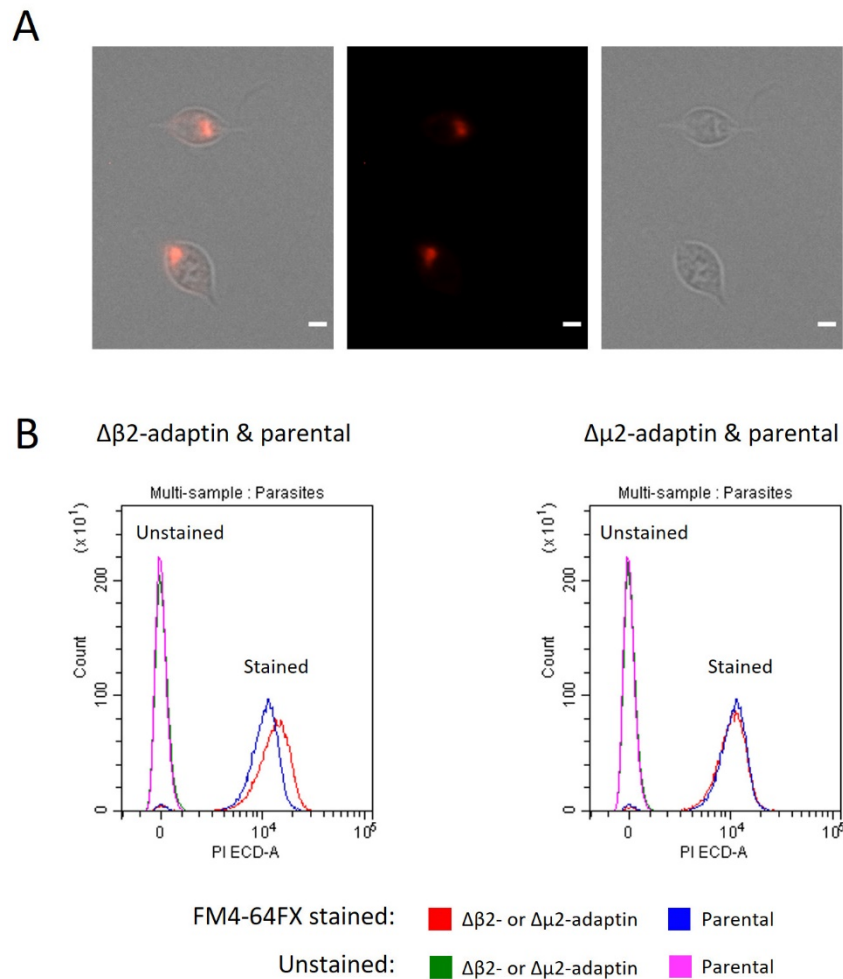


**Fig. 7 –  $\Delta\beta 2$ -adaplin promastigotes show increased FM4-64 fluorescence compared to the control.** (A) example showing the staining of *L. donovani* promastigotes with FM4-64FX. Parasites were treated for 15 min at 26°C and washed in promastigote culture medium before being imaged. Middle panel shows FM4-64FX signal, right panel shows the bright-field (BF) image and left panel shows a merge of the single channel images. Scale bar, 2  $\mu\text{m}$ . (B)  $\Delta\beta 2$ - and  $\Delta\mu 2$ -adaplin promastigotes were either incubated with 5  $\mu\text{M}$  FM4-64FX or not at 26°C for 30 min. The fluorescence intensity of the incorporated dye was then assessed by flow cytometry and with 30 000 events were acquired.

## 1.6. Discussion

LmCK1.2 is essential for *Leishmania* survival but little is known about the pathways it regulates. Because of its pleiotropic localisation in promastigotes and axenic amastigotes, LmCK1.2 needs to be tightly regulated. We recently showed that the low complexity regions (LCRs), in the C-terminus, were involved in the subcellular sequestration of LmCK1.2 (Martel et al., submitted). The LCRs are known to be implicated in protein-protein interactions, which is an major factor that drives CK1 localisation and regulates its activity (Behrend et al., 2000; Bischof et al., 2013; Cruciat et al., 2013; Fulcher et al., 2018; McKenzie et al., 2006; Sillibourne et al., 2002; Wolff et al., 2005, 2006, 2006; Yin et al., 2006). The data presented here confirm that LmCK1.2-associated proteins (LmCKAPs) are important for subcellular sequestration, as we identified LmCKAPs with functions consistent with the subcellular localisation of LmCK1.2. Moreover, our data present strong similarities to those obtained with PfCK1 (the orthologs of LmCK1.2 in *Plasmodium falciparum*). Both kinases interact with proteins involved in post-translational modification, nucleic-acid-binding and trafficking, suggesting that they could have similar roles in the two different parasites (Dorin-Semblat et al., 2015).

### 1.6.1. The subcellular localisation of LmCK1.2 is consistent with the functions of LmCKAPs

LmCK1.2 has been shown to localise to the flagellum, the basal body and the TAC (Martel et al. submitted). We identified several LmCKAPs, such as tubulins, FAZ2 (flagellum attachment zone), a dynein light chain and TAC60 (tripartite attachment complex protein), for which the function is consistent with such localisation. These proteins could therefore be implicated in the localisation or the regulation of LmCK1.2. For instance, LmCK1.2 was shown to localise between the kinetoplast and the basal bodies, a region where the exclusion zone filaments links the kinetoplast DNA to the basal bodies (Martel et al. submitted). We could confirm this localisation by the identification of TAC60 (LdBPK\_260530.1), a member of the tripartite attachment complex (TAC), which, in *T. brucei*, is located to the outer membrane of the mitochondrion, between the kDNA and basal body (Käser et al., 2017). TAC60 is required for kDNA segregation, supporting the hypothesis that LmCK1.2 could have a role in this process. As another example, LmCK1.2 was previously shown to colocalise with and

phosphorylate Hsp70 (HSPA1B), leading to the hypothesis that Hsp70 could also interact with LmCK1.2 to insure its subcellular localisation (Martel et al., submitted). This hypothesis is supported by the identification of HSPA2 and HSPA1B, as interacting partners. We also identified HSPA5, an ER-specific Hsp70, suggesting that LmCK1.2 could also localise to the ER. The identification of cytoplasmic Hsp70, as a major LmCK1.2 binding partner might be crucial to understand how LmCK1.2 is loaded into exosomes. Indeed, one mechanism described to load cargo proteins into exosomes in mammalian cells is through endosomal microautophagy-like processes, involving Hsc70 (Desdín-Micó and Mittelbrunn, 2017; Sahu et al., 2011). Hsc70 interacts with soluble cytoplasmic proteins to bring them to the endosomes through binding with the endosomal-limiting membrane (Sahu et al., 2011). Altogether these findings indicate that the localisation of LmCK1.2 is strongly linked to its functions.

### 1.6.2. Potential functions of LmCK1.2 in the nucleus

LmCK1.2 has been identified in the nucleus and nucleolus of *Leishmania* and potential functions could be inferred such as the regulation of chromosome segregation or rRNA processing. Our recent data support these hypotheses, LmCK1.2 could be implicated in RNA splicing in *Leishmania*. Indeed, we identified three interacting proteins involved in mRNA processing, Gemin2 (LdBPK\_361350.1), SMN-like (survival of motor neuron, LdBPK\_321890.1) and a small nuclear ribonucleoprotein-associated protein B (SmB, LdBPK\_271890.1). SMN and Gemin2 are involved in splice leader (SL) biogenesis in *T. brucei* (Palfi et al., 2009). In *P. falciparum*, Dorin-Semblat et al. showed that PfCK1, the ortholog of LmCK1.2 also co-purified with RNA splicing factors, which were over-represented in their dataset (Dorin-Semblat et al., 2015). The role of LmCK1.2 in RNA splicing is consistent with the functions of mammalian CK1. Indeed, CK1 $\alpha$  was shown to localise to nuclear speckles, compartments that supply splicing factors to active transcription sites (Fu et al., 2001; Gross et al., 1999; Spector and Lamond, 2011), and bind to and phosphorylate different regulators of mRNA processing (Gross et al., 1999; Kattapuram et al., 2005). LmCK1.2 could play a role in ribosome maturation, as we identified many ribosomal proteins in the LmCKAPs dataset in axenic amastigotes. This data is consistent with our previous result showing that LmCK1.2 localises at the periphery of the nucleolus in *L. donovani*, where pre-ribosomal ribonucleoproteins are matured and assembled with ribosomal proteins (Boisvert et al., 2007). Moreover, the interactome of PfCK1 contains

15 ribosomal proteins, confirming a role for CK1 in ribosomal processing (Dorin-Semblat et al., 2015). A link between CK1 and ribosomes biogenesis has also been described for other eukaryotes: (i) the two human CK1 $\delta$  and CK1 $\epsilon$  are components of pre-40S subunits required for cytoplasmic 40S maturation (Zemp et al., 2014); (ii) yeast CK1 $\delta/\epsilon$  homolog Hrr25 is essential for ribosome assembly (Ghalei et al., 2015), and (iii) Hrr25 plays a role in 60S ribosome biogenesis by phosphorylating Tif6p, the yeast homologue of mammalian eIF6 (Ray et al., 2008). Finally, we previously showed that nucleolar LmCK1.2 was redistributed to the mitotic spindle during mitosis leading to the hypothesis that the kinase could be implicated in the regulation of chromosome segregation (Martel et al., submitted). The functions of several LmCKAPs support this hypothesis. First, we identified alpha, beta tubulin, and tubulin-tyrosine ligase-like protein TTLB, which are important for spindle assembly and chromosome congression. We also identified, in axenic amastigotes, a spindle-associated protein NuSap2 (LdBPK\_151000.1) that was shown to localise to the spindle during mitosis in *T. brucei* (Zhou et al., 2018). TbNuSap2 is a highly divergent ASE1/PRC1/MAP65 ortholog, which plays a role in promoting the G2/M transition and is required for spindle elongation (Schuyler et al., 2003; Zhou et al., 2018). Although TbCK1.2 does not interact with TbNuSap2, it was only performed in procyclic form and not in bloodstream form.

### 1.6.3. Novel functions for CK1 family members: Regulation of the Nuclear Pore Complex

One of the most striking finding in our dataset is the identification of 14 components of the nuclear pore complex (NPC) in axenic amastigotes (see [Table 3](#)). For comparison, the NPC in *T. brucei* contains only 20 NUPs (Obado et al., 2016). The NPC is a cylindrical ring-like structure composed of lined-up nucleoporins (Nup) that mediate transport of all macromolecules between the nucleus and the cytoplasm (Strambio-De-Castillia et al., 2010). Apart from transport, the NPC plays important roles on either sides of the nuclear envelope (Strambio-De-Castillia et al., 2010). Most of the components that were co-precipitated with LmCK1.2 are components of the outer ring, suggesting that LmCK1.2 might also be a component of this ring (Strambio-De-Castillia et al., 2010). The identification of two inner ring components, Nup144 and Nup96, and one component from the nuclear basket, Nup110 suggests that LmCK1.2 could interact with the outer ring complex towards the nucleus. As for

its functions, LmCK1.2 could be regulating the outer ring and contribute to the change in conformational states of the NPC and thus its permeability (Lusk et al.). Evidence in the literature of the interaction between CK1 and Nups and its functions are scarce. The only example of such an interaction is in yeast, Hrr25p was shown to bind and phosphorylate Nup53p. However phosphorylation of Nup53p by Hrr25p results in the destabilisation of their interaction (Lusk et al.). Further work will be needed to investigate this exciting role for CK1.

#### 1.6.4. LmCK1.2 might be loaded into exosomes through the regulation of vesicular trafficking.

LmCK1.2 has been identified in the secretome and in exosomes, suggesting that this kinase could be released by the parasite. We showed that there is an over-representation of exosomal proteins in our dataset, 23% in promastigotes and 19% in amastigotes, suggesting that LmCK1.2 might be implicated in the post-translational regulation of exosomal or secreted proteins. How LmCK1.2 is loaded into exosomes remains to be elucidated. We cannot exclude the implication of some of these exosomal LmCKAPs in this process, but it seems more likely that it requires cellular trafficking. We identified several binding partners that were annotated as implicated in trafficking such as exocyst or proteins carrying domains required for membrane binding such as the FYVE domain. We specifically focused on the adaptor protein-2 complex, involved in the transport of cargos from the plasma membrane to the early endosomes through endocytosis by binding to clathrin-coated vesicles (Collins et al., 2002). AP2 coordinates clathrin-coated pit formation and binds to cargo proteins (Cocucci et al., 2012; Jackson et al., 2010). Knowing that vesicles generated at the plasma membrane could deliver their cargo to early endosomes, which mature into MVB, the AP2 complex might be involved in loading LmCK1.2 into exosomes (Desdín-Micó and Mittelbrunn, 2017). We showed that the 4 members of the AP2 complex,  $\alpha$ 2-,  $\beta$ 2-,  $\mu$ 2- and  $\sigma$ 2-adaptin subunits co-purified with LmCK1.2 in axenic amastigotes. Three of the four subunits,  $\alpha$ 2-,  $\beta$ 2- and  $\mu$ 2-adaptin were localised to the flagellar pocket, the site for endocytosis in trypanosomatids and also where PIP2 is concentrated (Demmel et al., 2016). The sequestration of PIP2 to the flagellar pocket explains also the localisation of three of the AP2 complex proteins to the flagellar pocket and not to the cell body as PIP2 is required for the targeting of AP2 complex to the plasma membrane (Cocucci et al., 2012; Jackson et al., 2010). Interestingly LmCK1.2 also localises to

the flagellar pocket and human CK1 activity is sensitive to PIP2 concentration in the plasma membrane, with high concentration leading to the inhibition of its activity (Martel et al., submitted) (Brockman and Anderson, 1991). We did not yet determine with which subunits LmCK1.2 interacts but we showed that LmCK1.2 only phosphorylated  $\beta$ 2-adaptin subunit *in vitro*. However, we cannot exclude that it could bind to another subunit.

We found that all the subunits might not be equally important. First, we observed different degree of conservation of the different subunits between *L. donovani* and *T. cruzi* or *Bodo saltans*. Second, we could not generate an  $\alpha$ 2-adaptin null mutant despite several attempts, whereas we could easily obtain null mutants for  $\beta$ 2- and  $\mu$ 2-adaptins.  $\alpha$ 2-adaptin might thus be essential for parasite survival contrary to  $\beta$ 2- and  $\mu$ 2-adaptins, suggesting that this adaptin might perform additional functions compared to the two other AP2 subunits. However, we can exclude that these additional functions could be performed as part of another complex as  $\alpha$ 2-,  $\beta$ 2- and  $\mu$ 2-adaptins appears to be part of only one complex, which might also include LmCK1.2. Although  $\beta$ 2-adaptin deleted cells were viable in promastigotes, they were bigger than the control and than the  $\Delta\mu$ 2-adaptins cells, and seemed to have a larger flagellar pocket. It would be interesting to perform electron microscopy to determine the cause of the increase in cell size. These phenotypes are compatible with a role of AP2 complex in endocytosis.  $\Delta\beta$ 2-adaptin and  $\Delta\mu$ 2-adaptin mutants displayed a similar growth defect in axenic amastigotes, somewhat more pronounced for  $\Delta\beta$ 2-adaptin mutant than for  $\Delta\mu$ 2-adaptin mutant, suggesting a hierarchy between the subunits with  $\alpha$ 2 >  $\beta$ 2 >  $\mu$ 2. Our data suggest that the AP2 complex is more important in axenic amastigotes than in promastigotes, and if we consider that it interacts with LmCK1.2 predominantly in axenic amastigote, it further suggests that LmCK1.2 could regulate an important function of the AP2 complex at that stage. This is probably not the whole story as we identified by gel filtration LmCK1.2 in complex with the three adaptins in promastigotes. In other eukaryotes, loss of one of the large AP2 subunits usually eliminates the function of the AP2 complex (González-Gaitán and Jäckle, 1997; Grant and Hirsh, 1999). In *Dictyostelium*, disruption of the  $\beta$  subunit ( $\beta$ 1/2), which is common to AP1 and AP2 complexes, results in severe defects in growth, development and cytokinesis (Thomas Sosa et al., 2012). In *C. elegans*, only the double disruption of  $\alpha$ 2- and  $\mu$ 2-adaptins led to the complete abrogation of AP2 functions (Gu et al.). This could explain the partial phenotypes we observed and suggests that the generation of a double mutant could exacerbate the phenotypes we observed in *Leishmania*. The implication of CK1 in endocytosis

through the regulation of AP2 has been shown in other eukaryotes. Several studies have linked CK1 and adaptor proteins, either by direct interaction or phosphorylation (Hagemann et al., 2014; Panek et al., 1997; Turner et al., 1999). Peng et *al.* showed that Hrr25 was involved in the regulation of endocytosis, being one of the earliest proteins on the site of endocytosis with Ede1, an early endocytic Eps15-like protein important for endocytic initiation. The phosphorylation of Ede1 by Hrr25 is even required for the Hrr25-Ede1 interaction and promotes the efficient initiation of endocytic sites. Moreover, reducing the abundance of human CK1 $\delta$  or CK1 $\epsilon$  by RNAi decreases the rate of initiation of clathrin-mediated endocytosis (Peng et al., 2015b). Considering (i) the absence of AP2 complex in *T. brucei*, (ii) that endocytosis is clathrin-independent in *T. cruzi* and (iii) the loss of the clathrin-binding domain in trypanosomatid  $\beta$ 2-adaptin, the requirement of AP2 in clathrin-mediated endocytosis in *Leishmania* remains an open question. To determine the functions of AP2 complex will require future investigations.

The present work increases the knowledge on LmCK1.2 by the identification of its binding partners and the characterisation of the AP2 complex. It also provides elements that could contribute to decipher the pathways leading to the excretion of LmCK1.2 and thus the survival of the parasite in its mammalian host.

## 1.7. Acknowledgments

This work was supported by the ANR-13-ISV3-0009 grant and the Institut Pasteur. D.M. is registered in the Ecole Doctorale BioSPC (Université de Paris, Sorbonne Paris Cité, Paris, France) and has a PhD grant from the “Integrative Biology of Emerging Infectious Diseases” (LabEX IBEID) funded in the framework of the French Government’s “Programme Investissements d’Avenir” under Grant Agreement number ANR-10-LABX-62-IBEID. Mass spectrometry analyses were performed by the Institut Curie “Laboratoire de Spectrométrie de Masse Protéomique”, supported by grants from “Region Ile-de-France” and the FRM.

## 1.8. Supplementary information

Supplemental Information includes 4 tables and 2 figures.

### 1.8.1. Supplemental tables

**Table S1:** Primers used for gene tagging, knockouts and verification in *LdB* pTB007 strain with pT/pPLOT plasmids.

Primer name	Sequence (5' - 3')
<b>CRISPR-Cas9 primers</b>	
$\alpha$ 2-adaptin (LdBPK_070060.1) 5' HF forward	TTCTCTTTCTGTATTTTCTCTCACCCGCCGgtataatgcagacctgctgc
$\alpha$ 2-adaptin (LdBPK_070060.1) 3' HF forward	GCCCTCGACACAATCAAGTTCGCCCTACAaggctctgtagtggtccgg
$\alpha$ 2-adaptin (LdBPK_070060.1) 3' HF reverse	GTTTTATAAAGCTTTCTGCCAGCACTCGGCccaatttgagacctgtgc
$\alpha$ 2-adaptin (LdBPK_070060.1) 5' sgRNA forward	gaaattaatacactcactataggTCGACAGGAGGTTGACGTgttttagactagaaatagc
$\alpha$ 2-adaptin (LdBPK_070060.1) 3' sgRNA forward	gaaattaatacactcactataggATGCTTGTCTCTGCGTAGgttttagactagaaatagc
$\beta$ 2-adaptin (LdBPK_110990.1) 5' HF forward	AATAGCAGCACACTGTCCCTTCTTCTGtataatgcagacctgctgc
$\beta$ 2-adaptin (LdBPK_110990.1) 3' HF forward	ATGCGCGCCTTGTGTCCGCTATCGACGGACggttctgtagtggtccgg
$\beta$ 2-adaptin (LdBPK_110990.1) 3' HF reverse	CCCTCTCCACGCAACGCCGTCCAGGACtccaatttgagacctgtgc
$\beta$ 2-adaptin (LdBPK_110990.1) 5' sgRNA forward	gaaattaatacactcactataggTATGACGTTACTGTCGGAGAgtttagactagaaatagc
$\beta$ 2-adaptin (LdBPK_110990.1) 3' sgRNA forward	gaaattaatacactcactataggTCTCGTGGCGGACGGCGTgttttagactagaaatagc
$\mu$ 2-adaptin (LdBPK_363180.1) 5' HF forward	CGTACACAAAACCTATTGCATCATTGGGCTgataatgcagacctgctgc
$\mu$ 2-adaptin (LdBPK_363180.1) 3' HF forward	GTCATGGCGGGTGATTATCAGTGCCGCATAggttctgtagtggtccgg
$\mu$ 2-adaptin (LdBPK_363180.1) 3' HF reverse	GAGCGGATGGTGAGTTGAATGGGGGAGCAGccaatttgagacctgtgc
$\mu$ 2-adaptin (LdBPK_363180.1) 5' sgRNA forward	gaaattaatacactcactataggTAGCTTGCAGGCGAAGCAGgttttagactagaaatagc
$\mu$ 2-adaptin (LdBPK_363180.1) 3' sgRNA forward	gaaattaatacactcactataggCGGGTGCGGTCTACACACAgtttagactagaaatagc
<i>Lm</i> CKAP1 (LdBPK_080130.1) 5' HF forward	CTGCGGCGCTCCGTCTGCCCTCTCCCCGtataatgcagacctgctgc
<i>Lm</i> CKAP1 (LdBPK_080130.1) 3' HF forward	TTCGCGGGACAGAACAGTCCGCTTGCTTTCggttctgtagtggtccgg
<i>Lm</i> CKAP1 (LdBPK_080130.1) 3' HF reverse	AGAGAGAGTAGGCACCAAGGAAGGAAACCGccaatttgagacctgtgc
<i>Lm</i> CKAP1 (LdBPK_080130.1) 5' sgRNA forward	gaaattaatacactcactataggACGCCTTCTGTCTGTTTCGAgtttagactagaaatagc
<i>Lm</i> CKAP1 (LdBPK_080130.1) 3' sgRNA forward	gaaattaatacactcactataggGGCAGGCGTCTGTACGCGTgttttagactagaaatagc

<i>LmSec3</i> (LdBPK_081060.1) 5' HF forward	TACAGATGCACATACATACGTCTATCCACCgtataatgcagacctgctgc
<i>LmSec3</i> (LdBPK_081060.1) 3' HF forward	TCCGACGTTGTGGAGATGCTCGCGCGTACggttctggtagtggttccgg
<i>LmSec3</i> (LdBPK_081060.1) 3' HF reverse	GCGGCGGTGATGCTGCCTTACGTGCCGACAccaatttgagagacctgtgc
<i>LmSec3</i> (LdBPK_081060.1) 5' sgRNA forward	gaaattaatacactcactataggTAGACTCTGATTGAGTTGCGgttttagagctagaaatagc
<i>LmSec3</i> (LdBPK_081060.1) 3' sgRNA forward	gaaattaatacactcactataggCCATCATGGGCTGCTGCTGCgttttagagctagaaatagc
<i>LmKin17</i> (LdBPK_170270.1) 5' HF forward	CTCTCTCCACGCACGAGCCCTTCTCCCTgtataatgcagacctgctgc
<i>LmKin17</i> (LdBPK_170270.1) 3' HF forward	GGTGCTTCGTCTGCCGCTACTACTCCATGggttctggtagtggttccgg
<i>LmKin17</i> (LdBPK_170270.1) 3' HF reverse	CAGAAGAGCTCTGCATCGTGTGCGAAGCCccaatttgagagacctgtgc
<i>LmKin17</i> (LdBPK_170270.1) 5' sgRNA forward	gaaattaatacactcactataggCTATGAGCTTACGGCGGCGgttttagagctagaaatagc
<i>LmKin17</i> (LdBPK_170270.1) 3' sgRNA forward	gaaattaatacactcactataggACGGCACGCTGTTTGAATCTgttttagagctagaaatagc
<i>LmKin21</i> (LdBPK_211280.1) 5' HF forward	TTCGCCACGCACCCACCGCACTCACCTCCgtataatgcagacctgctgc
<i>LmKin21</i> (LdBPK_211280.1) 3' HF forward	CTCGATTTTGGGGCCCTGGAAGGAAAGCGggttctggtagtggttccgg
<i>LmKin21</i> (LdBPK_211280.1) 3' HF reverse	AAAGGAAAAACAAAAAGAATAATCGAGCCccaatttgagagacctgtgc
<i>LmKin21</i> (LdBPK_211280.1) 5' sgRNA forward	gaaattaatacactcactataggTGATTGAGAGATGTCCCTCCgttttagagctagaaatagc
<i>LmKin21</i> (LdBPK_211280.1) 3' sgRNA forward	gaaattaatacactcactataggAGGGCACTCGCGGAGAGTGGgttttagagctagaaatagc
<i>LmKin30</i> (LdBPK_301510.1) 5' HF forward	GACGGCGTCCACGTTGCCAGCTTCTACCCgtataatgcagacctgctgc
<i>LmKin30</i> (LdBPK_301510.1) 3' HF forward	ACCGCGTTCGGCATCACGGTGCAGCAATCGggttctggtagtggttccgg
<i>LmKin30</i> (LdBPK_301510.1) 3' HF reverse	ACGTACACAGGACAGGCGTATAGCCTGACAccaatttgagagacctgtgc
<i>LmKin30</i> (LdBPK_301510.1) 5' sgRNA forward	gaaattaatacactcactataggAGGACGTGCGAGTAGAATGTgttttagagctagaaatagc
<i>LmKin30</i> (LdBPK_301510.1) 3' sgRNA forward	gaaattaatacactcactataggAGCGGAAAGTCGCTGCATCCgttttagagctagaaatagc
<i>LmDYNLL1</i> (LdBPK_320240.1) 5' HF forward	CCGTTCTCGCATCAGTGCCGCCGTTGCCTgtataatgcagacctgctgc
<i>LmDYNLL1</i> (LdBPK_320240.1) 3' HF forward	CAGGTCGCCGTTCTGCTCTTCAAGTGCGGGggttctggtagtggttccgg
<i>LmDYNLL1</i> (LdBPK_320240.1) 3' HF reverse	GGGATCTGATAACCGCGGCGTGAGTTCCTccaatttgagagacctgtgc
<i>LmDYNLL1</i> (LdBPK_320240.1) 5' sgRNA forward	gaaattaatacactcactataggATGGAAGGGGCTGTGTAGgttttagagctagaaatagc
<i>LmDYNLL1</i> (LdBPK_320240.1) 3' sgRNA forward	gaaattaatacactcactataggTGATAACAACAACACTAGgttttagagctagaaatagc
G00 primer sgRNA reverse	aaaagcaccgactcggtgcccttttcaagtgataacggactagccttatttaacttctatttctagctctaaac

#### Validation of gene knockouts : ORF amplification

<i>L. donovani</i> $\beta$ 2-adaptin ORF forward	GATGAGCTTGAAACGCTTCG
--	----------------------

<i>L. donovani</i> β2-adaptin ORF reverse	GAGTTGGCGCCGAGCTTTAC
<i>L. donovani</i> μ2-adaptin ORF forward	cttgctgtgccttgccaccaATGCTATCAGTTTTGATGTTCC
<i>L. donovani</i> μ2-adaptin ORF reverse	tccggggatcatcgattccTATGCGGCACTGATAATC
<i>L. donovani</i> LmCKAP1 ORF forward	CCGCCGAACGTGTTCTTCTC
<i>L. donovani</i> LmCKAP1 ORF reverse	tccggggatcatcgattccGAAAGCAAGCCGACTGTTCC
<i>L. donovani</i> LmKin30 ORF forward	ATGGCGGCTCTCTTGCCATC
<i>L. donovani</i> LmKin30 ORF reverse	CATGGAGTAGTAGCGGCAGA

**Validation of gene knockouts: amplification of sequence across integration junction**

Puromycin reverse	TCAATGTGTCGATCTGGGTCAAC
Blasticidin reverse	CCGTTGCTCTTTCAATGAGGGTG
<i>L. donovani</i> β2-adaptin 5'UTR forward	TTCCTCGACTCCTTATCGTG
<i>L. donovani</i> μ2-adaptin 5'UTR forward	TGTGCTGTGCCTCTCCCTT
<i>L. donovani</i> LmCKAP1 5'UTR forward	CGCTTCGTTCTCTGCTACGT
<i>L. donovani</i> LmKin30 5'UTR forward	TCACTATACTCCTTTAATCCCCT

Capital sequences indicate sgRNA target sites (or homology regions) and homology flanks (HF) in the genome. Underlined sequence indicate recognition sequence with sgRNA primers.

**Table S2:** Chromatographic conditions for mass spectrometry analysis.

	C18 Precolumn	Loading Buffer	Loading flow	Column	Column Buffer		Gradient		Column Flow	Column Temperature	Mass range
					A	B	%	Time			
<b>IP PRO</b>	300 μm inner diameter x 5 mm; Dionex	5% MeCN, 0.1% TFA	20 μl/min	75 μm i.d. x 50 cm, packed with C18 PepMap™, 3 μm, 100 Å; LC Packings	2% MeCN, 0.1% HCOOH	100% MeCN, 0.085% HCOOH	5 to 30%	157 min	400 nl/min	40°C	400-1200 m/z
<b>IP axAMA</b>	300 μm inner diameter x 5 mm; Dionex	5% MeCN, 0.1% TFA	20 μl/min	nanoViper Acclaim PepMap™ RSLC, 2 μm, 100Å, Thermo Scientific	2% MeCN, 0.1% HCOOH	100% MeCN, 0.085% HCOOH	5 to 35%	157 min	300 nl/min	45°C	400-1500 m/z

**Table S3:** Accession numbers of AP2 components in trypanosomatids, and in different eukaryote species for  $\beta$ 2-adaptin.

AP2 subunits	Name	Accession number	Species
<b><math>\alpha</math>2-adaptin</b>	alpha-adaptin-like protein	LdBPK_070060.1	<i>Leishmania donovani</i>
	alpha-adaptin-like protein	LINF_070005500	<i>Leishmania infantum</i>
	alpha-adaptin-like protein	LmjF.07.0050	<i>Leishmania major</i>
	alpha-adaptin-like protein	LmxM.07.0050	<i>Leishmania mexicana</i>
	alpha-adaptin-like protein	LbrM.07.0050	<i>Leishmania braziliensis</i>
	alpha-adaptin-like, putative	TcCLB.511391.140	<i>Trypanosoma cruzi</i>
	alpha adaptin, putative	BSAL_62690	<i>Bodo saltans</i>
<b><math>\beta</math>2-adaptin</b>	adaptin-related protein-like protein	LdBPK_110990.1	<i>Leishmania donovani</i>
	adaptin-related protein-like protein	LINF_110015900	<i>Leishmania infantum</i>
	adaptin-related protein-like protein	LmjF.11.0990	<i>Leishmania major</i>
	adaptin-related protein-like protein	LmxM.11.0990	<i>Leishmania mexicana</i>
	adaptin-related protein-like protein	LbrM.11.0790	<i>Leishmania braziliensis</i>
	beta-adaptin 1, putative	TcCLB.506297.180	<i>Trypanosoma cruzi</i>
	beta adaptin 1, putative	BSAL_57530	<i>Bodo saltans</i>
	AP-2 complex subunit beta	P63010	<i>Homo sapiens</i>
	Beta-adaptin-like protein B	Q9SUS3	<i>Arabidopsis thaliana</i>
	AP complex subunit beta	S8GQ34	<i>Toxoplasma gondii</i>
	Beta-adaptin	V6TQ21	<i>Giardia intestinalis</i>
AP-2 complex subunit beta	P27351	<i>Saccharomyces cerevisiae</i>	
<b><math>\mu</math>2-adaptin</b>	clathrin coat assembly protein-like protein	LdBPK_363180.1	<i>Leishmania donovani</i>
	clathrin coat assembly protein-like protein	LINF_360038400	<i>Leishmania infantum</i>
	clathrin coat assembly protein-like protein	LmjF.36.3030	<i>Leishmania major</i>
	clathrin coat assembly protein-like protein	LmxM.36.3030	<i>Leishmania mexicana</i>
	clathrin coat assembly protein-like protein	LbrM.35.3250	<i>Leishmania braziliensis</i>
	clathrin coat assembly protein, putative	TcCLB.509715.20	<i>Trypanosoma cruzi</i>
	clathrin coat assembly protein, putative	BSAL_13080	<i>Bodo saltans</i>
<b><math>\sigma</math>2-adaptin</b>	clathrin coat assembly protein AP17, putative	LdBPK_342100.1	<i>Leishmania donovani</i>
	clathrin coat assembly protein AP17 - putative	LINF_340028700	<i>Leishmania infantum</i>
	clathrin coat assembly protein AP17, putative	LmjF.34.2330	<i>Leishmania major</i>

clathrin coat assembly protein AP17, putative	LmxM.33.2330	<i>Leishmania mexicana</i>
clathrin coat assembly protein AP17, putative	LbrM.20.1830	<i>Leishmania braziliensis</i>
clathrin coat assembly protein AP17, putative	TcCLB.506559.330	<i>Trypanosoma cruzi</i>
clathrin coat assembly protein AP17, putative	BSAL_33010	<i>Bodo saltans</i>

---

**Table S4:** Raw data of the identification of proteins by mass spectrometry from the immunoprecipitation of LmCK1.2-V5-His<sub>6</sub>.

See [Appendix 1](#).

## 1.8.2. Supplemental figures

Figure S1:

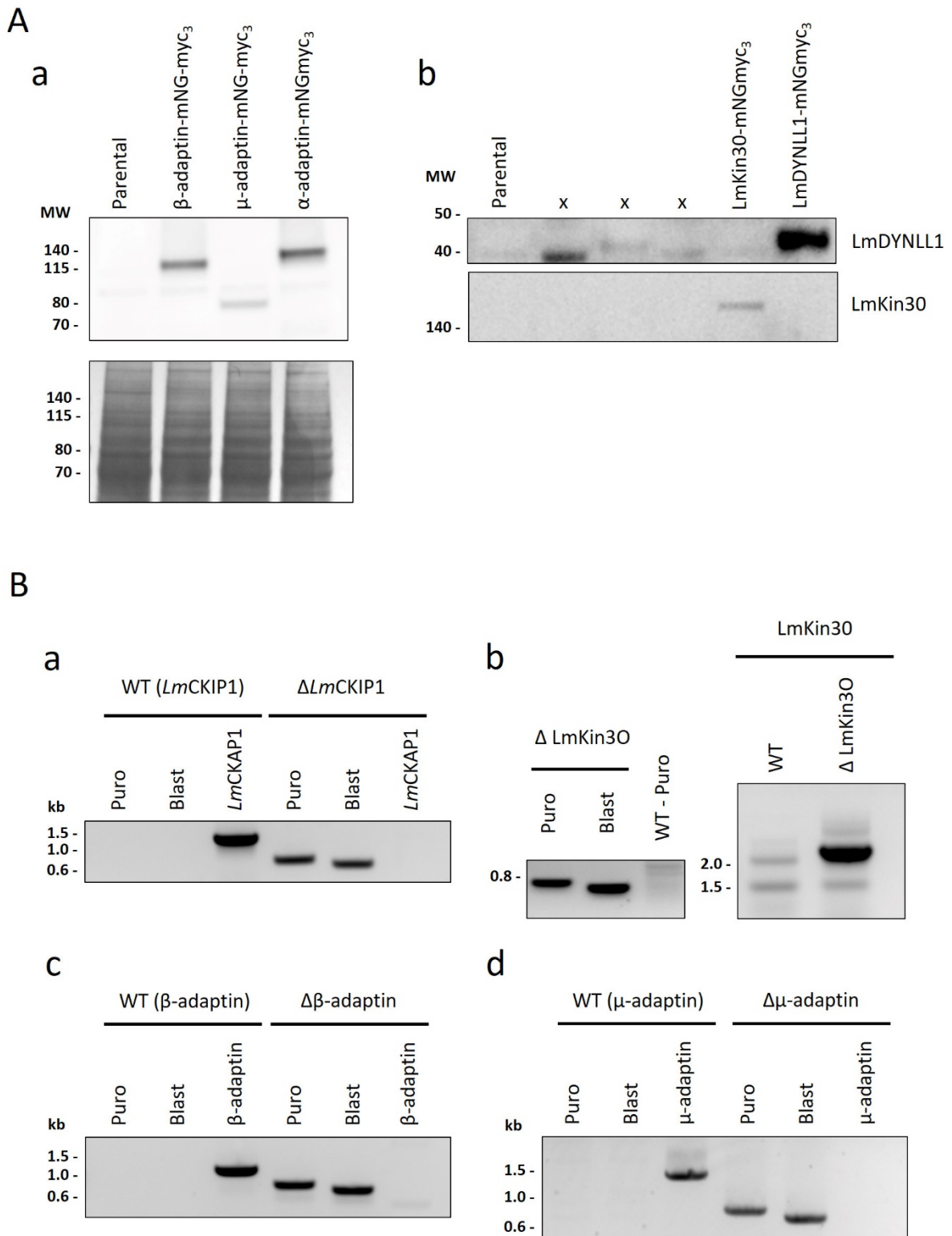


**Fig. S1** – *In locus* tagging and gene knockouts using the CRISPR-Cas9 toolkit.

(A) Proteins were extracted from LdB pTB007 or LdB  $\alpha 2$ -,  $\beta 2$  or  $\mu 2$ -adaptin-mNG-myc (a) and LdB LmKin30-mNG-myc or LdB LmDYNLL1-mNG-myc (b) promastigotes in logarithmic phase and twenty micrograms was analysed by Western blotting using an anti-Myc tag antibody (Top panels). The Coomassie-stained membrane of the blot is included as a loading control (bottom panels). Protein weight in kDa is indicated on the left. The expected size of the fusion proteins are: 140,4 kDa, 80,7 kDa, 139,4 kDa, 165,0 kDa and 42,5 kDa for  $\alpha 2$ -,  $\beta 2$  or  $\mu 2$ -adaptin-mNG-myc and LmKin30-mNG-myc and LmDYNLL1-mNG-myc, respectively.

(B) PCR analysis of the  $\Delta$ LmCKAP1 (a),  $\Delta$ LmKin30 (b),  $\Delta\beta 2$ -adaptin (c) or  $\Delta\mu 2$ -adaptin (d) cell lines. PCR products run on an agarose gel to assess the correct integration of the puromycin-resistance gene (Puro), blasticidin-resistance gene (Blast), and the presence/absence of the respective CDS. Fragments sizes in kb are indicated on the left.

Figure S2

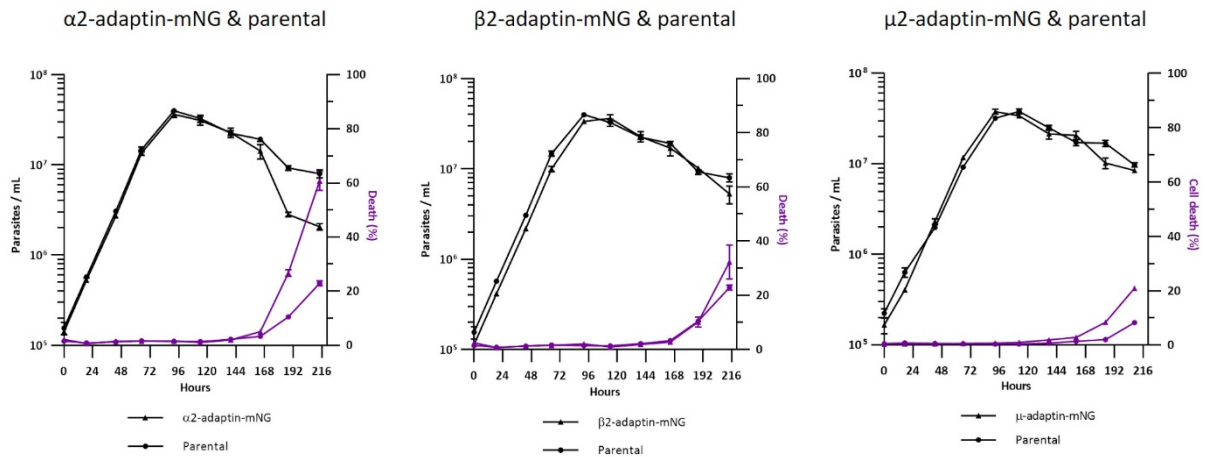


**Fig. S2** – Growth and cell death of the mNG-tagged  $\alpha 2$ -,  $\beta 2$ - and  $\mu 2$ -adaptin *L. donovani* cell lines in promastigotes.

Logarithmic phase promastigotes were seeded at  $1 \times 10^5$  cells/mL and cultured for 9 days. Samples were collected every 24 h to assess cell concentration (black symbols) and percentage of cell death (magenta symbols) by flow cytometry in triplicate in two independent experiments. Each values display the mean of triplicates and SD error bars. Cell lines: parental (circle),  $\alpha 2$ -adaptin-mNG (triangle, left panel),  $\beta 2$ -adaptin-mNG (triangle, middle panel) and  $\mu 2$ -adaptin-mNG (triangle, right panel).

## 1.8. References

- Agostinis, P., Pinna, L.A., Meggio, F., Marin, O., Goris, J., Vandenneede, J.R., and Merlevede, W. (1989). A synthetic peptide substrate specific for casein kinase-1. *FEBS Lett.* *259*, 75–78.
- Aslett, M., Aurrecochea, C., Berriman, M., Brestelli, J., Brunk, B.P., Carrington, M., Depledge, D.P., Fischer, S., Gajria, B., Gao, X., et al. (2010). TriTrypDB: a functional genomic resource for the Trypanosomatidae. *Nucleic Acids Res* *38*, D457-62.
- Atayde, V.D., Suau, H.A., Townsend, S., Hassani, K., Kamhawi, S., and Olivier, M. (2015). Exosome secretion by the parasitic protozoan *Leishmania* within the sand fly midgut. *Cell Rep.* *13*, 957–967.
- Behrend, L., Stöter, M., Kurth, M., Rutter, G., Heukeshoven, J., Deppert, W., and Knippschild, U. (2000). Interaction of casein kinase 1 delta (CK1 $\delta$ ) with post-Golgi structures, microtubules and the spindle apparatus. *Eur. J. Cell Biol.* *79*, 240–251.
- Beneke, T., Madden, R., Makin, L., Valli, J., Sunter, J., and Gluenz, E. (2017). A CRISPR Cas9 high-throughput genome editing toolkit for kinetoplastids. *R. Soc. Open Sci.* *4*, 170095.
- Bischof, J., Randoll, S.-J., Süßner, N., Henne-Bruns, D., Pinna, L.A., and Knippschild, U. (2013). CK1 $\delta$  Kinase Activity Is Modulated by Chk1-Mediated Phosphorylation. *PLoS ONE* *8*.
- Biswas, A., Mukherjee, S., Das, S., Shields, D., Chow, C.W., and Maitra, U. (2011). Opposing action of casein kinase 1 and calcineurin in nucleocytoplasmic shuttling of mammalian translation initiation factor eIF6. *J. Biol. Chem.* *286*, 3129–3138.
- Boehm, M., and Bonifacino, J.S. (2001). Adaptins: the final recount. *Mol. Biol. Cell* *12*, 2907–2920.
- Boisvert, F.-M., van Koningsbruggen, S., Navascués, J., and Lamond, A.I. (2007). The multifunctional nucleolus. *Nat. Rev. Mol. Cell Biol.* *8*, 574–585.
- Brockman, J.L., and Anderson, R.A. (1991). Casein kinase I is regulated by phosphatidylinositol 4,5-bisphosphate in native membranes. *J. Biol. Chem.* *266*, 2508–2512.
- Cocucci, E., Aguet, F., Boulant, S., and Kirchhausen, T. (2012). The First Five Seconds in the Life of a Clathrin-Coated Pit. *Cell* *150*, 495–507.
- Collins, B.M., McCoy, A.J., Kent, H.M., Evans, P.R., and Owen, D.J. (2002). Molecular Architecture and Functional Model of the Endocytic AP2 Complex. *Cell* *109*, 523–535.
- Cruciat, C.-M., Dolde, C., Groot, R.E.A. de, Ohkawara, B., Reinhard, C., Korswagen, H.C., and Niehrs, C. (2013). RNA Helicase DDX3 Is a Regulatory Subunit of Casein Kinase 1 in Wnt- $\beta$ -Catenin Signaling. *Science* *339*, 1436–1441.
- Dan-Goor, M., Nasereddin, A., Jaber, H., and Jaffe, C.L. (2013). Identification of a Secreted Casein Kinase 1 in *Leishmania donovani*: Effect of Protein over Expression on Parasite Growth and Virulence. *PLOS ONE* *8*, e79287.

- Demmel, L., Schmidt, K., Lucast, L., Havlicek, K., Zankel, A., Koestler, T., Reithofer, V., De, P.C., and Warren, G. (2016). The endocytic activity of the flagellar pocket in *Trypanosoma brucei* is regulated by an adjacent phosphatidylinositol phosphate kinase. *J. Cell Sci.* *129*, 2285–2285.
- Desdín-Micó, G., and Mittelbrunn, M. (2017). Role of exosomes in the protection of cellular homeostasis. *Cell Adhes. Migr.* *11*, 127–134.
- Dorin-Semblat, D., Demarta-Gatsi, C., Hamelin, R., Armand, F., Carvalho, T.G., Moniatte, M., and Doerig, C. (2015). Malaria Parasite-Infected Erythrocytes Secrete PfCK1, the Plasmodium Homologue of the Pleiotropic Protein Kinase Casein Kinase 1. *PLOS ONE* *10*, e0139591.
- Flegontov, P., Votýpka, J., Skalický, T., Logacheva, M.D., Penin, A.A., Tanifuji, G., Onodera, N.T., Kondrashov, A.S., Volf, P., Archibald, J.M., et al. (2013). Paratrypanosoma is a novel early-branching trypanosomatid. *Curr. Biol. CB* *23*, 1787–1793.
- Flotow, H., and Roach, P.J. (1991). Role of acidic residues as substrate determinants for casein kinase I. *J. Biol. Chem.* *266*, 3724–3727.
- Flotow, H., Graves, P.R., Wang, A.Q., Fiol, C.J., Roeske, R.W., and Roach, P.J. (1990). Phosphate groups as substrate determinants for casein kinase I action. *J. Biol. Chem.* *265*, 14264–14269.
- Fu, Z., Chakraborti, T., Morse, S., Bennett, G.S., and Shaw, G. (2001). Four Casein Kinase I Isoforms Are Differentially Partitioned between Nucleus and Cytoplasm. *Exp. Cell Res.* *269*, 275–286.
- Fulcher, L.J., Bozatz, P., Tachie-Menson, T., Wu, K.Z.L., Cummins, T.D., Bufton, J.C., Pinkas, D.M., Dunbar, K., Shrestha, S., Wood, N.T., et al. (2018). The DUF1669 domain of FAM83 family proteins anchor Casein Kinase 1 isoforms. *Sci. Signal.* *11*.
- Ghalei, H., Schaub, F.X., Doherty, J.R., Noguchi, Y., Roush, W.R., Cleveland, J.L., Stroupe, M.E., and Karbstein, K. (2015). Hrr25/CK1 $\delta$ -directed release of Ltv1 from pre-40S ribosomes is necessary for ribosome assembly and cell growth. *J. Cell Biol.* *208*, 745–759.
- González-Gaitán, M., and Jäckle, H. (1997). Role of *Drosophila*  $\alpha$ -Adaptin in Presynaptic Vesicle Recycling. *Cell* *88*, 767–776.
- Grant, B., and Hirsh, D. (1999). Receptor-mediated Endocytosis in the *Caenorhabditis elegans* Oocyte. *Mol. Biol. Cell* *10*, 4311–4326.
- Gross, S.D., Loijens, J.C., and Anderson, R.A. (1999). The casein kinase I $\alpha$  isoform is both physically positioned and functionally competent to regulate multiple events of mRNA metabolism. *J. Cell Sci.* *112*, 2647–2656.
- Gu, M., Liu, Q., Watanabe, S., Sun, L., Hollopeter, G., Grant, B.D., and Jorgensen, E.M. AP2 hemicomplexes contribute independently to synaptic vesicle endocytosis. *ELife* *2*.
- Hagemann, A.I., Kurz, J., Kauffeld, S., Chen, Q., Reeves, P.M., Weber, S., Schindler, S., Davidson, G., Kirchhausen, T., and Scholpp, S. (2014). In vivo analysis of formation and

endocytosis of the Wnt/ $\beta$ -catenin signaling complex in zebrafish embryos. *J. Cell Sci.* **127**, 3970–3982.

Jackson, L.P., Kelly, B.T., McCoy, A.J., Gaffry, T., James, L.C., Collins, B.M., Höning, S., Evans, P.R., and Owen, D.J. (2010). A Large-Scale Conformational Change Couples Membrane Recruitment to Cargo Binding in the AP2 Clathrin Adaptor Complex. *Cell* **141**, 1220–1229.

Jayaswal, S., Kamal, M.A., Dua, R., Gupta, S., Majumdar, T., Das, G., Kumar, D., and Rao, K.V.S. (2010). Identification of Host-Dependent Survival Factors for Intracellular Mycobacterium tuberculosis through an siRNA Screen. *PLOS Pathog.* **6**, e1000839.

Jiang, S., Zhang, M., Sun, J., and Yang, X. (2018). Casein kinase 1 $\alpha$ : biological mechanisms and theranostic potential. *Cell Commun. Signal.* **16**, 23.

Kalb, L.C., Frederico, Y.C.A., Boehm, C., Moreira, C.M. do N., Soares, M.J., and Field, M.C. (2016). Conservation and divergence within the clathrin interactome of *Trypanosoma cruzi*. *Sci. Rep.* **6**, 31212.

Käser, S., Willemin, M., Schnarwiler, F., Schimanski, B., Poveda-Huertes, D., Oeljeklaus, S., Haenni, B., Zuber, B., Warscheid, B., Meisinger, C., et al. (2017). Biogenesis of the mitochondrial DNA inheritance machinery in the mitochondrial outer membrane of *Trypanosoma brucei*. *PLOS Pathog.* **13**, e1006808.

Kattapuram, T., Yang, S., Maki, J.L., and Stone, J.R. (2005). Protein Kinase CK1 $\alpha$  Regulates mRNA Binding by Heterogeneous Nuclear Ribonucleoprotein C in Response to Physiologic Levels of Hydrogen Peroxide. *J. Biol. Chem.* **280**, 15340–15347.

Kawakami, F., Suzuki, K., and Ohtsuki, K. (2008). A Novel Consensus Phosphorylation Motif in Sulfatide- and Cholesterol-3-sulfate-Binding Protein Substrates for CK1 in Vitro. *Biol. Pharm. Bull.* **31**, 193–200.

Knippschild, U., Wolff, S., Giamas, G., Brockschmidt, C., Wittau, M., Würfl, P.U., Eismann, T., and Stöter, M. (2005). The Role of the Casein Kinase 1 (CK1) Family in Different Signaling Pathways Linked to Cancer Development. *Oncol. Res. Treat.* **28**, 508–514.

Knippschild, U., Kruger, M., Richter, J., Xu, P., Garcia-Reyes, B., Peifer, C., Halekotte, J., Bakulev, V., and Bischof, J. (2014). The CK1 Family: Contribution to Cellular Stress Response and Its Role in Carcinogenesis. *Front Oncol* **4**, 96.

Knockenbauer, K.E., and Schwartz, T.U. (2016). The Nuclear Pore Complex as a Flexible and Dynamic Gate. *Cell* **164**, 1162–1171.

Lemmon, S.K., and Traub, L.M. (2012). Getting in touch with the clathrin terminal domain. *Traffic Cph. Den.* **13**, 511–519.

Lu, P., Li, H., Li, N., Singh, R.N., Bishop, C.E., Chen, X., and Lu, B. (2017). MEX3C interacts with adaptor-related protein complex 2 and involves in miR-451a exosomal sorting. *PLoS ONE* **12**.

Lusk, C.P., Waller, D.D., Makhnevych, T., Dienemann, A., Whiteway, M., Thomas, D.Y., and Wozniak, R.W. Nup53p is a Target of Two Mitotic Kinases, Cdk1p and Hrr25p. *Traffic* 8, 647–660.

Madeira, F., Park, Y.M., Lee, J., Buso, N., Gur, T., Madhusoodanan, N., Basutkar, P., Tivey, A.R.N., Potter, S.C., Finn, R.D., et al. (2019). The EMBL-EBI search and sequence analysis tools APIs in 2019. *Nucleic Acids Res.*

Manna, P.T., Kelly, S., and Field, M.C. (2013). Adaptin evolution in kinetoplastids and emergence of the variant surface glycoprotein coat in African trypanosomatids. *Mol. Phylogenet. Evol.* 67, 123–128.

Marin, O., Bustos, V.H., Cesaro, L., Meggio, F., Pagano, M.A., Antonelli, M., Allende, C.C., Pinna, L.A., and Allende, J.E. (2003). A noncanonical sequence phosphorylated by casein kinase 1 in  $\beta$ -catenin may play a role in casein kinase 1 targeting of important signaling proteins. *Proc. Natl. Acad. Sci.* 100, 10193–10200.

Martel, D., Beneke, T., Gluenz, E., Späth, G.F., and Rachidi, N. (2017). Characterisation of Casein Kinase 1.1 in *Leishmania donovani* Using the CRISPR Cas9 Toolkit. *BioMed Res. Int.* 2017, 4635605.

McKenzie, J.A.G., Riento, K., and Ridley, A.J. (2006). Casein kinase I $\epsilon$  associates with and phosphorylates the tight junction protein occludin. *FEBS Lett.* 580, 2388–2394.

Mettlen, M., Chen, P.H., Srinivasan, S., Danuser, G., and Schmid, S.L. (2018). Regulation of Clathrin-Mediated Endocytosis. *Annu. Rev. Biochem.* 87, 871–896.

Morgan, G.W., Hall, B.S., Denny, P.W., Field, M.C., and Carrington, M. (2002). The endocytic apparatus of the kinetoplastida. Part II: machinery and components of the system. *Trends Parasitol.* 18, 540–546.

Mullin, K.A., Foth, B.J., Ilgoutz, S.C., Callaghan, J.M., Zawadzki, J.L., McFadden, G.I., and McConville, M.J. (2001). Regulated Degradation of an Endoplasmic Reticulum Membrane Protein in a Tubular Lysosome in *Leishmania mexicana*. *Mol. Biol. Cell* 12, 2364–2377.

Obado, S.O., Brillantes, M., Uryu, K., Zhang, W., Ketaren, N.E., Chait, B.T., Field, M.C., and Rout, M.P. (2016). Interactome Mapping Reveals the Evolutionary History of the Nuclear Pore Complex. *PLoS Biol.* 14, e1002365–e1002365.

Palfi, Z., Jaé, N., Preusser, C., Kaminska, K.H., Bujnicki, J.M., Lee, J.H., Günzl, A., Kambach, C., Urlaub, H., and Bindereif, A. (2009). SMN-assisted assembly of snRNP-specific Sm cores in trypanosomes. *Genes Dev.* 23, 1650–1664.

Panek, H.R., Stepp, J.D., Engle, H.M., Marks, K.M., Tan, P.K., Lemmon, S.K., and Robinson, L.C. (1997). Suppressors of YCK-encoded yeast casein kinase 1 deficiency define the four subunits of a novel clathrin AP-like complex. *EMBO J.* 16, 4194–4204.

Peng, D., and Tarleton, R. (2015). EuPaGDT: a web tool tailored to design CRISPR guide RNAs for eukaryotic pathogens. *Microb. Genomics* 1.

- Peng, Y., Grassart, A., Lu, R., Wong, C.C.L., Yates, J., Barnes, G., and Drubin, D.G. (2015). Casein Kinase 1 Promotes Initiation of Clathrin-Mediated Endocytosis. *Dev. Cell* 32, 231–240.
- Poullet, P., Carpentier, S., and Barillot, E. (2007). myProMS, a web server for management and validation of mass spectrometry-based proteomic data. *PROTEOMICS* 7, 2553–2556.
- Rachidi, N., Taly, J.F., Durieu, E., Leclercq, O., Aulner, N., Prina, E., Pescher, P., Notredame, C., Meijer, L., and Späth, G.F. (2014). Pharmacological Assessment Defines *Leishmania donovani* Casein Kinase 1 as a Drug Target and Reveals Important Functions in Parasite Viability and Intracellular Infection. *Antimicrob. Agents Chemother.* 58, 1501–1515.
- Ray, P., Basu, U., Ray, A., Majumdar, R., Deng, H., and Maitra, U. (2008). The *Saccharomyces cerevisiae* 60 S ribosome biogenesis factor Tif6p is regulated by Hrr25p-mediated phosphorylation. *J. Biol. Chem.* 283, 9681–9691.
- Sahu, R., Kaushik, S., Clement, C.C., Cannizzo, E.S., Scharf, B., Follenzi, A., Potolicchio, I., Nieves, E., Cuervo, A.M., and Santambrogio, L. (2011). Microautophagy of cytosolic proteins by late endosomes. *Dev. Cell* 20, 131–139.
- Santarém, N., Racine, G., Silvestre, R., Cordeiro-da-Silva, A., and Ouellette, M. (2013). Exoproteome dynamics in *Leishmania infantum*. *J. Proteomics* 84, 106–118.
- Schitteck, B., and Sinnberg, T. (2014). Biological functions of casein kinase 1 isoforms and putative roles in tumorigenesis. *Mol. Cancer* 13.
- Schumann Burkard, G., Jutzi, P., and Roditi, I. (2011). Genome-wide RNAi screens in bloodstream form trypanosomes identify drug transporters. *Mol. Biochem. Parasitol.* 175, 91–94.
- Schuyler, S.C., Liu, J.Y., and Pellman, D. (2003). The molecular function of Ase1p: evidence for a MAP-dependent midzone-specific spindle matrix. *Microtubule-associated proteins. J. Cell Biol.* 160, 517–528.
- Sillibourne, J.E., Milne, D.M., Takahashi, M., Ono, Y., and Meek, D.W. (2002). Centrosomal Anchoring of the Protein Kinase CK1 $\delta$  Mediated by Attachment to the Large, Coiled-coil Scaffolding Protein CG-NAP/AKAP450. *J. Mol. Biol.* 322, 785–797.
- Silverman, J.M., Chan, S.K., Robinson, D.P., Dwyer, D.M., Nandan, D., Foster, L.J., and Reiner, N.E. (2008). Proteomic analysis of the secretome of *Leishmania donovani*. *Genome Biol* 9, R35.
- Silverman, J.M., Clos, J., Horakova, E., Wang, A.Y., Wiesgigl, M., Kelly, I., Lynn, M.A., McMaster, W.R., Foster, L.J., Levings, M.K., et al. (2010a). *Leishmania* exosomes modulate innate and adaptive immune responses through effects on monocytes and dendritic cells. *J Immunol* 185, 5011–5022.
- Silverman, J.M., Clos, J., de'Oliveira, C.C., Shirvani, O., Fang, Y., Wang, C., Foster, L.J., and Reiner, N.E. (2010b). An exosome-based secretion pathway is responsible for protein export from *Leishmania* and communication with macrophages. *J Cell Sci* 123, 842–852.

- Simpson, R.J., Jensen, S.S., and Lim, J.W.E. (2008). Proteomic profiling of exosomes: Current perspectives. *PROTEOMICS* 8, 4083–4099.
- Spector, D.L., and Lamond, A.I. (2011). Nuclear Speckles. *Cold Spring Harb. Perspect. Biol.* 3, a000646.
- Strambio-De-Castillia, C., Niepel, M., and Rout, M.P. (2010). The nuclear pore complex: bridging nuclear transport and gene regulation. *Nat. Rev. Mol. Cell Biol.* 11, 490–501.
- Thomas Sosa, R., Weber, M.M., Wen, Y., and O’Halloran, T.J. (2012). A Single  $\beta$  Adaptin Contributes to AP1 and AP2 Complexes and Clathrin Function in Dictyostelium. *Traffic* 13, 305–316.
- Turner, K.M., Burgoyne, R.D., and Morgan, A. (1999). Protein phosphorylation and the regulation of synaptic membrane traffic. *Trends Neurosci.* 22, 459–464.
- Venerando, A., Ruzzene, M., and Pinna, L.A. (2014). Casein kinase: the triple meaning of a misnomer. *Biochem. J.* 460, 141–156.
- Vince, J.E., Tull, D.L., Spurck, T., Derby, M.C., McFadden, G.I., Gleeson, P.A., Gokool, S., and McConville, M.J. (2008). Leishmania Adaptor Protein-1 Subunits Are Required for Normal Lysosome Traffic, Flagellum Biogenesis, Lipid Homeostasis, and Adaptation to Temperatures Encountered in the Mammalian Host. *Eukaryot. Cell* 7, 1256–1267.
- Wolff, S., Xiao, Z., Wittau, M., Süssner, N., Stöter, M., and Knippschild, U. (2005). Interaction of casein kinase 1 delta (CK1 $\delta$ ) with the light chain LC2 of microtubule associated protein 1A (MAP1A). *Biochim. Biophys. Acta BBA - Mol. Cell Res.* 1745, 196–206.
- Wolff, S., Stöter, M., Giamas, G., Piesche, M., Henne-Bruns, D., Banting, G., and Knippschild, U. (2006). Casein kinase 1 delta (CK1 $\delta$ ) interacts with the SNARE associated protein snapin. *FEBS Lett.* 580, 6477–6484.
- Xia, C., Wolf, J.J., Vijayan, M., Studstill, C.J., Ma, W., and Hahm, B. (2018). Casein Kinase 1 $\alpha$  Mediates the Degradation of Receptors for Type I and Type II Interferons Caused by Hemagglutinin of Influenza A Virus. *J. Virol.* 92.
- Yin, H., Laguna, K.A., Li, G., and Kuret, J. (2006). Dysbindin Structural Homologue CK1BP Is an Isoform-Selective Binding Partner of Human Casein Kinase-1. *Biochemistry* 45, 5297–5308.
- Zemp, I., Wandrey, F., Rao, S., Ashiono, C., Wyler, E., Montellese, C., and Kutay, U. (2014). CK1 $\delta$  and CK1 $\epsilon$  are components of human 40S subunit precursors required for cytoplasmic 40S maturation. *J Cell Sci* 127, 1242–1253.
- Zhou, Q., Lee, K.J., Kurasawa, Y., Hu, H., An, T., and Li, Z. (2018). Faithful chromosome segregation in *Trypanosoma brucei* requires a cohort of divergent spindle-associated proteins with distinct functions. *Nucleic Acids Res.* 46, 8216–8231.



## 2. Characterisation of LmCKAP1

### 2.1. Introduction

Among the LmCKAPs potentially involved in endo- or exocytosis, and for which I performed CRISPR-Cas9 gene tagging and knockout (see [Chapter II section 1](#)), I also selected LmCKAP1 for further characterisation. I first tried to confirm tagging by Western blot analysis but I could not detect the protein, although the parasites were resistant to the drug. I then performed live imaging to determine the localisation of the protein. A staining could only be observed in dividing cells, with a polarised localisation at the membrane of the anterior end of the parasite (see [Chapter II section 1, Table 5](#)). This finding, which suggested that LmCKAP1 could be cell cycle regulated, prompted me to investigate further this hypothetical protein. LdBPK\_080130.1 contains a FYVE domain, which is known to bind to phosphatidylinositol 3-phosphate (Hall et al., 2006). It is a cysteine-rich zinc-finger-like motif that co-ordinates two zinc atoms and allows the insertion of proteins into cell membranes in a pH-dependent manner. Because the FYVE domain was identified as important for early endosomal localisation, LmCKAP1 could be implicated in targeting LmCK1.2 to the early endosomes and thus contribute to its loading into exosomes (Leevers et al., 1999).

### 2.2. Characterisation of LdBPK\_080130.1 (LmCKAP1) using bioinformatics

#### 2.2.1. Annotation of LmCKAP1.

In TriTrypDB (Aslett et al., 2010), LdBPK\_080130.1 is annotated as a hypothetical protein with unknown function. The protein is relatively large, 1150 amino acids, with a predicted molecular weight of 121.2 kDa and a basic isoelectric point of 11.62. It possesses an N-terminal FYVE/PHD zinc finger domain that could confer membrane-binding function, and additional InterProScan analysis of the protein sequence detected a signal peptide and predicted most of the protein to be non-cytoplasmic ([Fig. 14](#)).

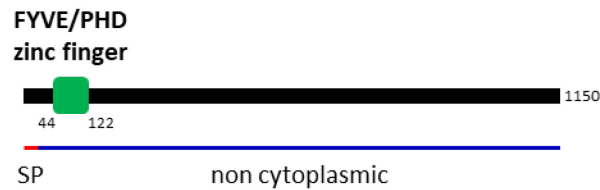


**Fig. 14 – Domain structure of LmCKAP1.**

The protein contains a FYVE/PHD zinc finger domain in N-terminus, a signal peptide (1-21, red) and is predicted to be non-cytoplasmic (blue).

In order to gain insights into LmCKAP1 phylogeny, I analysed its conservation across *Leishmania* species and other related trypanosomatids.

### 2.2.2. Paralogs and orthologs of LdBPK\_080130.1 (LmCKAP1)

I first searched LdBPK\_080130.1 orthologs in *Leishmania* and related trypanosomatids using TriTrypDB. I identified syntenic LmCKAP1 in *L. infantum*, *L. major*, *L. mexicana*, *L. braziliensis*, *L. tarentolae*, and *Crithidia fasciculata*. However in *L. amazonensis*, a gene deletion event has probably occurred during evolution, since the ORF was missing. I identified LmCKAP1 orthologs in *Trypanosoma brucei* and *T. cruzi* although they were not syntenic and were reduced in size. All the orthologs displayed a predicted FYVE/PHD zinc finger domain with an E-value  $\leq 6.0 \times 10^{-6}$ , except for *L. braziliensis*, *C. fasciculata* and *T. cruzi*, for which the domain was absent. Then, to investigate the conservation of LdBPK\_080130.1, I performed a multiple sequence alignment (MSA) using amino acid sequences retrieved from TriTrypDB and the multiple sequence alignment tool MUSCLE (MULTiple Sequence Comparison by Log-Expectation), which generated a percentage of identity matrix shown in Fig. 15 (the percentage of identity concerning LdBPK\_080130.1 are reported in Table 5) The MSA analysis revealed that the protein was not very conserved across *Leishmania* species with a percentage of identity varying between 65 and 99%, suggesting that the conservation of its amino acid composition might not be crucial for the function, or on the contrary that the protein has species-specific functions. In *C. fasciculata*, *T. brucei* and *T. cruzi*, the percentage of identity ranged between 22.63 to 48.6%. This evolutionary divergence and size reduction could possibly be associated with different functions in those parasites compared to *Leishmania*.

**Table 5 – Annotation of LmCKAP1 and orthologs in trypanosomatids.**

Species	Accession	Protein length	MW	Isoelectric point	Domains (region); E-value	% ID	Comments
<i>Leishmania donovani</i>	LdBPK_080130.1	1150	121,2	11,62	FYVE/PHD zinc finger (44-122); 1.2E-07	100	
<i>Leishmania infantum</i>	LINF_080006200	1150	121,3	11,64	FYVE/PHD zinc finger (44-122); 8.3E-08	99,57	
<i>Leishmania major</i>	LmjF.08.0130	1146	121,3	11,62	FYVE/PHD zinc finger (43-123); 2.9E-09	86,89	
<i>Leishmania mexicana</i>	LmxM.08.0130	1152	121,5	11,41	FYVE/PHD zinc finger (44-122); 8.3E-08	87,39	
<i>Leishmania braziliensis</i>	LbrM.08.0130	1147	121	11,42	absent	65,53	
<i>Leishmania tarentolae</i>	LtaP08.0130	1162	123,1	11,51	FYVE/PHD zinc finger (53-113); 3.6E-07	73,69	
<i>Leishmania amazonensis</i>	Absent	N/A	N/A	N/A	absent	N/A	Gene deleted in <i>L. amazonensis</i> MHOM/BR/71973/M2269 strain
<i>Crithidia fasciculata</i>	CFAC1_200007100	1151	119,3	12,08	absent	48,59	
<i>Trypanosoma brucei</i>	Tb927.5.3650 <i>not synthetic</i>	804	86,1	10,54	FYVE/PHD zinc finger (42-114); 6.0E-06	22,63	Targeted by RNAi in PCF T. brucei. No growth phenotype following induction of RNAi. PMID: 19309510
<i>Trypanosoma cruzi</i>	TcCLB.511653.50 <i>not synthetic</i>	797	87,6	11,43	absent	26,64	

Sequence informations obtained from TriTrypDB. Percent identity sequence of the different orthologs compared to LdBPK\_080130.1 were obtained through multiple sequence alignment (amino acid sequences) by MUSCLE (3.8) and the percent identity matrix created by Clustal2.1.



**Fig. 15 – Multiple alignment of LmCKAP1 protein sequences from different trypanosomatids species.**

CLUSTAL multiple sequence alignment by MUSCLE (3.8). Sequence species order from top to bottom: *T. brucei*, *T. cruzi*, *C. fasciculata*, *L. braziliensis*, *L. tarentolae*, *L. donovani* and *L. infantum*. Sequence of interest from *L. donovani* is highlighted by red squares.

### 2.2.3. Knowledge from other parasites

To gain insight into the functions of this hypothetical protein and due to the lack of sequence similarity with proteins from other organisms, I used the I-TASSER structure prediction server to predict LmCKAP1 structure (using LdBPK\_080130.1 sequence as input). The predicted structure was then compared to existing crystal structures and the server gave the best prediction based on 3D alignment. Interestingly, the server predicted a structural similarity between LmCKAP1 and *S. cerevisiae* VPS15 of the endosomal VPS34 complex II (PDB Hit #5dfzB: TM-score 0.907, coverage 0.933). Phosphatidylinositol 3-kinase Vps34 complexes regulate intracellular membrane trafficking in different pathways such as endocytic sorting, cytokinesis, and autophagy (Rostislavleva et al., 2015), and components of the Vps34 have been shown to be phosphorylated by CK1 (Backer, 2016). However, the characteristic of Vps15 does not correspond to that of LmCKAP1.

To gain further information on LmCKAP1, I collected data on its orthologs, Tb927.5.3650. Its knockdown by RNA interference (RNAi) in procyclic *T. brucei* parasites does not lead to any growth defect (Monnerat et al., 2009). The protein localises either to the cytoplasm, or to endocytic vesicles and contrary to LmCKAP1, it does not seem to be cell cycle regulated (Dean et al., 2017) (<http://www.tryptag.org/?id=Tb927.5.3650>). This finding suggests that Tb927.5.3650 might not be an ortholog or if it is, the function seems to have evolved considerably.

### 2.2.4. Post-translational regulation

Seven phospho-sites have been identified in the Tb927.5.3650 sequence, but only S482 complies to the canonical CK1 consensus site (Knippschild et al., 2014; Urbaniak, 2009), whereas only one site has been identified in the phosphoproteome of *L. infantum*, S698, which is a CK1 canonical site (Knippschild et al., 2014; Tsigankov et al., 2013). There was no information on the potential function of the phosphorylation of these sites.

## 2.3. Expression and localisation of LmCKAP1-mNG in *L. donovani*

### 2.3.1. LmCKAP1 is expressed at low level in *L. donovani*

I first compared the growth of LmCKAP1-mNG cell line to that of the parental cell line. To this end, parasites from logarithmic culture were inoculated in M199 medium supplemented with hygromycin B and incubated at 26°C during 216h. Growth, parasite survival (PI incorporation) and mNG fluorescence intensity (as a readout for LmCKAP1 abundance) were measured every 24h by FACS (Fig. 16).

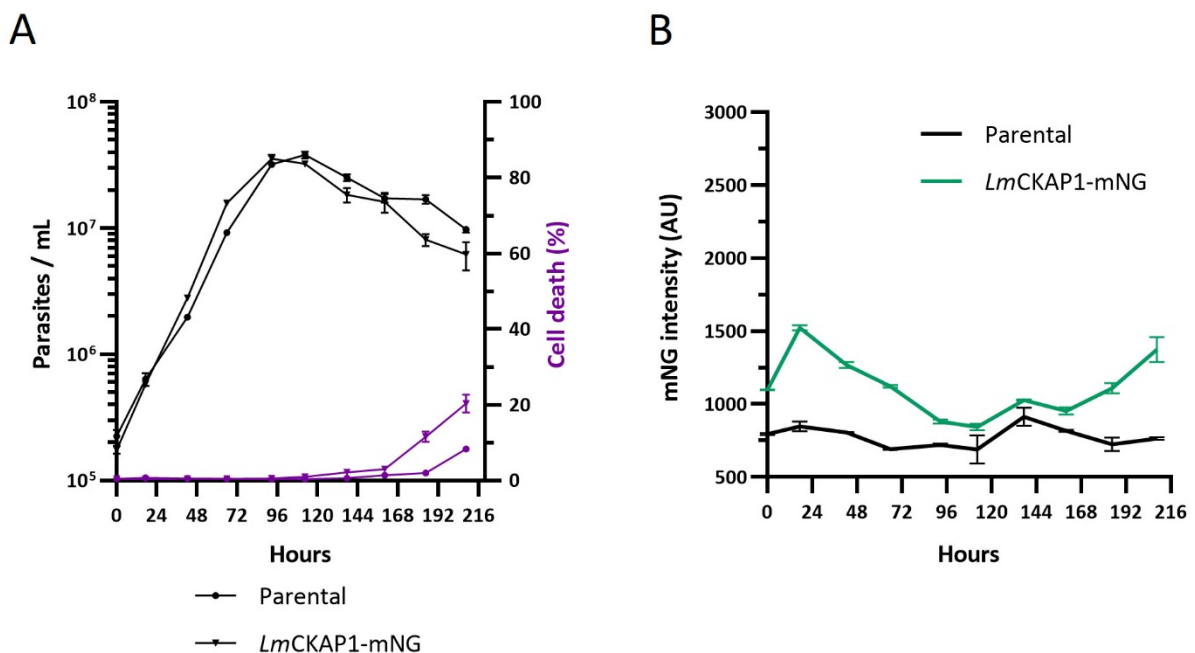


**Fig. 16 – Growth curve, cell survival and mNG intensity of promastigotes expressing mNG-tagged LmCKAP1.**

Promastigotes were cultured for 216h. Aliquots were taken every 24h for analysis. The cell number (A, left Y axis), the percentage of cell death (A, right Y axis) and the mNG mean fluorescence intensity (B) of the parental cell line (plain circle) or parasites expressing LmCKAP1-mNG (plain reverse triangle) were measured by FACS analysis. The experiment was performed in triplicates.

Promastigotes expressing LmCKAP1-mNG grew similarly to the mock control, with a similar percentage of cell death except in late stationary phase (Fig. 16A). The mean fluorescence intensity of the transgenic parasites expressing LmCKAP1-mNG was quite low, similar to that of parasites expressing  $\mu$ 2-adaptin-mNG (see Chapter II section 1). It reaches its maximum at about 1500 AU during the first 24h, decreases and increases again in late

stationary phase (green line, Fig. 16B). The fluorescence intensity of the parental cell line (black line, Fig. 16B) sets the background at around 600 AU. This result is in contradiction to that obtained from the Western blot analysis (see Chapter II section 1) and suggests that the protein could be expressed only in some parasites, and thus highly regulated. The specific gating of the mNG+ cells, which correspond to LmCKAP1+ cells, highlights only the bigger cells supporting the hypothesis that LmCKAP1 is only found in dividing cells (Fig. 17).

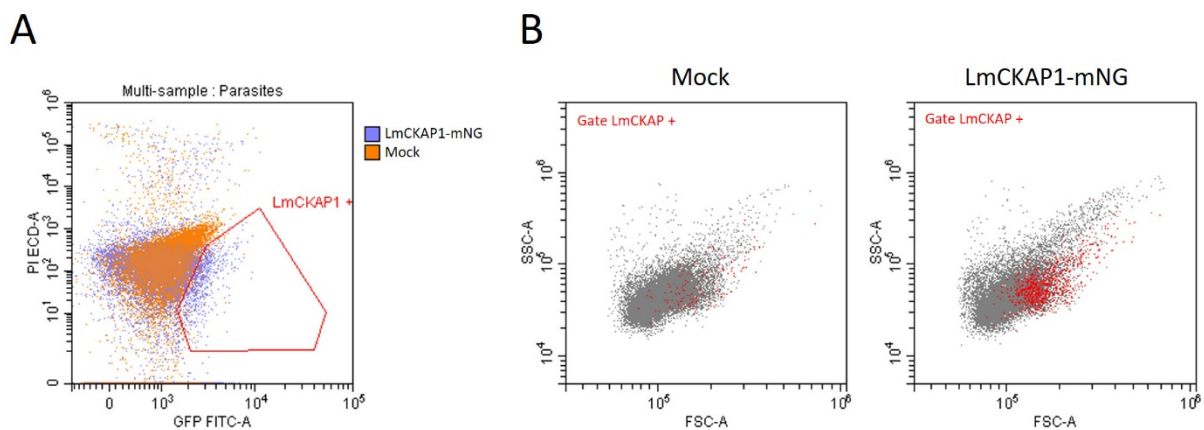


**Fig. 17 – Gating of the mNG fluorescent proteins among the parasite population highlights the bigger cells.**

Fluorescence intensity of mock or LmCKAP1-mNG promastigotes was assessed by flow cytometry. (A) Dot plot overlay representing the mNG fluorescence intensity (GFP-FITC-A) and propidium iodide incorporation (PI-ECD-A) of both parasite cell lines (Mock, orange; LmCKAP1-mNG, violet). Parasites expressing LmCKAP1-mNG are shown in “LmCKAP1 +” gate. (B) Dot plots of the SSC-A and FSC-A values for the Mock (left panel) and LmCKAP1-mNG (right panel) parasite populations. The cells that fit within the “LmCKAP1 +” gate are shown in red, showing that LmCKAP1 is expressed in bigger cells (high FSC-A values). Results representative of two independent experiments.

### 2.3.2. LmCKAP1-mNG is expressed in dividing parasites.

To gain insight into the potential functions of LmCKAP1 and determine precisely its localisation, I used live imaging microscopy. Briefly, transgenic promastigotes from logarithmic culture were washed in DPBS, placed on a microscope slide, covered with a coverslip, and imaged using an EVOS FL microscope (Thermo Fischer Scientific) or a Leica DMI 4000B microscope (Leica).

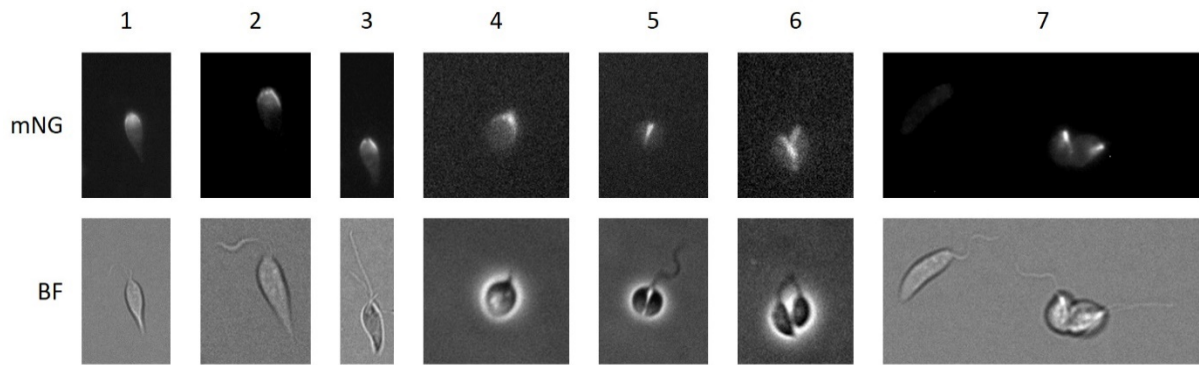


**Fig. 18 – Analysis of LmCKAP1-mNG localisation by fluorescence live microscopy.**

Parasites from transgenic promastigotes expressing LmCKAP1-mNG from logarithmic culture were placed on glass slide. Parasites were visualised by fluorescence microscopy using an EVOS FL or Leica DMI 4000B microscope. LmCKAP1-mNG localisation at different cell cycle stages is represented. BF, bright field; mNG, mNeonGreen.

The results shown in Fig. 18 indicate that indeed, LmCKAP1-mNG is detected in dividing cells, with different patterns of localisation that seem to be dependent on the mitosis stage. During the early steps of mitosis, LmCKAP1 displays a polarised localisation at the membrane of the anterior end of the parasite, on each side of the flagellum (Fig. 18, panel 1-4). Then during cytokinesis, the protein is re-distributed to the cleavage furrow (Fig. 18, panel 5) and seems to follow the cleavage furrow ingression even until late cytokinesis (Fig. 18, panel 6). Non-dividing cells showed no significant fluorescence (Fig. 18, panel 7). Although this result was obtained only once and should be repeated, it suggests that LmCKAP1 could be implicated in cytokinesis; it also supports the data obtained by cytometry, suggesting that the abundance of LmCKAP1 is cell cycle regulated.

To confirm this hypothesis, I needed to increase the proportion of mitotic cells in the logarithmic phase population. To this end, I treated logarithmic promastigotes from the parental or transgenic parasites expressing LmCKAP1-mNG cell lines with either flavopiridol, a cyclin-dependent kinase inhibitor that arrest the cell cycle in G2/M in *Leishmania* (Hassan et al., 2001) or DMSO as control. After 18h of treatment, the fluorescence intensity of arrested transgenic or parental parasites was measured by FACS.

As observed in Fig. 19A, flavopiridol treatment of the control parasites led to an increase in size compared to parasites treated by DMSO, globally, which is due to an increase in the number of cells in G2/M. This result indicates that the flavopiridol treatment was

efficient. The proportion of LmCKAP1-mNG positive cells in flavopiridol- and DMSO-treated parasites was assessed based on the mNG fluorescence intensity measured by FACS (Fig. 19B).

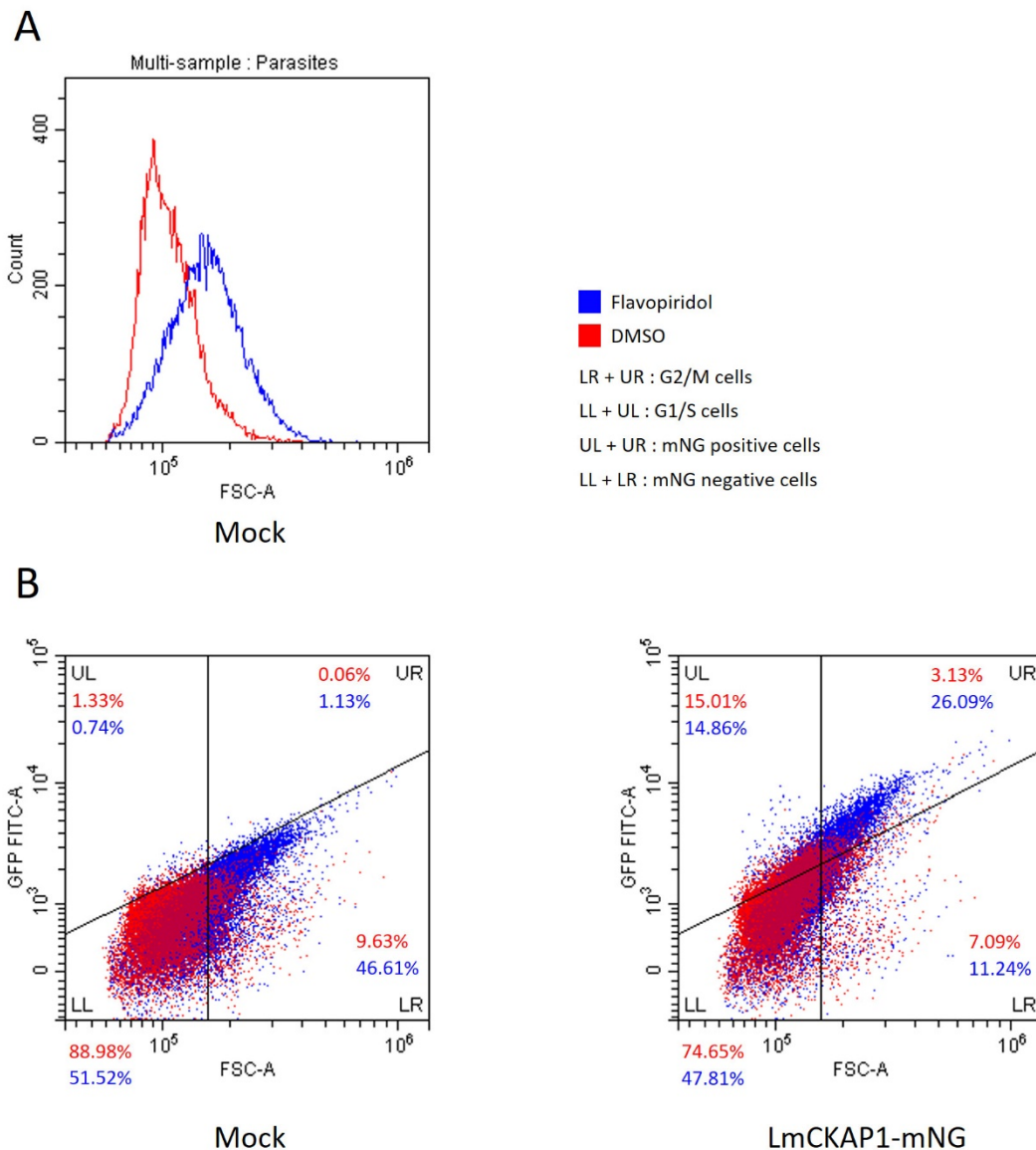


**Fig. 19 – Proportion of LmCKAP1-mNG positive cells increases upon flavopiridol treatment.**

Mock or LmCKAP1-mNG promastigotes were treated with flavopiridol or DMSO (negative control) for 18h, and the fluorescence intensity was then assessed by flow cytometry. (A) Histogram overlay representing the increased cell size (FSC-A) of flavopiridol-treated (blue) parasites compared to DMSO-treated (red) for the mock cells, indicating an increased proportion of cells in G2/M upon drug treatment. (B) Dot plot overlay representing the cell size (FSC-A) and mNG fluorescence intensity (GFP-FITC-A) of flavopiridol- or DMSO-treated (blue or red, respectively) for the mock cells (left panel) and LmCKAP1-mNG cells (right panel). The diagonal gate forms a separation between non-fluorescent and fluorescent LmCKAP1-mNG parasites and was applied to both dot plots. The diagonal form of the gating is due to increased amount of autofluorescent parasites in flavopiridol-treated samples. G1/S cells are represented in quadrants LL and UL. G2/M cells are represented in quadrants LR and UR. Populations of LmCKAP1-mNG positive cells are represented in quadrants UL and UR. This is representative of three independent experiments.

I compared the fluorescence intensity with the cell size (FSC-A) and showed that cells expressing LmCKAP1-mNG were more abundant after flavopiridol-treatment (41 %) than after DMSO treatment (18 %) (Fig. 19B). Remarkably, most of the cells expressing higher amounts of LmCKAP1-mNG corresponded to the largest cells (Fig. 19B, right panel), therefore supporting that LmCKAP1 is indeed expressed mostly in mitotic cells.

## 2.4. Knockout of LmCKAP1-mNG in *L. donovani*.

### 2.4.1. LmCKAP1 null mutants are larger cells and have minor growth defect as axenic amastigotes

Next, I investigated the phenotype of the deleted transgenic knockout cell line generated with the CRISPR-Cas9 toolkit ( $\Delta$ LmCKAP1, see Chapter II section 1). Both alleles were correctly replaced with the puromycin or blasticidin resistance genes. The absence of the ORF was validated by PCR analysis (see Chapter II section 1). I compared the growth of  $\Delta$ LmCKAP1 to that of the parental cell line, in promastigotes and axenic amastigotes. Parasites from logarithmic culture were inoculated in promastigote or axenic amastigote medium and incubated at 26°C (for 216h) or 37°C (for 192h) for promastigotes or axenic amastigotes, respectively. Growth, parasite survival (PI incorporation) and forward scatter area (FSC-A, to assess the cell size) were measured every 24h by FACS (Fig. 20). Null mutants grew similarly to the WT in promastigotes, with similar percentage of cell death observed throughout the different growth phases (Fig. 20A). As LmCKAP1 tends to accumulate in mitotic cells, I asked whether its deletion would lead to an accumulation of mitotic cells, as a result of a cell cycle defect. To this end, I compared the FSC-A values (corresponding to parasite size) of  $\Delta$ LmCKAP1 to those of the parental cells (Fig. 20B). In fact, a larger proportion of parasites in  $\Delta$ LmCKAP1 cells were mitotic compared to the parental cells, particularly during the entry into stationary phase (21.62 % for the  $\Delta$ LmCKAP1 cells compared to 5.93 % for the parental cells at 96h) (Fig. 20B). In stationary phase, parasites size heterogeneity tended to decrease (Fig. 20B, 144h and 192h), although slower in the mutant cells than in the parental cells.  $\Delta$ LmCKAP1 cells seem to accumulate more mitotic cells in logarithmic phase than the parental cells, suggesting that they might have a cell cycle defect. This will have to be confirmed by performing a cell cycle

assay. Next, I compared both cell lines during axenic amastigotes differentiation and observed

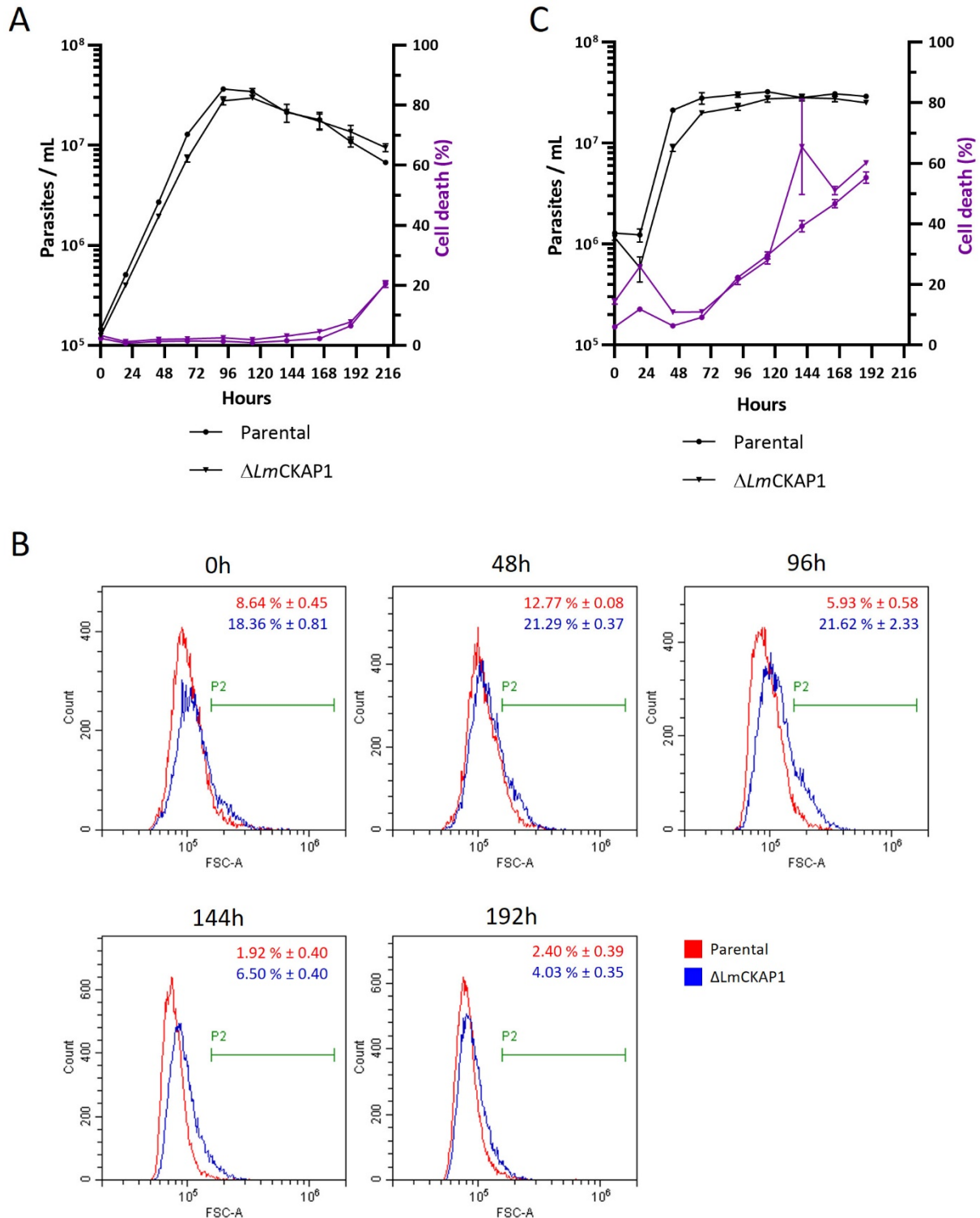


**Fig. 20 – Growth curve, cell survival and forward scatter area of  $\Delta$ LmCKAP1 promastigotes or amastigotes.**

Parasites were cultured for 216h. Aliquots were taken every 24h for analysis. The cell number (A and C, left Y axis), percentage of cell death (A and C, right Y axis) of the parental strain (plain circle) or  $\Delta$ LmCKAP1 (plain reverse triangle) in promastigotes (A, B) or axenic amastigotes (C) were measured by FACS analysis. (B) The forward scatter area (FSC-A) of the parental (red) or  $\Delta$ LmCKAP1 promastigotes were assessed by FACS analysis at 0h, 48h, 96h, 144h and 192h of growth. The percentage of cells in the gate P2 (high FSC-A values, positioned based on Fig. 19B gating) for three replicates is presented as the mean and standard deviation is shown. The experiment has been performed in triplicates.

that the null mutants show increased cell death during the first 48h of logarithmic phase, resulting in a delay reaching stationary phase (Fig. 20C). The surprising increase in percentage of cell death observed for the null mutant cell line at 144h is probably due to an experimental error. These results are preliminary and will need to be repeated to validate the phenotype in axenic amastigotes.

#### 2.4.2. Low ectopic overexpression of LmCK1.2 in $\Delta$ LmCKAP1 parasites leads to an increase in cell death only in axenic amastigotes

To determine whether LmCKAP1 could be involved in the localisation of LmCK1.2, I expressed the tagged kinase from an ectopic plasmid in LmCKAP1 null mutant cell line. To do so, I took advantage of the plasmid expressing LmCK1.2-V5 (Rachidi et al., 2014), which I modified to replace the hygromycin resistance gene (HygR) by a neomycin resistance cassette (NeoR), as the HygR was already used by the pTB007 plasmid. The cloning steps involved digestion of the plasmids pLEXY-CK1.2-V5-His<sub>6</sub> (HygR) and pLEXY-neo2 (Jena Bioscience) with BamHI restriction enzyme, gel purification of the pLEXY-neo2 vector backbone and the fragment containing LmCK1.2-V5-His<sub>6</sub> ORF and re-circularization by ligation followed by transformation into bacteria (see Fig. 21A and Materials and Methods). The correct orientation of the ORF was verified by digestion (data not shown).  $\Delta$ LmCKAP1 cells were transfected with the pLEXY-CK1.2-V5-His<sub>6</sub> and selected with neomycin drug selection. I characterised these cells by FACS to verify their growth behaviour (Fig. 21B and C).

In promastigotes, the ectopic expression of LmCK1.2-V5 had no visible effect on the growth of the null mutant as shown in Fig. 21B, except maybe at stationary phase, whereas it led to a strong growth defect in axenic amastigotes. Indeed, null mutant parasites grew slower than the parental cells and failed to reach the same stationary phase parasite concentration (Fig. 21C). The slower growth seems to be the consequence of an increase in the percentage of cell death (Fig. 21C) during differentiation (first 48h) but also during proliferation (from 96 to 192h). The expression of ectopic LmCK1.2, in addition to the endogenous protein, seems to exacerbate the growth defect I observed in axenic amastigote in the null mutant alone. This finding delivers additional evidence towards a link between LmCK1.2 and LmCKAP1.

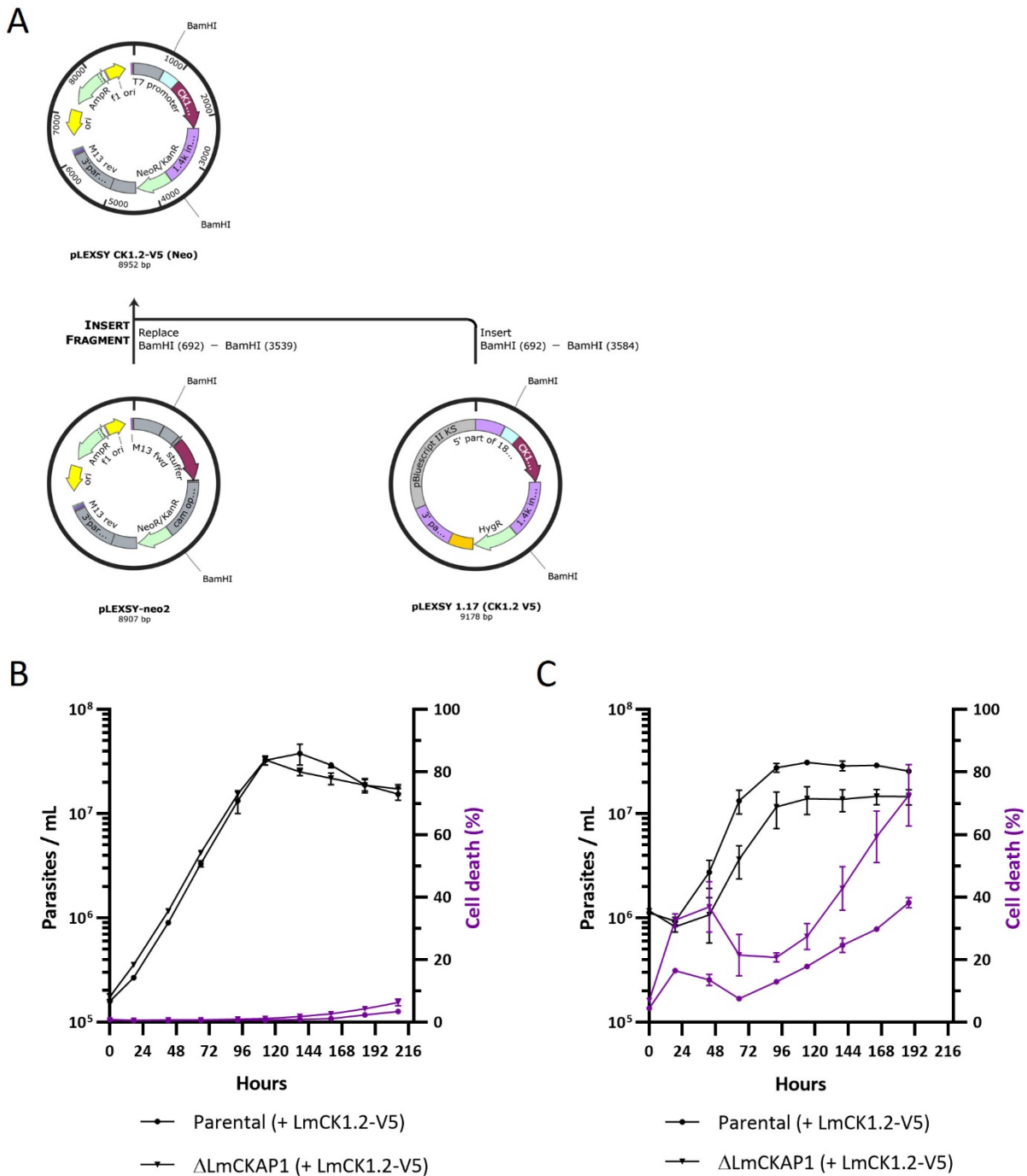


**Fig. 21 – Characterisation of the  $\Delta$ LmCKAP1 (+ LmCK1.2-V5) cells.**

(A) Cartoon depicting the cloning steps to replace the HygR cassette from the plasmid pLEXSY-CK1.2 by the NeoR cassette of the pLEXSY-neo2 vector. Both vectors were digested by BamHI, fragments of interest were purified, and the plasmid recircularised by ligation. (B and C) Growth curve and cell survival of  $\Delta$ LmCKAP1 (+ LmCK1.2-V5) and parental cells in promastigotes (B) or axenic amastigotes (C). Parasites were cultured for 216h. Aliquots were taken every 24h for analysis. The cell number (B and C, left Y axis), percentage of cell death (B and C, right Y axis) of the parental strain (plain circle) or expressing  $\Delta$ LmCKAP1 (plain reverse triangle) in promastigotes (A, B) or axenic amastigotes (C) were measured by FACS analysis. The experiment has been performed once in triplicate.

### 2.4.3. Analysis of $\Delta$ LmCKAP1 (+ LmCK1.2-V5) mutants shows aberrant mitotic parasites

The size increase observed in  $\Delta$ LmCKAP1 parasites could be due to an increase in the number of dividing cells, so I investigated this hypothesis using fluorescence microscopy. I used the cell line that also expressed LmCK1.2-V5 ( $\Delta$ LmCKAP1/CK) as it allowed me to simultaneously assess the localisation of LmCK1.2 in the mutant cells. I observed the mutant parasites by fluorescence microscopy; logarithmic phase promastigotes were fixed with PFA and the nucleus and kinetoplast stained with Hoechst 33342. I counted the number of nucleus and kinetoplast per parasite, as well as parasites with unusual shape or aberrant division pattern (Fig. 22A). The percentage of parasites in mitosis was higher in  $\Delta$ LmCKAP1/CK than in the parental cell line, 23% versus 8% respectively. This important difference was due to an increase in aberrant mitotic pattern in the mutant cells, 15.21% for  $\Delta$ LmCKAP1/CK versus 0.82% for the parental cells (Fig. 22A). These aberrant cells (for examples, see Fig. 22B) displayed divided nuclei with undivided kinetoplasts (2N1K<sup>M</sup>), cells without kinetoplasts (1N0K), and cells where cytokinesis started before full completion of chromosome segregation. For instance, in Fig. 22Ba, a 2N1K<sup>M</sup> cell can be observed with a protrusion, probably a remnant of premature cytokinesis that failed. The  $\alpha$ -tubulin staining shows the intersection between the main parasite body and this remnant body (white arrow). Based on the position of the 2 nuclei and the fact that kinetoplast segregation had failed, cytokinesis should not have been attempted. In Fig. 22Bb, this parasite shows two mitotic spindles and four nuclei, indicating that the parasite has started a new round of DNA replication and mitosis without fully completing the first cytokinesis. These results are preliminary and will have to be repeated, but together with the localisation data, they strongly suggest that LmCKAP1 and LmCK1.2 might have a role in cytokinesis.

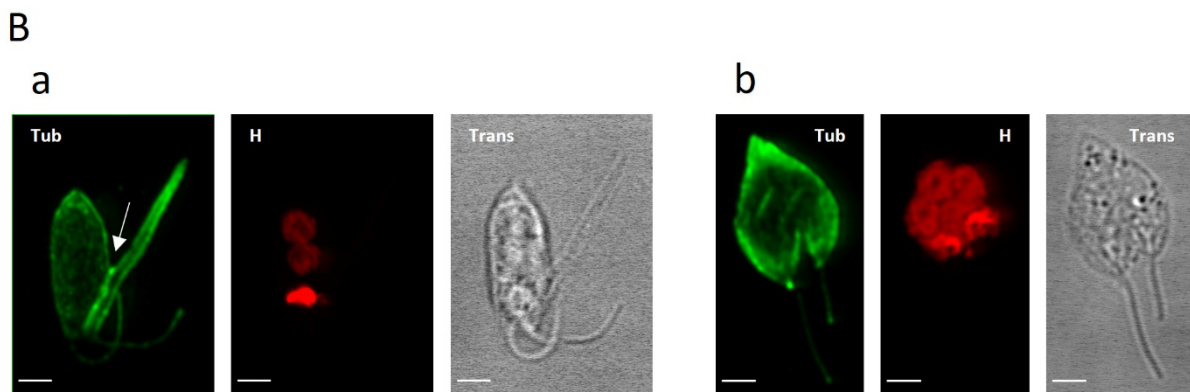
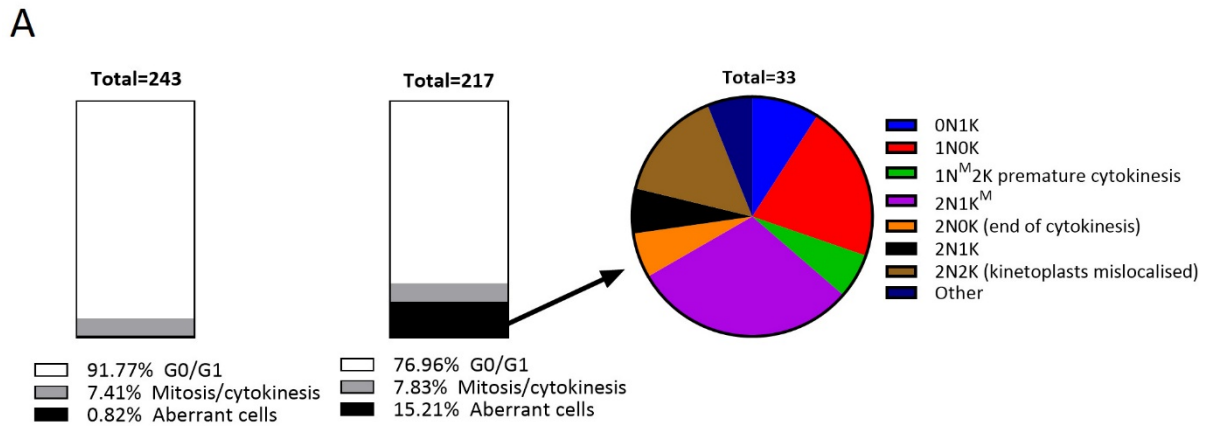


**Fig. 22 – IFA of  $\Delta$ LmCKAP1 cells show aberrant mitotic parasites.**

(A) Proportion of mitotic cells in the  $\Delta$ LmCKAP1 (+ *LmCK1.2-V5*) mutant and parental cells in promastigotes. Parasites were PFA-fixed and the nuclei stained with Hoechst 33342. Parasites were imaged and the quiescent, mitotic or aberrant cells were counted and plotted as vertical slices (left panels). The detail of aberrant cells found in the null mutant are shown in the pie graph (right coloured panel). N, nucleus; K, kinetoplast; M, mitosis. The experiment was done once. (B) IFA of  $\Delta$ LmCKAP1 (+ *LmCK1.2-V5*) cells, fixed with PFA (a) or treated with detergent (b) and stained with anti- $\alpha$ -tubulin (Tub) and Hoechst 33342 (H). The confocal images show the Tub and H stainings and transmission image (Trans). Scale bar, 2  $\mu$ m. The pictures are maximum intensity projection (MIP of the confocal stacks containing the parasites).

#### 2.4.4. Localisation of LmCK1.2-V5 in $\Delta$ LmCKAP1 cell line.

Next, to investigate whether the localisation of LmCK1.2 was dependent on LmCKAP1, I compared the localisation of LmCK1.2 in the parental and  $\Delta$ LmCKAP1 promastigote cell lines. I could not find any obvious differences in preliminary observations. However, a more thorough investigation will be necessary, particularly in amastigotes and focusing on the different steps of the cell cycle.

## 2.5. Discussion and perspectives.

Here, I characterised a novel protein that seems to be involved in cytokinesis, LmCKAP1. Several lines of evidences support this hypothesis. LmCKAP1-mNG is only detected during mitosis; to my knowledge, this is one of the rare cell-cycle-regulated proteins identified in *Leishmania*. Its regulation is very similar to that of cyclin B in eukaryotes, which increases in abundance at the onset of mitosis to be degraded in the metaphase to anaphase transition (Deshaies, 1997). The mechanisms of regulation could be similar, except that contrary to cyclin B, LmCKAP1 remains until the end of cytokinesis. LmCKAP1-mNG is localised to the plasma membrane situated at the anterior part of the parasite during the early stages of mitosis. Then it relocates to the cleavage furrow during cytokinesis until the separation of the two daughter cells. Furthermore,  $\Delta$ LmCKAP1 null mutants show an increase in cell size in promastigotes that was linked to a higher percentage of cells engaged in mitosis (23%), a majority of these mitotic cells displayed aberrant mitotic figures, mostly with multiple nuclei or with premature cytokinesis. This finding suggests that the mutant cells are unable to exit mitosis although they can reactivate S phase as shown by the multiple nuclei. Finally,  $\Delta$ LmCKAP1 cells display a growth defect during axenic amastigotes differentiation, which is amplified by the ectopic expression of LmCK1.2-V5. This data constitutes a genetic evidence of the interaction of the two proteins in *Leishmania*. However, if LmCKAP1 was essential for cytokinesis, the deletion of the corresponding gene would lead to cell death but it is not the case, as I obtained a  $\Delta$ LmCKAP1 mutant cell line. These data suggest therefore that LmCKAP1 could either be implicated in defining the site for cytokinesis or be important to trigger a potential cytokinesis checkpoint, although such a checkpoint has never been identified in *Leishmania*. However, because this gene was not identified in *L. amazonensis*, despite the fact that these parasites performed cytokinesis, it also suggests that LmCKAP1 might not be the only protein able to perform this function.

LmCKAP1 was co-purified with LmCK1.2 in axenic amastigotes, suggesting a physical link with this kinase. I have shown that a slight overexpression of LmCK1.2 increases the growth defect of  $\Delta$ LmCKAP1 mutant, suggesting a genetic link between the two proteins. I could not perform a kinase assay using recombinant LmCKAP1 as substrate, due to time constraints, but from phospho-proteomic data available for *L. infantum*, LmCKAP1 is

phosphorylated at S711 and S698, the last being a canonical consensus site for CK1 (S/TXXXS/T)(Knippschild et al., 2014).

Only few papers have described the involvement of CK1 in cytokinesis, which makes this study attractive to the CK1 field. Different isoforms of CK1 in human were predicted to be among the main regulators of cytokinesis by comparative phosphoproteomic analysis (Karayel et al., 2018). Furthermore, in *Schizosaccharomyces pombe*, CK1 was shown to be an integral component of a mitotic, ubiquitin-mediated checkpoint pathway. Upon mitotic checkpoint activation, the CK1 phosphorylation of Sid4 (a scaffold of Polo kinase) mediates its ubiquitination by Dma1, which in turn stops cytokinesis (Johnson et al., 2013).

Using the I-TASSER structure prediction server, I could predict LmCKAP1 to be structurally similar to *S. cerevisiae* VPS15, a protein kinase of the endosomal VPS34 complex II. Phosphatidylinositol 3-kinase Vps34 complexes regulate intracellular membrane trafficking for different pathways such as endocytic sorting, cytokinesis, and autophagy (Rostislavleva et al., 2015). Furthermore, components of the Vps34 complex have been shown to be phosphorylated by CK1 (Backer, 2016). However, the localisation, the structure and the cell cycle specific expression of LmCKAP1 do not correspond to the features of Vps15 (this study), therefore the precise functions of this protein still remain to be deciphered.

The FYVE domain interacts with PI3P, suggesting that the PI3P might be localised similarly to LmCKAP1, to the plasma membrane of the anterior part of the parasite. PI3P has been shown to be required for cytokinesis (Nezis et al., 2010). One hypothesis could be that the presence of PI3P in the membrane could define the location of cytokinesis and recruit proteins such as LmCKAP1. This hypothesis will be investigated by using FYVE-mNG to highlight PI3P localisation. We will also delete the FYVE domain of LmCKAP1 to see whether it can still localises and if not, whether it disturbs cytokinesis similarly to the deletion of the whole gene.

Future work will also investigate the difference of phenotypes between promastigotes and axenic amastigotes, as results presented here focused more on promastigotes, although the major effects were observed in axenic amastigotes and the physical interaction was shown for axenic amastigotes. With regards to LmCKAP1 regulation of expression, more investigations will be needed since LmCKAP1 is only expressed in mitotic cells, post-transcriptional and post-translational regulation are worth considering.



### 3. Development of LmCK1.2 immunoprecipitation conditions for mass spectrometry analysis.

This part summarises all the optimisation steps for [Chapter II](#).

To identify LmCK1.2 interacting partners, I performed immuno-precipitations followed by mass spectrometry analyses. Before sending the samples, I had to develop the protocol for immunoprecipitation (IP) of the fusion protein LmCK1.2-V5-His<sub>6</sub> (hereafter named LmCK1.2-V5) from parasite lysates. I took advantage of the transgenic *L. donovani* cell lines *LdBob* pLEXSY (mock) and *LdBob* pLEXSY-CK1.2-V5-His<sub>6</sub>, which had been previously characterized in the laboratory (Rachidi et al., 2014). I first optimized the protocol for promastigotes, and then adjusted it for axenic amastigotes cell extracts.

#### 3.1. LmCK1.2-V5-His<sub>6</sub> immunoprecipitation from promastigotes cell lysates

I first used protein G agarose beads non-covalently coupled to anti-V5 antibody. I lysed  $4 \times 10^9$  transgenic promastigotes from the two strains with 4 mL RIPA buffer (20 mM Tris-HCl pH 7.5, 150 mM NaCl, 1 mM Na<sub>2</sub>EDTA, 1 mM EGTA, 1% NP-40, 1% sodium deoxycholate, 2.5 mM sodium pyrophosphate, 1 mM  $\beta$ -glycerophosphate, 1 mM Na<sub>3</sub>VO<sub>4</sub> and 1  $\mu$ g / mL leupeptin), supplemented with a protease inhibitor cocktail (Roche), 0.1 mM PMSF and 500 U/mL benzonase (DNAse). After a sonication step, the samples were centrifuged to eliminate cell and DNA debris, and then assayed. Fourteen milligrams of total proteins were then pre-cleared with 50  $\mu$ L of packed protein-G agarose beads (Pierce) for 1h at 4°C with agitation. This pre-clearing step was necessary to eliminate proteins non-specifically bound to the beads. The pre-cleared protein lysate was then incubated with 8  $\mu$ g of mouse IgG2a anti-V5-tag monoclonal antibody (1.75  $\mu$ g antibody/mg of protein lysate) overnight at 4°C with agitation for optimal binding of the antibody to LmCK1.2-V5. The samples were then incubated with 50  $\mu$ L of protein-G agarose beads for 1h at 4°C and the beads were washed 3 times in washing buffer (50 mM Tris-HCl [pH 7.4], 5 mM NaF, 250 mM NaCl, 5 mM EDTA [pH 8.0], 0.1% NP-40, complete protease inhibitor cocktail). Proteins were eluted from the beads twice successively by addition of 50  $\mu$ L of NuPAGE loading buffer (1X NuPAGE LDS Sample Buffer, 1X NuPAGE

Sample Reducing Agent) and heating the sample for 5 minutes at 95°C. The samples were separated by SDS-PAGE and stained by SYPRO Ruby. The results are shown in Fig. 23.

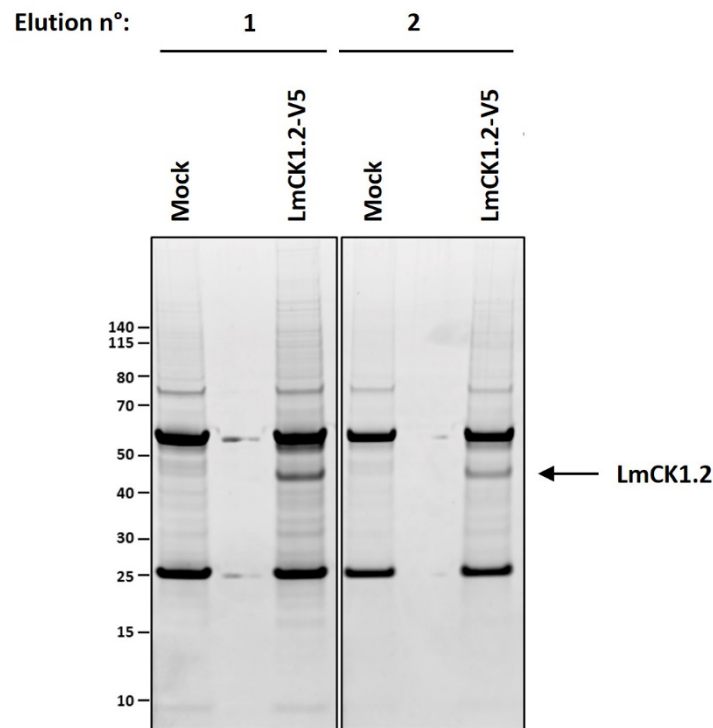


**Fig. 23 – LmCK1.2-V5 immunoprecipitation.**

Promastigotes from Mock or expressing LmCK1.2-V5 were used to purify LmCK1.2-V5 and associated proteins. Two elutions were performed successively (1 and 2). Proteins were separated by SDS-PAGE and stained with SYPRO Ruby.

As judged in Fig. 23, there is an enrichment of LmCK1.2-V5, indicated by the intense band at 45 kDa present in the LmCK1.2-V5 but not in the mock fractions. Despite the presence of a few bands specifically present in the LmCK1.2-V5 fraction, the patterns were quite similar between the two samples suggesting the presence of non-specific bindings due to inefficient washing or pre-clearing steps. Moreover, the presence of the antibody heavy and light chains (very intense bands at about 55 and 25 kDa) could prevent the optimal detection of LmCK1.2 binding proteins by mass spectrometry.

In order to optimise the protocol, I first changed two parameters independently: the amount of agarose beads used for the pre-clearing step (100  $\mu$ L instead of 50  $\mu$ L of packed beads) and the number of washes before the elutions (6 times instead of 3). These modifications individually did not improve the quality of the elutions, so I combined the two parameters using 2 mg of total protein. After immuno-precipitation, the elutions were

separated by SDS-PAGE and the proteins revealed either directly by SYPRO Ruby staining (Fig. 24A) or by Western blot analysis using an anti-V5 antibody ( $\alpha$ -V5, Fig 24B-C).

The results presented in Fig. 24A clearly show that the combination of these two parameters improved the immuno-precipitation of LmCK1.2, as it increased the number of proteins recovered from LmCK1.2-V5 fractions in elution 1. However, the third elution from the LmCK1.2-V5 fraction (Fig. 24B) as well as the flow through (FT, Fig. 24C) still contained the kinase, as visible by the 45 kDa band, suggesting that the elution step should be optimized.

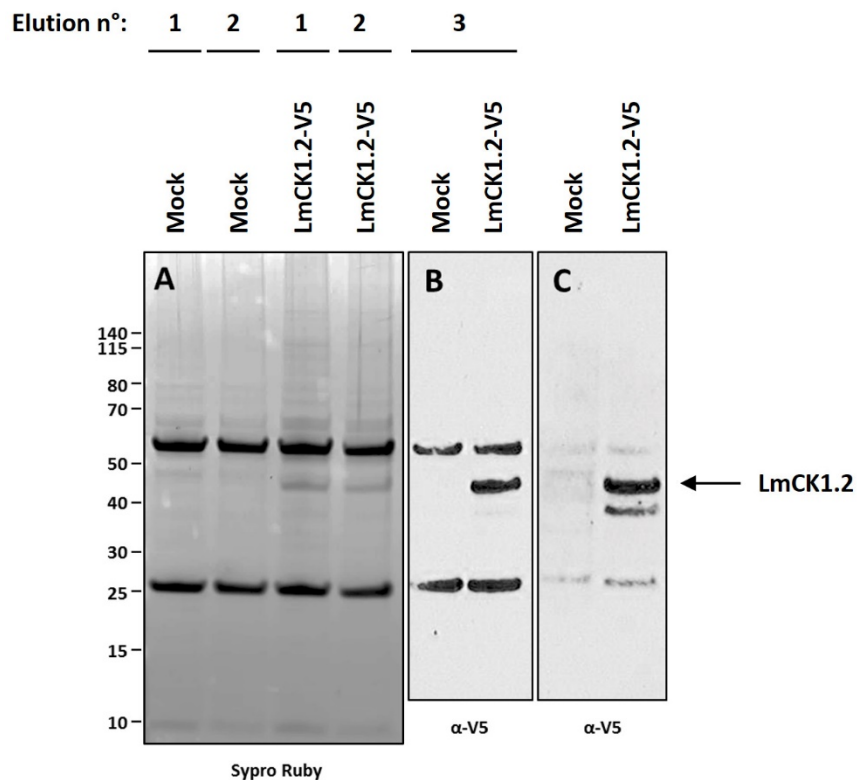


**Fig. 24 – LmCK1.2-V5 immunoprecipitation.**

Promastigotes from Mock or expressing LmCK1.2-V5 were used to purify LmCK1.2-V5 and associated proteins. Three elutions were performed successively (1, 2 and 3). The proteins were revealed by SYPRO Ruby staining for the elutions 1 and 2(A), or Western blot analysis with an  $\alpha$ -V5 antibody for the elutions 3 (B) and 30  $\mu$ g of the flow through (FT) (C). SYPRO Ruby Scan at 650V; Exposure time of Western blot 5 min.

Moreover, during the purification step, I always recovered a significant amount of non-specific proteins bound to the beads. To alleviate this problem that could be due to the use of agarose beads, I switched to magnetic beads, which I cross-linked to the anti-V5 antibody to eliminate the presence of the antibody light and heavy chains in the elutions.

As before, promastigotes were lysed and protein concentration assessed. For each strain, 6 mg of total protein were used and adjusted to an identical volume. I used protein G magnetic beads (Dynabeads, ThermoFisher Scientific). Following the manufacturer's protocol, I carried out a pre-clearing step by incubating the lysates with 50  $\mu$ L of magnetic beads for 30 minutes at 4°C with agitation. The pre-cleared lysates were recovered using a magnet and kept on ice until performing the immuno-precipitation. In parallel, 50  $\mu$ L of magnetic beads were incubated with 3  $\mu$ g of anti-V5 antibody for 10 minutes at room temperature (RT). After washing the  $\alpha$ V5-beads with 0.02% PBS-Tween 20 and with a conjugation buffer (20 mM Sodium Phosphate pH 7.4, 150 mM NaCl), I proceeded to the crosslinking step. To this end, the  $\alpha$ V5-beads were incubated with 250  $\mu$ L of 5 mM bisulfosuccinimidyl suberate (BS<sup>3</sup>) for 30 minutes at RT with agitation, and then the reaction was quenched with the addition of 12.5  $\mu$ L of 50 mM Tris pH7.4 for 15 minutes at RT. The  $\alpha$ V5-beads were washed again and added to the pre-cleared lysates. After 30 minutes of incubation at 4°C with agitation, the beads were washed six times 5 minutes at 4°C. The purified proteins were eluted with two times 30  $\mu$ L NuPAGE loading buffer and incubated 5 minutes at 70°C. The samples were separated on SDS-PAGE and the gel was either stained with SYPRO Ruby or transferred to a PVDF membrane for Western blot analysis with the anti-V5 antibody. The results are presented in [Fig. 25](#).

The use of magnetic beads cross-linked to the  $\alpha$ -V5 antibody substantially improved the quality of the immuno-precipitation ([Fig. 25](#)). This method was much faster compared to that using agarose beads, and allowing the recovery of more proteins in the LmCK1.2-V5 fraction. Nevertheless, the use of magnetic beads resulted in (i) the purification of non-specific proteins (<28 kDa, light chain of the antibody and other proteins), (ii) the purification of proteins specifically detected in the mock fraction, and (iii) the detection of LmCK1.2 in the second elution and in the FT.

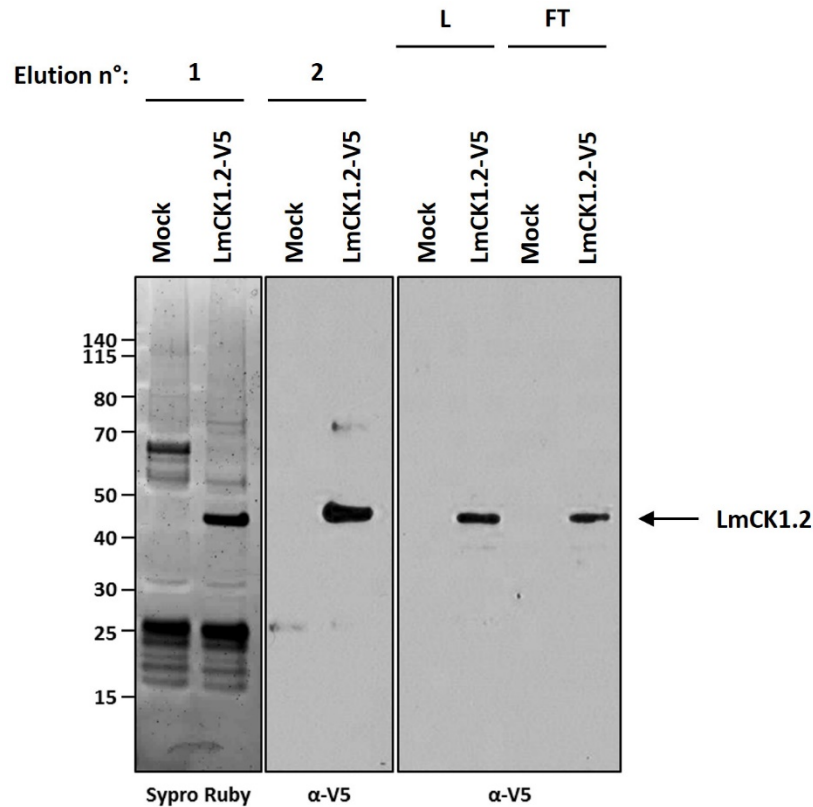


**Fig. 25 – LmCK1.2-V5 immunoprecipitation with magnetic beads.**

Promastigotes from Mock or expressing LmCK1.2-V5 were used to purify LmCK1.2-V5 and associated proteins. Two elutions were performed successively (1 and 2). The proteins were revealed by SYPRO Ruby staining for the elutions 1, or Western blot analysis with an  $\alpha$ -V5 antibody for the elutions 2, and 5  $\mu$ L of the protein lysate (L) or the flow through (FT). Western blot exposure time: 5 min.

To solve these issues, in particular to increase elution efficiency, I changed the buffer and the temperature at which it was performed. I followed the manufacturer's recommendations and tested the acidic glycine buffer (33.33 mM glycine [pH 2.8], 0.33X NuPAGE LDS Sample Buffer, 0.33X NuPAGE Sample Reducing Agent). I performed a similar IP and proceeded to three successive 10 minutes elutions at 70°C with 30  $\mu$ L of glycine elution buffer followed by a fourth elution with 30 $\mu$ L of the NuPAGE loading buffer for 5 minutes at 95°C. The results are shown in [Fig. 26](#).

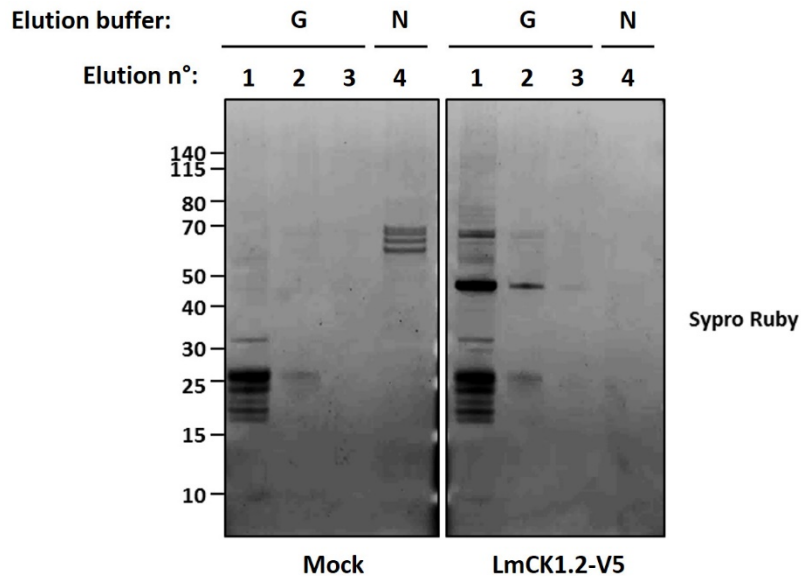


**Fig. 26 – LmCK1.2-V5 immunoprecipitation with magnetic beads.**

Promastigotes from Mock or expressing LmCK1.2-V5 were used to purify LmCK1.2-V5 and associated proteins. Four elutions were performed successively (1 to 4) using two different elutions buffer, glycine elution buffer (G, 1 to 3) or NuPAGE loading buffer (N, 4). The proteins were revealed by SYPRO Ruby staining.

The new protocol was very efficient and greatly improved the elution step, as visible by the enrichment of the LmCK1.2-V5 protein in elution 1 and the low quantity of protein in the elutions 2 and 3. The majority of the bound proteins were recovered in elution 1. Moreover the non-specific bands, recovered in the mock fraction previously (see Fig. 25) have greatly decreased, and could only be seen when using the NuPAGE elution buffer (see elution 4 of the mock strain in Fig. 26). Unfortunately, I was not able to eliminate the smaller non-specific bands (< 30 kDa) but the purification was sufficient to identify LmCK1.2 binding partners.

I thus used this protocol to immuno-precipitate LmCK1.2-V5 from the mock and LmCK1.2-V5-expressing cell lines from three biological replicates with two elutions per experiment with the glycine elution buffer. The second elution was used to assess the success of the purification before sending the samples for MS analysis, by detecting LmCK1.2-V5. The samples were separated by SDS-PAGE and the gel was stained with SYPRO Ruby. As visible in Fig. 27, LmCK1.2-V5 was recovered in the three replicates and the small amount of protein recovered in the second elution indicated that the majority of LmCK1.2 was recovered in the first elution. The first elution was then stored at -80°C and sent for mass spectrometry analysis (Institut Curie, Mass Spectrometry Platform).

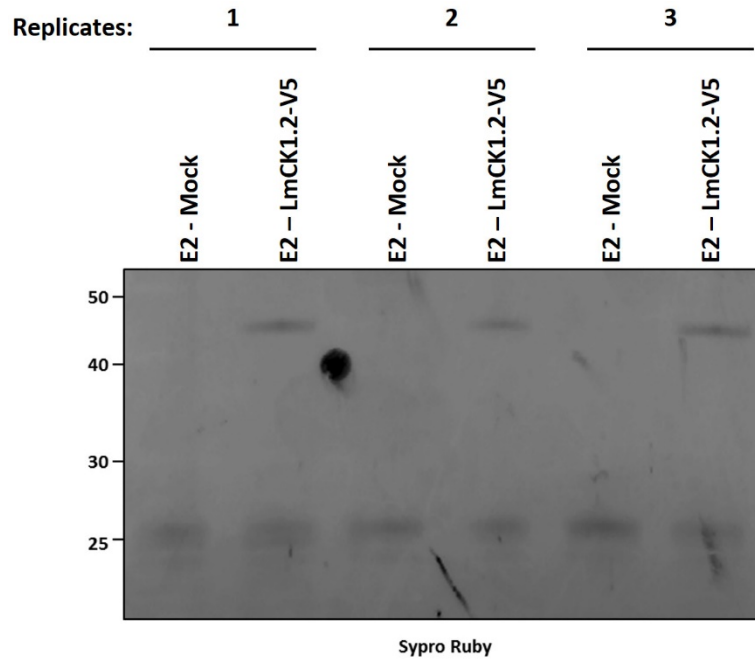


**Fig. 27 – LmCK1.2-V5 immunoprecipitation for mass spectrometry (PRO).**

Promastigotes from Mock or expressing LmCK1.2-V5 were used to purify LmCK1.2-V5 and associated proteins. SDS-PAGE and SYPRO Ruby staining of the elution 2 of LmCK1.2-V5 immunoprecipitation in biological triplicates.

### 3.2. LmCK1.2-V5-His<sub>6</sub> immuno-precipitation from amastigotes cell lysates

Next I performed the immuno-precipitation of LmCK1.2-V5 from axenic amastigote lysates using the last conditions defined in [Section 3.1](#), to verify that they were optimum. I used 48h differentiated axenic amastigotes that I lysed similarly as before, and assessed protein concentration. For the mock and for the parasites expressing LmCK1.2-V5 cell line, 6 mg of total protein were used and adjusted to an identical volume. I performed a similar IP with three successive elutions at 70°C for 10 minutes with 30 µL of glycine elution buffer, followed by a fourth elution with 30µL of NuPAGE loading buffer, at 95°C for 5 minutes. The results are as shown in [Fig. 28](#).

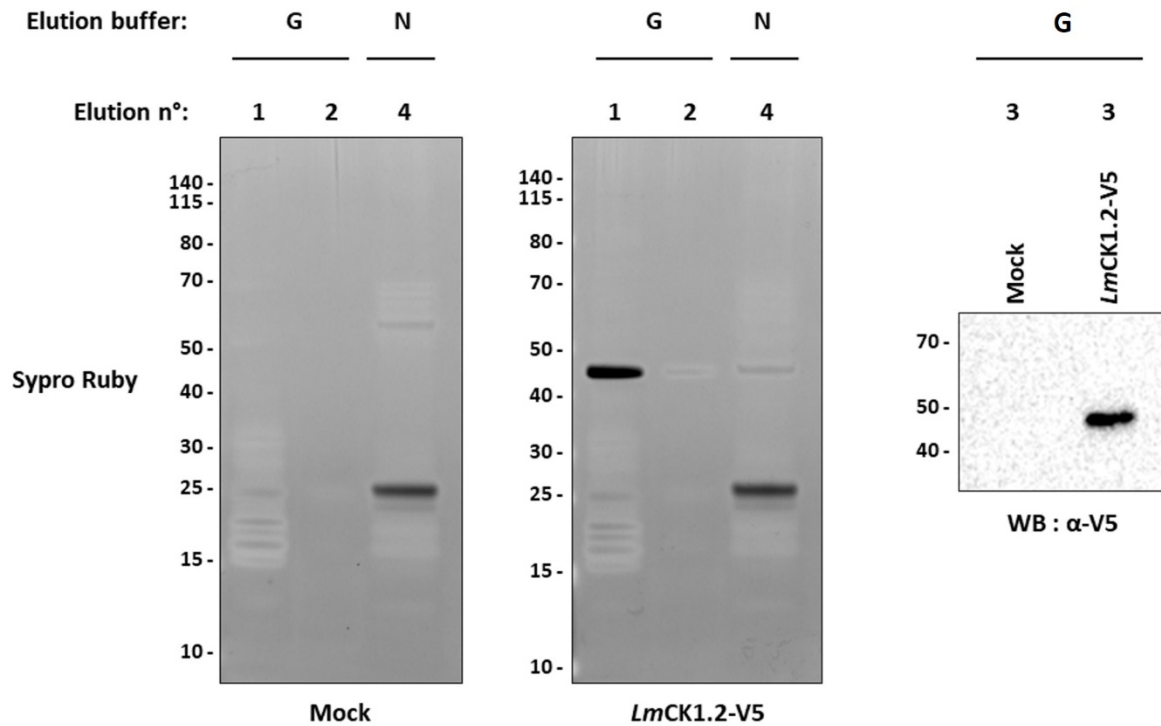


**Fig. 28 – LmCK1.2-V5 immunoprecipitation with magnetic beads.**

Axenic amastigotes from Mock or expressing LmCK1.2-V5 were used to purify LmCK1.2-V5 and associated proteins. Four elutions were performed successively (1 to 4) using two different elution buffer, glycine elution buffer (G, 1 to 3) or NuPAGE loading buffer (N, 4). The proteins were revealed by SYPRO Ruby staining for the elutions 1 to 4, or Western blot analysis with an  $\alpha$ -V5 antibody for the elutions 3. Western blot exposure time: 5 min.

These conditions were optimal for the immuno-precipitation of LmCK1.2 from axenic amastigotes, with only a few bands visible in the mock fraction. However, only few associated proteins were recovered from the *LmCK1.2-V5* fraction. A possible explanation could be that LmCK1.2 has less different binding partners in promastigotes than in amastigotes, suggesting that each binding partners is recovered with a lower abundance.

In an attempt to recover more LmCK1.2-v5 associated proteins, I kept the same IP conditions but increased the quantity of total protein by three fold (18 mg). Again, I performed three elutions in glycine elution buffer and one in NuPAGE loading buffer, as was done before (Fig. 29).

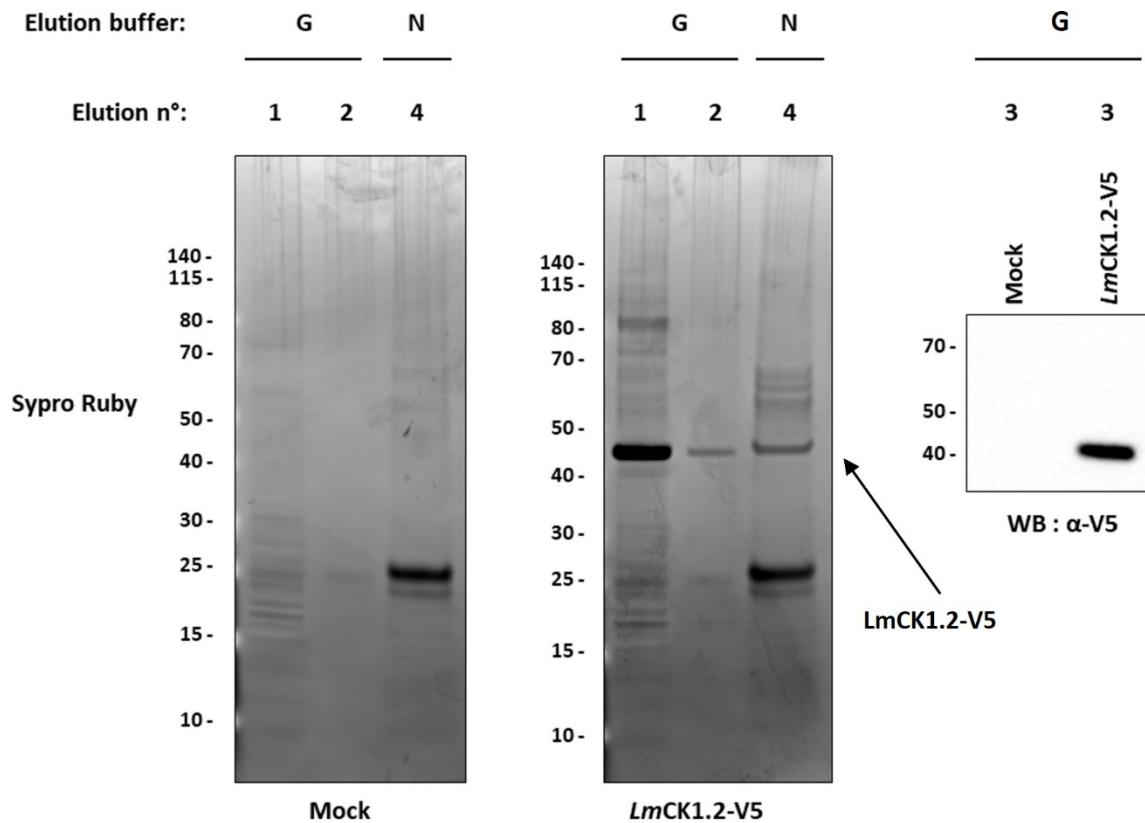


**Fig. 29 – LmCK1.2-V5 immunoprecipitation with magnetic beads from 18 mg total protein lysate.**

Axenic amastigotes from Mock or expressing LmCK1.2-V5 were used to purify LmCK1.2-V5 and associated proteins. Four elutions were performed successively (1 to 4) using two different elution buffer, glycine elution buffer (G, 1 to 3) or NuPAGE loading buffer (N, 4). The proteins were revealed by SYPRO Ruby staining for the elutions 1 to 4, or Western blot analysis with an  $\alpha$ -V5 antibody for the elutions 3. Western blot exposure time: 5 min.

The immuno-precipitation was very much improved by using higher quantity of total proteins as judged in Fig. 29. Interestingly, in elution 4 I purified a different set of proteins. I still purified non-specific proteins, although less than from promastigote lysates. This could be due to the amount of total protein I used. Therefore, for the final experiment, I used an intermediate concentration of 14 mg of total protein. I immuno-precipitated LmCK1.2-V5 from the mock and LmCK1.2-V5-expressing parasites from three biological replicates and performed three successive elutions for each experiments. I used the glycine elution buffer condition for elution 1 and the NuPAGE loading buffer condition for elution 2 and 3, to maximise the number of binding partners identified. I used elution 3 to verify the presence of LmCK1.2-V5 before sending elution 1 and 2 to MS. The samples were separated by SDS-PAGE and the gel stained with SYPRO Ruby. As visible in Fig. 30, LmCK1.2-V5 was recovered in the three replicates in very small amount, indicating that the majority of LmCK1.2 had been

recovered in the first two elutions. These two elutions were sent for mass spectrometry analysis (Institut Curie Mass Spectrometry Platform).

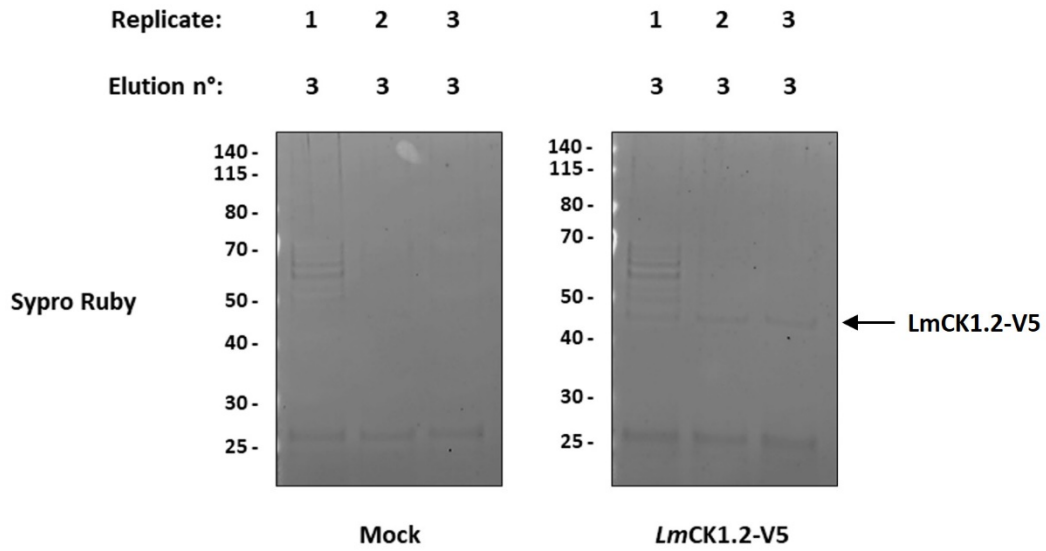


**Fig. 30 – LmCK1.2-V5 immunoprecipitation for mass spectrometry (axAMA).**

Axenic amastigotes from Mock or expressing LmCK1.2-V5 were used to purify LmCK1.2-V5 and associated proteins. SDS-PAGE and SYPRO Ruby staining of the elution 3 of LmCK1.2-V5 immunoprecipitation in biological triplicates.

## 4. Adaptation of the CRISPR-Cas9 toolkit to *Leishmania donovani* and characterisation of LmCK1.1

At first, one of the important goal of my PhD project was to generate a null mutant for LmCK1.2 in *Leishmania donovani*. The idea was to determine whether LmCK1.2 was essential for parasite survival and also required for macrophage infection. Indeed, previous studies in the laboratory had demonstrated the essentiality of LmCK1.2 in intracellular amastigote survival particularly (Rachidi et al., 2014). Treatment with CK1 specific inhibitor D4476 blocked promastigote growth and strongly affected axenic amastigote viability, and decreases the percentage of infected macrophages (Rachidi et al., 2014). When I started, the generation of null mutants in *L. donovani* was not an easy task, it was time consuming as it needed multiple steps of cloning, multiple round of transfection to integrate the two resistance cassettes into the locus and the selection could take months. Moreover, *L. donovani* has the ability to adapt to stressful conditions by copy number variation leading to gene amplification, deletion or aneuploidy (Bussotti et al., 2018; Dumetz et al., 2017; Rogers et al., 2011), so during the selection of the heteozygote, parasites can adapt and compensate for the deletion, masking the phenotype. As a result, studies involving *in locus* gene taggings or knockouts were scarce in *Leishmania*. Everything changed when genome editing using CRISPR-Cas9 (clustered regularly interspaced short palindromic repeats/CRISPR-associated gene 9) was introduced to the field of trypanosomatids: *Trypanosoma cruzi* (Lander et al., 2015; Peng et al., 2015a), *L. major* (Sollelis et al., 2015), *L. donovani* (Zhang and Matlashewski, 2015), *L. mexicana* (Beneke et al., 2017), *T. brucei* (Beneke et al., 2017; Rico et al., 2018; Vasquez et al., 2018), and even the honey bee trypanosomatid *Lotmaria passim* (Liu et al., 2019).

In that context, I adapted the CRISPR-Cas9 toolkit developed in Eva Gluenz's laboratory (University of Oxford) (Beneke et al., 2017) to our *L. donovani* LdBob. For this work, Tom Beneke from the Gluenz's lab visited our lab for two weeks to transfert the technology and assist me for troobleshootings, which led to this publication. Afterwards, I trained scientists and students from other laboratories to use this technique, and our lab is taking advantage of its position in the Institut Pasteur network to diffuse the toolbox to other countries. The

CRISPR-Cas9 has revolutionised the field and allowed for the dissection of molecular processes with unprecedented efficiency (Bryant et al., 2019).

Published in 2017 in BioMed Research International, vol. 2017, Article ID 4635605, 11 pages, 2017. <https://doi.org/10.1155/2017/4635605>.

**Characterisation of Casein Kinase 1.1 in *Leishmania donovani* Using the CRISPR Cas9 Toolkit.**

Daniel Martel<sup>1,2</sup>, Tom Beneke<sup>3</sup>, Eva Gluenz<sup>3</sup>, Gerald F. Späth<sup>1</sup>, and Najma Rachidi<sup>1</sup>.

<sup>1</sup> Institut Pasteur and INSERM U1201, Unité de Parasitologie moléculaire et Signalisation, Paris, France, <sup>2</sup> Université Paris Diderot, Sorbonne Paris Cité, Paris, France, <sup>3</sup> Sir William Dunn School of Pathology, University of Oxford, Oxford, UK.

Adress for correspondence: [najma.rachidi@pasteur.fr](mailto:najma.rachidi@pasteur.fr)

## Research Article

# Characterisation of Casein Kinase 1.1 in *Leishmania donovani* Using the CRISPR Cas9 Toolkit

Daniel Martel,<sup>1</sup> Tom Beneke,<sup>2</sup> Eva Gluenz,<sup>2</sup> Gerald F. Späth,<sup>1</sup> and Najma Rachidi<sup>1</sup>

<sup>1</sup>Institut Pasteur and INSERM U1201, Unité de Parasitologie Moléculaire et Signalisation, Paris, France

<sup>2</sup>Sir William Dunn School of Pathology, University of Oxford, Oxford, UK

Correspondence should be addressed to Najma Rachidi; najma.rachidi@pasteur.fr

Received 14 July 2017; Revised 22 September 2017; Accepted 12 October 2017; Published 29 November 2017

Academic Editor: Ernesto S. Nakayasu

Copyright © 2017 Daniel Martel et al. This is an open access article distributed under the Creative Commons Attribution License, which permits unrestricted use, distribution, and reproduction in any medium, provided the original work is properly cited.

The recent adaptation of CRISPR Cas9 genome editing to *Leishmania* spp. has opened a new era in deciphering *Leishmania* biology. The method was recently improved using a PCR-based CRISPR Cas9 approach, which eliminated the need for cloning. This new approach, which allows high-throughput gene deletion, was successfully validated in *L. mexicana* and *L. major*. In this study, we validated the toolkit in *Leishmania donovani* targeting the flagellar protein PF16, confirming that the tagged protein localizes to the flagellum and that null mutants lose their motility. We then used the technique to characterise CK1.1, a member of the casein kinase 1 family, which is involved in the regulation of many cellular processes. We showed that CK1.1 is a low-abundance protein present in promastigotes and in amastigotes. We demonstrated that CK1.1 is not essential for promastigote and axenic amastigote survival or for axenic amastigote differentiation, although it may have a role during stationary phase. Altogether, our data validate the use of PCR-based CRISPR Cas9 toolkit in *L. donovani*, which will be crucial for genetic modification of hamster-derived, disease-relevant parasites.

## 1. Introduction

The protozoan parasite *Leishmania* is the causative agent of leishmaniasis, which has several clinical forms depending on the species, including cutaneous (e.g., *L. major* and *L. mexicana*), diffuse cutaneous, mucocutaneous, and fatal visceral leishmaniasis (e.g., *L. donovani*) [1, 2]. *Leishmania* goes through several extracellular developmental stages in the insect vector, from nonvirulent procyclic to virulent metacyclic promastigote forms [3], and one intracellular stage, the amastigote form, which resides inside the phagolysosome of the mammalian host macrophages. In recent years, omics systems-wide analyses, particularly RNA-Seq, have been applied for many purposes such as the determination of disease phenotype, the mode of action of drugs, or the identification of drug-resistance markers [4, 5]. These technologies have also dramatically improved our knowledge of *Leishmania* biology [4]. However, knowing the genes that are differentially regulated under different conditions is only the prelude to understand their role. This is particularly important for *Leishmania* as more than 50%

of the genes encode hypothetical proteins [6]. One major bottleneck for their characterisation is the absence of a *Leishmania*-specific genetic toolbox that could overcome different parasite-specific limitations such as the absence of RNA-interference machinery in the subgenus *Leishmania*, a stark contrast to *Trypanosoma brucei*, where this technique greatly contributed to a better understanding of the biology of this parasite over the past decade [7, 8].

Although possible, genetic engineering has been particularly challenging and time-consuming in *Leishmania* parasites [9]. *In locus* tagging of a gene of interest (GOI) requires multiple steps of cloning to assemble a cassette that could be integrated at the 5' or the 3' end of the gene [10]. Furthermore, the traditional gene targeting method involving homologous recombination requires the generation of a cassette containing an antibiotic selection marker gene flanked by 300 to 900 bp of both the 5' and 3' UTR of the GOI to direct integration into the genome [10, 11]. This strategy has many drawbacks [12]: (i) for a diploid asexual organism such as *Leishmania*, at least two rounds of transfection are required [13], and (ii) heterozygous transfectants need to be selected before

the second round can be performed. The generation of a knockout strain is thus time-consuming and can favor misintegration of the targeting cassette elsewhere in the genome or parasite compensatory adaptations if the deleted gene is important for survival. This is particularly true for *L. donovani*, as several studies have shown its ability to adapt to stressful conditions by copy number variations leading to gene amplification, gene deletion, or aneuploidy [14, 15]. This genome instability further complicates genetic engineering, as the presence of additional chromosomes requires additional rounds of transfection to obtain a complete deletion of the GOI. A simpler and more efficient method is therefore required to decipher *L. donovani* biology.

The clustered regularly interspaced short palindromic repeats (CRISPR)/CRISPR-associated protein 9 (Cas9) has been used, since 2013, as a genome editing tool for a large number of organisms including yeast and mammalian cells, and has subsequently been adapted for several unicellular human pathogens such as *Plasmodium falciparum* and *Trypanosoma cruzi* [16]. The recent adaptation of CRISPR Cas9 for *Leishmania* spp. has opened a new era for *Leishmania* genetic manipulation [17–19]. However these early methods required the cloning of at least the single guide RNA (sgRNA) in an expression vector, which increases the time necessary to generate a knockout and prevent the use of these methods to perform high-throughput gene tagging or deletions. In a recent paper, Beneke et al. described the development of a new PCR-based CRISPR Cas9 toolkit allowing rapid and precise gene modification, which was successfully applied to *L. mexicana*, *L. major*, and *Trypanosoma brucei* [20]. Parasites stably expressing hSpCas9 and T7 RNA polymerase were transfected with PCR fragments corresponding to the sgRNA and the donor DNA cassettes to generate knockout or tagged parasites in only one week. This method is perfectly suited to generate knockout parasites in a high-throughput fashion, as no cloning is required [20]. The toolkit includes simple protocols for gene deletions, or N- and C-terminal tagging as well as a website to design overlapping oligonucleotides for the PCRs (<http://leishgedit.net/>, [20]).

Casein Kinase 1 isoform 1 (CK1.1, LdBPK\_351020.1) is a member of the CK1 family, which are signalling serine/threonine protein kinases involved in the regulation of various cellular processes such as the cell cycle or protein trafficking [21]. They contain a highly conserved kinase domain and a specific C-terminal domain that plays a key role in their regulation and their localization [21, 22]. In *Leishmania*, there are six isoforms, of which only two have been studied: LdCK1.4 (LdBPK\_2716800.1) and LdCK1.2 (LdBPK\_351030.1). LdCK1.4 is secreted by the promastigotes and may play an important role in virulence and parasite survival [23]. LdCK1.2 (LdBPK\_351030.1) is an ecto-/exokinase released in the host cell via exosomes [24]. We showed that this kinase is essential for parasite survival in mammalian cells [25] and represents a validated drug target [26]. In contrast, LdCK1.1 has not yet been studied. Data available from transcriptomic analyses suggest that CK1.1 is upregulated in metacyclic promastigotes and in intracellular amastigotes [27, 28], whereas proteomic data indicates that it is a very

low-abundance protein and, contrary to LdCK1.2, has not been detected in exosomes [24, 29].

In this study, we first generated a *Leishmania donovani* Bob cell line expressing Cas9 and T7 RNA polymerase. In order to validate the CRISPR Cas9 toolkit in *Leishmania donovani*, we targeted PF16 gene, which encodes a central pair protein of the axoneme, essential for parasite motility. We successfully deleted the PF16 gene, which resulted in loss of motility, and we obtained the expected flagellar localization of PF16, by C-terminal tagging. We then applied the CRISPR Cas9 toolkit for a first functional genetic analysis of CK1.1. We showed that tagged CK1.1 protein was detected in both life stages but at a very low level. We demonstrated that CK1.1 was not essential for parasite survival as the null mutant parasites could survive as promastigotes and axenic amastigotes but may have a function in stationary phase.

## 2. Material and Methods

**2.1. *Leishmania donovani* Culture and Axenic Amastigote Differentiation.** Axenic *L. donovani* strain 1S2D (MHOM/SD/62/1S-CL2D) clone LdBob was obtained from Steve Beverley, Washington University School of Medicine, St. Louis, MO, and cultured as described previously [30–32]. Briefly,  $10^5$  logarithmic promastigotes per mL were incubated at 26°C in M199 media (Gibco) supplemented with 10% heat-inactivated FCS, 20 mM HEPES, pH 6.9, 4.1 mM NaHCO<sub>3</sub>, 2 mM glutamine, 8 μM 6-biopterin, 10 μg/mL folic acid, 100 μM adenine, 30 μM hemin, 1x RPMI 1640 vitamins solutions (Sigma), 100 U/mL of Penicillin/Streptomycin (Pen/Step), and adjusted at pH 7.4. Axenic amastigotes were obtained by incubating  $10^6$  logarithmic promastigotes per mL at 37°C and 5% CO<sub>2</sub> in RPMI 1640 + GlutaMAX™-I medium (Gibco) supplemented with 20% of heat-inactivated FCS, 28 mM MES, 2 mM glutamine, 1x RPMI 1640 amino acid mix (Sigma), 1x RPMI 1640 vitamins solutions (Sigma), 10 μg/mL folic acid, 2 mM glutamine, 100 μM adenine, 100 U/mL of Pen/Step, and adjusted at pH 5.5. Relevant selective drugs were added to the medium at the following concentrations: 30 μg/mL hygromycin B (Invitrogen), 30 μg/mL puromycin dihydrochloride (Sigma), and 20 μg/mL blastidicin S hydrochloride (Invitrogen). When appropriate, axenic amastigotes cell aggregates were dispersed by passing cell suspensions five times through a 27-gauge needle before analysis.

**2.2. Analysis of the Percentage of Cell Death, Parasite Concentration, and mNeonGreen Fluorescence Intensity.** Cultured parasites were diluted in DPBS (Gibco) and incubated with 2 μg/mL propidium iodide (Sigma-Aldrich). Cells were analysed with a CytoFLEX flow cytometer (Beckman Coulter, Inc.) to determine the incorporation of propidium iodide (exλ = 488 nm; emλ = 617 nm) and to monitor mNG levels in PF16::mNG::3xMyc (PF16-mNG-myc) or CK1.1::mNG::3xMyc (CK1.1-mNG-myc) transgenic parasites (exλ = 506 nm; emλ = 517 nm). The percentage of cell death, cell growth, and the mean mNeonGreen (mNG) fluorescence intensity were calculated using CytExpert (v2.0.0.153)

software (Beckman Coulter, Inc.). Graphs were generated with GraphPad Prism (v7.03).

**2.3. Parasite Transfection.** Parasite transfections were performed as described previously [20].  $1 \times 10^7$  LdBob cells in logarithmic phase were transfected with 15  $\mu\text{g}$  of pTB007, with or without PCR reactions (mock) in 1x Tb-BSF buffer (90 mM sodium phosphate, 5 mM potassium chloride, 0.15 mM calcium chloride, 50 mM HEPES, pH 7.3) [33] using 2 mm gap cuvettes (MBP) with program X-001 of the Amaxa Nucleofector IIb (Lonza Cologne AG, Germany). Transfected cells were immediately transferred into 5 mL prewarmed medium in 25 cm<sup>2</sup> flasks and left to recover overnight at 26°C before adding or not the appropriate selection drugs. Survival of drug-resistant transfectants became apparent 7–10 days after transfection.

**2.4. PCR-Amplification of the Targeting Fragments and the sgRNA Templates.** PCR reactions were performed as described previously [20]. Briefly, for the PCR-amplification of the targeting fragments of pPLOT and pT cassettes, 30 ng circular pPLOT or pT plasmid, 0.2 mM dNTPs, 2  $\mu\text{M}$  each of gene-specific forward and reverse primers, and 1 unit HiFi polymerase (Roche) were mixed in 1x HiFi reaction buffer (Roche), supplemented with 1.875 mM MgCl<sub>2</sub> to reach a final concentration of 3.375 mM and 3% (v/v) DMSO. The PCR conditions were as follows: 5 min at 94°C then 40 cycles of 30 s at 94°C, 30 s at 65°C, and 2 min 15 s at 72°C, and lastly a final elongation step of 7 min at 72°C. The presence of the expected product was assessed by running 2  $\mu\text{L}$  of the 40  $\mu\text{L}$  reaction on a 1% agarose gel. The sample was then heat-sterilized at 94°C for 5 min and used for transfection without further purification. Primer sequences are detailed in Table S1 in Supplementary Materials.

In order to amplify the sgRNA templates, 0.2 mM dNTPs, 2  $\mu\text{M}$  each of primer G00 (sgRNA scaffold), 2  $\mu\text{M}$  of gene-specific forward primer, and 1 unit HiFi polymerase (Roche) were mixed in 1x HiFi reaction buffer with MgCl<sub>2</sub> (Roche). The PCR conditions were 30 s at 98°C followed by 35 cycles of 10 s at 98°C, 30 s at 60°C, and 15 s at 72°C and a final elongation step of 7 min at 72°C. To assess the presence of the expected product, 2  $\mu\text{L}$  of the 20  $\mu\text{L}$  reaction was run on a 1% agarose gel. The sample was heat-sterilized at 94°C for 5 min and transfected without further purification. Primer sequences are detailed in Supplementary Materials in Table S1.

**2.5. Diagnostic PCR.** To assess the loss of the target gene in the knockout cell lines, genomic DNA was isolated from parasites collected after 1 passage post-transfection with the DNeasy Blood & Tissue Kit (Qiagen). One hundred nanograms of genomic DNA was mixed with 0.3 mM dNTPs, 0.5  $\mu\text{M}$  forward primer and reverse primer, 3% (v/v) DMSO, 2.5 units LongAmp Taq DNA polymerase (NEB), and 1x LongAmp Taq Reaction Buffer supplemented with Mg<sup>2+</sup> (2 mM final, NEB). The PCR conditions were 5 min at 94°C followed by 35 cycles of 30 s at 94°C, 30 s at 60°C, 2 min 30 s at 65°C, and a final elongation step of 10 min at 72°C.

Three microliters of reaction was then run on a 1% agarose gel to assess for the presence of the expected product. Primer sequences are detailed in Supplementary Materials in Table S2.

**2.6. Protein Extraction, SDS-PAGE, and Western Blot Analysis.** Between  $5 \times 10^7$  and  $2 \times 10^8$  logarithmic phase parasites (depending on the experiment) were resuspended in RIPA lysis buffer containing 150 mM NaCl, 1% Triton X-100, 20 mM Tris HCl, pH 7.4, 1% Nonidet P-40, 1 mM EDTA, and inhibitor cocktails for proteases (Roche Applied Science, IN) and supplemented with 1 mM sodium orthovanadate and 1 mM PMSF. The cells were sonicated using the Bioruptor® (Diagenode) with the high power mode for 5 min (sonication cycle: 10 sec ON, 20 sec OFF) followed by 5 more minutes (sonication cycle: 30 sec ON, 30 sec OFF) and then centrifuged. Total protein quantity was assessed by the Pierce Coomassie Plus (Bradford) Assay. Twenty micrograms of total proteins was denatured, separated by SDS-PAGE, and transferred onto polyvinylidene difluoride (PVDF) membranes (Pierce). Depending on the experiment, proteins were revealed as described in Supplementary Materials in Table S3, using the following primary antibodies at the indicated dilutions: (i) anti-CK1.2 antibody (1/500, [25]), (ii) anti-myc antibody (1/1000, Bioss R-1319-100), anti-Flag M2 antibody (1/1000, Sigma F3165); and secondary antibodies: anti-rabbit antibody (1/20000, Thermo Scientific 31462) and anti-mouse antibody (1/20000, Thermo Scientific 32230). Proteins were revealed by SuperSignal™ West Pico Chemiluminescent Substrate (Thermo Scientific) using the PXi image analysis system (Syngene) at various exposure times.

**2.7. Fluorescence Microscopy.** *L. donovani* promastigotes expressing the fluorescent fusion protein PF16-mNG-myc were imaged by live microscopy. Samples were prepared as previously described [34]. Briefly, parasites were harvested from logarithmic phase culture by centrifugation at 800g for 5 min and washed three times in PBS with Hoechst 33342 at 5  $\mu\text{g}/\text{mL}$ . The cells were resuspended in 50  $\mu\text{L}$  PBS, and 2  $\mu\text{L}$  was placed on a microscope slide, then a coverslip was applied, and the cells were immediately imaged with a 60x NA 1.42 plan-apochromat oil immersion objective lens (Olympus AMEP4694) on a EVOS FL microscope (Thermo Fischer Scientific, AMF4300) with a ICX445 monochrome charge-coupled device (CCD) camera (Sony) at room temperature.

**2.8. Parasite Tracking.** *Leishmania* promastigotes from early stationary phase were filmed for 10 s (200 frames) with a Leica DMI 4000B microscope, using a 40x objective and an Evolv EMCCD camera, with Metaview software. Tracking was performed using the Spot Detector and Spot Tracking tools from Icy software [2], with defaults settings and the following modifications: Spot Detector: Scale 3, Sensitivity 80 (~7 pix); size filtering: min = 10 – max = 300.

**2.9. Bioinformatics.** Multiple sequence alignments (MSA) were computed using the PSI-Coffee mode of T-Coffee [35]. The resulting alignments were visualized using Clustalw (1.83).

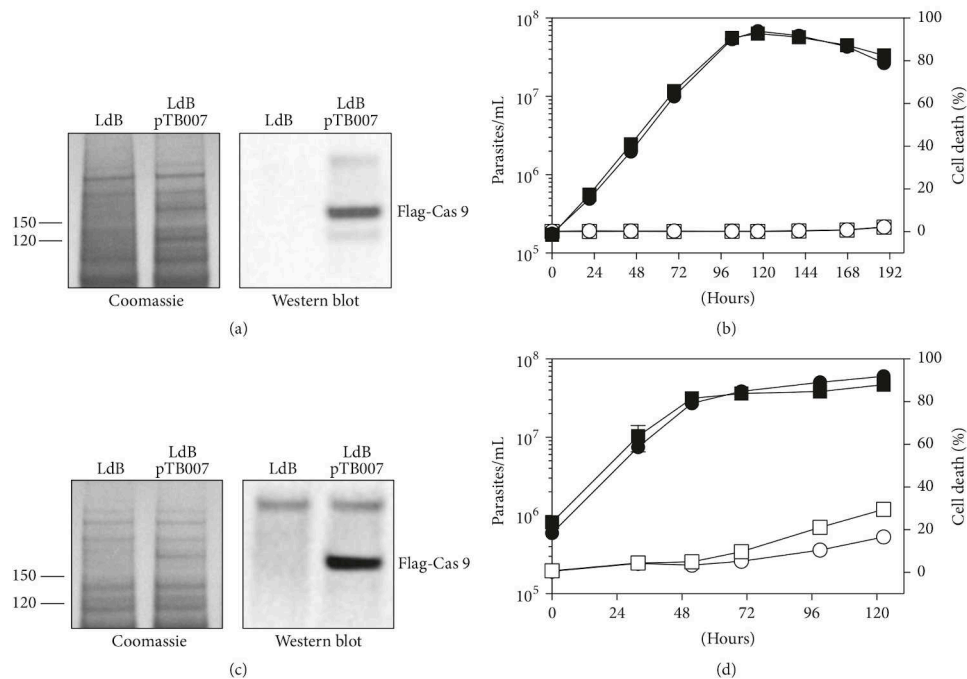


FIGURE 1: Constitutive expression of Cas9 in *L. donovani* Bob strain. (a) Proteins were extracted from LdB (LdB) or LdB expressing Cas9-FLAG (LdB pTB007, 162 kDa) promastigote in logarithmic phase. Twenty micrograms was analysed by Western blotting using the anti-FLAG M2 antibody (right panel). The Coomassie-stained membrane of the blot is included as a loading control (left panel). Protein weight in kDa is indicated on the left. (b) Logarithmic phase promastigotes were seeded at  $1 \times 10^5$  promastigotes/mL and cultured for 8 days. Samples were collected every 24 h to assess cell number (black symbol) and percentage of cell death (white symbol) by flow cytometry in triplicate in two independent experiments. Cell lines: LdB (square) and LdB pTB007 (circle). (c) Proteins were extracted from LdB or LdB expressing Cas9-FLAG (LdB pTB007, 162 kDa) axenic amastigotes (48 h after temperature and pH shift) and processed as described in (a). (d) Logarithmic phase promastigotes were seeded at  $1 \times 10^6$  promastigotes/mL, shifted to 37°C and pH 5.5 and cultured for 5 days. Samples were collected and treated as described in (c).

### 3. Results and Discussion

**3.1. Expression of Cas9 and T7 RNA Polymerase Does Not Affect Parasite Growth and Differentiation.** We first transfected LdB promastigotes with the plasmid pTB007 (LdB pTB007) expressing (i) the humanized *Streptococcus pyogenes* Cas9 nuclease gene (*hSpCas9*) [36] with a nuclear localization signal and three copies of the FLAG epitope at the N-terminus, (ii) T7 RNA polymerase (T7 RNAP) and (iii), a hygromycin resistance gene [20]. We confirmed the expression of Cas9 by Western blot analysis (Figure 1(a)) and showed that this expression did not alter the growth of *L. donovani* promastigotes (Figure 1(b)), similar to what has been shown with *L. mexicana* promastigotes [20]. We found that Cas9 is also expressed in axenic amastigotes (Figure 1(c)). The presence of pTB007 did not interfere with axenic amastigote differentiation or proliferation (Figure 1(d)) but surprisingly has a slight positive effect on cell survival in late stationary phase.

**3.2. Validation of the CRISPR Cas9 Gene Editing Toolkit in *L. donovani*.** To assess the efficiency of the CRISPR Cas9 gene editing toolkit in *L. donovani*, we performed C-terminal tagging and the generation of null mutants on the well-studied *PF16* gene (LdBPK\_201450.1), which encodes a central pair protein of the flagellar axoneme. Previous experiments in *L. mexicana* showed flagellar localization of PF16, and its deletion abrogates parasite motility [20]. We sought to replicate these phenotypes in *L. donovani* using the same gene editing strategy to validate the toolkit in this parasite species.

To fuse PF16 with the mNeonGreen-3xmyc (mNG-myc) in LdB, we produced two PCR fragments: the donor DNA cassette, containing mNG-myc and the puromycin-resistance marker, as well as the sgRNA template to generate a Cas9 cleavage downstream of the *PF16* gene [20]. It is crucial to know the exact sgRNA sequence and protospacer-adjacent motif (PAM) to successfully tag or delete genes in *Leishmania* spp. using CRISPR Cas9. There are important differences between the genome of LdBPK282A1

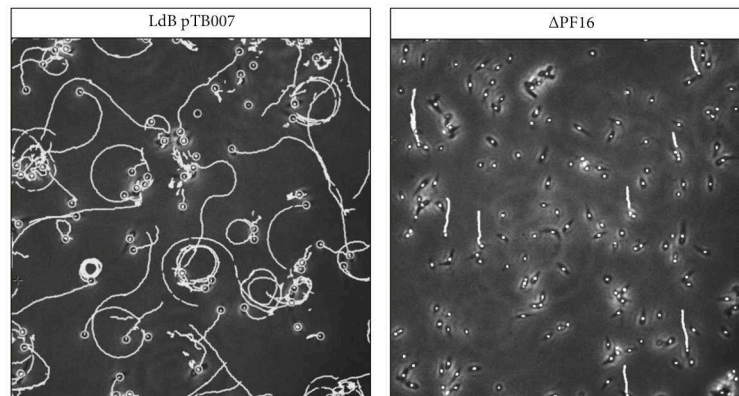


FIGURE 2: *L. donovani* *PF16* null mutants are immotile. LdB pTB007 or LdB pTB007  $\Delta$ *PF16* promastigotes in logarithmic phase were filmed for 10 s (200 frames). The tracking of individual parasites was performed using the Spot Detector and Spot Tracking tools from Icy software. Images were taken with a Leica DMI 4000B microscope, using a 40x objective and an Evolv EMCCD camera, with Metaview software.

reference strains from South-Eastern Nepal [37] and that of LdBob, a strain derived from the Sudanese isolate LdIS2D (MHOM/SD/62/IS-CL2D [38]). Thus, we used an unpublished LdIS2D reference genome (PRJNA396645, <https://www.ncbi.nlm.nih.gov/bioproject/396645>) to design the primers required to generate the donor DNA and the corresponding sgRNAs. Sequences were identified using the EuPaGDT CRISPR gRNA Design Tool [39] with similar target parameters as those used in the LeishGEdit strategy [20]. LdB pTB007 promastigotes were then transfected with the two PCR fragments. The transgenic parasites were selected using puromycin; the correct integration of the tagging cassette was confirmed by the detection of the tagged protein using microscopy and Western blot analysis with an anti-myc antibody (Figures S1A and B). The localization of the tagged protein was consistent with the known localization of *PF16* [20]. Fluorescence intensity measurements showed that its abundance is constant during promastigote growth and that the expression of the mNG-myc reporter fused to the C-terminus of *PF16* does not lead to any growth defects (Figure S1C). These data indicate that the tagging of *PF16* using CRISPR Cas9 was successful in *L. donovani*. This approach is simple and fast and will greatly improve the way we study *Leishmania* genes compared to previous methods of gene tagging (e.g., by expressing GOI fused to a fluorescent tag from an episome), since part of their endogenous regulation may be better maintained through the conservation of either the 5' or 3' UTR (depending whether the tagging is at the C- or N-terminus, resp.).

Next, we targeted the *PF16* locus to generate null mutants in a single round of transfection. LdB pTB007 promastigotes were transfected with four PCR fragments corresponding to the two sgRNA templates to generate a double-strand break upstream and downstream of the *PF16* CDS, and the two repair cassettes containing the resistance marker genes for blasticidin and puromycin [20]. We confirmed the generation of a double drug-resistant cell population by PCR (Figure S2A), indicating that *PF16* has been successfully deleted in

the whole population, without the need for subcloning as observed previously with *L. mexicana* and *L. major* [20]. The  $\Delta$ *PF16* mutant grew similarly to the parental strain (data not shown), only displaying a loss of motility (Figure 2), which is consistent with published data [20, 40, 41]. Altogether, these data validate the use of the CRISPR Cas9 toolkit developed by Beneke et al. in *L. donovani* [20]. This approach will overcome the two main limitations for the genetic manipulation of *L. donovani*. First, because *L. donovani* adapts very fast to its environment by copy number variations [15], the ability to generate homozygote knockouts in one single transfection will minimise the introduction of compensatory mutations, which could mask the phenotype of the knockouts. This is therefore a major improvement compared to previous methods for gene deletion [42]. Second, *L. donovani* strain LdIS2D, purified from the spleen or the liver of infected hamsters, is particularly sensitive to *in vitro* culture, as this strain loses virulence after only 5 to 10 passages in culture to become unable to infect hamsters ([38] and our unpublished data). Thus, minimising time in culture is a prerequisite for virulence studies; hence this CRISPR Cas9 method will enhance our ability to conduct such studies in *L. donovani*, one of the causative agents of the only lethal form of leishmaniasis.

**3.3. *Leishmania* CK1.1 Member of the Casein Kinase Family Is More Closely Related to CK1.2 Than to Other CK1s.** LdCK1.1 (LdBPK\_351020.1) is 324 amino acids long and has a predicted molecular weight of 37.2 kDa. It contains a kinase domain, a N-terminal domain longer than that of CK1 of other eukaryotes including LdCK1.2, but similar to that of TbCK1.1, and a C-terminal domain shorter than that of the human CK1 ( $\alpha$ ,  $\delta$ , and  $\epsilon$ ), LdCK1.2, or TbCK1.2, but similar to that of TbCK1.1 (Figure 3(a)). LdCK1.1 is closely related to LdCK1.2, with 67% identity in protein sequence [25]. As the two encoding genes are adjacent on chromosome 35, they probably originated from the same gene that duplicated and then evolved differently [25]. The most striking difference



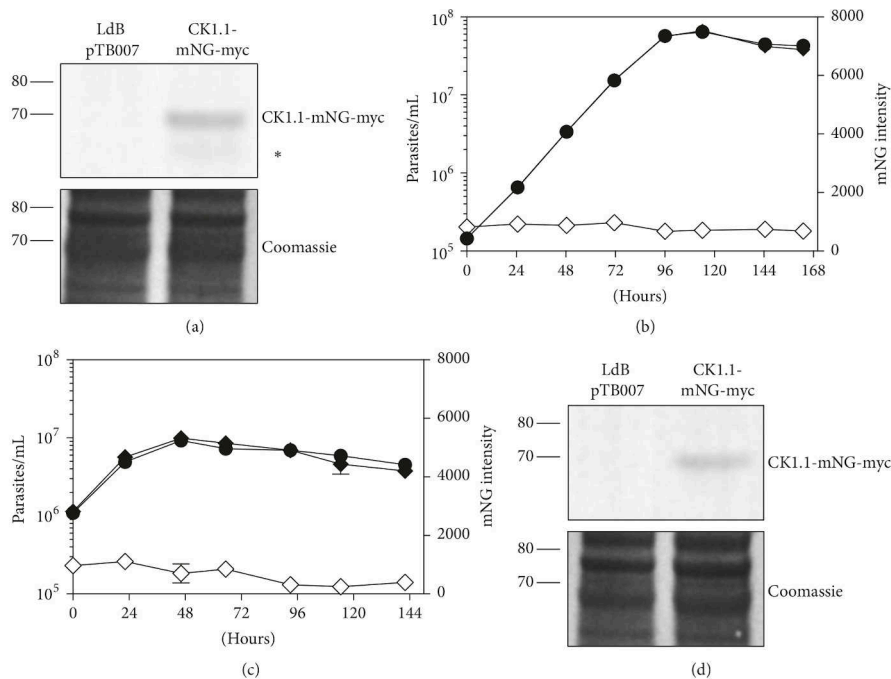


FIGURE 4: Successful in locus tagging of *L. donovani* CK1.1 with mNG-myc tag. (a) Proteins were extracted from LdB pTB007 or LdB CK1.1-mNG-myc promastigotes in logarithmic phase and twenty micrograms was analysed by Western blotting using an anti-Myc tag antibody (Top panel). The Coomassie-stained membrane of the blot is included as a loading control (bottom panel). Protein weight in kDa is indicated on the left. The expected size of the fusion protein is 69,8 kDa. The lower band indicated with an asterisk (\*) may be a result of protein degradation. (b) Promastigotes were seeded at  $1 \times 10^5$  promastigotes/mL and cultured for 7 days, and aliquots were taken every 24 h for analysis. Cell number (black symbol) and mNeonGreen fluorescence intensity (white symbol) were assessed by flow cytometry in triplicate in two independent experiments. Fluorescence intensity of the LdB pTB007 strain was used for normalization. Cell lines: LdB pTB007 (circle) and LdB pTB007 CK1.1-mNG-myc (diamond). (c) Similar to (b), except that promastigotes were seeded at  $1 \times 10^6$  promastigotes/mL, shifted to  $37^\circ\text{C}$  and pH5.5 and cultured for 6 days. (d) Similar to (a), except that proteins were extracted from LdB pTB007 or LdB CK1.1-mNG-myc axenic amastigotes (48 h after temperature and pH shift).

is the lack of 33 amino acids in the C-terminal domain of LdCK1.1 compared to that of LdCK1.2 (Figure 3(b)). Since the C-terminal domain is particularly important for the localization and the regulation of CK1 family members, these data suggest that CK1.1 and CK1.2 could have different localization and function [22]. LdCK1.1 has an orthologue in *T. brucei* TbCK1.1 (Tb9275.790, 60% identity) and in *T. cruzi* TcCK1.1 (TcCLB.508541.220, 63% identity), which are also adjacent to TbCK1.2 and TcCK1.2, respectively. The two isoforms present in *T. cruzi* have a distinct feature compared to the orthologues in other trypanosomatids; TcCK1.2 is encoded by an array of five copies, while TcCK1.1 is encoded by a single copy (CL Brener-Esmeraldo-like strain [43]). Finally, LdCK1.1 shows 57% identity with the human CK1  $\delta$ , compared to 67% for LdCK1.2. Previously we showed that *Leishmania* CK1.2 is the most conserved kinase in *Leishmania*, and the kinase with the most similarity to its human orthologues [25], leading to the hypothesis that CK1.2 could have a function outside of the parasite by mimicking the host CK1. These characteristics are

not shared by CK1.1, suggesting that it could be essentially intracellular; this hypothesis is supported by proteomics data showing that CK1.1 is not detected in *Leishmania* exosomes [24].

3.4. *Leishmania donovani* CK1.1 Is a Nonessential Kinase Which May Play a Role in Stationary Phase. Next, we applied the CRISPR Cas9 toolkit to gain insight into CK1.1 function in the parasite. We tagged the protein to determine its localization and we deleted it to determine whether this kinase is essential for promastigote or amastigote survival.

To generate transgenic parasites expressing CK1.1-mNG-myc from the endogenous locus, we cotransfected LdB pTB007 promastigotes with a sgRNA cassette targeting the 3' end of *CK1.1* and a repair cassette containing the puromycin-resistance marker and the mNG-myc tag in frame. We then performed a Western blot analysis to determine whether CK1.1-mNG-myc was expressed in the transfected promastigotes and revealed a band at about 70 kDa corresponding to the expected size of the tagged protein (Figure 4(a)). Using FACS

analysis to measure cell density, we showed that the parasites expressing CK1.1-mNG-myc displayed no change in growth phenotype at the promastigote stage (Figure 4(b)). CK1.1 shows comparable expression in logarithmic and stationary phase (Figure 4(b)), although at a lower level than PF16-mNG-myc, as judged by Western blot and FACS analysis (Figures S1B and S1C). Promastigotes expressing CK1.1-mNG-myc could differentiate into axenic amastigotes that proliferated at a rate similar to the control cells (Figure 4(c)). CK1.1-mNG-myc is also detected in amastigotes, as shown Figure 4(d), with slightly higher levels in logarithmic phase than in stationary phase (Figure 4(c)). Altogether, these data suggest that CK1.1 is a low-abundance protein, explaining why we could barely detect the protein above background, using a fluorescence microscope (data not shown). This finding is consistent with proteomic data showing that CK1.1 in *L. donovani* or in *L. major* [30] could only be detected with 1 peptide [29] and in *T. brucei* where TbCK1.1 was not detected contrary to TbCK1.2 [44, 45].

To determine whether CK1.1 is essential for parasite survival, we generated a CK1.1 null mutant in *L. donovani*. We performed a cotransfection of LdB pTB007 promastigotes with two sgRNA cassettes targeting the 5' and the 3' end of *CK1.1* and two repair cassettes containing, respectively, the puromycin and the blasticidin-resistance genes. We obtained parasites that were resistant to both drugs and confirmed the correct integration of the puromycin and blasticidin-resistance genes at *CK1.1* locus and the complete loss of *CK1.1* by PCR as shown in Figure 5(a). Similarly to *PF16*, *CK1.1* was deleted in the whole population in one single transfection, confirming once again the remarkable efficiency of this method. The generation of homozygous  $\Delta$ CK1.1 parasites indicates that LdCK1.1 is not essential for promastigote survival. We did not observe any growth defect except in stationary phase, where the cell density of the  $\Delta$ CK1.1 was lower than that of the control parasites (Figure 5(b)). Although the percentage of cell death, as measured by propidium iodide (PI) incorporation, was slightly higher in  $\Delta$ CK1.1 parasites (4%) than in control parasites (2%), it remained below 5% which thus could not entirely explain the decrease in cell density. However, when cells contain fragmented DNA or when they lose their DNA (zooids), the percentage of PI<sup>+</sup> cells no longer corresponds to the real percentage of dead cells. We investigated this hypothesis by measuring the  $\Delta$ CK1.1 DNA content in stationary phase using FACS analysis, and found no differences in the DNA content of  $\Delta$ CK1.1 compared to that of control parasites (data not shown). We did not observe an increase in fragmented DNA or cell debris (data not shown), suggesting that the difference in cell density might not be a consequence of cell death. Interestingly, these data indicate that CK1.2 cannot compensate for the loss of CK1.1 and conversely, the absence of CK1.1 does not influence the regulation of CK1.2 abundance. Indeed, there is no difference in CK1.2 level between the mutant and the control strains in promastigotes (Figure 5(c), left panel) or in amastigotes (Figure 5(c), right panel). These results suggest the absence of a regulatory feedback loop between the two kinases, supporting the hypothesis that they might have different

functions. We did not observe any morphological differences between  $\Delta$ CK1.1 and control parasites (data not shown).

We investigated whether promastigotes could undergo axenic amastigote differentiation in the absence of CK1.1. We showed that they could differentiate and similar to what we observed in promastigotes, they could proliferate as well as control parasites (Figure 5(d)); however,  $\Delta$ CK1.1 parasites present a higher percentage of cell death in stationary phase (about 40%) than the control parasites (about 20%). This cell mortality, exclusively restricted to the amastigote stage, as we did not observe this phenomenon in promastigotes (Figure 5(b)), indicates that CK1.1 could have a role in late stationary phase. These data demonstrate that CK1.1 is not essential for amastigote survival, which is consistent with observations in *T. brucei* showing that TbCK1.1 is not essential for bloodstream form survival contrary to TbCK1.2 [46].

Overall, our data demonstrate that CK1.1 is not essential for parasite survival and axenic amastigote differentiation but could have a role in the regulation of processes linked to stationary growth phase. Conversely, we have previously shown that CK1.2 is essential for the survival of axenic and intracellular amastigotes [25], suggesting these two related kinases have evolved independently. Evolution of the two isoforms is similar in *T. brucei* where TbCK1.2 is essential for cell survival, but not TbCK1.1 [46]. Altogether, these data suggest that CK1.1 and CK1.2 have evolved similarly in the two major trypanosomatids.

#### 4. Conclusion

In this study, we validated the CRISPR Cas9 toolkit for *Leishmania donovani* targeting PF16. Gene editing and particularly PCR-based CRISPR Cas9 methods will have a major impact on our ability to study the biology of *L. donovani*. The fact that only one single transfection is required to obtain knockout mutants will (i) dramatically limit parasite adaptation, by decreasing any compensatory mutation that could mask the phenotype, and (ii) allow the use of hamster-derived parasites for genetic manipulation by preventing the nonspecific loss of virulence occurring during *in vitro* culture. The use of CRISPR Cas9 in hamster-derived *L. donovani* opens new possibilities of studying the phenotype of nonessential genes in the context of the relevant mammalian host, thus moving beyond *in vitro* studies for the medically most relevant *Leishmania* spp.

#### Conflicts of Interest

The authors declare that there are no conflicts of interest regarding the publication of this paper.

#### Acknowledgments

This work was supported by the ANR-13-ISV3-0009. Daniel Martel was supported by the French Government's Investissements d'Avenir Program, Laboratoire d'Excellence Integrative Biology of Emerging Infectious Diseases (Grant no. ANR-10-LABX-62-IBEID studentship). Eva Gluenz is a Royal Society

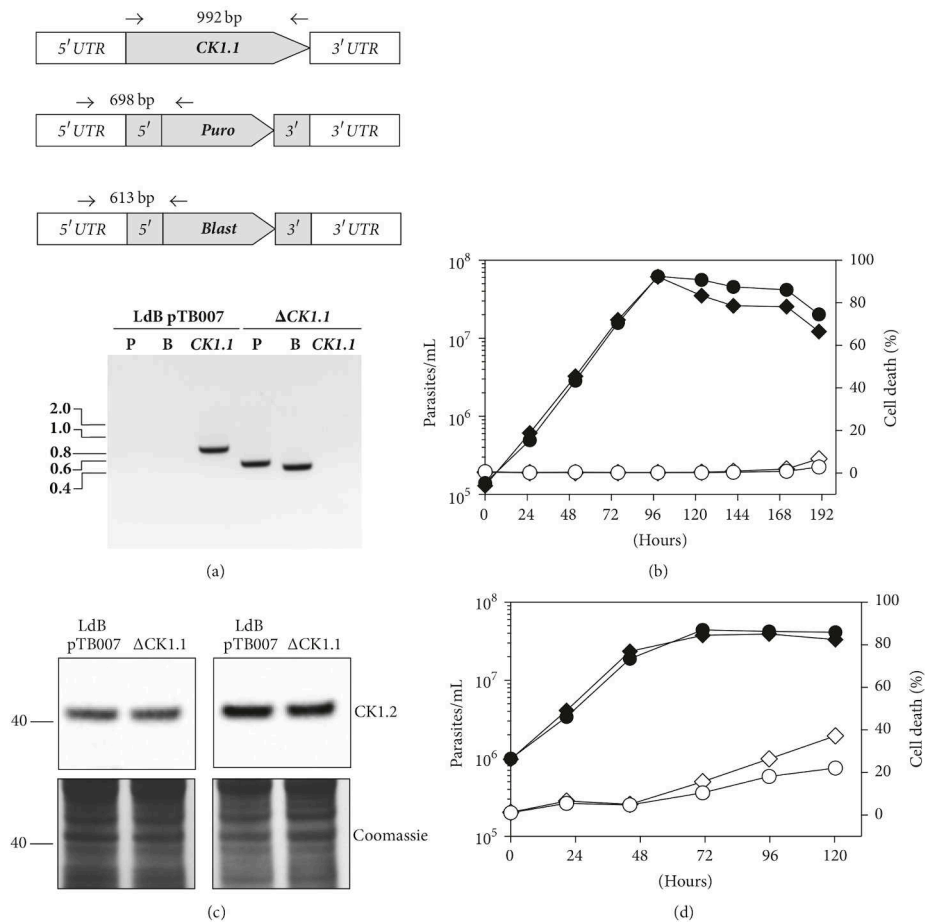


FIGURE 5: *CK1.1* is nonessential in *L. donovani*. (a) PCR analysis of the  $\Delta$ CK1.1 cell line. Diagrams showing the *CK1.1* locus and PCR primers (small arrows) used to test for the presence of the *CK1.1* CDS or the correct integration of puromycin and blasticidin drug-resistance genes (top panel). PCR products run on an agarose gel to assess the correct integration of the puromycin-resistance gene (P), blasticidin-resistance gene (B), and the presence/absence of the *CK1.1* CDS (bottom panel). Fragments sizes in kb are indicated on the left. (b) Promastigotes were seeded at  $1 \times 10^5$  promastigotes/mL and were cultured for 8 days. Aliquots were taken every 24 h to assess cell number (black symbol) and percentage of death (white symbol) by flow cytometry in triplicate from two independent experiments. Cell lines: LdB pTB007 (circle), LdB pTB007  $\Delta$ CK1.1 (diamond). (c) Proteins were extracted from LdB pTB007 or LdB pTB007  $\Delta$ CK1.1 promastigotes in logarithmic phase (right panel) and axenic amastigotes 48 h after temperature and pH shift (left panel) and twenty micrograms was analysed by Western blotting using an anti-CK1.2 antibody (Top panel). The Coomassie-stained membrane of the blot is included as a loading control (bottom panel). Protein weight in kDa is indicated on the left. (d) Similar to (b), except that promastigotes were seeded at  $1 \times 10^6$  promastigotes/mL, shifted to 37°C and pH 5.5 and cultured for 6 days.

University Research Fellow and Tom Beneke was supported by an MRC studentship (15/16\_MSD\_836338). The authors thank Thierry Blisnick and Philippe Bastin for providing access to the Leica DMI 4000B microscope, and Thierry Blisnick for his help in generating the video used for parasite tracking.

### Supplementary Materials

Figure S1. Characterisation of PF16-mNG-myc. Figure S2. Generating PF16 null mutant in *L. donovani*. Table S1. Primers used to tag and knockout PF16 and CK1.1 in *L. donovani* using pT/pPLOT plasmids. Table S2. Primers used for

the validation of PF16 and CK1.1 Knockouts. Table S3. Conditions for Western blot analysis. (*Supplementary Materials*)

## References

- [1] D. Pace, "Leishmaniasis," *Infection*, vol. 69, supplement 1, pp. S10–S18, 2014.
- [2] N. Galindo-Sevilla et al., "Low serum levels of dehydroepiandrosterone and cortisol in human diffuse cutaneous leishmaniasis by *Leishmania mexicana*," *Am J Trop Med Hyg*, vol. 76, no. 3, pp. 566–572, 2007.
- [3] S. M. Gossage, M. E. Rogers, and P. A. Bates, "Two separate growth phases during the development of *Leishmania* in sand flies: Implications for understanding the life cycle," *International Journal for Parasitology*, vol. 33, no. 10, pp. 1027–1034, 2003.
- [4] C. Cantacessi, F. Dantas-Torres, M. J. Nolan, and D. Otranto, "The past, present, and future of *Leishmania* genomics and transcriptomics," *Trends in Parasitology*, vol. 31, no. 3, pp. 100–108, 2015.
- [5] A. Mondelaers, M. P. Sanchez-Cañete, S. Hendrickx et al., "Genomic and Molecular Characterization of Miltefosine Resistance in *Leishmania infantum* Strains with Either Natural or Acquired Resistance through Experimental Selection of Intracellular Amastigotes," *PLoS ONE*, vol. 11, no. 4, p. e0154101, 2016.
- [6] N. Ravooru, S. Ganji, N. Sathyanarayanan, and H. G. Nagendra, "Insilico analysis of hypothetical proteins unveils putative metabolic pathways and essential genes in *Leishmania donovani*," *Frontiers in Genetics*, vol. 5, article 291, 2014.
- [7] S. Alsford, D. J. Turner, S. O. Obado et al., "High-throughput phenotyping using parallel sequencing of RNA interference targets in the African trypanosome," *Genome Research*, vol. 21, no. 6, pp. 915–924, 2011.
- [8] E. Rico, A. Ivens, L. Glover, D. Horn, and K. R. Matthews, "Genome-wide RNAi selection identifies a regulator of transmission stage-enriched gene families and cell-type differentiation in *Trypanosoma brucei*," *PLoS Pathogens*, vol. 13, no. 3, Article ID e1006279, 2017.
- [9] S. M. Beverley, "Protozoomics: Trypanosomatid parasite genetics comes of age," *Nature Reviews Genetics*, vol. 4, no. 1, pp. 11–19, 2003.
- [10] S. Dean, J. Sunter, R. J. Wheeler, I. Hodgkinson, E. Gluenz, and K. Gull, "A toolkit enabling efficient, scalable and reproducible gene tagging in trypanosomatids," *Open Biology*, vol. 5, no. 1, Article ID 140197, 2015.
- [11] M. Dacher, M. A. Morales, P. Pescher et al., "Probing druggability and biological function of essential proteins in *Leishmania* combining facilitated null mutant and plasmid shuffle analyses," *Molecular Microbiology*, vol. 93, no. 1, pp. 146–166, 2014.
- [12] K. A. Robinson and S. M. Beverley, "Improvements in transfection efficiency and tests of RNA interference (RNAi) approaches in the protozoan parasite *Leishmania*," *Molecular and Biochemical Parasitology*, vol. 128, no. 2, pp. 217–228, 2003.
- [13] A. Cruz, C. M. Coburn, and S. M. Beverley, "Double targeted gene replacement for creating null mutants," *Proceedings of the National Academy of Sciences of the United States of America*, vol. 88, no. 16, pp. 7170–7174, 1991.
- [14] M. B. Rogers et al., "Chromosome and gene copy number variation allow major structural change between species and strains of *Leishmania*," *Genome Res*, vol. 21, no. 12, pp. 2129–2142, 2011.
- [15] F. Dumetz, H. Imamura, M. Sanders et al., "Modulation of Aneuploidy in," *mBio*, vol. 8, no. 3, p. e00599-17, 2017.
- [16] N. Lander, M. A. Chiurillo, and R. Docampo, "Genome Editing by CRISPR/Cas9: A Game Change in the Genetic Manipulation of Protists," *Journal of Eukaryotic Microbiology*, vol. 63, no. 5, pp. 679–690, 2016.
- [17] L. Sollelis et al., "First efficient CRISPR-Cas9-mediated genome editing in *Leishmania* parasites," *Cell Microbiol*, vol. 17, no. 10, pp. 1405–1412, 2015.
- [18] W.-W. Zhang and G. Matlashewski, "CRISPR-Cas9-mediated genome editing in *Leishmania donovani*," *mBio*, vol. 6, no. 4, Article ID e00861-15, 2015.
- [19] W. Zhang, P. Lypaczewski, G. Matlashewski, and I. J. Blader, "Optimized CRISPR-Cas9 Genome Editing for *Leishmania* and Its Use To Target a Multigene Family, Induce Chromosomal Translocation, and Study DNA Break Repair Mechanisms," *mSphere*, vol. 2, no. 1, 2017.
- [20] T. Beneke et al., "A CRISPR Cas9 high-throughput genome editing toolkit for kinetoplastids," *R Soc Open Sci*, vol. 4, no. 5, Article ID 170095, 2017.
- [21] U. Knippschild, A. Gocht, S. Wolff, N. Huber, J. Löhler, and M. Stöter, "The casein kinase 1 family: Participation in multiple cellular processes in eukaryotes," *Cellular Signalling*, vol. 17, no. 6, pp. 675–689, 2005.
- [22] U. Knippschild, M. Krüger, J. Richter et al., "The CK1 family: Contribution to cellular stress response and its role in carcinogenesis," *Frontiers in Oncology*, vol. 4, article no. 96, 2014.
- [23] M. Dan-Goor, A. Nasereddin, H. Jaber, and C. L. Jaffe, "Identification of a secreted casein kinase 1 in *Leishmania donovani*: Effect of protein over expression on parasite growth and virulence," *PLoS ONE*, vol. 8, no. 11, Article ID e79287, 2013.
- [24] J. M. Silverman, J. Clos, C. C. DeOliveira et al., "An exosome-based secretion pathway is responsible for protein export from *Leishmania* and communication with macrophages," *Journal of Cell Science*, vol. 123, no. 6, pp. 842–852, 2010.
- [25] N. Rachidi, J. F. Taly, E. Durieu et al., "Pharmacological assessment defines *Leishmania donovani* casein kinase 1 as a drug target and reveals important functions in parasite viability and intracellular infection," *Antimicrobial Agents and Chemotherapy*, vol. 58, no. 3, pp. 1501–1515, 2014.
- [26] E. Durieu, E. Prina, O. Leclercq et al., "From drug screening to target deconvolution: a target-based drug discovery pipeline using *Leishmania* casein kinase 1 isoform 2 to identify compounds with antileishmanial activity," *Antimicrobial Agents and Chemotherapy*, vol. 60, no. 5, pp. 2822–2833, 2016.
- [27] L. A. Dillon, K. Okrah, V. K. Hughitt et al., "Transcriptomic profiling of gene expression and RNA processing during *Leishmania major* differentiation," *Nucleic Acids Research*, vol. 43, no. 14, pp. 6799–6813, 2015.
- [28] M. Fiebig, S. Kelly, E. Gluenz, and P. J. Myler, "Comparative life cycle transcriptomics revises *Leishmania mexicana* genome annotation and links a chromosome duplication with parasitism of vertebrates," *PLoS Pathogens*, vol. 11, no. 10, Article ID e1005186, 2015.
- [29] H. Pawar, S. Renuse, S. N. Khobragade et al., "Neglected tropical diseases and omics science: Proteogenomics analysis of the promastigote stage of *leishmania major* parasite," *OMICS: A Journal of Integrative Biology*, vol. 18, no. 8, pp. 499–512, 2014.
- [30] Y. Saar, A. Ransford, E. Waldman et al., "Characterization of developmentally-regulated activities in axenic amastigotes of *Leishmania donovani*," *Molecular and Biochemical Parasitology*, vol. 95, no. 1, pp. 9–20, 1998.

- [31] S. Goyard, H. Segawa, J. Gordon et al., “An in vitro system for developmental and genetic studies of *Leishmania donovani* phosphoglycans,” *Molecular and Biochemical Parasitology*, vol. 130, no. 1, pp. 31–42, 2003.
- [32] M. A. Morales, R. Watanabe, C. Laurent et al., “Phosphoproteomic analysis of *Leishmania donovani* pro- and amastigote stages,” *Proteomics*, vol. 8, no. 2, pp. 350–363, 2008.
- [33] G. Schumann Burkard, P. Jutzi, and I. Roditi, “Genome-wide RNAi screens in bloodstream form trypanosomes identify drug transporters,” *Molecular and Biochemical Parasitology*, vol. 175, no. 1, pp. 91–94, 2011.
- [34] R. J. Wheeler, E. Gluenz, and K. Gull, “Basal body multipotency and axonemal remodelling are two pathways to a 9+0 flagellum,” *Nature Communications*, vol. 6, article 8964, 2015.
- [35] C. Kemena and C. Notredame, “Upcoming challenges for multiple sequence alignment methods in the high-throughput era,” *Bioinformatics*, vol. 25, no. 19, pp. 2455–2465, 2009.
- [36] L. Cong, F. A. Ran, D. Cox et al., “Multiplex genome engineering using CRISPR/Cas systems,” *Science*, vol. 339, no. 6121, pp. 819–823, 2013.
- [37] T. Downing, H. Imamura, S. Decuypere et al., “Whole genome sequencing of multiple *Leishmania donovani* clinical isolates provides insights into population structure and mechanisms of drug resistance,” *Genome Research*, vol. 21, no. 12, pp. 2143–2156, 2011.
- [38] P. Pescher, T. Blisnick, P. Bastin, and G. F. Späth, “Quantitative proteome profiling informs on phenotypic traits that adapt *Leishmania donovani* for axenic and intracellular proliferation,” *Cellular Microbiology*, vol. 13, no. 7, pp. 978–991, 2011.
- [39] D. Peng and R. Tarleton, “EuPaGDT: a web tool tailored to design CRISPR guide RNAs for eukaryotic pathogens,” *Microb Genom*, vol. 1, no. 4, 2015.
- [40] C. Branche, L. Kohl, G. Toutirais, J. Buisson, J. Cosson, and P. Bastin, “Conserved and specific functions of axoneme components in trypanosome motility,” *Journal of Cell Science*, vol. 119, no. 16, pp. 3443–3455, 2006.
- [41] K. S. Ralston, A. G. Lerner, D. R. Diener, and K. L. Hill, “Flagellar motility contributes to cytokinesis in *Trypanosoma brucei* and is modulated by an evolutionarily conserved dynein regulatory system,” *Eukaryotic Cell*, vol. 5, no. 4, pp. 696–711, 2006.
- [42] G. F. Späth and J. Clos, “Joining forces: first application of a rapamycin-induced dimerizable Cre system for conditional null mutant analysis in *Leishmania*,” *Molecular Microbiology*, vol. 100, no. 6, pp. 923–927, 2016.
- [43] M. Aslett et al., “TriTrypDB: a functional genomic resource for the Trypanosomatidae,” *Nucleic Acids Res*, 2010.
- [44] M. D. Urbaniak, T. Mathieson, M. Bantscheff et al., “Chemical proteomic analysis reveals the drugability of the kinome of *trypanosoma brucei*,” *ACS Chemical Biology*, vol. 7, no. 11, pp. 1858–1865, 2012.
- [45] K. Gunasekera, D. Wüthrich, S. Braga-Lagache, M. Heller, and T. Ochsenreiter, “Proteome remodelling during development from blood to insect-form *Trypanosoma brucei* quantified by SILAC and mass spectrometry,” *BMC Genomics*, vol. 13, no. 1, article no. 556, 2012.
- [46] M. D. Urbaniak, “Casein kinase 1 isoform 2 is essential for bloodstream form *Trypanosoma brucei*,” *Molecular and Biochemical Parasitology*, vol. 166, no. 2, pp. 183–185, 2009.

Figure S1

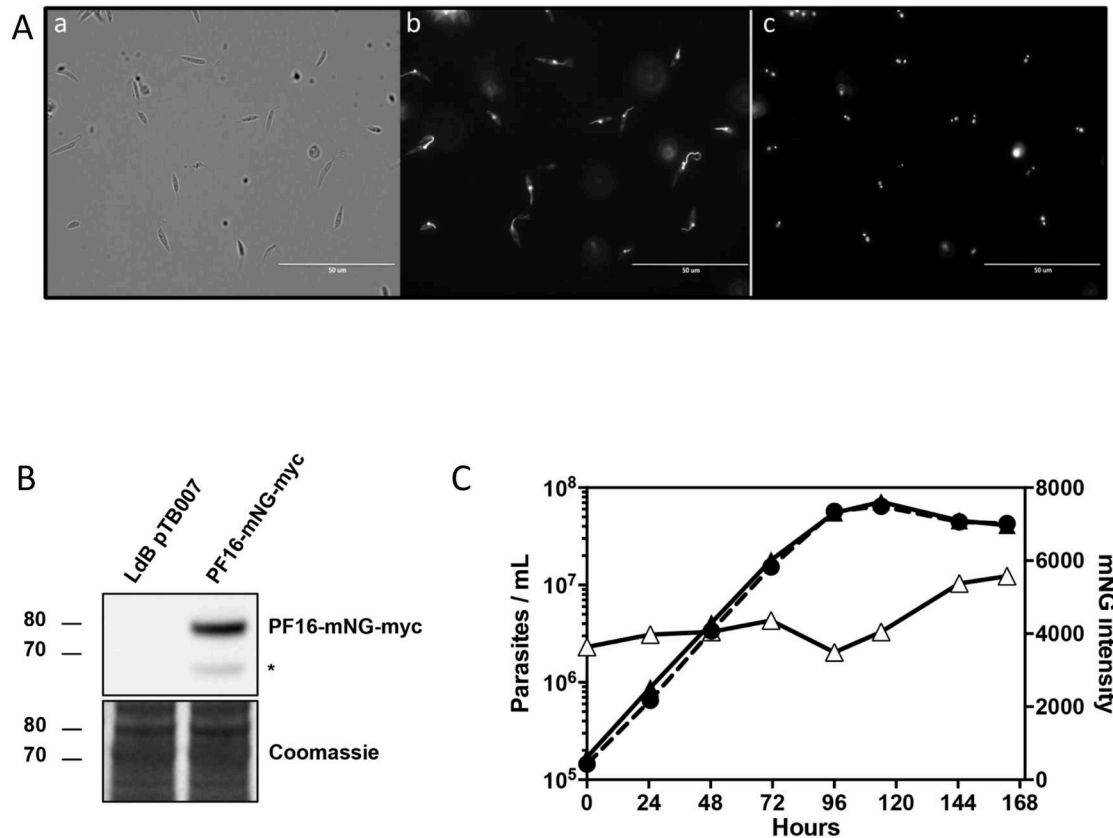


**FIGURE S1. Characterisation of PF16-mNG-myc.**

(A) Fluorescence micrographs of *LdB* pTB007 promastigotes expressing PF16-mNG-myc. 100% parasites showed a flagellar localisation in passage 1 after transfection. (a) Transmitted light, (b) mNeonGreen fluorescence, (c) Hoechst-stained DNA fluorescence. (B) Proteins were extracted from *LdB* pTB007 or *LdB* pTB007 PF16-mNG-myc promastigotes in logarithmic phase and twenty micrograms were analysed by Western blotting using an anti-Myc antibody (Top panel). The Coomassie-stained membrane of the blot is included as a loading control (Bottom panel). The lower band indicated with an asterisk (\*) may be a result of protein degradation. Protein weight in kDa is indicated on the left. (C) Promastigotes were seeded at  $1 \times 10^5$  promastigotes/ml and were cultured for 7 days. Aliquots were taken every 24h to assess cell number (black symbol) and mNeonGreen fluorescence intensity (white symbol) by flow cytometry in triplicates from two independent experiments. Cell lines: *LdB* pTB007 (circle), *LdB* pTB007 PF16-mNG-myc (triangle). The dotted line denotes data that are identical to those used in Figure 4B.

Figure S2

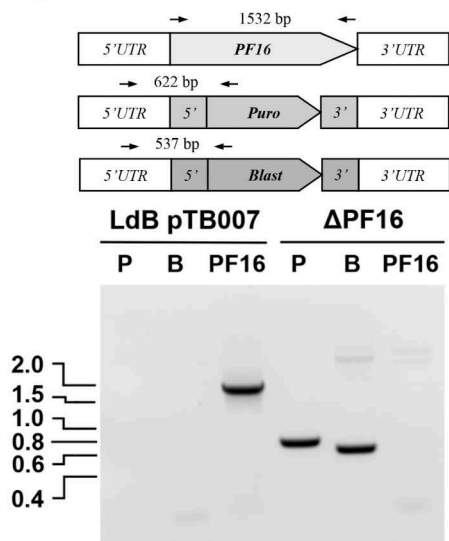


**FIGURE S2. Generating PF16 null mutant in *L. donovani***

PCR analysis of the  $\Delta$ PF16 cell line. Diagrams showing the PF16 locus and PCR primers (small arrows) used to test for the presence of the PF16 CDS or the correct integration of puromycin and blasticidin drug-resistance genes (Top panel). PCR products run on an agarose gel to assess the correct integration of the puromycin-resistance gene (P), blasticidin-resistance gene (B) and the presence/absence of the PF16 CDS (Bottom panel). Fragments sizes in kb are indicated on the left.

**Table S1: Primers used to tag and knockout PF16 and CK1.1 in *L. donovani* using pT/pPLOT plasmids**

<i>L. donovani</i> PF16 5'HF forward	5' ATCGCTGCAGAAGTGATTCTCCCCGTCCCCgtataatgcagacctgtgc 3'
<i>L. donovani</i> PF16 3'HF forward	5' AAGATCGAGAACTACCACGTGCAGCAGCACggttctgtagtggtccgg 3'
<i>L. donovani</i> PF16 3'HF reverse	5' CGAGCAGCGTGAGTTGGCGTGGCCGTGCCGccaattgagagacctgtgc 3'
<i>L. donovani</i> PF16 5'sgRNA forward	5' gaaattaatacactcactataggTGTGGGCACGGCTATTGAGTgtttagagctagaaatagc 3'
<i>L. donovani</i> PF16 3'sgRNA forward	5' gaaattaatacactcactataggGCTGATGCTCAGCCGCCATTgtttagagctagaaatagc 3'
<i>L. donovani</i> CK1.1 5'HF forward	5' CGCCTCTTTCCTGAACCCTGCCGTCAGCCAgataatgcagacctgtgc 3'
<i>L. donovani</i> CK1.1 3'HF forward	5' AATGCAGCGAAGCGCGGAAAGAAACAGAAAggttctgtagtggtccgg 3'
<i>L. donovani</i> CK1.1 3'HF reverse	5' ACTTCGCCTATTCACCTAACAAGCCTATCCAccaattgagagacctgtgc 3'
<i>L. donovani</i> CK1.1 5'sgRNA forward	5' gaaattaatacactcactataggGCTACTTCTCTTGTGTTCgtttagagctagaaatagc 3'
<i>L. donovani</i> CK1.1 3'sgRNA forward	5' gaaattaatacactcactataggTGTATGTCTGTGTTTCGTTAAgtttagagctagaaatagc

Underlined sequences indicate sgRNA target sites or homology regions in the genome

**Table S2 Primers used for the validation of PF16 and CK1.1 Knockouts**

ORF amplification	<i>L. donovani</i> PF16 ORF forward	5' <u>cttgctgtgccttgccaccaATGTCTGAATCGGGTTATTCTGC</u> 3'
	<i>L. donovani</i> PF16 ORF reverse	5' <u>tcccgggatatcatcgattccGTGCTGCTGCACGTGGTAG</u> 3'
	<i>L. donovani</i> CK1.1 ORF forward	5' <u>cttgctgtgccttgccaccaATGGAGTGAAGAGCAAG</u> 3'
	<i>L. donovani</i> CK1.1 ORF reverse	5' <u>tcccgggatatcatcgattccCTTCTGTTTCTTTCCGCG</u> 3'
Amplification of sequence across integration junction, <i>L. donovani</i> PF16	<i>L. donovani</i> PF16 5'UTR forward	5' TGACATCGCTGCAGAAGTGA 3'
	Puromycin reverse	5' TCAATGTGTCGATCTGGGTCAAC 3'
	Blasticidin reverse	5' CCGTTGCTCTTTCAATGAGGGTG 3'
Amplification of sequence across integration junction, <i>L. donovani</i> CK1.1	<i>L. donovani</i> CK1.1 5'UTR forward	5' TGCTCAACGACTCTCCGACGT 3'
	Puromycin reverse	5' TCAATGTGTCGATCTGGGTCAAC 3'
	Blasticidin reverse	5' CCGTTGCTCTTTCAATGAGGGTG 3'

**Table S3 : Conditions for Western blot analysis**

\*PBST: PBS with 0.25% Tween 20

\*\*TBST: Tris-buffered saline with 0.075% Tween 20

Western blot description	Blocking buffer	1 <sup>st</sup> antibody dilution	Washing buffer	2 <sup>nd</sup> antibody dilution
Anti-myc Tag	PBST* + 5% BSA (Sigma) 1h @RT	Anti-myc Tag (Biosensis R-1319-100) 1:1000 in PBST + 2.5% BSA (Sigma) O/N @4°C	PBST 3 x 5 min	Anti-rabbit (Thermo Scientific 31462) 1:20000 in PBST + 2,5% BSA (Sigma) 1h @RT
Anti-FLAG M2	TBST** + 5% Milk (Lactel) 1h @RT	Anti-FLAG M2 (Sigma F3165) 1:1000 in TBST + 5% Milk (Lactel) O/N @4°C	TBST + 5% Milk (Lactel) 3 x 5 min	Anti-mouse (Thermo Scientific 32230) 1:20000 in TBST + 5% Milk (Lactel) 1h @RT
Anti-CK1.2	PBST + 5% BSA (Sigma) 1h @RT	Anti-CK1.2 (SY3535) 1:500 in PBST + 2,5% BSA (Sigma) O/N @4°C	PBST 3 x 5 min	Anti-rabbit (Thermo Scientific 31462) 1:20000 in PBST + 2,5% BSA (Sigma) 1h @RT

## 5. Conclusion

As a final conclusion for this chapter, I would like to emphasize the discovery we made, by establishing the interactome of LmCK1.2 in the parasite. These results provide the first evidence on the pathways regulated by this important signalling kinase. As shown by the diversity of LmCKAPs, LmCK1.2 seems to regulate most of the pathways essential for parasite survival from cell cycle to endocytosis. I started to investigate some pathways by characterising AP2 complex and LmCKAP1, involved respectively in endocytosis and cytokinesis.

However, this work is not completely finished and many aspects need to be confirmed, experiments to be performed in triplicate to ascertain some of the conclusions I draw in the two parts of this chapter. I also need to confirm the results obtained with the different knockouts by using addbacks. I have made the constructs but because of time constraints I was unable to transfect the parasites. For the AP2 complex, we have only preliminary data supporting the implication of this complex in endocytosis. The FM4-64 data need to be confirmed in triplicate, and experiments using other dyes such as concanavaline A to perform an assay measuring the rate of endocytosis in the AP2 deleted mutants. I started the optimisation of this assay, but could not complete it due to time constraints. We are also currently tagging and knocking out the potential last member of the complex, AP17. It will be important to test the behaviour of these different mutants during macrophage infection to see whether they can survive under the harsh environmental conditions in the phagolysosomes. Olivier Leclercq has already generated the LD1S transgenic parasites and they will be tested in the near future. For the hypothetical protein LmCKAP1, several experiments need to be repeated to ascertain our conclusion. We also need to determine why the expression of LmCK1.2 in LmCKAP1 mutant is so detrimental for parasite survival in axenic amastigotes and whether it is similar in intracellular amastigotes. Because this protein binds to LmCK1.2, it is also a potential substrate. I generated a plasmid allowing the expression of LmCKAP1 in *E. coli* but could not purify the protein, probably because the buffer we were using was not adapted to such a basic protein. We will thus adapt our protocol.



# Chapter III

---



## A role for LmCK1.2 in host-pathogen interactions

*Leishmania* parasites are transmitted to mammals by the bites of phlebotomine sand flies, which inject the extracellular and flagellated metacyclic promastigotes into the dermis of the skin. Promastigotes are then phagocytosed mainly by macrophages in which they differentiate into intracellular and immotile amastigotes. Within the phagocytic cells (macrophages), *Leishmania* amastigotes reside and replicate in parasitophorous vacuoles. To establish a persistent infection in mammals, *Leishmania* parasites directly manipulate macrophages, by altering host signalling pathways and block microbicidal functions and innate inflammatory responses during infection, thus converting the microbicidal phagocytes into safe target cells (Isnard et al., 2012; Olivier et al., 2005). For example, *Leishmania* major surface protease GP63 was shown to manipulate macrophage responses in order to promote infection via direct activation of protein tyrosine phosphatases (Gomez et al., 2009). This resulted in the down regulation of the JAK and MAP kinase pathways and cleavage of signalling proteins such as NF- $\kappa$ B and AP-1 transcription factors (Contreras et al., 2010; Shio et al., 2015).

CK1 has multiple roles in the cell, and there are several evidences that suggest a role in immune response and inflammation (Knippschild et al., 2014). For instance, after RNA virus infection, RIG-I pathway stimulation was followed by CK1 $\gamma$ 1 phosphorylation of the NF- $\kappa$ B subunit p65, that targeted it for degradation (Wang et al., 2014), thus demonstrating that CK1 $\gamma$ 1 is a negative regulator of innate immunity. Due to the importance of innate immune attenuation upon *Leishmania* infection and persistence within the mammalian host, and because *Leishmania* secretes effectors that modulate macrophage response, we asked whether *Leishmania* CK1.2 could play a role in host-cell subversion.

Different lines of evidence support this hypothesis: (1) *Leishmania* parasites secrete exosomes that are enriched in virulence factors and manipulate host signalling and immune cellular functions mainly favouring an immunosuppressive status allowing the parasite to better propagate within its infected host (Atayde et al., 2015; Hassani et al., 2014; Silverman et al., 2010a, 2010b). (2) LmCK1.2 has been described as an ecto-kinase, secreted as free protein or through exosomes (Sacerdoti-Sierra and Jaffe, 1997; Silverman et al., 2008, 2010a; Vieira et al., 2002). (3) LmCK1.2 can phosphorylate host proteins, for instance its

phosphorylation of the human receptor IFNAR1 results in parasite internalisation and subsequent attenuation of the cellular responses to IFN $\alpha$  *in vitro* (Liu et al., 2009).

These evidences suggest that LmCK1.2 could play an important role in host cell dysfunction, however due to its broad range of action it is challenging to speculate which pathways affected by the kinase causes host cell immune subversion. One way to further define the role of LmCK1.2 in the host cell is to identify its binding partners from the mammalian host cell. Indeed, as previously discussed, CK1 localisation and function is frequently linked to its interacting partners (Knippschild et al., 2014), and it seems to be also the case for *Leishmania* CK1.2 (see [Chapter I](#)). Thus, I investigated LmCK1.2 associated proteins from the host cell.

The immuno-precipitation of secreted LmCK1.2 from *L. donovani* infected macrophages without recovering the non-secreted kinase can be challenging. Besides, protein extracts from *L. donovani* exosomes successfully identified specific LmCK1.2 kinase activity, however we could not detect the protein by Western blot analysis, suggesting that the protein is low abundant in the exosomes (unpublished results). To bypass this problem, I used an *ex vivo* method that was previously applied for *Mycobacterium tuberculosis* (Bach et al., 2008).

I thus developed a similar method to pull-down recombinant LmCK1.2-V5 and host cell interacting partners, using murine bone marrow-derived macrophage (BMDM) lysates. Hereafter describe the different steps that were necessary to optimise the protocol before mass spectrometry analysis. It allowed me to identify potential LmCK1.2 associated proteins from the host cell (LmCKAHost).

# 1. Development of an *ex vivo* method to identify the LmCKAHost proteins

## 1.1. Generation of the recombinant proteins and macrophage lysates

### 1.1.1. Production of rLmCK1.2-V5

I used the pBAD-thio-LmaCK1.2 vector to produce the recombinant LmCK1.2 protein fused with the 11.7 kDa thioredoxin in N-terminus and a V5-His<sub>6</sub>-tag in C-terminus (rLmCK1.2-V5, (Rachidi et al., 2014)). The thioredoxin protein was used to increase translation efficiency and solubility of eukaryotic proteins expressed in *E. coli*.

The protocol used to purify the kinase was the following. The bacterial pellets were resuspended in ÄKTA lysis buffer (AL) at pH 7.4 containing 50 mM sodium phosphate, 300 mM NaCl, 10 mM imidazole, 1 mM sodium vanadate, 1 mM sodium fluoride supplemented with protease inhibitor cocktail. Samples were sonicated at 20 V for two cycles of 2 min (10/10 s ON/OFF; 30/30 s ON/OFF). Triton X-100 (0.1% final) was then added and the samples were placed for 30 min at 4°C with agitation and then centrifuged 30 min at 15,000 g at 4°C. The supernatants were then cleared through a 0.22 µm filter. Next, rLmCK1.2-V5 was purified by affinity using an ÄKTA Purifier with a HiTrap TALON crude column. The column was pre-equilibrated in ÄKTA washing buffer (AW) (50 mM sodium phosphate, 300 mM NaCl, 20 mM imidazole, 1 mM sodium vanadate, 1 mM sodium fluoride supplemented with protease inhibitor cocktail and adjusted at pH 7.4), and the lysate injected in the column. The column was then washed with AW buffer and the recombinant protein eluted with ÄKTA elution buffer (AE) (50 mM sodium phosphate, 300 mM NaCl, 300 mM imidazole, 1 mM sodium vanadate, 1 mM sodium fluoride supplemented with protease inhibitor cocktail and adjusted at pH 7.4), recovering 1 mL fractions corresponding to the peak of elution. I used 7 µL of four elution fractions (A2 to A4) to verify the purity of the elutions by SDS-PAGE and SYPRO Ruby staining (Fig. 31).

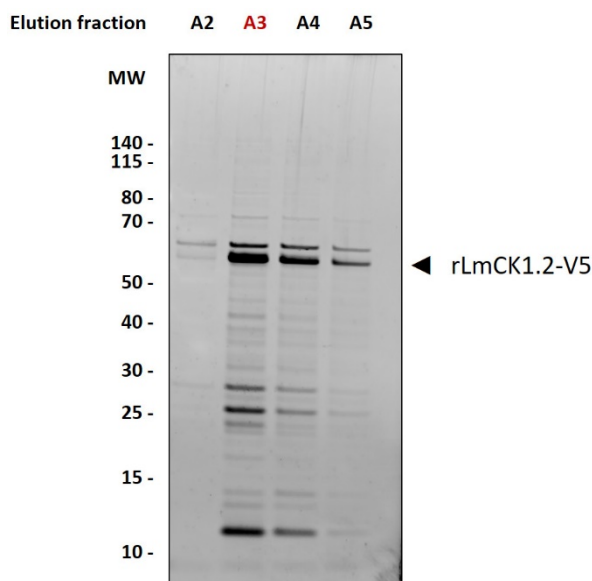


**Fig. 31 – Elution fractions of the purification of recombinant LmCK1.2-V5.**

*E. coli* expressing the fusion protein thioredoxin-LmCK1.2-V5-His<sub>6</sub> (rLmCK1.2-V5, 55.9 kDa) were lysed and the protein purified with a HiTrap TALON crude column placed on a ÄKTA Purifier. Four elution fractions (A2 to A5), corresponding to the peak of elution, were reduced, separated by SDS-PAGE and stained with SYPRO Ruby. Elution fraction A3 (red) was selected for further experiments. MW, molecular weight.

There was a clear enrichment of rLmCK1.2-V5, particularly in the elution A3 and A4, as seen by the intense band between 50-70 kDa. Although contaminants remain in the elution fractions. For the purpose of a pull down I considered that the purification was satisfying and I selected the elution fraction A3 for the next experiments.

### 1.1.2. Production of the recombinant control protein thioredoxin-V5-His<sub>6</sub>

To avoid the identification of false positives due to non-specific binding to the thioredoxin or the V5-His<sub>6</sub>-tag present in rLmCK1.2-V5, I generated the pBADthio-V5-His<sub>6</sub> plasmid allowing the expression of recombinant thioredoxin-V5-His<sub>6</sub> alone that I used as an additional control. The cloning steps involved the PCR amplification of the backbone of pBAD-thio-LmaCK1.2 plasmid using 5' phosphorylated primers DM1/DM2 (see Fig. 32A and Materials and Methods). The PCR fragment was re-circularized by ligation and transformed into bacteria. The resulting plasmid, pBADthio-V5-His<sub>6</sub>, was verified by DNA sequencing. I then produced the recombinant thioredoxin-V5-His<sub>6</sub> in *E. coli*, using the same protocol as described before (Rachidi et al., 2014). Proteins from elution fraction A2 to A5 were separated on SDS-PAGE and stained with SYPRO Ruby (Fig. 32B). The purification of recombinant thioredoxin-V5-His<sub>6</sub> (16.2 kDa) was very efficient, as judged by the band above 15 kDa and the absence of

contaminants, except in fraction A3. I selected the elution fraction A2 for the future experiments.

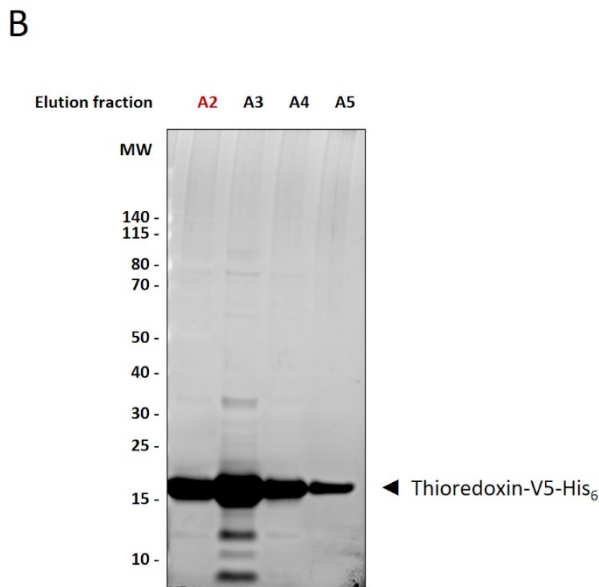
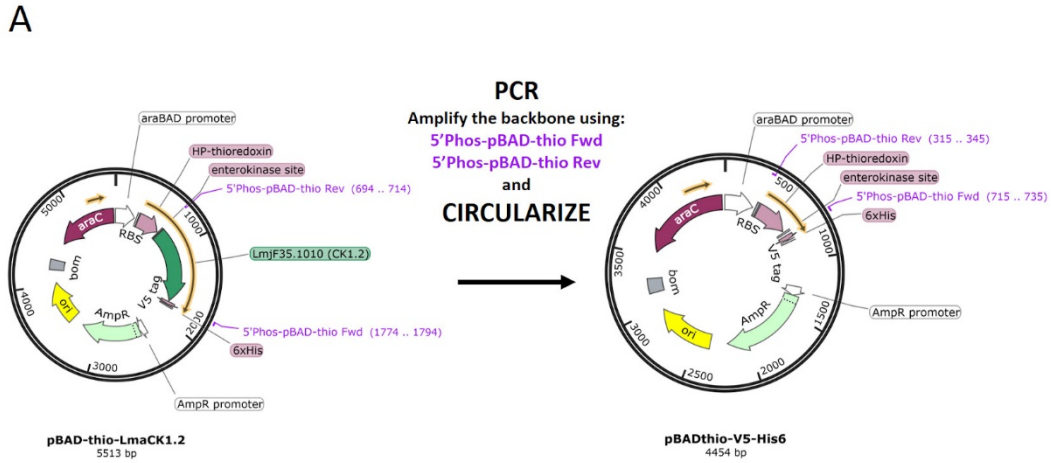


**Fig. 32 – Production of recombinant Thioredoxin-V5-His<sub>6</sub> protein.**

(A) Schematic representation of the cloning steps to generate the pBADthio-V5-His<sub>6</sub> plasmid from the pBAD-thio-LmaCK1.2 plasmid. (B) *E. coli* cells expressing thioredoxin-V5-His<sub>6</sub> (16.2 kDa) were lysed and the protein purified with a HiTrap TALON crude column placed on a ÄKTA Purifier. Four elution fractions (A2 to A5), corresponding to the peak of elution, were reduced, separated by SDS-PAGE and stained with SYPRO Ruby. Elution fraction A2 (red) was selected for further experiments. MW, molecular weight.

### 1.1.3. Production of macrophage extracts

I used bone-marrow derived macrophages (BMDM) from BALB/c ByJRj mice. The protocol for BMDM differentiation is well established in the lab and BMDMs are routinely used for macrophage infections with *Leishmania* species ((Aulner et al., 2013) and see **Materials and Methods**). Macrophages were lysed with RIPA buffer (150 mM NaCl, 1% Triton X-100, 20 mM Tris HCl [pH 7.4], 1% NP-40, 1 mM EDTA) supplemented with complete protease inhibitor cocktail (Roche Applied Science, IN) and with 1 mM sodium orthovanadate and 1 mM PMSF. Macrophage lysates were then vortexed and, after sonication, clarified by centrifugation.

### 1.2. Optimisation of the protocol to immuno-precipitate rLmCK1.2-V5 from BMDM lysates.

I first incubated 1 µg rLmCK1.2-V5 with 130 µg BMDM extracts for 2.5h at 4°C before proceeding to the immuno-precipitation (IP) as described in **Chapter II**. As a control, I incubated the BMDM protein lysates without the recombinant protein, replacing it with the same volume of the elution buffer (AE buffer) to account for proteins that bind to the beads (control). Three successive elutions of 10 minutes at 70°C with glycine elution buffer followed by one elution of 5 minutes at 95°C with NuPAGE loading buffer were performed. The samples were separated on SDS-PAGE and the gel was stained with SYPRO Ruby, as shown in **Fig. 33**.

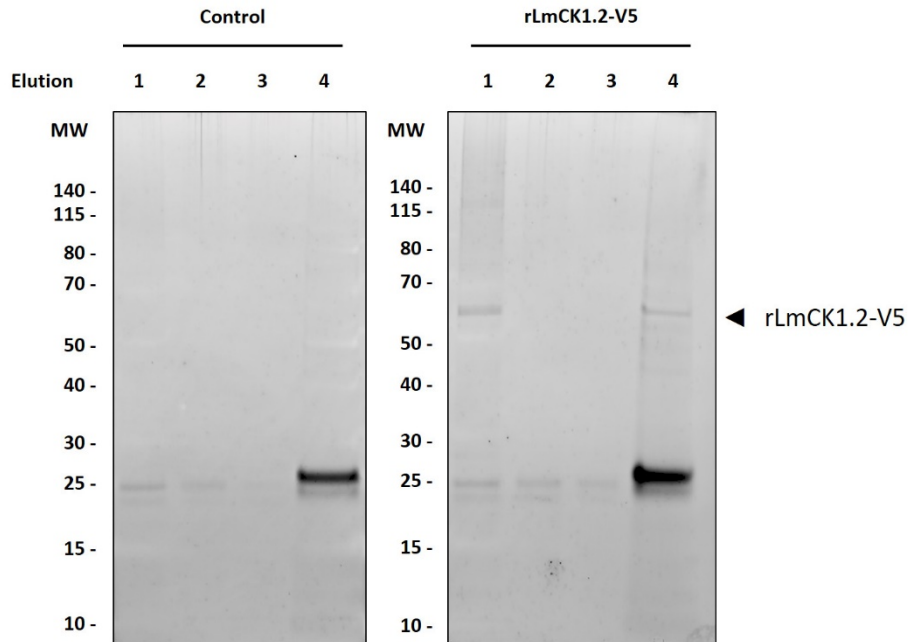


**Fig. 33 – Immunoprecipitation of host proteins by recombinant LmCK1.2-V5 from macrophage lysates.**

Four successive elutions were performed, with the glycine elution buffer (1 to 3) and NuPAGE loading buffer (4), and the proteins were resolved by SDS-PAGE and SYPRO Ruby staining. MW, molecular weight.

The rLmCK1.2-V5 is detected as a faint band at ~60 kDa (right panel) and absent in the control IP. Several other bands were detected in the IP performed in presence of rLmCK1.2-V5. One elution with the glycine buffer was sufficient to elute most of the bound rLmCK1.2-V5, as we did not observe the band in elutions 2 and 3. However, in elution 4 (NuPAGE loading buffer) rLmCK1.2-V5 could be detected, suggesting that there was still some protein bound to the antibody. There is also an intense band at ~25 kDa in elution 4, which could correspond to the light chain of the antibody, even though there was a crosslinking step. This was observed previously (see [Chapter II](#)). Although rLmCK1.2 was detectable with these IP conditions, the amount of binding proteins purified was not compatible with mass spectrometry analysis.

To optimise the protocol, I proceeded similarly as before, except I incubated the recombinant kinase and BMDM lysates longer from 2.5h to overnight (~18h) and I tested two quantities of rLmCK1.2-V5 (1 and 2  $\mu$ g). The results are shown in [Fig. 34](#).

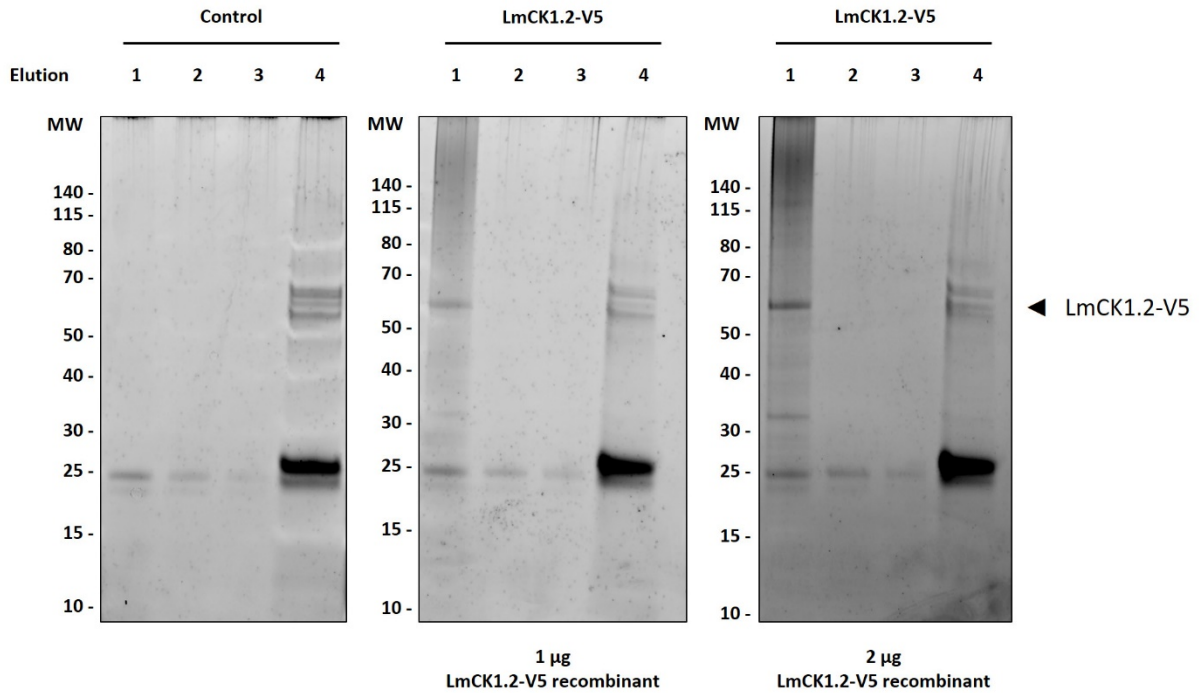


**Fig. 34 – Immunoprecipitation of host proteins by recombinant LmCK1.2-V5 from macrophage lysates.**

Murine BMDM protein lysates (130 µg) were incubated with recombinant LmCK1.2-V5 (LmCK1.2-V5, 1 or 2 µg), or without recombinant protein (Control). Proteins were incubated overnight at 4°C before proceeding to the immunoprecipitation steps with an anti-V5 antibody. Four successive elutions were performed, with the glycine elution buffer (1 to 3) and NuPAGE loading buffer (4), and the proteins were resolved by SDS-PAGE and SYPRO Ruby staining. MW, molecular weight.

By increasing the incubation time, and the quantity of rLmCK1.2-V5, more interacting proteins were eluted. However, before performing the final experiment for MS analysis, I did the IP with the recombinant thioredoxin-V5-His<sub>6</sub> protein. I used 142 µg of BMDM total proteins and 2 µg of rLmCK1.2-V5 or thioredoxin-V5-His<sub>6</sub>. The results of the elutions are presented in [Fig. 35](#).

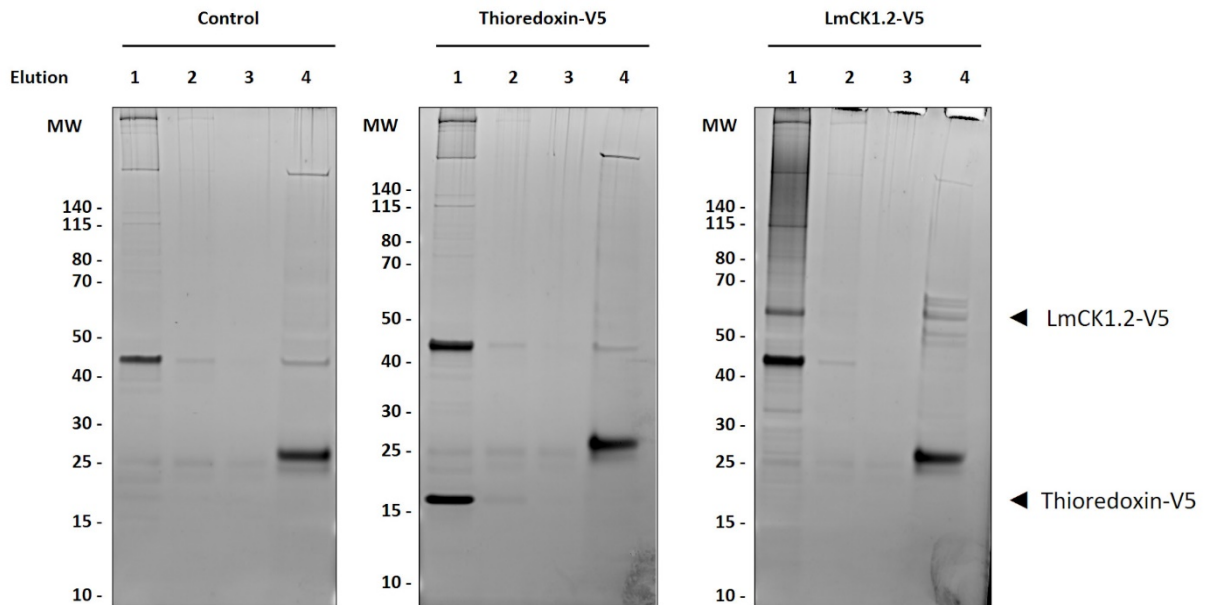


**Fig. 35 – Immunoprecipitation of host proteins by recombinant LmCK1.2-V5 from macrophage lysates.**

Mice BMDM protein lysates (142  $\mu$ g) were incubated with recombinant LmCK1.2-V5 (LmCK1.2-V5, 2  $\mu$ g), or without recombinant protein (Control). An additional control was added, recombinant Thioredoxin-V5 protein (Thioredoxin-V5, 2  $\mu$ g). Proteins were incubated for over-night at 4°C before proceeding to the immunoprecipitation steps with an anti-V5 antibody. Four successive elutions were performed, with the glycine elution buffer (1 to 3) and NuPAGE loading buffer (4), and the proteins were resolved by SDS-PAGE and SYPRO Ruby staining. MW, molecular weight.

The IP of recombinant thioredoxin-V5-His<sub>6</sub> (control-thio) was successful, as seen by the intense band recovered in elution 1 at the expected molecular weight, just above 15 kDa (middle panel). The pattern obtained with the control is similar to that of the thioredoxin-V5-His<sub>6</sub> control, suggesting that the proteins detected in presence of rLmCK1.2-V5 (Fig. 35, right panel) are mainly specific interactors of LmCK1.2. The optimisation was completed, I nevertheless added a pre-clearing step to the final experiment to remove more contaminants.



## 2. Identification of LmCKAHost proteins

### 2.1. Immuno-precipitation of rLmCK1.2-V5 from BMDM lysates.

To identify LmCKAHost proteins by mass spectrometry (MS) analysis, I performed the immuno-precipitation of rLmCK1.2-V5 as previously described in triplicates. For each experiment, I used two controls, one without recombinant protein and the other with the recombinant thioredoxin-V5-His<sub>6</sub> described before. For each replicate, the recombinant protein batches were the same, and the BMDM protein lysates came from two different batches, one that was used for the first experiment and the other batch for the last two.

The rLmCK1.2-V5, the control-thio and the control were incubated overnight with 142 µg BMDM protein lysates in 150 µL final volume. The proteins were then pre-cleared on 50 µL magnetic beads coupled to protein G for 30 minutes at 4°C with agitation. The pre-cleared samples were incubated with 50 µL magnetic beads coupled to protein G and cross-linked to 3 µg anti-V5 antibody for 30 minutes at 4°C with agitation. The beads were then washed six times 5 minutes at 4°C, and the proteins eluted by two successive elutions of 10 minutes at 70°C with glycine elution buffer (elution 1 and 2) followed by one elution of 5 minutes at 95°C with NuPAGE loading buffer (elution 3). The elutions 1 and 3 were used for MS analysis and proteins from elution 2 were separated by SDS-PAGE and stained with SYPRO Ruby to assess the IP (Fig. 36).

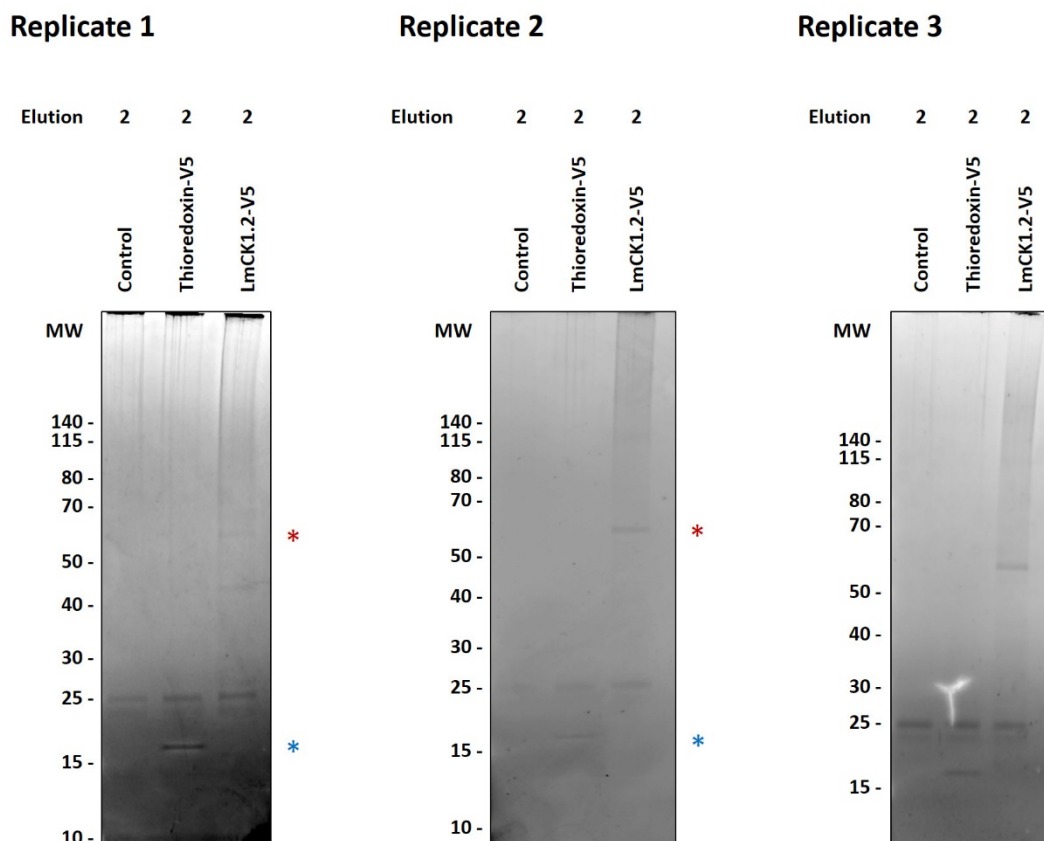


**Fig. 36 – Immunoprecipitation for mass spectrometry analysis of host proteins with recombinant LmCK1.2-V5 from macrophage lysates, in three biological replicates.**

Three successive elutions were performed, with the glycine elution buffer (1 and 2) and NuPAGE loading buffer (3). Elutions 1 and 3 were sent for MS analysis, and elution 2 were resolved by SDS-PAGE and SYPRO Ruby staining. Red stars, recombinant LmCK1.2-V5; Blue stars, recombinant thioredoxin-V5. MW, molecular weight.

For the three replicates, a band at the expected molecular weight for recombinant thioredoxin-V5-His<sub>6</sub> and rLmCK1.2-V5 was detected in their respective lane, which indicated that the IPs were successful. The elutions 1 and 3 were used for nanoscale liquid chromatography coupled to tandem mass spectrometry (nanoLC-MS/MS). MS analysis of the samples were done at the “Laboratoire de Spectrométrie de Masse Protéomique (LSMP)” platform at Institut Curie in Paris. SDS-PAGE was used without separation as a clean-up step and only one gel slice containing the entire elution fraction was excised. Peptide sequences predicted by MS were used to query the in house databases, containing SwissProt Mus Musculus (16745 sequences) and Uniprot *L. donovani* CK1.2 by using SequestHT from Proteome Discoverer (version 1.4 or 2.1) (see **Materials and Methods** for more details). The raw data are available in **Appendix 2**.

## 2.2. Analysis of the proteins identified by MS analysis

### 2.2.1. Selection criteria used for the identification of LmCK1.2 binding partners.

To identify LmCKAHost among the different proteins detected by mass spectrometry, and because the method is *ex vivo*, I selected only the proteins identified exclusively in rLmCK1.2-V5 IP in two or three replicates, and not in the controls. The numbers of distinct proteins identified in each replicates of the IP with rLmCK1.2-V5 and in both controls are represented in a Venn diagram in Fig. 37.

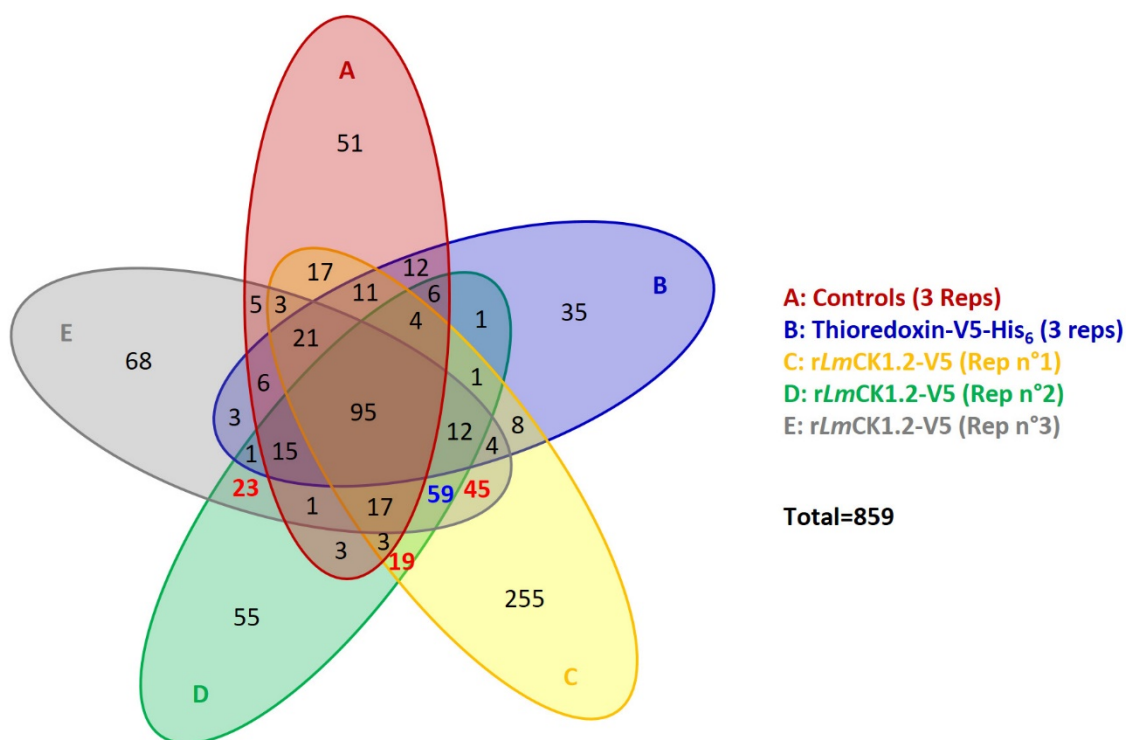


**Fig. 37 – Venn diagram of the proteins detected by MS analysis.**

The total proteins detected in three replicates of control (A) or thioredoxin-V5-His<sub>6</sub> (B), and each replicates of rLmCK1.2-V5 (C, D and E) identified by mass spectrometry. The numbers represent the distinct proteins in the overlapping and non-overlapping areas. The number of distinct proteins only found in rLmCK1.2-V5 IP in two or three replicates are shown in red or blue, respectively.

A total of 59 host proteins were immuno-precipitated with rLmCK1.2-V5 in all three replicates, and an additional 87 proteins were identified in at least two replicates (Fig. 37). In total, 146 potential LmCK1.2-V5 associated proteins were identified from the host (LmCKAHost). The list of LmCK1.2 associated host proteins is presented in Table 8 along with the mean number of peptides (mPep) identified in the three or two replicates and their respective standard deviation (SD) (see Table 8 in Appendices of Chapter III).

I used existing protein-protein interaction data to visualize protein complexes that had been co-precipitated with rLmCK1.2-V5. The human identifiers were used as input to identify protein-protein interaction from STRING database, and were merged to the interaction networks of LmCKAHost using Cytoscape software (version 3.7.1) (Fig. 38). Overall, very few proteins are clustering except 13 ribosomal proteins that may have been co-precipitated together, one of which is a known interacting partner of mammalian CK1, RPL27. This observation is consistent with the protocol used for this experiment, which is *ex vivo*. LmCK1.2 could bind to individual proteins but might not be integrated into complexes as it was added to a lysate. Therefore it is more likely that the proteins identified are bound directly to rLmCK1.2-V5. However, the LmCKAHost dataset is probably not complete and will need more experimental work to establish the physiological relevance of these interactions.

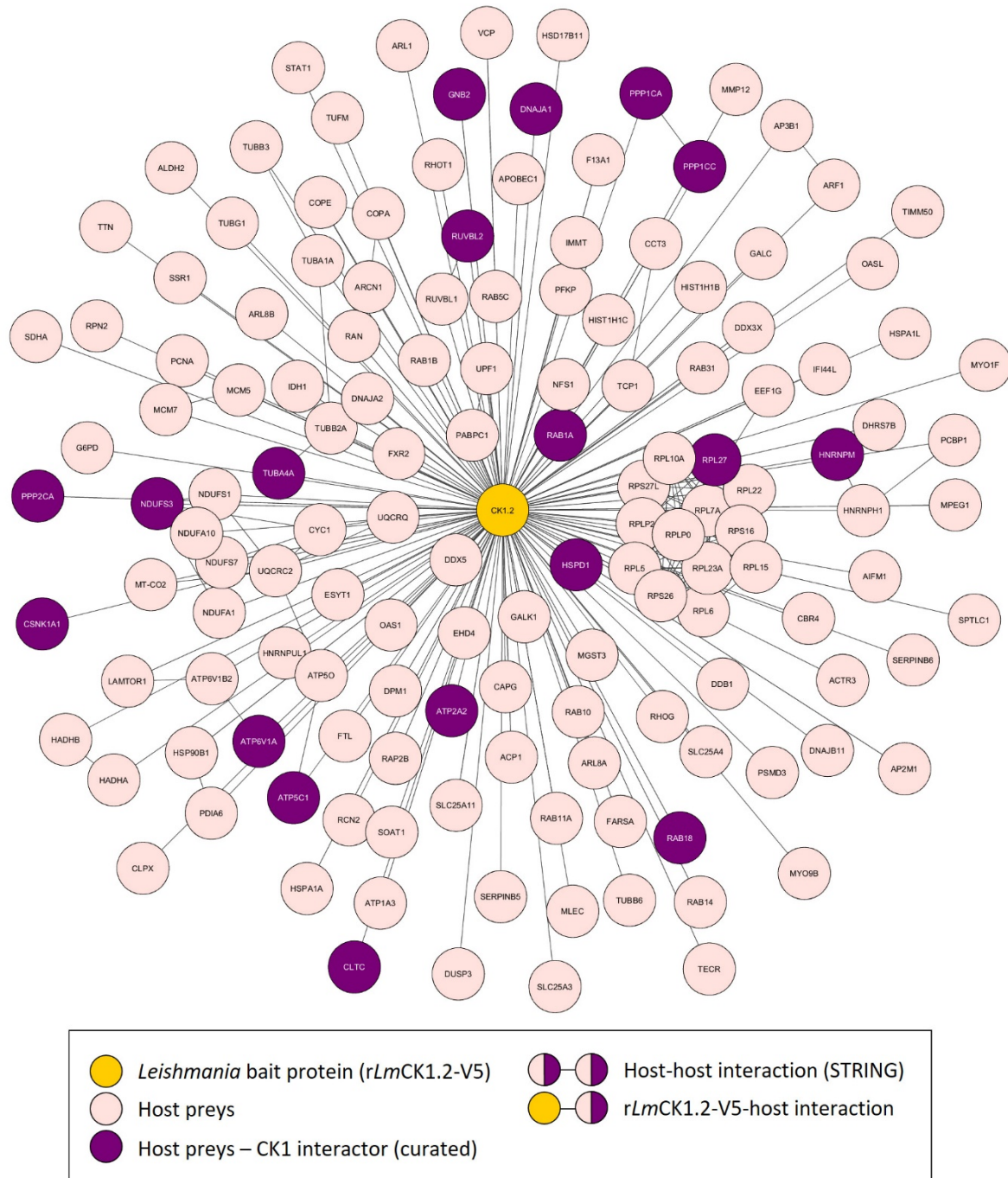


**Fig. 38 – Interaction network of LmCK1.2 and host proteins.**

Network representation of the rLmCK1.2-V5 interactome from BMDM cell lysates generated with Cytoscape. Human orthologs of the mouse identifiers were used here. The representation shows rLmCK1.2-V5 as bait protein (yellow node) and the 145 interacting host proteins (pink or purple nodes). One protein had no human ortholog and is thus not included in the figure. Bait-prey interactions are indicated by black lines between yellow and pink or purple nodes. Host-host interactions imported from STRING database are indicated by black lines between pink and/or purple nodes. Proteins that were identified as human CK1 interactors from BioGRID database (18 proteins found, for all 6 CK1 isoforms) are indicated by purple nodes.

## 2.2.2. Identification of 18 LmCKAHost proteins that also interact with mammalian CK1

To assess whether the LmCKAHost dataset is enriched in true CK1 binding partners, I assessed whether some of the proteins I identified were known CK1 interacting partners. To this end, I searched for known mammalian CK1 binding partners among the LmCKAHost proteins using the Biological General Repository for Interaction Datasets (BioGRID 3.5). I verified among all the interactors of the six human CK1 isoforms (CSNK1A1, CSNK1G1, CSNK1G2, CSNK1G3, CSNK1D and CSNK1E) for the presence of common proteins. 18 proteins were described as interacting with human CK1, which represents 12.3% of the total LmCKAHost proteins. This data suggests that the LmCKAHost dataset is relevant and that *LmCK1.2* and host CK1 may regulate common pathways. Most of the proteins (15) were identified as interactors of CK1 $\alpha$ , the others of CK1 $\delta$  or  $\epsilon$ , which suggests that *LmCK1.2* might perform the functions of CK1 $\alpha$  in the host cell during *Leishmania* infection. In the literature, it is frequent to find proteins described to interact with several CK1 paralogs. Here, only 3 of the 18 proteins were described to interact with more than one paralog. I implemented the 18 proteins that were described as interacting with CK1 in the literature in the interaction network in [Fig. 38](#), and the detailed isoforms involved are shown in [Table 6](#).

**Table 6 – LmCKAHost proteins also described as human CK1 interactors.**

UniProt Accession ( <i>Mus musculus</i> )	UniProt Accession ( <i>Homo sapiens</i> ortholog )	Protein name ( <i>Homo sapiens</i> )	Annotation	Found in Membrane trafficking Reactome Pathway?	no. Rep	mPep (CK) $\pm$ SD	Also interact with CK1 isoform: (reference)
P68368	P68366	TUBA4A	Tubulin alpha-4A chain	Yes	2 (1 & 3)	15,0 $\pm$ 2,8	CSNK1A1 (Rosenbluh et al., 2016)
Q68FD5	Q00610	CLTC	Clathrin heavy chain 1	Yes	2 (1 & 3)	8,5 $\pm$ 10,6	CSNK1A1; CSNK1E (Hein et al., 2015)
Q9WTM5	Q9Y230	RUVBL2	RuvB-like 2	-	3	7,3 $\pm$ 5,0	CSNK1A1 (Rosenbluh et al., 2016)
Q91VR2	P36542	ATP5C1	ATP synthase subunit gamma, mitochondrial	-	3	5,7 $\pm$ 3,2	CSNK1A1 (Rosenbluh et al., 2016)
Q9D0E1	P52272	HNRNPM	Heterogeneous nuclear ribonucleoprotein M	-	2 (1 & 3)	4,0 $\pm$ 1,4	CSNK1A1 (Rosenbluh et al., 2016)
P63330	P67775	PPP2CA	Serine/threonine-protein phosphatase 2A catalytic subunit alpha isoform	-	3	3,7 $\pm$ 3,1	CSNK1A1 (Dubois et al., 2002)
P50516	P38606	ATP6V1A	V-type proton ATPase catalytic subunit A	-	3	3,0 $\pm$ 1,7	CSNK1A1 (Rosenbluh et al., 2016)

P62821	P62820	RAB1A	Ras-related protein Rab-1A	Yes	2 (1 & 2)	3,0 ± 0,0	CSNK1D (Wang et al., 2015)
P35293	Q9NP72	RAB18	Ras-related protein Rab-18	Yes	3	2,3 ± 0,6	CSNK1A1 (Rosenbluh et al., 2016)
P61358	P61353	RPL27	60S ribosomal protein L27	-	3	2,3 ± 1,5	CSNK1A1 (Rosenbluh et al., 2016)
P62880	P62879	GNB2	Guanine nucleotide-binding protein G(I)/G(S)/G(T) subunit beta-2	-	2 (1 & 3)	2,0 ± 1,4	CSNK1A1 (Wang et al., 2011)
P62137	P62136	PPP1CA	Serine/threonine-protein phosphatase PP1-alpha catalytic subunit	-	2 (1 & 2)	2,0 ± 0,0	CSNK1E (Luo et al., 2007)
Q8BK63	P48729	CSNK1A1	Casein kinase I isoform alpha	-	3	2,0 ± 1,0	CSNK1E; CSNK1D (Rosenbluh et al., 2016; Varjosalo et al., 2013);
P63038	P10809	HSPD1	60 kDa heat shock protein, mitochondrial	-	3	1,7 ± 1,2	CSNK1A1 (Rosenbluh et al., 2016)
Q9DCT2	O75489	NDUFS3	NADH dehydrogenase [ubiquinone] iron-sulfur protein 3, mitochondrial	-	3	1,7 ± 0,6	CSNK1A1 (Rosenbluh et al., 2016)
O55143	P16615	ATP2A2	Sarcoplasmic/endoplasmic reticulum calcium ATPase 2	-	2 (1 & 3)	1,5 ± 0,7	CSNK1A1 (Rosenbluh et al., 2016)
P63037	P31689	DNAJA1	DnaJ homolog subfamily A member 1	-	2 (1 & 3)	1,5 ± 0,7	CSNK1A1 (Cai et al., 2018)
P63087	P36873	PPP1CC	Serine/threonine-protein phosphatase PP1-gamma catalytic subunit	-	3	1,0 ± 0,0	CSNK1A1; CSNK1E (Fardilha et al., 2011; Wallach et al., 2013)

Identifiers are formatted in UniProt Accession. Proteins also identified in the Reactome pathway “Membrane trafficking” are indicated with “Yes”. For each proteins, the number of replicates is shown, and the precise replicates in which they were identified, in the case of proteins identified in 2 replicates, is also shown. The mean number of peptides (mPep) identified in every replicates and corresponding standard deviation (SD) are given. A search of the LmCKAHost presence among the human CK1 known interactors from BioGRID database was performed, and the specific CK1 isoforms involved in the interaction are shown by their protein name, along with the reference.

Among the 18 LmCKAHost proteins that were described in the literature to be mammalian CK1 interacting partners, four were part of the membrane trafficking pathway (Reactome), the  $\alpha$ -tubulin TUBA4A, the clathrin heavy chain CLTC, RAB1A and RAB18 (Table 6). RAB1A is a member of the Rab GTPase family and was shown to bind and activate CK1 $\delta$  to spatially regulate its kinase activity, in the context of ER-Golgi traffic (Wang et al., 2015). There were also two chaperones, the chaperonin HSPD1 and the Hsp40 DNAJA1, and three nucleic acid binding proteins: RUVBL2, a component of the NuA4 histone acetyltransferase complex involved in transcriptional activation, HNRNPM, a pre-mRNA binding protein involved in splicing, and a component of the large ribosomal subunit, RPL27, required for rRNA processing. Three protein phosphatases were also found, the alpha and gamma catalytic subunits of the serine/threonine protein phosphatase PP1, and the alpha catalytic subunit of

the phosphatase PP2. Three components of the energy metabolism pathway, the F-type ATPase ATP5C1 and the V-type ATPase ATP6V1A, and the NADH dehydrogenase NDUF53 were identified. It is important to note that the CK1 $\alpha$  isoform was identified among the LmCKAHost proteins, and has been described to interact with two other CK1 isoforms, CK1 $\delta$  and CK1 $\epsilon$  (Rosenbluh et al., 2016; Varjosalo et al., 2013). Interaction between CK1 paralogs has not been studied in detail, but it was shown that homo-dimerisation of CK1 $\delta$  negatively regulated its activity in simian-virus 40 (SV40)-transformed cell lines (Deppert et al., 1991). Studying the role of LmCK1.2 interaction with host CK1 $\alpha$  *in vivo* would be very interesting in the future, especially since the host CK1 $\alpha$  has been showed to be down regulated upon *Leishmania* infection (Isnard et al., 2015).

### 2.2.3. LmCKAHost proteins are implicated in multiple cellular pathways

I used UniProt to recover the human orthologs of the mouse proteins to further analyse the proteins identified. H2-D1 (UniProtKB #P01900), a member of the MHC class I family involved in the presentation of foreign antigens to the immune system has only a distant orthologs in human, HLA-A, with 68% of identity (UniProtKB #B2NJ13). For the other proteins, I performed a pathway analysis using Reactome version 69 (<http://reactome.org/>), which is a curated database of pathways and reactions in human biology (Fabregat et al., 2018). All LmCKAHost human identifiers (UniProt accession) were subjected to Reactome and were used for an over-representation analysis. Reactome uses a statistical test (hypergeometric distribution) to determine whether certain pathways are enriched in the submitted dataset. 132 proteins out of the 145 were found in Reactome, and 665 pathways were hit with at least one of our proteins. The result of this analysis is presented as a genome-wide overview of the different pathways over-represented among the LmCKAHost proteins (Fig. 39A).

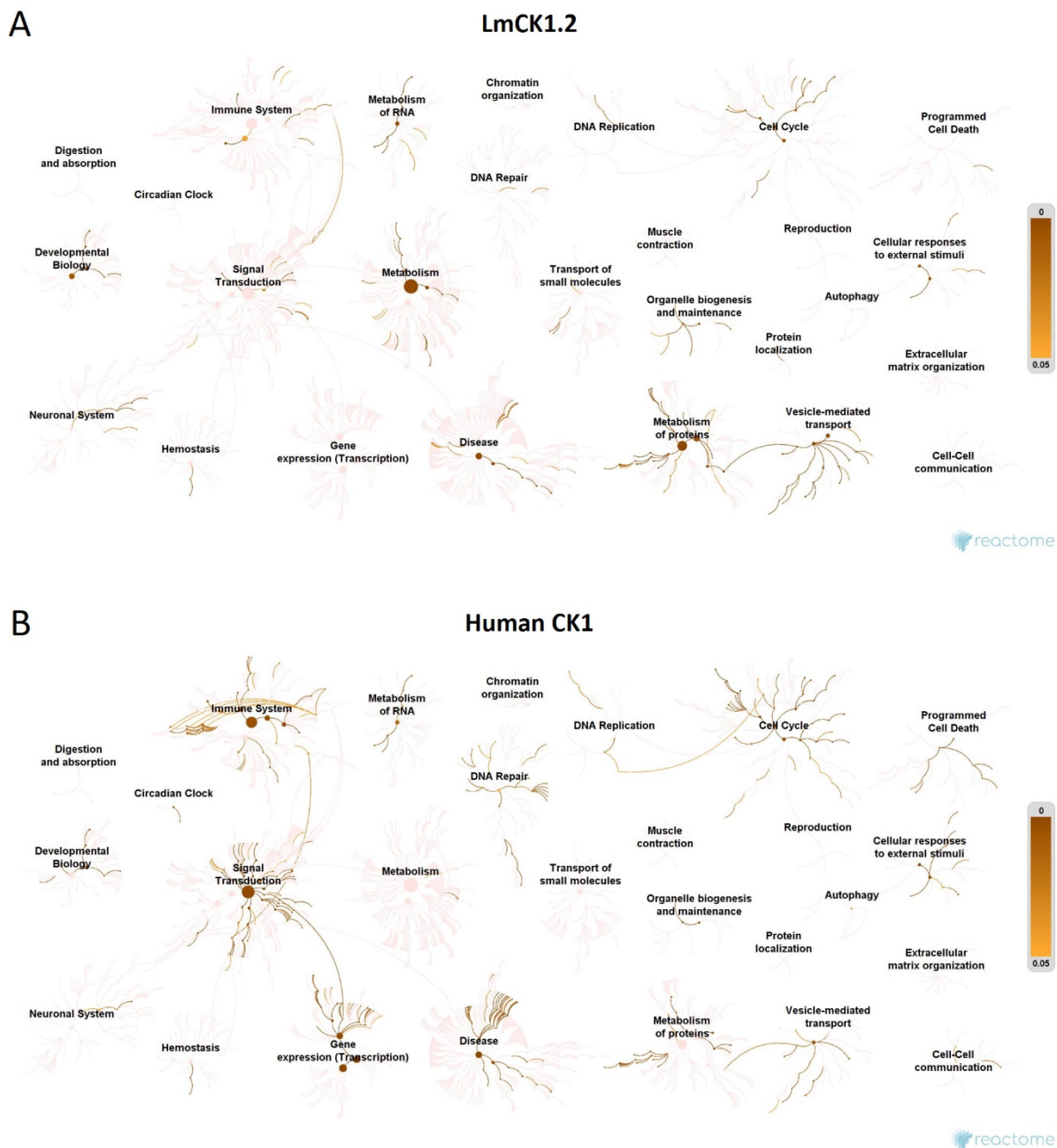


**Fig. 39 – Genome-wide overview of the results of the LmCKAHost pathway analysis and comparison with human CK1 interactors.**

Reactome pathways are displayed in a hierarchy, for the LmCKAHost (A) or human CK1 $\alpha$ ,  $\delta$  and  $\epsilon$  interactors from BioGRID database (B). The roots of one top-level pathway is represented as the center of each tree. Every step away from the center shows the the next lower level in the pathway hierarchy. The color code denotes over-representation of a pathway in the input LmCKAHost proteins (corresponding to the p-value of each entities). Not significantly over-represented pathways are shown in light pink. Generated by Reactome (Fabregat et al., 2018).

This analysis highlights the main pathways that are targeted by LmCK1.2. As seen in Fig. 39A, only few pathways seem to be strongly targeted by LmCK1.2 protein metabolism, vesicle-mediated transport and cell cycle. LmCK1.2 targets also organelle biogenesis and maintenance, immune response, signal transduction, metabolism of RNA and stress response. I next performed the same analysis with the human CK1 $\alpha$ ,  $\delta$ , and CK1 $\epsilon$  interacting partners obtained from BioGRID database (see Table 9 for accession numbers, in Appendices of Chapter III) to investigate whether similar pathways were regulated by the human and *Leishmania* CK1s. The results are presented in Fig. 39B. Human CK1s are involved in more pathways than LmCK1.2, which indicates that LmCK1.2 might target only specific pathways essential for parasite survival and not all the available CK1 pathways. It could also be the consequence of our methodology which prevented the identification of protein complexes. I can only interpret the pathways that are over-represented with LmCK1.2. Several pathways are over-represented in human CK1s dataset compared to that of LmCK1.2: DNA repair, gene expression, cell cycle, immune response and programmed cell death. Conversely, certain pathways are more represented in LmCK1.2 than in human CK1s datasets: vesicle-mediated transport, metabolism of proteins and organelle biogenesis and maintenance. This latter finding suggests that LmCK1.2 might interact with human proteins that are not interacting with the human CK1s. To illustrate such a hypothesis, I showed that human Hsp90 interacts with LmCK1.2, while the *Leishmania* Hsp90 does not (see Chapter II section 1, Tables 1 and 2). The other possibility is that some of LmCK1.2 interacting partners have not yet been identified as human CK1 interacting partners. This will have to be investigated further to discriminate between the two possibilities. Altogether, these results could highlight specific pathways that could be important for parasite survival.

#### 2.2.4. Enrichment of LmCKAHost dataset in proteins involved in membrane trafficking.

This pathway is particularly interesting as it is mostly targeted by LmCK1.2 and not extensively by human CK1s. Moreover, this pathway is also represented among LmCKAPs. The vesicle-mediated transport pathway that comprises the membrane trafficking pathway is particularly over-represented among the LmCKAHost proteins, with 24 proteins, involved in different processes of trafficking (Fig. 40A). Particularly, there are nine Rab GTPases mostly

involved in ER to Golgi anterograde transport; two coatomer subunits ( $\alpha$  and  $\epsilon$ ), which are required for budding from Golgi membranes, and are essential for the Golgi-to-ER transport of dilysine-tagged proteins; one clathrin heavy chain, which is the main protein of the coat of coated pits and vesicles; the  $\mu$ -adaptin of the AP2 complex, which we identified as a parasite LmCKAP (see Chapter II section 1, Tables 1 and 2); and the  $\beta$ -adaptin of the AP3 complex, which transports cargo-selective proteins from the Golgi to the vacuole/lysosome (Fig. 40B). This finding suggests that LmCK1.2 could target host trafficking generally, for instance to insure supply of nutrients to the parasitophorous vacuole. This will have to be verified *in vivo*, during *Leishmania* infection.

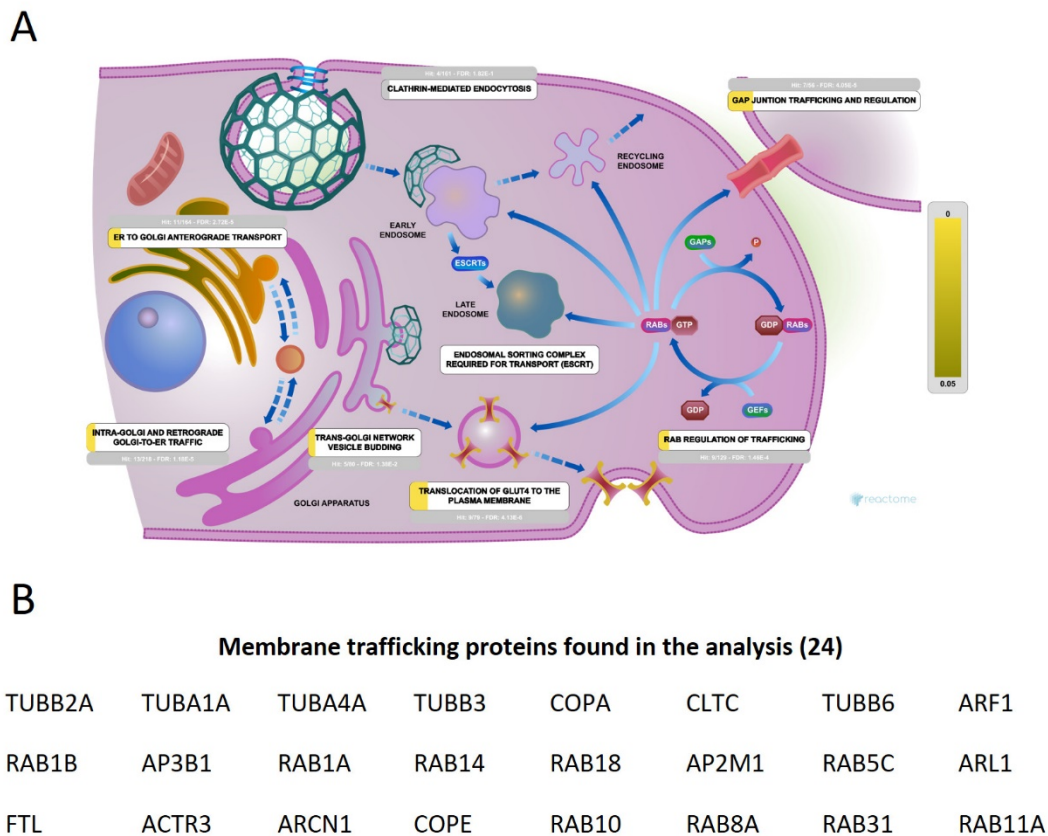


**Fig. 40 – Over-representation of the membrane trafficking pathway among the LmCKAHost proteins (Reactome pathway analysis).**

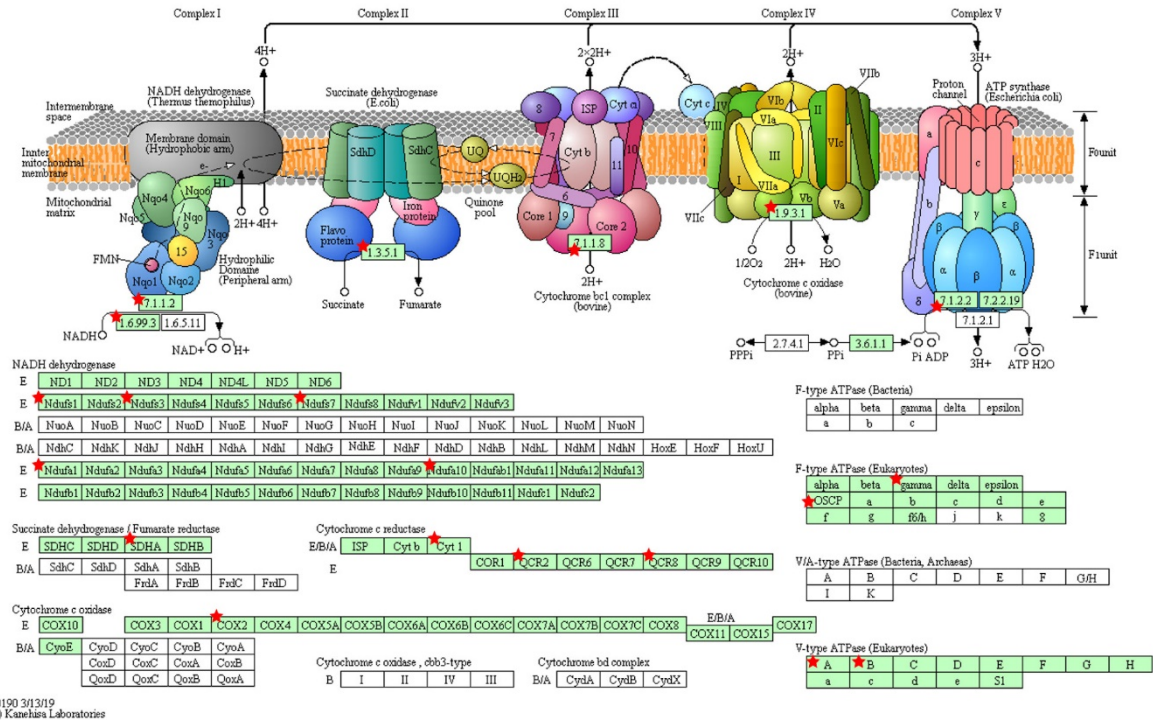
(A) Cartoon representing the membrane trafficking pathway. For each lower level pathways, the over-representation of these pathways is shown with the colour code, as well as the number of proteins identified and the false discovery rate (FDR). Cartoon generated by Reactome (Fabregat et al., 2018). (B) Identifiers of the 24 proteins identified in the membrane trafficking pathway (Reactome).

### 2.2.5. Enrichment of LmCKAHost dataset in proteins involved in oxidative phosphorylation pathway.

Protein metabolism is another pathway for which I identified many proteins. I searched for functional annotation using the DAVID Bioinformatics resources 6.8 and the human identifiers as input, and visualised proteins enriched in the oxidative phosphorylation pathway (KEGG pathway). 14 LmCKAHost proteins matched this pathway, and are presented in **Fig. 41**. Interestingly, LmCKAHost proteins are present in the entire electron transport chain, in complexes I to IV, suggesting that LmCK1.2 could play an important role in the energy metabolism. ATP6V1A, ATP5C1 and NDUFS3 were also found to bind to human CK1 $\alpha$  although the role of the interaction was not investigated (Rosenbluh et al., 2016). Moreover, ATP6V1A transcription has been shown to be up regulated during *Leishmania* infection, which could contribute to maintain the acidification of the parasitophorous vacuole (Osorio et al., 2009).

A

Oxidative Phosphorylation



B

Oxidative phosphorylation (Energy metabolism) proteins found in the analysis (14)

<b>NADH dehydrogenase</b>	NDUFS1	NDUFS3	NDUFS7	NDUFA1	NDUFA10
<b>Succinate dehydrogenase</b>	SDHA				
<b>Cytochrome C reductase</b>	CYC1	UQCRCQ	UQCRC2		
<b>Cytochrome C oxidase</b>	MT-CO2				
<b>F-type ATPase</b>	ATP5C1	ATP5O			
<b>V-type ATPase</b>	ATP6V1A	ATP6V1B2			

Fig. 41 – Over-representation of proteins from the energy metabolism in the LmCKAHost proteins (DAVID pathway analysis).

(A) Cartoon representing the oxidative phosphorylation pathway of the energy metabolism (generated by KEGG). Proteins shown with red stars were found among *LmCKAHost* proteins, and are listed in (B) Identifiers of the 14 proteins identified in the membrane trafficking pathway (Reactome)

### 2.2.6. More than a third of LmCKAHost proteins might play a role during *Leishmania* infection

Then, I most focused on LmCKAHost proteins that could be of physiological relevance in the context of *Leishmania* infection. As LmCK1.2 is exported into the host cell, we hypothesised that it could play a role in host subversion by phosphorylating host proteins. Several proteins could be of importance during macrophage subversion and for the persistence of the parasites. Hereafter I described the identification of these proteins and the protein names and accession are presented in [Table 7](#).

Several proteins could play a role in parasitophorous vacuole maturation, and thus could be regulated by secreted LmCK1.2 ([Table 7](#)). Two V-ATPase were found, the ATP6V1A and ATP6V1B2, which are involved in the acidification of early phagosomes and to lysosomes. *L. donovani* promastigote glycolipid virulence factor lipophosphoglycan (LPG) was shown to be involved in impairment of phagolysosome biogenesis, including acquisition of V-ATPase to the early phagosomes, thus inducing a maturation delay allowing the promastigotes to differentiate into resistant amastigotes. *L. donovani* promastigotes lacking LPG led to normal maturation of the phagolysosomes resulting in promastigote killing (Vinet et al., 2009). Other proteins such as RAB5C, which are recruited to early phagosomes, and the  $\alpha$ - and  $\beta$ -tubulin TUBA1A, TUBA4A, TUBB2A, TUBB3 and TUBB6 have been shown to play a role in phagocytosis, phagosome formation and maturation (Bucci et al., 1995; Harrison and Grinstein, 2002). Another protein that may play a role in phagocytosis is the extended synaptotagmin 1, ESYT1, which was shown to negatively modulate virus-induced membrane fusion (El Kasmi et al., 2018).

I identified proteins that could play a role in host immune response subversion ([Table 7](#)). For instance, the signal transducer and activator of transcription 1, STAT1, involved in interferon gamma signalling that play critical role in the control of *Leishmania* infection. STAT1 function was shown to be attenuated upon *Leishmania* infection thus blocking the biological functions of IFN $\gamma$  (Bhardwaj et al., 2005; Nandan and Reiner, 1995). Furthermore, STAT1 was also shown to function in phagosome acidification, a feature that proved to be crucial for host resistance to intracellular infection by *L. major* (Späth et al., 2009). Interferon-induced protein 44-like, IFI44L has been shown to be down regulated in Zika virus-infected male germ cells and its overexpression reduced Zika virus production (Robinson et al., 2018). H2-D1, the H-2 class

I histocompatibility antigen (D-D alpha chain), the mouse orthologs of human HLA-A. HLA-A proteins are involved in the presentation of foreign antigens to the immune system. There were also two proteins that could be modulated upon *Leishmania* infection, as they were described to be implicated in apoptosis, the cytochrome c (CYC1) and the apoptosis inducing factor mitochondria associated 1 (AIFM1), which is a flavoprotein essential for nuclear disassembly in apoptotic cells (Benítez-Guzmán et al., 2018; Cai et al., 1998). One of the key features that *Leishmania* parasites use to develop in phagocytic macrophages is to inhibit host cell apoptosis (Moore and Matlashewski, 1994).

Because *Leishmania* intracellular amastigotes are auxotrophic for various essential nutrients and are thus dependent upon host resources to grow and to persist, several studies have shown that the protein expression profile of major metabolic pathways were modified upon *Leishmania* infection (Menezes et al., 2013; Moreira et al., 2015; Singh et al., 2015). In LmCKAHost dataset, many proteins were involved in metabolic pathways or in energy metabolism (as shown before). Some proteins were involved in fatty acid elongation like the proteins HADHA, HADHB and TECP, or others in the carbon metabolism like G6PD, IDH1, PFKFB and SDHA. Overall, 27 proteins were involved in protein metabolic pathways and could be potentially regulated by LmCK1.2 upon *Leishmania* infection (Table 7).

Finally, from the phagocytosis of *Leishmania* promastigotes to the growth of intracellular amastigotes in the parasitophorous vacuole and further propagation and persistence of the parasites, the host cell employs a wide range of proteins involved in vesicle trafficking (Matte and Descoteaux, 2016; Russell et al., 1992). In that context, secreted LmCK1.2 could play a role in regulating several vesicle trafficking pathways (see Table 7).

Globally, more than a third of all LmCKAHost proteins appear to be physiologically relevant (57 proteins), or at least we could hypothesise putative functions for these proteins in the context of *Leishmania* infection. It suggests that LmCK1.2, which is released by the parasite, could play a significant role in *Leishmania* survival and persistence in the host cell, by binding host proteins.

**Table 7 – Selection of LmCKAHost proteins with potential physiological relevance.**

UniProt Accession <i>Mus musculus</i>	UniProt Accession <i>Homo sapiens</i> ortholog	Protein name <i>Homo sapiens</i>	Annotation
<b>Phagosomes (9)</b>			
P50516	P38606	ATP6V1A	V-type proton ATPase catalytic subunit A
P62814	P21281	ATP6V1B2	V-type proton ATPase subunit B, brain isoform
P35278	P51148	RAB5C	Ras-related protein Rab-5C
P68369	Q71U36	TUBA1A	Tubulin alpha-1A chain
P68368	P68366	TUBA4A	Tubulin alpha-4A chain
Q7TMM9	Q13885	TUBB2A	Tubulin beta-2A chain
Q9ERD7	Q13509	TUBB3	Tubulin beta-3 chain
Q922F4	Q9BUE5	TUBB6	Tubulin beta-6 chain
Q3U7R1	Q9BSJ8	ESYT1	Extended synaptotagmin-1
<b>Host immune response (5)</b>			
P42225	P42224	STAT1	Signal transducer and activator of transcription 1
Q9BDB7	Q53G44	IFI44L	Interferon-induced protein 44-like
P01900	*P30498	H2-D1 / *HLA-B	H-2 class I histocompatibility antigen, D-D alpha chain / *MHC class I antigen B*78
Q9D0M3	P08574	CYC1	Cytochrome c1, heme protein, mitochondrial
Q920X1	O95831	AIFM1	Apoptosis-inducing factor 1, mitochondrial
<b>Metabolic pathways (27)</b>			
Q9DB20	P48047	ATP5O	ATP synthase subunit O, mitochondrial
Q91VR2	P36542	ATP5C1	ATP synthase subunit gamma, mitochondrial
P50516	P38606	ATP6V1A	V-type proton ATPase catalytic subunit A
P62814	P21281	ATP6V1B2	V-type proton ATPase subunit B, brain isoform
Q91VD9	P28331	NDUFS1	NADH-ubiquinone oxidoreductase 75 kDa subunit, mitochondrial
Q9DCT2	O75489	NDUFS3	NADH dehydrogenase [ubiquinone] iron-sulfur protein 3, mitochondrial
Q9DC70	O75251	NDUFS7	NADH dehydrogenase [ubiquinone] iron-sulfur protein 7, mitochondrial
O35683	O15239	NDUFA1	NADH dehydrogenase [ubiquinone] 1 alpha subcomplex subunit 1
Q99LC3	O95299	NDUFA10	NADH dehydrogenase [ubiquinone] 1 alpha subcomplex subunit 10, mitochondrial
Q9Z1J3	Q9Y697	NFS1	Cysteine desulfurase, mitochondrial
P47738	P05091	ALDH2	Aldehyde dehydrogenase, mitochondrial
P00405	P00403	MT-CO2	Cytochrome c oxidase subunit 2
O70152	O60762	DPM1	Dolichol-phosphate mannosyltransferase subunit 1
Q9R0N0	P51570	GALK1	Galactokinase
P54818	P54803	GALC	Galactocerebrosidase
Q00612	P11413	G6PD	Glucose-6-phosphate 1-dehydrogenase X
Q8BM51	P40939	HADHA	Trifunctional enzyme subunit alpha, mitochondrial
Q99JY0	P55084	HADHB	Trifunctional enzyme subunit beta, mitochondrial
Q9CY27	Q9NZ01	TECR	Very-long-chain enoyl-CoA reductase
O88844	O75874	IDH1	Isocitrate dehydrogenase [NADP] cytoplasmic
Q9WUA3	Q01813	PFKP	ATP-dependent 6-phosphofructokinase, platelet type
Q9DBG6	P04844	RPN2	Dolichyl-diphosphooligosaccharide--protein glycosyltransferase subunit 2
O35704	O15269	SPTLC1	Serine palmitoyltransferase 1
Q8K2B3	P31040	SDHA	Succinate dehydrogenase [ubiquinone] flavoprotein subunit, mitochondrial
Q9DB77	P22695	UQCRC2	Cytochrome b-c1 complex subunit 2, mitochondrial
Q9CQ69	O14949	UQCRCQ	Cytochrome b-c1 complex subunit 8
Q61263	P35610	SOAT1	Sterol O-acyltransferase 1
<b>Membrane trafficking pathway (24)</b>			
Q7TMM9	Q13885	TUBB2A	Tubulin beta-2A chain
P68369	Q71U36	TUBA1A	Tubulin alpha-1A chain
P68368	P68366	TUBA4A	Tubulin alpha-4A chain

Q9ERD7	Q13509	TUBB3	Tubulin beta-3 chain
Q8CIE6	P53621	COPA	Coatomer subunit alpha
Q68FD5	Q00610	CLTC	Clathrin heavy chain 1
Q922F4	Q9BUF5	TUBB6	Tubulin beta-6 chain
P84078	P84077	ARF1	ADP-ribosylation factor 1
Q9D1G1	Q9H0U4	RAB1B	Ras-related protein Rab-1B
Q9Z1T1	O00203	AP3B1	AP-3 complex subunit beta-1
P62821	P62820	RAB1A	Ras-related protein Rab-1A
Q91V41	P61106	RAB14	Ras-related protein Rab-14
P35293	Q9NP72	RAB18	Ras-related protein Rab-18
P84091	Q96CW1	AP2M1	AP-2 complex subunit mu
P35278	P51148	RAB5C	Ras-related protein Rab-5C
P61211	P40616	ARL1	ADP-ribosylation factor-like protein 1
P29391	P02792	FTL	Ferritin light chain 1
Q99JY9	P61158	ACTR3	Actin-related protein 3
Q5XJY5	P48444	ARCN1	Coatomer subunit delta
O89079	O14579	COPE	Coatomer subunit epsilon
P61027	P61026	RAB10	Ras-related protein Rab-10
P62492	P62491	RAB11A	Ras-related protein Rab-11A
Q921E2	Q13636	RAB31	Ras-related protein Rab-31
P55258	P61006	RAB8A	Ras-related protein Rab-8A

I next investigated whether in the proteome of macrophages infected by *Leishmania* published by Isnard *et al.*, I could identify LmCKAHosts (Isnard *et al.*, 2015). I found nine proteins that were either degraded or down regulated upon *Leishmania* infection: TUBB3, TUBB6, RUVBL2, CSNK1A1, HNRNPUL1, CLTC, VCP, HIST1H1C and DDX3X (Table 8); and eleven proteins that were either up-regulated or produced upon *Leishmania* infection: RUVBL1, SLC25A4, ATP6V1A, RPN2, HNRNPM, RPLP2, EEF1G, SOAT1, ATP6V1B2, ACTR3 and DDX5. The identification of these 20 proteins suggests that the LmCKAHost dataset contains physiologically relevant proteins.



### 3. Conclusion and perspectives

Here I developed a method to identify the LmCK1.2 interactome, and I identified 146 high confidence proteins (LmCKAHost).

I used an *ex vivo* method, which is somewhat artificial as it does not reflect the interactions that occur *in vivo* between excreted LmCK1.2 and host proteins, however this approach was considered as the most suited for several reasons: (i) LmCK1.2 null mutant parasites are lethal, therefore it was not possible to use any approaches that would compare null versus wild types parasites, (ii) the *ex vivo* method had been successful in identifying physiologically relevant binding proteins. This approach provided valuable results and has the advantage to select mostly direct interaction as I obtained less complexes in the LmCKAHost dataset than for that of the parasitic LmCKAPs. Moreover it gave us clues about the pathways regulated by LmCK1.2 in host-pathogen interactions for further investigations.

The analysis of the 146 LmCKAHost proteins showed that LmCK1.2 is involved in multiple host cellular pathways, the pleiotropic nature of the parasitic LmCKAP appears to be conserved. Remarkably, I identified 18 LmCKAHost proteins that were also known human CK1 interactors, which strengthen the confidence that my dataset is indeed enriched in LmCK1.2 interactors. The fact that LmCK1.2 and host CK1 share similar interactors suggests that the *Leishmania* kinase could function in the same pathways and replace the host CK1. Furthermore, human CK1 $\alpha$ , CK1 $\epsilon$  and CK1 $\delta$  were found to interact with these eighteen proteins, suggesting that LmCK1.2 could cover functions that are usually distinct between different paralogs. Nevertheless, it seems that within our dataset, human CK1 $\alpha$  interacting proteins are over-represented suggesting that LmCK1.2 might mainly regulate its pathways. This is consistent with the data showing that host CK1 $\alpha$  is down regulated upon *Leishmania* infection (Isnard et al., 2015), and that it interacts with LmCK1.2, although the function of this interaction remains to be elucidated.

The identification of LmCKAHost not already known as human CK1 interactors, suggests three possibilities: (i) these LmCKAHost proteins could be novel human CK1 interactors, and therefore it would be interesting to investigate this further as we may have discovered new functions for the kinase, (ii) LmCK1.2 could interact with host proteins that

are not usual partners for the host CK1, and thus LmCK1.2 could regulate pathways that ultimately would lead to parasite survival, growth and persistence in the host organism, (iii) the method, I used, selected proteins that are not normally accessible to the host CK1s, as they could be buried inside protein complexes or spatially separated from the kinase.

I searched for proteins that could have a particular physiological significance in *Leishmania* infection, as these proteins would be the most interesting to study in the future. I identified more than a third of the dataset that could be implicated in functions linked to infection. These proteins were required for phagosome formation and maturation, crucial steps for *Leishmania* differentiation into amastigotes (Vinet et al., 2009). Several proteins were involved in metabolism, such as the fatty acid, carbon or energy metabolism. The importance of such pathways had been demonstrated during *Leishmania* infection. The metabolic dependence of the parasite on the host cell was shown by transcriptomic and proteomic studies, which demonstrated that *Leishmania* turn their host cells into metabolic factories to insure its proliferation (Dillon et al., 2015; Menezes et al., 2013; Moreira et al., 2015; Osorio et al., 2009; Rabhi et al., 2012; Singh et al., 2015). LmCK1.2 could be involved in the subversion of the metabolic pathways and further investigations will be needed to determine its real impact. The last important pathway carries out vesicular and protein trafficking, which is over-represented in my dataset. This finding is consistent with similar work performed with PfCK1. Batty *et al.* identified 10 host proteins that reproducibly interact with PfCK1, among which GAPVD1 and SNX22, involved in trafficking (Batty et al., 2019). They hypothesised that these proteins could coordinate the trafficking of PfCK1 during infection. It might also be the case for *Leishmania* CK1.2.

As this work was mainly *in vitro*, we ignore whether these interactions happen *in vivo* and whether they are important for parasite survival. However there are several promising leads that suggest that the interactome could be of physiological relevance and worth of further investigation. I identified twenty proteins that have been shown experimentally to be up- or down regulated upon *Leishmania* infection, suggesting that the LmCKAHost dataset is physiologically relevant. We need to confirm the interactions by reverse pull-down, yeast-two-hybrid, or even by localisation studies. I have preliminary results showing the localization of LmCK1.2 in the host cell macrophages outside the parasites, supporting its excretion by the parasites. These results need to be confirmed. Then, investigate the localisation of exported

LmCK1.2 in the host cell, with regards to some of the interacting partners that I found, would be very informative. We have preliminary results that show that several LmCKA<sub>Phost</sub> proteins are also substrates of rLmCK1.2-V5, which further strengthen the relevance of my dataset (unpublished data from Smirlis and Rachidi). Ultimately, to confirm the physiological relevance, we will use different tools available in mammalian cells, such as RNAi, CRISPR Cas9 and observe the effect of the knockdown of LmCK1.2 partners on parasite survival.

To conclude, the systematic identification of LmCK1.2 in proteomics analysis of the exosomal content from *Leishmania* parasites and the probable importance of these exosomes in host cell subversion suggest a role for this kinase in host-pathogen interactions. The identification of LmCKA<sub>Phost</sub> proteins supports this hypothesis and provides evidence on the pathways controlled by LmCK1.2. This work paves the way for future investigations that could be translated into drug discovery.



## 4. Appendices of Chapter III

**Table 8 – List of LmCKAHost proteins identified by mass spectrometry.**

UniProt Accession <i>M. musculus</i>	UniProt Accession <i>H. sapiens</i> ortholog	Protein name <i>H. sapiens</i>	Annotation	no. Rep	mPep (CK) $\pm$ SD
Q7TMM9	Q13885	TUBB2A	Tubulin beta-2A chain	3	18,0 $\pm$ 1,0
P68369	Q71U36	TUBA1A	Tubulin alpha-1A chain	3	17,0 $\pm$ 6,1
Q8CIE6	P53621	COPA	Coatomer subunit alpha	3	11,7 $\pm$ 10,5
Q9ERD7	Q13509	TUBB3	Tubulin beta-3 chain	3	11,7 $\pm$ 2,9
P84096	P84095	RHOG	Rho-related GTP-binding protein RhoG	3	8,0 $\pm$ 6,1
Q922F4	Q9BUF5	TUBB6	Tubulin beta-6 chain	3	7,7 $\pm$ 1,2
Q9WTM5	Q9Y230	RUVBL2	RuvB-like 2	3	7,3 $\pm$ 5,0
P60122	Q9Y265	RUVBL1	RuvB-like 1	3	6,7 $\pm$ 2,3
Q99KV1	Q9UBS4	DNAJB11	DnaJ homolog subfamily B member 11	3	6,0 $\pm$ 1,7
Q91VR2	P36542	ATP5C1	ATP synthase subunit gamma, mitochondrial	3	5,7 $\pm$ 3,2
P01900		H2-D1*	H-2 class I histocompatibility antigen, D-D alpha chain	3	5,7 $\pm$ 2,1
P48962	P12235	SLC25A4	ADP/ATP translocase 1	3	5,3 $\pm$ 2,9
Q9DB77	P22695	UQCRC2	Cytochrome b-c1 complex subunit 2, mitochondrial	3	5,3 $\pm$ 2,3
P11928	P00973	OAS1	2'-5'-oligoadenylate synthase 1A	3	5,0 $\pm$ 1,7
P62827	P62826	RAN	GTP-binding nuclear protein Ran	3	4,7 $\pm$ 3,8
Q8BH61	P00488	F13A1	Coagulation factor XIII A chain	3	4,3 $\pm$ 3,1
P14685	O43242	PSMD3	26S proteasome non-ATPase regulatory subunit 3	3	3,7 $\pm$ 0,6
P63330	P67775	PPP2CA	PPP1CC	3	3,7 $\pm$ 3,1
Q9D1G1	Q9H0U4	RAB1B	Ras-related protein Rab-1B	3	3,7 $\pm$ 2,5
P11983	P17987	TCP1	T-complex protein 1 subunit alpha	3	3,7 $\pm$ 2,1
Q9CR62	Q02978	SLC25A11	Mitochondrial 2-oxoglutarate/malate carrier protein	3	3,0 $\pm$ 1,0
P50516	P38606	ATP6V1A	V-type proton ATPase catalytic subunit A	3	3,0 $\pm$ 1,7
P47911	Q02878	RPL6	60S ribosomal protein L6	3	2,7 $\pm$ 1,5
Q9EQ06	Q8NBQ5	HSD17B11	Estradiol 17-beta-dehydrogenase 11	3	2,7 $\pm$ 1,5
Q9D880	Q3ZCQ8	TIMM50	Mitochondrial import inner membrane translocase subunit TIM50	3	2,7 $\pm$ 1,5
P14131	P62249	RPS16	40S ribosomal protein S16	3	2,3 $\pm$ 1,5
P61358	P61353	RPL27	60S ribosomal protein L27	3	2,3 $\pm$ 1,5
P47738	P05091	ALDH2	Aldehyde dehydrogenase, mitochondrial	3	2,3 $\pm$ 2,3
O70152	O60762	DPM1	Dolichol-phosphate mannosyltransferase subunit 1	3	2,3 $\pm$ 0,6
P54818	P54803	GALC	Galactocerebrosidase	3	2,3 $\pm$ 1,5
Q99LC3	O95299	NDUFA10	NADH dehydrogenase [ubiquinone] 1 alpha subcomplex subunit 10, mitochondrial	3	2,3 $\pm$ 0,6
P35293	Q9NP72	RAB18	Ras-related protein Rab-18	3	2,3 $\pm$ 0,6
P61211	P40616	ARL1	ADP-ribosylation factor-like protein 1	3	2,0 $\pm$ 1,0
P84091	Q96CW1	AP2M1	AP-2 complex subunit mu	3	2,0 $\pm$ 1,0
Q8BK63	P48729	CSNK1A1	Casein kinase I isoform alpha	3	2,0 $\pm$ 1,0
Q9D7X3	P51452	DUSP3	Dual specificity protein phosphatase 3	3	2,0 $\pm$ 1,7
P60335	Q15365	PCBP1	Poly(rC)-binding protein 1	3	2,0 $\pm$ 1,0
Q6PIC6	P13637	ATP1A3	Sodium/potassium-transporting ATPase subunit alpha-3	3	2,0 $\pm$ 1,0

Continuation of Table 6 (2/4)					
UniProt Accession <i>Mus musculus</i>	UniProt Accession <i>Homo sapiens</i> ortholog	Protein name <i>Homo sapiens</i>	Annotation	no. Rep	mPep (CK) ± SD
P63038	P10809	HSPD1	60 kDa heat shock protein, mitochondrial	3	1,7 ± 1,2
Q9Z1J3	Q9Y697	NFS1	Cysteine desulfurase, mitochondrial	3	1,7 ± 0,6
Q9DBG6	P04844	RPN2	Dolichyl-diphosphooligosaccharide--protein glycosyltransferase subunit 2	3	1,7 ± 0,6
P29391	P02792	FTL	Ferritin light chain 1	3	1,7 ± 1,2
Q9D358	P24666	ACP1	Low molecular weight phosphotyrosine protein phosphatase	3	1,7 ± 1,2
Q91VD9	P28331	NDUFS1	NADH-ubiquinone oxidoreductase 75 kDa subunit, mitochondrial	3	1,7 ± 0,6
P17918	P12004	PCNA	Proliferating cell nuclear antigen	3	1,7 ± 1,2
Q8BMS1	P40939	HADHA	Trifunctional enzyme subunit alpha, mitochondrial	3	1,7 ± 0,6
P67984	P35268	RPL22	60S ribosomal protein L22	3	1,3 ± 0,6
Q9Z0X1	O95831	AIFM1	Apoptosis-inducing factor 1, mitochondrial	3	1,3 ± 0,6
Q9QYJ0	O60884	DNAJA2	DnaJ homolog subfamily A member 2	3	1,3 ± 0,6
Q9R0N0	P51570	GALK1	Galactokinase	3	1,3 ± 0,6
O35737	P31943	HNRNPH1	Heterogeneous nuclear ribonucleoprotein H	3	1,3 ± 0,6
Q8VEK3	Q00839	HNRNPUL1	Heterogeneous nuclear ribonucleoprotein U	3	1,3 ± 0,6
O35704	O15269	SPTLC1	Serine palmitoyltransferase 1	3	1,3 ± 0,6
Q9CY27	Q9NZ01	TECR	Very-long-chain enoyl-CoA reductase	3	1,3 ± 0,6
Q9DB20	P48047	ATP5O	ATP synthase subunit O, mitochondrial	3	1,0 ± 0,0
Q8BFR5	P49411	TUFM	Elongation factor Tu, mitochondrial	3	1,0 ± 0,0
P63087	P36873	PPP1CC	Serine/threonine-protein phosphatase PP1-gamma catalytic subunit	3	1,0 ± 0,0
Q8K2B3	P31040	SDHA	Succinate dehydrogenase [ubiquinone] flavoprotein subunit, mitochondrial	3	1,0 ± 0,0
P68368	P68366	TUBA4A	Tubulin alpha-4A chain	2 (1 & 3)	15,0 ± 2,8
Q68FD5	Q00610	CLTC	Clathrin heavy chain 1	2 (1 & 3)	8,5 ± 10,6
P70248	O00160	MYO1F	Unconventional myosin-1f	2 (1 & 3)	8,5 ± 9,2
P14869	P05388	RPLP0	60S acidic ribosomal protein P0	2 (1 & 3)	7,5 ± 3,5
P29341	P11940	PABPC1	Polyadenylate-binding protein 1	2 (1 & 3)	6,5 ± 0,7
Q8VI94	Q15646	OASL	2'-5'-oligoadenylate synthase-like protein 1	2 (1 & 3)	5,5 ± 4,9
O88844	O75874	IDH1	Isocitrate dehydrogenase [NADP] cytoplasmic	2 (1 & 2)	5,0 ± 1,4
Q61696	P0DMV8	HSPA1A	Heat shock 70 kDa protein 1A	2 (1 & 3)	5,0 ± 1,4
P84078	P84077	ARF1	ADP-ribosylation factor 1	2 (1 & 2)	4,0 ± 0,0
P12970	P62424	RPL7A	60S ribosomal protein L7a	2 (1 & 3)	4,0 ± 1,4
Q3U1J4	Q16531	DDB1	DNA damage-binding protein 1	2 (1 & 3)	4,0 ± 0,0
P08113	P14625	HSP90B1	Endoplasmic	2 (1 & 3)	4,0 ± 4,2
Q9D0E1	P52272	HNRNPM	Heterogeneous nuclear ribonucleoprotein M	2 (1 & 3)	4,0 ± 1,4
Q01853	P55072	VCP	Transitional endoplasmic reticulum ATPase	2 (1 & 3)	4,0 ± 1,4
Q9EQP2	Q9H223	EHD4	EH domain-containing protein 4	2 (1 & 2)	3,5 ± 3,5
P53026	P62906	RPL10A	60S ribosomal protein L10a	2 (1 & 3)	3,5 ± 2,1
Q9Z1T1	O00203	AP3B1	AP-3 complex subunit beta-1	2 (1 & 3)	3,5 ± 2,1
Q6ZQJ3	Q14165	MLEC	Malectin	2 (2 & 3)	3,0 ± 0,0
P62821	P62820	RAB1A	Ras-related protein Rab-1A	2 (2 & 3)	3,0 ± 0,0
P00405	P00403	MT-CO2	Cytochrome c oxidase subunit 2	2 (1 & 2)	3,0 ± 2,8
Q9WUA3	Q01813	PFKP	ATP-dependent 6-phosphofructokinase, platelet type	2 (1 & 3)	3,0 ± 1,4

Continuation of Table 6 (3/4)					
UniProt Accession <i>Mus musculus</i>	UniProt Accession <i>Homo sapiens</i> ortholog	Protein name <i>Homo sapiens</i>	Annotation	no. Rep	mPep (CK) ± SD
P16627	P34931	HSPA1L	Heat shock 70 kDa protein 1-like	2 (1 & 3)	3,0 ± 0,0
P62855	P62854	RPS26	40S ribosomal protein S26	2 (2 & 3)	2,5 ± 0,0
Q8VEH3	Q96BM9	ARL8A	ADP-ribosylation factor-like protein 8A	2 (2 & 3)	2,5 ± 0,0
P51908	P41238	APOBEC1	C->U-editing enzyme APOBEC-1	2 (2 & 3)	2,5 ± 0,0
Q9D0M3	P08574	CYC1	Cytochrome c1, heme protein, mitochondrial	2 (2 & 3)	2,5 ± 0,0
Q8VEM8	Q00325	SLC25A3	Phosphate carrier protein, mitochondrial	2 (2 & 3)	2,5 ± 0,0
Q8BP92	Q14257	RCN2	Reticulocalbin-2	2 (2 & 3)	2,5 ± 0,0
Q9CQW2	Q9NVJ2	ARL8B	ADP-ribosylation factor-like protein 8B	2 (1 & 2)	2,5 ± 2,1
Q91V41	P61106	RAB14	Ras-related protein Rab-14	2 (1 & 2)	2,5 ± 2,1
Q60854	P35237	SERPINB6	Serpin B6	2 (1 & 2)	2,5 ± 0,7
P99027	P05387	RPLP2	60S acidic ribosomal protein P2	2 (1 & 3)	2,5 ± 0,7
Q9D8N0	P26641	EEF1G	Elongation factor 1-gamma	2 (1 & 3)	2,5 ± 0,7
P15864	P16403	HIST1H1C	Histone H1.2	2 (1 & 3)	2,5 ± 0,7
Q9EPU0	Q92900	UPF1	Regulator of nonsense transcripts 1	2 (1 & 3)	2,5 ± 2,1
P35278	P51148	RAB5C	Ras-related protein Rab-5C	2 (2 & 3)	2,0 ± 0,0
P62137	P62136	PPP1CA	Serine/threonine-protein phosphatase PP1-alpha catalytic subunit	2 (2 & 3)	2,0 ± 0,0
P24452	P40121	CAPG	Macrophage-capping protein	2 (1 & 2)	2,0 ± 0,0
P61226	P61225	RAP2B	Ras-related protein Rap-2b	2 (1 & 2)	2,0 ± 0,0
Q99JY0	P55084	HADHB	Trifunctional enzyme subunit beta, mitochondrial	2 (1 & 2)	2,0 ± 0,0
P83887	P23258	TUBG1	Tubulin gamma-1 chain	2 (1 & 2)	2,0 ± 1,4
Q9CZM2	P61313	RPL15	60S ribosomal protein L15	2 (1 & 3)	2,0 ± 1,4
P62880	P62879	GNB2	Guanine nucleotide-binding protein G(I)/G(S)/G(T) subunit beta-2	2 (1 & 3)	2,0 ± 1,4
Q922R8	Q15084	PDIA6	Protein disulfide-isomerase A6	2 (1 & 3)	2,0 ± 0,0
P16381	O00571	DDX3X	Putative ATP-dependent RNA helicase PI10	2 (1 & 3)	2,0 ± 1,4
P70124	P36952	SERPINB5	Serpin B5	2 (1 & 3)	2,0 ± 1,4
A1L314	Q2M385	MPEG1	Macrophage-expressed gene 1 protein	2 (2 & 3)	1,5 ± 0,0
Q35683	O15239	NDUFA1	NADH dehydrogenase [ubiquinone] 1 alpha subcomplex subunit 1	2 (2 & 3)	1,5 ± 0,0
Q61263	P35610	SOAT1	Sterol O-acyltransferase 1	2 (2 & 3)	1,5 ± 0,0
Q9CY50	P43307	SSR1	Translocon-associated protein subunit alpha	2 (2 & 3)	1,5 ± 0,0
Q00612	P11413	G6PD	Glucose-6-phosphate 1-dehydrogenase X	2 (1 & 2)	1,5 ± 0,7
Q8C0C7	Q9Y285	FARSA	Phenylalanine--tRNA ligase alpha subunit	2 (1 & 2)	1,5 ± 0,7
P62814	P21281	ATP6V1B2	V-type proton ATPase subunit B, brain isoform	2 (1 & 2)	1,5 ± 0,7
Q99JY9	P61158	ACTR3	Actin-related protein 3	2 (1 & 3)	1,5 ± 0,7
Q9CQ69	O14949	UQCRQ	Cytochrome b-c1 complex subunit 8	2 (1 & 3)	1,5 ± 0,7
P63037	P31689	DNAJA1	DnaJ homolog subfamily A member 1	2 (1 & 3)	1,5 ± 0,7
Q61656	P17844	DDX5	Probable ATP-dependent RNA helicase DDX5	2 (1 & 3)	1,5 ± 0,7
O55143	P16615	ATP2A2	Sarcoplasmic/endoplasmic reticulum calcium ATPase 2	2 (1 & 3)	1,5 ± 0,7
P42225	P42224	STAT1	Signal transducer and activator of transcription 1	2 (1 & 3)	1,5 ± 0,7
Q9JHS4	O76031	CLPX	ATP-dependent Clp protease ATP-binding subunit clpX-like, mitochondrial	2 (2 & 3)	1,0 ± 0,0
O89079	O14579	COPE	Coatmer subunit epsilon	2 (2 & 3)	1,0 ± 0,0
Q61881	P33993	MCM7	DNA replication licensing factor MCM7	2 (2 & 3)	1,0 ± 0,0
P34960	P39900	MMP12	Macrophage metalloelastase	2 (2 & 3)	1,0 ± 0,0

Continuation of Table 6 (4/4)					
UniProt Accession <i>Mus musculus</i>	UniProt Accession <i>Homo sapiens</i> ortholog	Protein name <i>Homo sapiens</i>	Annotation	no. Rep	mPep (CK) ± SD
Q9CPU4	O14880	MGST3	Microsomal glutathione S-transferase 3	2 (2 & 3)	1,0 ± 0,0
Q8BG51	Q8IXI2	RHOT1	Mitochondrial Rho GTPase 1	2 (2 & 3)	1,0 ± 0,0
Q921E2	Q13636	RAB31	Ras-related protein Rab-31	2 (2 & 3)	1,0 ± 0,0
P55258	P61006	RAB8A	Ras-related protein Rab-8A	2 (2 & 3)	1,0 ± 0,0
A2ASS6	Q8WZ42	TTN	Titin	2 (2 & 3)	1,0 ± 0,0
P62751	P62750	RPL23A	60S ribosomal protein L23a	2 (1 & 2)	1,0 ± 0,0
Q3U7R1	Q9BSJ8	ESYT1	Extended synaptotagmin-1	2 (1 & 2)	1,0 ± 0,0
Q9BDB7	Q53G44	IFI44L	Interferon-induced protein 44-like	2 (1 & 2)	1,0 ± 0,0
P61027	P61026	RAB10	Ras-related protein Rab-10	2 (1 & 2)	1,0 ± 0,0
P62492	P62491	RAB11A	Ras-related protein Rab-11A	2 (1 & 2)	1,0 ± 0,0
Q6ZWY3	Q71UM5	RPS27L	40S ribosomal protein S27-like	2 (1 & 3)	1,0 ± 0,0
P47962	P46777	RPL5	60S ribosomal protein L5	2 (1 & 3)	1,0 ± 0,0
Q91VT4	Q8N4T8	CBR4	Carbonyl reductase family member 4	2 (1 & 3)	1,0 ± 0,0
Q5XJY5	P48444	ARCN1	Coatmer subunit delta	2 (1 & 3)	1,0 ± 0,0
Q99J47	Q6IAN0	DHRS7B	Dehydrogenase/reductase SDR family member 7B	2 (1 & 3)	1,0 ± 0,0
P49718	P33992	MCM5	DNA replication licensing factor MCM5	2 (1 & 3)	1,0 ± 0,0
Q61584	P51116	FXR2	Fragile X mental retardation syndrome-related protein 1	2 (1 & 3)	1,0 ± 0,0
Q8VDM6	Q9BUJ2	HNRNPUL1	Heterogeneous nuclear ribonucleoprotein U-like protein 1	2 (1 & 3)	1,0 ± 0,0
P43276	P16401	HIST1H1B	Histone H1.5	2 (1 & 3)	1,0 ± 0,0
Q8CAQ8	Q16891	IMMT	MICOS complex subunit Mic60	2 (1 & 3)	1,0 ± 0,0
Q9DC70	O75251	NDUFS7	NADH dehydrogenase [ubiquinone] iron-sulfur protein 7, mitochondrial	2 (1 & 3)	1,0 ± 0,0
Q9CQ22	Q6IAA8	LAMTOR1	Ragulator complex protein LAMTOR1	2 (1 & 3)	1,0 ± 0,0
P80318	P49368	CCT3	T-complex protein 1 subunit gamma	2 (1 & 3)	1,0 ± 0,0
Q9QY06	Q13459	MYO9B	Unconventional myosin-IXb	2 (1 & 3)	1,0 ± 0,0

\* Protein name of the *Mus musculus* protein.

**Table 9 – List of curated human CK1 interactors obtained from BioGRID v3.5 database.**

See [Appendix 3](#).

# Conclusion & Perspectives

---



Using multi-disciplinary strategy combining microscopic, biochemical and gene editing approaches, I revealed *LmCK1.2* as an essential signalling protein for *Leishmania* parasites both inside and outside of the parasites. I could confirm the pleiotropic localisation *LmCK1.2* by the identification of corresponding binding partners. The parasite and host interactomes allowed me to gain insights into the functions of *LmCK1.2* in the parasite as well as in the host cell. Surprisingly, some of these functions appear to be similar, for instance the vesicular and protein trafficking pathway for which we found many proteins in both cell types. However, at present we cannot conclude whether these interactions are the consequence of the trafficking of *LmCK1.2* or whether *LmCK1.2* regulates this pathway. I favour the second hypothesis for two main reasons: (1) yeast CK1 $\delta/\epsilon$  orthologs Hrr25 has been involved in the regulation of endocytic processes (Peng et al., 2015c) and (2) *LmCK1.2* phosphorylates  $\beta$ 2-adaptin (Martel *et al.*, in preparation). Nevertheless more experiments will be required to conclude, such as inhibiting *LmCK1.2* by a specific inhibitor and investigate whether the endocytic pathways are still functioning, using dyes such as FM4-64.

Remarkably, the composition of the *LmCKAP* identified in *L. donovani* axenic amastigotes resembles to that of the *LmCKAPhost* proteins. In both datasets I identified proteins involved in mRNA splicing, translation or linked to the cytoskeleton. It is not only the composition that is similar, but several proteins are common interactors to the parasite and the host CK1s: the  $\mu$ -adaptin of the AP2 complex (LdBPK\_363180.1 (*L. donovani*); AP2M1 (host)), an ATP-dependent 6-phosphofructokinase (LdBPK\_292620.1; PFKP) or the dual specificity protein phosphatase 3 (LdBPK\_210760.1; DUSP3). One major question that arises from chapter 3 is the physiological relevance of the *LmCKAPhost* dataset. We have some elements suggesting that this dataset is relevant as we found *LmCKAPhost* that are up- or down-regulated upon *Leishmania* infection. However, all the other proteins will have to be investigated.

It appears that *Leishmania* CK1.2 has similarities with three different mammalian CK1 paralogs, that are involved in different pathways (reviewed in (Knippschild et al., 2005b)). Whether *LmCK1.2* can substitute for these different isoforms, and what could be the resulting benefit for *Leishmania* survival, growth and persistence in the host cell remains to be elucidated. However, only the CK1 $\alpha$  isoform is down-regulated during *Leishmania* infections (Isnard et al., 2015), and it is also the paralog that shares the most interactors with *LmCK1.2*,

suggesting that the *Leishmania* kinase might replace CK1 $\alpha$  during macrophage infection. This paralog seems to be also important during viral infection. The viral protein VP5 of the infectious bursal disease virus (IBDV) interacts with the host CK1 $\alpha$  and a knockdown of the host kinase leads to the decrease of IBDV replication. The relation between CK1 and viral proteins has been shown for two other viruses, hepatitis C virus (HCV) and yellow fever virus (YFV) (Bhattacharya et al., 2009; Sudha et al., 2012). CK1 $\alpha$  phosphorylates NS5A (HCV) and the methyl-transferase of YFV, phosphorylation essential for viral replication. Notably, one of the binding partners we identified as host binding partners of LmCK1.2 is CK1 $\alpha$ . Altogether, these findings suggest that CK1 could be a master regulator of intracellular pathogen survival and could greatly contribute to regulate host-pathogen interactions.

Protein kinases are already very important therapeutic targets for diseases such as cancer or Alzheimer's disease and are starting to become important for infectious disease. Our unit is directly interested in finding new antileishmanial therapies as the current available therapies for leishmaniasis are not optimal and cause parasite resistance. LmCK1.2 is an excellent target: as it performs functions in the host cells it is less prone to mutations (Rachidi et al., 2014). The knowledge that I generated on LmCK1.2 during my PhD will be used to identify novel therapeutic strategies. For instance, targeting the host instead of the parasite (reviewed in (Lamotte et al., 2017)). The LmCKAHost could constitute prime targets for protein-protein interactions inhibitors. Moreover, the proteins required for the exosomal release of LmCK1.2 could be exploited as targets to prevent its release and inhibits intracellular parasite survival.

Finally, given the proximity between LmCK1.2 and other parasitic CK1s (TbCK1.2 and TcCK1.2 and PfCK1), knowledge acquired with *Leishmania* will be transferable to those parasitic CK1s. Moreover, the high level of identity between LmCK1.2 and mammalian CK1s, the localisation study and the two interactomes, suggest that only part of the results obtained with LmCK1.2 might be applicable to mammalian CK1s. Nevertheless, the similarities and differences will tell us a many informations about host-*Leishmania* interactions which could be exploited for drug discovery.

# References

---



- Agostinis, P., Pinna, L.A., Meggio, F., Marin, O., Goris, J., Vandenheede, J.R., and Merlevede, W. (1989). A synthetic peptide substrate specific for casein kinase-1. *FEBS Lett.* *259*, 75–78.
- Akhoundi, M., Kuhls, K., Cannet, A., Votýpka, J., Marty, P., Delaunay, P., and Sereno, D. (2016). A Historical Overview of the Classification, Evolution, and Dispersion of Leishmania Parasites and Sandflies. *PLoS Negl. Trop. Dis.* *10*, e0004349–e0004349.
- Al-Kamel, M.A. (2016). Impact of leishmaniasis in women: a practical review with an update on my ISD-supported initiative to combat leishmaniasis in Yemen (ELYP). *Int. J. Womens Dermatol.* *2*, 93–101.
- Alvar, J., Yactayo, S., and Bern, C. (2006). Leishmaniasis and poverty. *Trends Parasitol.* *22*, 552–557.
- Alvar, J., Vélez, I.D., Bern, C., Herrero, M., Desjeux, P., Cano, J., Jannin, J., and Den, M.B. (2012). Leishmaniasis worldwide and global estimates of its incidence. *PloS One* *7*, e35671–e35671.
- Andrade, B.B., de Oliveira, C.I., Brodskyn, C.I., Barral, A., and Barral-Netto, M. (2007). Role of sand fly saliva in human and experimental leishmaniasis: current insights. *Scand. J. Immunol.* *66*, 122–127.
- Antoine, J.C., Prina, E., Jouanne, C., and Bongrand, P. (1990). Parasitophorous vacuoles of *Leishmania amazonensis*-infected macrophages maintain an acidic pH. *Infect. Immun.* *58*, 779–787.
- Ardito, F., Giuliani, M., Perrone, D., Troiano, G., and Muzio, L.L. (2017). The crucial role of protein phosphorylation in cell signaling and its use as targeted therapy (Review). *Int. J. Mol. Med.* *40*, 271–280.
- Aslett, M., Aurrecochea, C., Berriman, M., Brestelli, J., Brunk, B.P., Carrington, M., Depledge, D.P., Fischer, S., Gajria, B., Gao, X., et al. (2010). TriTrypDB: a functional genomic resource for the Trypanosomatidae. *Nucleic Acids Res* *38*, D457–62.
- Atayde, V.D., Suau, H.A., Townsend, S., Hassani, K., Kamhawi, S., and Olivier, M. (2015). Exosome secretion by the parasitic protozoan *Leishmania* within the sand fly midgut. *Cell Rep.* *13*, 957–967.
- Atayde, V.D., Hassani, K., da Silva Lira Filho, A., Borges, A.R., Adhikari, A., Martel, C., and Olivier, M. (2016). *Leishmania* exosomes and other virulence factors: Impact on innate immune response and macrophage functions. *Cell. Immunol.* *309*, 7–18.
- Aulner, N., Danckaert, A., Rouault-Hardoin, E., Desrivot, J., Helynck, O., Commere, P.H., Munier-Lehmann, H., Spath, G.F., Shorte, S.L., Milon, G., et al. (2013). High content analysis of primary macrophages hosting proliferating *Leishmania* amastigotes: application to anti-leishmanial drug discovery. *PLoS Negl Trop Dis* *7*, e2154.
- Bach, H., Papavinasandaram, K.G., Wong, D., Hmama, Z., and Av-Gay, Y. (2008). Mycobacterium tuberculosis Virulence Is Mediated by PtpA Dephosphorylation of Human Vacuolar Protein Sorting 33B. *Cell Host Microbe* *3*, 316–322.

- Backer, J.M. (2016). The intricate regulation and complex functions of the Class III phosphoinositide 3-kinase Vps34. *Biochem. J.* *473*, 2251–2271.
- Banuls, A.L., Hide, M., and Prugnolle, F. (2007). Leishmania and the leishmaniasis: a parasite genetic update and advances in taxonomy, epidemiology and pathogenicity in humans. *Adv Parasitol* *64*, 1–109.
- Barak, E., Amin-Spector, S., Gerliak, E., Goyard, S., Holland, N., and Zilberstein, D. (2005). Differentiation of *Leishmania donovani* in host-free system: analysis of signal perception and response. *Mol. Biochem. Parasitol.* *141*, 99–108.
- Barik, S., Taylor, R.E., and Chakrabarti, D. (1997). Identification, cloning, and mutational analysis of the casein kinase 1 cDNA of the malaria parasite, *Plasmodium falciparum*. Stage-specific expression of the gene. *J. Biol. Chem.* *272*, 26132–26138.
- Barja, P.P., Pescher, P., Bussotti, G., Dumetz, F., Imamura, H., Kedra, D., Domagalska, M., Chaumeau, V., Himmelbauer, H., Pages, M., et al. (2017). Haplotype selection as an adaptive mechanism in the protozoan pathogen *Leishmania donovani*. *Nat. Ecol. Evol.* *1*, 1961–1969.
- Batty, M.B., Schittenhelm, R.B., Doerig, C., and Garcia-Bustos, J. (2019). Interaction of *Plasmodium falciparum* Casein kinase 1 (PfCK1) with components of host cell protein trafficking machinery. *BioRxiv* 617571.
- Behrend, L., Stöter, M., Kurth, M., Rutter, G., Heukeshoven, J., Deppert, W., and Knippschild, U. (2000). Interaction of casein kinase 1 delta (CK1 $\delta$ ) with post-Golgi structures, microtubules and the spindle apparatus. *Eur. J. Cell Biol.* *79*, 240–251.
- Ben Salah, A., Ben Messaoud, N., Guedri, E., Zaatour, A., Ben Alaya, N., Bettaieb, J., Gharbi, A., Belhadj Hamida, N., Boukthir, A., Chlif, S., et al. (2013). Topical Paromomycin with or without Gentamicin for Cutaneous Leishmaniasis. *N. Engl. J. Med.* *368*, 524–532.
- Beneke, T., Madden, R., Makin, L., Valli, J., Sunter, J., and Gluenz, E. (2017). A CRISPR Cas9 high-throughput genome editing toolkit for kinetoplastids. *R. Soc. Open Sci.* *4*, 170095.
- Benítez-Guzmán, A., Arriaga-Pizano, L., Morán, J., and Gutiérrez-Pabello, J.A. (2018). Endonuclease G takes part in AIF-mediated caspase-independent apoptosis in *Mycobacterium bovis*-infected bovine macrophages. *Vet. Res.* *49*.
- Besteiro, S., Williams, R.A.M., Coombs, G.H., and Mottram, J.C. (2007). Protein turnover and differentiation in *Leishmania*. *Int. J. Parasitol.* *37*, 1063–1075.
- Bhardwaj, N., Rosas, L.E., Lafuse, W.P., and Satoskar, A.R. (2005). *Leishmania* inhibits STAT1-mediated IFN- $\gamma$  signaling in macrophages: increased tyrosine phosphorylation of dominant negative STAT1 $\beta$  by *Leishmania mexicana*. *Int. J. Parasitol.* *35*, 75–82.
- Bhattacharya, D., Ansari, I.H., and Striker, R. (2009). The flaviviral methyltransferase is a substrate of Casein Kinase 1. *Virus Res.* *141*, 101–104.
- Bhattacharya, S.K., Sinha, P.K., Sundar, S., Thakur, C.P., Jha, T.K., Pandey, K., Das, V.R., Kumar, N., Lal, C., Verma, N., et al. (2007). Phase 4 trial of miltefosine for the treatment of Indian visceral leishmaniasis. *J. Infect. Dis.* *196*, 591–598.

- Bischof, J., Randoll, S.-J., Süßner, N., Henne-Bruns, D., Pinna, L.A., and Knippschild, U. (2013). CK1 $\delta$  Kinase Activity Is Modulated by Chk1-Mediated Phosphorylation. *PLoS ONE* 8.
- Biswas, A., Mukherjee, S., Das, S., Shields, D., Chow, C.W., and Maitra, U. (2011). Opposing action of casein kinase 1 and calcineurin in nucleo-cytoplasmic shuttling of mammalian translation initiation factor eIF6. *J. Biol. Chem.* 286, 3129–3138.
- Bobrie, A., Colombo, M., Raposo, G., and Théry, C. (2011). Exosome Secretion: Molecular Mechanisms and Roles in Immune Responses. *Traffic* 12, 1659–1668.
- Boehm, M., and Bonifacino, J.S. (2001). Adaptins: the final recount. *Mol. Biol. Cell* 12, 2907–2920.
- Boisvert, F.-M., van Koningsbruggen, S., Navascués, J., and Lamond, A.I. (2007). The multifunctional nucleolus. *Nat. Rev. Mol. Cell Biol.* 8, 574–585.
- Borba, J.V.B., Silva, A.C., Ramos, P.I.P., Grazzia, N., Miguel, D.C., Muratov, E.N., Furnham, N., and Andrade, C.H. (2019). Unveiling the Kinomes of *Leishmania infantum* and *L. braziliensis* Empowers the Discovery of New Kinase Targets and Antileishmanial Compounds. *Comput. Struct. Biotechnol. J.* 17, 352–361.
- Boucher, N., Wu, Y., Dumas, C., Dubé, M., Sereno, D., Breton, M., and Papadopoulou, B. (2002). A Common Mechanism of Stage-regulated Gene Expression in *Leishmania* Mediated by a Conserved 3'-Untranslated Region Element. *J. Biol. Chem.* 277, 19511–19520.
- Boynak, N.Y., Rojas, F., D'Alessio, C., Vilchez, S.L., Rodriguez, V., Ghiringhelli, P.D., and Téllez-Iñón, M.T. (2013). Identification of a Wee1-like kinase gene essential for procyclic *Trypanosoma brucei* survival. *PloS One* 8, e79364–e79364.
- Bozatzki, P., and Sapkota, G.P. (2018). The FAM83 family of proteins: from pseudo-PLDs to anchors for CK1 isoforms. *Biochem. Soc. Trans.* 46, 761–771.
- Brockman, J.L., and Anderson, R.A. (1991). Casein kinase I is regulated by phosphatidylinositol 4,5-bisphosphate in native membranes. *J. Biol. Chem.* 266, 2508–2512.
- Bryant, J.M., Baumgarten, S., Glover, L., Hutchinson, S., and Rachidi, N. (2019). CRISPR in Parasitology: Not Exactly Cut and Dried! *Trends Parasitol.* 35, 409–422.
- Bucci, C., Lütcke, A., Steele-Mortimer, O., Olkkonen, V.M., Dupree, P., Chiariello, M., Bruni, C.B., Simons, K., and Zerial, M. (1995). Co-operative regulation of endocytosis by three RAB5 isoforms. *FEBS Lett.* 366, 65–71.
- Budini, M., Jacob, G., Jedlicki, A., Pérez, C., Allende, C.C., and Allende, J.E. (2009). Autophosphorylation of carboxy-terminal residues inhibits the activity of protein kinase CK1 $\alpha$ . *J. Cell. Biochem.* 106, 399–408.
- Burnett, G., and Kennedy, E.P. (1954). The Enzymatic Phosphorylation of Proteins. *J. Biol. Chem.* 211, 969–980.
- Bussotti, G., Gouzélou, E., Côrtes, M.B., Kherachi, I., Harrat, Z., Eddaikra, N., Mottram, J.C., Antoniou, M., Christodoulou, V., Bali, A., et al. (2018). *Leishmania* Genome Dynamics

during Environmental Adaptation Reveal Strain-Specific Differences in Gene Copy Number Variation, Karyotype Instability, and Telomeric Amplification. *MBio* 9.

Cai, J., Yang, J., and Jones, DeanP. (1998). Mitochondrial control of apoptosis: the role of cytochrome c. *Biochim. Biophys. Acta BBA - Bioenerg.* 1366, 139–149.

Cai, J., Li, R., Xu, X., Zhang, L., Lian, R., Fang, L., Huang, Y., Feng, X., Liu, X., Li, X., et al. (2018). CK1 $\alpha$  suppresses lung tumour growth by stabilizing PTEN and inducing autophagy. *Nat. Cell Biol.* 20, 465.

Carregaro, V., Costa, D.L., Brodskyn, C., Barral, A.M., Barral-Netto, M., Cunha, F.Q., and Silva, J.S. (2013). Dual effect of *Lutzomyia longipalpis* saliva on *Leishmania braziliensis* infection is mediated by distinct saliva-induced cellular recruitment into BALB/c mice ear. *BMC Microbiol.* 13, 102–102.

Cecílio, P., Pérez-Cabezas, B., Fernández, L., Moreno, J., Carrillo, E., Requena, J.M., Fichera, E., Reed, S.G., Coler, R.N., Kamhawi, S., et al. (2017). Pre-clinical antigenicity studies of an innovative multivalent vaccine for human visceral leishmaniasis. *PLoS Negl. Trop. Dis.* 11, e0005951–e0005951.

Cegielska, A., Gietzen, K.F., Rivers, A., and Virshup, D.M. (1998). Autoinhibition of Casein Kinase I  $\epsilon$  (CKI $\epsilon$ ) Is Relieved by Protein Phosphatases and Limited Proteolysis. *J. Biol. Chem.* 273, 1357–1364.

Charest, H., Zhang, W.W., and Matlashewski, G. (1996). The developmental expression of *Leishmania donovani* A2 amastigote-specific genes is post-transcriptionally mediated and involves elements located in the 3'-untranslated region. *J. Biol. Chem.* 271, 17081–17090.

Cobb, M.H., and Rosen, O.M. (1983). Description of a protein kinase derived from insulin-treated 3T3-L1 cells that catalyzes the phosphorylation of ribosomal protein S6 and casein. *J. Biol. Chem.* 258, 12472–12481.

Cocucci, E., Aguet, F., Boulant, S., and Kirchhausen, T. (2012). The First Five Seconds in the Life of a Clathrin-Coated Pit. *Cell* 150, 495–507.

Collins, B.M., McCoy, A.J., Kent, H.M., Evans, P.R., and Owen, D.J. (2002). Molecular Architecture and Functional Model of the Endocytic AP2 Complex. *Cell* 109, 523–535.

Contreras, I., Gómez, M.A., Nguyen, O., Shio, M.T., McMaster, R.W., and Olivier, M. (2010). *Leishmania*-induced inactivation of the macrophage transcription factor AP-1 is mediated by the parasite metalloprotease GP63. *PLoS Pathog.* 6, e1001148–e1001148.

Croft, S.L., and Olliaro, P. (2011). *Leishmaniasis* chemotherapy--challenges and opportunities. *Clin. Microbiol. Infect. Off. Publ. Eur. Soc. Clin. Microbiol. Infect. Dis.* 17, 1478–1483.

Cruciat, C.-M., Dolde, C., Groot, R.E.A. de, Ohkawara, B., Reinhard, C., Korswagen, H.C., and Niehrs, C. (2013). RNA Helicase DDX3 Is a Regulatory Subunit of Casein Kinase 1 in Wnt- $\beta$ -Catenin Signaling. *Science* 339, 1436–1441.

- Dan-Goor, M., Nasereddin, A., Jaber, H., and Jaffe, C.L. (2013). Identification of a Secreted Casein Kinase 1 in *Leishmania donovani*: Effect of Protein over Expression on Parasite Growth and Virulence. *PLOS ONE* *8*, e79287.
- Davidson, G., Wu, W., Shen, J., Bilic, J., Fenger, U., Stannek, P., Glinka, A., and Niehrs, C. (2005). Casein kinase 1  $\gamma$  couples Wnt receptor activation to cytoplasmic signal transduction. *Nature* *438*, 867–872.
- Dean, S., Sunter, J.D., and Wheeler, R.J. (2017). TrypTag.org: A Trypanosome Genome-wide Protein Localisation Resource. *Trends Parasitol.* *33*, 80–82.
- DeMaggio, A.J., Lindberg, R.A., Hunter, T., and Hoekstra, M.F. (1992). The budding yeast HRR25 gene product is a casein kinase I isoform. *Proc. Natl. Acad. Sci.* *89*, 7008–7012.
- Demmel, L., Schmidt, K., Lucast, L., Havlicek, K., Zankel, A., Koestler, T., Reithofer, V., De, P.C., and Warren, G. (2016). The endocytic activity of the flagellar pocket in *Trypanosoma brucei* is regulated by an adjacent phosphatidylinositol phosphate kinase. *J. Cell Sci.* *129*, 2285–2285.
- Deppert, W., Kurth, M., Graessmann, M., Graessmann, A., and Knippschild, U. (1991). Altered phosphorylation at specific sites confers a mutant phenotype to SV40 wild-type large T antigen in a flat revertant of SV40-transformed cells. *Oncogene* *6*, 1931–1938.
- Desdín-Micó, G., and Mittelbrunn, M. (2017). Role of exosomes in the protection of cellular homeostasis. *Cell Adhes. Migr.* *11*, 127–134.
- Deshaias, R.J. (1997). Phosphorylation and proteolysis: partners in the regulation of cell division in budding yeast. *Curr. Opin. Genet. Dev.* *7*, 7–16.
- Dillon, L.A.L., Okrah, K., Hughitt, V.K., Suresh, R., Li, Y., Fernandes, M.C., Belew, A.T., Corrada Bravo, H., Mosser, D.M., and El-Sayed, N.M. (2015). Transcriptomic profiling of gene expression and RNA processing during *Leishmania* major differentiation. *Nucleic Acids Res.* *43*, 6799–6813.
- Dinesh, D.S., Das, M.L., Picado, A., Roy, L., Rijal, S., Singh, S.P., Das, P., Boelaert, M., and Coosemans, M. (2010). Insecticide Susceptibility of *Phlebotomus argentipes* in Visceral Leishmaniasis Endemic Districts in India and Nepal. *PLoS Negl. Trop. Dis.* *4*, e859.
- Donald, R.G.K., Zhong, T., Meijer, L., and Liberator, P.A. (2005). Characterization of two *T. gondii* CK1 isoforms. *Mol. Biochem. Parasitol.* *141*, 15–27.
- Dong, G., Filho, A.L., and Olivier, M. (2019). Modulation of Host-Pathogen Communication by Extracellular Vesicles (EVs) of the Protozoan Parasite *Leishmania*. *Front. Cell. Infect. Microbiol.* *9*.
- Dorin-Semlat, D., Demarta-Gatsi, C., Hamelin, R., Armand, F., Carvalho, T.G., Moniatte, M., and Doerig, C. (2015). Malaria Parasite-Infected Erythrocytes Secrete PfCK1, the Plasmodium Homologue of the Pleiotropic Protein Kinase Casein Kinase 1. *PLOS ONE* *10*, e0139591.
- Dostálová, A., and Volf, P. (2012). *Leishmania* development in sand flies: parasite-vector interactions overview. *Parasit. Vectors* *5*, 276.

- Doyle, P.S., Engel, J.C., Pimenta, P.F., da Silva, P.P., and Dwyer, D.M. (1991). *Leishmania donovani*: long-term culture of axenic amastigotes at 37 degrees C. *Exp. Parasitol.* *73*, 326–334.
- Dubois, T., Howell, S., Zemlickova, E., and Aitken, A. (2002). Identification of casein kinase I $\alpha$  interacting protein partners. *FEBS Lett.* *517*, 167–171.
- Dumetz, F., Imamura, H., Sanders, M., Seblova, V., Myskova, J., Pescher, P., Vanaerschot, M., Meehan, C.J., Cuyppers, B., De, G.M., et al. (2017). Modulation of Aneuploidy in *Leishmania donovani* during Adaptation to Different In Vitro and In Vivo Environments and Its Impact on Gene Expression. *MBio* *8*.
- Dunning, N. (2009). *Leishmania* vaccines: from leishmanization to the era of DNA technology. *Biosci. Horiz. Int. J. Stud. Res.* *2*, 73–82.
- Durieu, E., Prina, E., Leclercq, O., Oumata, N., Gaboriaud-Kolar, N., Vougianniopoulou, K., Aulner, N., Defontaine, A., No, J.H., Ruchaud, S., et al. (2016). From Drug Screening to Target Deconvolution: a Target-Based Drug Discovery Pipeline Using *Leishmania* Casein Kinase 1 Isoform 2 To Identify Compounds with Antileishmanial Activity. *Antimicrob. Agents Chemother.* *60*, 2822–2833.
- El Kasmi, I., Khadivjam, B., Lackman, M., Duron, J., Bonneil, E., Thibault, P., and Lippé, R. (2018). Extended Synaptotagmin 1 Interacts with Herpes Simplex Virus 1 Glycoprotein M and Negatively Modulates Virus-Induced Membrane Fusion. *J. Virol.* *92*.
- Fabregat, A., Jupe, S., Matthews, L., Sidiropoulos, K., Gillespie, M., Garapati, P., Haw, R., Jassal, B., Korninger, F., May, B., et al. (2018). The Reactome Pathway Knowledgebase. *Nucleic Acids Res.* *46*, D649–D655.
- Fardilha, M., Esteves, S.L.C., Korrodi-Gregório, L., Vintém, A.P., Domingues, S.C., Rebelo, S., Morrice, N., Cohen, P.T.W., Silva, O.A.B. da C. e, and Silva, E.F. da C. e (2011). Identification of the human testis protein phosphatase 1 interactome. *Biochem. Pharmacol.* *82*, 1403–1415.
- Fiuza, J.A., Dey, R., Davenport, D., Abdeladhim, M., Meneses, C., Oliveira, F., Kamhawi, S., Valenzuela, J.G., Gannavaram, S., and Nakhasi, H.L. (2016). Intra-dermal Immunization of *Leishmania donovani* Centrin Knock-Out Parasites in Combination with Salivary Protein LJM19 from Sand Fly Vector Induces a Durable Protective Immune Response in Hamsters. *PLoS Negl. Trop. Dis.* *10*, e0004322.
- Flegontov, P., Votýpka, J., Skalický, T., Logacheva, M.D., Penin, A.A., Tanifuji, G., Onodera, N.T., Kondrashov, A.S., Volf, P., Archibald, J.M., et al. (2013). *Paratrypanosoma* is a novel early-branching trypanosomatid. *Curr. Biol. CB* *23*, 1787–1793.
- Flotow, H., and Roach, P.J. (1991). Role of acidic residues as substrate determinants for casein kinase I. *J. Biol. Chem.* *266*, 3724–3727.
- Flotow, H., Graves, P.R., Wang, A.Q., Fiol, C.J., Roeske, R.W., and Roach, P.J. (1990). Phosphate groups as substrate determinants for casein kinase I action. *J. Biol. Chem.* *265*, 14264–14269.

- Forestier, C.-L., Gao, Q., and Boons, G.-J. (2015). Leishmania lipophosphoglycan: how to establish structure-activity relationships for this highly complex and multifunctional glycoconjugate? *Front. Cell. Infect. Microbiol.* *4*.
- Fu, Z., Chakraborti, T., Morse, S., Bennett, G.S., and Shaw, G. (2001). Four Casein Kinase I Isoforms Are Differentially Partitioned between Nucleus and Cytoplasm. *Exp. Cell Res.* *269*, 275–286.
- Fulcher, L.J., Bozatz, P., Tachie-Menson, T., Wu, K.Z.L., Cummins, T.D., Bufton, J.C., Pinkas, D.M., Dunbar, K., Shrestha, S., Wood, N.T., et al. (2018). The DUF1669 domain of FAM83 family proteins anchor Casein Kinase 1 isoforms. *Sci. Signal.* *11*.
- Fulcher, L.J., He, Z., Mei, L., Macartney, T.J., Wood, N.T., Prescott, A.R., Whigham, A.J., Varghese, J., Gourlay, R., Ball, G., et al. (2019). FAM83D directs protein kinase CK1 $\alpha$  to the mitotic spindle for proper spindle positioning. *EMBO Rep.* e47495–e47495.
- Galluzzi, L., Ceccarelli, M., Diotallevi, A., Menotta, M., and Magnani, M. (2018). Real-time PCR applications for diagnosis of leishmaniasis. *Parasit. Vectors* *11*, 273–273.
- Ghalei, H., Schaub, F.X., Doherty, J.R., Noguchi, Y., Roush, W.R., Cleveland, J.L., Stroupe, M.E., and Karbstein, K. (2015). Hrr25/CK1 $\delta$ -directed release of Ltv1 from pre-40S ribosomes is necessary for ribosome assembly and cell growth. *J. Cell Biol.* *208*, 745–759.
- Giamas, G., Hirner, H., Shoshiashvili, L., Grothey, A., Gessert, S., Kühl, M., Henne-Bruns, D., Vorgias, C.E., and Knippschild, U. (2007). Phosphorylation of CK1 $\delta$ : identification of Ser370 as the major phosphorylation site targeted by PKA in vitro and in vivo. *Biochem. J.* *406*, 389–398.
- Gietzen, K.F., and Virshup, D.M. (1999). Identification of Inhibitory Autophosphorylation Sites in Casein Kinase I  $\epsilon$ . *J. Biol. Chem.* *274*, 32063–32070.
- Gomes, R., and Oliveira, F. (2012). The immune response to sand fly salivary proteins and its influence on leishmania immunity. *Front. Immunol.* *3*, 110.
- Gomez, M.A., Contreras, I., Hallé, M., Tremblay, M.L., McMaster, R.W., and Olivier, M. (2009). Leishmania GP63 alters host signaling through cleavage-activated protein tyrosine phosphatases. *Sci. Signal.* *2*, ra58–ra58.
- González-Gaitán, M., and Jäckle, H. (1997). Role of Drosophila  $\alpha$ -Adaptin in Presynaptic Vesicle Recycling. *Cell* *88*, 767–776.
- Gossage, S.M., Rogers, M.E., and Bates, P.A. (2003). Two separate growth phases during the development of Leishmania in sand flies: implications for understanding the life cycle. *Int. J. Parasitol.* *33*, 1027–1034.
- Grant, B., and Hirsh, D. (1999). Receptor-mediated Endocytosis in the Caenorhabditis elegans Oocyte. *Mol. Biol. Cell* *10*, 4311–4326.
- Graves, P.R., and Roach, P.J. (1995). Role of COOH-terminal Phosphorylation in the Regulation of Casein Kinase I $\delta$ . *J. Biol. Chem.* *270*, 21689–21694.

- Gross, S.D., Hoffman, D.P., Fiset, P.L., Baas, P., and Anderson, R.A. (1995). A phosphatidylinositol 4,5-bisphosphate-sensitive casein kinase I alpha associates with synaptic vesicles and phosphorylates a subset of vesicle proteins. *J. Cell Biol.* *130*, 711–724.
- Gross, S.D., Loijens, J.C., and Anderson, R.A. (1999). The casein kinase Ialpha isoform is both physically positioned and functionally competent to regulate multiple events of mRNA metabolism. *J. Cell Sci.* *112*, 2647–2656.
- Gu, M., Liu, Q., Watanabe, S., Sun, L., Hollopeter, G., Grant, B.D., and Jorgensen, E.M. AP2 hemicomplexes contribute independently to synaptic vesicle endocytosis. *ELife* *2*.
- Guerin, P.J., Olliaro, P., Sundar, S., Boelaert, M., Croft, S.L., Desjeux, P., Wasunna, M.K., and Bryceson, A.D.M. (2002). Visceral leishmaniasis: current status of control, diagnosis, and treatment, and a proposed research and development agenda. *Lancet Infect. Dis.* *2*, 494–501.
- Hagemann, A.I., Kurz, J., Kauffeld, S., Chen, Q., Reeves, P.M., Weber, S., Schindler, S., Davidson, G., Kirchhausen, T., and Scholpp, S. (2014). In vivo analysis of formation and endocytosis of the Wnt/ $\beta$ -catenin signaling complex in zebrafish embryos. *J. Cell Sci.* *127*, 3970–3982.
- Hall, B.S., Gabernet-Castello, C., Voak, A., Goulding, D., Natesan, S.K., and Field, M.C. (2006). TbVps34, the trypanosome orthologue of Vps34, is required for Golgi complex segregation. *J. Biol. Chem.* *281*, 27600–27612.
- Hammarsten, O. (1883). Zur Frage ob Casein ein einheitlicher Stoff sei. *Hoppe Seylers Z Physiol Chem* *7*, 227–273.
- Hanks, S.K., and Hunter, T. (1995). Protein kinases 6. The eukaryotic protein kinase superfamily: kinase (catalytic) domain structure and classification. *FASEB J.* *9*, 576–596.
- Hanks, S.K., Quinn, A.M., and Hunter, T. (1988). The protein kinase family: conserved features and deduced phylogeny of the catalytic domains. *Science* *241*, 42–52.
- Hardin, A.O., Meals, E.A., Yi, T., Knapp, K.M., and English, B.K. (2006). SHP-1 inhibits LPS-mediated TNF and iNOS production in murine macrophages. *Biochem. Biophys. Res. Commun.* *342*, 547–555.
- Harrison, R.E., and Grinstein, S. (2002). Phagocytosis and the microtubule cytoskeleton. *Biochem. Cell Biol. Biochim. Biol. Cell.* *80*, 509–515.
- Hassan, P., Fergusson, D., Grant, K.M., and Mottram, J.C. (2001). The CRK3 protein kinase is essential for cell cycle progression of *Leishmania mexicana*. *Mol. Biochem. Parasitol.* *113*, 189–198.
- Hassani, K., Shio, M.T., Martel, C., Faubert, D., and Olivier, M. (2014). Absence of metalloprotease GP63 alters the protein content of *Leishmania* exosomes. *PloS One* *9*, e95007–e95007.
- Hein, M.Y., Hubner, N.C., Poser, I., Cox, J., Nagaraj, N., Toyoda, Y., Gak, I.A., Weisswange, I., Mansfeld, J., Buchholz, F., et al. (2015). A Human Interactome in Three Quantitative Dimensions Organized by Stoichiometries and Abundances. *Cell* *163*, 712–723.

- Hirner, H., Günes, C., Bischof, J., Wolff, S., Grothey, A., Köhl, M., Oswald, F., Wegwitz, F., Bösl, M.R., Trauzold, A., et al. (2012). Impaired CK1 Delta Activity Attenuates SV40-Induced Cellular Transformation In Vitro and Mouse Mammary Carcinogenesis In Vivo. *PLOS ONE* 7, e29709.
- Hodgkinson, V.H., Soong, L., Duboise, S.M., and McMahon-Pratt, D. (1996). *Leishmania amazonensis*: cultivation and characterization of axenic amastigote-like organisms. *Exp. Parasitol.* 83, 94–105.
- Hoekstra, M.F., Liskay, R.M., Ou, A.C., DeMaggio, A.J., Burbee, D.G., and Heffron, F. (1991). HRR25, a putative protein kinase from budding yeast: association with repair of damaged DNA. *Science* 253, 1031–1034.
- Ilg, T. (2000). Proteophosphoglycans of *Leishmania*. *Parasitol. Today Pers. Ed* 16, 489–497.
- Inbar, E., Hughitt, V.K., Dillon, L.A.L., Ghosh, K., El-Sayed, N.M., and Sacks, D.L. (2017). The Transcriptome of *Leishmania major* Developmental Stages in Their Natural Sand Fly Vector. *MBio* 8, e00029-17.
- Isnard, A., Shio, M.T., and Olivier, M. (2012). Impact of *Leishmania* metalloprotease GP63 on macrophage signaling. *Front. Cell. Infect. Microbiol.* 2.
- Isnard, A., Christian, J.G., Kodiha, M., Stochaj, U., McMaster, W.R., and Olivier, M. (2015). Impact of *Leishmania* infection on host macrophage nuclear physiology and nucleopore complex integrity. *PLoS Pathog.* 11, e1004776–e1004776.
- Ives, A., Ronet, C., Prevel, F., Ruzzante, G., Fuertes-Marraco, S., Schutz, F., Zangger, H., Revaz-Breton, M., Lye, L.F., Hickerson, S.M., et al. (2011). *Leishmania* RNA virus controls the severity of mucocutaneous leishmaniasis. *Science* 331, 775–778.
- Jackson, L.P., Kelly, B.T., McCoy, A.J., Gaffry, T., James, L.C., Collins, B.M., Höning, S., Evans, P.R., and Owen, D.J. (2010). A Large-Scale Conformational Change Couples Membrane Recruitment to Cargo Binding in the AP2 Clathrin Adaptor Complex. *Cell* 141, 1220–1229.
- Jayaswal, S., Kamal, M.A., Dua, R., Gupta, S., Majumdar, T., Das, G., Kumar, D., and Rao, K.V.S. (2010). Identification of Host-Dependent Survival Factors for Intracellular *Mycobacterium tuberculosis* through an siRNA Screen. *PLOS Pathog.* 6, e1000839.
- Jha, T.K., Sundar, S., Thakur, C.P., Bachmann, P., Karbwang, J., Fischer, C., Voss, A., and Berman, J. (1999). Miltefosine, an oral agent, for the treatment of Indian visceral leishmaniasis. *N. Engl. J. Med.* 341, 1795–1800.
- Jiang, S., Zhang, M., Sun, J., and Yang, X. (2018). Casein kinase 1 $\alpha$ : biological mechanisms and theranostic potential. *Cell Commun. Signal.* 16, 23.
- Johnson, A.E., Chen, J.-S., and Gould, K.L. (2013). CK1 Is Required for a Mitotic Checkpoint that Delays Cytokinesis. *Curr. Biol.* 23, 1920–1926.
- Kalb, L.C., Frederico, Y.C.A., Boehm, C., Moreira, C.M. do N., Soares, M.J., and Field, M.C. (2016). Conservation and divergence within the clathrin interactome of *Trypanosoma cruzi*. *Sci. Rep.* 6, 31212.

- Karayel, Ö., Şanal, E., Giese, S.H., Kagiyalı, Z.C.Ü., Polat, A.N., Hu, C.-K., Renard, B.Y., Tuncbag, N., and Özlü, N. (2018). Comparative phosphoproteomic analysis reveals signaling networks regulating monopolar and bipolar cytokinesis. *Sci. Rep.* 8, 2269.
- Käser, S., Willemin, M., Schnarwiler, F., Schimanski, B., Poveda-Huertes, D., Oeljeklaus, S., Haenni, B., Zuber, B., Warscheid, B., Meisinger, C., et al. (2017). Biogenesis of the mitochondrial DNA inheritance machinery in the mitochondrial outer membrane of *Trypanosoma brucei*. *PLOS Pathog.* 13, e1006808.
- Kassi, M., Kassi, M., Afghan, A.K., Rehman, R., and Kasi, P.M. (2008). Marring leishmaniasis: the stigmatization and the impact of cutaneous leishmaniasis in Pakistan and Afghanistan. *PLoS Negl. Trop. Dis.* 2, e259–e259.
- Kattapuram, T., Yang, S., Maki, J.L., and Stone, J.R. (2005). Protein Kinase CK1 $\alpha$  Regulates mRNA Binding by Heterogeneous Nuclear Ribonucleoprotein C in Response to Physiologic Levels of Hydrogen Peroxide. *J. Biol. Chem.* 280, 15340–15347.
- Kawakami, F., Suzuki, K., and Ohtsuki, K. (2008). A Novel Consensus Phosphorylation Motif in Sulfatide- and Cholesterol-3-sulfate-Binding Protein Substrates for CK1 in Vitro. *Biol. Pharm. Bull.* 31, 193–200.
- Killick-Kendrick, R. (1999). The biology and control of phlebotomine sand flies. *Clin. Dermatol.* 17, 279–289.
- Kishore, K., Kumar, V., Kesari, S., Dinesh, D.S., Kumar, A.J., Das, P., and Bhattacharya, S.K. (2006). Vector control in leishmaniasis. *Indian J. Med. Res.* 123, 467–472.
- Knippschild, U., Milne, D.M., Campbell, L.E., DeMaggio, A.J., Christenson, E., Hoekstra, M.F., and Meek, D.W. (1997). p53 is phosphorylated in vitro and in vivo by the delta and epsilon isoforms of casein kinase 1 and enhances the level of casein kinase 1 delta in response to topoisomerase-directed drugs. *Oncogene* 15, 1727–1736.
- Knippschild, U., Wolff, S., Giamas, G., Brockschmidt, C., Wittau, M., Würfl, P.U., Eismann, T., and Stöter, M. (2005a). The Role of the Casein Kinase 1 (CK1) Family in Different Signaling Pathways Linked to Cancer Development. *Oncol. Res. Treat.* 28, 508–514.
- Knippschild, U., Gocht, A., Wolff, S., Huber, N., Löhler, J., and Stöter, M. (2005b). The casein kinase 1 family: participation in multiple cellular processes in eukaryotes. *Cell. Signal.* 17, 675–689.
- Knippschild, U., Kruger, M., Richter, J., Xu, P., Garcia-Reyes, B., Peifer, C., Halekotte, J., Bakulev, V., and Bischof, J. (2014). The CK1 Family: Contribution to Cellular Stress Response and Its Role in Carcinogenesis. *Front Oncol* 4, 96.
- Knockenbauer, K.E., and Schwartz, T.U. (2016). The Nuclear Pore Complex as a Flexible and Dynamic Gate. *Cell* 164, 1162–1171.
- de La Llave, E., Lecoœur, H., Besse, A., Milon, G., Prina, E., and Lang, T. (2011). A combined luciferase imaging and reverse transcription polymerase chain reaction assay for the study of *Leishmania amastigote* burden and correlated mouse tissue transcript fluctuations. *Cell. Microbiol.* 13, 81–91.

- Lamotte, S., Späth, G.F., Rachidi, N., and Prina, E. (2017). The enemy within: Targeting host–parasite interaction for antileishmanial drug discovery. *PLoS Negl. Trop. Dis.* *11*.
- Lander, N., Li, Z.H., Niyogi, S., and Docampo, R. (2015). CRISPR/Cas9-Induced Disruption of Paraflagellar Rod Protein 1 and 2 Genes in *Trypanosoma cruzi* Reveals Their Role in Flagellar Attachment. *MBio* *6*, e01012–e01012.
- Lasa, M., Marin, O., and Pinna, L.A. (1997). Rat Liver Golgi Apparatus Contains a Protein Kinase Similar to the Casein Kinase of Lactating Mammary Gland. *Eur. J. Biochem.* *243*, 719–725.
- Leevers, S.J., Vanhaesebroeck, B., and Waterfield, M.D. (1999). Signalling through phosphoinositide 3-kinases: the lipids take centre stage. *Curr. Opin. Cell Biol.* *11*, 219–225.
- Lemmon, S.K., and Traub, L.M. (2012). Getting in touch with the clathrin terminal domain. *Traffic Cph. Den.* *13*, 511–519.
- Li, X., Wilmanns, M., Thornton, J., and Köhn, M. (2013). Elucidating Human Phosphatase-Substrate Networks. *Sci. Signal.* *6*, rs10–rs10.
- Lindberg, R.A., Quinn, A.M., and Hunter, T. (1992). Dual-specificity protein kinases: will any hydroxyl do? *Trends Biochem. Sci.* *17*, 114–119.
- Liu, J., Carvalho, L.P., Bhattacharya, S., Carbone, C.J., Kumar, K.G.S., Leu, N.A., Yau, P.M., Donald, R.G.K., Weiss, M.J., Baker, D.P., et al. (2009). Mammalian Casein Kinase 1 $\alpha$  and Its Leishmanial Ortholog Regulate Stability of IFNAR1 and Type I Interferon Signaling. *Mol. Cell. Biol.* *29*, 6401–6412.
- Liu, Q., Lei, J., and Kadowaki, T. (2019). Gene Disruption of Honey Bee Trypanosomatid Parasite, *Lotmaria passim*, by CRISPR/Cas9 System. *Front. Cell. Infect. Microbiol.* *9*, 126–126.
- Löhler, J., Hirner, H., Schmidt, B., Kramer, K., Fischer, D., Thal, D.R., Leithäuser, F., and Knippschild, U. (2009). Immunohistochemical Characterisation of Cell-Type Specific Expression of CK1 $\delta$  in Various Tissues of Young Adult BALB/c Mice. *PLOS ONE* *4*, e4174.
- Longenecker, K.L., Roach, P.J., and Hurley, T.D. (1996). Three-dimensional Structure of Mammalian Casein Kinase I: Molecular Basis for Phosphate Recognition. *J. Mol. Biol.* *257*, 618–631.
- Lu, P., Li, H., Li, N., Singh, R.N., Bishop, C.E., Chen, X., and Lu, B. (2017). MEX3C interacts with adaptor-related protein complex 2 and involves in miR-451a exosomal sorting. *PLoS ONE* *12*.
- Luo, W., Peterson, A., Garcia, B.A., Coombs, G., Kofahl, B., Heinrich, R., Shabanowitz, J., Hunt, D.F., Yost, H.J., and Virshup, D.M. (2007). Protein phosphatase 1 regulates assembly and function of the  $\beta$ -catenin degradation complex. *EMBO J.* *26*, 1511–1521.
- Lusk, C.P., Waller, D.D., Makhnevych, T., Dienemann, A., Whiteway, M., Thomas, D.Y., and Wozniak, R.W. Nup53p is a Target of Two Mitotic Kinases, Cdk1p and Hrr25p. *Traffic* *8*, 647–660.

- Madeira, F., Park, Y.M., Lee, J., Buso, N., Gur, T., Madhusoodanan, N., Basutkar, P., Tivey, A.R.N., Potter, S.C., Finn, R.D., et al. (2019). The EMBL-EBI search and sequence analysis tools APIs in 2019. *Nucleic Acids Res.*
- Manna, P.T., Kelly, S., and Field, M.C. (2013). Adaptin evolution in kinetoplastids and emergence of the variant surface glycoprotein coat in African trypanosomatids. *Mol. Phylogenet. Evol.* *67*, 123–128.
- Manning, G., Whyte, D.B., Martinez, R., Hunter, T., and Sudarsanam, S. (2002). The protein kinase complement of the human genome. *Science* *298*, 1912–1934.
- Marin, O., Meggio, F., and Pinna, L.A. (1994). Design and Synthesis of Two New Peptide Substrates for the Specific and Sensitive Monitoring of Casein Kinases 1 and 2. *Biochem. Biophys. Res. Commun.* *198*, 898–905.
- Marin, O., Bustos, V.H., Cesaro, L., Meggio, F., Pagano, M.A., Antonelli, M., Allende, C.C., Pinna, L.A., and Allende, J.E. (2003). A noncanonical sequence phosphorylated by casein kinase 1 in  $\beta$ -catenin may play a role in casein kinase 1 targeting of important signaling proteins. *Proc. Natl. Acad. Sci.* *100*, 10193–10200.
- Maroli, M., Feliciangeli, M.D., Bichaud, L., Charrel, R.N., and Gradoni, L. (2013). Phlebotomine sandflies and the spreading of leishmaniasis and other diseases of public health concern. *Med. Vet. Entomol.* *27*, 123–147.
- Martel, D., Beneke, T., Gluenz, E., Späth, G.F., and Rachidi, N. (2017). Characterisation of Casein Kinase 1.1 in *Leishmania donovani* Using the CRISPR Cas9 Toolkit. *BioMed Res. Int.* *2017*, 4635605.
- Matkin, A., Das, A., and Bellofatto, V. (2001). The *Leptomonas seymouri* spliced leader RNA promoter requires a novel transcription factor. *Int. J. Parasitol.* *31*, 545–549.
- Matte, C., and Descoteaux, A. (2016). Exploitation of the Host Cell Membrane Fusion Machinery by *Leishmania* Is Part of the Infection Process. *PLoS Pathog.* *12*.
- McKenzie, J.A.G., Riento, K., and Ridley, A.J. (2006). Casein kinase I $\epsilon$  associates with and phosphorylates the tight junction protein occludin. *FEBS Lett.* *580*, 2388–2394.
- Mendes-Sousa, A.F., Do, V.V., Silva, N.C.S., Guimaraes-Costa, A.B., Pereira, M.H., Sant’Anna, M.R.V., Oliveira, F., Kamhawi, S., Ribeiro, J.M.C., Andersen, J.F., et al. (2017). The Sand Fly Salivary Protein Lufaxin Inhibits the Early Steps of the Alternative Pathway of Complement by Direct Binding to the Proconvertase C3b-B. *Front. Immunol.* *8*, 1065–1065.
- Menezes, J.P.B., Almeida, T.F., Petersen, A.L.O.A., Guedes, C.E.S., Mota, M.S.V., Lima, J.G.B., Palma, L.C., Buck, G.A., Krieger, M.A., Probst, C.M., et al. (2013). Proteomic analysis reveals differentially expressed proteins in macrophages infected with *Leishmania amazonensis* or *Leishmania major*. *Microbes Infect.* *15*, 579–591.
- Mettlen, M., Chen, P.H., Srinivasan, S., Danuser, G., and Schmid, S.L. (2018). Regulation of Clathrin-Mediated Endocytosis. *Annu. Rev. Biochem.* *87*, 871–896.

- Minia, I., and Clayton, C. (2016). Regulating a Post-Transcriptional Regulator: Protein Phosphorylation, Degradation and Translational Blockage in Control of the Trypanosome Stress-Response RNA-Binding Protein ZC3H11. *PLoS Pathog.* *12*, e1005514–e1005514.
- Minzel, W., Venkatachalam, A., Fink, A., Hung, E., Brachya, G., Burstain, I., Shaham, M., Rivlin, A., Omer, I., Zinger, A., et al. (2018). Small Molecules Co-targeting CKI $\alpha$  and the Transcriptional Kinases CDK7/9 Control AML in Preclinical Models. *Cell* *175*, 171–185.e25.
- Miranda-Saavedra, D., and Barton, G.J. (2007). Classification and functional annotation of eukaryotic protein kinases. *Proteins Struct. Funct. Bioinforma.* *68*, 893–914.
- Moafi, M., Rezvan, H., Sherkat, R., and Taleban, R. (2019). Leishmania Vaccines Entered in Clinical Trials: A Review of Literature. *Int. J. Prev. Med.* *10*, 95–95.
- Molina, R., Gradoni, L., and Alvar, J. (2003). HIV and the transmission of Leishmania. *Ann. Trop. Med. Parasitol.* *97 Suppl 1*, 29–45.
- Mondelaers, A., Sanchez-Cañete, M.P., Hendrickx, S., Eberhardt, E., Garcia-Hernandez, R., Lachaud, L., Cotton, J., Sanders, M., Cuyper, B., Imamura, H., et al. (2016). Genomic and Molecular Characterization of Miltefosine Resistance in Leishmania infantum Strains with Either Natural or Acquired Resistance through Experimental Selection of Intracellular Amastigotes. *PloS One* *11*, e0154101.
- Monnerat, S., Clucas, C., Brown, E., Mottram, J.C., and Hammarton, T.C. (2009). Searching for novel cell cycle regulators in Trypanosoma brucei with an RNA interference screen. *BMC Res. Notes* *2*, 46–46.
- Moore, K.J., and Matlashewski, G. (1994). Intracellular infection by Leishmania donovani inhibits macrophage apoptosis. *J. Immunol.* *152*, 2930–2937.
- Moreira, D., Rodrigues, V., Abengoza, M., Rivas, L., Rial, E., Laforge, M., Li, X., Foretz, M., Viollet, B., Estaquier, J., et al. (2015). Leishmania infantum Modulates Host Macrophage Mitochondrial Metabolism by Hijacking the SIRT1-AMPK Axis. *PLOS Pathog.* *11*, e1004684.
- Morgan, G.W., Hall, B.S., Denny, P.W., Field, M.C., and Carrington, M. (2002). The endocytic apparatus of the kinetoplastida. Part II: machinery and components of the system. *Trends Parasitol.* *18*, 540–546.
- Mottram, J.C., and Smith, G. (1995). A family of trypanosome cdc2-related protein kinases. *Gene* *162*, 147–152.
- Mullin, K.A., Foth, B.J., Ilgoutz, S.C., Callaghan, J.M., Zawadzki, J.L., McFadden, G.I., and McConville, M.J. (2001). Regulated Degradation of an Endoplasmic Reticulum Membrane Protein in a Tubular Lysosome in Leishmania mexicana. *Mol. Biol. Cell* *12*, 2364–2377.
- Nagill, R., and Kaur, S. (2011). Vaccine candidates for leishmaniasis: a review. *Int. Immunopharmacol.* *11*, 1464–1488.
- Nandan, D., and Reiner, N.E. (1995). Attenuation of gamma interferon-induced tyrosine phosphorylation in mononuclear phagocytes infected with Leishmania donovani: selective inhibition of signaling through Janus kinases and Stat1. *Infect. Immun.* *63*, 4495–4500.

- Nandan, D., Yi, T., Lopez, M., Lai, C., and Reiner, N.E. (2002). Leishmania EF-1 $\alpha$  Activates the Src Homology 2 Domain Containing Tyrosine Phosphatase SHP-1 Leading to Macrophage Deactivation. *J. Biol. Chem.* *277*, 50190–50197.
- Nett, I.R., Davidson, L., Lamont, D., and Ferguson, M.A. (2009a). Identification and specific localization of tyrosine-phosphorylated proteins in *Trypanosoma brucei*. *Eukaryot. Cell* *8*, 617–626.
- Nett, I.R., Martin, D.M., Miranda-Saavedra, D., Lamont, D., Barber, J.D., Mehlert, A., and Ferguson, M.A. (2009b). The phosphoproteome of bloodstream form *Trypanosoma brucei*, causative agent of African sleeping sickness. *Mol. Cell. Proteomics MCP* *8*, 1527–1538.
- Nezis, I.P., Sagona, A.P., Schink, K.O., and Stenmark, H. (2010). Divide and ProsPer: the emerging role of PtdIns3P in cytokinesis. *Trends Cell Biol.* *20*, 642–649.
- Nishi, H., Shaytan, A., and Panchenko, A.R. (2014). Physicochemical mechanisms of protein regulation by phosphorylation. *Front. Genet.* *5*, 270.
- Obado, S.O., Brillantes, M., Uryu, K., Zhang, W., Ketaren, N.E., Chait, B.T., Field, M.C., and Rout, M.P. (2016). Interactome Mapping Reveals the Evolutionary History of the Nuclear Pore Complex. *PLoS Biol.* *14*, e1002365–e1002365.
- Okwor, I., and Uzonna, J. (2016). Social and Economic Burden of Human Leishmaniasis. *Am. J. Trop. Med. Hyg.* *94*, 489–493.
- Olivier, M., Gregory, D.J., and Forget, G. (2005). Subversion Mechanisms by Which *Leishmania* Parasites Can Escape the Host Immune Response: a Signaling Point of View. *Clin. Microbiol. Rev.* *18*, 293–305.
- Osman, M., Mistry, A., Keding, A., Gabe, R., Cook, E., Forrester, S., Wiggins, R., Di, S.M., Colloca, S., Siani, L., et al. (2017). A third generation vaccine for human visceral leishmaniasis and post kala azar dermal leishmaniasis: First-in-human trial of ChAd63-KH. *PLoS Negl. Trop. Dis.* *11*, e0005527–e0005527.
- Osorio, J. y F., De, E.L.L., Regnault, B., Coppée, J.Y., Milon, G., Lang, T., and Prina, E. (2009). Transcriptional signatures of BALB/c mouse macrophages housing multiplying *Leishmania amazonensis* amastigotes. *BMC Genomics* *10*, 119–119.
- Paape, D., Barrios-Llerena, M.E., Le, T.B., Mackay, L., and Aebischer, T. (2010). Gel free analysis of the proteome of intracellular *Leishmania mexicana*. *Mol. Biochem. Parasitol.* *169*, 108–114.
- Palfi, Z., Jaé, N., Preusser, C., Kaminska, K.H., Bujnicki, J.M., Lee, J.H., Günzl, A., Kambach, C., Urlaub, H., and Bindereif, A. (2009). SMN-assisted assembly of snRNP-specific Sm cores in trypanosomes. *Genes Dev.* *23*, 1650–1664.
- Panek, H.R., Stepp, J.D., Engle, H.M., Marks, K.M., Tan, P.K., Lemmon, S.K., and Robinson, L.C. (1997). Suppressors of YCK-encoded yeast casein kinase 1 deficiency define the four subunits of a novel clathrin AP-like complex. *EMBO J.* *16*, 4194–4204.
- Papadopoulou, B., Roy, G., and Ouellette, M. (1994). Autonomous replication of bacterial DNA plasmid oligomers in *Leishmania*. *Mol. Biochem. Parasitol.* *65*, 39–49.

- Parsons, M., Valentine, M., Deans, J., Schieven, G.L., and Ledbetter, J.A. (1991). Distinct patterns of tyrosine phosphorylation during the life cycle of *Trypanosoma brucei*. *Mol. Biochem. Parasitol.* *45*, 241–248.
- Parsons, M., Worthey, E.A., Ward, P.N., and Mottram, J.C. (2005). Comparative analysis of the kinomes of three pathogenic trypanosomatids: *Leishmania major*, *Trypanosoma brucei* and *Trypanosoma cruzi*. *BMC Genomics* *6*, 127.
- Peng, D., and Tarleton, R. (2015). EuPaGDT: a web tool tailored to design CRISPR guide RNAs for eukaryotic pathogens. *Microb. Genomics* *1*.
- Peng, D., Kurup, S.P., Yao, P.Y., Minning, T.A., and Tarleton, R.L. (2015a). CRISPR-Cas9-mediated single-gene and gene family disruption in *Trypanosoma cruzi*. *MBio* *6*, e02097-14.
- Peng, Y., Grassart, A., Lu, R., Wong, C.C.L., Yates, J., Barnes, G., and Drubin, D.G. (2015b). Casein Kinase 1 Promotes Initiation of Clathrin-Mediated Endocytosis. *Dev. Cell* *32*, 231–240.
- Peng, Y., Moritz, M., Han, X., Giddings, T.H., Lyon, A., Kollman, J., Winey, M., Yates, J., Agard, D.A., Drubin, D.G., et al. (2015c). Interaction of CK1 $\delta$  with  $\gamma$ TuSC ensures proper microtubule assembly and spindle positioning. *Mol. Biol. Cell* *26*, 2505–2518.
- Petzold, G., Fischer, E.S., and Thomä, N.H. (2016). Structural basis of lenalidomide-induced CK1 $\alpha$  degradation by the CRL4<sup>CRBN</sup> ubiquitin ligase. *Nature* *532*, 127–130.
- Pimenta, P.F., Turco, S.J., McConville, M.J., Lawyer, P.G., Perkins, P.V., and Sacks, D.L. (1992). Stage-specific adhesion of *Leishmania* promastigotes to the sandfly midgut. *Science* *256*, 1812–1815.
- Pouillet, P., Carpentier, S., and Barillot, E. (2007). myProMS, a web server for management and validation of mass spectrometry-based proteomic data. *PROTEOMICS* *7*, 2553–2556.
- Ptacek, J., Devgan, G., Michaud, G., Zhu, H., Zhu, X., Fasolo, J., Guo, H., Jona, G., Breitkreutz, A., Sopko, R., et al. (2005). Global analysis of protein phosphorylation in yeast. *Nature* *438*, 679–684.
- Rabhi, I., Rabhi, S., Ben-Othman, R., Rasche, A., Daskalaki, A., Trentin, B., Piquemal, D., Regnault, B., Descoteaux, A., and Guizani-Tabbane, L. (2012). Transcriptomic signature of *Leishmania* infected mice macrophages: a metabolic point of view. *PLoS Negl. Trop. Dis.* *6*, e1763–e1763.
- Rachidi, N., Taly, J.F., Durieu, E., Leclercq, O., Aulner, N., Prina, E., Pescher, P., Notredame, C., Meijer, L., and Späth, G.F. (2014). Pharmacological Assessment Defines *Leishmania donovani* Casein Kinase 1 as a Drug Target and Reveals Important Functions in Parasite Viability and Intracellular Infection. *Antimicrob. Agents Chemother.* *58*, 1501–1515.
- Ranjan, A., Sur, D., Singh, V.P., Siddique, N.A., Manna, B., Lal, C.S., Sinha, P.K., Kishore, K., and Bhattacharya, S.K. (2005). Risk factors for Indian kala-azar. *Am. J. Trop. Med. Hyg.* *73*, 74–78.

- Ray, P., Basu, U., Ray, A., Majumdar, R., Deng, H., and Maitra, U. (2008). The *Saccharomyces cerevisiae* 60 S ribosome biogenesis factor Tif6p is regulated by Hrr25p-mediated phosphorylation. *J. Biol. Chem.* *283*, 9681–9691.
- Ready, P.D. (2013). Biology of phlebotomine sand flies as vectors of disease agents. *Annu. Rev. Entomol.* *58*, 227–250.
- Reed, S.G., Coler, R.N., Mondal, D., Kamhawi, S., and Valenzuela, J.G. (2016). Leishmania vaccine development: exploiting the host–vector–parasite interface. *Expert Rev. Vaccines* *15*, 81–90.
- Rico, E., Jeacock, L., Kovářová, J., and Horn, D. (2018). Inducible high-efficiency CRISPR-Cas9-targeted gene editing and precision base editing in African trypanosomes. *Sci. Rep.* *8*, 7960–7960.
- Rivers, A., Gietzen, K.F., Vielhaber, E., and Virshup, D.M. (1998). Regulation of Casein Kinase I  $\epsilon$  and Casein Kinase I  $\delta$  by an in Vivo Futile Phosphorylation Cycle. *J. Biol. Chem.* *273*, 15980–15984.
- Robinson, C.L., Chong, A.C.N., Ashbrook, A.W., Jeng, G., Jin, J., Chen, H., Tang, E.I., Martin, L.A., Kim, R.S., Kenyon, R.M., et al. (2018). Male germ cells support long-term propagation of Zika virus. *Nat. Commun.* *9*, 2090.
- Robinson, L.C., Hubbard, E.J., Graves, P.R., DePaoli-Roach, A.A., Roach, P.J., Kung, C., Haas, D.W., Hagedorn, C.H., Goebel, M., and Culbertson, M.R. (1992). Yeast casein kinase I homologues: an essential gene pair. *Proc. Natl. Acad. Sci.* *89*, 28–32.
- Rogers, M.B., Hilley, J.D., Dickens, N.J., Wilkes, J., Bates, P.A., Depledge, D.P., Harris, D., Her, Y., Herzyk, P., Imamura, H., et al. (2011). Chromosome and gene copy number variation allow major structural change between species and strains of *Leishmania*. *Genome Res.* *21*, 2129–2142.
- Roque, A.L.R., and Jansen, A.M. (2014). Wild and synanthropic reservoirs of *Leishmania* species in the Americas. *Int. J. Parasitol. Parasites Wildl.* *3*, 251–262.
- Rosenbluh, J., Mercer, J., Shrestha, Y., Oliver, R., Tamayo, P., Doench, J.G., Tirosh, I., Piccioni, F., Hartenian, E., Horn, H., et al. (2016). Genetic and Proteomic Interrogation of Lower Confidence Candidate Genes Reveals Signaling Networks in  $\beta$ -Catenin-Active Cancers. *Cell Syst.* *3*, 302-316.e4.
- Rosenzweig, D., Smith, D., Myler, P.J., Olafson, R.W., and Zilberstein, D. (2008a). Post-translational modification of cellular proteins during *Leishmania donovani* differentiation. *Proteomics* *8*, 1843–1850.
- Rosenzweig, D., Smith, D., Opperdoes, F., Stern, S., Olafson, R.W., and Zilberstein, D. (2008b). Retooling *Leishmania* metabolism: from sand fly gut to human macrophage. *FASEB J. Off. Publ. Fed. Am. Soc. Exp. Biol.* *22*, 590–602.
- Roskoski, R. (2015). A historical overview of protein kinases and their targeted small molecule inhibitors. *Pharmacol. Res.* *100*, 1–23.

- Rostislavleva, K., Soler, N., Ohashi, Y., Zhang, L., Pardon, E., Burke, J.E., Masson, G.R., Johnson, C., Steyaert, J., Ktistakis, N.T., et al. (2015). Structure and flexibility of the endosomal Vps34 complex reveals the basis of its function on membranes. *Science* *350*, aac7365.
- Roy, A., Kucukural, A., and Zhang, Y. (2010). I-TASSER: a unified platform for automated protein structure and function prediction. *Nat. Protoc.* *5*, 725–738.
- Russell, D.G., Xu, S., and Chakraborty, P. (1992). Intracellular trafficking and the parasitophorous vacuole of *Leishmania mexicana*-infected macrophages. *J. Cell Sci.* *103*, 1193–1210.
- Sacco, F., Perfetto, L., Castagnoli, L., and Cesareni, G. (2012). The human phosphatase interactome: An intricate family portrait. *FEBS Lett.* *586*, 2732–2739.
- Sacerdoti-Sierra, N., and Jaffe, C.L. (1997). Release of ecto-protein kinases by the protozoan parasite *Leishmania major*. *J. Biol. Chem.* *272*, 30760–30765.
- Sahu, R., Kaushik, S., Clement, C.C., Cannizzo, E.S., Scharf, B., Follenzi, A., Potalicchio, I., Nieves, E., Cuervo, A.M., and Santambrogio, L. (2011). Microautophagy of cytosolic proteins by late endosomes. *Dev. Cell* *20*, 131–139.
- Santarém, N., Racine, G., Silvestre, R., Cordeiro-da-Silva, A., and Ouellette, M. (2013). Exoproteome dynamics in *Leishmania infantum*. *J. Proteomics* *84*, 106–118.
- Saxena, A., Lahav, T., Holland, N., Aggarwal, G., Anupama, A., Huang, Y., Volpin, H., Myler, P.J., and Zilberstein, D. (2007). Analysis of the *Leishmania donovani* transcriptome reveals an ordered progression of transient and permanent changes in gene expression during differentiation. *Mol. Biochem. Parasitol.* *152*, 53–65.
- Schitteck, B., and Sinnberg, T. (2014). Biological functions of casein kinase 1 isoforms and putative roles in tumorigenesis. *Mol. Cancer* *13*.
- Schlein, Y., Jacobson, R.L., and Shlomai, J. (1991). Chitinase secreted by *Leishmania* functions in the sandfly vector. *Proc. Biol. Sci.* *245*, 121–126.
- Schumann Burkard, G., Jutzi, P., and Roditi, I. (2011). Genome-wide RNAi screens in bloodstream form trypanosomes identify drug transporters. *Mol. Biochem. Parasitol.* *175*, 91–94.
- Schuyler, S.C., Liu, J.Y., and Pellman, D. (2003). The molecular function of Ase1p: evidence for a MAP-dependent midzone-specific spindle matrix. Microtubule-associated proteins. *J. Cell Biol.* *160*, 517–528.
- Schwartz, P.A., and Murray, B.W. (2011). Protein kinase biochemistry and drug discovery. *Bioorganic Chem.* *39*, 192–210.
- Scianimanico, S., Desrosiers, M., Dermine, J.F., Meresse, S., Descoteaux, A., and Desjardins, M. (1999). Impaired recruitment of the small GTPase rab7 correlates with the inhibition of phagosome maturation by *Leishmania donovani* promastigotes. *Cell Microbiol* *1*, 19–32.

- Seyed, N., Peters, N.C., and Rafati, S. (2018). Translating Observations From Leishmanization Into Non-Living Vaccines: The Potential of Dendritic Cell-Based Vaccination Strategies Against Leishmania. *Front. Immunol.* *9*, 1227–1227.
- Shao, S., Sun, X., Chen, Y., Zhan, B., and Zhu, X. (2019). Complement Evasion: An Effective Strategy That Parasites Utilize to Survive in the Host. *Front. Microbiol.* *10*.
- Shio, M.T., Christian, J.G., Jung, J.Y., Chang, K.P., and Olivier, M. (2015). PKC/ROS-Mediated NLRP3 Inflammasome Activation Is Attenuated by Leishmania Zinc-Metalloprotease during Infection. *PLoS Negl. Trop. Dis.* *9*, e0003868–e0003868.
- Sillibourne, J.E., Milne, D.M., Takahashi, M., Ono, Y., and Meek, D.W. (2002). Centrosomal Anchoring of the Protein Kinase CK1 $\delta$  Mediated by Attachment to the Large, Coiled-coil Scaffolding Protein CG-NAP/AKAP450. *J. Mol. Biol.* *322*, 785–797.
- Silverman, J.M., Chan, S.K., Robinson, D.P., Dwyer, D.M., Nandan, D., Foster, L.J., and Reiner, N.E. (2008). Proteomic analysis of the secretome of *Leishmania donovani*. *Genome Biol* *9*, R35.
- Silverman, J.M., Clos, J., de'Oliveira, C.C., Shirvani, O., Fang, Y., Wang, C., Foster, L.J., and Reiner, N.E. (2010a). An exosome-based secretion pathway is responsible for protein export from *Leishmania* and communication with macrophages. *J Cell Sci* *123*, 842–852.
- Silverman, J.M., Clos, J., Horakova, E., Wang, A.Y., Wiesgigl, M., Kelly, I., Lynn, M.A., McMaster, W.R., Foster, L.J., Levings, M.K., et al. (2010b). *Leishmania* exosomes modulate innate and adaptive immune responses through effects on monocytes and dendritic cells. *J Immunol* *185*, 5011–5022.
- Simpson, A.G.B., Stevens, J.R., and Lukeš, J. (2006). The evolution and diversity of kinetoplastid flagellates. *Trends Parasitol.* *22*, 168–174.
- Simpson, R.J., Jensen, S.S., and Lim, J.W.E. (2008). Proteomic profiling of exosomes: Current perspectives. *PROTEOMICS* *8*, 4083–4099.
- Singh, A.K., Pandey, R.K., Siqueira-Neto, J.L., Kwon, Y.-J., Freitas-Junior, L.H., Shaha, C., and Madhubala, R. (2015). Proteomic-Based Approach To Gain Insight into Reprogramming of THP-1 Cells Exposed to *Leishmania donovani* over an Early Temporal Window. *Infect. Immun.* *83*, 1853–1868.
- Singh, N., Kumar, M., and Singh, R.K. (2012). Leishmaniasis: current status of available drugs and new potential drug targets. *Asian Pac. J. Trop. Med.* *5*, 485–497.
- Smith, D.F., Peacock, C.S., and Cruz, A.K. (2007). Comparative genomics: From genotype to disease phenotype in the leishmaniasis. *Int. J. Parasitol.* *37*, 1173–1186.
- Sollelis, L., Ghorbal, M., MacPherson, C.R., Martins, R.M., Kuk, N., Crobu, L., Bastien, P., Scherf, A., Lopez-Rubio, J.J., and Sterkers, Y. (2015). First efficient CRISPR-Cas9-mediated genome editing in *Leishmania* parasites. *Cell Microbiol* *17*, 1405–1412.
- Solyakov, L., Halbert, J., Alam, M.M., Semblat, J.P., Dorin-Semblat, D., Reininger, L., Bottrill, A.R., Mistry, S., Abdi, A., Fennell, C., et al. (2011). Global kinomic and phospho-

- proteomic analyses of the human malaria parasite *Plasmodium falciparum*. *Nat. Commun.* *2*, 565–565.
- Songyang, Z., Lu, K.P., Kwon, Y.T., Tsai, L.H., Filhol, O., Cochet, C., Brickey, D.A., Soderling, T.R., Bartleson, C., Graves, D.J., et al. (1996). A structural basis for substrate specificities of protein Ser/Thr kinases: primary sequence preference of casein kinases I and II, NIMA, phosphorylase kinase, calmodulin-dependent kinase II, CDK5, and Erk1. *Mol. Cell. Biol.* *16*, 6486–6493.
- Spadafora, C., Repetto, Y., Torres, C., Pino, L., Robello, C., Morello, A., Gamarro, F., and Castanys, S. (2002). Two casein kinase 1 isoforms are differentially expressed in *Trypanosoma cruzi*. *Mol. Biochem. Parasitol.* *124*, 23–36.
- Späth, G.F., Schlesinger, P., Schreiber, R., and Beverley, S.M. (2009). A Novel Role for Stat1 in Phagosome Acidification and Natural Host Resistance to Intracellular Infection by *Leishmania major*. *PLOS Pathog.* *5*, e1000381.
- Spector, D.L., and Lamond, A.I. (2011). Nuclear Speckles. *Cold Spring Harb. Perspect. Biol.* *3*, a000646.
- Strambio-De-Castillia, C., Niepel, M., and Rout, M.P. (2010). The nuclear pore complex: bridging nuclear transport and gene regulation. *Nat. Rev. Mol. Cell Biol.* *11*, 490–501.
- Stuart, K., Brun, R., Croft, S., Fairlamb, A., Gürtler, R.E., McKerrow, J., Reed, S., and Tarleton, R. (2008). Kinetoplastids: related protozoan pathogens, different diseases. *J. Clin. Invest.* *118*, 1301–1310.
- Sudha, G., Yamunadevi, S., Tyagi, N., Das, S., and Srinivasan, N. (2012). Structural and molecular basis of interaction of HCV non-structural protein 5A with human casein kinase 1 $\alpha$  and PKR. *BMC Struct. Biol.* *12*, 28–28.
- Sundar, S., More, D.K., Singh, M.K., Singh, V.P., Sharma, S., Makharia, A., Kumar, P.C., and Murray, H.W. (2000). Failure of pentavalent antimony in visceral leishmaniasis in India: report from the center of the Indian epidemic. *Clin. Infect. Dis. Off. Publ. Infect. Dis. Soc. Am.* *31*, 1104–1107.
- Sundar, S., Agrawal, N., Arora, R., Agarwal, D., Rai, M., and Chakravarty, J. (2009). Short-course paromomycin treatment of visceral leishmaniasis in India: 14-day vs 21-day treatment. *Clin. Infect. Dis. Off. Publ. Infect. Dis. Soc. Am.* *49*, 914–918.
- Sunter, J., and Gull, K. (2017). Shape, form, function and *Leishmania* pathogenicity: from textbook descriptions to biological understanding. *Open Biol.* *7*.
- Talevich, E., Tobin, A.B., Kannan, N., and Doerig, C. (2012). An evolutionary perspective on the kinome of malaria parasites. *Philos. Trans. R. Soc. Lond. B. Biol. Sci.* *367*, 2607–2618.
- Talevich, E., Kannan, N., and Miranda-Saavedra, D. (2013). Computational Analysis of Apicomplexan Kinomes. In *Protein Phosphorylation in Parasites*, (John Wiley & Sons, Ltd), pp. 1–36.

- Tamar, S., Dumas, C., and Papadopoulou, B. (2000). Chromosome structure and sequence organization between pathogenic and non-pathogenic *Leishmania* spp. *Mol. Biochem. Parasitol.* *111*, 401–414.
- Taylor, S.S., and Radzio-Andzelm, E. (1994). Three protein kinase structures define a common motif. *Structure* *2*, 345–355.
- Teixeira, C., Gomes, R., Oliveira, F., Meneses, C., Gilmore, D.C., Elnaiem, D.E., Valenzuela, J.G., and Kamhawi, S. (2014). Characterization of the early inflammatory infiltrate at the feeding site of infected sand flies in mice protected from vector-transmitted *Leishmania major* by exposure to uninfected bites. *PLoS Negl. Trop. Dis.* *8*, e2781–e2781.
- Thakur, B.B. (2003). Breakthrough in the management of visceral leishmaniasis. *J. Assoc. Physicians India* *51*, 649–651.
- Thomas Sosa, R., Weber, M.M., Wen, Y., and O’Halloran, T.J. (2012). A Single  $\beta$  Adaptin Contributes to AP1 and AP2 Complexes and Clathrin Function in *Dictyostelium*. *Traffic* *13*, 305–316.
- Tlili, A., Marzouki, S., Chabaane, E., Abdeladhim, M., Kammoun-Rebai, W., Sakkouhi, R., Belhadj, N.H., Oliveira, F., Kamhawi, S., Louzir, H., et al. (2018). Phlebotomus papatasi Yellow-Related and Apyrase Salivary Proteins Are Candidates for Vaccination against Human Cutaneous Leishmaniasis. *J. Invest. Dermatol.* *138*, 598–606.
- Tsigankov, P., Gherardini, P.F., Helmer-Citterich, M., and Zilberstein, D. (2012). What has proteomics taught us about *Leishmania* development? *Parasitology* *139*, 1146–1157.
- Tsigankov, P., Gherardini, P.F., Helmer-Citterich, M., Späth, G.F., and Zilberstein, D. (2013). Phosphoproteomic Analysis of Differentiating *Leishmania* Parasites Reveals a Unique Stage-Specific Phosphorylation Motif. *J. Proteome Res.* *12*, 3405–3412.
- Tuazon, P.T., and Traugh, J.A. (1991). Casein kinase I and II--multipotential serine protein kinases: structure, function, and regulation. *Adv. Second Messenger Phosphoprotein Res.* *23*, 123–164.
- Turner, K.M., Burgoyne, R.D., and Morgan, A. (1999). Protein phosphorylation and the regulation of synaptic membrane traffic. *Trends Neurosci.* *22*, 459–464.
- Ubersax, J.A., Woodbury, E.L., Quang, P.N., Paraz, M., Blethrow, J.D., Shah, K., Shokat, K.M., and Morgan, D.O. (2003). Targets of the cyclin-dependent kinase Cdk1. *Nature* *425*, 859–864.
- Ullu, E., Matthews, K.R., and Tschudi, C. (1993). Temporal order of RNA-processing reactions in trypanosomes: rapid trans splicing precedes polyadenylation of newly synthesized tubulin transcripts. *Mol. Cell. Biol.* *13*, 720–725.
- Urbaniak, M.D. (2009). Casein kinase 1 isoform 2 is essential for bloodstream form *Trypanosoma brucei*. *Mol. Biochem. Parasitol.* *166*, 183–185.
- Utz, A.C., Hirner, H., Blatz, A., Hillenbrand, A., Schmidt, B., Deppert, W., Henne-Bruns, D., Fischer, D., Thal, D.R., Leithäuser, F., et al. (2010). Analysis of Cell Type-specific

- Expression of CK1 $\epsilon$  in Various Tissues of Young Adult BALB/c Mice and in Mammary Tumors of SV40 T-Ag-transgenic Mice. *J. Histochem. Cytochem.* *58*, 1–15.
- Vancura, A., Sessler, A., Leichus, B., and Kuret, J. (1994). A prenylation motif is required for plasma membrane localization and biochemical function of casein kinase I in budding yeast. *J. Biol. Chem.* *269*, 19271–19278.
- Varjosalo, M., Sacco, R., Stukalov, A., van Drogen, A., Planyavsky, M., Hauri, S., Aebersold, R., Bennett, K.L., Colinge, J., Gstaiger, M., et al. (2013). Interlaboratory reproducibility of large-scale human protein-complex analysis by standardized AP-MS. *Nat. Methods* *10*, 307–314.
- Vasquez, J.J., Wedel, C., Cosentino, R.O., and Siegel, T.N. (2018). Exploiting CRISPR-Cas9 technology to investigate individual histone modifications. *Nucleic Acids Res.* *46*, e106–e106.
- Venerando, A., Ruzzene, M., and Pinna, L.A. (2014). Casein kinase: the triple meaning of a misnomer. *Biochem. J.* *460*, 141–156.
- Vieira, L.L., Sacerdoti-Sierra, N., and Jaffe, C.L. (2002). Effect of pH and temperature on protein kinase release by *Leishmania donovani*. *Int. J. Parasitol.* *32*, 1085–1093.
- Vince, J.E., Tull, D.L., Spurck, T., Derby, M.C., McFadden, G.I., Gleeson, P.A., Gokool, S., and McConville, M.J. (2008). *Leishmania* Adaptor Protein-1 Subunits Are Required for Normal Lysosome Traffic, Flagellum Biogenesis, Lipid Homeostasis, and Adaptation to Temperatures Encountered in the Mammalian Host. *Eukaryot. Cell* *7*, 1256–1267.
- Vinet, A.F., Fukuda, M., Turco, S.J., and Descoteaux, A. (2009). The *Leishmania donovani* Lipophosphoglycan Excludes the Vesicular Proton-ATPase from Phagosomes by Impairing the Recruitment of Synaptotagmin V. *PLOS Pathog.* *5*, e1000628.
- Wallach, T., Schellenberg, K., Maier, B., Kalathur, R.K.R., Porras, P., Wanker, E.E., Futschik, M.E., and Kramer, A. (2013). Dynamic Circadian Protein–Protein Interaction Networks Predict Temporal Organization of Cellular Functions. *PLOS Genet.* *9*, e1003398.
- Wang, J., Huo, K., Ma, L., Tang, L., Li, D., Huang, X., Yuan, Y., Li, C., Wang, W., Guan, W., et al. (2011). Toward an understanding of the protein interaction network of the human liver. *Mol. Syst. Biol.* *7*.
- Wang, J., Davis, S., Menon, S., Zhang, J., Ding, J., Cervantes, S., Miller, E., Jiang, Y., and Ferro-Novick, S. (2015). Ypt1/Rab1 regulates Hrr25/CK1 $\delta$  kinase activity in ER–Golgi traffic and macroautophagy. *J. Cell Biol.* *210*, 273–285.
- Wang, P.C., Vancura, A., Mitcheson, T.G., and Kuret, J. (1992). Two genes in *Saccharomyces cerevisiae* encode a membrane-bound form of casein kinase-1. *Mol. Biol. Cell* *3*, 275–286.
- Wang, P.C., Vancura, A., Desai, A., Carmel, G., and Kuret, J. (1994). Cytoplasmic forms of fission yeast casein kinase-1 associate primarily with the particulate fraction of the cell. *J. Biol. Chem.* *269*, 12014–12023.

- Wang, X., Hoekstra, M.F., DeMaggio, A.J., Dhillon, N., Vancura, A., Kuret, J., Johnston, G.C., and Singer, R.A. (1996). Prenylated isoforms of yeast casein kinase I, including the novel Yck3p, suppress the *gcs1* blockage of cell proliferation from stationary phase. *Mol. Cell. Biol.* *16*, 5375–5385.
- Wang, Y., Hu, L., Tong, X., and Ye, X. (2014). Casein Kinase 1 $\gamma$ 1 Inhibits the RIG-I/TLR Signaling Pathway through Phosphorylating p65 and Promoting Its Degradation. *J. Immunol.* *192*, 1855–1861.
- Wang, Z., Wang, S., Wang, W., Gu, Y., Liu, H., Wei, F., and Liu, Q. (2016). Targeted disruption of CK1 $\alpha$  in *Toxoplasma gondii* increases acute virulence in mice. *Eur. J. Protistol.* *56*, 90–101.
- Ward, P., Equinet, L., Packer, J., and Doerig, C. (2004). Protein kinases of the human malaria parasite *Plasmodium falciparum*: the kinome of a divergent eukaryote. *BMC Genomics* *5*, 79–79.
- Wasan, K.M., Morton, R.E., Rosenblum, M.G., and Lopez-Berestein, G. (1994). Decreased toxicity of liposomal amphotericin B due to association of amphotericin B with high-density lipoproteins: role of lipid transfer protein. *J. Pharm. Sci.* *83*, 1006–1010.
- Werneck, G.L., Costa, C.H.N., de Carvalho, F.A.A., Pires e Cruz, M. do S., Maguire, J.H., and Castro, M.C. (2014). Effectiveness of Insecticide Spraying and Culling of Dogs on the Incidence of *Leishmania infantum* Infection in Humans: A Cluster Randomized Trial in Teresina, Brazil. *PLoS Negl. Trop. Dis.* *8*.
- Wolff, S., Xiao, Z., Wittau, M., Süßner, N., Stöter, M., and Knippschild, U. (2005). Interaction of casein kinase 1 delta (CK1 $\delta$ ) with the light chain LC2 of microtubule associated protein 1A (MAP1A). *Biochim. Biophys. Acta BBA - Mol. Cell Res.* *1745*, 196–206.
- Wolff, S., Stöter, M., Giamas, G., Piesche, M., Henne-Bruns, D., Banting, G., and Knippschild, U. (2006). Casein kinase 1 delta (CK1 $\delta$ ) interacts with the SNARE associated protein snapin. *FEBS Lett.* *580*, 6477–6484.
- World Health Organization (2010). Control of the leishmaniases. World Health Organ. Tech. Rep. Ser. xii–xiii, 1–186, back cover.
- Xia, C., Wolf, J.J., Vijayan, M., Studstill, C.J., Ma, W., and Hahm, B. (2018). Casein Kinase 1 $\alpha$  Mediates the Degradation of Receptors for Type I and Type II Interferons Caused by Hemagglutinin of Influenza A Virus. *J. Virol.* *92*.
- Xu, R. m., Carmel, G., Sweet, R. m., Kuret, J., and Cheng, X. (1995). Crystal structure of casein kinase-1, a phosphate-directed protein kinase. *EMBO J.* *14*, 1015–1023.
- Yin, H., Laguna, K.A., Li, G., and Kuret, J. (2006). Dysbindin Structural Homologue CK1BP Is an Isoform-Selective Binding Partner of Human Casein Kinase-1. *Biochemistry* *45*, 5297–5308.
- Zemp, I., Wandrey, F., Rao, S., Ashiono, C., Wyler, E., Montellese, C., and Kutay, U. (2014). CK1 $\delta$  and CK1 $\epsilon$  are components of human 40S subunit precursors required for cytoplasmic 40S maturation. *J Cell Sci* *127*, 1242–1253.

- Zhai, L., Graves, P.R., Robinson, L.C., Italiano, M., Culbertson, M.R., Rowles, J., Cobb, M.H., DePaoli-Roach, A.A., and Roach, P.J. (1995). Casein Kinase I $\gamma$  Subfamily. MOLECULAR CLONING, EXPRESSION, AND CHARACTERIZATION OF THREE MAMMALIAN ISOFORMS AND COMPLEMENTATION OF DEFECTS IN THE SACCHAROMYCES CEREVISIAE YCK GENES. *J. Biol. Chem.* *270*, 12717–12724.
- Zhang, W.W., and Matlashewski, G. (2015). CRISPR-Cas9-Mediated Genome Editing in *Leishmania donovani*. *MBio* *6*, e00861.
- Zhou, Q., Lee, K.J., Kurasawa, Y., Hu, H., An, T., and Li, Z. (2018). Faithful chromosome segregation in *Trypanosoma brucei* requires a cohort of divergent spindle-associated proteins with distinct functions. *Nucleic Acids Res.* *46*, 8216–8231.
- Zilberstein, D., and Shapira, M. (1994). The role of pH and temperature in the development of *Leishmania* parasites. *Annu. Rev. Microbiol.* *48*, 449–470.



# Appendices

---



# Appendix 1

---



**Table S4:** Raw data of the identification of proteins by mass spectrometry from the immunoprecipitation of LmCK1.2-V5-His<sub>6</sub>.

**IP from promastigotes**

Gene ID	Peptides, Distribution				MW (kDa)	Protein name
	Group #1 (Mock): Replicates 1-2-3		Group #2 (LmCK1.2-V5): Replicates 1-2-3			
	Distribution in group	Number of peptides identified in rep. 1-2-3	Distribution in group	Number of peptides identified in rep. 1-2-3		
LdBPK_151330.1		3	23-9-34	92,6	MGT1 magnesium transporter	
LdBPK_352220.1		3	6-5-27	114,9	hypothetical protein, conserved	
LdBPK_361350.1		3	21-14-25	67,5	hypothetical protein, conserved	
LdBPK_081300.1		3	18-13-16	66,9	histone deacetylase, putative	
LdBPK_341610.1		3	14-5-15	55,2	hypothetical protein, conserved	
LdBPK_363660.1		3	9-4-15	88,6	hypothetical protein, conserved	
LdBPK_290210.1		3	4-13-14	174,2	hypothetical protein, conserved	
LdBPK_341080.1		2	1-0-10	66,9	hypothetical protein, conserved	
LdBPK_252460.1		3	7-5-9	39,7	hypothetical protein, conserved	
LdBPK_180100.1		3	5-2-8	50,2	hypothetical protein, conserved	
LdBPK_321780.1		3	3-1-6	89,8	hypothetical protein, conserved	
LdBPK_330990.1		3	2-3-6	122,1	hypothetical protein, conserved	
LdBPK_100800.1		3	4-1-5	208,9	hypothetical protein, conserved	
LdBPK_130650.1		3	2-1-5	218,0	hypothetical protein, conserved	
LdBPK_110310.1		1	0-0-4	195,1	hypothetical protein, conserved	
LdBPK_250870.1		3	3-2-2	41,6	hypothetical protein, conserved	
LdBPK_321890.1		2	3-0-3	16,7	hypothetical protein, conserved	
LdBPK_020640.1		1	2-0-0	34,5	mitochondrial carrier protein, putative	
LdBPK_040940.1		1	0-2-0	52,1	chaperone protein DNAJ, putative	
LdBPK_081680.1		2	1*-0-2	33,3	unspecified product	
LdBPK_282480.1		1	2-0-0	46,4	eukaryotic translation initiation factor, putative	
LdBPK_290470.1		2	2-0-1	78,4	hypothetical protein, conserved	
LdBPK_331960.1		1	0-0-2	71,1	ATP-binding cassette protein subfamily D, member 3, putative	
LdBPK_332020.1		1	2-0-0	64,9	Ribosome assembly protein rrb1, putative	
LdBPK_351190.1		1	2-0-0	123,1	NADH-dependent fumarate reductase, putative	
LdBPK_353750.1		2	1-2-0	24,8	Gim5A protein, putative	
LdBPK_360770.1		1	2-0-0	28,3	Protein C21orf2 homolog, putative	
LdBPK_361580.1		1	2-0-0	56,5	hypothetical protein, conserved	
LdBPK_364480.1		1	0-0-2	178,6	hypothetical protein, conserved	
LdBPK_010130.1		1	0-0-1	38,9	hypothetical protein, conserved	
LdBPK_010510.1		1	1*-0-0	77,0	long chain fatty acid CoA ligase, putative	
LdBPK_030060.1		1	1-0-0	93,2	hypothetical protein, conserved	
LdBPK_030960.1		1	1-0-0	46,6	elongation initiation factor 2 alpha subunit, putative	
LdBPK_040760.1		1	1*-0-0	20,4	nascent polypeptide associated complex subunit- like protein, copy 2 (fragment)	
LdBPK_040770.1		1	1-0-0	18,2	nascent polypeptide associated complex subunit- like protein, copy 1	
LdBPK_070060.1		1	1-0-0	107,7	alpha-adaptin-like protein	
LdBPK_071150.1		1	0-0-1	38,9	RNA binding protein-like protein	

LdBPK_101090.1			1	1-0-0	36,9	nucleoside phosphorylase-like protein
LdBPK_111050.1			1	0-0-1	54,0	pretranslocation protein, alpha subunit, putative, protein transport protein SEC61 subunit alpha, putative
LdBPK_140190.1			1	1-0-0	22,4	hypothetical protein, conserved
LdBPK_140670.1			1	0-0-1	32,4	fatty acid elongase, putative
LdBPK_140760.1			1	0-0-1	37,2	fatty acid elongase, putative
LdBPK_181270.1			1	1-0-0	26,2	hypothetical protein, conserved (fragment)
LdBPK_181410.1			1	0-0-1	121,9	chaperone DNAJ protein, putative
LdBPK_250270.1			1	0-0-1	126,6	hypothetical protein, conserved
LdBPK_251460.1			1	1-0-0	24,2	GTP-binding protein, putative
LdBPK_261940.1			1	1-0-0	37,7	hypothetical protein, conserved
LdBPK_270681.1			1	1-0-0	52,3	hypothetical protein, conserved
LdBPK_272020.1			1	0-0-1	44,1	RNA-binding protein, putative
LdBPK_272680.1			1	0-0-1*	55,4	unspecified product
LdBPK_282370.1			1	1-0-0	48,0	glycoprotein 96-92, putative
LdBPK_290830.1			1	0-0-1	62,9	hypothetical protein, conserved
LdBPK_290870.1			1	1-0-0	51,7	hypothetical protein, conserved
LdBPK_292690.1			1	0-0-1	45,8	hypothetical protein, conserved (fragment)
LdBPK_301180.1			1	1-0-0	58,1	importin alpha, putative
LdBPK_303770.1			1	0-0-1	144,9	CPSF-domain protein, putative
LdBPK_310170.1			1	0-0-1	133,3	DNA-directed RNA polymerase II subunit 2, putative (RPB2)
LdBPK_310360.1			1	0-0-1	11,4	amino acid transporter aATP11, putative (fragment)
LdBPK_311240.1			1	0-1-0	83,3	Pyrophosphate-energized vacuolar membrane proton pump 1, putative, Vacuolar proton pyrophosphatase 1, putative (VP1)
LdBPK_320050.1			1	0-0-1	36,4	protein transport protein SEC13, putative
LdBPK_321940.1			1	1*-0-0	64,3	heat shock protein 60, Chaperonin HSP60, mitochondrial (HSP60)
LdBPK_333240.1			3	1-1-1	230,2	hypothetical protein, unknown function
LdBPK_341880.1			2	0-1-1	8,7	ubiquitin-like protein
LdBPK_342410.1			1	0-1-0	22,6	hypothetical protein, conserved
LdBPK_350850.1			1	1*-0-0	129,7	NADH-dependent fumarate reductase-like protein
LdBPK_351020.1			2	1*-0-1*	37,2	casein kinase I, putative
LdBPK_360190.1			1	1*-0-0	13,1	elongation factor 2
LdBPK_361320.1			1	1-0-0	40,7	fructose-1,6-bisphosphate aldolase
LdBPK_362130.1			1	1*-0-0	60,6	chaperonin HSP60, mitochondrial precursor
LdBPK_363100.1			1	1-0-0	44,1	succinyl-CoA ligase [GDP-forming] beta-chain, putative
LdBPK_363820.1			1	0-0-1	22,8	hypothetical protein, conserved
LdBPK_366240.1			1	0-0-1	46,7	hypothetical protein, unknown function
LdBPK_351030.1	3	4-6-2	3	70-58-64	39,8	casein kinase, putative
LdBPK_367240.1	1	0-1-0	2	0-3-5	58,2	T-complex protein 1, theta subunit, putative, CCT-theta, putative
LDPBQ7IC8_280018400	1	0-2-0	3	7-2-5	71,8	
LdBPK_010540.1	1	0-1-0	1	3-0-0	77,8	long chain fatty acid CoA ligase, putative
LdBPK_291170.1	2	1*-1*-0	2	1*-0-3*	9,7	ribosomal protein L1a, putative (fragment)
LdBPK_291180.1	2	1*-1*-0	2	1*-0-3*	9,2	ribosomal protein L1a, putative (fragment)
LdBPK_362140.1	2	0-1-1	3	2-1-3	59,3	chaperonin HSP60, mitochondrial precursor
LdBPK_363620.1	2	1-1-0	2	3-2-0	23,1	hypothetical protein, conserved
LdBPK_363930.1	1	1-0-0	2	3-1-0	19,2	60S ribosomal protein L34, putative
LDPBQ7IC8_280036500 (LinJ.28.2960)	3	15-18-7	3	50-34-40	71,3	
LdBPK_262350.1	3	1-2-1	3	5-3-1	15,2	60S ribosomal protein L35, putative
LdBPK_040750.1	2	4-5-0	3	12-5-4	24,6	60S ribosomal protein L10, putative
LdBPK_271940.1	2	3-3-0	2	7-4-0	53,8	D-lactate dehydrogenase-like protein
LdBPK_330350.1	3	3-3-3	3	7-4-3	80,4	unspecified product
LdBPK_330360.1	3	3*-3*-3*	3	7*-4*-3*	80,6	heat shock protein 83-1
LdBPK_333300.1	3	13-11-12	3	30-9-17	17,4	40S ribosomal protein S13, putative
LDPBQ7IC8_260018000	2	2-7-0	3	16-8-13	70,4	
LdBPK_211300.1	1	4-0-0	3	9-2-2	15,9	40S ribosomal protein S23, putative

LdBPK_361310.1	3	5-4-4	3	11-4-7	22,1	40S ribosomal protein S9, putative
LdBPK_111110.1	3	6-5-2	3	12-5-6	16,4	60S ribosomal protein L28, putative
LdBPK_303390.1	3	5*-5*-6*	3	12*-4*-5*	10,4	60S ribosomal protein L9, putative (fragment)
LdBPK_080130.1	3	2-1-1	3	4-2-4	121,2	hypothetical protein, conserved
LdBPK_212020.1	2	1-2-0	2	4-4-0	33,8	mitochondrial structure specific endonuclease I (SSE-1), putative
LdBPK_291600.1	1	0-2-0	2	0-3-4	73,8	hypothetical protein, conserved
LdBPK_010790.1	1	0-1-0	2	2-1-0	45,3	eukaryotic initiation factor 4a, putative
LdBPK_050510.1	1	1-0-0	2	2-0-1	62,5	ATPase alpha subunit
LdBPK_160560.1	1	0-1-0	2	1-0-2	49,7	orotidine-5-phosphate decarboxylase/orotate phosphoribosyltransferase, putative
LdBPK_231400.1	1	1-0-0	1	2-0-0	56,2	coronin, putative
LdBPK_270390.1	1	0-1-0	1	0-0-2	159,1	Nuclear pore complex protein 158, serine peptidase, Clan SP, family S59, putative (Nup158)
LdBPK_281700.1	2	1-1-0	1	2-0-0	38,3	hydrolase, alpha/beta fold family, putative
LdBPK_302320.1	1	0-1-0	1	2-0-0	52,5	hypothetical protein, conserved
LdBPK_310560.1	1	0-1-0	1	0-0-2	93,9	ATP-binding cassette protein subfamily D, member 2, putative
LdBPK_332600.1	1	0-1-0	2	2-1-0	42,5	hypothetical protein, conserved (POMP11)
LdBPK_353840.1	3	14-13-11	3	26-10-11	15,0	60S ribosomal protein L23, putative
LdBPK_210760.1	3	5-4-4	3	9-4-7	66,8	dual specificity protein phosphatase, putative
LdBPK_211290.1	3	14-12-10	3	25-13-14	21,5	60S ribosomal protein L9, putative
LdBPK_111180.1	3	4-3-2	3	7-5-4	14,7	40S ribosomal protein S15A, putative
LdBPK_280570.1	3	3-4-4	3	7-3-5	12,8	ribosomal protein S26, putative
LdBPK_350370.1	2	3-4-0	3	7-3-2	46,4	ATP-dependent DEAD-box RNA helicase, putative
LdBPK_351440.1	2	1*-4*-0	2	7*-0-1*	11,5	60S ribosomal protein L2, putative (fragment)
LdBPK_351450.1	2	1-4-0	2	7-0-1	10,8	60S ribosomal protein L2, putative (fragment)
LdBPK_281100.1	3	5-5-4	3	8-6-6	13,0	ribosomal protein S20, putative
LdBPK_353810.1	3	6-3-3	3	9-3-5	16,1	60S ribosomal protein L27A/L29, putative
LdBPK_212190.1	3	4-3-2	3	6-1-1	10,3	60S ribosomal protein L37a, putative
LdBPK_367220.1	1	0-4-0	2	0-2-6	143,8	nuclear pore complex protein (NUP155), putative, nucleoporin, putative
LdBPK_061020.1	1	2-0-0	1	3-0-0	132,1	hypothetical protein, conserved
LdBPK_070910.1	2	2-2-0	2	3-3-0	61,0	flavoprotein subunit-like protein
LdBPK_111130.1	2	1*-2*-0	2	3*-0-2*	5,2	60S ribosomal protein L28, putative (fragment)
LdBPK_131400.1	1	0-2-0	3	3-3-3	58,8	chaperonin TCP20, putative
LdBPK_131410.1	2	2-1-0	3	3-1-1	12,3	60S ribosomal protein L44, putative
LdBPK_332160.1	1	0-2-0	1	0-0-3	86,6	hypothetical protein, conserved
LdBPK_191590.1	3	15-10-2	3	22-10-3	55,6	inosine-5'-monophosphate dehydrogenase
LdBPK_342620.1	3	7-4-5	3	10-4-6	20,1	40S ribosomal protein S19 protein, putative
LdBPK_343440.1	3	12-8-6	3	17-5-12	18,0	60S ribosomal protein L21, putative
LdBPK_353330.1	3	5-3-2	2	7-0-3	20,8	60S ribosomal subunit protein L31, putative
LdBPK_240040.1	3	11-7-4	3	15-5-9	19,1	60S ribosomal protein L17, putative
LdBPK_360990.1	3	10-12-5	3	16-11-12	19,0	40S ribosomal protein S18, putative
LdBPK_350600.1	3	9-6-3	3	12-4-7	20,8	60S ribosomal protein L18a, putative
LdBPK_362640.1	1	0-6-0	1	0-0-8	97,1	nucleoporin interacting component (NUP93), putative
LdBPK_030240.1	2	3-2-0	2	4-0-1	9,5	ribosomal protein L38, putative
LdBPK_130890.1	2	3-2-0	1	4-0-0	50,0	hypothetical protein, conserved
LdBPK_161220.1	3	2-3-1	3	4-1-3	6,5	60S ribosomal protein L39, putative
LdBPK_302470.1	3	2*-2*-3*	3	4*-2*-3*	9,5	heat shock 70-related protein 1, mitochondrial precursor, putative (fragment)
LdBPK_302540.1	3	2*-2*-3*	3	4*-2*-3*	9,0	heat shock 70-related protein 1, mitochondrial precursor, putative (fragment)
LdBPK_361050.1	2	3*-0-1*	2	4-1*-0	18,6	40S ribosomal protein S10, putative
LdBPK_363020.1	2	2-3-0	3	4-2-1	15,8	40S ribosomal protein S24e
LdBPK_365620.1	2	1-3-0	2	4-2-0	57,5	NADH dehydrogenase, putative
LdBPK_131120.1	3	14-17-12	3	22-11-16	30,6	40S ribosomal protein S4, putative
LdBPK_270790.1	3	4-2-1	2	5-0-1	44,5	isovaleryl-coA dehydrogenase, putative
LdBPK_352610.1	3	4-2-1	3	5-4-4	24,3	hypothetical protein, conserved
LdBPK_212090.1	3	12-6-4	3	14-6-9	15,3	60S ribosomal protein L32

LdBPK_010440.1	3	6-7-2	3	8-4-7	23,8	ribosomal protein S7, putative
LdBPK_292620.1	2	4-7-0	3	8-1-3	54,0	ATP-dependent phosphofructokinase
LdBPK_242140.1	3	8-9-8	3	10-7-6	13,1	60S ribosomal protein L26, putative (fragment)
LdBPK_281050.1	3	5-9-7	3	10-6-7	15,6	40S ribosomal protein S14
LdBPK_303650.1	3	5*-9*-7*	3	10*-6*-7*	15,6	40S ribosomal protein S14
LdBPK_170170.1	3	27-23-16	3	27-15-20	49,1	elongation factor 1-alpha
LdBPK_190130.1	3	13-9-4	3	13-5-5	68,5	protein kinase, putative
LdBPK_330960.1	3	11-13-7	3	13-6-13	37,7	40S ribosomal protein S3, putative
LdBPK_060590.1	3	6-7-9	3	8-9-7	16,4	60S ribosomal protein L23a, putative
LdBPK_291160.1	3	2-9-3	3	9-4-9	41,1	ribosomal protein L1a, putative
LdBPK_350400.1	2	3-8-0	3	8-2-5	30,0	40S ribosomal protein S3A, putative
LdBPK_010430.1	3	4*-5*-2*	3	5*-3*-4*	11,5	ribosomal protein S7, putative (fragment)
LdBPK_190190.1	3	2*-5*-5*	3	4*-4*-5*	11,3	ADP,ATP carrier protein 1, mitochondrial precursor, putative (fragment)
LdBPK_350240.1	3	5-5-2	3	5-4-4	11,4	60S ribosomal protein L30
LdBPK_020430.1	1	0-3-0	1	0-0-3	31,9	voltage-dependent anion-selective channel, putative, Mitochondrial outer membrane protein porin, putative (VDAC)
LdBPK_220340.1	3	3-3-2	3	3-3-3	7,5	40S ribosomal protein S15, putative (fragment)
LdBPK_251220.1	2	3-3-0	2	3-0-1	13,0	ribosomal protein S25
LdBPK_290290.1	2	3-3-0	3	3-3-1	53,4	D-lactate dehydrogenase-like protein
LdBPK_330770.1	1	0-3-0	2	3-2-0	5,4	60S ribosomal protein L6, putative (fragment)
LdBPK_360210.1	3	2-3-2	2	3-1-0	94,1	elongation factor 2
LdBPK_361040.1	2	3-0-1	2	3*-1-0	17,4	40S ribosomal protein S10, putative (fragment)
LdBPK_091020.1	2	0-1-2	1	0-2-0	51,3	elongation factor-1 gamma
LdBPK_171300.1	2	1-2-0	1	2-0-0	90,4	hypothetical protein, conserved
LdBPK_191150.1	1	0-2-0	1	2-0-0	41,4	hypothetical protein, conserved
LdBPK_210800.1	3	1-2-2	2	2-0-1	12,0	60S ribosomal protein L36, putative
LdBPK_230050.1	3	1-2-1	2	1-2-0	25,4	peroxidoxin
LdBPK_230060.1	2	2-2-0	2	2-2-0	32,0	cyclophilin, putative
LdBPK_282360.1	3	1-2-1	3	2-1-1	6,7	ribosomal protein S29, putative
LdBPK_282700.1	1	0-2-0	1	2-0-0	68,8	acyl-CoA dehydrogenase, putative
LdBPK_282750.1	1	0-2-0	1	2-0-0	16,5	40S ribosomal protein S17, putative
LdBPK_322830.1	2	0-2-1	2	2-0-2	15,4	ribosomal protein L27, putative
LdBPK_351900.1	3	1*-2*-2*	2	2*-0-1*	11,9	60S ribosomal protein L36, putative
LdBPK_060030.1	1	1-0-0	1	1-0-0	75,4	hypothetical protein, conserved
LdBPK_090420.1	2	1-0-1	2	1-0-1	66,5	integral membrane transport protein, putative
LdBPK_100310.1	1	0-1-0	2	1-1-0	48,5	isocitrate dehydrogenase [NADP], mitochondrial precursor, putative
LdBPK_100560.1	1	1-0-0	1	1-0-0	39,3	glycerol-3-phosphate dehydrogenase [NAD+], glycosomal
LdBPK_110780.1	1	0-1-0	1	0-0-1	22,4	40S ribosomal protein S21, putative (fragment)
LdBPK_110970.1	2	0-1*-1*	3	1*-1*-1*	5,3	40S ribosomal protein S5 (fragment)
LdBPK_180230.1	2	1-1-0	1	1-0-0	34,4	60S ribosomal protein L7, putative
LdBPK_210550.1	1	0-1-0	1	0-1-0	49,8	DnaJ protein, putative
LdBPK_211790.1	3	1-1-1	3	1-1-1	4,0	40S ribosomal protein S11, putative (fragment)
LdBPK_220009.1	1	0-1-0	1	0-0-1	36,5	heat shock protein DNAJ, putative
LdBPK_220260.1	1	0-1-0	1	0-0-1	138,0	hypothetical protein, conserved
LdBPK_262140.1	1	1-0-0	1	1-0-0	27,6	hypothetical protein, conserved
LdBPK_281760.1	1	0-1-0	1	1-0-0	66,6	hypothetical protein, conserved
LdBPK_282950.1	2	1*-1*-0	3	1*-1*-1*	13,4	heat-shock protein hsp70, putative (fragment)
LdBPK_321060.1	1	1-0-0	1	0-1-0	59,3	chaperonin containing t-complex protein, putative
LdBPK_332400.1	1	0-0-1	1	1-0-0	33,3	hypothetical protein, conserved
LdBPK_340910.1	2	1-1-0	2	1-0-1	10,8	60S ribosomal protein L13a, putative (fragment)
LdBPK_342380.1	1	0-1-0	1	1-0-0	68,6	hypothetical protein, unknown function
LdBPK_342530.1	2	1-1-0	2	1-1-0	28,9	hypothetical protein, conserved
LdBPK_353590.1	1	0-1-0	1	1-0-0	24,5	Pre-rRNA-processing protein PNO1, putative (PNO1)
LdBPK_362790.1	1	0-1-0	1	0-1-0	48,6	dihydrolipoamide acetyltransferase precursor, putative

LdBPK_363360.1	1	1-0-0	2	1-0-1	29,7	14-3-3 protein-like protein
LdBPK_365150.1	1	0-1-0	1	0-1-0	76,5	hypothetical protein, conserved
LDPBQ71C8_300033100	3	10-16-23	3	21-15-22	71,8	
LdBPK_320790.1	3	12-7-8	3	11-8-8	25,2	RNA binding protein, putative
LdBPK_320410.1	3	17-23-5	3	21-8-6	66,8	ATP-dependent RNA helicase, putative
LdBPK_151000.1	3	11-11-4	3	8-9-10	129,2	hypothetical protein, conserved
LdBPK_342370.1	1	0-21-0	3	8-5-19	100,1	hypothetical protein, conserved
LdBPK_302480.1	3	6*-12*-18*	3	16*-10*-16*	54,2	heat shock 70-related protein 1, mitochondrial precursor, putative (fragment)
LdBPK_290020.1	3	4-8-2	1	7-0-0	114,8	transcription factor-like protein
LdBPK_050770.1	3	7-3-2	2	6-0-4	139,6	hypothetical protein, unknown function
LdBPK_302990.1	2	6-7-0	3	6-4-2	39,1	unspecified product
LdBPK_190710.1	3	13-7-3	3	11-5-1	33,6	glycosomal malate dehydrogenase
LdBPK_242160.1	2	6-4-0	3	4-1-5	25,0	40S ribosomal protein S8, putative
LdBPK_260840.1	3	4-5-3	3	4-2-4	16,7	40S ribosomal protein S16, putative
LdBPK_320460.1	3	4-5-3	3	4-1-4	28,6	40S ribosomal protein S2
LdBPK_352040.1	3	14-6-4*	3	11-5-8	15,4	60S ribosomal protein L32
LdBPK_212240.1	3	2*-9*-6*	3	7*-3*-5*	8,7	beta tubulin (fragment)
LdBPK_251210.1	2	4-3-0	2	2-0-3	56,3	ATP synthase subunit beta, mitochondrial, putative, ATP synthase F1, beta subunit, putative (ATPB)
LdBPK_363940.1	2	3-4-0	3	3-2-2	9,8	40S ribosomal protein S27-1, putative
LdBPK_081290.1	3	3-12-7	3	9-4-7	15,9	beta tubulin (fragment)
LdBPK_190200.1	3	6-12-9	3	9-7-8	35,2	ADP,ATP carrier protein 1, mitochondrial precursor, putative
LdBPK_030220.1	1	0-3-0	2	1-0-2	79,0	long chain fatty Acyl CoA synthetase, putative
LdBPK_110960.1	3	3-3-2	3	2-2-1	10,4	40S ribosomal protein S5 (fragment)
LdBPK_211820.1	3	2-3-1	3	2-1-1	58,8	ATP-dependent RNA helicase SUB2, putative (SUB2)
LdBPK_252090.1	3	3-3-2	3	2-1-1	30,4	hypothetical protein, conserved
LdBPK_311050.1	2	3-2-0	1	2-0-0	38,6	hypothetical protein, unknown function
LdBPK_333390.1	1	3-0-0	1	2-0-0	14,1	h1 histone-like protein
LdBPK_354200.1	1	0-3-0	1	0-0-2	64,6	poly(a) binding protein, putative
LdBPK_300120.1	3	4-6-4	3	4-4-3	69,5	alkyldihydroxyacetonephosphate synthase
LdBPK_353150.1	3	1-16-1	2	10-0-6	99,9	ATP-dependent RNA helicase, putative
LdBPK_320020.1	3	2-5-2	2	3-1-0	56,4	nuclear segregation protein, putative
LdBPK_210300.1	2	6-10-0	2	6-5-0	51,7	hexokinase, putative
LdBPK_120720.1	1	0-24-0	3	5-2-13	144,0	hypothetical protein, conserved
LdBPK_060410.1	1	0-2-0	1	1-0-0	28,1	60S ribosomal protein L19, putative
LdBPK_072500.1	2	2-2-0	3	1-1-1	58,3	glycosomal phosphoenolpyruvate carboxykinase, putative
LdBPK_131420.1	2	1-2-0	2	0-1-1	28,7	pyrroline-5-carboxylate reductase
LdBPK_171320.1	3	1*-2*-2*	1	1*-0-0	12,5	histone H2B
LdBPK_180300.1	1	0-2-0	1	1-0-0	40,0	hypothetical protein, conserved
LdBPK_241560.1	3	1-2-2	3	1-1-1	19,4	IgE-dependent histamine-releasing factor, putative
LdBPK_251850.1	1	0-2-0	2	0-1-1	34,2	3-oxo-5-alpha-steroid 4-dehydrogenase, putative
LdBPK_252520.1	1	0-2-0	1	1-0-0	109,3	hypothetical protein, conserved
LdBPK_271720.1	1	0-2-0	1	0-0-1	219,8	hypothetical protein, unknown function
LdBPK_282970.1	2	0-2-1	1	0-1-0	34,4	activated protein kinase c receptor (LACK)
LdBPK_310140.1	1	0-2-0	1	0-0-1	92,5	hypothetical protein, unknown function
LdBPK_311930.1	1	0-2-0	1	0-0-1	14,7	ubiquitin-fusion protein
LdBPK_312450.1	2	1-2-0	1	1-0-0	55,6	hypothetical protein, conserved
LdBPK_332070.1	2	1-2-0	1	1-0-0	9,8	60S ribosomal protein L37
LdBPK_363550.1	2	2-1-0	1	1-0-0	8,0	ribosomal protein L29, putative
LdBPK_070550.1	3	2-4-1	1	2-0-0	39,1	60S ribosomal protein L7a, putative
LdBPK_170750.1	3	1-4-1	1	2-0-0	48,2	hypothetical protein, conserved (fragment)
LdBPK_221370.1	3	1-4-1	2	2-2-0	26,0	40S ribosomal protein L14, putative
LdBPK_363570.1	3	2-4-2	2	2-0-1	33,1	short chain dehydrogenase-like protein
LdBPK_091410.1	3	3*-6*-4*	1	3*-0-0	12,3	histone H2B

LdBPK_190040.1	3	3-6-4	1	3-0-0	11,9	histone H2B
LdBPK_070130.1	2	2-11-0	2	5-0-1	59,6	ATP-dependent DEAD/H RNA helicase, putative
LdBPK_130330.1	3	12-35-13	3	15-15-14	49,8	alpha tubulin
LdBPK_366110.1	3	4-22-4	3	7-5-9	58,3	flagellum targeting protein kharon1, putative (KH1)
LdBPK_260160.1	3	4-5-1	3	2-1-1	28,9	60S ribosomal protein L7, putative
LdBPK_211420.1	2	3-3-0	2	1-1-0	29,0	hypothetical protein, conserved
LdBPK_252470.1	1	0-3-0	1	0-0-1	64,6	hypothetical protein, conserved
LdBPK_342240.1	1	0-3-0	1	0-0-1	16,5	ribosomal protein l35a, putative
LdBPK_361550.1	1	0-3-0	1	0-0-1	132,4	hypothetical protein, conserved
LdBPK_365240.1	1	0-3-0	1	1-0-0	12,1	40S ribosomal protein SA, putative (fragment)
LdBPK_220004.1	3	1-6-1	2	2-0-1	21,7	60S ribosomal protein L11 (L5, L16)
LdBPK_364540.1	1	0-13-0	1	0-0-3	177,5	hypothetical protein, conserved
LdBPK_303740.1	1	0-9-0	1	0-2-0	50,8	hypothetical protein, conserved
LdBPK_290710.1	1	0-5-0	1	0-0-1	82,0	RNA-binding protein, putative
LdBPK_342680.1	1	0-5-0	1	0-0-1	71,5	regulatory subunit of protein kinase a-like protein
LdBPK_251240.1	1	0-11-0	1	2-0-0	113,0	hypothetical protein, conserved
LdBPK_180940.1	1	0-8-0	1	1-0-0	139,7	hypothetical protein, conserved
LdBPK_181340.1	1	0-8-0	1	0-0-1	107,7	hypothetical protein, conserved
LdBPK_110600.1	1	0-9-0	1	1-0-0	58,4	3-methylcrotonoyl-CoA carboxylase beta subunit, putative
LdBPK_310450.1	2	0-9-2	1	1-0-0	80,0	cytoskeleton-associated protein CAP5.5, putative, cysteine peptidase, Clan CA, family C2, putative, Calpain-like protein 1 (CAP5.5)
LdBPK_332570.1	1	0-9-0	1	1-0-0	56,5	hypothetical protein, conserved
LdBPK_282120.1	1	0-19-0	1	2-0-0	81,2	hypothetical protein, conserved
LdBPK_151430.1	1	0-10-0	1	0-0-1	48,9	nucleolar RNA binding protein, putative
LdBPK_261960.1	1	0-10-0	1	0-1-0	89,1	hypothetical protein, conserved
LdBPK_323200.1	1	0-11-0	2	0-1-1	96,2	hypothetical protein, conserved
LdBPK_100210.1	1	0-15-0	1	0-0-1	52,6	Nucleolar protein 56, putative (NOP56)
LdBPK_303360.1	1	0-22-0	1	0-0-1	40,8	MORN repeat-containing protein 1 (MORN1)
LdBPK_020680.1	1	1*-0-0			90,8	ATP-dependent Clp protease subunit, heat shock protein 78 (HSP78), putative
LdBPK_030260.1	1	0-1-0			24,3	hypothetical protein (fragment)
LdBPK_030300.1	1	0-1-0			116,4	hypothetical protein, conserved
LdBPK_040970.1	1	0-1-0			51,6	hypothetical protein, conserved
LdBPK_041200.1	1	0-1-0			253,9	hypothetical protein, conserved
LdBPK_041250.1	1	1-0-0			42,0	actin
LdBPK_050080.1	1	0-1-0			21,9	hypothetical protein, conserved
LdBPK_050280.1	1	0-1-0			25,1	protein tyrosine phosphatase, putative
LdBPK_050360.1	1	0-1-0			66,5	ATP-dependent RNA helicase, putative
LdBPK_050640.1	1	0-1-0			199,5	hypothetical protein, conserved
LdBPK_050850.1	1	0-1-0			68,7	hypothetical protein, conserved
LdBPK_060110.1	1	0-1-0			66,4	hypothetical protein, conserved
LdBPK_060220.1	1	0-1-0			32,1	hypothetical protein, conserved
LdBPK_060580.1	2	0-1-1			30,3	deoxyuridine triphosphatase, putative
LdBPK_070620.1	1	0-1-0			51,2	hypothetical protein, conserved
LdBPK_070760.1	1	0-1-0			209,3	unspecified product
LdBPK_080400.1	1	0-1-0			203,7	hypothetical protein, conserved
LdBPK_090230.1	1	0-1-0			33,2	hypothetical protein, conserved
LdBPK_090970.1	1	0-1-0			16,8	calmodulin, putative
LdBPK_091170.1	1	0-1-0			51,3	hypothetical protein, conserved
LdBPK_091630.1	1	0-1-0			69,0	hypothetical protein, conserved
LdBPK_100550.1	1	0-1-0			713,3	hypothetical protein, conserved
LdBPK_101280.1	1	0-1-0			47,0	flagellar protofilament ribbon protein-like protein
LdBPK_110720.1	1	0-1-0			62,7	hypothetical protein, conserved
LdBPK_120310.1	1	0-1-0			41,5	hypothetical protein, conserved
LdBPK_120661.1	1	0-1-0			50,7	hypothetical protein, conserved

LdBPK_130290.1	1	0-1-0		66,9	flagellar radial spoke protein, putative
LdBPK_130460.1	1	0-1-0		15,6	40S ribosomal protein S12, putative
LdBPK_130950.1	1	0-1-0		26,0	hypothetical protein, conserved
LdBPK_131580.1	1	0-1-0		104,3	hypothetical protein, conserved
LdBPK_140810.1	1	0-1-0		207,7	hypothetical protein, conserved
LdBPK_150610.1	1	0-1-0		25,9	hypothetical protein, conserved
LdBPK_150750.1	1	1-0-0		336,5	hypothetical protein, conserved
LdBPK_151120.1	1	1*-0-0		12,7	tryparedoxin peroxidase
LdBPK_151530.1	1	0-1-0		13,5	ribosomal protein S6, putative
LdBPK_160150.1	1	0-0-1		18,7	eukaryotic translation initiation factor 1A, putative
LdBPK_160390.1	1	0-1-0		88,0	tubulin tyrosine ligase, putative
LdBPK_170260.1	1	0-1-0		43,1	hypothetical protein, conserved
LdBPK_171000.1	1	0-1-0		73,1	hypothetical protein, conserved
LdBPK_171140.1	1	0-1-0		46,4	hydrolase-like protein
LdBPK_171210.1	1	0-1-0		158,3	kinesin, putative
LdBPK_180530.1	1	0-1-0		56,9	tubulin cofactor C domain-containing protein RP2, putative (rp2)
LdBPK_180820.1	1	0-1-0		290,0	hypothetical protein, conserved
LdBPK_181360.1	1	0-1-0		42,7	pyruvate dehydrogenase E1 component alpha subunit, putative
LdBPK_190670.1	1	0-1-0		21,7	U3 snoRNA-associated protein UTP11, putative
LdBPK_191080.1	1	0-1-0		136,5	hypothetical protein, conserved
LdBPK_201430.1	1	0-1-0		129,6	hypothetical protein, conserved
LdBPK_210260.1	1	1-0-0		104,9	major vault protein-like protein
LdBPK_210310.1	1	0-1*-0		36,1	hexokinase, putative (fragment)
LdBPK_210490.1	1	0-1-0		46,6	hypothetical protein, conserved
LdBPK_211250.1	1	0-1-0		51,8	epsilon tubulin, putative
LdBPK_211460.1	1	0-1-0		146,5	hypothetical protein, conserved
LdBPK_211480.1	1	0-1-0		138,9	hypothetical protein, conserved
LdBPK_211720.1	1	0-1-0		95,3	hypothetical protein, conserved
LdBPK_212200.1	1	1-0-0		26,8	proteasome subunit alpha type-5, putative
LdBPK_220050.1	1	0-1-0		131,6	hypothetical protein, conserved
LdBPK_221230.1	1	0-1-0		32,4	hypothetical protein, conserved
LdBPK_221310.1	1	0-1-0		23,0	i/6 autoantigen-like protein
LdBPK_240630.1	1	0-1-0		89,9	ubiquitin carboxyl-terminal hydrolase, putative, cysteine peptidase, Clan CA, family C19, putative
LdBPK_241000.1	1	0-1-0		165,5	hypothetical protein, conserved
LdBPK_241050.1	1	0-1-0		23,9	dynein light chain, putative
LdBPK_242040.1	1	0-1-0		103,2	hypothetical protein, conserved
LdBPK_242350.1	1	0-1-0		58,8	notchless homolog, putative
LdBPK_250250.1	1	0-1-0		96,2	hypothetical protein, conserved
LdBPK_250430.1	1	0-1-0		173,8	hypothetical protein, conserved
LdBPK_250550.1	3	1-1-1		32,5	hypothetical protein, conserved
LdBPK_250610.1	1	0-1-0		44,7	hypothetical protein, conserved
LdBPK_250710.1	1	0-1-0		56,1	hypothetical protein, conserved
LdBPK_250730.1	1	0-1-0		31,3	hypothetical protein, conserved
LdBPK_251660.1	1	0-1-0		135,3	hypothetical protein, conserved
LdBPK_252030.1	1	0-1-0		113,5	kinesin, putative
LdBPK_260920.1	1	0-1-0		67,0	hypothetical protein, conserved
LdBPK_261170.1	1	0-1-0		182,3	hypothetical protein, conserved
LdBPK_261320.1	1	0-1-0		67,8	DNA ligase k alpha, putative
LdBPK_261950.1	1	0-1-0		287,1	microtubule-associated protein, putative (GB4)
LdBPK_262260.1	1	0-1-0		88,7	hypothetical protein, conserved
LdBPK_262430.1	1	0-1-0		51,1	hypothetical protein, conserved
LdBPK_270460.1	1	0-1-0		39,3	Ribosome production factor 1, putative
LdBPK_270800.1	1	0-1-0		62,4	hypothetical protein, conserved
LdBPK_270970.1	1	0-1-0		69,1	hypothetical protein, conserved

LdBPK_271360.1	1	0-1-0		93,1	hypothetical protein, conserved
LdBPK_271530.1	1	0-1-0		93,1	hypothetical protein, conserved
LdBPK_271700.1	1	0-1-0		182,6	protein kinase-like protein
LdBPK_271930.1	1	0-1-0		28,0	hypothetical protein, conserved
LdBPK_272310.1	1	0-1-0		41,1	hypothetical protein, conserved
LdBPK_281860.1	1	0-1-0		65,1	hypothetical protein, conserved
LdBPK_281900.1	1	0-1-0		96,3	DNA topoisomerase III, putative
LdBPK_282560.1	1	0-1-0		145,8	hypothetical protein, conserved
LdBPK_282610.1	1	1-0-0		55,6	Vacuolar proton pump subunit B, putative, V-type proton ATPase subunit B, putative
LdBPK_283030.1	1	1-0-0		22,5	hypothetical protein, conserved
LdBPK_290440.1	1	0-1-0		65,3	hypothetical protein, conserved
LdBPK_291060.1	1	0-1-0		192,8	kinesin, putative
LdBPK_300640.1	1	0-1-0		25,0	ribosome biogenesis regulatory protein (RRS1), putative
LdBPK_301210.1	1	0-1-0		94,2	hypothetical protein, conserved
LdBPK_303230.1	1	1-0-0		45,9	3-hydroxy-3-methylglutaryl-CoA reductase, putative
LdBPK_310200.1	1	0-1-0		70,2	nucleolar protein, putative
LdBPK_310770.1	1	0-1-0		35,3	hypothetical protein, conserved
LdBPK_311190.1	1	0-1-0		12,4	hypothetical protein, unknown function
LdBPK_311640.1	1	1-0-0		29,5	diphthine synthase-like protein
LdBPK_311650.1	1	0-1-0		19,2	hypothetical protein, conserved
LdBPK_312700.1	1	0-0-1		40,8	serine/threonine protein phosphatase pp1(5.9), putative
LdBPK_312890.1	1	1-0-0		20,2	ADP-ribosylation factor, putative
LdBPK_320140.1	1	0-1-0		111,6	hypothetical protein, conserved
LdBPK_320240.1	1	0-1-0		10,6	dynein light chain, flagellar outer arm, putative
LdBPK_320270.1	1	0-1-0		147,0	Serine/threonine-protein kinase Nek1-related, putative
LdBPK_320620.1	1	0-1-0		36,8	hypothetical protein, conserved
LdBPK_322740.1	1	0-1-0		68,4	hypothetical protein, conserved
LdBPK_323630.1	1	0-1-0		86,3	hypothetical protein, conserved
LdBPK_332730.1	1	0-1-0		120,2	hypothetical protein, conserved
LdBPK_333400.1	1	0-1-0		49,7	hypothetical protein, conserved
LdBPK_340150.1	1	1-0-0		33,3	malate dehydrogenase
LdBPK_340710.1	1	0-1*-0		80,5	hypothetical protein, conserved
LdBPK_341540.1	1	0-1-0		106,7	hypothetical protein, conserved
LdBPK_342160.1	1	0-1-0		20,8	centrin, putative
LdBPK_342540.1	1	0-1-0		49,8	hypothetical protein, conserved
LdBPK_342590.1	1	0-1-0		33,6	hypothetical protein, conserved
LdBPK_343900.1	1	0-1-0		79,2	hypothetical protein, conserved
LdBPK_344120.1	1	0-1-0		20,2	nucleolar protein family a, putative (fragment)
LdBPK_351600.1	1	0-1-0		84,4	hypothetical protein, conserved
LdBPK_351800.1	1	0-1-0		54,0	trypanin-like protein
LdBPK_352030.1	1	0-1-0		404,6	ankyrin repeat protein, putative
LdBPK_352250.1	1	0-1-0		11,2	kinetoplastid membrane protein-11
LdBPK_352260.1	1	0-1*-0		11,2	kinetoplastid membrane protein-11
LdBPK_352820.1	1	0-1-0		143,1	hypothetical protein, conserved
LdBPK_353030.1	1	0-1-0		51,0	chaperone protein DNAj, putative
LdBPK_353290.1	1	0-1-0		90,5	hypothetical protein, conserved
LdBPK_354190.1	1	1-0-0		59,7	conserved hypothetical protein
LdBPK_354670.1	1	0-1-0		56,7	hypothetical protein, conserved
LdBPK_360910.1	1	0-1-0		94,5	hypothetical protein, conserved
LdBPK_360950.1	1	0-1-0		27,1	Eukaryotic translation initiation factor 6 (eIF-6), putative
LdBPK_361130.1	2	1-1-0		2,2	ribosomal protein L24, putative (fragment)
LdBPK_361440.1	1	0-1-0		118,5	hypothetical protein, conserved
LdBPK_361930.1	1	0-1-0		59,4	DEAD box RNA helicase, putative
LdBPK_362480.1	1	0-1*-0		35,5	glyceraldehyde 3-phosphate dehydrogenase, cytosolic

LdBPK_362680.1	1	0-1-0		42,5	hypothetical protein, conserved
LdBPK_363270.1	1	0-1-0		62,5	hypothetical protein, conserved
LdBPK_363830.1	1	0-1-0		63,0	hypothetical protein, conserved
LdBPK_364100.1	1	0-1-0		47,8	S-adenosylhomocysteine hydrolase
LdBPK_364270.1	1	0-1-0		38,7	phosphoglycerate mutase family member 5, putative
LdBPK_365020.1	1	0-1-0		101,8	hypothetical protein, conserved
LdBPK_365380.1	1	0-1-0		71,2	hypothetical protein, conserved
LdBPK_366100.1	2	1-1-0		14,1	kinetoplast-associated protein, putative
LdBPK_366180.1	2	1-1-0		18,4	kinetoplast DNA-associated protein, putative
LdBPK_366230.1	1	0-1-0		70,4	hypothetical protein, conserved
LdBPK_367070.1	1	1-0-0		29,1	hypothetical protein, conserved
LDPBQ7IC8_280037600	1	0-1-0		72,1	
LdBPK_010260.1	1	0-2-0		30,6	hypothetical protein, conserved
LdBPK_020630.1	1	0-2-0		100,7	hypothetical protein, conserved
LdBPK_040890.1	1	0-2-0		140,3	hypothetical protein, conserved
LdBPK_060680.1	1	0-2-0		70,9	hypothetical protein, conserved
LdBPK_071080.1	1	0-2-0		36,7	hypothetical protein, conserved
LdBPK_100920.1	2	1*-2*-0		14,6	histone H3
LdBPK_101110.1	1	0-2-0		41,4	RNA-binding protein-like protein
LdBPK_110410.1	1	0-2-0		91,4	hypothetical protein, conserved
LdBPK_120240.1	1	0-2-0		169,8	hypothetical protein, unknown function
LdBPK_120570.1	1	0-2-0		155,0	hypothetical protein, conserved
LdBPK_140840.1	1	0-2-0		21,0	hypothetical protein, conserved
LdBPK_150580.1	1	0-2-0		57,4	hypothetical protein, conserved
LdBPK_160120.1	1	0-2-0		94,7	hypothetical protein, conserved
LdBPK_160610.1	2	1-2-0		12,0	histone H3, putative (fragment)
LdBPK_170010.1	1	0-2-0		87,6	hypothetical protein, conserved
LdBPK_170270.1	1	0-2-0		114,9	hypothetical protein, conserved
LdBPK_181600.1	1	0-2-0		73,3	hypothetical protein, conserved
LdBPK_190230.1	1	0-2-0		72,8	hypothetical protein, conserved
LdBPK_190340.1	1	0-2-0		49,9	hypothetical protein, conserved
LdBPK_191030.1	1	0-2-0		131,9	hypothetical protein, conserved
LdBPK_191410.1	1	0-2-0		81,1	hypothetical protein, conserved
LdBPK_210980.1	2	1-2-0		23,6	hypoxanthine-guanine phosphoribosyltransferase
LdBPK_211160.1	1	0-2-0		13,9	histone H2A
LdBPK_211170.1	1	0-2*-0		13,9	histone H2A, putative
LdBPK_211220.1	1	0-2-0		199,9	intraflagellar transport protein 172, putative (IFT172)
LdBPK_220080.1	1	0-2-0		171,6	hypothetical protein, conserved
LdBPK_220180.1	1	0-2-0		60,7	hypothetical protein, conserved
LdBPK_231380.1	1	0-2-0		52,2	hypothetical protein, unknown function
LdBPK_231850.1	1	0-2-0		59,1	hypothetical protein, conserved
LdBPK_242000.1	1	0-2-0		57,4	hypothetical protein, conserved
LdBPK_250080.1	1	0-2-0		60,9	poly(A)-binding protein, putative
LdBPK_250630.1	1	0-2-0		181,6	RNA polymerase I second largest subunit, putative
LdBPK_260020.1	1	0-2-0		40,3	brix domain containing-like protein
LdBPK_261180.1	1	0-2-0		71,6	hypothetical protein, conserved
LdBPK_261530.1	1	0-2-0		79,3	trifunctional enzyme alpha subunit, mitochondrial precursor-like protein
LdBPK_261610.1	2	1-2-0		9,7	40S ribosomal protein S33, putative
LdBPK_280050.1	1	0-2-0		56,1	hypothetical protein, conserved
LdBPK_280790.1	1	0-2-0		44,0	hypothetical protein, conserved
LdBPK_281150.1	1	0-2-0		43,8	hypothetical protein, conserved
LdBPK_281360.1	1	0-2-0		49,2	hypothetical protein, conserved
LdBPK_282220.1	1	0-2-0		60,3	DEAD-box ATP-dependent RNA helicase, mitochondrial (MHLE1)
LdBPK_282430.1	1	0-2-0		23,8	glycosomal membrane protein, putative

LdBPK_282490.1	1	0-2-0		94,9	hypothetical protein, conserved
LdBPK_282730.1	1	0-2-0		165,0	hypothetical protein, conserved
LdBPK_290200.1	1	0-2-0		105,6	hypothetical protein, conserved
LdBPK_291890.1	1	0-2-0		69,1	paraflagellar rod protein 1D, putative
LdBPK_301900.1	1	0-2-0		66,4	hypothetical protein, unknown function
LdBPK_302840.1	1	0-2-0		91,9	hypothetical protein, conserved
LdBPK_302940.1	1	0-2-0		49,0	hypothetical protein, conserved
LdBPK_303700.1	1	0-2-0		63,7	hypothetical protein, conserved
LdBPK_303710.1	1	0-2-0		24,4	ribosomal protein L15, putative
LdBPK_310210.1	1	0-2-0		52,4	hypothetical protein, conserved
LdBPK_310570.1	1	0-2-0		135,3	hypothetical protein, conserved
LdBPK_310700.1	1	0-2-0		126,7	hypothetical protein, conserved
LdBPK_313240.1	1	0-2-0		95,9	hypothetical protein, conserved
LdBPK_320360.1	1	0-2-0		51,0	hypothetical protein, conserved
LdBPK_320430.1	1	0-2-0		80,9	hypothetical protein, conserved
LdBPK_321120.1	1	0-2-0		67,9	dynein, putative
LdBPK_322670.1	1	0-2-0		101,9	hypothetical protein, conserved
LdBPK_323050.1	1	0-2-0		70,4	outer dynein arm docking complex, putative (DC2)
LdBPK_330070.1	1	0-2-0		75,8	hypothetical protein, conserved
LdBPK_330630.1	1	0-2-0		101,4	hypothetical protein, conserved
LdBPK_330840.1	1	0-2-0		176,0	hypothetical protein, conserved
LdBPK_331290.1	1	0-2-0		66,8	hypothetical protein, conserved
LdBPK_332660.1	1	0-2-0		144,5	hypothetical protein, conserved
LdBPK_340260.1	1	0-2-0		148,8	hypothetical protein, conserved
LdBPK_340640.1	1	0-2-0		251,4	hypothetical protein, conserved
LdBPK_340780.1	1	0-2-0		52,8	hypothetical protein, conserved
LdBPK_340970.1	1	0-2-0		74,7	hypothetical protein, conserved
LdBPK_342870.1	1	0-2-0		63,9	hypothetical protein, conserved
LdBPK_350630.1	1	0-2-0		66,0	hypothetical protein, conserved
LdBPK_352240.1	2	0-2-1		30,3	RNA-binding protein, putative
LdBPK_353970.1	1	0-2-0		51,2	hypothetical protein, conserved
LdBPK_354080.1	1	0-2-0		78,9	ATP-dependent RNA helicase, putative
LdBPK_354760.1	1	0-2-0		34,6	hypothetical protein, conserved
LdBPK_354930.1	1	0-2-0		111,6	hypothetical protein, conserved
LdBPK_360430.1	1	0-2-0		48,2	hypothetical protein, conserved
LdBPK_362730.1	1	0-2-0		74,7	cyclin-e binding protein 1-like protein
LdBPK_364180.1	2	2-0-1		24,1	hslVU complex proteolytic subunit, threonine peptidase, Clan T(1), family T1B, ATP-dependent protease subunit HslV, putative (HslV)
LdBPK_364550.1	1	0-2-0		61,0	hypothetical protein, unknown function
LdBPK_364810.1	1	0-2-0		48,7	hypothetical protein, conserved
LdBPK_365350.1	1	0-2-0		26,3	40S ribosomal protein SA, putative
LdBPK_366150.1	1	0-2-0		208,8	hypothetical protein, conserved
LdBPK_366480.1	1	0-2-0		150,7	flagellum transition zone component, putative
LdBPK_050100.1	1	0-3-0		71,8	phosphoprotein phosphatase, putative
LdBPK_080900.1	1	0-3-0		63,1	hypothetical protein, conserved
LdBPK_101240.1	1	0-3-0		57,0	hypothetical protein, conserved
LdBPK_120120.1	1	0-3-0		149,7	hypothetical protein, conserved
LdBPK_120400.1	1	0-3-0		69,3	hypothetical protein, conserved
LdBPK_131010.1	1	0-3-0		60,1	hypothetical protein, conserved
LdBPK_131350.1	2	1-3-0		80,8	Kinesin-13 5, putative (KIN13-5)
LdBPK_140120.1	1	0-3-0		37,5	hypothetical protein, conserved
LdBPK_151140.1	1	3-0-0		22,2	tryparedoxin peroxidase
LdBPK_170460.1	1	0-3-0		82,5	hypothetical protein, conserved
LdBPK_191140.1	1	0-3-0		290,3	hypothetical protein, conserved

LdBPK_212130.1	1	0-3-0		48,5	centromere/microtubule binding protein cbf5, putative
LdBPK_240240.1	1	0-3-0		66,6	ATP-dependent DEAD/H RNA helicase, putative
LdBPK_240270.1	1	0-3-0		75,1	dynein intermediate-chain-like protein
LdBPK_240410.1	1	0-3-0		79,7	hypothetical protein, conserved
LdBPK_242060.1	1	0-3-0		29,9	hypothetical protein, conserved
LdBPK_261230.1	1	0-3-0		76,7	hypothetical protein, conserved
LdBPK_262010.1	1	0-3-0		77,0	hypothetical protein, conserved
LdBPK_262440.1	1	0-3-0		71,2	hypothetical protein, conserved
LdBPK_271390.1	1	0-3-0		74,3	hypothetical protein, conserved
LdBPK_271690.1	1	0-3-0		92,3	hypothetical protein, conserved
LdBPK_271800.1	1	0-3-0		148,6	hypothetical protein, conserved
LdBPK_271900.1	1	0-3-0		105,2	FtsJ cell division protein, putative
LdBPK_291090.1	1	0-3-0		67,7	hypothetical protein, conserved
LdBPK_291360.1	1	3-0-0		97,0	ATP-dependent Clp protease subunit, heat shock protein 100 (HSP100), putative
LdBPK_292100.1	1	0-3-0		213,0	hypothetical protein, conserved
LdBPK_301360.1	1	0-3-0		33,1	U3 small nuclear ribonucleoprotein (snRNP), putative
LdBPK_303210.1	1	0-3-0		49,0	hypothetical protein, conserved
LdBPK_313100.1	1	0-3-0		217,4	hypothetical protein, conserved
LdBPK_320390.1	1	0-3-0		57,5	hypothetical protein, conserved
LdBPK_321490.1	1	0-3-0		121,4	hypothetical protein, conserved
LdBPK_322370.1	1	0-3-0		45,2	hypothetical protein, unknown function (fragment)
LdBPK_323320.1	1	0-3*-0		12,0	ribosomal protein L3, putative (fragment)
LdBPK_331300.1	1	0-3-0		89,0	hypothetical protein, conserved
LdBPK_332630.1	1	0-3-0		35,8	hypothetical protein, conserved
LdBPK_340270.1	1	0-3-0		42,7	hypothetical protein, conserved
LdBPK_340490.1	1	0-3-0		75,9	hypothetical protein, conserved
LdBPK_340720.1	1	0-3*-0		35,3	hypothetical protein, conserved (fragment)
LdBPK_341210.1	1	0-3-0		271,1	hypothetical protein, conserved
LdBPK_341470.1	1	0-3-0		276,8	hypothetical protein, conserved
LdBPK_342730.1	1	0-3-0		11,1	ribosomal protein L3, putative (fragment)
LdBPK_342780.1	1	0-3-0		46,9	hypothetical protein, conserved
LdBPK_351870.1	2	1-3-0		34,0	60S ribosomal protein L5, putative
LdBPK_353530.1	1	0-3-0		76,6	hypothetical protein, conserved
LdBPK_353920.1	1	0-3-0		50,2	hypothetical protein, conserved
LdBPK_360840.1	1	0-3-0		121,1	hypothetical protein, unknown function
LdBPK_363340.1	1	0-3-0		63,1	hypothetical protein, conserved
LdBPK_366690.1	1	0-3-0		58,2	hypothetical protein, conserved
LdBPK_366950.1	1	0-3-0		22,4	hypothetical protein, conserved
LdBPK_050580.1	1	0-4-0		86,4	hypothetical protein, conserved
LdBPK_051180.1	1	0-4-0		212,3	hypothetical protein, conserved
LdBPK_060330.1	1	0-4-0		129,5	hypothetical protein, conserved
LdBPK_070590.1	1	0-4-0		117,2	hypothetical protein, conserved
LdBPK_101150.1	1	0-4-0		65,1	hypothetical protein, unknown function
LdBPK_110150.1	1	0-4-0		93,6	hypothetical protein, conserved
LdBPK_120070.1	1	0-4-0		71,4	hypothetical protein, unknown function
LdBPK_120470.1	1	0-4-0		108,8	hypothetical protein, conserved
LdBPK_131330.1	1	0-4-0		83,3	hypothetical protein, conserved
LdBPK_140260.1	1	0-4-0		74,8	hypothetical protein, conserved
LdBPK_160990.1	1	0-4-0		110,0	hypothetical protein, conserved
LdBPK_161420.1	1	0-4-0		200,1	DNA-directed rna polymerase I largest subunit, putative
LdBPK_200330.1	1	0-4-0		35,0	leucine-rich repeat-containing protein
LdBPK_210670.1	1	0-4-0		75,1	RNA helicase, putative
LdBPK_230090.1	1	0-4-0		48,6	hypothetical protein, conserved
LdBPK_231120.1	1	0-4-0		60,0	cytosolic leucyl aminopeptidase

LdBPK_231490.1	1	0-4-0		148,7	hypothetical protein, conserved
LdBPK_240300.1	1	0-4-0		34,9	hypothetical protein, conserved
LdBPK_241930.1	1	0-4-0		57,7	hypothetical protein, conserved
LdBPK_251110.1	1	0-4-0		95,2	hypothetical protein, conserved
LdBPK_252300.1	1	0-4-0		34,5	hypothetical protein, conserved
LdBPK_280770.1	1	0-4-0		62,3	hypothetical protein, conserved
LdBPK_281420.1	1	0-4-0		99,8	ATP-dependent RNA helicase, putative
LdBPK_300240.1	1	0-4-0		66,7	hypothetical protein, conserved
LdBPK_301890.1	1	0-4-0		106,9	hypothetical protein, conserved
LdBPK_320150.1	1	0-4-0		110,6	hypothetical protein, conserved
LdBPK_321830.1	1	0-4-0		84,7	hypothetical protein, conserved
LdBPK_322040.1	1	0-4-0		84,6	hypothetical protein, conserved
LdBPK_331460.1	1	0-4-0		44,7	hypothetical protein, conserved
LdBPK_340620.1	1	0-4-0		91,2	hypothetical protein, conserved
LdBPK_340700.1	1	0-4-0		52,1	hypothetical protein, conserved (fragment)
LdBPK_342010.1	1	0-4-0		205,9	hypothetical protein, conserved
LdBPK_342350.1	1	0-4-0		78,6	unspecified product
LdBPK_342360.1	1	0-4*-0		78,7	hypothetical protein, unknown function
LdBPK_342400.1	1	0-4-0		64,0	hypothetical protein, conserved
LdBPK_350200.1	1	0-4-0		239,8	hypothetical protein, conserved
LdBPK_361630.1	1	0-4-0		53,0	hypothetical protein, conserved
LdBPK_364960.1	1	0-4-0		159,1	hypothetical protein, conserved
LdBPK_040060.1	1	0-5-0		58,9	hypothetical protein, conserved
LdBPK_051080.1	1	0-5-0		80,3	Phosphatidylinositol 4-phosphate 5-kinase, putative, MORN repeat-containing protein
LdBPK_081030.1	1	0-5-0		96,8	hypothetical protein, conserved
LdBPK_140430.1	1	0-5-0		84,7	hypothetical protein, conserved
LdBPK_201450.1	1	0-5-0		55,2	axoneme central apparatus protein, flagellar protein 16, putative (FP16)
LdBPK_251520.1	1	0-5-0		88,3	cAMP response protein, putative (CARP4)
LdBPK_260620.1	1	0-5-0		158,2	hypothetical protein, conserved
LdBPK_260740.1	1	0-5-0		62,4	hypothetical protein, unknown function
LdBPK_261280.1	1	0-5-0		125,6	hypothetical protein, conserved
LdBPK_280290.1	1	0-5-0		85,9	hypothetical protein, conserved
LdBPK_282000.1	1	0-5-0		139,7	hypothetical protein, conserved
LdBPK_291130.1	1	0-5-0		203,4	hypothetical protein, conserved
LdBPK_312660.1	1	0-5-0		102,7	hypothetical protein, conserved
LdBPK_313260.1	1	0-5-0		76,0	methylcrotonoyl-coa carboxylase biotinylated subunitprotein-like protein
LdBPK_313290.1	1	0-5-0		161,8	hypothetical protein, conserved
LdBPK_332590.1	1	0-5-0		114,4	hypothetical protein, conserved
LdBPK_366250.1	1	0-5-0		73,0	hypothetical protein, conserved
LdBPK_366660.1	1	0-5-0		84,1	hypothetical protein, conserved
LdBPK_050730.1	1	0-6-0		65,7	hypothetical protein, conserved
LdBPK_061080.1	1	0-6-0		80,0	hypothetical protein, conserved
LdBPK_131090.1	1	0-6-0		78,5	adenylosuccinate synthetase, putative
LdBPK_131250.1	1	0-6-0		125,0	hypothetical protein, conserved
LdBPK_141540.1	1	0-6-0		82,2	hypothetical protein, conserved (fragment)
LdBPK_160660.1	1	0-6-0		64,7	hypothetical protein, conserved
LdBPK_190090.1	2	1-6-0		31,3	fibrillarlin, putative
LdBPK_210590.1	1	0-6-0		121,8	hypothetical protein, conserved
LdBPK_221460.1	1	0-6-0		77,1	hypothetical protein, conserved
LdBPK_230040.1	1	0-6-0		53,7	beta propeller protein, putative
LdBPK_230520.1	1	0-6-0		155,5	hypothetical protein, conserved
LdBPK_252080.1	1	0-6-0		144,8	hypothetical protein, conserved
LdBPK_262310.1	1	0-6-0		137,5	hypothetical protein, conserved
LdBPK_271100.1	1	0-6-0		46,4	hypothetical protein, conserved

LdBPK_282900.1	1	0-6-0		49,0	hypothetical protein, unknown function
LdBPK_322460.1	1	0-6-0		129,0	hypothetical protein, conserved
LdBPK_351320.1	1	0-6*-0		11,4	histone H4
LdBPK_351980.1	1	0-6-0		115,7	hypothetical protein, conserved
LdBPK_363220.1	1	0-6-0		25,8	fibrillarin
LdBPK_040710.1	1	0-7-0		86,3	hypothetical protein, conserved
LdBPK_060010.1	1	0-7-0		11,4	histone H4
LdBPK_110470.1	1	0-7-0		81,1	pumilio-repeat, RNA-binding protein, putative
LdBPK_150010.1	1	0-7-0		11,4	histone H4
LdBPK_161510.1	1	0-7-0		68,9	paraflagellar rod protein 2C
LdBPK_210020.1	1	0-7*-0		11,5	histone H4
LdBPK_290780.1	1	0-7-0		74,9	U3 small nucleolar ribonucleoprotein protein MPP10, putative
LdBPK_291960.1	1	0-7-0		37,6	hypothetical protein, conserved
LdBPK_302110.1	1	0-7-0		68,8	hypothetical protein, conserved
LdBPK_331580.1	1	0-7-0		91,4	hypothetical protein, conserved
LdBPK_340500.1	1	0-7-0		291,3	calcium channel protein, putative
LdBPK_350020.1	1	0-7*-0		11,4	unspecified product
LdBPK_361920.1	1	0-7-0		73,1	DEAD box RNA helicase, putative
LdBPK_363370.1	1	0-7-0		62,3	hypothetical protein, conserved
LdBPK_181150.1	1	0-8-0		107,0	hypothetical protein, conserved
LdBPK_230790.1	1	0-8-0		76,6	hypothetical protein, conserved
LdBPK_311320.1	1	0-8-0		108,0	hypothetical protein, conserved
LdBPK_365140.1	1	0-8-0		43,0	hypothetical protein, conserved
LdBPK_101040.1	1	0-9-0		87,3	hypothetical protein, conserved
LdBPK_110810.1	1	0-9-0		104,5	hypothetical protein, conserved
LdBPK_180830.1	1	0-9-0		102,9	Periodic tryptophan protein 2 homolog, putative
LdBPK_242270.1	1	0-9-0		163,9	basal body component, putative
LdBPK_261790.1	1	0-9-0		297,4	hypothetical protein, conserved
LdBPK_311010.1	1	0-9-0		80,4	hypothetical protein, conserved
LdBPK_320260.1	1	0-9-0		194,4	hypothetical protein, conserved
LdBPK_331970.1	1	0-9-0		74,5	nucleolar GTP-binding protein, putative
LdBPK_050050.1	1	0-10-0		94,0	hypothetical protein, conserved
LdBPK_071250.1	1	0-10-0		91,2	hypothetical protein, conserved
LdBPK_171350.1	1	0-10-0		116,7	hypothetical protein, conserved
LdBPK_210830.1	1	0-10-0		78,7	hypothetical protein, conserved
LdBPK_221160.1	1	0-10-0		116,4	hypothetical protein, unknown function (fragment)
LdBPK_250440.1	1	0-10-0		109,7	hypothetical protein, conserved
LdBPK_281210.1	1	0-10-0		68,5	hypothetical protein, conserved
LdBPK_140580.1	1	0-11-0		126,9	hypothetical protein, conserved
LdBPK_290390.1	1	0-11-0		104,7	hypothetical protein, conserved
LdBPK_340320.1	1	0-11-0		81,3	hypothetical protein, conserved
LdBPK_351210.1	1	0-12-0		79,8	pre-mRNA splicing factor ATP-dependent RNA helicase, putative
LdBPK_364420.1	1	0-12-0		107,1	hypothetical protein, conserved
LdBPK_090570.1	1	0-13-0		86,9	hypothetical protein, conserved
LdBPK_311390.1	1	0-13-0		156,8	hypothetical protein, conserved
LdBPK_200710.1	1	0-14-0		81,0	rRNA biogenesis protein-like protein
LdBPK_270720.1	1	0-14-0		84,9	hypothetical protein, conserved
LdBPK_311400.1	1	0-15-0		97,3	hypothetical protein, unknown function
LdBPK_090120.1	1	0-23-0		65,7	hypothetical protein, conserved

## IP from axenic amastigotes

Gene ID	Group #1 (Mock): Replicate 1		Group #2 (Mock): Replicate 2		Group #3 (Mock): Replicate 3		Group #1 (LmCK1.2-V5): Replicate 1		Group #2 (LmCK1.2-V5): Replicate 2		Group #3 (LmCK1.2-V5): Replicate 3		MW (kDa)	Protein name
	Number of peptides identified in elutions 1-2	Sum peptide	Number of peptides identified in elutions 1-2	Sum peptide	Number of peptides identified in elutions 1-2	Sum peptide	Number of peptides identified in elutions 1-2	Sum peptide	Number of peptides identified in elutions 1-2	Sum peptide	Number of peptides identified in elutions 1-2	Sum peptide		
LdBPK_351030.1	-	0	1-0	1	-	0	74-44	118	74-46	120	74-46	120	39,8	casein kinase, putative
LdBPK_151330.1	-	0	-	0	-	0	63-34	97	73-22	95	59-29	88	92,6	MGT1 magnesium transporter
LdBPK_361350.1	-	0	-	0	-	0	45-18	63	50-15	65	50-16	66	67,5	hypothetical protein, conserved
LdBPK_100800.1	-	0	-	0	-	0	41-29	70	41-24	65	39-22	61	208,9	hypothetical protein, conserved
LdBPK_341610.1	-	0	-	0	-	0	42-17	59	42-13	55	45-13	58	55,2	hypothetical protein, conserved
LdBPK_352220.1	-	0	-	0	-	0	41-14	55	45-8	53	45-6	51	114,9	hypothetical protein, conserved
LDPBQ71C8_28003650 (LinJ_28.2960)	12-2	14	5-2	7	8-0	8	36-10	46	38-9	47	38-8	46	71,3	hsp70
LDPBQ71C8_30003310	17-3	20	3-4	7	13-1	14	22-4	26	30-4	34	25-7	32	71,8	hsp70
LdBPK_333300.1	16-3	19	10-5	15	11-3	14	25-6	31	25-4	29	19-7	26	17,4	40S ribosomal protein S13, putative
LdBPK_081300.1	-	0	-	0	-	0	24-6	30	23-6	29	21-6	27	66,9	histone deacetylase, putative
LDPBQ71C8_28001840	4-1	5	1-0	1	3-0	3	22-5	27	26-3	29	22-2	24	71,8	hsp70
LdBPK_070060.1	-	0	-	0	-	0	21-5	26	26-3	29	19-2	21	107,7	alpha-adaptin-like protein
LdBPK_250870.1	-	0	-	0	-	0	17-7	24	21-8	29	16-12	28	41,6	hypothetical protein, conserved
LdBPK_321780.1	-	0	-	0	-	0	11-14	25	19-10	29	15-17	32	89,8	hypothetical protein, conserved
LdBPK_211290.1	8-11	19	3-9	12	7-6	13	13-13	26	13-14	27	10-14	24	21,5	60S ribosomal protein L9, putative
LdBPK_170170.1	14-10	24	6-11	17	8-5	13	13-10	23	14-11	25	14-14	28	49,1	elongation factor 1-alpha
LdBPK_353840.1	13-5	18	4-8	12	8-10	18	12-11	23	13-11	24	16-17	33	15,0	60S ribosomal protein L23, putative
LdBPK_363660.1	-	0	-	0	-	0	26-2	28	20-3	23	24-2	26	88,6	hypothetical protein, conserved
LdBPK_302480.1	14*-3*	17	2*-4*	6	9*-1*	10	15*-4*	19	19*-4*	23	15*-6*	21	54,2	heat shock 70-related protein 1, mitochondrial precursor, putative (fragment)
LdBPK_110990.1	-	0	-	0	-	0	18-0	18	21-1	22	23-0	23	108,5	adaptin-related protein-like protein
LdBPK_343440.1	10-5	15	7-6	13	10-5	15	16-7	23	15-7	22	14-6	20	18,0	60S ribosomal protein L21, putative
LdBPK_151000.1	-	0	2-4	6	2-0	2	14-4	18	18-4	22	27-8	35	129,2	hypothetical protein, conserved
LDPBQ71C8_26001800	-	0	-	0	-	0	17-6	23	19-2	21	14-2	16	70,4	hsp70
LdBPK_240040.1	7-4	11	6-9	15	7-2	9	12-6	18	15-5	20	13-8	21	19,1	60S ribosomal protein L17, putative
LdBPK_210900.1	-	0	-	0	-	0	15-4	19	13-4	17	18-6	24	115,9	hypothetical protein, conserved
LdBPK_180100.1	-	0	-	0	-	0	14-3	17	13-4	17	17-3	20	50,2	hypothetical protein, conserved
LdBPK_131120.1	8-3	11	4-3	7	5-4	9	13-4	17	12-5	17	12-3	15	30,6	40S ribosomal protein S4, putative
LdBPK_252520.1	3-0	3	1-0	1	-	0	10-0	10	15-1	16	13-0	13	109,3	hypothetical protein, conserved
LdBPK_040750.1	6-5	11	5-6	11	6-4	10	8-6	14	10-6	16	10-7	17	24,6	60S ribosomal protein L10, putative
LdBPK_330960.1	8-4	12	5-7	12	4-3	7	11-7	18	10-5	15	12-9	21	37,7	40S ribosomal protein S3, putative
LdBPK_366240.1	-	0	-	0	-	0	5-6	11	7-7	14	6-9	15	46,7	hypothetical protein, unknown function
LdBPK_341080.1	-	0	-	0	-	0	18-2	20	13-0	13	20-3	23	66,9	hypothetical protein, conserved
LdBPK_130330.1	3-1	4	1-0	1	2-0	2	10-2	12	9-4	13	13-2	15	49,8	alpha tubulin
LdBPK_350400.1	-	0	-	0	-	0	10-1	11	12-1	13	10-0	10	30,0	40S ribosomal protein S3A, putative
LdBPK_111110.1	5-3	8	4-2	6	3-2	5	9-3	12	10-3	13	6-4	10	16,4	60S ribosomal protein L28, putative
LdBPK_320460.1	4-3	7	1-3	4	3-2	5	8-5	13	10-3	13	10-2	12	28,6	40S ribosomal protein S2

LdBPK_354190.1	-	0	0-3	3	0-1	1	1-7	8	5-8	13	3-14	17	59,7	conserved hypothetical protein
LdBPK_252460.1	-	0	-	0	-	0	10-4	14	10-2	12	11-4	15	39,7	hypothetical protein, conserved
LdBPK_342620.1	8-4	12	3-4	7	1-3	4	10-3	13	7-5	12	6-0	6	20,1	40S ribosomal protein S19 protein, putative
LdBPK_290210.1	-	0	-	0	-	0	6-4	10	10-2	12	6-8	14	174,2	hypothetical protein, conserved
LdBPK_322920.1	-	0	-	0	-	0	3-0	3	12-0	12	13-0	13	115,2	hypothetical protein, conserved
LdBPK_367220.1	-	0	-	0	-	0	2-0	2	12-0	12	14-0	14	143,8	nuclear pore complex protein (NUP155), putative, nucleoporin, putative
LdBPK_362640.1	-	0	-	0	-	0	1-0	1	12-0	12	15-0	15	97,1	nucleoporin interacting component (NUP93), putative
LdBPK_363180.1	-	0	-	0	-	0	12-0	12	11-0	11	8-0	8	48,9	clathrin coat assembly protein-like protein
LdBPK_291160.1	0-1	1	-	0	1-0	1	7-2	9	10-1	11	7-1	8	41,1	ribosomal protein L1a, putative
LdBPK_190200.1	9-6	15	2-1	3	2-1	3	10-4	14	8-2	10	9-4	13	35,2	ADP,ATP carrier protein 1, mitochondrial precursor, putative
LdBPK_320410.1	3-6	9	1-2	3	2-1	3	10-5	15	7-3	10	6-5	11	66,8	ATP-dependent RNA helicase, putative
LdBPK_281050.1	1-2	3	1-3	4	2-2	4	5-0	5	6-4	10	5-4	9	15,6	40S ribosomal protein S14
LdBPK_303390.1	3*-5*	8	0-5*	5	2*-2*	4	5*-5*	10	4*-6*	10	3*-5*	8	10,4	60S ribosomal protein L9, putative (fragment)
LdBPK_303650.1	1*-2*	3	1*-3*	4	2*-2*	4	5*-0	5	6*-4*	10	5*-4*	9	15,6	40S ribosomal protein S14
LdBPK_181410.1	-	0	-	0	-	0	3-3	6	6-4	10	2-3	5	121,9	chaperone DNAJ protein, putative
LdBPK_366110.1	0-1	1	0-5	5	0-3	3	1-1	2	4-6	10	1-12	13	58,3	flagellum targeting protein kharon1, putative (KH1)
LdBPK_151320.1	-	0	-	0	-	0	5-1	6	8-1	9	2-2	4	154,7	ubiquitin hydrolase, putative
LdBPK_350240.1	5-3	8	1-5	6	3-4	7	3-5	8	5-4	9	3-6	9	11,4	60S ribosomal protein L30
LdBPK_360990.1	2-4	6	1-3	4	2-0	2	5-4	9	4-5	9	3-6	9	19,0	40S ribosomal protein S18, putative
LdBPK_361310.1	2-2	4	1-1	2	1-1	2	4-1	5	6-3	9	4-2	6	22,1	40S ribosomal protein S9, putative
LdBPK_060440.1	-	0	0-3	3	1-4	5	0-3	3	4-5	9	3-5	8	58,8	hypothetical protein, conserved
LdBPK_320270.1	0-1	1	0-3	3	0-4	4	0-9	9	0-8	8	0-11	11	147,0	Serine/threonine-protein kinase Nek1-related, putative
LdBPK_352040.1	9-1*	10	3-1*	4	5-1*	6	9-1*	10	8*-0	8	9-0	9	15,4	60S ribosomal protein L32
LdBPK_352100.1	-	0	-	0	-	0	9-0	9	8-0	8	4-0	4	80,3	hypothetical protein, conserved
LdBPK_212090.1	8-2	10	3-1	4	6-1	7	8-1	9	8-0	8	8-0	8	15,3	60S ribosomal protein L32
LdBPK_270790.1	5-0	5	2-2	4	2-0	2	5-0	5	8-0	8	5-0	5	44,5	isovaleryl-coA dehydrogenase, putative
LdBPK_320790.1	4-2	6	3-2	5	1-0	1	4-1	5	7-1	8	6-4	10	25,2	RNA binding protein, putative
LdBPK_251220.1	4-3	7	2-2	4	2-2	4	3-3	6	4-4	8	4-3	7	13,0	ribosomal protein S25
LdBPK_271740.1	-	0	0-2	2	0-2	2	2-1	3	4-4	8	4-4	8	180,9	hypothetical protein, conserved
LdBPK_342370.1	-	0	-	0	-	0	0-1	1	4-4	8	2-3	5	100,1	hypothetical protein, conserved
LdBPK_060590.1	4-0	4	3-1	4	1-1	2	8-0	8	7-0	7	6-0	6	16,4	60S ribosomal protein L23a, putative
LdBPK_290470.1	-	0	-	0	-	0	8-4	12	7-0	7	6-4	10	78,4	hypothetical protein, conserved
LdBPK_330990.1	-	0	-	0	-	0	7-2	9	6-1	7	3-3	6	122,1	hypothetical protein, conserved
LdBPK_321890.1	-	0	-	0	-	0	6-0	6	5-2	7	4-2	6	16,7	hypothetical protein, conserved
LdBPK_190130.1	2-2	4	0-2	2	0-1	1	5-2	7	5-2	7	5-0	5	68,5	protein kinase, putative
LdBPK_210300.1	-	0	-	0	-	0	5-0	5	7-0	7	5-0	5	51,7	hexokinase, putative
LdBPK_301580.1	-	0	-	0	-	0	3-5	8	5-2	7	4-3	7	181,7	protein kinase, putative
LdBPK_171300.1	-	0	0-3	3	0-1	1	2-3	5	3-4	7	2-3	5	90,4	hypothetical protein, conserved
LdBPK_050770.1	0-2	2	0-2	2	0-3	3	0-2	2	1-6	7	2-11	13	139,6	hypothetical protein, unknown function
LdBPK_292620.1	-	0	-	0	-	0	2-0	2	7-0	7	3-1	4	54,0	ATP-dependent phosphofructokinase
LdBPK_364480.1	-	0	-	0	-	0	-	0	7-0	7	9-0	9	178,6	hypothetical protein, conserved
LdBPK_072500.1	-	0	-	0	-	0	5-0	5	6-0	6	3-0	3	58,3	glycosomal phosphoenolpyruvate carboxykinase, putative
LdBPK_170750.1	2-0	2	0-1	1	-	0	5-1	6	5-1	6	5-0	5	48,2	hypothetical protein, conserved (fragment)
LdBPK_261940.1	-	0	-	0	-	0	5-0	5	6-0	6	8-0	8	37,7	hypothetical protein, conserved
LdBPK_280570.1	6-0	6	3-0	3	5-0	5	5-0	5	6-0	6	6-0	6	12,8	ribosomal protein S26, putative
LdBPK_081290.1	1-0	1	2-0	2	1-0	1	4-0	4	5-1	6	7-0	7	15,9	beta tubulin (fragment)
LdBPK_211300.1	1-1	2	0-2	2	2-0	2	4-2	6	3-3	6	3-2	5	15,9	40S ribosomal protein S23, putative
LdBPK_281100.1	2-5	7	1-2	3	1-3	4	4-3	7	1-5	6	0-5	5	13,0	ribosomal protein S20, putative
LdBPK_353810.1	2-4	6	0-3	3	2-2	4	4-4	8	3-3	6	2-3	5	16,1	60S ribosomal protein L27A/L29, putative
LdBPK_270390.1	-	0	-	0	-	0	3-0	3	6-0	6	6-1	7	159,1	Nuclear pore complex protein 158, serine peptidase, Clan SP, family S59, putative (Nup158)
LdBPK_332160.1	-	0	-	0	-	0	3-0	3	6-0	6	9-0	9	86,6	hypothetical protein, conserved

LdBPK_110600.1	-	0	-	0	-	0	2-0	2	6-0	6	2-0	2	58,4	3-methylcrotonoyl-CoA carboxylase beta subunit, putative
LdBPK_350370.1	-	0	-	0	-	0	2-0	2	6-0	6	4-0	4	46,4	ATP-dependent DEAD-box RNA helicase, putative
LdBPK_242160.1	4-1	5	4-0	4	2-0	2	6-0	6	5-0	5	4-0	4	25,0	40S ribosomal protein S8, putative
LdBPK_242380.1	-	0	-	0	-	0	5-0	5	4-1	5	5-2	7	85,5	cullin-like protein-like protein
LdBPK_261530.1	9-0	9	-	0	-	0	5-0	5	5-0	5	5-0	5	79,3	trifunctional enzyme alpha subunit, mitochondrial precursor-like protein
LdBPK_130650.1	-	0	-	0	-	0	4-0	4	5-0	5	6-1	7	218,0	hypothetical protein, conserved
LdBPK_363020.1	1-1	2	-	0	2-0	2	4-0	4	4-1	5	3-0	3	15,8	40S ribosomal protein S24e
LdBPK_030240.1	2-3	5	2-2	4	0-2	2	2-3	5	2-3	5	3-3	6	9,5	ribosomal protein L38, putative
LdBPK_111130.1	3*-2*	5	3*-1*	4	2*-1*	3	3*-1*	4	4*-1*	5	3*-2*	5	5,2	60S ribosomal protein L28, putative (fragment)
LdBPK_111180.1	2-2	4	1-3	4	1-2	3	3-2	5	3-2	5	3-1	4	14,7	40S ribosomal protein S15A, putative
LdBPK_190710.1	2-0	2	1-0	1	-	0	3-0	3	5-0	5	2-0	2	33,6	glycosomal malate dehydrogenase
LdBPK_251160.1	4-3	7	5-3	8	2-3	5	2-3	5	2-3	5	3-2	5	54,2	aldehyde dehydrogenase, mitochondrial precursor
LdBPK_302990.1	2-1	3	0-2	2	1-0	1	3-2	5	2-3	5	3-1	4	39,1	unspecified product
LdBPK_350600.1	2-3	5	3-3	6	3-1	4	3-1	4	4-1	5	3-2	5	20,8	60S ribosomal protein L18a, putative
LdBPK_363940.1	3-4	7	1-3	4	3-1	4	3-3	6	2-3	5	2-4	6	9,8	40S ribosomal protein S27-1, putative
LdBPK_170290.1	-	0	-	0	-	0	0-2	2	0-5	5	0-7	7	121,5	hypothetical protein, conserved
LdBPK_262350.1	1-1	2	1-2	3	2-1	3	2-2	4	2-3	5	1-1	2	15,2	60S ribosomal protein L35, putative
LdBPK_300120.1	-	0	-	0	-	0	2-0	2	5-0	5	3-0	3	69,5	alkyldihydroxyacetonephosphate synthase
LdBPK_340270.1	-	0	0-1	1	0-1	1	0-2	2	1-4	5	0-7	7	42,7	hypothetical protein, conserved
LdBPK_362140.1	-	0	0-2	2	0-1	1	0-1	1	3-2	5	3-1	4	59,3	chaperonin HSP60, mitochondrial precursor
LdBPK_171330.1	-	0	-	0	-	0	-	0	3-2	5	-	0	172,2	hypothetical protein, conserved
LdBPK_320050.1	-	0	-	0	-	0	-	0	5-0	5	4-0	4	36,4	protein transport protein SEC13, putative
LdBPK_353330.1	4-0	4	2-0	2	2-0	2	5-0	5	4-0	4	5-0	5	20,8	60S ribosomal subunit protein L31, putative
LdBPK_080800.1	-	0	-	0	-	0	4-0	4	4-0	4	3-0	3	32,6	hypothetical protein, unknown function
LdBPK_302440.1	-	0	-	0	0-1	1	0-4	4	0-4	4	0-2	2	128,6	hypothetical protein, conserved
LdBPK_364650.1	-	0	0-4	4	0-1	1	1-4	5	1-3	4	0-4	4	41,2	asparaginase-like protein
LdBPK_170270.1	-	0	-	0	0-1	1	0-2	2	0-4	4	0-5	5	114,9	hypothetical protein, conserved
LdBPK_211790.1	1-1	2	1-2	3	2-2	4	2-0	2	3-1	4	2-2	4	4,0	40S ribosomal protein S11, putative (fragment)
LdBPK_212240.1	1*-0	1	1*-0	1	-	0	2*-0	2	3*-1*	4	5*-0	5	8,7	beta tubulin (fragment)
LdBPK_270700.1	-	0	-	0	-	0	2-1	3	3-1	4	0-2	2	62,6	hypothetical protein, conserved
LdBPK_323840.1	-	0	0-3	3	0-2	2	0-2	2	0-4	4	0-3	3	100,3	hypothetical protein, conserved
LdBPK_120720.1	-	0	-	0	-	0	0-1	1	0-4	4	0-2	2	144,0	hypothetical protein, conserved
LdBPK_242050.1	-	0	-	0	-	0	1-0	1	4-0	4	4-0	4	81,0	hypothetical protein, conserved
LdBPK_311930.1	-	0	-	0	-	0	1-0	1	2-2	4	1-0	1	14,7	ubiquitin-fusion protein
LdBPK_080130.1	-	0	-	0	-	0	-	0	0-4	4	3-4	7	121,2	hypothetical protein, conserved
LdBPK_090120.1	-	0	-	0	2-0	2	-	0	4-0	4	5-0	5	65,7	hypothetical protein, conserved
LdBPK_220260.1	-	0	-	0	-	0	-	0	4-0	4	3-0	3	138,0	hypothetical protein, conserved
LdBPK_190190.1	3*-1*	4	-	0	-	0	4*-1*	5	3*-0	3	3*-0	3	11,3	ADP,ATP carrier protein 1, mitochondrial precursor, putative (fragment)
LdBPK_010440.1	2-0	2	1-1	2	2-0	2	3-1	4	2-1	3	5-0	5	23,8	ribosomal protein S7, putative
LdBPK_150010.1	6-0	6	-	0	-	0	3-0	3	3-0	3	2-0	2	11,4	histone H4
LdBPK_210020.1	6*-0	6	-	0	-	0	3*-0	3	3*-0	3	2*-0	2	11,5	histone H4
LdBPK_211280.1	-	0	0-1	1	0-1	1	0-3	3	0-3	3	0-2	2	231,1	kinesin, putative
LdBPK_221030.1	-	0	-	0	-	0	0-3	3	0-3	3	1-0	1	130,2	hypothetical protein, conserved
LdBPK_262410.1	0-1	1	0-3	3	0-2	2	0-3	3	0-3	3	0-4	4	97,2	hypothetical protein, conserved
LdBPK_271890.1	-	0	-	0	-	0	3-0	3	3-0	3	2-0	2	11,8	small nuclear ribonucleoprotein protein, putative
LdBPK_323680.1	-	0	-	0	-	0	3-0	3	3-0	3	3-0	3	67,4	hypothetical protein, conserved
LdBPK_350020.1	6*-0	6	-	0	-	0	3*-0	3	3*-0	3	2*-0	2	11,4	unspecified product
LdBPK_010430.1	1*-0	1	0-1*	1	2*-0	2	2*-1*	3	2*-1*	3	2*-0	2	11,5	ribosomal protein S7, putative (fragment)
LdBPK_161220.1	3-0	3	-	0	-	0	2-0	2	3-0	3	3-0	3	6,5	60S ribosomal protein L39, putative
LdBPK_211160.1	2-0	2	-	0	-	0	2-0	2	3-0	3	2-0	2	13,9	histone H2A
LdBPK_211170.1	2*-0	2	-	0	-	0	2*-0	2	3*-0	3	2*-0	2	13,9	histone H2A, putative
LdBPK_211910.1	-	0	-	0	-	0	2-0	2	3-0	3	3-0	3	102,2	hypothetical protein, conserved

LdBPK_251280.1	-	0	-	0	-	0	2-2	4	3-0	3	3-0	3	235,3	hypothetical protein, conserved
LdBPK_260160.1	-	0	-	0	-	0	2-0	2	3-0	3	1-0	1	28,9	60S ribosomal protein L7, putative
LdBPK_281700.1	1-0	1	1-0	1	2-0	2	2-0	2	3-0	3	2-0	2	38,3	hydrolase, alpha/beta fold family, putative
LdBPK_282700.1	3-0	3	-	0	-	0	2-0	2	3-0	3	3-0	3	68,8	acyl-CoA dehydrogenase, putative
LdBPK_351020.1	-	0	-	0	-	0	2*-0	2	3-0	3	2*-1*	6	37,2	casein kinase I, putative
LdBPK_351600.1	-	0	-	0	-	0	2-0	2	3-0	3	7-0	7	84,4	hypothetical protein, conserved
LdBPK_181340.1	-	0	0-1	1	0-1	1	0-1	1	0-3	3	1-2	3	107,7	hypothetical protein, conserved
LdBPK_301510.1	-	0	-	0	-	0	1-0	1	3-0	3	-	0	133,0	kinesin, putative
LdBPK_321490.1	-	0	0-2	2	0-2	2	0-1	1	0-3	3	0-3	3	121,4	hypothetical protein, conserved
LdBPK_362130.1	-	0	0-2*	2	0-1*	1	0-1*	1	2*-1*	3	2*-1*	3	60,6	chaperonin HSP60, mitochondrial precursor
LdBPK_100580.1	-	0	-	0	-	0	-	0	3-0	3	-	0	126,2	hypothetical protein, conserved
LdBPK_150840.1	-	0	-	0	-	0	-	0	3-0	3	1-0	1	225,5	hypothetical protein, conserved
LdBPK_210580.1	-	0	-	0	-	0	-	0	3-0	3	7-0	7	47,3	hypothetical protein, conserved
LdBPK_290020.1	7-0	7	2-0	2	2-0	2	6-0	6	2-0	2	4-0	4	114,8	transcription factor-like protein
LdBPK_322830.1	-	0	1-0	1	-	0	4-0	4	2-0	2	2-0	2	15,4	ribosomal protein L27, putative
LdBPK_363570.1	2-0	2	-	0	-	0	4-0	4	2-0	2	1-0	1	33,1	short chain dehydrogenase-like protein
LdBPK_050100.1	-	0	-	0	-	0	3-0	3	2-0	2	2-1	3	71,8	phosphoprotein phosphatase, putative
LdBPK_060010.1	2*-0	2	-	0	-	0	2*-0	2	2*-0	2	1*-0	1	11,4	histone H4
LdBPK_070550.1	-	0	-	0	-	0	2-0	2	2-0	2	2-0	2	39,1	60S ribosomal protein L7a, putative
LdBPK_091410.1	3*-3*	6	1*-0	1	-	0	2*-0	2	2*-0	2	-	0	12,3	histone H2B
LdBPK_111190.1	-	0	-	0	-	0	2-0	2	2-0	2	-	0	77,0	hypothetical protein, conserved
LdBPK_190040.1	3-3	6	1-0	1	-	0	2-0	2	2-0	2	-	0	11,9	histone H2B
LdBPK_220340.1	1-1	2	0-1	1	1-1	2	2-1	3	2-0	2	2-0	2	7,5	40S ribosomal protein S15, putative (fragment)
LdBPK_230050.1	-	0	-	0	-	0	2-0	2	2-0	2	3-0	3	25,4	peroxidoxin
LdBPK_260840.1	1-2	3	0-2	2	1-0	1	1-2	3	0-2	2	0-1	1	16,7	40S ribosomal protein S16, putative
LdBPK_320240.1	-	0	-	0	-	0	2-0	2	2-0	2	2-0	2	10,6	dynein light chain, flagellar outer arm, putative
LdBPK_342300.1	-	0	-	0	-	0	0-2	2	2-0	2	3-1	4	56,8	hypothetical protein, conserved
LdBPK_351320.1	3*-0	3	-	0	-	0	2*-0	2	2*-0	2	1*-0	0	11,4	histone H4
LdBPK_351440.1	1*-0	1	-	0	-	0	2*-1*	3	2*-0	2	2*-0	2	11,5	60S ribosomal protein L2, putative (fragment)
LdBPK_351450.1	1-0	1	-	0	-	0	2-1	3	2-0	2	2-0	2	10,8	60S ribosomal protein L2, putative (fragment)
LdBPK_366860.1	-	0	-	0	-	0	2-0	2	2-0	2	4-0	4	28,5	protein-L-isoaspartate o-methyltransferase, putative
LdBPK_091010.1	-	0	-	0	-	0	1-0	1	2-0	2	3-0	3	63,5	hypothetical protein, conserved
LdBPK_100700.1	-	0	-	0	-	0	1-0	1	1-1	2	1-0	1	41,7	hypothetical protein, unknown function
LdBPK_212190.1	1-0	1	-	0	-	0	1-0	1	1-1	2	1-0	1	10,3	60S ribosomal protein L37a, putative
LdBPK_231720.1	-	0	-	0	-	0	0-1	1	0-2	2	0-1	1	187,3	hypothetical protein, conserved
LdBPK_250270.1	-	0	-	0	-	0	1-0	1	2-0	2	-	0	126,6	hypothetical protein, conserved
LdBPK_272040.1	-	0	-	0	-	0	1-0	1	2-0	2	1-0	1	36,5	hypothetical protein, conserved
LdBPK_322820.1	-	0	-	0	-	0	1-0	1	2-0	2	-	0	41,9	hypothetical protein, conserved
LdBPK_323110.1	-	0	-	0	-	0	1-1	2	1-1	2	1-0	1	16,6	nucleoside diphosphate kinase b
LdBPK_330350.1	2-1	3	2-1	3	2-0	2	0-1	1	1-1	2	1-1	2	80,4	unspecified product
LdBPK_330360.1	2*-1*	3	2*-1*	3	2*-0	2	0-1*	1	1*-1*	2	1*-1*	2	80,6	heat shock protein 83-1
LdBPK_352650.1	-	0	-	0	-	0	1-0	1	2-0	2	1-0	1	34,8	hypothetical protein, unknown function
LdBPK_363360.1	-	0	-	0	-	0	1-0	1	1-1	2	-	0	29,7	14-3-3 protein-like protein
LdBPK_050510.1	-	0	-	0	-	0	-	0	2-0	2	1-0	1	62,5	ATPase alpha subunit
LdBPK_050560.1	-	0	-	0	-	0	-	0	2-0	2	2-0	2	44,4	hypothetical protein, conserved
LdBPK_090420.1	0-1	1	0-1	1	1-0	1	-	0	1-1	2	0-1	1	66,5	integral membrane transport protein, putative
LdBPK_150740.1	-	0	-	0	-	0	-	0	2-0	2	-	0	103,2	hypothetical protein, conserved
LdBPK_190970.1	2-2	4	-	0	-	0	-	0	2-0	2	1-0	1	66,1	4-coumarate:coa ligase-like protein
LdBPK_210550.1	-	0	-	0	-	0	-	0	2-0	2	-	0	49,8	DnaJ protein, putative
LdBPK_210800.1	-	0	0-1	1	0-1	1	-	0	2-0	2	1-0	1	12,0	60S ribosomal protein L36, putative
LdBPK_260530.1	-	0	-	0	-	0	-	0	2-0	2	4-2	6	74,1	hypothetical protein, conserved
LdBPK_261960.1	-	0	-	0	-	0	-	0	2-0	2	2-0	2	89,1	hypothetical protein, conserved
LdBPK_281740.1	-	0	-	0	-	0	-	0	2-0	2	-	0	35,7	hypothetical protein, conserved

LdBPK_290790.1	4-0	4	1-0	1	4-1	5	-	0	2-0	2	4-1	5	87,0	heat shock protein 90, putative (LPG3)
LdBPK_310320.1	-	0	-	0	-	0	-	0	2-0	2	-	0	127,3	hypothetical protein, conserved
LdBPK_310450.1	-	0	-	0	-	0	-	0	2-0	2	2-0	2	80,0	cytoskeleton-associated protein CAP5.5, putative, cysteine peptidase, Clan CA, family C2, putative, Calpain-like protein 1 (CAP5.5)
LdBPK_323080.1	-	0	0-1	1	0-1	1	-	0	0-2	2	0-2	2	56,7	tubulin-tyrosine ligase-like protein
LdBPK_351900.1	-	0	0-1*	1	0-1*	1	-	0	2*-0	2	1*-0	1	11,9	60S ribosomal protein L36, putative
LdBPK_366150.1	-	0	-	0	-	0	-	0	2-0	2	1-0	1	208,8	hypothetical protein, conserved
LDPBQ7IC8_180019500	-	0	-	0	-	0	-	0	2-0	2	-	0	91,7	
LdBPK_081680.1	1*-0	1	-	0	-	0	4-0	4	1*-0	1	2*-0	2	33,3	unspecified product
LdBPK_081060.1	-	0	-	0	-	0	3-0	3	1-0	1	1-0	1	126,9	hypothetical protein, conserved
LdBPK_181270.1	1-0	1	-	0	-	0	3*-0	3	1-0	1	2-0	2	26,2	hypothetical protein, conserved (fragment)
LdBPK_110960.1	1-1	2	0-1	1	-	0	1-2	3	1-0	1	2-0	2	10,4	40S ribosomal protein S5 (fragment)
LdBPK_242140.1	4-1	5	-	0	2-0	2	2-0	2	1-0	1	1-0	1	13,1	60S ribosomal protein L26, putative (fragment)
LdBPK_251880.1	-	0	-	0	-	0	2-0	2	1-0	1	-	0	106,1	hypothetical protein, conserved
LdBPK_272350.1	-	0	-	0	-	0	2-0	2	1-0	1	2-0	2	43,6	heat shock protein DNAJ, putative
LdBPK_332070.1	1-1	2	-	0	1-0	1	2-0	2	1-0	1	1-0	1	9,8	60S ribosomal protein L37
LdBPK_342380.1	-	0	-	0	-	0	0-2	2	0-1	1	0-2	2	68,6	hypothetical protein, unknown function
LdBPK_060410.1	-	0	-	0	-	0	1-0	1	1-0	1	1-0	1	28,1	60S ribosomal protein L19, putative
LdBPK_100920.1	1*-0	1	-	0	-	0	1*-0	1	1*-0	1	1*-0	1	14,6	histone H3
LdBPK_160610.1	1-0	1	-	0	-	0	1-0	1	1-0	1	1-0	1	12,0	histone H3, putative (fragment)
LdBPK_170570.1	-	0	-	0	-	0	0-1	1	1-0	1	0-1	1	107,1	hypothetical protein, unknown function
LdBPK_221370.1	-	0	-	0	-	0	1-0	1	1-0	1	-	0	26,0	40S ribosomal protein L14, putative
LdBPK_251210.1	-	0	-	0	-	0	1-0	1	1-0	1	2-0	2	56,3	ATP synthase subunit beta, mitochondrial, putative, ATP synthase F1, beta subunit, putative (ATPB)
LdBPK_251850.1	-	0	-	0	-	0	1-0	1	1-0	1	2-0	2	34,2	3-oxo-5-alpha-steroid 4-dehydrogenase, putative
LdBPK_282360.1	0-1	1	0-1	1	-	0	1-1	2	0-1	1	0-1	1	6,7	ribosomal protein S29, putative
LdBPK_282390.1	-	0	-	0	-	0	0-1	1	1-0	1	-	0	99,7	cyclin dependent kinase-binding protein, putative
LdBPK_302470.1	1*-1*	2	0-1*	1	2*-0	2	1*-0	1	1*-0	1	2*-0	2	9,5	heat shock 70-related protein 1, mitochondrial precursor, putative (fragment)
LdBPK_302540.1	1*-1*	2	0-1*	1	2*-0	2	1*-0	1	1*-0	1	2*-0	2	9,0	heat shock 70-related protein 1, mitochondrial precursor, putative (fragment)
LdBPK_323920.1	0-1	1	0-1	1	1-1	2	0-1	1	1-0	1	0-1	1	15,0	kinetoplast-associated protein p18-2, putative
LdBPK_332600.1	2-0	2	-	0	-	0	1-0	1	1-0	1	2-0	2	42,5	hypothetical protein, conserved (POMP11)
LdBPK_340910.1	1-0	1	-	0	-	0	1-0	1	1-0	1	1-0	1	10,8	60S ribosomal protein L13a, putative (fragment)
LdBPK_341880.1	-	0	-	0	-	0	1-0	1	1-0	1	1-0	1	8,7	ubiquitin-like protein
LdBPK_352020.1	-	0	-	0	-	0	0-1	1	0-1	1	-	0	150,5	hypothetical protein, unknown function
LdBPK_352610.1	-	0	1-0	1	-	0	1-0	1	1-0	1	2-0	2	24,3	hypothetical protein, conserved
LdBPK_354200.1	-	0	-	0	-	0	1-0	1	1-0	1	-	0	64,6	poly(a) binding protein, putative
LdBPK_361020.1	-	0	-	0	0-1	1	1-0	1	1-0	1	1-1	2	99,3	hypothetical protein, unknown function
LdBPK_361130.1	1-1	2	1-1	2	0-1	1	1-1	2	1-0	1	1-0	1	2,2	ribosomal protein L24, putative (fragment)
LdBPK_363930.1	1-0	1	-	0	-	0	1-0	1	1-0	1	1-0	1	19,2	60S ribosomal protein L34, putative
LdBPK_020640.1	-	0	-	0	-	0	-	0	1-0	1	-	0	34,5	mitochondrial carrier protein, putative
LdBPK_030220.1	-	0	-	0	-	0	-	0	1-0	1	-	0	79,0	long chain fatty Acyl CoA synthetase, putative
LdBPK_041250.1	1-1	2	0-1	1	-	0	-	0	1-0	1	1-0	1	42,0	actin
LdBPK_050280.1	-	0	-	0	-	0	-	0	1-0	1	-	0	25,1	protein tyrosine phosphatase, putative
LdBPK_051180.1	-	0	0-1	1	0-1	1	-	0	0-1	1	0-4	4	212,3	hypothetical protein, conserved
LdBPK_060660.1	-	0	-	0	-	0	-	0	1-0	1	-	0	326,2	protein kinase, putative
LdBPK_060950.1	-	0	-	0	-	0	-	0	1-0	1	1-0	1	48,9	hypothetical protein, conserved
LdBPK_070130.1	3-0	3	-	0	-	0	-	0	1-0	1	-	0	59,6	ATP-dependent DEAD/H RNA helicase, putative
LdBPK_071050.1	-	0	-	0	-	0	-	0	0-1	1	-	0	141,4	protein kinase, putative
LdBPK_091300.1	-	0	-	0	-	0	-	0	1-0	1	-	0	218,1	ATP-dependent helicase, putative (fragment)
LdBPK_111050.1	-	0	-	0	-	0	-	0	1-0	1	-	0	54,0	pretranslocation protein, alpha subunit, putative, protein transport protein SEC61 subunit alpha, putative
LdBPK_130250.1	-	0	-	0	-	0	-	0	1-0	1	3-0	3	56,3	hypothetical protein, conserved
LdBPK_140490.1	-	0	-	0	-	0	-	0	1-0	1	-	0	9,2	hypothetical protein, unknown function (fragment)

LdBPK_140500.1	-	0	-	0	-	0	-	0	1*-0	1	-	0	30,4	hypothetical protein, unknown function
LdBPK_181510.1	-	0	-	0	-	0	-	0	1-0	1	-	0	107,3	P-type H <sup>+</sup> -ATPase 1B, putative (H1B)
LdBPK_210250.1	-	0	-	0	-	0	-	0	1-0	1	-	0	78,6	hypothetical protein, conserved
LdBPK_210760.1	-	0	-	0	1-0	1	-	0	1-0	1	2-1	3	66,8	dual specificity protein phosphatase, putative
LdBPK_211320.1	-	0	-	0	-	0	-	0	1-0	1	-	0	34,4	cell division protein kinase 2
LdBPK_231460.1	-	0	-	0	-	0	-	0	1-0	1	-	0	60,2	T-complex protein 1, gamma subunit, putative
LdBPK_270710.1	-	0	-	0	-	0	-	0	1-0	1	-	0	70,1	hypothetical protein, conserved
LdBPK_282430.1	1-0	1	-	0	-	0	-	0	1-0	1	-	0	23,8	glycosomal membrane protein, putative
LdBPK_282490.1	-	0	-	0	-	0	-	0	0-1	1	0-1	1	94,9	hypothetical protein, conserved
LdBPK_283190.1	-	0	-	0	-	0	-	0	1-0	1	-	0	33,2	hypothetical protein, conserved
LdBPK_290190.1	-	0	-	0	-	0	-	0	1-0	1	-	0	57,1	hypothetical protein, conserved
LdBPK_291170.1	-	0	-	0	-	0	-	0	1*-0	1	-	0	9,7	ribosomal protein L1a, putative (fragment)
LdBPK_291180.1	-	0	-	0	-	0	-	0	1*-0	1	-	0	9,2	ribosomal protein L1a, putative (fragment)
LdBPK_291720.1	-	0	-	0	-	0	-	0	0-1	1	-	0	105,2	hypothetical protein, unknown function
LdBPK_291820.1	-	0	-	0	-	0	-	0	1-0	1	1-0	1	39,5	hypothetical protein, conserved
LdBPK_300600.1	-	0	-	0	-	0	-	0	1-0	1	-	0	54,1	hypothetical protein, conserved
LdBPK_301180.1	-	0	-	0	-	0	-	0	1-0	1	-	0	58,1	importin alpha, putative
LdBPK_301900.1	-	0	-	0	0-1	1	-	0	0-1	1	0-2	2	66,4	hypothetical protein, unknown function
LdBPK_302320.1	-	0	-	0	-	0	-	0	1-0	1	2-0	2	52,5	hypothetical protein, conserved
LdBPK_302710.1	-	0	-	0	-	0	-	0	0-1	1	0-1	1	96,7	hypothetical protein, conserved
LdBPK_303360.1	-	0	-	0	-	0	-	0	1-0	1	-	0	40,8	MORN repeat-containing protein 1 (MORN1)
LdBPK_312700.1	1-0	1	-	0	-	0	-	0	1-0	1	1-0	1	40,8	serine/threonine protein phosphatase pp1(5.9), putative
LdBPK_313100.1	-	0	0-5	5	0-3	3	-	0	0-1	1	0-3	3	217,4	hypothetical protein, conserved
LdBPK_322350.1	-	0	-	0	-	0	-	0	1-0	1	-	0	110,1	U5 small nuclear ribonucleoprotein component, putative, U5 snrnp-specific protein, putative
LdBPK_323200.1	-	0	-	0	-	0	-	0	1-0	1	1-0	1	96,2	hypothetical protein, conserved
LdBPK_330940.1	-	0	-	0	-	0	-	0	1-0	1	-	0	63,2	dnaj chaperone-like protein
LdBPK_332740.1	-	0	-	0	-	0	-	0	0-1	1	-	0	72,2	enoyl-CoA hydratase/Enoyl-CoA isomerase/3-hydroxyacyl-CoA dehydrogenase, putative
LdBPK_340010.1	3-0	3	-	0	-	0	-	0	1-0	1	-	0	33,5	hypothetical protein, conserved
LdBPK_340060.1	-	0	-	0	-	0	-	0	1-0	1	-	0	115,1	hypothetical protein, conserved
LdBPK_340140.1	-	0	-	0	-	0	-	0	1-0	1	-	0	36,1	malate dehydrogenase, putative
LdBPK_341470.1	-	0	-	0	-	0	-	0	1-0	1	-	0	276,8	hypothetical protein, conserved
LdBPK_344040.1	-	0	-	0	-	0	-	0	0-1	1	-	0	50,9	hypothetical protein, conserved
LdBPK_350630.1	-	0	-	0	-	0	-	0	1-0	1	-	0	66,0	hypothetical protein, conserved
LdBPK_351720.1	-	0	-	0	-	0	-	0	1-0	1	1-0	1	42,6	casein kinase II, putative
LdBPK_353150.1	1-0	1	-	0	-	0	-	0	1-0	1	1-0	1	99,9	ATP-dependent RNA helicase, putative
LdBPK_354880.1	-	0	-	0	-	0	-	0	1-0	1	1-0	1	36,5	hypothetical protein, conserved
LdBPK_364100.1	-	0	-	0	-	0	-	0	1-0	1	-	0	47,8	S-adenosylhomocysteine hydrolase
LdBPK_365300.1	-	0	-	0	0-1	1	-	0	1-0	1	-	0	43,5	hypothetical protein, conserved
LdBPK_365620.1	-	0	-	0	-	0	-	0	1-0	1	1-0	1	57,5	NADH dehydrogenase, putative
LdBPK_041170.1	-	0	-	0	-	0	3-0	3	-	0	3-0	3	38,9	fructose-1,6-bisphosphatase, cytosolic, putative
LdBPK_160560.1	-	0	-	0	-	0	2-0	2	-	0	-	0	49,7	orotidine-5-phosphate decarboxylase/orotate phosphoribosyltransferase, putative
LdBPK_220790.1	-	0	-	0	-	0	0-2	2	-	0	0-1	1	91,4	hypothetical protein, conserved
LdBPK_240250.1	-	0	-	0	-	0	2-0	2	-	0	-	0	353,5	hypothetical protein, conserved
LdBPK_361050.1	1*-0	1	-	0	-	0	2-0	2	-	0	1*-0	1	18,6	40S ribosomal protein S10, putative
LdBPK_090440.1	-	0	-	0	-	0	0-1	1	-	0	-	0	203,9	hypothetical protein, conserved
LdBPK_100210.1	-	0	-	0	-	0	1-0	1	-	0	-	0	52,6	Nucleolar protein 56, putative (NOP56)
LdBPK_131360.1	1-0	1	-	0	-	0	1-0	1	-	0	-	0	63,5	squalene monooxygenase-like protein
LdBPK_131410.1	-	0	-	0	-	0	1-0	1	-	0	-	0	12,3	60S ribosomal protein L44, putative
LdBPK_150090.1	-	0	-	0	-	0	1-0	1	-	0	-	0	47,5	ATP-dependent protease ATPase subunit HslU1, putative (HslU1)
LdBPK_171320.1	1-0	1	-	0	-	0	1-0	1	-	0	-	0	12,5	histone H2B
LdBPK_180870.1	-	0	-	0	-	0	1-0	1	-	0	-	0	57,1	hypothetical protein, conserved
LdBPK_180950.1	-	0	-	0	-	0	1-0	1	-	0	-	0	38,9	hypothetical protein, conserved

LdBPK_210330.1	-	0	-	0	-	0	1-0	1	-	0	-	0	119,5	protein kinase, putative
LdBPK_220004.1	-	0	-	0	-	0	0-1	1	-	0	2-0	2	21,7	60S ribosomal protein L11 (L5, L16)
LdBPK_220009.1	-	0	-	0	-	0	1-0	1	-	0	1-0	1	36,5	heat shock protein DNAJ, putative
LdBPK_261180.1	-	0	-	0	-	0	1-0	1	-	0	-	0	71,6	hypothetical protein, conserved
LdBPK_270681.1	-	0	-	0	-	0	0-1	1	-	0	2-0	2	52,3	hypothetical protein, conserved
LdBPK_291000.1	1-0	1	-	0	-	0	1-0	1	-	0	-	0	56,7	hypothetical protein, conserved
LdBPK_312320.1	-	0	-	0	-	0	1-0	1	-	0	-	0	38,6	3,2-trans-enoyl-CoA isomerase, mitochondrial precursor, putative
LdBPK_312400.1	-	0	-	0	-	0	1*0	1	-	0	-	0	39,5	3,2-trans-enoyl-CoA isomerase, mitochondrial precursor, putative
LdBPK_320640.1	-	0	-	0	-	0	1-0	1	-	0	4-0	4	39,6	hypothetical protein, conserved
LdBPK_342100.1	-	0	-	0	-	0	1-0	1	-	0	1-0	1	16,8	clathrin coat assembly protein AP17, putative
LdBPK_342240.1	-	0	-	0	-	0	1-0	1	-	0	1-0	1	16,5	ribosomal protein l35a, putative
LdBPK_343530.1	-	0	-	0	-	0	1-0	1	-	0	-	0	53,9	serine palmitoyltransferase-like protein
LdBPK_350930.1	-	0	-	0	-	0	1-1	2	-	0	-	0	199,8	hypothetical protein, conserved
LdBPK_351380.1	-	0	-	0	-	0	1-0	1	-	0	1-0	1	13,7	hypothetical protein, unknown function
LdBPK_361040.1	1-0	1	-	0	-	0	1*0	1	-	0	1-0	1	17,4	40S ribosomal protein S10, putative (fragment)
LdBPK_364410.1	-	0	-	0	-	0	1-0	1	-	0	-	0	89,7	hypothetical protein, conserved
LdBPK_364930.1	-	0	-	0	-	0	1-0	1	-	0	0-1	1	106,2	hypothetical protein, conserved
LdBPK_365020.1	-	0	-	0	-	0	0-1	1	-	0	-	0	101,8	hypothetical protein, conserved
LdBPK_366480.1	-	0	-	0	-	0	0-1	1	-	0	-	0	150,7	flagellum transition zone component, putative
LdBPK_020490.1	-	0	-	0	0-1	1	-	0	-	0	0-3	3	218,1	hypothetical protein, conserved
LdBPK_050700.1	-	0	-	0	-	0	-	0	-	0	0-2	2	177,9	hypothetical protein, conserved
LdBPK_050850.1	-	0	-	0	-	0	-	0	-	0	2-0	2	68,7	hypothetical protein, conserved
LdBPK_051040.1	-	0	-	0	-	0	-	0	-	0	1-0	1	39,7	stomatin-like protein
LdBPK_071070.1	-	0	-	0	-	0	-	0	-	0	2-1	3	269,4	hypothetical protein, conserved
LdBPK_110400.1	0-1	1	-	0	-	0	-	0	-	0	0-2	2	120,2	tubulin-tyrsoine ligase-like protein
LdBPK_110780.1	1-0	1	-	0	-	0	-	0	-	0	-	0	22,4	40S ribosomal protein S21, putative (fragment)
LdBPK_131400.1	-	0	-	0	-	0	-	0	-	0	1-0	1	58,8	chaperonin TCP20, putative
LdBPK_151180.1	-	0	-	0	-	0	-	0	-	0	1-0	1	287,4	protein kinase, putative
LdBPK_160330.1	-	0	-	0	-	0	-	0	-	0	0-1	1	135,2	hypothetical protein, conserved
LdBPK_170330.1	1-0	1	-	0	-	0	-	0	-	0	-	0	18,7	histone H2A, putative
LdBPK_170870.1	-	0	1-0	1	-	0	-	0	-	0	-	0	52,0	guanosine monophosphate reductase, putative
LdBPK_181360.1	2-0	2	-	0	-	0	-	0	-	0	-	0	42,7	pyruvate dehydrogenase E1 component alpha subunit, putative
LdBPK_201350.1	-	0	-	0	-	0	-	0	-	0	1-0	1	15,0	calpain-like cysteine peptidase, putative
LdBPK_210520.1	-	0	-	0	-	0	-	0	-	0	0-1	1	76,1	hypothetical protein, unknown function
LdBPK_220380.1	1-0	1	-	0	-	0	-	0	-	0	-	0	55,5	hypothetical protein, conserved
LdBPK_220610.1	1-0	1	-	0	-	0	-	0	-	0	-	0	73,7	hypothetical protein, conserved
LdBPK_231170.1	1-0	1	-	0	-	0	-	0	-	0	-	0	25,8	hypothetical protein, unknown function
LdBPK_241470.1	-	0	-	0	0-1	1	-	0	-	0	-	0	342,6	kinesin, putative
LdBPK_241710.1	-	0	-	0	-	0	-	0	-	0	1-0	1	64,7	hypothetical protein, conserved
LdBPK_251620.1	-	0	-	0	-	0	-	0	-	0	1-0	1	89,0	protein kinase, putative
LdBPK_251790.1	1-0	1	-	0	-	0	-	0	-	0	-	0	37,9	pyruvate dehydrogenase E1 beta subunit, putative
LdBPK_261590.1	0-1	1	-	0	-	0	-	0	-	0	-	0	63,7	proline oxidase, mitochondrial precursor-like protein
LdBPK_270930.1	1-0	1	-	0	-	0	-	0	-	0	-	0	47,8	cysteine desulfurase, putative
LdBPK_271070.1	-	0	-	0	-	0	-	0	-	0	1-0	1	7,0	histone H1, putative
LdBPK_271100.1	-	0	-	0	-	0	-	0	-	0	1-0	1	46,4	hypothetical protein, conserved
LdBPK_271390.1	-	0	-	0	-	0	-	0	-	0	0-1	1	74,3	hypothetical protein, conserved
LdBPK_271650.1	-	0	-	0	-	0	-	0	-	0	1-0	1	498,6	dynein heavy chain, putative
LdBPK_280610.1	-	0	-	0	-	0	-	0	-	0	0-1	1	165,4	Mitogen-activated protein kinase 8, putative (MPK8)
LdBPK_280980.1	-	0	-	0	1-0	1	-	0	-	0	-	0	91,0	ribonucleoside-diphosphate reductase large chain, putative
LdBPK_282120.1	-	0	-	0	-	0	-	0	-	0	0-3	3	81,2	hypothetical protein, conserved
LdBPK_282370.1	0-2	2	-	0	-	0	-	0	-	0	-	0	48,0	glycoprotein 96-92, putative
LdBPK_290830.1	-	0	-	0	-	0	-	0	-	0	3-0	3	62,9	hypothetical protein, conserved

LdBPK_290890.1	2-0	2	-	0	-	0	-	0	-	0	-	0	34,0	high mobility group protein homolog tdp-1, putative
LdBPK_292570.1	-	0	-	0	-	0	-	0	-	0	1*-0	1	7,7	60S ribosomal protein L13, putative (fragment)
LdBPK_292580.1	-	0	-	0	-	0	-	0	-	0	1-0	1	7,3	60S ribosomal protein L13, putative (fragment)
LdBPK_302370.1	-	0	-	0	-	0	-	0	-	0	1-0	1	60,6	zinc-finger protein, conserved
LdBPK_303430.1	3-0	3	-	0	-	0	-	0	-	0	-	0	57,6	PAS-domain containing phosphoglycerate kinase, putative
LdBPK_311050.1	-	0	0-2	2	0-1	1	-	0	-	0	-	0	38,6	hypothetical protein, unknown function
LdBPK_311730.1	-	0	-	0	0-1	1	-	0	-	0	0-1	1	76,1	hypothetical protein, conserved
LdBPK_320020.1	0-1	1	-	0	-	0	-	0	-	0	-	0	56,4	nuclear segregation protein, putative
LdBPK_323630.1	-	0	0-1	1	-	0	-	0	-	0	-	0	86,3	hypothetical protein, conserved
LdBPK_330340.1	1-0	1	-	0	-	0	-	0	-	0	-	0	74,7	ATP-binding cassette sub-family F member 1, putative (ABCF1)
LdBPK_330770.1	-	0	-	0	-	0	-	0	-	0	1-0	1	5,4	60S ribosomal protein L6, putative (fragment)
LdBPK_340990.1	1-0	1	-	0	-	0	-	0	-	0	-	0	105,7	Wee1-like protein kinase, putative
LdBPK_343970.1	-	0	-	0	-	0	-	0	-	0	0-3	3	51,4	hypothetical protein, conserved
LdBPK_351460.1	-	0	-	0	-	0	-	0	-	0	0-1	1	323,7	hypothetical protein, conserved
LdBPK_355300.1	1-0	1	-	0	-	0	-	0	-	0	-	0	39,6	isopentenyl-diphosphate delta-isomerase (type II), putative (idi1)
LdBPK_362480.1	-	0	-	0	-	0	-	0	-	0	0-1*	1	35,5	glyceraldehyde 3-phosphate dehydrogenase, cytosolic
LdBPK_362790.1	2-0	2	-	0	-	0	-	0	-	0	-	0	48,6	dihydrolipoamide acetyltransferase precursor, putative
LdBPK_364540.1	-	0	-	0	-	0	-	0	-	0	0-1	1	177,5	hypothetical protein, conserved
LdBPK_365240.1	1-0	1	-	0	-	0	-	0	-	0	-	0	12,1	40S ribosomal protein SA, putative (fragment)
LdBPK_366650.1	-	0	-	0	-	0	-	0	-	0	1-0	1	62,0	hypothetical protein, conserved



# Appendix 2

---



## Appendix 2

Raw data of the identification of proteins by mass spectrometry from the immunoprecipitation of recombinant LmCK1.2-V5-His<sub>6</sub> and associated protein from the mammalian host.

All proteins	Control IPs		rLmCK1.2-V5-His6 IPs			MW (kDa)	Protein name	Species
	Number of peptides identified in control: Rep.1(E1-E2)-Rep.2(E1-E2)-Rep.3(E1-E2)	Number of peptides identified in thioredoxin-V5-His6 control: Rep.1(E1-E2)-Rep.2(E1-E2)-Rep.3(E1-E2)	Number of peptides identified in rCK1.2-V5-His6 IP: Rep. 1	Number of peptides identified in rCK1.2-V5-His6 IP: Rep. 2	Number of peptides identified in rCK1.2-V5-His6 IP: Rep. 3			
A4IAZ8_LEIIN	0-0-0-2-0-4	0-1-1-4-1-5	34-27	39-41	38-39	39,8	Putative casein kinase	<i>Leishmania infantum</i>
G3P_MOUSE	0-0-5-6-1-1	3-1-3-7-1-1	15-2	22-19	12-5	35,8	Glyceraldehyde-3-phosphate dehydrogenase	<i>Mus musculus</i>
TBB5_MOUSE	0-0-4-6-3-1	0-0-1-2-1-1	18-4	22-12	21-9	49,7	Tubulin beta-5 chain	<i>Mus musculus</i>
DESP_MOUSE	14-6-11-7-2-11	6-17-2-26-4-11	16-3	21-12	12-16	332,9	Desmoplakin	<i>Mus musculus</i>
ACTB_MOUSE	14-8-7-11-4-9	9-4-5-10-6-7	16-8	19-17	18-7	41,7	Actin, cytoplasmic 1	<i>Mus musculus</i>
K2C5_MOUSE	9-5-12-19-11-19	4-13-6-22-9-19	5-4	19-18	14-15	61,8	Keratin, type II cytoskeletal 5	<i>Mus musculus</i>
PLAK_MOUSE	12-6-9-8-1-6	8-13-1-14-4-4	17-2	17-8	5-5	81,8	Junction plakoglobin	<i>Mus musculus</i>
TBB2A_MOUSE			19-0	17-0	18-0	49,9	Tubulin beta-2A chain	<i>Mus musculus</i>
ATPA_MOUSE	2-0-2-4-2-0	2-1-1-0-1-0	13-4	16-5	10-1	59,8	ATP synthase subunit alpha, mitochondrial	<i>Mus musculus</i>
TBB4B_MOUSE	0-0-4-0-0-0		17-0	16-0	17-7	49,8	Tubulin beta-4B chain	<i>Mus musculus</i>
TBA1B_MOUSE	0-0-0-4-0-5	0-0-0-0-0-1	15-0	15-10	14-5	50,2	Tubulin alpha-1B chain	<i>Mus musculus</i>
ATPB_MOUSE	1-0-4-2-3-1	1-1-3-1-2-0	12-0	14-3	10-2	56,3	ATP synthase subunit beta, mitochondrial	<i>Mus musculus</i>
GRP78_MOUSE	5-0-7-2-1-3	3-2-3-0-6-0	17-0	14-3	10-6	72,4	78 kDa glucose-regulated protein	<i>Mus musculus</i>
TBA1A_MOUSE			14-0	14-10	13-0	50,1	Tubulin alpha-1A chain	<i>Mus musculus</i>
ENOA_MOUSE	3-2-2-3-2-2	3-3-1-2-1-0	4-0	13-7	3-4	47,1	Alpha-enolase	<i>Mus musculus</i>
HSP7C_MOUSE	5-1-5-2-2-0	5-3-3-1-4-1	14-2	13-3	15-3	70,9	Heat shock cognate 71 kDa protein	<i>Mus musculus</i>
TBA1C_MOUSE	3-0-2-0-1-0	4-1-2-0-3-0	14-2	13-9	12-5	49,9	Tubulin alpha-1C chain	<i>Mus musculus</i>
K2C6A_MOUSE	7-1-10-10-6-13	7-13-5-18-5-13	0-7	9-11	14-13	59,3	Keratin, type II cytoskeletal 6A	<i>Mus musculus</i>
ACTC_MOUSE	8-0-4-0-0-0	6-2-0-5-0-0	9-0	10-9	8-3	42,0	Actin, alpha cardiac muscle 1	<i>Mus musculus</i>
iRT-Kit_WR_fusion	10-9-10-9-10-10	11-9-7-9-9-8	9-10	9-10	9-9	14,2	no description	<i>unknown organism</i>
RS3_MOUSE	1-0-2-7-6-5	3-1-2-7-1-6	11-4	10-8	13-4	26,7	40S ribosomal protein S3	<i>Mus musculus</i>
TBB3_MOUSE			15-0	10-0	10-0	50,4	Tubulin beta-3 chain	<i>Mus musculus</i>
ADT2_MOUSE	2-0-0-0-3-0	2-1-0-0-1-1	6-0	9-5	7-0	32,9	ADP/ATP translocase 2	<i>Mus musculus</i>
GCAA_MOUSE	1-6-0-7-1-14	3-8-1-6-3-13	3-7	3-9	4-13	36,4	Ig gamma-2A chain C region, A allele	<i>Mus musculus</i>
K1C14_MOUSE	7-5-10-9-4-10	6-7-4-18-6-8	4-5	9-8	9-12	52,9	Keratin, type I cytoskeletal 14	<i>Mus musculus</i>
ANXA2_MOUSE	7-3-4-7-2-5	3-7-5-6-2-4	4-2	7-8	6-5	38,7	Annexin A2	<i>Mus musculus</i>
DJB11_MOUSE			5-0	8-0	5-0	40,6	Dnaj homolog subfamily B member 11	<i>Mus musculus</i>
FCGR1_MOUSE	5-2-3-3-5-2	5-1-1-5-2-3	10-3	8-2	6-3	44,9	High affinity immunoglobulin gamma Fc receptor I	<i>Mus musculus</i>
GBLP_MOUSE	0-0-0-1-0-0	0-3-0-0-0-0	11-3	8-8	9-1	35,1	Guanine nucleotide-binding protein subunit beta-2-like 1	<i>Mus musculus</i>
IGKC_MOUSE	3-5-2-7-3-6	2-5-1-8-3-9	2-5	6-8	5-7	11,8	Ig kappa chain C region	<i>Mus musculus</i>

K1C17_MOUSE	7-4-9-8-0-10	8-11-2-7-6-8	5-5	8-5	8-9	48,2	Keratin, type I cytoskeletal 17	<i>Mus musculus</i>
K2C75_MOUSE	0-0-8-0-0-0	0-7-0-11-0-0	0-5	8-6		59,7	Keratin, type II cytoskeletal 75	<i>Mus musculus</i>
RHOG_MOUSE			4-0	7-8	3-2	21,3	Rho-related GTP-binding protein RhoG	<i>Mus musculus</i>
ADT1_MOUSE			2-0	7-0	7-0	32,9	ADP/ATP translocase 1	<i>Mus musculus</i>
EF1A1_MOUSE	2-1-3-4-3-1	1-2-1-4-2-1	9-3	7-6	10-2	50,1	Elongation factor 1-alpha 1	<i>Mus musculus</i>
HS90B_MOUSE	0-2-0-0-0-0	0-0-0-1-0-0	6-1	7-2	3-1	83,3	Heat shock protein HSP 90-beta	<i>Mus musculus</i>
K1C10_MOUSE	7-6-9-10-6-12	5-8-5-9-6-13	5-5	7-6	10-11	57,8	Keratin, type I cytoskeletal 10	<i>Mus musculus</i>
K22E_MOUSE	7-3-7-5-3-7	4-6-1-6-5-6	2-3	7-5	7-6	70,9	Keratin, type II cytoskeletal 2 epidermal	<i>Mus musculus</i>
K2C71_MOUSE	0-0-2-3-0-0	0-0-2-2-0-4		3-7	0-3	57,4	Keratin, type II cytoskeletal 71	<i>Mus musculus</i>
QCR2_MOUSE			4-0	7-1	4-0	48,2	Cytochrome b-c1 complex subunit 2, mitochondrial	<i>Mus musculus</i>
RL3_MOUSE	0-0-1-2-0-0	0-0-2-5-0-0	3-0	7-5	11-2	46,1	60S ribosomal protein L3	<i>Mus musculus</i>
RS4X_MOUSE	1-0-3-0-3-5	1-0-0-1-5-3	1-2	7-1	9-1	29,6	40S ribosomal protein S4, X isoform	<i>Mus musculus</i>
TBB6_MOUSE			9-0	7-0	7-0	50,1	Tubulin beta-6 chain	<i>Mus musculus</i>
ATPG_MOUSE			2-0	6-1	6-2	32,9	ATP synthase subunit gamma, mitochondrial	<i>Mus musculus</i>
EHD4_MOUSE			1-0	6-0		61,5	EH domain-containing protein 4	<i>Mus musculus</i>
K1C16_MOUSE	4-0-6-8-2-7	5-7-0-7-4-6	2-0	5-6	5-6	51,6	Keratin, type I cytoskeletal 16	<i>Mus musculus</i>
K22O_MOUSE	5-1-4-6-0-7	0-6-2-7-0-9		6-5	6-7	62,8	Keratin, type II cytoskeletal 2 oral	<i>Mus musculus</i>
K2C73_MOUSE	5-2-5-4-4-6	3-5-2-5-4-6	3-4	4-6	6-5	58,9	Keratin, type II cytoskeletal 73	<i>Mus musculus</i>
LG3BP_MOUSE	0-0-0-0-1-0	0-0-0-0-1-0	2-0	6-0	5-0	64,5	Galectin-3-binding protein	<i>Mus musculus</i>
RAN_MOUSE			2-0	6-3	2-1	24,4	GTP-binding nuclear protein Ran	<i>Mus musculus</i>
RL4_MOUSE	0-0-1-1-0-0	1-0-2-1-0-0	8-1	6-2	10-0	47,2	60S ribosomal protein L4	<i>Mus musculus</i>
RL8_MOUSE	0-0-2-1-0-0	0-0-1-2-0-0	1-0	6-3	2-1	28,0	60S ribosomal protein L8	<i>Mus musculus</i>
COF1_MOUSE	1-0-1-2-0-0	0-1-0-3-0-1	2-1	5-2	4-2	18,6	Cofilin-1	<i>Mus musculus</i>
HA12_MOUSE			5-0	5-3	2-2	41,1	H-2 class I histocompatibility antigen, D-D alpha chain	<i>Mus musculus</i>
K1C42_MOUSE	6-5-7-6-4-8	5-7-4-10-2-5	4-5	5-4	8-8	50,1	Keratin, type I cytoskeletal 42	<i>Mus musculus</i>
K2C1_MOUSE	6-4-7-6-5-7	5-6-3-6-6-7	5-5	5-4	5-6	65,6	Keratin, type II cytoskeletal 1	<i>Mus musculus</i>
KPYM_MOUSE	3-0-2-2-1-2	1-1-1-1-4-0	1-0	5-3	3-2	57,8	Pyruvate kinase PKM	<i>Mus musculus</i>
OST48_MOUSE	1-0-0-0-0-0		2-0	5-0	2-0	49,0	Dolichyl-diphosphooligosaccharide--protein glycosyltransferase 48 kDa subunit	<i>Mus musculus</i>
PP2AA_MOUSE			3-0	5-2	1-0	35,6	Serine/threonine-protein phosphatase 2A catalytic subunit alpha isoform	<i>Mus musculus</i>
RAB1B_MOUSE			1-0	5-1	4-0	22,2	Ras-related protein Rab-1B	<i>Mus musculus</i>
RAB5A_MOUSE		0-1-0-0-0-0	1-0	5-0		23,6	Ras-related protein Rab-5A	<i>Mus musculus</i>
RL32_MOUSE	0-0-2-3-0-0	0-0-0-1-0-0		5-1	2-0	15,9	60S ribosomal protein L32	<i>Mus musculus</i>
RPN1_MOUSE	0-0-0-0-1-0		5-0	5-2	4-0	68,5	Dolichyl-diphosphooligosaccharide--protein glycosyltransferase subunit 1	<i>Mus musculus</i>
RS11_MOUSE	0-0-0-3-1-1	0-0-1-3-3-0	3-1	5-3	5-2	18,4	40S ribosomal protein S11	<i>Mus musculus</i>
RS6_MOUSE	0-0-1-3-1-0	0-0-0-4-0-0	2-0	5-2	3-0	28,7	40S ribosomal protein S6	<i>Mus musculus</i>
RS8_MOUSE	1-0-1-1-1-1	2-0-0-1-2-1	5-2	5-3	7-4	24,2	40S ribosomal protein S8	<i>Mus musculus</i>
SFPQ_MOUSE	0-0-2-0-1-0	2-0-0-0-0-0	3-0	5-0	3-0	75,4	Splicing factor, proline- and glutamine-rich	<i>Mus musculus</i>
VIME_MOUSE	15-5-0-0-0-2	14-0-0-0-1-0	26-0	5-0		53,7	Vimentin	<i>Mus musculus</i>
ANXA1_MOUSE	3-0-0-2-1-3	0-1-0-0-0-0	0-1	4-1	1-3	38,7	Annexin A1	<i>Mus musculus</i>
ARF1_MOUSE			4-0	4-0		20,7	ADP-ribosylation factor 1	<i>Mus musculus</i>
ARF5_MOUSE				4-0		20,5	ADP-ribosylation factor 5	<i>Mus musculus</i>
CATB_MOUSE		1-0-0-0-0-0	2-1	4-1	1-0	37,3	Cathepsin B	<i>Mus musculus</i>
COX2_MOUSE			1-0	4-1		26,0	Cytochrome c oxidase subunit 2	<i>Mus musculus</i>
DHB12_MOUSE		0-0-0-0-1-0	2-0	4-1	5-0	34,7	Very-long-chain 3-oxoacyl-CoA reductase	<i>Mus musculus</i>
DUS3_MOUSE			1-0	4-0	1-0	20,5	Dual specificity protein phosphatase 3	<i>Mus musculus</i>
GRP75_MOUSE	0-0-0-1-0-0		5-0	4-0	5-0	73,5	Stress-70 protein, mitochondrial	<i>Mus musculus</i>
HS90A_MOUSE		0-2-0-0-0-0	9-0	4-0	2-0	84,8	Heat shock protein HSP 90-alpha	<i>Mus musculus</i>
IDHC_MOUSE			4-0	4-2		46,7	Isocitrate dehydrogenase [NADP] cytoplasmic	<i>Mus musculus</i>
K1C13_MOUSE	6-3-4-5-0-8	5-8-0-4-4-5	4-4	4-4	5-5	47,8	Keratin, type I cytoskeletal 13	<i>Mus musculus</i>
K2C72_MOUSE	3-1-1-3-2-3	0-3-1-2-3-4	2-2	2-4	5-2	56,8	Keratin, type II cytoskeletal 72	<i>Mus musculus</i>
OAS1A_MOUSE			3-0	4-2	5-1	42,4	2'-5'-oligoadenylate synthase 1A	<i>Mus musculus</i>
PRDX1_MOUSE	2-0-1-3-0-1	2-1-1-3-0-2	5-1	4-4	3-2	22,2	Peroxiredoxin-1	<i>Mus musculus</i>
RAB14_MOUSE			1-0	4-0		23,9	Ras-related protein Rab-14	<i>Mus musculus</i>

RAB1A_MOUSE				4-0	2-0	22,7	Ras-related protein Rab-1A	<i>Mus musculus</i>
RINI_MOUSE		0-0-0-3-0-0	3-0	3-4	6-0	49,8	Ribonuclease inhibitor	<i>Mus musculus</i>
RL10_MOUSE		0-0-1-2-0-0	4-0	3-4	5-1	24,6	60S ribosomal protein L10	<i>Mus musculus</i>
RL13A_MOUSE	0-0-2-0-3-1	1-0-0-0-2-0	2-0	4-1	2-1	23,5	60S ribosomal protein L13a	<i>Mus musculus</i>
RL18A_MOUSE	2-1-2-3-1-2	2-1-1-2-0-2	3-3	4-4	3-1	20,7	60S ribosomal protein L18a	<i>Mus musculus</i>
RL27_MOUSE			1-0	4-0	2-0	15,8	60S ribosomal protein L27	<i>Mus musculus</i>
RS14_MOUSE	0-0-0-1-0-0		4-0	4-1	4-0	16,3	40S ribosomal protein S14	<i>Mus musculus</i>
RS18_MOUSE	0-0-3-0-0-0	0-0-1-0-0-0	1-1	4-0	3-0	17,7	40S ribosomal protein S18	<i>Mus musculus</i>
RSSA_MOUSE	1-1-1-1-0-0	1-1-0-0-0-0	3-0	4-0	2-1	32,8	40S ribosomal protein SA	<i>Mus musculus</i>
RUVB1_MOUSE			8-0	4-0	8-0	50,2	RuvB-like 1	<i>Mus musculus</i>
SGPL1_MOUSE	0-0-0-0-2-0	0-0-0-0-1-0	2-0	4-2	4-0	63,7	Sphingosine-1-phosphate lyase 1	<i>Mus musculus</i>
SQRD_MOUSE	0-0-0-0-2-0	2-0-0-0-1-0	6-0	4-1	4-0	50,3	Sulfide:quinone oxidoreductase, mitochondrial	<i>Mus musculus</i>
TCPA_MOUSE			2-0	4-2	3-0	60,4	T-complex protein 1 subunit alpha	<i>Mus musculus</i>
ARL8A_MOUSE				3-0	2-0	21,4	ADP-ribosylation factor-like protein 8A	<i>Mus musculus</i>
ARL8B_MOUSE			1-0	3-1		21,5	ADP-ribosylation factor-like protein 8B	<i>Mus musculus</i>
ENOB_MOUSE	2-2-1-1-0-1	2-0-1-0-1-0	2-0	3-2	1-1	47,0	Beta-enolase	<i>Mus musculus</i>
GNMB_MOUSE	0-0-0-3-3-3	0-0-1-2-2-1	2-0	2-3	2-1	63,7	Transmembrane glycoprotein NMB	<i>Mus musculus</i>
H2B1B_MOUSE	2-0-1-1-1-1	0-0-1-1-1-1	4-1	3-1	4-0	14,0	Histone H2B type 1-B	<i>Mus musculus</i>
H4_MOUSE	4-0-1-0-0-2	1-0-0-0-2-1	8-0	3-0	2-1	11,4	Histone H4	<i>Mus musculus</i>
K1C15_MOUSE	6-0-4-6-0-11	0-0-0-4-4-6		3-3	4-0	49,1	Keratin, type I cytoskeletal 15	<i>Mus musculus</i>
K2C1B_MOUSE	6-2-0-4-4-6	0-6-2-3-0-4	3-3	3-2	4-4	61,4	Keratin, type II cytoskeletal 1b	<i>Mus musculus</i>
K2C79_MOUSE	4-2-4-4-3-7	2-4-2-5-3-6	3-2	2-3	6-4	57,6	Keratin, type II cytoskeletal 79	<i>Mus musculus</i>
LAMA1_MOUSE	0-0-2-1-0-0	0-0-1-1-0-0		3-0		338,2	Laminin subunit alpha-1	<i>Mus musculus</i>
MPCP_MOUSE				3-0	2-0	39,6	Phosphate carrier protein, mitochondrial	<i>Mus musculus</i>
NDUAA_MOUSE			2-0	3-0	2-0	40,6	NADH dehydrogenase [ubiquinone] 1 alpha subcomplex subunit 10, mitochondrial	<i>Mus musculus</i>
PKP1_MOUSE	1-0-1-0-0-0	1-2-0-1-0-0	3-0	3-0	2-1	80,9	Plakophilin-1	<i>Mus musculus</i>
PSMD3_MOUSE			4-0	3-0	4-0	60,7	26S proteasome non-ATPase regulatory subunit 3	<i>Mus musculus</i>
RAB18_MOUSE			2-0	3-0	2-0	23,0	Ras-related protein Rab-18	<i>Mus musculus</i>
RL13_MOUSE	0-0-2-1-0-0	0-0-1-2-0-0	1-0	3-1	1-0	24,3	60S ribosomal protein L13	<i>Mus musculus</i>
RL24_MOUSE	0-0-0-1-0-0	0-0-2-1-2-0	2-0	3-1	3-0	17,8	60S ribosomal protein L24	<i>Mus musculus</i>
RL27A_MOUSE	1-0-1-1-0-2	1-1-1-2-0-1	3-1	3-3	0-3	16,6	60S ribosomal protein L27a	<i>Mus musculus</i>
RS13_MOUSE	0-0-0-1-1-3	0-0-1-0-1-2	3-1	3-1	2-1	17,2	40S ribosomal protein S13	<i>Mus musculus</i>
RS24_MOUSE	0-0-1-0-0-0		1-0	3-0	5-0	15,4	40S ribosomal protein S24	<i>Mus musculus</i>
SPB6_MOUSE			2-0	3-0		42,6	Serpin B6	<i>Mus musculus</i>
VAT1_MOUSE	0-0-0-0-1-0	0-0-1-0-0-0	4-0	3-1	2-0	43,1	Synaptic vesicle membrane protein VAT-1 homolog	<i>Mus musculus</i>
VATA_MOUSE			4-0	3-1	1-0	68,3	V-type proton ATPase catalytic subunit A	<i>Mus musculus</i>
VDAC1_MOUSE	1-0-0-0-0-0		4-0	3-0	2-0	32,4	Voltage-dependent anion-selective channel protein 1	<i>Mus musculus</i>
ACADL_MOUSE				2-0		47,9	Long-chain specific acyl-CoA dehydrogenase, mitochondrial	<i>Mus musculus</i>
ALDOA_MOUSE	1-0-0-1-0-0		2-0	2-0	1-2	39,4	Fructose-bisphosphate aldolase A	<i>Mus musculus</i>
AP2M1_MOUSE			1-0	2-0	3-0	49,7	AP-2 complex subunit mu	<i>Mus musculus</i>
ARF6_MOUSE		0-1-0-0-0-0	2-0	2-1	1-0	20,1	ADP-ribosylation factor 6	<i>Mus musculus</i>
ARL1_MOUSE			2-0	2-1	1-0	20,4	ADP-ribosylation factor-like protein 1	<i>Mus musculus</i>
ARLY_MOUSE				2-0		51,7	Argininosuccinate lyase	<i>Mus musculus</i>
ASSY_MOUSE				2-1		46,6	Argininosuccinate synthase	<i>Mus musculus</i>
AT1A3_MOUSE			1-0	2-1	2-0	111,7	Sodium/potassium-transporting ATPase subunit alpha-3	<i>Mus musculus</i>
CAPG_MOUSE			2-0	2-0		39,2	Macrophage-capping protein	<i>Mus musculus</i>
CDC42_MOUSE				2-0		21,3	Cell division control protein 42 homolog	<i>Mus musculus</i>
CHTOP_MOUSE	0-0-1-0-0-0	0-0-1-0-0-0		2-0		26,6	Chromatin target of PRMT1 protein	<i>Mus musculus</i>
CY1_MOUSE				2-1	2-0	35,3	Cytochrome c1, heme protein, mitochondrial	<i>Mus musculus</i>
DPM1_MOUSE			2-0	2-0	3-0	29,2	Dolichol-phosphate mannosyltransferase subunit 1	<i>Mus musculus</i>
DSG1A_MOUSE	2-1-3-3-0-1	0-1-1-4-0-3	0-1	2-2	1-3	114,6	Desmoglein-1-alpha	<i>Mus musculus</i>
ECHA_MOUSE			1-0	2-0	2-0	82,7	Trifunctional enzyme subunit alpha, mitochondrial	<i>Mus musculus</i>
ECHB_MOUSE			2-0	2-0		51,4	Trifunctional enzyme subunit beta, mitochondrial	<i>Mus musculus</i>

FCGR3_MOUSE	0-1-0-0-0-0		1-0	2-0		30,0	Low affinity immunoglobulin gamma Fc region receptor III	<i>Mus musculus</i>
GALC_MOUSE			4-0	2-0	1-0	77,3	Galactocerebrosidase	<i>Mus musculus</i>
GNAI2_MOUSE	1-0-0-0-0-0		1-0	0-2	4-1	40,5	Guanine nucleotide-binding protein G(i) subunit alpha-2	<i>Mus musculus</i>
K1C27_MOUSE				0-2		49,1	Keratin, type I cytoskeletal 27	<i>Mus musculus</i>
K2C80_MOUSE	0-0-2-2-0-3	0-0-0-1-1-0	1-1	2-1	1-2	50,7	Keratin, type II cytoskeletal 80	<i>Mus musculus</i>
KSYK_MOUSE				2-0		71,4	Tyrosine-protein kinase SYK	<i>Mus musculus</i>
LPXN_MOUSE				0-2		43,5	Leupaxin	<i>Mus musculus</i>
M2OM_MOUSE			3-0	2-0	4-0	34,2	Mitochondrial 2-oxoglutarate/malate carrier protein	<i>Mus musculus</i>
MLEC_MOUSE				2-0	4-0	32,3	Malectin	<i>Mus musculus</i>
NDUA4_MOUSE	0-0-0-0-1-0		1-0	2-0	2-0	9,3	Cytochrome c oxidase subunit NDUA4	<i>Mus musculus</i>
NDUS1_MOUSE			2-0	2-0	1-0	79,8	NADH-ubiquinone oxidoreductase 75 kDa subunit, mitochondrial	<i>Mus musculus</i>
NDUS3_MOUSE			1-0	2-0	2-0	30,1	NADH dehydrogenase [ubiquinone] iron-sulfur protein 3, mitochondrial	<i>Mus musculus</i>
PP1A_MOUSE				0-2	2-0	37,5	Serine/threonine-protein phosphatase PP1-alpha catalytic subunit	<i>Mus musculus</i>
RAB5B_MOUSE				2-0		23,7	Ras-related protein Rab-5B	<i>Mus musculus</i>
RAB5C_MOUSE				2-0	2-0	23,4	Ras-related protein Rab-5C	<i>Mus musculus</i>
RAB9A_MOUSE				2-1		22,9	Ras-related protein Rab-9A	<i>Mus musculus</i>
RAC1_MOUSE	1-0-0-0-1-0		2-0	2-2	1-1	21,5	Ras-related C3 botulinum toxin substrate 1	<i>Mus musculus</i>
RAP2B_MOUSE			2-0	2-0		20,5	Ras-related protein Rap-2b	<i>Mus musculus</i>
RL11_MOUSE	0-1-1-3-0-0	0-0-0-3-0-0	2-2	2-2	2-1	20,3	60S ribosomal protein L11	<i>Mus musculus</i>
RL12_MOUSE	0-0-1-1-0-0		3-0	2-0	4-0	17,8	60S ribosomal protein L12	<i>Mus musculus</i>
RL14_MOUSE	1-0-1-0-0-1	0-1-1-0-0-1	2-1	2-1	4-0	23,6	60S ribosomal protein L14	<i>Mus musculus</i>
RL22_MOUSE			1-0	2-0	0-1	14,8	60S ribosomal protein L22	<i>Mus musculus</i>
RL28_MOUSE	0-0-0-1-0-0	0-0-1-2-0-0		2-1	3-1	15,7	60S ribosomal protein L28	<i>Mus musculus</i>
RL37A_MOUSE	0-0-1-0-0-1	0-0-1-0-1-0	1-0	2-1	4-1	10,3	60S ribosomal protein L37a	<i>Mus musculus</i>
RPN2_MOUSE			1-0	2-0	2-0	69,1	Dolichyl-diphosphooligosaccharide--protein glycosyltransferase subunit 2	<i>Mus musculus</i>
RS15A_MOUSE	1-0-0-0-0-0		3-0	2-0	3-0	14,8	40S ribosomal protein S15a	<i>Mus musculus</i>
RS2_MOUSE	0-0-0-0-1-0	2-0-0-1-1-1	7-1	2-2	10-1	31,2	40S ribosomal protein S2	<i>Mus musculus</i>
RS9_MOUSE	2-0-3-1-0-0	1-0-0-1-0-0	4-0	2-0	4-0	22,6	40S ribosomal protein S9	<i>Mus musculus</i>
RUVB2_MOUSE			8-0	2-0	12-0	51,1	RuvB-like 2	<i>Mus musculus</i>
SOAT1_MOUSE				2-0	1-0	63,8	Sterol O-acyltransferase 1	<i>Mus musculus</i>
SSRA_MOUSE				2-0	1-0	32,1	Translocon-associated protein subunit alpha	<i>Mus musculus</i>
SSRD_MOUSE		0-1-0-0-0-0	1-0	2-0	1-0	18,9	Translocon-associated protein subunit delta	<i>Mus musculus</i>
TBG1_MOUSE			1-0	1-2		51,1	Tubulin gamma-1 chain	<i>Mus musculus</i>
TECR_MOUSE			1-0	2-0	1-0	36,1	Very-long-chain enoyl-CoA reductase	<i>Mus musculus</i>
TIM50_MOUSE			1-0	2-2	3-0	39,8	Mitochondrial import inner membrane translocase subunit TIM50	<i>Mus musculus</i>
VDAC2_MOUSE	1-0-0-0-0-0	1-3-0-0-0-0	3-0	1-2	1-0	31,7	Voltage-dependent anion-selective channel protein 2	<i>Mus musculus</i>
2ABA_MOUSE	0-0-0-1-0-0			0-1		51,7	Serine/threonine-protein phosphatase 2A 55 kDa regulatory subunit B alpha isoform	<i>Mus musculus</i>
ABEC1_MOUSE				0-1	4-0	27,5	C->U-editing enzyme APOBEC-1	<i>Mus musculus</i>
AIFM1_MOUSE			1-0	1-0	2-0	66,8	Apoptosis-inducing factor 1, mitochondrial	<i>Mus musculus</i>
ALBU_MOUSE	0-1-1-1-1-1	0-1-1-1-1-1	0-1	1-1	1-1	68,7	Serum albumin	<i>Mus musculus</i>
ALDH2_MOUSE			5-0	1-0	1-0	56,5	Aldehyde dehydrogenase, mitochondrial	<i>Mus musculus</i>
ANKR1_MOUSE				1-0		36,0	Ankyrin repeat domain-containing protein 1	<i>Mus musculus</i>
APT_MOUSE				1-0		19,7	Adenine phosphoribosyltransferase	<i>Mus musculus</i>
ARG1_MOUSE	1-0-0-0-1-0	0-0-0-0-1-1		1-0	1-1	34,8	Arginase-1	<i>Mus musculus</i>
ATPO_MOUSE			1-0	1-0	1-0	23,4	ATP synthase subunit O, mitochondrial	<i>Mus musculus</i>
BLMH_MOUSE	1-0-2-0-0-0	0-1-0-0-0-0	3-0	1-0	1-0	52,5	Bleomycin hydrolase	<i>Mus musculus</i>
CALX_MOUSE				1-0		67,3	Calnexin	<i>Mus musculus</i>
CAP1_MOUSE	0-0-0-0-0-1	0-0-0-0-2-1		1-0	1-0	51,6	Adenylyl cyclase-associated protein 1	<i>Mus musculus</i>
CATA_MOUSE	1-0-0-0-0-0	1-1-0-1-0-0		1-0		59,8	Catalase	<i>Mus musculus</i>
CATD_MOUSE	0-0-1-1-0-0	0-0-1-0-0-0		1-0	1-0	45,0	Cathepsin D	<i>Mus musculus</i>
CH60_MOUSE			3-0	1-0	1-0	61,0	60 kDa heat shock protein, mitochondrial	<i>Mus musculus</i>
CLPX_MOUSE				0-1	0-1	69,2	ATP-dependent Clp protease ATP-binding subunit clpX-like, mitochondrial	<i>Mus musculus</i>
COPA_MOUSE			12-0	1-0	20-2	138,4	Coatomer subunit alpha	<i>Mus musculus</i>

COPE_MOUSE				1-0	1-0	34,6	Coatomer subunit epsilon	<i>Mus musculus</i>
COPG2_MOUSE				1-0		97,7	Coatomer subunit gamma-2	<i>Mus musculus</i>
CP059_MOUSE				1-0		47,8	Uncharacterized protein C16orf59 homolog	<i>Mus musculus</i>
CREG1_MOUSE				1-0		24,5	Protein CREG1	<i>Mus musculus</i>
DHB11_MOUSE			2-1	1-0	4-0	32,9	Estradiol 17-beta-dehydrogenase 11	<i>Mus musculus</i>
DNJA2_MOUSE			2-0	1-0	1-0	45,7	Dnaj homolog subfamily A member 2	<i>Mus musculus</i>
EF2_MOUSE		0-1-0-0-0-0	9-0	0-1	1-1	95,3	Elongation factor 2	<i>Mus musculus</i>
EFTU_MOUSE			1-0	0-1	1-0	49,5	Elongation factor Tu, mitochondrial	<i>Mus musculus</i>
ESYT1_MOUSE			1-0	1-0		121,6	Extended synaptotagmin-1	<i>Mus musculus</i>
F13A_MOUSE			7-0	1-0	5-0	83,2	Coagulation factor XIII A chain	<i>Mus musculus</i>
FBX50_MOUSE	1-0-1-1-1-1	0-1-0-0-0-0		1-0	0-1	30,4	F-box only protein 50	<i>Mus musculus</i>
FRIL1_MOUSE			1-0	1-0	3-0	20,8	Ferritin light chain 1	<i>Mus musculus</i>
G6PC3_MOUSE				0-1		38,8	Glucose-6-phosphatase 3	<i>Mus musculus</i>
G6PD1_MOUSE			2-0	1-0		59,3	Glucose-6-phosphate 1-dehydrogenase X	<i>Mus musculus</i>
GALK1_MOUSE			1-0	1-0	2-0	42,3	Galactokinase	<i>Mus musculus</i>
GELS_MOUSE	1-0-0-0-0-0	1-0-0-0-0-0	7-0	0-1		85,9	Gelsolin	<i>Mus musculus</i>
GGCT_MOUSE				0-1		21,2	Gamma-glutamylcyclotransferase	<i>Mus musculus</i>
GLE1_MOUSE				1-0		79,6	Nucleoporin GLE1	<i>Mus musculus</i>
GRN_MOUSE	0-2-0-1-0-3	0-1-0-2-0-0	0-1	0-1	0-2	63,5	Granulins	<i>Mus musculus</i>
GRPE1_MOUSE				1-0		24,3	GrpE protein homolog 1, mitochondrial	<i>Mus musculus</i>
GSDA2_MOUSE	1-0-0-1-0-0	0-1-0-0-0-0	1-0	0-1	1-1	49,8	Gasdermin-A2	<i>Mus musculus</i>
HNRH1_MOUSE			1-0	0-1	2-0	49,2	Heterogeneous nuclear ribonucleoprotein H	<i>Mus musculus</i>
HNRPU_MOUSE			0-1	1-0	2-0	87,9	Heterogeneous nuclear ribonucleoprotein U	<i>Mus musculus</i>
HPCL1_MOUSE	0-0-0-0-0-1			0-1		22,3	Hippocalcin-like protein 1	<i>Mus musculus</i>
HVM16_MOUSE	0-0-0-1-0-2	0-0-0-1-0-2	1-1	0-1	1-2	15,1	Ig heavy chain V region MOPC 21 (Fragment)	<i>Mus musculus</i>
IF44L_MOUSE			1-0	1-0		49,7	Interferon-induced protein 44-like	<i>Mus musculus</i>
IFI44_MOUSE				1-1		47,9	Interferon-induced protein 44	<i>Mus musculus</i>
IGHG1_MOUSE	2-0-0-1-1-2	1-0-1-1-1-3		1-1	2-2	35,7	Ig gamma-1 chain C region secreted form	<i>Mus musculus</i>
IQGA1_MOUSE		2-0-0-0-2-0	8-1	0-1	2-0	188,7	Ras GTPase-activating-like protein IQGAP1	<i>Mus musculus</i>
JIP2_MOUSE				0-1		89,9	C-Jun-amino-terminal kinase-interacting protein 2	<i>Mus musculus</i>
K0930_MOUSE				1-0		46,0	Uncharacterized protein KIAA0930 homolog	<i>Mus musculus</i>
K1C12_MOUSE	0-0-0-1-0-0	0-1-0-0-0-0		1-0	1-1	52,5	Keratin, type I cytoskeletal 12	<i>Mus musculus</i>
KC1A_MOUSE			2-0	1-0	1-2	38,9	Casein kinase I isoform alpha	<i>Mus musculus</i>
KC1E_MOUSE				1-0		47,3	Casein kinase I isoform epsilon	<i>Mus musculus</i>
KV2A1_MOUSE				0-1		12,3	Ig kappa chain V-II region MOPC 167	<i>Mus musculus</i>
KV2A4_MOUSE	1-1-1-1-1-1	1-1-1-1-1-1	1-1	1-1	1-1	12,2	Ig kappa chain V-II region 2S1.3	<i>Mus musculus</i>
KV2A5_MOUSE	0-0-0-1-0-0	0-0-0-1-0-0		0-1	0-1	12,4	Ig kappa chain V-II region 17S29.1	<i>Mus musculus</i>
LAMB1_MOUSE				1-0		197,1	Laminin subunit beta-1	<i>Mus musculus</i>
LBR_MOUSE				1-0		71,4	Lamin-B receptor	<i>Mus musculus</i>
LICH_MOUSE				1-0		45,3	Lysosomal acid lipase/cholesteryl ester hydrolase	<i>Mus musculus</i>
LRP12_MOUSE				1-0		94,6	Low-density lipoprotein receptor-related protein 12	<i>Mus musculus</i>
LYZ1_MOUSE	1-1-1-1-1-1	1-1-1-1-1-1	0-1	1-1	1-1	16,8	Lysozyme C-1	<i>Mus musculus</i>
MCM7_MOUSE				1-0	1-0	81,2	DNA replication licensing factor MCM7	<i>Mus musculus</i>
MGST3_MOUSE				0-1	1-0	17,0	Microsomal glutathione S-transferase 3	<i>Mus musculus</i>
MIRO1_MOUSE				1-0	1-0	72,2	Mitochondrial Rho GTPase 1	<i>Mus musculus</i>
MMP12_MOUSE				1-0	1-0	55,0	Macrophage metalloelastase	<i>Mus musculus</i>
MOES_MOUSE	1-0-0-0-0-0		1-0	1-0		67,8	Moesin	<i>Mus musculus</i>
MPEG1_MOUSE				1-1	1-0	78,4	Macrophage-expressed gene 1 protein	<i>Mus musculus</i>
MRV1_MOUSE				1-0		97,4	Protein MRV1	<i>Mus musculus</i>
MYO1E_MOUSE	2-0-0-0-0-0		6-0	1-0		126,8	Unconventional myosin-1e	<i>Mus musculus</i>
NAMPT_MOUSE				1-1		55,4	Nicotinamide phosphoribosyltransferase	<i>Mus musculus</i>
NCPR_MOUSE				1-0		77,0	NADPH--cytochrome P450 reductase	<i>Mus musculus</i>
NDP_MOUSE				1-0		14,7	Norrin	<i>Mus musculus</i>

NDUA1_MOUSE				1-0	2-0	8,1	NADH dehydrogenase [ubiquinone] 1 alpha subcomplex subunit 1	<i>Mus musculus</i>
NDUB4_MOUSE				1-0		15,1	NADH dehydrogenase [ubiquinone] 1 beta subcomplex subunit 4	<i>Mus musculus</i>
NFS1_MOUSE			1-0	1-1	1-1	50,6	Cysteine desulfurase, mitochondrial	<i>Mus musculus</i>
NIPBL_MOUSE				1-0		315,4	Nipped-B-like protein	<i>Mus musculus</i>
NONO_MOUSE	0-0-0-0-2-1		2-0	1-0	1-0	54,5	Non-POU domain-containing octamer-binding protein	<i>Mus musculus</i>
NSDHL_MOUSE				1-0		40,7	Sterol-4-alpha-carboxylate 3-dehydrogenase, decarboxylating	<i>Mus musculus</i>
OSTC_MOUSE	0-0-0-0-1-0		1-0	1-0	1-0	16,8	Oligosaccharyltransferase complex subunit OSTC	<i>Mus musculus</i>
PCBP1_MOUSE			3-0	0-1	2-0	37,5	Poly(rC)-binding protein 1	<i>Mus musculus</i>
PCNA_MOUSE			1-0	1-0	3-0	28,8	Proliferating cell nuclear antigen	<i>Mus musculus</i>
PODN_MOUSE				0-1		68,7	Podocan	<i>Mus musculus</i>
PP1G_MOUSE			1-0	1-0	0-1	37,0	Serine/threonine-protein phosphatase PP1-gamma catalytic subunit	<i>Mus musculus</i>
PPAC_MOUSE			3-0	1-0	1-0	18,2	Low molecular weight phosphotyrosine protein phosphatase	<i>Mus musculus</i>
PRDX2_MOUSE	1-0-1-1-0-1	1-1-1-1-0-1	0-1	1-1	0-1	21,8	Peroxiredoxin-2	<i>Mus musculus</i>
PRS7_MOUSE				1-0		48,6	26S protease regulatory subunit 7	<i>Mus musculus</i>
PRS8_MOUSE				1-0		45,6	26S protease regulatory subunit 8	<i>Mus musculus</i>
PSA4_MOUSE		0-1-0-0-0-0		1-0		29,5	Proteasome subunit alpha type-4	<i>Mus musculus</i>
PSA5_MOUSE	1-1-0-0-1-1	0-1-0-0-0-0	1-0	1-0	0-1	26,4	Proteasome subunit alpha type-5	<i>Mus musculus</i>
PSB6_MOUSE	1-0-0-0-0-0	0-1-0-0-0-0		1-0		25,4	Proteasome subunit beta type-6	<i>Mus musculus</i>
RAB10_MOUSE			1-0	1-0		22,5	Ras-related protein Rab-10	<i>Mus musculus</i>
RAB15_MOUSE	0-0-0-1-0-0	1-0-0-0-0-0	1-0	1-1		24,3	Ras-related protein Rab-15	<i>Mus musculus</i>
RAB21_MOUSE				1-0		24,1	Ras-related protein Rab-21	<i>Mus musculus</i>
RAB31_MOUSE				1-0	1-0	21,3	Ras-related protein Rab-31	<i>Mus musculus</i>
RAB7A_MOUSE		0-1-0-0-0-0		1-0	1-1	23,5	Ras-related protein Rab-7a	<i>Mus musculus</i>
RAB8A_MOUSE				1-0	1-0	23,7	Ras-related protein Rab-8A	<i>Mus musculus</i>
RALB_MOUSE				1-0		23,3	Ras-related protein Ral-B	<i>Mus musculus</i>
RAP1A_MOUSE				1-0		21,0	Ras-related protein Rap-1A	<i>Mus musculus</i>
RB11A_MOUSE			1-0	1-0		24,4	Ras-related protein Rab-11A	<i>Mus musculus</i>
RCN2_MOUSE				1-0	4-0	37,3	Reticulocalbin-2	<i>Mus musculus</i>
RDH11_MOUSE				1-0		35,1	Retinol dehydrogenase 11	<i>Mus musculus</i>
RHOA_MOUSE				1-0		21,8	Transforming protein RhoA	<i>Mus musculus</i>
RHOC_MOUSE				0-1		22,0	Rho-related GTP-binding protein RhoC	<i>Mus musculus</i>
RL18_MOUSE		0-0-1-1-0-0	1-0	1-0	3-0	21,6	60S ribosomal protein L18	<i>Mus musculus</i>
RL21_MOUSE	0-0-1-1-0-0	0-0-0-2-0-0	1-0	1-1	1-0	18,6	60S ribosomal protein L21	<i>Mus musculus</i>
RL23A_MOUSE			1-0	1-0		17,7	60S ribosomal protein L23a	<i>Mus musculus</i>
RL26_MOUSE	0-0-1-0-1-0	0-0-0-0-1-0		1-0	3-0	17,3	60S ribosomal protein L26	<i>Mus musculus</i>
RL30_MOUSE	0-0-0-0-3-0	0-0-1-0-1-1	0-1	1-0	3-0	12,8	60S ribosomal protein L30	<i>Mus musculus</i>
RL31_MOUSE				1-0		14,5	60S ribosomal protein L31	<i>Mus musculus</i>
RL35_MOUSE	0-0-0-0-1-0	0-0-0-1-1-0		1-0	1-0	14,6	60S ribosomal protein L35	<i>Mus musculus</i>
RL36A_MOUSE	0-0-1-2-0-0			1-0		12,4	60S ribosomal protein L36a	<i>Mus musculus</i>
RL39_MOUSE	0-0-0-0-1-0			1-0	1-0	6,4	60S ribosomal protein L39	<i>Mus musculus</i>
RL40_MOUSE	0-0-0-1-1-1	1-1-1-1-0-0	2-0	1-0	2-1	14,7	Ubiquitin-60S ribosomal protein L40	<i>Mus musculus</i>
RL6_MOUSE			3-0	1-0	4-0	33,5	60S ribosomal protein L6	<i>Mus musculus</i>
RL7_MOUSE	0-0-1-0-0-0	2-0-0-0-0-0	1-0	1-0	7-0	31,4	60S ribosomal protein L7	<i>Mus musculus</i>
RL9_MOUSE	0-0-0-0-3-0	0-0-0-0-1-0	1-0	1-0	1-0	21,9	60S ribosomal protein L9	<i>Mus musculus</i>
RS10_MOUSE		0-0-0-0-1-0	3-0	1-0	1-0	18,9	40S ribosomal protein S10	<i>Mus musculus</i>
RS16_MOUSE			2-0	0-1	4-0	16,4	40S ribosomal protein S16	<i>Mus musculus</i>
RS19_MOUSE	0-0-0-0-1-0		1-0	1-0	1-0	16,1	40S ribosomal protein S19	<i>Mus musculus</i>
RS20_MOUSE	0-0-0-1-0-1	0-0-0-0-1-0	2-0	1-1	3-1	13,4	40S ribosomal protein S20	<i>Mus musculus</i>
RS23_MOUSE	0-0-0-1-0-0	0-0-0-1-0-0		1-0		15,8	40S ribosomal protein S23	<i>Mus musculus</i>
RS25_MOUSE		0-1-0-0-0-1	2-1	1-0	1-0	13,7	40S ribosomal protein S25	<i>Mus musculus</i>
RS26_MOUSE				1-1	3-0	13,0	40S ribosomal protein S26	<i>Mus musculus</i>
RS3A_MOUSE	0-0-0-0-1-0	0-0-0-0-3-0	1-0	1-1	3-0	29,9	40S ribosomal protein S3a	<i>Mus musculus</i>
RS5_MOUSE	0-1-0-0-1-1	0-0-0-0-0-1	2-0	1-0	1-1	22,9	40S ribosomal protein S5	<i>Mus musculus</i>
S10AE_MOUSE	0-0-0-1-0-1	0-1-0-1-0-1		1-1	1-1	11,6	Protein S100-A14	<i>Mus musculus</i>

SCAM3_MOUSE				1-0		38,5	Secretory carrier-associated membrane protein 3	<i>Mus musculus</i>
SDCB1_MOUSE				1-0		32,4	Syntenin-1	<i>Mus musculus</i>
SDHA_MOUSE			1-0	1-0	1-0	72,6	Succinate dehydrogenase [ubiquinone] flavoprotein subunit, mitochondrial	<i>Mus musculus</i>
SFXN3_MOUSE	0-0-0-0-1-0		1-0	1-0	2-0	35,4	Sideroflexin-3	<i>Mus musculus</i>
SPB11_MOUSE	0-0-1-0-0-0	0-0-1-0-0-0		1-0		43,5	Serpin B11	<i>Mus musculus</i>
SPTC1_MOUSE			1-0	1-1	1-0	52,5	Serine palmitoyltransferase 1	<i>Mus musculus</i>
SSRG_MOUSE				1-0		21,1	Translocan-associated protein subunit gamma	<i>Mus musculus</i>
STOM_MOUSE	1-0-0-0-0-0	0-1-0-0-0-0	1-0	1-0	2-0	31,4	Erythrocyte band 7 integral membrane protein	<i>Mus musculus</i>
STT3A_MOUSE				1-0		80,6	Dolichyl-diphosphooligosaccharide--protein glycosyltransferase subunit STT3A	<i>Mus musculus</i>
SVIL_MOUSE				1-0		243,2	Supervillin	<i>Mus musculus</i>
SYFA_MOUSE			2-0	1-0		57,6	Phenylalanine--tRNA ligase alpha subunit	<i>Mus musculus</i>
SYNC_MOUSE				0-1		64,3	Asparagine--tRNA ligase, cytoplasmic	<i>Mus musculus</i>
TGM1_MOUSE	2-1-0-1-0-0	2-2-0-1-0-0	1-0	1-0	0-1	89,8	Protein-glutamine gamma-glutamyltransferase K	<i>Mus musculus</i>
TITIN_MOUSE				1-0	1-0	3906,5	Titin	<i>Mus musculus</i>
TRAP1_MOUSE	1-1-1-1-1-0	1-1-1-1-1-0	2-1	1-0	1-1	80,2	Heat shock protein 75 kDa, mitochondrial	<i>Mus musculus</i>
UN93B_MOUSE				1-0		67,0	Protein unc-93 homolog B1	<i>Mus musculus</i>
VATB2_MOUSE			1-0	1-1		56,6	V-type proton ATPase subunit B, brain isoform	<i>Mus musculus</i>
VATH_MOUSE				1-0		55,9	V-type proton ATPase subunit H	<i>Mus musculus</i>
ZDHCS_MOUSE				1-0		77,5	Palmitoyltransferase ZDHC5	<i>Mus musculus</i>
1433E_MOUSE			7-0			29,2	14-3-3 protein epsilon	<i>Mus musculus</i>
1433G_MOUSE			4-0			28,3	14-3-3 protein gamma	<i>Mus musculus</i>
1433S_MOUSE			6-0			27,7	14-3-3 protein sigma	<i>Mus musculus</i>
1433Z_MOUSE	2-0-0-0-0-0	0-2-1-0-1-0	4-0		2-1	27,8	14-3-3 protein zeta/delta	<i>Mus musculus</i>
2AAA_MOUSE					1-0	65,3	Serine/threonine-protein phosphatase 2A 65 kDa regulatory subunit A alpha isoform	<i>Mus musculus</i>
6PGD_MOUSE	1-0-0-0-0-0				0-1	53,2	6-phosphogluconate dehydrogenase, decarboxylating	<i>Mus musculus</i>
AAAT_MOUSE			1-0			58,5	Neutral amino acid transporter B(0)	<i>Mus musculus</i>
AATC_MOUSE	1-0-0-0-0-1					46,2	Aspartate aminotransferase, cytoplasmic	<i>Mus musculus</i>
ABCG1_MOUSE			1-0			74,0	ATP-binding cassette sub-family G member 1	<i>Mus musculus</i>
ABD12_MOUSE					1-0	45,3	Monoacylglycerol lipase ABHD12	<i>Mus musculus</i>
ABHEB_MOUSE			1-0			22,5	Alpha/beta hydrolase domain-containing protein 14B	<i>Mus musculus</i>
ACOC_MOUSE	1-0-0-0-0-0					98,1	Cytoplasmic aconitate hydratase	<i>Mus musculus</i>
ACOT8_MOUSE		1-0-0-0-0-0				35,8	Acyl-coenzyme A thioesterase 8	<i>Mus musculus</i>
ACTBL_MOUSE	5-3-0-4-0-0	4-0-0-0-0-0	5-0			42,0	Beta-actin-like protein 2	<i>Mus musculus</i>
ACTN4_MOUSE	3-0-0-0-0-1	1-1-0-0-0-0	12-0		0-2	105,0	Alpha-actinin-4	<i>Mus musculus</i>
ACTZ_MOUSE			1-0			42,6	Alpha-centractin	<i>Mus musculus</i>
AHSA1_MOUSE			1-0			38,1	Activator of 90 kDa heat shock protein ATPase homolog 1	<i>Mus musculus</i>
AKAP9_MOUSE					1-0	436,2	A-kinase anchor protein 9	<i>Mus musculus</i>
AL3A2_MOUSE					1-0	54,0	Fatty aldehyde dehydrogenase	<i>Mus musculus</i>
AL3B1_MOUSE			1-0			52,3	Aldehyde dehydrogenase family 3 member B1	<i>Mus musculus</i>
AL9A1_MOUSE	0-1-0-0-0-0					53,5	4-trimethylaminobutyraldehyde dehydrogenase	<i>Mus musculus</i>
AMPL_MOUSE			4-0			56,1	Cytosol aminopeptidase	<i>Mus musculus</i>
ANLN_MOUSE			0-1			122,8	Actin-binding protein anillin	<i>Mus musculus</i>
ANXA3_MOUSE	1-0-0-0-0-0					36,4	Annexin A3	<i>Mus musculus</i>
ANXA6_MOUSE	1-0-0-0-0-0					75,9	Annexin A6	<i>Mus musculus</i>
ANXA8_MOUSE					0-1	36,7	Annexin A8	<i>Mus musculus</i>
AP1M1_MOUSE			1-0			48,5	AP-1 complex subunit mu-1	<i>Mus musculus</i>
AP2A1_MOUSE			2-0			107,7	AP-2 complex subunit alpha-1	<i>Mus musculus</i>
AP3B1_MOUSE			2-0		5-0	122,7	AP-3 complex subunit beta-1	<i>Mus musculus</i>
AP3D1_MOUSE			1-0			135,1	AP-3 complex subunit delta-1	<i>Mus musculus</i>
APMAP_MOUSE	1-0-0-0-0-0					46,4	Adipocyte plasma membrane-associated protein	<i>Mus musculus</i>
APOE_MOUSE			1-0			35,9	Apolipoprotein E	<i>Mus musculus</i>
ARC_MOUSE	1-0-0-0-0-0					45,3	Activity-regulated cytoskeleton-associated protein	<i>Mus musculus</i>
ARF4_MOUSE					3-0	20,4	ADP-ribosylation factor 4	<i>Mus musculus</i>

ARL11_MOUSE			1-0			19,2	ADP-ribosylation factor-like protein 11	<i>Mus musculus</i>
ARM10_MOUSE					1-0	33,3	Armadillo repeat-containing protein 10	<i>Mus musculus</i>
ARMC9_MOUSE		0-0-0-0-0-1				91,9	LisH domain-containing protein ARMC9	<i>Mus musculus</i>
ARP2_MOUSE			1-0			44,8	Actin-related protein 2	<i>Mus musculus</i>
ARP3_MOUSE			2-0		0-1	47,4	Actin-related protein 3	<i>Mus musculus</i>
ARPC2_MOUSE			1-0			34,4	Actin-related protein 2/3 complex subunit 2	<i>Mus musculus</i>
ARPC4_MOUSE	2-0-0-0-0-0					19,7	Actin-related protein 2/3 complex subunit 4	<i>Mus musculus</i>
ASAH1_MOUSE		1-0-0-0-0-0				44,7	Acid ceramidase	<i>Mus musculus</i>
ASAP2_MOUSE	1-1-0-0-0-0	0-0-0-0-0-1				106,8	Arf-GAP with SH3 domain, ANK repeat and PH domain-containing protein 2	<i>Mus musculus</i>
ASB16_MOUSE					1-0	49,1	Ankyrin repeat and SOCS box protein 16	<i>Mus musculus</i>
ASM3B_MOUSE			1-0			51,6	Acid sphingomyelinase-like phosphodiesterase 3b	<i>Mus musculus</i>
ASNS_MOUSE			1-0			64,3	Asparagine synthetase [glutamine-hydrolyzing]	<i>Mus musculus</i>
ASPH_MOUSE					1-0	83,0	Aspartyl/asparaginyl beta-hydroxylase	<i>Mus musculus</i>
AT2A2_MOUSE			2-0		1-0	114,9	Sarcoplasmic/endoplasmic reticulum calcium ATPase 2	<i>Mus musculus</i>
AT2B4_MOUSE			2-0			133,1	Plasma membrane calcium-transporting ATPase 4	<i>Mus musculus</i>
ATPK_MOUSE			1-0			10,3	ATP synthase subunit f, mitochondrial	<i>Mus musculus</i>
BAF_MOUSE			1-0			10,1	Barrier-to-autointegration factor	<i>Mus musculus</i>
BAG2_MOUSE			1-0			23,5	BAG family molecular chaperone regulator 2	<i>Mus musculus</i>
BIEA_MOUSE			1-0			33,5	Biliverdin reductase A	<i>Mus musculus</i>
BINCA_MOUSE					1-0	20,9	Bcl10-interacting CARD protein	<i>Mus musculus</i>
BRI3_MOUSE					1-0	13,6	Brain protein I3	<i>Mus musculus</i>
BSN_MOUSE			0-1			418,8	Protein bassoon	<i>Mus musculus</i>
C1QA_MOUSE	3-0-0-0-1-0	2-0-0-0-2-0	3-0		2-0	26,0	Complement C1q subcomponent subunit A	<i>Mus musculus</i>
C1QB_MOUSE	2-0-0-0-1-1	2-0-0-0-1-0	2-0		2-0	26,7	Complement C1q subcomponent subunit B	<i>Mus musculus</i>
C1QC_MOUSE	1-1-0-0-2-0	2-0-0-0-1-0	3-1		1-0	26,0	Complement C1q subcomponent subunit C	<i>Mus musculus</i>
CALL3_MOUSE					0-1	16,7	Calmodulin-like protein 3	<i>Mus musculus</i>
CALM_MOUSE		0-1-0-0-0-0	3-0			16,8	Calmodulin	<i>Mus musculus</i>
CAN1_MOUSE	1-0-0-0-1-0	0-1-0-0-0-0	2-1		1-0	82,1	Calpain-1 catalytic subunit	<i>Mus musculus</i>
CAND1_MOUSE			2-0			136,3	Cullin-associated NEDD8-dissociated protein 1	<i>Mus musculus</i>
CAPZB_MOUSE	5-0-0-0-0-0		8-0			31,3	F-actin-capping protein subunit beta	<i>Mus musculus</i>
CASPE_MOUSE	1-0-0-0-0-0					29,5	Caspase-14	<i>Mus musculus</i>
CATG_MOUSE	1-0-0-0-0-0	1-0-0-0-0-0	3-0			29,1	Cathepsin G	<i>Mus musculus</i>
CATS_MOUSE			1-0			38,5	Cathepsin S	<i>Mus musculus</i>
CAZA1_MOUSE			3-0			32,9	F-actin-capping protein subunit alpha-1	<i>Mus musculus</i>
CAZA2_MOUSE	4-0-1-0-0-0	1-0-0-0-0-0	7-0		0-1	33,0	F-actin-capping protein subunit alpha-2	<i>Mus musculus</i>
CBPA4_MOUSE					1-0	47,3	Carboxypeptidase A4	<i>Mus musculus</i>
CBR4_MOUSE			1-0		1-0	25,4	Carbonyl reductase family member 4	<i>Mus musculus</i>
CD38_MOUSE	1-0-0-0-0-0					34,4	ADP-ribosyl cyclase/cyclic ADP-ribose hydrolase 1	<i>Mus musculus</i>
CDIPT_MOUSE			1-0			23,6	CDP-diacylglycerol--inositol 3-phosphatidyltransferase	<i>Mus musculus</i>
CDSN_MOUSE	1-1-0-0-0-0		0-1			54,3	Corneodesmosin	<i>Mus musculus</i>
CEPT1_MOUSE			1-0			46,4	Choline/ethanolaminephosphotransferase 1	<i>Mus musculus</i>
CH10_MOUSE			1-0			11,0	10 kDa heat shock protein, mitochondrial	<i>Mus musculus</i>
CHMP5_MOUSE			0-1			24,6	Charged multivesicular body protein 5	<i>Mus musculus</i>
CHP1_MOUSE			1-0			22,4	Calcineurin B homologous protein 1	<i>Mus musculus</i>
CIR1A_MOUSE	0-0-0-0-0-1	0-0-0-0-0-1				76,9	Cirhin	<i>Mus musculus</i>
CISY_MOUSE			1-0			51,7	Citrate synthase, mitochondrial	<i>Mus musculus</i>
CKAP5_MOUSE					1-0	225,6	Cytoskeleton-associated protein 5	<i>Mus musculus</i>
CLCN7_MOUSE			1-0			88,7	H(+)/Cl(-) exchange transporter 7	<i>Mus musculus</i>
CLH1_MOUSE			15-1		1-0	191,6	Clathrin heavy chain 1	<i>Mus musculus</i>
CLIC1_MOUSE			1-0			27,0	Chloride intracellular channel protein 1	<i>Mus musculus</i>
CLIC3_MOUSE			1-0			26,8	Chloride intracellular channel protein 3	<i>Mus musculus</i>
CLUS_MOUSE	0-0-2-0-0-0					51,7	Clusterin	<i>Mus musculus</i>
CMC1_MOUSE			2-0			74,6	Calcium-binding mitochondrial carrier protein Aralar1	<i>Mus musculus</i>

CMC2_MOUSE			3-0			74,5	Calcium-binding mitochondrial carrier protein Aralar2	<i>Mus musculus</i>
CMTR1_MOUSE	0-0-0-0-1-0	0-0-0-0-0-1				95,7	Cap-specific mRNA (nucleoside-2'-O-)-methyltransferase 1	<i>Mus musculus</i>
CN37_MOUSE					2-0	47,1	2',3'-cyclic-nucleotide 3'-phosphodiesterase	<i>Mus musculus</i>
CNBP1_MOUSE			1-0			9,2	Beta-catenin-interacting protein 1	<i>Mus musculus</i>
CNDP2_MOUSE			2-0			52,8	Cytosolic non-specific dipeptidase	<i>Mus musculus</i>
CO6A2_MOUSE	0-0-0-1-0-0					110,3	Collagen alpha-2(VI) chain	<i>Mus musculus</i>
COPB2_MOUSE		1-0-0-0-0-0	1-0		0-1	102,4	Coatomer subunit beta'	<i>Mus musculus</i>
COPD_MOUSE			1-0		1-0	57,2	Coatomer subunit delta	<i>Mus musculus</i>
COR1A_MOUSE	1-0-0-0-0-0					51,0	Coronin-1A	<i>Mus musculus</i>
COR1C_MOUSE			1-0			53,1	Coronin-1C	<i>Mus musculus</i>
CPNE3_MOUSE	2-0-0-0-0-0	0-1-0-0-0-0				59,6	Copine-3	<i>Mus musculus</i>
CREM_MOUSE					1-0	38,5	cAMP-responsive element modulator	<i>Mus musculus</i>
CRYAB_MOUSE			3-0			20,1	Alpha-crystallin B chain	<i>Mus musculus</i>
CSEN_MOUSE			0-1			29,5	Calsenilin	<i>Mus musculus</i>
CSMD3_MOUSE			0-1			405,8	CUB and sushi domain-containing protein 3	<i>Mus musculus</i>
CT024_MOUSE			0-1			14,8	Uncharacterized protein C20orf24 homolog	<i>Mus musculus</i>
CTNA1_MOUSE			4-0			100,1	Catenin alpha-1	<i>Mus musculus</i>
CTNA2_MOUSE			3-0			105,3	Catenin alpha-2	<i>Mus musculus</i>
CTNB1_MOUSE			5-0			85,5	Catenin beta-1	<i>Mus musculus</i>
CTND1_MOUSE			1-0			104,9	Catenin delta-1	<i>Mus musculus</i>
CXA1_MOUSE			1-0			43,0	Gap junction alpha-1 protein	<i>Mus musculus</i>
CXAR_MOUSE			1-0			39,9	Coxsackievirus and adenovirus receptor homolog	<i>Mus musculus</i>
CYFP1_MOUSE			1-0			145,2	Cytoplasmic FMR1-interacting protein 1	<i>Mus musculus</i>
CYTC_MOUSE	0-0-1-0-0-0					15,5	Cystatin-C	<i>Mus musculus</i>
DCAF8_MOUSE			1-0			66,0	DDB1- and CUL4-associated factor 8	<i>Mus musculus</i>
DCLK2_MOUSE		1-0-0-0-0-0				83,0	Serine/threonine-protein kinase DCLK2	<i>Mus musculus</i>
DD19A_MOUSE			1-0			53,9	ATP-dependent RNA helicase DDX19A	<i>Mus musculus</i>
DDA1_MOUSE					1-0	11,8	DET1- and DDB1-associated protein 1	<i>Mus musculus</i>
DDB1_MOUSE			4-0		4-0	126,9	DNA damage-binding protein 1	<i>Mus musculus</i>
DDIT4_MOUSE			1-0			24,9	DNA damage-inducible transcript 4 protein	<i>Mus musculus</i>
DDX3L_MOUSE			1-0		2-1	73,1	Putative ATP-dependent RNA helicase P110	<i>Mus musculus</i>
DDX5_MOUSE			2-0		1-0	69,3	Probable ATP-dependent RNA helicase DDX5	<i>Mus musculus</i>
DERL1_MOUSE					1-0	28,8	Derlin-1	<i>Mus musculus</i>
DEST_MOUSE		0-1-0-0-0-0	1-0			18,5	Dextrin	<i>Mus musculus</i>
DGKG_MOUSE		0-0-0-0-0-1				88,5	Diacylglycerol kinase gamma	<i>Mus musculus</i>
DHB4_MOUSE		0-1-0-0-0-0				79,5	Peroxisomal multifunctional enzyme type 2	<i>Mus musculus</i>
DHX8_MOUSE			1-0			142,6	ATP-dependent RNA helicase DHX8	<i>Mus musculus</i>
DHX9_MOUSE			1-0			149,5	ATP-dependent RNA helicase A	<i>Mus musculus</i>
DI3L2_MOUSE	0-0-1-0-0-0					97,8	DIS3-like exonuclease 2	<i>Mus musculus</i>
DIC_MOUSE					1-0	31,7	Mitochondrial dicarboxylate carrier	<i>Mus musculus</i>
DIRA2_MOUSE					1-0	22,5	GTP-binding protein Di-Ras2	<i>Mus musculus</i>
DJB12_MOUSE					1-0	42,0	Dnaj homolog subfamily B member 12	<i>Mus musculus</i>
DLGP1_MOUSE	0-0-0-0-0-1					110,4	Disks large-associated protein 1	<i>Mus musculus</i>
DLRB1_MOUSE			1-0			11,0	Dynein light chain roadblock-type 1	<i>Mus musculus</i>
DMRT2_MOUSE			0-1			61,6	Doublesex- and mab-3-related transcription factor 2	<i>Mus musculus</i>
DMXL1_MOUSE					1-0	336,0	DmX-like protein 1	<i>Mus musculus</i>
DNJA1_MOUSE			1-0		2-0	44,9	Dnaj homolog subfamily A member 1	<i>Mus musculus</i>
DNJA3_MOUSE			1-0			52,4	Dnaj homolog subfamily A member 3, mitochondrial	<i>Mus musculus</i>
DNJB1_MOUSE			1-0			38,2	Dnaj homolog subfamily B member 1	<i>Mus musculus</i>
DR9C7_MOUSE		0-1-0-0-0-0				35,1	Short-chain dehydrogenase/reductase family 9C member 7	<i>Mus musculus</i>
DRS7B_MOUSE			1-0		1-0	35,0	Dehydrogenase/reductase SDR family member 7B	<i>Mus musculus</i>
DSC1_MOUSE			1-0			98,9	Desmocollin-1	<i>Mus musculus</i>
DSG4_MOUSE			2-0			114,4	Desmoglein-4	<i>Mus musculus</i>
DTD1_MOUSE		0-1-0-0-0-0				23,4	D-tyrosyl-tRNA(Tyr) deacylase 1	<i>Mus musculus</i>

DX39A_MOUSE	0-0-0-0-0-1		4-0		49,1	ATP-dependent RNA helicase DDX39A	<i>Mus musculus</i>
DYHC1_MOUSE			8-0		532,0	Cytoplasmic dynein 1 heavy chain 1	<i>Mus musculus</i>
DYN2_MOUSE			3-0		98,1	Dynamin-2	<i>Mus musculus</i>
E9BM96_LEIDB			1-0		42,2	Casein kinase 1 isoform 2, putative	<i>Leishmania donovani</i>
ECH1_MOUSE			1-0		36,1	Delta(3,5)-Delta(2,4)-dienoyl-CoA isomerase, mitochondrial	<i>Mus musculus</i>
ECHD1_MOUSE			1-0		35,5	Ethylmalonyl-CoA decarboxylase	<i>Mus musculus</i>
ECM2_MOUSE				1-0	76,7	Extracellular matrix protein 2	<i>Mus musculus</i>
EF1B_MOUSE			1-0		24,7	Elongation factor 1-beta	<i>Mus musculus</i>
EF1D_MOUSE			1-0		31,3	Elongation factor 1-delta	<i>Mus musculus</i>
EF1G_MOUSE			3-0	1-1	50,1	Elongation factor 1-gamma	<i>Mus musculus</i>
EFGM_MOUSE		0-1-0-0-0-0			83,5	Elongation factor G, mitochondrial	<i>Mus musculus</i>
EFHD2_MOUSE	2-0-0-0-0-0		6-0		26,8	EF-hand domain-containing protein D2	<i>Mus musculus</i>
EH1L1_MOUSE				1-0	184,8	EH domain-binding protein 1-like protein 1	<i>Mus musculus</i>
EIF3A_MOUSE			3-0		161,9	Eukaryotic translation initiation factor 3 subunit A	<i>Mus musculus</i>
EIF3B_MOUSE			1-0		91,4	Eukaryotic translation initiation factor 3 subunit B	<i>Mus musculus</i>
EIF3C_MOUSE			2-0		105,5	Eukaryotic translation initiation factor 3 subunit C	<i>Mus musculus</i>
EIF3D_MOUSE			1-0		64,0	Eukaryotic translation initiation factor 3 subunit D	<i>Mus musculus</i>
EIF3F_MOUSE			1-0		38,0	Eukaryotic translation initiation factor 3 subunit F	<i>Mus musculus</i>
EIF3K_MOUSE	0-1-0-0-0-0				25,1	Eukaryotic translation initiation factor 3 subunit K	<i>Mus musculus</i>
EIF3L_MOUSE			1-0		66,6	Eukaryotic translation initiation factor 3 subunit L	<i>Mus musculus</i>
ENDD1_MOUSE			1-0		55,3	Endonuclease domain-containing 1 protein	<i>Mus musculus</i>
ENPL_MOUSE			7-0	1-0	92,5	Endoplasmic reticulum protein	<i>Mus musculus</i>
EPIPL_MOUSE	0-0-0-0-1-1				724,6	Epiplakin	<i>Mus musculus</i>
ERO1A_MOUSE	0-0-0-0-0-1				54,1	ERO1-like protein alpha	<i>Mus musculus</i>
ERP44_MOUSE			1-0		46,9	Endoplasmic reticulum resident protein 44	<i>Mus musculus</i>
ETFA_MOUSE				1-0	35,0	Electron transfer flavoprotein subunit alpha, mitochondrial	<i>Mus musculus</i>
ETFB_MOUSE			1-0		27,6	Electron transfer flavoprotein subunit beta	<i>Mus musculus</i>
EVPL_MOUSE		0-1-0-0-0-0			232,0	Envoplakin	<i>Mus musculus</i>
EWS_MOUSE			1-0		68,5	RNA-binding protein EWS	<i>Mus musculus</i>
F120A_MOUSE			2-0		121,6	Constitutive coactivator of PPAR-gamma-like protein 1	<i>Mus musculus</i>
FA83H_MOUSE			1-0		131,1	Protein FAM83H	<i>Mus musculus</i>
FABP4_MOUSE			1-0		14,6	Fatty acid-binding protein, adipocyte	<i>Mus musculus</i>
FACR1_MOUSE	0-0-0-0-1-0			3-0	59,4	Fatty acyl-CoA reductase 1	<i>Mus musculus</i>
FAF2_MOUSE				1-0	52,5	FAS-associated factor 2	<i>Mus musculus</i>
FAS_MOUSE			1-0		272,4	Fatty acid synthase	<i>Mus musculus</i>
FBRL_MOUSE			4-0		34,3	rRNA 2'-O-methyltransferase fibrillar	<i>Mus musculus</i>
FCERG_MOUSE				2-1	9,7	High affinity immunoglobulin epsilon receptor subunit gamma	<i>Mus musculus</i>
FKB1A_MOUSE			1-0		11,9	Peptidyl-prolyl cis-trans isomerase FKBP1A	<i>Mus musculus</i>
FKBP4_MOUSE			1-0		51,6	Peptidyl-prolyl cis-trans isomerase FKBP4	<i>Mus musculus</i>
FLII_MOUSE	1-0-0-0-0-0		4-0		144,8	Protein flightless-1 homolog	<i>Mus musculus</i>
FLNA_MOUSE	4-0-0-0-0-0	0-1-0-0-0-0	1-0		281,2	Filamin-A	<i>Mus musculus</i>
FLNB_MOUSE	1-0-1-0-0-0				277,8	Filamin-B	<i>Mus musculus</i>
FSIP2_MOUSE				0-1	784,9	Fibrous sheath-interacting protein 2	<i>Mus musculus</i>
FUMH_MOUSE			1-0		54,4	Fumarate hydratase, mitochondrial	<i>Mus musculus</i>
FXR1_MOUSE			1-0	1-0	76,2	Fragile X mental retardation syndrome-related protein 1	<i>Mus musculus</i>
FYN_MOUSE			2-0		60,7	Tyrosine-protein kinase Fyn	<i>Mus musculus</i>
G3PT_MOUSE				2-0	47,7	Glyceraldehyde-3-phosphate dehydrogenase, testis-specific	<i>Mus musculus</i>
GAN_MOUSE			2-0		67,7	Gigaxonin	<i>Mus musculus</i>
GANAB_MOUSE		1-0-0-0-0-0			106,9	Neutral alpha-glucosidase AB	<i>Mus musculus</i>
GBB1_MOUSE	1-0-0-0-0-0			3-0	37,4	Guanine nucleotide-binding protein G(I)/G(S)/G(T) subunit beta-1	<i>Mus musculus</i>
GBB2_MOUSE			1-0	3-0	37,3	Guanine nucleotide-binding protein G(I)/G(S)/G(T) subunit beta-2	<i>Mus musculus</i>
GDF3_MOUSE				1-0	41,6	Growth/differentiation factor 3	<i>Mus musculus</i>
GDIB_MOUSE			1-0		50,5	Rab GDP dissociation inhibitor beta	<i>Mus musculus</i>

GDIR1_MOUSE			1-0			23,4	Rho GDP-dissociation inhibitor 1	<i>Mus musculus</i>
GILT_MOUSE			1-0			27,8	Gamma-interferon-inducible lysosomal thiol reductase	<i>Mus musculus</i>
GLRX1_MOUSE			1-0			11,9	Glutaredoxin-1	<i>Mus musculus</i>
GNA13_MOUSE	1-0-0-0-0-0		1-0			44,1	Guanine nucleotide-binding protein subunit alpha-13	<i>Mus musculus</i>
GOGA7_MOUSE			1-0			15,8	Golgin subfamily A member 7	<i>Mus musculus</i>
GPSM2_MOUSE	0-0-0-1-0-0					75,6	G-protein-signaling modulator 2	<i>Mus musculus</i>
GRPE2_MOUSE	0-0-1-0-0-0					25,0	GrpE protein homolog 2, mitochondrial	<i>Mus musculus</i>
GSHB_MOUSE			1-0			52,2	Glutathione synthetase	<i>Mus musculus</i>
GTR3_MOUSE	1-0-0-0-0-0					53,5	Solute carrier family 2, facilitated glucose transporter member 3	<i>Mus musculus</i>
GUF1_MOUSE		0-0-0-0-1-0				72,5	Translation factor Guf1, mitochondrial	<i>Mus musculus</i>
H11_MOUSE	0-0-0-1-0-0					21,8	Histone H1.1	<i>Mus musculus</i>
H12_MOUSE			3-0		2-0	21,3	Histone H1.2	<i>Mus musculus</i>
H15_MOUSE			1-0		1-0	22,6	Histone H1.5	<i>Mus musculus</i>
H2A1H_MOUSE	1-0-0-0-0-0	0-1-0-1-0-0	0-1		2-1	14,0	Histone H2A type 1-H	<i>Mus musculus</i>
H2A2C_MOUSE			2-0			14,0	Histone H2A type 2-C	<i>Mus musculus</i>
H2AY_MOUSE			3-0			39,7	Core histone macro-H2A.1	<i>Mus musculus</i>
H2B2E_MOUSE	2-0-0-0-0-0					14,0	Histone H2B type 2-E	<i>Mus musculus</i>
H31_MOUSE	0-0-0-1-1-1		1-0			15,4	Histone H3.1	<i>Mus musculus</i>
HBB1_MOUSE		1-0-0-0-0-0			0-1	15,8	Hemoglobin subunit beta-1	<i>Mus musculus</i>
HCK_MOUSE			1-0			59,1	Tyrosine-protein kinase HCK	<i>Mus musculus</i>
HEXA_MOUSE			1-0			60,6	Beta-hexosaminidase subunit alpha	<i>Mus musculus</i>
HEXB_MOUSE			1-0			61,1	Beta-hexosaminidase subunit beta	<i>Mus musculus</i>
HMGGB1_MOUSE E			1-0			24,9	High mobility group protein B1	<i>Mus musculus</i>
HNRL1_MOUSE			1-0		1-0	96,0	Heterogeneous nuclear ribonucleoprotein U-like protein 1	<i>Mus musculus</i>
HNRPD_MOUSE			1-0			38,4	Heterogeneous nuclear ribonucleoprotein D0	<i>Mus musculus</i>
HNRPF_MOUSE					2-0	45,7	Heterogeneous nuclear ribonucleoprotein F	<i>Mus musculus</i>
HNRPK_MOUSE			2-0			51,0	Heterogeneous nuclear ribonucleoprotein K	<i>Mus musculus</i>
HNRPM_MOUSE E			3-0		4-1	77,6	Heterogeneous nuclear ribonucleoprotein M	<i>Mus musculus</i>
HNRPQ_MOUSE			1-0			69,6	Heterogeneous nuclear ribonucleoprotein Q	<i>Mus musculus</i>
HP1B3_MOUSE					1-0	60,9	Heterochromatin protein 1-binding protein 3	<i>Mus musculus</i>
HPHL1_MOUSE			2-0			130,9	Hephaestin-like protein 1	<i>Mus musculus</i>
HPLN3_MOUSE					1-0	40,7	Hyaluronan and proteoglycan link protein 3	<i>Mus musculus</i>
HS71A_MOUSE			4-0		3-3	70,1	Heat shock 70 kDa protein 1A	<i>Mus musculus</i>
HS71L_MOUSE			3-0		0-3	70,6	Heat shock 70 kDa protein 1-like	<i>Mus musculus</i>
HSP72_MOUSE			9-0			69,6	Heat shock-related 70 kDa protein 2	<i>Mus musculus</i>
HSPB1_MOUSE			1-0			23,0	Heat shock protein beta-1	<i>Mus musculus</i>
HUNK_MOUSE	0-0-0-0-0-1					79,6	Hormonally up-regulated neu tumor-associated kinase	<i>Mus musculus</i>
HUTH_MOUSE	5-1-0-0-0-0	3-2-0-0-0-0			1-0	72,3	Histidine ammonia-lyase	<i>Mus musculus</i>
HVM17_MOUSE	1-0-0-0-0-0	1-0-0-0-0-0				13,0	Ig heavy chain V region MOPC 47A	<i>Mus musculus</i>
HXK1_MOUSE			1-0			108,3	Hexokinase-1	<i>Mus musculus</i>
IASPP_MOUSE			1-0			89,0	RelA-associated inhibitor	<i>Mus musculus</i>
IDE_MOUSE	2-0-0-0-0-0				0-1	117,8	Insulin-degrading enzyme	<i>Mus musculus</i>
IDHP_MOUSE			1-0			50,9	Isocitrate dehydrogenase [NADP], mitochondrial	<i>Mus musculus</i>
IF2A_MOUSE			3-0			36,1	Eukaryotic translation initiation factor 2 subunit 1	<i>Mus musculus</i>
IF2B_MOUSE			1-0			38,1	Eukaryotic translation initiation factor 2 subunit 2	<i>Mus musculus</i>
IF2G_MOUSE			1-0			51,1	Eukaryotic translation initiation factor 2 subunit 3, X-linked	<i>Mus musculus</i>
IF2P_MOUSE			1-0			137,6	Eukaryotic translation initiation factor 5B	<i>Mus musculus</i>
IF4A1_MOUSE	0-0-0-1-0-0	1-1-0-0-0-0	7-0		2-1	46,2	Eukaryotic initiation factor 4A-I	<i>Mus musculus</i>
IF4A3_MOUSE			2-0			46,8	Eukaryotic initiation factor 4A-III	<i>Mus musculus</i>
IF4G1_MOUSE			1-0			176,1	Eukaryotic translation initiation factor 4 gamma 1	<i>Mus musculus</i>
IF5_MOUSE			1-0			49,0	Eukaryotic translation initiation factor 5	<i>Mus musculus</i>
ILEUA_MOUSE			3-0			42,6	Leukocyte elastase inhibitor A	<i>Mus musculus</i>
IMDH1_MOUSE			2-0			55,3	Inosine-5'-monophosphate dehydrogenase 1	<i>Mus musculus</i>

IQCC_MOUSE					0-1	46,9	IQ domain-containing protein C	<i>Mus musculus</i>
ISC2B_MOUSE		1-0-0-0-0-0				23,2	Isochorismatase domain-containing protein 2B	<i>Mus musculus</i>
K1C19_MOUSE		0-6-0-0-0-0			4-0	44,5	Keratin, type I cytoskeletal 19	<i>Mus musculus</i>
K1C24_MOUSE					0-1	54,0	Keratin, type I cytoskeletal 24	<i>Mus musculus</i>
K1C40_MOUSE		0-0-0-0-0-2				48,9	Keratin, type I cytoskeletal 40	<i>Mus musculus</i>
K1H1_MOUSE	0-1-0-0-0-0		5-0			47,1	Keratin, type I cuticular Ha1	<i>Mus musculus</i>
K2C4_MOUSE		0-3-0-5-0-0	0-3		0-5	56,3	Keratin, type II cytoskeletal 4	<i>Mus musculus</i>
K2C7_MOUSE	0-0-0-0-0-4	0-0-0-0-0-4	3-0		4-0	50,7	Keratin, type II cytoskeletal 7	<i>Mus musculus</i>
K2C8_MOUSE	0-0-3-0-0-0	0-4-0-3-0-0			0-2	54,6	Keratin, type II cytoskeletal 8	<i>Mus musculus</i>
KAPCA_MOUSE			1-0			40,6	cAMP-dependent protein kinase catalytic subunit alpha	<i>Mus musculus</i>
KAPCB_MOUSE					1-0	40,7	cAMP-dependent protein kinase catalytic subunit beta	<i>Mus musculus</i>
KAT6B_MOUSE			1-0			208,5	Histone acetyltransferase KAT6B	<i>Mus musculus</i>
KCRB_MOUSE			1-0			42,7	Creatine kinase B-type	<i>Mus musculus</i>
KCRU_MOUSE	2-0-0-0-0-0	0-1-0-0-0-0	3-0			47,0	Creatine kinase U-type, mitochondrial	<i>Mus musculus</i>
KIME_MOUSE			1-0			41,9	Mevalonate kinase	<i>Mus musculus</i>
KPCD_MOUSE			1-0			77,5	Protein kinase C delta type	<i>Mus musculus</i>
KPRA_MOUSE			1-0			39,4	Phosphoribosyl pyrophosphate synthase-associated protein 1	<i>Mus musculus</i>
KRT34_MOUSE			4-0			44,6	Keratin, type I cuticular Ha4	<i>Mus musculus</i>
KRT35_MOUSE	0-0-2-2-0-3	0-0-0-1-1-0	4-0			50,5	Keratin, type I cuticular Ha5	<i>Mus musculus</i>
KRT81_MOUSE			4-0			52,9	Keratin, type II cuticular Hb1	<i>Mus musculus</i>
KRT82_MOUSE			2-0			57,1	Keratin, type II cuticular Hb2	<i>Mus musculus</i>
KRT85_MOUSE			4-0			55,8	Keratin, type II cuticular Hb5	<i>Mus musculus</i>
KV2A7_MOUSE	2-1-0-0-1-1	1-1-1-0-0-1	1-1		2-1	12,3	Ig kappa chain V-II region 26-10	<i>Mus musculus</i>
LACTB_MOUSE	0-0-0-1-0-0					60,7	Serine beta-lactamase-like protein LACTB, mitochondrial	<i>Mus musculus</i>
LAMC1_MOUSE	0-0-1-0-0-0					177,3	Laminin subunit gamma-1	<i>Mus musculus</i>
LANC1_MOUSE			1-0			45,3	LanC-like protein 1	<i>Mus musculus</i>
LAP2B_MOUSE			1-0			50,4	Lamina-associated polypeptide 2, isoforms beta/delta/epsilon/gamma	<i>Mus musculus</i>
LASP1_MOUSE	0-0-0-1-0-0					30,0	LIM and SH3 domain protein 1	<i>Mus musculus</i>
LDHA_MOUSE	0-0-0-0-1-0		1-0		0-2	36,5	L-lactate dehydrogenase A chain	<i>Mus musculus</i>
LDHB_MOUSE			1-0			36,6	L-lactate dehydrogenase B chain	<i>Mus musculus</i>
LEG1_MOUSE			1-0			14,9	Galectin-1	<i>Mus musculus</i>
LEG3_MOUSE	1-1-0-0-1-0	0-0-0-1-1-0	3-0			27,5	Galectin-3	<i>Mus musculus</i>
LEGL_MOUSE			1-0			19,0	Galectin-related protein	<i>Mus musculus</i>
LGUL_MOUSE			1-0			20,8	Lactoylglutathione lyase	<i>Mus musculus</i>
LIPL_MOUSE					1-0	53,1	Lipoprotein lipase	<i>Mus musculus</i>
LIS1_MOUSE		0-1-0-0-0-0				46,7	Platelet-activating factor acetylhydrolase IB subunit alpha	<i>Mus musculus</i>
LMNA_MOUSE	0-0-0-0-0-1	1-0-0-0-0-0	5-0		0-4	74,2	Prelamin-A/C	<i>Mus musculus</i>
LMNB1_MOUSE			1-0			66,8	Lamin-B1	<i>Mus musculus</i>
LRC15_MOUSE			2-0			64,2	Leucine-rich repeat-containing protein 15	<i>Mus musculus</i>
LRRK2_MOUSE	0-0-0-1-0-0					284,7	Leucine-rich repeat serine/threonine-protein kinase 2	<i>Mus musculus</i>
LRRN3_MOUSE			0-1			79,2	Leucine-rich repeat neuronal protein 3	<i>Mus musculus</i>
LSP1_MOUSE			1-0			36,7	Lymphocyte-specific protein 1	<i>Mus musculus</i>
LTOR1_MOUSE			1-0		1-0	17,7	Ragulator complex protein LAMTOR1	<i>Mus musculus</i>
LYST_MOUSE			1-0			425,3	Lysosomal-trafficking regulator	<i>Mus musculus</i>
LYZ2_MOUSE	0-0-0-0-1-0					16,7	Lysozyme C-2	<i>Mus musculus</i>
LZTL1_MOUSE		0-1-0-0-0-0				34,8	Leucine zipper transcription factor-like protein 1	<i>Mus musculus</i>
MAK_MOUSE	1-0-0-0-0-0					70,1	Serine/threonine-protein kinase MAK	<i>Mus musculus</i>
MAL2_MOUSE		0-1-0-0-0-0	1-0			19,1	Protein MAL2	<i>Mus musculus</i>
MAOX_MOUSE	1-0-0-0-0-0					64,0	NADP-dependent malic enzyme	<i>Mus musculus</i>
MARK4_MOUSE			0-1			82,6	MAP/microtubule affinity-regulating kinase 4	<i>Mus musculus</i>
MCM5_MOUSE			1-0		1-0	82,3	DNA replication licensing factor MCM5	<i>Mus musculus</i>
MDFI_MOUSE					1-0	26,0	MyoD family inhibitor	<i>Mus musculus</i>
MDHM_MOUSE	2-0-0-1-0-0		3-0		1-0	35,6	Malate dehydrogenase, mitochondrial	<i>Mus musculus</i>
MEGF6_MOUSE	0-0-0-0-0-1					164,7	Multiple epidermal growth factor-like domains protein 6	<i>Mus musculus</i>

MERL_MOUSE					1-0	69,8	Merlin	<i>Mus musculus</i>
METH_MOUSE	0-0-0-1-0-0					139,1	Methionine synthase	<i>Mus musculus</i>
MIC60_MOUSE			1-0		1-0	83,9	MICOS complex subunit Mic60	<i>Mus musculus</i>
ML12B_MOUSE	3-2-0-0-0-0		3-0			19,8	Myosin regulatory light chain 12B	<i>Mus musculus</i>
MSPD2_MOUSE			1-0			59,9	Motile sperm domain-containing protein 2	<i>Mus musculus</i>
MTAP_MOUSE			1-0			31,1	S-methyl-5'-thioadenosine phosphorylase	<i>Mus musculus</i>
MY18A_MOUSE			2-0			232,8	Unconventional myosin-XVIIIa	<i>Mus musculus</i>
MYH9_MOUSE	10-3-0-0-0-0	1-1-0-0-0-0	33-0		0-2	226,4	Myosin-9	<i>Mus musculus</i>
MYL6_MOUSE	2-0-0-0-0-0		8-0		0-1	16,9	Myosin light polypeptide 6	<i>Mus musculus</i>
MYO1C_MOUSE	4-0-0-0-0-0		19-0			121,9	Unconventional myosin-Ic	<i>Mus musculus</i>
MYO1F_MOUSE			15-0		2-0	125,9	Unconventional myosin-I f	<i>Mus musculus</i>
MYO1G_MOUSE E			17-0			117,2	Unconventional myosin-Ig	<i>Mus musculus</i>
MYO5A_MOUSE E	2-0-0-0-0-0		19-0			215,5	Unconventional myosin-Va	<i>Mus musculus</i>
MYO9B_MOUSE			1-0		1-0	238,8	Unconventional myosin-IXb	<i>Mus musculus</i>
NACA_MOUSE		0-1-0-0-0-0			0-1	23,4	Nascent polypeptide-associated complex subunit alpha	<i>Mus musculus</i>
NDE1_MOUSE			1-0			38,5	Nuclear distribution protein nudE homolog 1	<i>Mus musculus</i>
NDKA_MOUSE			2-0			17,2	Nucleoside diphosphate kinase A	<i>Mus musculus</i>
NDRG2_MOUSE	1-0-0-0-0-0					40,8	Protein NDRG2	<i>Mus musculus</i>
NDUS7_MOUSE			1-0		1-0	24,7	NADH dehydrogenase [ubiquinone] iron-sulfur protein 7, mitochondrial	<i>Mus musculus</i>
NIBL1_MOUSE			1-0			84,8	Niban-like protein 1	<i>Mus musculus</i>
NID1_MOUSE	0-0-1-0-0-0	0-0-0-1-0-0				136,5	Nidogen-1	<i>Mus musculus</i>
NODAL_MOUSE					1-0	40,5	Nodal	<i>Mus musculus</i>
NP11_MOUSE			1-0			45,3	Nucleosome assembly protein 1-like 1	<i>Mus musculus</i>
NPC1_MOUSE			1-0			142,9	Niemann-Pick C1 protein	<i>Mus musculus</i>
NPM_MOUSE	1-0-0-0-0-0				1-1	32,6	Nucleophosmin	<i>Mus musculus</i>
NPTN_MOUSE			1-0			44,4	Neuroplastin	<i>Mus musculus</i>
NR6A1_MOUSE		0-1-0-0-0-0				56,0	Nuclear receptor subfamily 6 group A member 1	<i>Mus musculus</i>
NRDC_MOUSE		0-0-0-0-0-1				132,9	Nardilysin	<i>Mus musculus</i>
NTPCR_MOUSE			1-0			20,7	Cancer-related nucleoside-triphosphatase homolog	<i>Mus musculus</i>
NU155_MOUSE			1-0			155,1	Nuclear pore complex protein Nup155	<i>Mus musculus</i>
NUCB1_MOUSE			1-0			53,4	Nucleobindin-1	<i>Mus musculus</i>
NUCL_MOUSE					2-0	76,7	Nucleolin	<i>Mus musculus</i>
NUP98_MOUSE			1-0			197,2	Nuclear pore complex protein Nup98-Nup96	<i>Mus musculus</i>
OASL1_MOUSE			2-0		9-0	59,1	2'-5'-oligoadenylate synthase-like protein 1	<i>Mus musculus</i>
OASL2_MOUSE					1-0	58,8	2'-5'-oligoadenylate synthase-like protein 2	<i>Mus musculus</i>
OBSL1_MOUSE	0-0-0-0-1-0	1-1-0-0-0-1			1-0	197,9	Obscurin-like protein 1	<i>Mus musculus</i>
ODPB_MOUSE			1-0			38,9	Pyruvate dehydrogenase E1 component subunit beta, mitochondrial	<i>Mus musculus</i>
OPSB_MOUSE		1-0-0-0-0-0				38,9	Short-wave-sensitive opsin 1	<i>Mus musculus</i>
OTOP1_MOUSE					0-1	65,8	Otopetrin-1	<i>Mus musculus</i>
OTUB2_MOUSE			1-0			27,3	Ubiquitin thioesterase OTUB2	<i>Mus musculus</i>
P5CR1_MOUSE		1-0-0-0-0-0	1-0			32,4	Pyrrroline-5-carboxylate reductase 1, mitochondrial	<i>Mus musculus</i>
PA2G4_MOUSE			1-0			43,7	Proliferation-associated protein 2G4	<i>Mus musculus</i>
PABP1_MOUSE			7-0		6-0	70,7	Polyadenylate-binding protein 1	<i>Mus musculus</i>
PADI1_MOUSE			2-0			73,8	Protein-arginine deiminase type-1	<i>Mus musculus</i>
PADI3_MOUSE	1-0-0-0-0-0					75,1	Protein-arginine deiminase type-3	<i>Mus musculus</i>
PCBP2_MOUSE			2-0			38,2	Poly(rC)-binding protein 2	<i>Mus musculus</i>
PDC6I_MOUSE			2-0			96,0	Programmed cell death 6-interacting protein	<i>Mus musculus</i>
PDE1B_MOUSE		0-0-0-0-1-0				61,2	Calcium/calmodulin-dependent 3',5'-cyclic nucleotide phosphodiesterase 1B	<i>Mus musculus</i>
PDI A1_MOUSE	1-0-0-0-0-0		2-0			57,1	Protein disulfide-isomerase	<i>Mus musculus</i>
PDI A3_MOUSE	0-0-0-0-1-0		1-0			56,7	Protein disulfide-isomerase A3	<i>Mus musculus</i>
PDI A6_MOUSE			2-0		1-1	48,1	Protein disulfide-isomerase A6	<i>Mus musculus</i>
PEPD_MOUSE	1-0-0-0-0-0		1-0			55,0	Xaa-Pro dipeptidase	<i>Mus musculus</i>
PERM_MOUSE	2-0-0-0-1-0	1-1-0-0-1-0	1-1		1-0	81,2	Myeloperoxidase	<i>Mus musculus</i>

PFKAL_MOUSE			5-0			85,4	ATP-dependent 6-phosphofructokinase, liver type	<i>Mus musculus</i>
PFKAP_MOUSE			4-0		2-0	85,5	ATP-dependent 6-phosphofructokinase, platelet type	<i>Mus musculus</i>
PGAM1_MOUSE					0-1	28,8	Phosphoglycerate mutase 1	<i>Mus musculus</i>
PGK1_MOUSE			6-0			44,6	Phosphoglycerate kinase 1	<i>Mus musculus</i>
PGRC2_MOUSE			1-0			23,3	Membrane-associated progesterone receptor component 2	<i>Mus musculus</i>
PGRP1_MOUSE	0-0-1-0-0-0					20,5	Peptidoglycan recognition protein 1	<i>Mus musculus</i>
PHB2_MOUSE		0-0-0-0-1-0	2-0		2-0	33,3	Prohibitin-2	<i>Mus musculus</i>
PHB_MOUSE			2-0			29,8	Prohibitin	<i>Mus musculus</i>
PI3R4_MOUSE			0-1			152,6	Phosphoinositide 3-kinase regulatory subunit 4	<i>Mus musculus</i>
PITH1_MOUSE			1-0			24,2	PITH domain-containing protein 1	<i>Mus musculus</i>
PKDRE_MOUSE					1-0	241,4	Polycystic kidney disease and receptor for egg jelly-related protein	<i>Mus musculus</i>
PKP3_MOUSE		0-1-0-0-0-0	8-0			87,3	Plakophilin-3	<i>Mus musculus</i>
PLBL1_MOUSE	0-0-1-0-2-0	0-0-1-0-0-0				63,0	Phospholipase B-like 1	<i>Mus musculus</i>
PLCD1_MOUSE			1-0			85,9	1-phosphatidylinositol 4,5-bisphosphate phosphodiesterase delta-1	<i>Mus musculus</i>
PLD4_MOUSE	0-0-0-0-1-0					56,2	Phospholipase D4	<i>Mus musculus</i>
PLEC_MOUSE		0-1-0-0-0-0	6-0			534,2	Plectin	<i>Mus musculus</i>
PLSL_MOUSE	3-0-0-0-0-0		4-0			70,1	Plastin-2	<i>Mus musculus</i>
PNPH_MOUSE	0-0-0-0-0-1					32,3	Purine nucleoside phosphorylase	<i>Mus musculus</i>
POF1B_MOUSE		0-1-0-0-0-0				67,8	Protein POF1B	<i>Mus musculus</i>
PP13G_MOUSE			1-0			37,8	Protein phosphatase 1 regulatory subunit 3G	<i>Mus musculus</i>
PPAP_MOUSE			1-0			43,7	Prostatic acid phosphatase	<i>Mus musculus</i>
PPIA_MOUSE			4-0			18,0	Peptidyl-prolyl cis-trans isomerase A	<i>Mus musculus</i>
PPIB_MOUSE			1-0			23,7	Peptidyl-prolyl cis-trans isomerase B	<i>Mus musculus</i>
PPIE_MOUSE			1-0			33,4	Peptidyl-prolyl cis-trans isomerase E	<i>Mus musculus</i>
PPR35_MOUSE	0-0-1-0-0-0					28,4	Protein phosphatase 1 regulatory subunit 35	<i>Mus musculus</i>
PPT2_MOUSE			1-0			34,4	Lysosomal thioesterase PPT2	<i>Mus musculus</i>
PRDX4_MOUSE	0-0-0-1-0-0					31,1	Peroxiredoxin-4	<i>Mus musculus</i>
PRDX6_MOUSE			3-0			24,9	Peroxiredoxin-6	<i>Mus musculus</i>
PROF1_MOUSE	1-0-0-0-0-0		2-0			15,0	Profilin-1	<i>Mus musculus</i>
PRPS1_MOUSE			1-0			34,8	Ribose-phosphate pyrophosphokinase 1	<i>Mus musculus</i>
PRS10_MOUSE			2-0			44,2	26S protease regulatory subunit 10B	<i>Mus musculus</i>
PRSR2_MOUSE			1-0			50,4	Proline and serine-rich protein 2	<i>Mus musculus</i>
PSA1_MOUSE	1-0-0-0-0-0	0-1-0-0-0-0				29,5	Proteasome subunit alpha type-1	<i>Mus musculus</i>
PSA2_MOUSE		0-1-0-0-0-0				25,9	Proteasome subunit alpha type-2	<i>Mus musculus</i>
PSA3_MOUSE	1-0-0-0-0-0	0-1-0-0-0-0				28,4	Proteasome subunit alpha type-3	<i>Mus musculus</i>
PSA6_MOUSE	2-0-0-0-0-0	0-2-0-0-0-1	1-0		0-1	27,4	Proteasome subunit alpha type-6	<i>Mus musculus</i>
PSA7_MOUSE	2-0-0-0-0-1	0-2-0-0-0-0	1-0			27,9	Proteasome subunit alpha type-7	<i>Mus musculus</i>
PSA_MOUSE	1-0-0-0-0-0	0-1-0-0-0-0	1-0		0-1	103,3	Puromycin-sensitive aminopeptidase	<i>Mus musculus</i>
PSB1_MOUSE	0-0-0-0-0-1					26,4	Proteasome subunit beta type-1	<i>Mus musculus</i>
PSB2_MOUSE	1-0-0-0-0-0	0-1-0-0-0-0	1-0			22,9	Proteasome subunit beta type-2	<i>Mus musculus</i>
PSB3_MOUSE		0-0-1-1-0-0	1-0		1-0	23,0	Proteasome subunit beta type-3	<i>Mus musculus</i>
PSB5_MOUSE	1-0-0-0-0-0	0-3-0-0-0-0				28,5	Proteasome subunit beta type-5	<i>Mus musculus</i>
PSMD2_MOUSE			1-0			100,2	26S proteasome non-ATPase regulatory subunit 2	<i>Mus musculus</i>
PSPC1_MOUSE			2-0			58,8	Paraspeckle component 1	<i>Mus musculus</i>
PTPRE_MOUSE			1-0			80,7	Receptor-type tyrosine-protein phosphatase epsilon	<i>Mus musculus</i>
PTPRK_MOUSE					1-0	164,2	Receptor-type tyrosine-protein phosphatase kappa	<i>Mus musculus</i>
QCR8_MOUSE			2-0		1-0	9,8	Cytochrome b-c1 complex subunit 8	<i>Mus musculus</i>
RA54B_MOUSE	0-0-0-0-0-1					99,3	DNA repair and recombination protein RAD54B	<i>Mus musculus</i>
RAB2A_MOUSE		0-1-0-0-0-0				23,5	Ras-related protein Rab-2A	<i>Mus musculus</i>
RAB43_MOUSE					1-0	23,3	Ras-related protein Rab-43	<i>Mus musculus</i>
RAB7B_MOUSE					1-0	22,5	Ras-related protein Rab-7b	<i>Mus musculus</i>
RALA_MOUSE			1-0			23,6	Ras-related protein Ral-A	<i>Mus musculus</i>
RASF8_MOUSE					0-1	48,1	Ras association domain-containing protein 8	<i>Mus musculus</i>

RASH_MOUSE			1-0			21,3	GTPase HRas	<i>Mus musculus</i>
RENT1_MOUSE			1-0		4-0	124,0	Regulator of nonsense transcripts 1	<i>Mus musculus</i>
RFFL_MOUSE			0-1			42,2	E3 ubiquitin-protein ligase rifyflylin	<i>Mus musculus</i>
RFIP5_MOUSE			1-0			69,6	Rab11 family-interacting protein 5	<i>Mus musculus</i>
RGPA2_MOUSE	0-0-0-0-0-1					210,3	Ral GTPase-activating protein subunit alpha-2	<i>Mus musculus</i>
RHG17_MOUSE			2-0			92,2	Rho GTPase-activating protein 17	<i>Mus musculus</i>
RISC_MOUSE		0-1-0-0-0-0				51,0	Retinoid-inducible serine carboxypeptidase	<i>Mus musculus</i>
RL10A_MOUSE			2-0		5-0	24,9	60S ribosomal protein L10a	<i>Mus musculus</i>
RL15_MOUSE			1-0		3-0	24,1	60S ribosomal protein L15	<i>Mus musculus</i>
RL17_MOUSE					1-0	21,4	60S ribosomal protein L17	<i>Mus musculus</i>
RL19_MOUSE	1-0-0-0-0-0	1-0-0-0-0-0	1-0		3-0	23,5	60S ribosomal protein L19	<i>Mus musculus</i>
RL23_MOUSE	0-0-0-2-0-0	0-0-0-1-0-0			2-0	14,9	60S ribosomal protein L23	<i>Mus musculus</i>
RL34_MOUSE					1-0	13,3	60S ribosomal protein L34	<i>Mus musculus</i>
RL35A_MOUSE					2-0	12,6	60S ribosomal protein L35a	<i>Mus musculus</i>
RL36_MOUSE					1-0	12,2	60S ribosomal protein L36	<i>Mus musculus</i>
RL38_MOUSE			1-0			8,2	60S ribosomal protein L38	<i>Mus musculus</i>
RL5_MOUSE			1-0		1-0	34,4	60S ribosomal protein L5	<i>Mus musculus</i>
RL7A_MOUSE			3-0		5-0	30,0	60S ribosomal protein L7a	<i>Mus musculus</i>
RLA0_MOUSE			5-0		10-0	34,2	60S acidic ribosomal protein P0	<i>Mus musculus</i>
RLA1_MOUSE					2-0	11,5	60S acidic ribosomal protein P1	<i>Mus musculus</i>
RLA2_MOUSE			2-0		3-0	11,7	60S acidic ribosomal protein P2	<i>Mus musculus</i>
RO60_MOUSE		0-1-0-0-0-0				60,1	60 kDa SS-A/Ro ribonucleoprotein	<i>Mus musculus</i>
ROA1_MOUSE			2-0			34,2	Heterogeneous nuclear ribonucleoprotein A1	<i>Mus musculus</i>
ROA2_MOUSE			2-0			37,4	Heterogeneous nuclear ribonucleoproteins A2/B1	<i>Mus musculus</i>
ROA3_MOUSE			2-0			39,7	Heterogeneous nuclear ribonucleoprotein A3	<i>Mus musculus</i>
RPTOR_MOUSE			1-0			149,5	Regulatory-associated protein of mTOR	<i>Mus musculus</i>
RRAGC_MOUSE			1-0			44,1	Ras-related GTP-binding protein C	<i>Mus musculus</i>
RS27L_MOUSE			1-0		1-0	9,5	40S ribosomal protein S27-like	<i>Mus musculus</i>
RS28_MOUSE	0-1-0-0-0-0	0-1-0-0-0-0	1-0			7,8	40S ribosomal protein S28	<i>Mus musculus</i>
RS30_MOUSE			1-0			6,6	40S ribosomal protein S30	<i>Mus musculus</i>
RS7_MOUSE	0-0-0-0-1-0	0-0-0-0-1-0	3-0		1-0	22,1	40S ribosomal protein S7	<i>Mus musculus</i>
RTN3_MOUSE			1-0			103,9	Reticulon-3	<i>Mus musculus</i>
RUXE_MOUSE			1-0			10,8	Small nuclear ribonucleoprotein E	<i>Mus musculus</i>
RXFP2_MOUSE			1-0			82,9	Relaxin receptor 2	<i>Mus musculus</i>
S10AB_MOUSE					0-1	11,1	Protein S100-A11	<i>Mus musculus</i>
S12A7_MOUSE		0-0-0-0-0-1	0-1			119,5	Solute carrier family 12 member 7	<i>Mus musculus</i>
S29A2_MOUSE	0-0-1-0-0-0					50,3	Equilibrative nucleoside transporter 2	<i>Mus musculus</i>
S38A3_MOUSE		0-1-0-0-0-0				55,6	Sodium-coupled neutral amino acid transporter 3	<i>Mus musculus</i>
S41A1_MOUSE					0-1	54,9	Solute carrier family 41 member 1	<i>Mus musculus</i>
SAHH3_MOUSE			2-0			66,9	Putative adenosylhomocysteinase 3	<i>Mus musculus</i>
SAHH_MOUSE	0-1-0-0-0-0	0-1-0-0-0-0	5-0			47,7	Adenosylhomocysteinase	<i>Mus musculus</i>
SAM50_MOUSE					1-0	51,9	Sorting and assembly machinery component 50 homolog	<i>Mus musculus</i>
SAP_MOUSE		0-0-0-0-1-0				61,4	Prosaposin	<i>Mus musculus</i>
SBP1_MOUSE			2-0			52,5	Selenium-binding protein 1	<i>Mus musculus</i>
SC22B_MOUSE		0-1-0-0-0-0				24,7	Vesicle-trafficking protein SEC22b	<i>Mus musculus</i>
SC61B_MOUSE			1-0			10,0	Protein transport protein Sec61 subunit beta	<i>Mus musculus</i>
SCFD1_MOUSE			2-0			72,3	Sec1 family domain-containing protein 1	<i>Mus musculus</i>
SEPT7_MOUSE			1-0			50,5	Septin-7	<i>Mus musculus</i>
SF3B3_MOUSE			1-0			135,6	Splicing factor 3B subunit 3	<i>Mus musculus</i>
SFXN1_MOUSE					1-0	35,6	Sideroflexin-1	<i>Mus musculus</i>
SH321_MOUSE	0-0-1-1-0-0	0-0-0-0-0-1			0-1	60,3	SH3 domain-containing protein 21	<i>Mus musculus</i>
SH3G2_MOUSE			1-0			40,0	Endophilin-A1	<i>Mus musculus</i>
SMHD1_MOUSE		0-0-0-0-0-1				225,6	Structural maintenance of chromosomes flexible hinge domain-containing protein 1	<i>Mus musculus</i>

SNX11_MOUSE		0-1-0-0-0-0			30,4	Sorting nexin-11	<i>Mus musculus</i>
SNX19_MOUSE				0-1	109,8	Sorting nexin-19	<i>Mus musculus</i>
SP20H_MOUSE			1-0		59,5	Transcription factor SPT20 homolog	<i>Mus musculus</i>
SPB5_MOUSE			3-0	0-1	42,1	Serpin B5	<i>Mus musculus</i>
SPCS_MOUSE	0-0-0-0-1-0				55,3	O-phosphoseryl-tRNA(Sec) selenium transferase	<i>Mus musculus</i>
SPHK2_MOUSE			1-0		65,6	Sphingosine kinase 2	<i>Mus musculus</i>
SPTN1_MOUSE			4-0		284,6	Spectrin alpha chain, non-erythrocytic 1	<i>Mus musculus</i>
SRS12_MOUSE	1-0-0-0-0-0				29,7	Serine/arginine-rich splicing factor 12	<i>Mus musculus</i>
STAT1_MOUSE			2-0	1-0	87,2	Signal transducer and activator of transcription 1	<i>Mus musculus</i>
SUCA_MOUSE			1-0		36,2	Succinyl-CoA ligase [ADP/GDP-forming] subunit alpha, mitochondrial	<i>Mus musculus</i>
SUN2_MOUSE			1-0		81,6	SUN domain-containing protein 2	<i>Mus musculus</i>
SWAHC_MOUSE E		0-1-0-0-0-0			54,9	Ankyrin repeat domain-containing protein SOWAHC	<i>Mus musculus</i>
SYCC_MOUSE			1-0		94,9	Cysteine--tRNA ligase, cytoplasmic	<i>Mus musculus</i>
SYG_MOUSE			1-0		81,9	Glycine--tRNA ligase	<i>Mus musculus</i>
SYHM_MOUSE	1-0-0-0-0-0	0-1-0-0-0-0			57,0	Probable histidine--tRNA ligase, mitochondrial	<i>Mus musculus</i>
SYNE1_MOUSE			1-0		1009,9	Nesprin-1	<i>Mus musculus</i>
SYPM_MOUSE			0-1		53,5	Probable proline--tRNA ligase, mitochondrial	<i>Mus musculus</i>
SYRC_MOUSE			2-0		75,7	Arginine--tRNA ligase, cytoplasmic	<i>Mus musculus</i>
SYSC_MOUSE			2-0		58,4	Serine--tRNA ligase, cytoplasmic	<i>Mus musculus</i>
SYTC_MOUSE			2-0		83,4	Threonine--tRNA ligase, cytoplasmic	<i>Mus musculus</i>
TADBP_MOUSE			1-0		44,5	TAR DNA-binding protein 43	<i>Mus musculus</i>
TAGL2_MOUSE			1-0		22,4	Transgelin-2	<i>Mus musculus</i>
TALDO_MOUSE	1-0-0-0-0-0				37,4	Transaldolase	<i>Mus musculus</i>
TAOK3_MOUSE		0-1-0-0-0-0			105,3	Serine/threonine-protein kinase TAO3	<i>Mus musculus</i>
TBA4A_MOUSE			13-0	12-5	49,9	Tubulin alpha-4A chain	<i>Mus musculus</i>
TBB4A_MOUSE	1-0-0-0-0-0	1-1-0-0-0-0	15-0	13-0	49,6	Tubulin beta-4A chain	<i>Mus musculus</i>
TBC23_MOUSE			1-0		76,4	TBC1 domain family member 23	<i>Mus musculus</i>
TCPD_MOUSE			1-0		58,1	T-complex protein 1 subunit delta	<i>Mus musculus</i>
TCPE_MOUSE			1-0		59,6	T-complex protein 1 subunit epsilon	<i>Mus musculus</i>
TCPG_MOUSE			1-0	1-0	60,6	T-complex protein 1 subunit gamma	<i>Mus musculus</i>
TCPQ_MOUSE			1-0		59,6	T-complex protein 1 subunit theta	<i>Mus musculus</i>
TCPZ_MOUSE			1-0		58,0	T-complex protein 1 subunit zeta	<i>Mus musculus</i>
TCTP_MOUSE			1-0		19,5	Translationally-controlled tumor protein	<i>Mus musculus</i>
TERA_MOUSE			5-0	0-3	89,3	Transitional endoplasmic reticulum ATPase	<i>Mus musculus</i>
TFR1_MOUSE			1-0		85,7	Transferrin receptor protein 1	<i>Mus musculus</i>
TGM3_MOUSE	1-0-0-0-0-0	0-0-0-1-0-0			77,3	Protein-glutamine gamma-glutamyltransferase E	<i>Mus musculus</i>
THIKA_MOUSE			1-0		44,0	3-ketoacyl-CoA thiolase A, peroxisomal	<i>Mus musculus</i>
THIL_MOUSE			1-0		44,8	Acetyl-CoA acetyltransferase, mitochondrial	<i>Mus musculus</i>
TIBAB_MOUSE			1-0		11,3	Putative mitochondrial import inner membrane translocase subunit Tim8 A-B	<i>Mus musculus</i>
TIGD2_MOUSE			1-0		59,7	Tigger transposable element-derived protein 2	<i>Mus musculus</i>
TIM_MOUSE	1-0-0-0-0-0				137,5	Protein timeless homolog	<i>Mus musculus</i>
TKT_MOUSE	0-0-1-1-0-1	0-0-0-0-0-1		0-1	67,6	Transketolase	<i>Mus musculus</i>
TLR7_MOUSE			1-0		121,8	Toll-like receptor 7	<i>Mus musculus</i>
TM14C_MOUSE				1-0	11,6	Transmembrane protein 14C	<i>Mus musculus</i>
TMCO1_MOUSE				1-0	21,2	Transmembrane and coiled-coil domain-containing protein 1	<i>Mus musculus</i>
TMED9_MOUSE		0-1-0-0-0-0			27,1	Transmembrane emp24 domain-containing protein 9	<i>Mus musculus</i>
TMEDA_MOUSE	0-0-1-0-0-0		1-0		24,9	Transmembrane emp24 domain-containing protein 10	<i>Mus musculus</i>
TMM33_MOUSE E				1-0	28,0	Transmembrane protein 33	<i>Mus musculus</i>
TMM43_MOUSE E				1-0	44,8	Transmembrane protein 43	<i>Mus musculus</i>
TMOD3_MOUSE E			3-0		39,5	Tropomodulin-3	<i>Mus musculus</i>
TNPO2_MOUSE			1-0		100,5	Transportin-2	<i>Mus musculus</i>
TOM40_MOUSE				1-0	37,9	Mitochondrial import receptor subunit TOM40 homolog	<i>Mus musculus</i>
TPD52_MOUSE			1-0		24,3	Tumor protein D52	<i>Mus musculus</i>

TPD54_MOUSE			1-0			24,0	Tumor protein D54	<i>Mus musculus</i>
TPIS_MOUSE	2-0-0-0-0-1	0-0-1-1-0-0	2-0		1-1	32,2	Triosephosphate isomerase	<i>Mus musculus</i>
TPM1_MOUSE	3-0-0-0-0-0	0-2-0-0-0-0	2-0			32,7	Tropomyosin alpha-1 chain	<i>Mus musculus</i>
TPM3_MOUSE		0-2-0-0-0-0				33,0	Tropomyosin alpha-3 chain	<i>Mus musculus</i>
TRAF5_MOUSE					1-0	64,1	TNF receptor-associated factor 5	<i>Mus musculus</i>
TRIS0_MOUSE			0-1			54,6	E3 ubiquitin-protein ligase TRIM50	<i>Mus musculus</i>
TRXR1_MOUSE			1-0			66,9	Thioredoxin reductase 1, cytoplasmic	<i>Mus musculus</i>
TSP1_MOUSE	0-0-1-0-0-0					129,6	Thrombospondin-1	<i>Mus musculus</i>
TTL12_MOUSE			1-0			74,0	Tubulin--tyrosine ligase-like protein 12	<i>Mus musculus</i>
TLL1_MOUSE			1-0			49,1	Probable tubulin polyglutamylase TLL1	<i>Mus musculus</i>
TX1B3_MOUSE			1-0			13,7	Tax1-binding protein 3	<i>Mus musculus</i>
TXTP_MOUSE					1-0	33,9	Tricarboxylate transport protein, mitochondrial	<i>Mus musculus</i>
UAP1_MOUSE			0-1			58,6	UDP-N-acetylhexosamine pyrophosphorylase	<i>Mus musculus</i>
UB2L3_MOUSE			1-0			17,9	Ubiquitin-conjugating enzyme E2 L3	<i>Mus musculus</i>
UB2V2_MOUSE			1-0			16,4	Ubiquitin-conjugating enzyme E2 variant 2	<i>Mus musculus</i>
UBE3A_MOUSE		0-0-0-0-0-1				99,8	Ubiquitin-protein ligase E3A	<i>Mus musculus</i>
UBP5_MOUSE			1-0			95,8	Ubiquitin carboxyl-terminal hydrolase 5	<i>Mus musculus</i>
USO1_MOUSE			1-0			107,0	General vesicular transport factor p115	<i>Mus musculus</i>
VAOD1_MOUSE			1-0			40,3	V-type proton ATPase subunit d 1	<i>Mus musculus</i>
VAPB_MOUSE			1-0			26,9	Vesicle-associated membrane protein-associated protein B	<i>Mus musculus</i>
VAV_MOUSE			1-0			98,1	Proto-oncogene vav	<i>Mus musculus</i>
VDAC3_MOUSE	1-0-0-0-0-0	1-1-0-0-0-0	1-0		1-0	30,8	Voltage-dependent anion-selective channel protein 3	<i>Mus musculus</i>
VGFR2_MOUSE			1-0			152,5	Vascular endothelial growth factor receptor 2	<i>Mus musculus</i>
VINC_MOUSE		0-1-0-0-0-0	4-0			116,7	Vinculin	<i>Mus musculus</i>
VPP1_MOUSE			1-0			96,5	V-type proton ATPase 116 kDa subunit a isoform 1	<i>Mus musculus</i>
VPRBP_MOUSE			1-0			168,9	Protein VPRBP	<i>Mus musculus</i>
VPS35_MOUSE			2-0			91,7	Vacuolar protein sorting-associated protein 35	<i>Mus musculus</i>
WDR1_MOUSE			1-0			66,4	WD repeat-containing protein 1	<i>Mus musculus</i>
XDH_MOUSE			1-0			146,6	Xanthine dehydrogenase/oxidase	<i>Mus musculus</i>
YBOX1_MOUSE					3-0	35,7	Nuclease-sensitive element-binding protein 1	<i>Mus musculus</i>
ZCH18_MOUSE					1-0	105,7	Zinc finger CCCH domain-containing protein 18	<i>Mus musculus</i>



# Appendix 3

---



**Table 9** – List of curated human CK1 $\alpha$ ,  $\delta$  and  $\epsilon$  interactors obtained from BioGRID v3.5 database.

CSNK1A1 (P48729)				
Interactor	Role	Organism	Experimental Evidence Code	Dataset
ACACA	HIT	H. sapiens	Affinity Capture-MS	Varjosalo M (2013)
ACACA	HIT	H. sapiens	Affinity Capture-MS	Rosenbluh J (2016)
ACTA1	HIT	H. sapiens	Affinity Capture-MS	Dubois T (2002)
ACTG1	HIT	H. sapiens	Affinity Capture-MS	Rosenbluh J (2016)
ADAP1	BAIT	H. sapiens	Affinity Capture-Western	Dubois T (2001)
ADAP1	HIT	H. sapiens	Co-purification	Dubois T (2002)
ADAP1	BAIT	H. sapiens	Reconstituted Complex	Dubois T (2001)
AFG3L2	HIT	H. sapiens	Affinity Capture-MS	Rosenbluh J (2016)
AGR2	HIT	H. sapiens	Affinity Capture-MS	Rosenbluh J (2016)
AGR2	BAIT	H. sapiens	Proximity Label-MS	Tiemann K (2018)
AHSA1	HIT	H. sapiens	Affinity Capture-MS	Rosenbluh J (2016)
ANKRD17	HIT	H. sapiens	Affinity Capture-MS	Rosenbluh J (2016)
APC	HIT	H. sapiens	Biochemical Activity	Godin KS (2009)
ARHGAP22	BAIT	H. sapiens	Affinity Capture-MS	Huttlin EL (2017)
ATAD3A	HIT	H. sapiens	Affinity Capture-MS	Rosenbluh J (2016)
ATOH1	BAIT	H. sapiens	Affinity Capture-Western	Cheng YF (2016)
ATP1A1	HIT	H. sapiens	Affinity Capture-MS	Rosenbluh J (2016)
ATP2A2	HIT	H. sapiens	Affinity Capture-MS	Rosenbluh J (2016)
ATP5A1	HIT	H. sapiens	Affinity Capture-MS	Rosenbluh J (2016)
ATP5B	HIT	H. sapiens	Affinity Capture-MS	Rosenbluh J (2016)
ATP5C1	HIT	H. sapiens	Affinity Capture-MS	Rosenbluh J (2016)
ATP6V1A	HIT	H. sapiens	Affinity Capture-MS	Rosenbluh J (2016)
AXIN1	BAIT	H. sapiens	Affinity Capture-MS	Hein MY (2015)
AXIN1	HIT	H. sapiens	Affinity Capture-Western	Zhang Y (2002)
AXIN1	BAIT	H. sapiens	Phenotypic Suppression	Zhang Y (2002)
BACH1	HIT	H. sapiens	Affinity Capture-MS	Varjosalo M (2013)
BCL10	HIT	H. sapiens	Affinity Capture-Western	Carvalho G (2010)
BCL10	HIT	H. sapiens	Affinity Capture-Western	Hatchi EM (2014)
BCL10	HIT	H. sapiens	Affinity Capture-Western	Bidere N (2009)
BCR	BAIT	H. sapiens	Affinity Capture-MS	Boldt K (2016)
BTRC	BAIT	H. sapiens	Affinity Capture-MS	Coyaud E (2015)
BTRC	BAIT	H. sapiens	Proximity Label-MS	Coyaud E (2015)
C1orf111	BAIT	H. sapiens	Affinity Capture-MS	Huttlin EL (2015)
C1orf111	BAIT	H. sapiens	Affinity Capture-MS	Huttlin EL (2017)
CAD	HIT	H. sapiens	Affinity Capture-MS	Rosenbluh J (2016)
CAND1	HIT	H. sapiens	Affinity Capture-MS	Rosenbluh J (2016)
CARD11	BAIT	H. sapiens	Affinity Capture-MS	Bidere N (2009)
CARD11	HIT	H. sapiens	Affinity Capture-Western	Hatchi EM (2014)
CARD11	BAIT	H. sapiens	Affinity Capture-Western	Bidere N (2009)
CARD11	HIT	H. sapiens	Affinity Capture-Western	Bidere N (2009)
Card11	BAIT	M. musculus	Affinity Capture-Western	Bidere N (2009)
Cbx1	BAIT	M. musculus	Affinity Capture-MS	Hutchins JR (2010)
CBY1	HIT	H. sapiens	Affinity Capture-MS	Boldt K (2016)
CDC25A	HIT	H. sapiens	Biochemical Activity	Honaker Y (2010)
CDH1	HIT	H. sapiens	Affinity Capture-MS	Rosenbluh J (2016)
CDH1	BAIT	H. sapiens	Proximity Label-MS	Guo Z (2014)
CDK9	HIT	H. sapiens	Affinity Capture-MS	Rosenbluh J (2016)
CEP128	BAIT	H. sapiens	Proximity Label-MS	Gupta GD (2015)

CEP135	BAIT	H. sapiens	Proximity Label-MS	Gupta GD (2015)
CEP170	BAIT	H. sapiens	Proximity Label-MS	Gupta GD (2015)
CGN	HIT	H. sapiens	Affinity Capture-MS	Boldt K (2016)
CHRM3	BAIT	H. sapiens	Reconstituted Complex	Budd DC (2000)
CLTC	BAIT	H. sapiens	Affinity Capture-MS	Hein MY (2015)
COPS5	BAIT	H. sapiens	Affinity Capture-Western	Huang X (2009)
CPSF6	BAIT	H. sapiens	Co-fractionation	Havugimana PC (2012)
CRBN	BAIT	H. sapiens	Affinity Capture-Western	Nguyen TV (2016)
CRBN	HIT	H. sapiens	Affinity Capture-Western	Kroenke J (2015)
CRBN	BAIT	H. sapiens	Biochemical Activity	Kroenke J (2015)
CRBN	BAIT	H. sapiens	Biochemical Activity	Petzold G (2016)
CRBN	BAIT	H. sapiens	Reconstituted Complex	Petzold G (2016)
CSNK1D	HIT	H. sapiens	Affinity Capture-MS	Varjosalo M (2013)
CSNK1E	HIT	H. sapiens	Affinity Capture-MS	Varjosalo M (2013)
CSNK1E	HIT	H. sapiens	Affinity Capture-MS	Rosenbluh J (2016)
CTNNB1	BAIT	H. sapiens	Affinity Capture-MS	Rosenbluh J (2016)
CTNNB1	HIT	H. sapiens	Affinity Capture-Western	Li Z (2018)
CYFIP1	HIT	H. sapiens	Affinity Capture-MS	Rosenbluh J (2016)
DBNDD1	BAIT	H. sapiens	Affinity Capture-MS	Huttlin EL (2014/pre-pub)
DBR1	HIT	H. sapiens	Affinity Capture-MS	Varjosalo M (2013)
DDX1	HIT	H. sapiens	Affinity Capture-MS	Cai J (2018)
DENND4C	BAIT	H. sapiens	Affinity Capture-MS	Boldt K (2016)
DNAJA1	HIT	H. sapiens	Affinity Capture-MS	Cai J (2018)
DYNLL1	HIT	H. sapiens	Affinity Capture-MS	Varjosalo M (2013)
DYNLL2	HIT	H. sapiens	Affinity Capture-MS	Varjosalo M (2013)
E2F1	BAIT	H. sapiens	Affinity Capture-Western	Huart AS (2009)
EFTUD2	BAIT	H. sapiens	Affinity Capture-MS	Malinova A (2017)
EGFR	BAIT	H. sapiens	Affinity Capture-MS	Tong J (2014)
EGLN3	BAIT	H. sapiens	Affinity Capture-MS	Rodriguez J (2016)
EIF3J	HIT	H. sapiens	Affinity Capture-MS	Rosenbluh J (2016)
ELAVL1	BAIT	H. sapiens	Affinity Capture-RNA	Abdelmohsen K (2009)
EPM2AIP1	HIT	H. sapiens	Affinity Capture-MS	Varjosalo M (2013)
ERF	HIT	H. sapiens	Co-purification	Dubois T (2002)
ESR2	BAIT	H. sapiens	Affinity Capture-MS	Giurato G (2018)
FABP5	HIT	H. sapiens	Affinity Capture-MS	Rosenbluh J (2016)
FAM83B	HIT	H. sapiens	Affinity Capture-MS	Varjosalo M (2013)
FAM83B	HIT	H. sapiens	Affinity Capture-MS	Rosenbluh J (2016)
FAM83D	HIT	H. sapiens	Affinity Capture-MS	Varjosalo M (2013)
Fam83d	BAIT	M. musculus	Affinity Capture-MS	Hein MY (2015)
FAM83D	HIT	H. sapiens	Affinity Capture-MS	Huttlin EL (2017)
FAM83D	HIT	H. sapiens	Affinity Capture-MS	Rosenbluh J (2016)
FAM83G	HIT	H. sapiens	Affinity Capture-MS	Varjosalo M (2013)
FAM83G	HIT	H. sapiens	Affinity Capture-MS	Huttlin EL (2017)
FAM83H	HIT	H. sapiens	Affinity Capture-MS	Varjosalo M (2013)
FAM83H	BAIT	H. sapiens	Affinity Capture-MS	Hein MY (2015)
FAM83H	HIT	H. sapiens	Affinity Capture-MS	Huttlin EL (2017)
FAM83H	HIT	H. sapiens	Affinity Capture-MS	Rosenbluh J (2016)
FAM110D	BAIT	H. sapiens	Affinity Capture-MS	Huttlin EL (2014/pre-pub)
FAM170A	BAIT	H. sapiens	Affinity Capture-MS	Huttlin EL (2015)
FAM170A	BAIT	H. sapiens	Affinity Capture-MS	Huttlin EL (2017)
FBXW7	BAIT	H. sapiens	Affinity Capture-MS	Khan OM (2018)
FKBP5	HIT	H. sapiens	Affinity Capture-MS	Rosenbluh J (2016)
FLII	HIT	H. sapiens	Affinity Capture-MS	Rosenbluh J (2016)
FOXA1	BAIT	H. sapiens	Affinity Capture-MS	Jozwik KM (2016)
GAPVD1	HIT	H. sapiens	Affinity Capture-MS	Huttlin EL (2017)
GAPVD1	HIT	H. sapiens	Affinity Capture-MS	Rosenbluh J (2016)

GCN1L1	HIT	H. sapiens	Affinity Capture-MS	Rosenbluh J (2016)
GFPT1	HIT	H. sapiens	Affinity Capture-MS	Rosenbluh J (2016)
GIGYF1	HIT	H. sapiens	Affinity Capture-MS	Boldt K (2016)
GLI3	HIT	H. sapiens	Biochemical Activity	Wang B (2006)
GMPPB	HIT	H. sapiens	Affinity Capture-MS	Rosenbluh J (2016)
GNB2	HIT	H. sapiens	Two-hybrid	Wang J (2011)
GTSE1	BAIT	H. sapiens	Affinity Capture-MS	Hein MY (2015)
HABP4	BAIT	H. sapiens	Affinity Capture-MS	Saito A (2017)
HDAC2	HIT	H. sapiens	Affinity Capture-MS	Rosenbluh J (2016)
HDAC4	HIT	H. sapiens	Affinity Capture-MS	Rosenbluh J (2016)
HERC1	HIT	H. sapiens	Affinity Capture-MS	Huttlin EL (2017)
HIST1H1D	HIT	H. sapiens	Affinity Capture-MS	Rosenbluh J (2016)
HMGB1	HIT	H. sapiens	Co-purification	Dubois T (2002)
HMGB2	HIT	H. sapiens	Co-purification	Dubois T (2002)
HMMR	HIT	H. sapiens	Affinity Capture-MS	Varjosalo M (2013)
HMMR	HIT	H. sapiens	Affinity Capture-MS	Huttlin EL (2017)
HMMR	HIT	H. sapiens	Affinity Capture-MS	Rosenbluh J (2016)
HNF1B	BAIT	H. sapiens	Affinity Capture-MS	Rosenbluh J (2016)
HNRNPC	HIT	H. sapiens	Biochemical Activity	Kattapuram T (2005)
HNRNPL	BAIT	H. sapiens	Affinity Capture-RNA	Fei T (2017)
HNRNPM	HIT	H. sapiens	Affinity Capture-MS	Rosenbluh J (2016)
HSP90AA1	BAIT	H. sapiens	Affinity Capture-Luminescence	Taipale M (2012)
HSP90AA1	BAIT	H. sapiens	Affinity Capture-MS	Gano JJ (2010)
HSP90AA1	HIT	H. sapiens	Affinity Capture-MS	Cai J (2018)
HSP90AA1	HIT	H. sapiens	Biochemical Activity	Muller P (2012)
HSPA4	HIT	H. sapiens	Biochemical Activity	Muller P (2012)
HSPD1	HIT	H. sapiens	Affinity Capture-MS	Rosenbluh J (2016)
IDH3B	HIT	H. sapiens	Affinity Capture-MS	Rosenbluh J (2016)
IMPA1	HIT	H. sapiens	Affinity Capture-MS	Rosenbluh J (2016)
IMPA2	HIT	H. sapiens	Affinity Capture-MS	Rosenbluh J (2016)
IPO7	HIT	H. sapiens	Affinity Capture-MS	Rosenbluh J (2016)
IRS1	BAIT	H. sapiens	Affinity Capture-MS	Yoneyama Y (2018)
ITGA4	BAIT	H. sapiens	Affinity Capture-MS	Byron A (2012)
ITGB1	HIT	H. sapiens	Affinity Capture-MS	Rosenbluh J (2016)
KCTD3	HIT	H. sapiens	Affinity Capture-MS	Boldt K (2016)
KDM1A	HIT	H. sapiens	Affinity Capture-Western	Zhou A (2016)
KIF1B	HIT	H. sapiens	Affinity Capture-MS	Rosenbluh J (2016)
KIF13B	HIT	H. sapiens	Affinity Capture-MS	Boldt K (2016)
KPNA2	HIT	H. sapiens	Affinity Capture-MS	Dubois T (2002)
KPNB1	HIT	H. sapiens	Affinity Capture-MS	Cai J (2018)
KRAS	BAIT	H. sapiens	Proximity Label-MS	Kovalski JR (2019)
KSR1	BAIT	H. sapiens	Affinity Capture-MS	Boldt K (2016)
LARP1	HIT	H. sapiens	Affinity Capture-MS	Rosenbluh J (2016)
LBR	HIT	H. sapiens	Affinity Capture-MS	Rosenbluh J (2016)
LMO7	HIT	H. sapiens	Affinity Capture-MS	Rosenbluh J (2016)
LRP5	HIT	H. sapiens	Affinity Capture-MS	Huttlin EL (2017)
LRP6	HIT	H. sapiens	Affinity Capture-MS	Huttlin EL (2017)
MALT1	HIT	H. sapiens	Affinity Capture-Western	Carvalho G (2010)
MALT1	HIT	H. sapiens	Affinity Capture-Western	Hatchi EM (2014)
MALT1	HIT	H. sapiens	Affinity Capture-Western	Bidere N (2009)
MALT1	BAIT	H. sapiens	Affinity Capture-Western	Bidere N (2009)
MAP2K1	HIT	H. sapiens	Affinity Capture-MS	Rosenbluh J (2016)
MAPT	HIT	H. sapiens	Biochemical Activity	Wang JZ (1998)
MAPT	HIT	H. sapiens	Biochemical Activity	Sadik G (2009)
MARS	HIT	H. sapiens	Affinity Capture-MS	Rosenbluh J (2016)
MAT2A	HIT	H. sapiens	Affinity Capture-MS	Rosenbluh J (2016)

MDM2	BAIT	H. sapiens	Affinity Capture-Western	Huart AS (2009)
MDM2	BAIT	H. sapiens	Affinity Capture-Western	Huart AS (2012)
MDM2	HIT	H. sapiens	Affinity Capture-Western	Huart AS (2012)
MDM4	BAIT	H. sapiens	Affinity Capture-MS	Gilkes DM (2006)
MDM4	BAIT	H. sapiens	Affinity Capture-MS	Huttlin EL (2017)
MDM4	BAIT	H. sapiens	Affinity Capture-Western	Chen L (2005)
MDM4	BAIT	H. sapiens	Affinity Capture-Western	Li M (2011)
MDM4	BAIT	H. sapiens	Affinity Capture-Western	Wu S (2012)
MDM4	BAIT	H. sapiens	Affinity Capture-Western	Chen L (2015)
MDM4	HIT	H. sapiens	Reconstituted Complex	Chen L (2005)
MED12	BAIT	H. sapiens	Affinity Capture-MS	Rosenbluh J (2016)
MLH1	HIT	H. sapiens	Affinity Capture-MS	Rosenbluh J (2016)
MPRIIP	HIT	H. sapiens	Affinity Capture-MS	Rosenbluh J (2016)
MT1X	HIT	H. sapiens	Affinity Capture-MS	Rosenbluh J (2016)
MYO18A	BAIT	H. sapiens	Affinity Capture-MS	Hein MY (2015)
MZT2A	HIT	H. sapiens	Affinity Capture-MS	Varjosalo M (2013)
MZT2B	HIT	H. sapiens	Affinity Capture-MS	Varjosalo M (2013)
NCKIPSD	BAIT	H. sapiens	Affinity Capture-MS	Huttlin EL (2017)
NDUFB4	HIT	H. sapiens	Affinity Capture-MS	Rosenbluh J (2016)
NDUFS3	HIT	H. sapiens	Affinity Capture-MS	Rosenbluh J (2016)
NFATC1	BAIT	H. sapiens	Affinity Capture-MS	Gabriel CH (2016)
NFATC3	BAIT	H. sapiens	Affinity Capture-MS	Huttlin EL (2015)
NFKBIA	HIT	H. sapiens	Affinity Capture-Western	Carvalho G (2010)
NFKBIA	BAIT	H. sapiens	Affinity Capture-Western	Carvalho G (2010)
NIN	BAIT	H. sapiens	Proximity Label-MS	Gupta GD (2015)
NPEPPS	HIT	H. sapiens	Affinity Capture-MS	Rosenbluh J (2016)
NTRK1	BAIT	H. sapiens	Affinity Capture-MS	Emdal KB (2015)
OCLN	BAIT	H. sapiens	Reconstituted Complex	McKenzie JA (2006)
OPA1	HIT	H. sapiens	Affinity Capture-MS	Rosenbluh J (2016)
PCM1	BAIT	H. sapiens	Affinity Capture-MS	Gupta GD (2015)
PDE4D	HIT	H. sapiens	Biochemical Activity	Zhu H (2010)
PFKL	HIT	H. sapiens	Affinity Capture-MS	Rosenbluh J (2016)
PHF6	HIT	H. sapiens	Affinity Capture-MS	Rosenbluh J (2016)
PHGDH	HIT	H. sapiens	Affinity Capture-MS	Rosenbluh J (2016)
PHLPP1	HIT	H. sapiens	Biochemical Activity	Li X (2009)
PIP5K1A	HIT	H. sapiens	Co-fractionation	Havugimana PC (2012)
POTEB3	BAIT	H. sapiens	Affinity Capture-MS	Huttlin EL (2017)
POTEC	BAIT	H. sapiens	Affinity Capture-MS	Huttlin EL (2017)
PPIE	BAIT	H. sapiens	Affinity Capture-MS	Rosenbluh J (2016)
PPP1CC	BAIT	H. sapiens	Two-hybrid	Fardilha M (2011)
PPP1R14A	HIT	H. sapiens	Co-purification	Dubois T (2002)
PPP1R14A	BAIT	H. sapiens	Reconstituted Complex	Zemlickova E (2004)
PPP2CA	HIT	H. sapiens	Affinity Capture-MS	Dubois T (2002)
PRKDC	HIT	H. sapiens	Affinity Capture-MS	Rosenbluh J (2016)
PSMC5	HIT	H. sapiens	Affinity Capture-MS	Rosenbluh J (2016)
PTCH1	BAIT	H. sapiens	Affinity Capture-MS	Yamaki Y (2016)
PTEN	HIT	H. sapiens	Affinity Capture-MS	Cai J (2018)
PTEN	HIT	H. sapiens	Affinity Capture-Western	Cai J (2018)
PTEN	BAIT	H. sapiens	Affinity Capture-Western	Cai J (2018)
PTEN	HIT	H. sapiens	Reconstituted Complex	Cai J (2018)
PTEN	BAIT	H. sapiens	Reconstituted Complex	Cai J (2018)
RAB18	HIT	H. sapiens	Affinity Capture-MS	Rosenbluh J (2016)
RAC1	HIT	H. sapiens	Affinity Capture-MS	Rosenbluh J (2016)
RAF1	HIT	H. sapiens	Affinity Capture-MS	Rosenbluh J (2016)
RANGAP1	HIT	H. sapiens	Affinity Capture-MS	Rosenbluh J (2016)
RASAL2	HIT	H. sapiens	Affinity Capture-MS	Varjosalo M (2013)

RASAL2	HIT	H. sapiens	Affinity Capture-MS	Huttlin EL (2017)
RCC1	HIT	H. sapiens	Co-purification	Dubois T (2002)
RFC1	HIT	H. sapiens	Affinity Capture-MS	Rosenbluh J (2016)
RIPK4	BAIT	H. sapiens	Affinity Capture-MS	Rodriguez J (2016)
RPA1	BAIT	H. sapiens	Affinity Capture-MS	Marechal A (2014)
RPA2	BAIT	H. sapiens	Affinity Capture-MS	Marechal A (2014)
RPA3	BAIT	H. sapiens	Affinity Capture-MS	Marechal A (2014)
RPL3	HIT	H. sapiens	Affinity Capture-MS	Rosenbluh J (2016)
RPL4	HIT	H. sapiens	Affinity Capture-MS	Rosenbluh J (2016)
RPL27	HIT	H. sapiens	Affinity Capture-MS	Rosenbluh J (2016)
RPN1	HIT	H. sapiens	Affinity Capture-MS	Rosenbluh J (2016)
RPS3	HIT	H. sapiens	Affinity Capture-MS	Rosenbluh J (2016)
RPS15A	HIT	H. sapiens	Affinity Capture-MS	Rosenbluh J (2016)
RPS28	HIT	H. sapiens	Affinity Capture-MS	Rosenbluh J (2016)
RUVBL2	HIT	H. sapiens	Affinity Capture-MS	Rosenbluh J (2016)
SEC13	HIT	H. sapiens	Affinity Capture-MS	Varjosalo M (2013)
SEC13	HIT	H. sapiens	Affinity Capture-MS	Rosenbluh J (2016)
SEC16A	HIT	H. sapiens	Affinity Capture-MS	Varjosalo M (2013)
SEC16A	BAIT	H. sapiens	Affinity Capture-MS	Hein MY (2015)
SEC16A	HIT	H. sapiens	Affinity Capture-MS	Rosenbluh J (2016)
SEC23B	HIT	H. sapiens	Affinity Capture-MS	Varjosalo M (2013)
Sec24c	BAIT	M. musculus	Affinity Capture-MS	Hein MY (2015)
SEC61A1	HIT	H. sapiens	Affinity Capture-MS	Rosenbluh J (2016)
sept-11	HIT	H. sapiens	Affinity Capture-MS	Rosenbluh J (2016)
SERBP1	BAIT	H. sapiens	Affinity Capture-MS	Saito A (2017)
SETD8	BAIT	H. sapiens	Affinity Capture-Western	Wang Z (2015)
SH3BP4	HIT	H. sapiens	Affinity Capture-MS	Rosenbluh J (2016)
SH3GL1	HIT	H. sapiens	Affinity Capture-MS	Rosenbluh J (2016)
SH3KBP1	BAIT	H. sapiens	Affinity Capture-MS	Havrylov S (2009)
SHQ1	HIT	S. cerevisiae	Biochemical Activity	Godin KS (2009)
SIK2	BAIT	H. sapiens	Affinity Capture-MS	So J (2015)
SLC25A1	HIT	H. sapiens	Affinity Capture-MS	Rosenbluh J (2016)
SLC25A13	HIT	H. sapiens	Affinity Capture-MS	Rosenbluh J (2016)
SMC3	HIT	H. sapiens	Affinity Capture-MS	Rosenbluh J (2016)
smo	HIT	D. melanogaster	Biochemical Activity	Fan J (2013)
SNCA	HIT	H. sapiens	Biochemical Activity	Okochi M (2000)
SNCA	HIT	H. sapiens	Biochemical Activity	Kim EJ (2006)
SNX22	HIT	H. sapiens	Affinity Capture-MS	Varjosalo M (2013)
SNX24	HIT	H. sapiens	Affinity Capture-MS	Varjosalo M (2013)
SNX24	BAIT	H. sapiens	Affinity Capture-MS	Huttlin EL (2017)
SQSTM1	HIT	H. sapiens	Biochemical Activity	Watanabe Y (2017)
SSMEM1	BAIT	H. sapiens	Affinity Capture-MS	Huttlin EL (2017)
STAT1	HIT	H. sapiens	Affinity Capture-MS	Rosenbluh J (2016)
STUB1	HIT	H. sapiens	Affinity Capture-MS	Rosenbluh J (2016)
SYT9	HIT	H. sapiens	Co-purification	Dubois T (2002)
TEX264	BAIT	H. sapiens	Affinity Capture-MS	Huttlin EL (2015)
TEX264	BAIT	H. sapiens	Affinity Capture-MS	Huttlin EL (2017)
TIAM1	BAIT	H. sapiens	Affinity Capture-MS	Magliozzi R (2014)
TIAM1	HIT	H. sapiens	Affinity Capture-Western	Magliozzi R (2014)
TIAM1	HIT	H. sapiens	Biochemical Activity	Magliozzi R (2014)
TMPO	HIT	H. sapiens	Affinity Capture-MS	Rosenbluh J (2016)
TNFRSF1B	HIT	H. sapiens	Biochemical Activity	Beyaert R (1995)
TNFRSF1B	BAIT	H. sapiens	Reconstituted Complex	Darnay BG (1997)
TNPO1	HIT	H. sapiens	Affinity Capture-MS	Rosenbluh J (2016)
TOM20	HIT	S. cerevisiae	Biochemical Activity	Gerbeth C (2013)
TP53	HIT	H. sapiens	Affinity Capture-MS	Cai J (2018)

TP53	BAIT	H. sapiens	Affinity Capture-Western	Huart AS (2009)
TP53	BAIT	H. sapiens	Affinity Capture-Western	Wei X (2016)
TP53	HIT	H. sapiens	Biochemical Activity	Sakaguchi K (2000)
TRIM25	BAIT	H. sapiens	Affinity Capture-RNA	Choudhury NR (2017)
TTC9C	HIT	H. sapiens	Affinity Capture-MS	Huttlin EL (2017)
TTC27	HIT	H. sapiens	Affinity Capture-MS	Rosenbluh J (2016)
TUBA4A	HIT	H. sapiens	Affinity Capture-MS	Rosenbluh J (2016)
TUBB	HIT	H. sapiens	Affinity Capture-MS	Rosenbluh J (2016)
TUBG1	HIT	H. sapiens	Affinity Capture-MS	Rosenbluh J (2016)
UBAC2	HIT	H. sapiens	Affinity Capture-MS	Rosenbluh J (2016)
UNC45A	HIT	H. sapiens	Affinity Capture-MS	Varjosalo M (2013)
UNC45A	HIT	H. sapiens	Affinity Capture-MS	Rosenbluh J (2016)
Uso1	BAIT	M. musculus	Affinity Capture-MS	Hein MY (2015)
USP34	HIT	H. sapiens	Affinity Capture-MS	Varjosalo M (2013)
USP34	HIT	H. sapiens	Affinity Capture-MS	Huttlin EL (2017)
VCAM1	BAIT	H. sapiens	Affinity Capture-MS	Humphries JD (2009)
WDR45	HIT	H. sapiens	Affinity Capture-MS	Cai J (2018)
WDR92	BAIT	H. sapiens	Affinity Capture-MS	Cloutier P (2017)
WEE1	BAIT	H. sapiens	Affinity Capture-MS	Boldt K (2016)
XPO1	BAIT	H. sapiens	Affinity Capture-MS	Kirli K (2015)
XRCC6	BAIT	H. sapiens	Affinity Capture-MS	Hein MY (2015)
YWHAE	BAIT	H. sapiens	Affinity Capture-MS	Gloeckner CJ (2007)
YWHAQ	HIT	H. sapiens	Affinity Capture-MS	Rosenbluh J (2016)
ZBTB21	HIT	H. sapiens	Affinity Capture-MS	Boldt K (2016)
ZDBF2	HIT	H. sapiens	Affinity Capture-MS	Huttlin EL (2017)
ZNF217	BAIT	H. sapiens	Affinity Capture-MS	Rosenbluh J (2016)
ZNF618	HIT	H. sapiens	Affinity Capture-MS	Varjosalo M (2013)
ZNF618	HIT	H. sapiens	Affinity Capture-MS	Huttlin EL (2017)

**CSNK1D (P48730)**

<b>Interactor</b>	<b>Role</b>	<b>Organism</b>	<b>Experimental Evidence Code</b>	<b>Dataset</b>
AKAP9	HIT	H. sapiens	Affinity Capture-MS	Huttlin EL (2017)
AKAP9	BAIT	H. sapiens	Affinity Capture-Western	Sillibourne JE (2002)
ANKRD49	HIT	H. sapiens	Affinity Capture-MS	Huttlin EL (2017)
APC	BAIT	H. sapiens	Affinity Capture-MS	Novellasdemunt L (2017)
APP	HIT	H. sapiens	Reconstituted Complex	Olah J (2011)
APP	BAIT	H. sapiens	Reconstituted Complex	Virok DP (2011)
ATG4B	HIT	H. sapiens	Affinity Capture-MS	Huttlin EL (2014/pre-pub)
ATM	BAIT	H. sapiens	Biochemical Activity	Wang Z (2012)
ATOH1	BAIT	H. sapiens	Affinity Capture-MS	Cheng YF (2016)
ATOH1	BAIT	H. sapiens	Affinity Capture-Western	Cheng YF (2016)
AXIN1	BAIT	H. sapiens	Affinity Capture-MS	Hein MY (2015)
BACE1	BAIT	H. sapiens	Co-localization	Chen TC (2014)
BRCA1	BAIT	H. sapiens	Affinity Capture-MS	Hill SJ (2014)
BRCA1	HIT	H. sapiens	Two-hybrid	Hill SJ (2014)
BYSL	BAIT	H. sapiens	Co-fractionation	Havugimana PC (2012)
CACNG2	BAIT	H. sapiens	Affinity Capture-MS	Huttlin EL (2015)
CACNG2	BAIT	H. sapiens	Affinity Capture-MS	Huttlin EL (2017)
CACNG4	BAIT	H. sapiens	Affinity Capture-MS	Huttlin EL (2015)
CACNG5	BAIT	H. sapiens	Affinity Capture-MS	Huttlin EL (2017)
Ccdc9	BAIT	M. musculus	Affinity Capture-MS	Hein MY (2015)
CDH1	BAIT	H. sapiens	Proximity Label-MS	Guo Z (2014)
CEP128	BAIT	H. sapiens	Proximity Label-MS	Gupta GD (2015)
Cry1	BAIT	M. musculus	Affinity Capture-MS	Hein MY (2015)
CRY1	HIT	H. sapiens	Affinity Capture-MS	Huttlin EL (2017)
CRY2	HIT	H. sapiens	Affinity Capture-MS	Huttlin EL (2017)
CSNK1A1	BAIT	H. sapiens	Affinity Capture-MS	Varjosalo M (2013)

CSNK1E	BAIT	H. sapiens	Affinity Capture-MS	Varjosalo M (2013)
CSNK1E	BAIT	H. sapiens	Affinity Capture-MS	Huttlin EL (2017)
DAP3	BAIT	H. sapiens	Affinity Capture-MS	Hein MY (2015)
DBNDD1	BAIT	H. sapiens	Affinity Capture-MS	Huttlin EL (2014/pre-pub)
DBNDD2	BAIT	H. sapiens	Affinity Capture-Western	Yin H (2006)
DBNDD2	HIT	H. sapiens	Two-hybrid	Yin H (2006)
DRICH1	BAIT	H. sapiens	Affinity Capture-MS	Huttlin EL (2015)
DVL1	HIT	H. sapiens	Affinity Capture-Western	Gao ZH (2002)
DVL3	HIT	H. sapiens	Two-hybrid	Rual JF (2005)
DVL3	HIT	H. sapiens	Two-hybrid	Rolland T (2014)
EZH2	BAIT	H. sapiens	Affinity Capture-MS	Oliviero G (2016)
FAM83D	HIT	H. sapiens	Affinity Capture-MS	Huttlin EL (2017)
FAM83H	BAIT	H. sapiens	Affinity Capture-MS	Hein MY (2015)
FAM83H	HIT	H. sapiens	Affinity Capture-MS	Huttlin EL (2017)
FAM110B	HIT	H. sapiens	Affinity Capture-MS	Huttlin EL (2017)
FAM110D	BAIT	H. sapiens	Affinity Capture-MS	Huttlin EL (2014/pre-pub)
FAM199X	HIT	H. sapiens	Affinity Capture-MS	Huttlin EL (2017)
Fgfr1op	BAIT	M. musculus	Affinity Capture-MS	Hein MY (2015)
FHL1	HIT	H. sapiens	Affinity Capture-Western	Ding L (2009)
FHL1	BAIT	H. sapiens	Affinity Capture-Western	Ding L (2009)
FHL1	HIT	H. sapiens	Reconstituted Complex	Ding L (2009)
FKBPL	HIT	H. sapiens	Affinity Capture-MS	Huttlin EL (2017)
GAPVD1	HIT	H. sapiens	Affinity Capture-MS	Huttlin EL (2017)
GEMIN7	BAIT	H. sapiens	Affinity Capture-MS	Hein MY (2015)
GJA1	BAIT	H. sapiens	Affinity Capture-Western	Cooper CD (2002)
GJA1	HIT	H. sapiens	Biochemical Activity	Cooper CD (2002)
HIF1A	HIT	H. sapiens	Biochemical Activity	Kalouisi A (2010)
HMMR	HIT	H. sapiens	Affinity Capture-MS	Huttlin EL (2017)
HN1L	HIT	H. sapiens	Two-hybrid	Vinayagam A (2011)
HNRNPL	BAIT	H. sapiens	Affinity Capture-RNA	Fei T (2017)
HSPA8	HIT	H. sapiens	Affinity Capture-MS	Huttlin EL (2017)
HSPA8	BAIT	H. sapiens	Affinity Capture-MS	Rosenbluh J (2016)
KCTD17	BAIT	H. sapiens	Affinity Capture-MS	Huttlin EL (2015)
KDR	HIT	H. sapiens	Affinity Capture-Western	Shaik S (2012)
KDR	HIT	H. sapiens	Biochemical Activity	Shaik S (2012)
KLC1	BAIT	H. sapiens	Affinity Capture-MS	Hein MY (2015)
LDLRAD4	BAIT	H. sapiens	Affinity Capture-MS	Huttlin EL (2015)
LNX1	BAIT	H. sapiens	Affinity Capture-MS	Lenihan JA (2017)
LURAP1	HIT	H. sapiens	Two-hybrid	Rolland T (2014)
MAF1	BAIT	H. sapiens	Affinity Capture-MS	Huttlin EL (2015)
MAF1	BAIT	H. sapiens	Affinity Capture-MS	Huttlin EL (2017)
MAPT	HIT	H. sapiens	Biochemical Activity	Yin H (2006)
MAPT	HIT	H. sapiens	Biochemical Activity	Wolff S (2006)
MCC	BAIT	H. sapiens	Affinity Capture-MS	Ewing RM (2007)
MDM2	BAIT	H. sapiens	Affinity Capture-Western	Inuzuka H (2010)
MDM2	HIT	H. sapiens	Affinity Capture-Western	Wang Z (2012)
MDM2	BAIT	H. sapiens	Affinity Capture-Western	Wang Z (2012)
MDM2	HIT	H. sapiens	Biochemical Activity	Inuzuka H (2010)
MDM2	HIT	H. sapiens	Biochemical Activity	Kulikov R (2006)
MICU2	BAIT	H. sapiens	Affinity Capture-MS	Huttlin EL (2015)
MTMR3	HIT	H. sapiens	Affinity Capture-MS	Huttlin EL (2014/pre-pub)
MTSS1	BAIT	H. sapiens	Affinity Capture-Western	Zhong J (2013)
NEDD4	BAIT	H. sapiens	Affinity Capture-Western	Liu J (2014)
NFATC1	BAIT	H. sapiens	Affinity Capture-MS	Gabriel CH (2016)
NFATC2	BAIT	H. sapiens	Affinity Capture-MS	Gabriel CH (2016)
NOB1	HIT	H. sapiens	Co-fractionation	Wan C (2015)

NXF2	BAIT	H. sapiens	Affinity Capture-MS	Huttlin EL (2017)
PCM1	BAIT	H. sapiens	Affinity Capture-MS	Gupta GD (2015)
PCM1	BAIT	H. sapiens	Proximity Label-MS	Gupta GD (2015)
PDE4DIP	HIT	H. sapiens	Affinity Capture-MS	Huttlin EL (2017)
PER1	HIT	H. sapiens	Affinity Capture-MS	Huttlin EL (2017)
PER1	BAIT	H. sapiens	Affinity Capture-Western	Camacho F (2001)
PER2	HIT	H. sapiens	Two-hybrid	Wallach T (2013)
PML	BAIT	H. sapiens	Affinity Capture-Western	Alsheich-Bartok O (2008)
PML	HIT	H. sapiens	Affinity Capture-Western	Alsheich-Bartok O (2008)
PPM1B	HIT	H. sapiens	Co-fractionation	Wan C (2015)
PPP1R14A	BAIT	H. sapiens	Reconstituted Complex	Zemlickova E (2004)
PPP5C	BAIT	H. sapiens	Affinity Capture-Western	Dushukyan N (2017)
PPP5C	HIT	H. sapiens	Biochemical Activity	Dushukyan N (2017)
PPP6C	BAIT	H. sapiens	Affinity Capture-Western	Bhandari D (2013)
PRKAR2B	BAIT	H. sapiens	Affinity Capture-MS	Hein MY (2015)
PRKAR2B	HIT	H. sapiens	Affinity Capture-MS	Huttlin EL (2017)
PTPN14	BAIT	H. sapiens	Affinity Capture-MS	Wang W (2012)
PTPRD	BAIT	H. sapiens	Reconstituted Complex	Meehan M (2012)
RAB1A	HIT	H. sapiens	Reconstituted Complex	Wang J (2015)
RECQL4	BAIT	H. sapiens	Affinity Capture-MS	Lu H (2017)
RHOJ	BAIT	H. sapiens	Affinity Capture-MS	Huttlin EL (2015)
RIPK4	BAIT	H. sapiens	Affinity Capture-MS	Rodriguez J (2016)
RL2	HIT	HHV-1	Biochemical Activity	Chaurushiya MS (2012)
RP2	BAIT	H. sapiens	Affinity Capture-MS	Huttlin EL (2015)
RP2	BAIT	H. sapiens	Affinity Capture-MS	Huttlin EL (2017)
SETD8	BAIT	H. sapiens	Affinity Capture-Western	Wang Z (2015)
SMAD2	BAIT	H. sapiens	Affinity Capture-MS	Brown KA (2008)
SMAD2	HIT	H. sapiens	Affinity Capture-Western	Ding L (2009)
SMAD2	HIT	H. sapiens	Biochemical Activity	Ding L (2009)
SMAD3	BAIT	H. sapiens	Affinity Capture-MS	Brown KA (2008)
SMAD3	HIT	H. sapiens	Affinity Capture-Western	Ding L (2009)
SMAD3	HIT	H. sapiens	Biochemical Activity	Ding L (2009)
SMAD4	HIT	H. sapiens	Affinity Capture-Western	Ding L (2009)
SMURF1	BAIT	H. sapiens	Biochemical Activity	Andrews PS (2010)
SNCA	HIT	H. sapiens	Biochemical Activity	Yin H (2006)
SNCA	BAIT	H. sapiens	Co-localization	Chen TC (2014)
SNX24	HIT	H. sapiens	Affinity Capture-MS	Huttlin EL (2017)
SSMEM1	BAIT	H. sapiens	Affinity Capture-MS	Huttlin EL (2017)
TDP1	HIT	H. sapiens	Affinity Capture-MS	Huttlin EL (2017)
TEX264	BAIT	H. sapiens	Affinity Capture-MS	Huttlin EL (2015)
TP53	BAIT	H. sapiens	Affinity Capture-Western	Alsheich-Bartok O (2008)
TP53	HIT	H. sapiens	Affinity Capture-Western	Alsheich-Bartok O (2008)
TP53	HIT	H. sapiens	Biochemical Activity	Kulikov R (2006)
TP53	HIT	H. sapiens	Biochemical Activity	Wolff S (2006)
TP53	BAIT	H. sapiens	Co-localization	Chen TC (2014)
TRA2A	BAIT	H. sapiens	Affinity Capture-MS	Huttlin EL (2015)
TRIM9	HIT	H. sapiens	Two-hybrid	Rolland T (2014)
TRIM25	BAIT	H. sapiens	Affinity Capture-RNA	Choudhury NR (2017)
Tyw3	BAIT	M. musculus	Affinity Capture-MS	Hein MY (2015)
USP16	HIT	H. sapiens	Co-fractionation	Havugimana PC (2012)
VPS13B	HIT	H. sapiens	Affinity Capture-MS	Huttlin EL (2017)
XPO1	BAIT	H. sapiens	Affinity Capture-MS	Kirli K (2015)
YWHAZ	BAIT	H. sapiens	Reconstituted Complex	Zemlickova E (2004)
ZDHHC17	BAIT	H. sapiens	Affinity Capture-Western	Butland SL (2014)
ZDHHC17	BAIT	H. sapiens	Two-hybrid	Butland SL (2014)
ZNF618	HIT	H. sapiens	Affinity Capture-MS	Huttlin EL (2017)

CSNK1E (P49674)				
Interactor	Role	Organism	Experimental Evidence Code	Dataset
ACACA	HIT	H. sapiens	Affinity Capture-MS	Varjosalo M (2013)
ADAM22	HIT	H. sapiens	Affinity Capture-MS	Varjosalo M (2013)
AHCYL1	HIT	H. sapiens	Affinity Capture-MS	Varjosalo M (2013)
AHCYL2	HIT	H. sapiens	Affinity Capture-MS	Varjosalo M (2013)
ALYREF	BAIT	H. sapiens	Co-fractionation	Wan C (2015)
ANKRD6	BAIT	H. sapiens	Affinity Capture-Western	Schwarz-Romond T (2002)
ANKRD49	BAIT	H. sapiens	Affinity Capture-MS	Huttlin EL (2017)
APC	BAIT	H. sapiens	Affinity Capture-MS	Novellasdemunt L (2017)
APC	BAIT	H. sapiens	Co-localization	Chen TC (2014)
APP	HIT	H. sapiens	Reconstituted Complex	Olah J (2011)
APP	BAIT	H. sapiens	Reconstituted Complex	Virok DP (2011)
ARHGAP22	BAIT	H. sapiens	Affinity Capture-MS	Huttlin EL (2017)
ARHGEF1	HIT	H. sapiens	Two-hybrid	Vinayagam A (2011)
ARNTL	HIT	H. sapiens	Biochemical Activity	Eide EJ (2002)
ARNTL	BAIT	H. sapiens	Two-hybrid	Wallach T (2013)
ATOH1	BAIT	H. sapiens	Affinity Capture-MS	Cheng YF (2016)
ATOH1	BAIT	H. sapiens	Affinity Capture-Western	Cheng YF (2016)
AXIN1	BAIT	H. sapiens	Affinity Capture-MS	Hein MY (2015)
AXIN1	HIT	H. sapiens	Affinity Capture-Western	Zhang Y (2002)
AXIN1	BAIT	H. sapiens	Phenotypic Suppression	Zhang Y (2002)
AXIN1	BAIT	H. sapiens	Two-hybrid	Wang J (2011)
BAIAP2	BAIT	H. sapiens	Affinity Capture-MS	Hein MY (2015)
Bap1	BAIT	M. musculus	Affinity Capture-MS	Hein MY (2015)
BBS10	HIT	H. sapiens	Two-hybrid	Vinayagam A (2011)
BHLHE41	HIT	H. sapiens	Two-hybrid	Wallach T (2013)
BID	BAIT	H. sapiens	Co-localization	Chen TC (2014)
BTBD1	HIT	H. sapiens	Affinity Capture-MS	Huttlin EL (2017)
BYSL	BAIT	H. sapiens	Co-fractionation	Havugimana PC (2012)
C2orf44	HIT	H. sapiens	Two-hybrid	Vinayagam A (2011)
C7orf60	BAIT	H. sapiens	Affinity Capture-MS	Huttlin EL (2017)
CACNG2	BAIT	H. sapiens	Affinity Capture-MS	Huttlin EL (2015)
CACNG2	BAIT	H. sapiens	Affinity Capture-MS	Huttlin EL (2017)
CACNG4	BAIT	H. sapiens	Affinity Capture-MS	Huttlin EL (2015)
CACNG5	BAIT	H. sapiens	Affinity Capture-MS	Huttlin EL (2017)
CADM4	HIT	H. sapiens	Two-hybrid	Vinayagam A (2011)
CAMKK1	BAIT	H. sapiens	Affinity Capture-MS	Hein MY (2015)
CCDC61	HIT	H. sapiens	Affinity Capture-MS	Hein MY (2015)
CEP72	HIT	H. sapiens	Affinity Capture-MS	Hein MY (2015)
Cep72	BAIT	M. musculus	Affinity Capture-MS	Hein MY (2015)
CEP128	BAIT	H. sapiens	Proximity Label-MS	Gupta GD (2015)
CEP131	HIT	H. sapiens	Affinity Capture-MS	Hein MY (2015)
Cep152	BAIT	M. musculus	Affinity Capture-MS	Hutchins JR (2010)
CEP162	BAIT	H. sapiens	Affinity Capture-MS	Gupta GD (2015)
CEP290	BAIT	H. sapiens	Affinity Capture-MS	Gupta GD (2015)
CLOCK	HIT	H. sapiens	Affinity Capture-Luminescence	Wallach T (2013)
CLOCK	BAIT	H. sapiens	Two-hybrid	Wallach T (2013)
CLTC	BAIT	H. sapiens	Affinity Capture-MS	Hein MY (2015)
CRY1	HIT	H. sapiens	Affinity Capture-MS	Varjosalo M (2013)
CRY1	HIT	H. sapiens	Affinity Capture-MS	Hein MY (2015)
Cry1	BAIT	M. musculus	Affinity Capture-MS	Hein MY (2015)
CRY1	HIT	H. sapiens	Affinity Capture-MS	Huttlin EL (2017)
Cry1	BAIT	M. musculus	Affinity Capture-Western	Eide EJ (2002)
CRY1	BAIT	H. sapiens	Two-hybrid	Wallach T (2013)
CRY2	HIT	H. sapiens	Affinity Capture-MS	Hein MY (2015)

CRY2	HIT	H. sapiens	Affinity Capture-MS	Huttlin EL (2017)
CSNK1A1	BAIT	H. sapiens	Affinity Capture-MS	Varjosalo M (2013)
CSNK1A1	BAIT	H. sapiens	Affinity Capture-MS	Rosenbluh J (2016)
CSNK1D	HIT	H. sapiens	Affinity Capture-MS	Varjosalo M (2013)
Csnk1d	BAIT	M. musculus	Affinity Capture-MS	Hein MY (2015)
CSNK1D	HIT	H. sapiens	Affinity Capture-MS	Huttlin EL (2017)
Csnk1e	BAIT	M. musculus	Affinity Capture-MS	Hutchins JR (2010)
CSNK1E	HIT	H. sapiens	Biochemical Activity	McKenzie JA (2006)
CSNK1E	HIT	H. sapiens	Two-hybrid	Wallach T (2013)
CSNK2B	HIT	H. sapiens	Two-hybrid	Wallach T (2013)
CTNND1	BAIT	H. sapiens	Affinity Capture-Western	Del Valle-Perez B (2011)
CUL2	HIT	H. sapiens	Affinity Capture-MS	Varjosalo M (2013)
DBNDD1	BAIT	H. sapiens	Affinity Capture-MS	Huttlin EL (2014/pre-pub)
DBNDD2	BAIT	H. sapiens	Affinity Capture-Western	Yin H (2006)
DBNDD2	HIT	H. sapiens	Two-hybrid	Yin H (2006)
DEC1	HIT	H. sapiens	Two-hybrid	Wallach T (2013)
DHX16	BAIT	H. sapiens	Co-fractionation	Wan C (2015)
DRICH1	BAIT	H. sapiens	Affinity Capture-MS	Huttlin EL (2015)
DRICH1	BAIT	H. sapiens	Affinity Capture-MS	Huttlin EL (2017)
DTD1	BAIT	H. sapiens	Co-fractionation	Wan C (2015)
DVL1	HIT	H. sapiens	Affinity Capture-Western	Gao ZH (2002)
DVL2	HIT	H. sapiens	Affinity Capture-MS	Varjosalo M (2013)
DVL2	HIT	H. sapiens	Two-hybrid	Rual JF (2005)
DVL3	HIT	H. sapiens	Two-hybrid	Rolland T (2014)
DVL3	HIT	H. sapiens	Two-hybrid	Sahni N (2015)
Edc4	BAIT	M. musculus	Affinity Capture-MS	Hutchins JR (2010)
EIF1AD	BAIT	H. sapiens	Affinity Capture-MS	Huttlin EL (2014/pre-pub)
ELAVL1	BAIT	H. sapiens	Affinity Capture-RNA	Abdelmohsen K (2009)
FAM83B	HIT	H. sapiens	Affinity Capture-MS	Varjosalo M (2013)
FAM83D	HIT	H. sapiens	Affinity Capture-MS	Varjosalo M (2013)
FAM83D	HIT	H. sapiens	Two-hybrid	Vinayagam A (2011)
FAM83H	HIT	H. sapiens	Affinity Capture-MS	Varjosalo M (2013)
FAM83H	BAIT	H. sapiens	Affinity Capture-MS	Hein MY (2015)
FAM83H	HIT	H. sapiens	Affinity Capture-MS	Huttlin EL (2017)
FAM110A	HIT	H. sapiens	Two-hybrid	Vinayagam A (2011)
FAM110A	HIT	H. sapiens	Two-hybrid	Wang J (2011)
FAM110B	HIT	H. sapiens	Affinity Capture-MS	Varjosalo M (2013)
FAM110B	HIT	H. sapiens	Affinity Capture-MS	Huttlin EL (2017)
FAM110C	HIT	H. sapiens	Affinity Capture-MS	Varjosalo M (2013)
FAM110C	HIT	H. sapiens	Two-hybrid	Wang J (2011)
FAM110D	BAIT	H. sapiens	Affinity Capture-MS	Huttlin EL (2014/pre-pub)
FAM199X	HIT	H. sapiens	Affinity Capture-MS	Varjosalo M (2013)
FAM199X	HIT	H. sapiens	Affinity Capture-MS	Huttlin EL (2017)
FARP2	HIT	H. sapiens	Affinity Capture-MS	Varjosalo M (2013)
FBP1	HIT	H. sapiens	Two-hybrid	Vinayagam A (2011)
FBXO7	BAIT	H. sapiens	Biochemical Activity	Teixeira FR (2016)
FBXW11	HIT	H. sapiens	Two-hybrid	Wallach T (2013)
FKBPL	BAIT	H. sapiens	Affinity Capture-MS	Huttlin EL (2017)
FOPNL	HIT	H. sapiens	Affinity Capture-MS	Hein MY (2015)
FOXP2	BAIT	H. sapiens	Affinity Capture-MS	Huttlin EL (2017)
GAPVD1	HIT	H. sapiens	Affinity Capture-MS	Hein MY (2015)
GAPVD1	HIT	H. sapiens	Affinity Capture-MS	Huttlin EL (2017)
GTF3C1	HIT	H. sapiens	Two-hybrid	Vinayagam A (2011)
GTSE1	BAIT	H. sapiens	Affinity Capture-MS	Hein MY (2015)
HES1	HIT	H. sapiens	Two-hybrid	Vinayagam A (2011)
HMMR	HIT	H. sapiens	Affinity Capture-MS	Varjosalo M (2013)

HSPA8	HIT	H. sapiens	Affinity Capture-MS	Huttlin EL (2017)
JAK3	BAIT	H. sapiens	Affinity Capture-MS	Hein MY (2015)
KAT7	HIT	H. sapiens	Two-hybrid	Vinayagam A (2011)
Kctd5	BAIT	M. musculus	Affinity Capture-MS	Hein MY (2015)
KIAA0753	HIT	H. sapiens	Affinity Capture-MS	Hein MY (2015)
KIF2A	BAIT	H. sapiens	Affinity Capture-MS	Hein MY (2015)
KLHDC3	HIT	H. sapiens	Affinity Capture-MS	Varjosalo M (2013)
KLHL42	HIT	H. sapiens	Affinity Capture-MS	Huttlin EL (2017)
LDLRAD4	BAIT	H. sapiens	Affinity Capture-MS	Huttlin EL (2015)
LDLRAD4	BAIT	H. sapiens	Affinity Capture-MS	Huttlin EL (2017)
LPIN1	BAIT	H. sapiens	Affinity Capture-Western	Shimizu K (2017)
LTBR	BAIT	H. sapiens	Affinity Capture-MS	Huttlin EL (2015)
MAPK9	BAIT	H. sapiens	Affinity Capture-MS	Huttlin EL (2015)
MAVS	BAIT	H. sapiens	Affinity Capture-Western	Zhou Y (2016)
MCC	BAIT	H. sapiens	Affinity Capture-MS	Ewing RM (2007)
MCC	HIT	H. sapiens	Affinity Capture-MS	Varjosalo M (2013)
MCC	HIT	H. sapiens	Affinity Capture-MS	Hein MY (2015)
MCC	HIT	H. sapiens	Two-hybrid	Vinayagam A (2011)
MICU2	BAIT	H. sapiens	Affinity Capture-MS	Huttlin EL (2015)
MICU2	BAIT	H. sapiens	Affinity Capture-MS	Huttlin EL (2017)
MIER1	HIT	H. sapiens	Affinity Capture-MS	Hein MY (2015)
MRPL4	BAIT	H. sapiens	Affinity Capture-MS	Huttlin EL (2015)
MTA2	HIT	H. sapiens	Affinity Capture-MS	Varjosalo M (2013)
MTMR3	HIT	H. sapiens	Affinity Capture-MS	Huttlin EL (2014/pre-pub)
MTMR4	HIT	H. sapiens	Affinity Capture-MS	Huttlin EL (2017)
MYCN	HIT	H. sapiens	Synthetic Growth Defect	Toyoshima M (2012)
MYC	BAIT	H. sapiens	Dosage Lethality	Toyoshima M (2012)
NCOA3	BAIT	H. sapiens	Affinity Capture-Western	Li C (2011)
NCOA3	HIT	H. sapiens	Biochemical Activity	Li C (2011)
NLRP1	BAIT	H. sapiens	Co-fractionation	Wan C (2015)
NOB1	HIT	H. sapiens	Co-fractionation	Wan C (2015)
NR1D2	HIT	H. sapiens	Two-hybrid	Wallach T (2013)
NSUN2	BAIT	H. sapiens	Co-fractionation	Wan C (2015)
NTRK1	BAIT	H. sapiens	Affinity Capture-MS	Emdal KB (2015)
NXF2	BAIT	H. sapiens	Affinity Capture-MS	Huttlin EL (2017)
OCLN	BAIT	H. sapiens	Affinity Capture-MS	Huttlin EL (2017)
OCLN	HIT	H. sapiens	Affinity Capture-Western	McKenzie JA (2006)
OCLN	HIT	H. sapiens	Biochemical Activity	McKenzie JA (2006)
OCLN	BAIT	H. sapiens	Co-localization	Chen TC (2014)
OCLN	BAIT	H. sapiens	Reconstituted Complex	McKenzie JA (2006)
OCLN	BAIT	H. sapiens	Two-hybrid	McKenzie JA (2006)
OFD1	HIT	H. sapiens	Affinity Capture-MS	Hein MY (2015)
PCM1	HIT	H. sapiens	Affinity Capture-MS	Hein MY (2015)
PCM1	BAIT	H. sapiens	Proximity Label-MS	Gupta GD (2015)
PCMT1	BAIT	H. sapiens	Affinity Capture-MS	Huttlin EL (2015)
PCMT1	HIT	H. sapiens	Affinity Capture-MS	Huttlin EL (2017)
PDE4DIP	HIT	H. sapiens	Affinity Capture-MS	Huttlin EL (2017)
PER1	HIT	H. sapiens	Affinity Capture-MS	Varjosalo M (2013)
PER1	HIT	H. sapiens	Affinity Capture-MS	Hein MY (2015)
PER1	HIT	H. sapiens	Affinity Capture-MS	Huttlin EL (2017)
PER1	BAIT	H. sapiens	Affinity Capture-Western	Vielhaber E (2000)
PER1	HIT	H. sapiens	Biochemical Activity	Vielhaber E (2000)
PER1	BAIT	H. sapiens	Reconstituted Complex	Vielhaber E (2000)
PER1	BAIT	H. sapiens	Reconstituted Complex	Shirogane T (2005)
PER1	HIT	H. sapiens	Two-hybrid	Vielhaber E (2000)
PER1	HIT	H. sapiens	Two-hybrid	Wallach T (2013)

PER2	HIT	H. sapiens	Affinity Capture-MS	Huttlin EL (2017)
PER2	HIT	H. sapiens	Two-hybrid	Wallach T (2013)
PER3	HIT	H. sapiens	Affinity Capture-Western	Lee C (2004)
PNO1	BAIT	H. sapiens	Co-fractionation	Wan C (2015)
PNO1	HIT	H. sapiens	Two-hybrid	Vinayagam A (2011)
POTEF	HIT	H. sapiens	Affinity Capture-MS	Huttlin EL (2017)
PPM1B	HIT	H. sapiens	Co-fractionation	Wan C (2015)
PPP1CA	BAIT	H. sapiens	Biochemical Activity	Luo W (2007)
PPP1CC	HIT	H. sapiens	Two-hybrid	Wallach T (2013)
PPP1R14A	BAIT	H. sapiens	Reconstituted Complex	Zemlickova E (2004)
PPP2R5D	HIT	H. sapiens	Two-hybrid	Wallach T (2013)
PPP2R5E	HIT	H. sapiens	Two-hybrid	Wallach T (2013)
PPP6R3	HIT	H. sapiens	Affinity Capture-MS	Varjosalo M (2013)
PRDX4	HIT	H. sapiens	Affinity Capture-MS	Varjosalo M (2013)
PRKAR2A	HIT	H. sapiens	Affinity Capture-MS	Hein MY (2015)
PRKAR2B	HIT	H. sapiens	Affinity Capture-MS	Huttlin EL (2017)
PRMT5	HIT	H. sapiens	Affinity Capture-MS	Varjosalo M (2013)
PTPRD	BAIT	H. sapiens	Reconstituted Complex	Meehan M (2012)
RAD54B	HIT	H. sapiens	Two-hybrid	Rual JF (2005)
RASAL2	HIT	H. sapiens	Affinity Capture-MS	Varjosalo M (2013)
RASAL2	HIT	H. sapiens	Affinity Capture-MS	Hein MY (2015)
RBX1	HIT	H. sapiens	Two-hybrid	Vinayagam A (2011)
REST	HIT	H. sapiens	Affinity Capture-Western	Kaneko N (2014)
REST	BAIT	H. sapiens	Affinity Capture-Western	Kaneko N (2014)
RIPK4	BAIT	H. sapiens	Affinity Capture-MS	Rodriguez J (2016)
RNF7	BAIT	H. sapiens	Affinity Capture-MS	Huttlin EL (2014/pre-pub)
RNF43	BAIT	H. sapiens	Affinity Capture-MS	Huttlin EL (2017)
RORA	HIT	H. sapiens	Two-hybrid	Wallach T (2013)
RORC	HIT	H. sapiens	Two-hybrid	Wallach T (2013)
RP2	BAIT	H. sapiens	Affinity Capture-MS	Huttlin EL (2015)
RP2	BAIT	H. sapiens	Affinity Capture-MS	Huttlin EL (2017)
RPS4Y2	HIT	H. sapiens	Affinity Capture-MS	Huttlin EL (2017)
SAV1	BAIT	H. sapiens	Affinity Capture-MS	Couzens AL (2013)
SAV1	HIT	H. sapiens	Affinity Capture-MS	Varjosalo M (2013)
SDCCAG3	HIT	H. sapiens	Two-hybrid	Wang J (2011)
SEC13	HIT	H. sapiens	Affinity Capture-MS	Varjosalo M (2013)
SEC16A	HIT	H. sapiens	Affinity Capture-MS	Varjosalo M (2013)
SGOL2	BAIT	H. sapiens	Affinity Capture-MS	Huttlin EL (2015)
SMARCD1	BAIT	H. sapiens	Affinity Capture-MS	Huttlin EL (2015)
SNX22	HIT	H. sapiens	Affinity Capture-MS	Varjosalo M (2013)
SNX24	HIT	H. sapiens	Affinity Capture-MS	Varjosalo M (2013)
SNX24	HIT	H. sapiens	Affinity Capture-MS	Hein MY (2015)
SNX24	HIT	H. sapiens	Affinity Capture-MS	Huttlin EL (2017)
SPICE1	HIT	H. sapiens	Affinity Capture-MS	Hein MY (2015)
SSMEM1	BAIT	H. sapiens	Affinity Capture-MS	Huttlin EL (2017)
STK3	HIT	H. sapiens	Affinity Capture-MS	Varjosalo M (2013)
STOX2	HIT	H. sapiens	Affinity Capture-MS	Varjosalo M (2013)
STOX2	HIT	H. sapiens	Affinity Capture-MS	Hein MY (2015)
TAOK1	HIT	H. sapiens	Two-hybrid	Vinayagam A (2011)
TAZ	BAIT	H. sapiens	Affinity Capture-Western	Liu CY (2010)
TAZ	HIT	H. sapiens	Biochemical Activity	Liu CY (2010)
TCEB2	HIT	H. sapiens	Affinity Capture-MS	Varjosalo M (2013)
TENC1	HIT	H. sapiens	Two-hybrid	Wang J (2011)
TEX264	BAIT	H. sapiens	Affinity Capture-MS	Huttlin EL (2015)
TIAM1	BAIT	H. sapiens	Affinity Capture-MS	Magliozzi R (2014)
TMEM208	BAIT	H. sapiens	Affinity Capture-MS	Huttlin EL (2014/pre-pub)

TNFRSF1A	BAIT	H. sapiens	Affinity Capture-MS	Huttlin EL (2017)
TP53	BAIT	H. sapiens	Co-localization	Chen TC (2014)
TRA2A	BAIT	H. sapiens	Affinity Capture-MS	Huttlin EL (2015)
TRA2A	BAIT	H. sapiens	Affinity Capture-MS	Huttlin EL (2017)
TRAF3	BAIT	H. sapiens	Affinity Capture-Western	Zhou Y (2016)
TRAF3	HIT	H. sapiens	Affinity Capture-Western	Zhou Y (2016)
TRAF3	HIT	H. sapiens	Biochemical Activity	Zhou Y (2016)
TRIM3	HIT	H. sapiens	Affinity Capture-MS	Hein MY (2015)
Trp53	HIT	M. musculus	Biochemical Activity	Knippschild U (1997)
UBE2S	BAIT	H. sapiens	Affinity Capture-MS	Huttlin EL (2015)
UBXN7	BAIT	H. sapiens	Affinity Capture-MS	Raman M (2015)
UNC45A	HIT	H. sapiens	Affinity Capture-MS	Varjosalo M (2013)
UQCC1	HIT	H. sapiens	Affinity Capture-MS	Huttlin EL (2017)
Uso1	BAIT	M. musculus	Affinity Capture-MS	Hein MY (2015)
USP9X	HIT	H. sapiens	Affinity Capture-MS	Varjosalo M (2013)
USP9Y	HIT	H. sapiens	Affinity Capture-MS	Varjosalo M (2013)
USP39	BAIT	H. sapiens	Co-fractionation	Wan C (2015)
VPS13B	HIT	H. sapiens	Affinity Capture-MS	Varjosalo M (2013)
WDR5	HIT	H. sapiens	Affinity Capture-MS	Varjosalo M (2013)
WDR90	HIT	H. sapiens	Affinity Capture-MS	Hein MY (2015)
WWC1	BAIT	H. sapiens	Affinity Capture-MS	Toloczko A (2017)
XPO1	BAIT	H. sapiens	Affinity Capture-MS	Kirli K (2015)
ZMYND8	HIT	H. sapiens	Two-hybrid	Vinayagam A (2011)
ZNF227	HIT	H. sapiens	Two-hybrid	Vinayagam A (2011)
ZNF618	HIT	H. sapiens	Affinity Capture-MS	Huttlin EL (2017)
ZSWIM8	HIT	H. sapiens	Affinity Capture-MS	Varjosalo M (2013)